A 3D medical illustration of a blood vessel. The vessel is shown in a cross-section, with a white, fibrous-looking wall. Inside the vessel, numerous red blood cells (erythrocytes) are depicted as bright red, biconcave discs. Several white blood cells (leukocytes) are also visible, appearing as irregular, white, textured spheres. The background is a soft, warm gradient of orange and yellow, suggesting a light source from the left. The overall composition is dynamic, with the vessel curving from the top left towards the bottom right.

Endothelial plasticity in fibrosis and epigenetics as a therapeutic target

Melanie S. Hulshoff



university of
 groningen



Endothelial plasticity in fibrosis and epigenetics as a therapeutic target

PhD thesis

to obtain the degree of PhD at the
 University of Groningen
 on the authority of the
 Rector Magnificus Prof. C. Wijmenga
 and in accordance
 with the decision by the College of Deans

and

for the award of the degree
 “Doctor rerum naturalium” (Dr.rer.nat)
 of the Georg-August-Universität Göttingen
 within the doctoral program Molecular Medicine
 of the Georg-August University School of Science (GAUSS)

Double PhD degree

This thesis will be defended in public on
 Monday 7 December 2020 at 16.15 hours

by

Melissa Stephanie Hulshoff

born on 12 December 1992
 in Groningen, The Netherlands

SUPERVISORS

Prof. Elisabeth M. Zeisberg

Prof. Martin C. Harmsen

CO-SUPERVISOR

Dr. Guido Krenning

THESIS COMMITTEE

(ONLY FOR THE UNIVERSITY OF GÖTTINGEN)

Prof. Elisabeth M. Zeisberg

Dr. Guido Krenning

Prof. Steven A. Johnsen

ASSESSMENT COMMITTEE

Prof. Steven A. Johnsen

Prof. Bernd Wollnik

Prof. Jan-Luuk Hillebrands

Prof. Marie-José T. H. Goumans

EXAMINING COMMITTEE

Prof. Steven A. Johnsen

Prof. Bernd Wollnik

Prof. Jan-Luuk Hillebrands

Prof. Marie-José T. H. Goumans

Prof. Viacheslav O. Nikolaev

Prof. André Fischer

Prof. Marianne G. Rots

Prof. Robert H. Henning

CONTENTS

9 CHAPTER 1

Abstract, introduction and aims of the thesis

PART I: (EPI)GENETIC REGULATION OF ENDOTHELIAL PLASTICITY

19 CHAPTER 2

Epigenetic regulation of endothelial-to-mesenchymal transition in chronic heart disease

Histone modifications, DNA methylation, and noncoding RNAs

Arterioscler Thromb Vasc Biol 2018

49 CHAPTER 3

Hypoxia-induced endothelial-mesenchymal transition is associated with RASAL1 promoter hypermethylation in human coronary endothelial cells

FEBS Letters 2016

75 CHAPTER 4

miR-132-3p and KLF7 as novel potential regulators of aortic stiffening-associated EndMT in type 2 diabetes

101 CHAPTER 5

Non-coding RNA in endothelial-to-mesenchymal transition

Cardiovasc Res 2019

147 CHAPTER 6

Stage-specific mapping of the endothelial-to-mesenchymal transition

PART II: (EPI)GENETICS AS A THERAPEUTIC TARGET IN FIBROSIS

171 CHAPTER 7

Serelaxin alleviates cardiac fibrosis through inhibiting endothelial-to-mesenchymal transition via RFXP1

Theranostics 2020

223	CHAPTER 8 Causal connections from chronic kidney disease to cardiac fibrosis <i>Semin Nephrol 2018</i>
245	CHAPTER 9 CRISPR/Cas derivatives as novel gene modulating tools: possibilities and <i>in vivo</i> applications <i>Int J Mol Sci 2020</i>
279	CHAPTER 10 High-fidelity CRISPR/Cas9-based gene-specific hydroxymethylation rescues gene expression and attenuates renal fibrosis <i>Nat Commun 2018</i>
337	CHAPTER 11 Split-intein mediated AAV delivery of dCas9-TET3 as antifibrotic therapy <i>Submitted</i>
377	CHAPTER 12 Research summary
383	CHAPTER 13 Epilogue (general discussion)
393	CHAPTER 14 Nederlandse samenvatting (ook voor niet ingewijden)
399	CHAPTER 15 Deutsche Zusammenfassung
403	APPENDICES Abbreviations Acknowledgements Curriculum Vitae Publication list

CHAPTER

1

ABSTRACT, INTRODUCTION AND OUTLINE

ABSTRACT

In this thesis, we aim to (1) uncover novel (epi)genetic regulatory mechanisms that affect endothelial plasticity as an underlying cause of organ fibrosis, and (2) to therapeutically target (epi)genetic regulatory mechanisms to combat organ fibrosis. We identified relevant epigenetic changes during endothelial-to-mesenchymal transition (EndMT), a specific form of endothelial plasticity, in different disease contexts and investigated the impact of different EndMT triggers (such as hypoxia and high glucose) and unraveled the epigenetic changes they induce. Moreover, we have investigated their relevance to the induction and progression of EndMT. Also, we performed stage-specific mapping of EndMT to identify genetic regulatory mechanisms that drive the active stage of transition. For the second aim, we demonstrate that Serelaxin, a recombinant form of the human Relaxin-2 hormone, alleviates cardiac fibrosis in part through the inhibition of EndMT. We also discussed the mechanisms involved in the reciprocal relationship between chronic kidney disease and cardiac fibrosis and identified microRNAs as potential profibrotic kidney-heart messengers. Moreover, we identified relevant possibilities and in vivo applications of CRISPR/Cas derivatives. This gene modulating tool is applied to target epigenetic modifications which alleviate both renal and cardiac fibrosis. In conclusion, in this thesis we have shown that in fibroproliferative diseases, endothelial plasticity is highly regulated by epigenetic modifications (part I). These epigenetic modifications may offer new therapeutic approaches. Indeed, we demonstrate that epigenetic modifications can be targeted in vivo, which results in alleviated organ fibrosis (part II).

INTRODUCTION AND AIMS

Organ fibrosis is characterized by the progressive deposition of extracellular matrix which replaces functional tissue and results in structural alterations and eventually loss of function, contributing to organ dysfunction (*e.g.* heart failure). The excessive extracellular matrix is produced by different cell types, such as activated fibroblasts, so-called myofibroblasts, and myofibroblast-like cells derived from endothelial cells via a process called endothelial-to-mesenchymal transition (EndMT) [1-4]. As of yet, no specific anti-fibrotic therapy is available.

Endothelial cells line the inner side of blood (or lymphatic) vessels and are in direct contact with the blood. Endothelial cells form the barrier between the blood and the surrounding tissue, and have several important functions such as regulating vascular permeability and the trafficking of leukocytes to the surrounding tissue [5,6]. The dynamic environment (including both biochemical stimuli and mechanical forces) requires endothelial cells to be highly adaptive [7]. This endothelial plasticity can be advantageous, but adverse plasticity can also contribute to disease.

EndMT is a specific form of endothelial plasticity, and was originally discovered during cardiac valve development, but is now increasingly recognized for its contribution to pathologies such as cardiovascular disease [8-10], organ fibrosis [3,4,11] and cancer [12,13]. EndMT is characterized by the loss of endothelial markers and the upregulation of EndMT transcription factors as well as mesenchymal markers. EndMT-derived mesenchymal cells acquire a highly migratory and invasive phenotype which is accompanied by morphological changes from a cobble-stone endothelial morphology into a spindle-shaped myofibroblast-like morphology. EndMT is triggered by a variety of external stimuli such as the lack of oxygen (hypoxia), high glucose concentrations or pro-inflammatory cytokines [14-16]. These environmental factors trigger the activation of signaling pathways which induce EndMT such as the canonical Transforming Growth Factor Beta (TGF- β) pathway or the non-canonical pathways such as Notch [17]. However, the underlying molecular mechanisms that drive EndMT remain largely unknown.

Epigenetics is a way of regulating gene expression independent of changes in the nucleotide sequence, and has been increasingly linked to EndMT [18,19]. Epigenetic regulation includes DNA promoter methylation, histone modifications

and non-coding RNAs, which each individually or in concert influence gene transcription. Epigenetic regulation was originally identified as a determinant for cellular differentiation during development but is increasingly recognized for its association with cardiovascular disease, organ fibrosis and cancer [20-25]. Because EndMT (1) is originally a developmental process, (2) is a form of cellular plasticity by which extensive gene expression changes are necessary, and (3) contributes to diseases which are associated with epigenetic regulation, epigenetics is considered as a strong candidate regulator of EndMT [18].

The aims of this thesis are to (1) uncover novel (epi)genetic regulatory mechanisms that affect EndMT and (2) to therapeutically target (epi)genetic regulatory mechanisms to combat organ fibrosis.

OUTLINE OF THE THESIS

The first part of the thesis focuses on the epigenetic regulation of EndMT in the context of cardiovascular disease. **Chapter 2** starts with an overview of the signaling pathways and modulators of EndMT including profibrotic cytokines (*e.g.* TGF- β), hypoxia (the lack of oxygen) and high glucose. The focus of **Chapter 2** includes a summary of the epigenetic mechanisms (*i.e.* histone modifications, DNA methylation and non-coding RNAs) which influence EndMT in the context of chronic heart disease. Having identified the relevant epigenetic changes (**Chapter 2**), in the next two chapters we investigated the impact of different EndMT triggers (*i.e.* hypoxia and high glucose) and unraveled the epigenetic changes they induce. In **Chapter 3** we examine the possible involvement of DNA promoter methylation of the anti-fibrotic gene RASAL1 in hypoxia-induced EndMT. In **Chapter 4** we investigate the contribution of the non-coding RNA miR-132-3p and the transcription factor KLF7 in glucose-induced EndMT and the related aortic stiffening in diabetes. Besides cardiovascular disease, EndMT contributes to other pathologies including chronic kidney disease. **Chapter 5** describes the mechanisms by which non-coding RNAs facilitate or inhibit EndMT during development and diseases. In the last chapter of *part I*, **Chapter 6**, we performed stage-specific mapping of EndMT to identify regulatory mechanisms that drive the active stage of transition.

The second part of the thesis focuses on the therapeutic targeting of epigenetic mechanisms to combat organ fibrosis. We explore in **Chapter 7** the anti-fibrotic effect of Serelaxin, a recombinant form of the human Relaxin-2 hormone, in the heart. Serelaxin exerts vasodilating, anti-inflammatory and anti-fibrotic effects and might therefore be of interest to target chronic heart failure. **Chapter 8** describes the mechanisms by which chronic kidney disease may cause cardiac fibrosis. Several (potential) modulators are discussed including non-coding RNAs. **Chapter 9** describes different genome editing tools, the variety of Cas proteins and most importantly the possibilities and *in vivo* applications of CRISPR/Cas derivatives to perform gene modulation. The CRISPR/Cas system was originally discovered in bacteria and is now used to cleave mammalian DNA or RNA. Deactivation of the cleavage capacity of the CRISPR/Cas system enables to fuse Cas to other effector domains thereby enabling distinct possibilities to use the CRISPR/Cas system. In **Chapter 10** we use the deactivated CRISPR/Cas system to perform gene-specific reactivation of the anti-fibrotic genes (including RASAL1) which results in the amelioration of kidney fibrosis. After the successful establishment of this system to prevent experimental kidney fibrosis, we transfer this system to the heart to treat experimental cardiac fibrosis (**Chapter 11**).

The final part of the thesis includes a **Research Summary** and an **Epilogue** including discussion and future perspectives.

REFERENCES

1. Zeisberg EM, Kalluri R. Origins of cardiac fibroblasts. *Circ Res* 2010;107:1304–1312.
2. Krenning G, Zeisberg EM, Kalluri R. The origin of fibroblasts and mechanism of cardiac fibrosis. *J Cell Physiol* 2010;225:631–637.
3. Zeisberg EM, Tarnavski O, Zeisberg M, Dorfman AL, McMullen JR, Gustafsson E, et al. Endothelial-to-mesenchymal transition contributes to cardiac fibrosis. *Nat Med* 2007;13:952-961.
4. Zeisberg EM, Potenta SE, Sugimoto H, Zeisberg M, Kalluri R. Fibroblasts in kidney fibrosis emerge via endothelial-to-mesenchymal transition. *J Am Soc Nephrol* 2008;19:2282-2287.
5. Sukriti S, Tauseef M, Yazbeck P, Mehta D. Mechanisms regulating endothelial permeability. *Pulm Circ* 2014;4(4):535-551.
6. Aird WC. Phenotypic heterogeneity of the endothelium: I. Structure, function and mechanisms. *Circ Res* 2007;100:158-173.
7. Aird WC. Spatial and temporal dynamics of the endothelium. *J Thromb Haemost* 2005;3:1392-1406.
8. Ranchoux B, Antigny F, Rucker-Martin C, Hautefort A, Pechoux C, Bogaard HJ, et al. Endothelial-to-mesenchymal transition in pulmonary hypertension. *Circulation* 2015;131:1006-1018.
9. Chen PY, Qin L, Baeyens N, Li G, Afolabi T, Budatha M, et al. Endothelial-to-mesenchymal transition drives atherosclerosis progression. *The Journal of clinical investigation* 2015;125:4514-4528.
10. Souilhol C, Harmsen MC, Evans PC, Krenning G. Endothelial-mesenchymal transition in atherosclerosis. *Cardiovascular research* 2018;114:565-577.
11. Hashimoto N, Phan SH, Imaizumi K, Matsuo M, Nakashima H, Kawabe T, et al. Endothelial-mesenchymal transition in bleomycin-induced pulmonary fibrosis. *American journal of respiratory cell and molecular biology* 2010;43:161-172.
12. Zeisberg EM, Potenta S, Xie L, Zeisberg M, Kalluri R. Discovery of endothelial to mesenchymal transition as a source for carcinoma-associated fibroblasts. *Cancer research* 2007;67:10123-10128.
13. Hong L, Du X, Li W, Mao Y, Sun L, Li X. EndMT: A promising and controversial field. *Eur J Cell Biol* 2018;97:493-500.
14. Xu X, Tan X, Tampe B, et al. Snail is a direct target of hypoxia-inducible factor 1alpha (HIF1alpha) in hypoxia-induced endothelial to mesenchymal transition of human coronary endothelial cells. *J Biol Chem.* 2015;290:16653-64.
15. Xu X, Tan X, Tampe B, et al. Epigenetic balance of aberrant Rasal1 promoter methylation and hydroxymethylation regulates cardiac fibrosis. *Cardiovasc Res.* 2015;105:279-91.
16. Suthanthiran M, Gerber LM, Schwartz JE, et al. Circulating transforming growth factor-beta1 levels and the risk for kidney disease in African Americans. *Kidney Int.* 2009;76:72-80.

17. Rieder F, Kessler SP, West GA, et al. Inflammation-induced endothelial-to-mesenchymal transition: a novel mechanism of intestinal fibrosis. *Am J Pathol.* 2011;179:2660-73.
18. Hulshoff MS, Xu X, Krenning G, Zeisberg EM. Epigenetic regulation of endothelial-to-mesenchymal transition in chronic heart disease. *Arterioscler Thromb Vasc Biol.* 2018;38(9):1986-1996.
19. Hulshoff MS, Del Monte-Nieto G, Kovacic J, Krenning G. Non-coding RNA in endothelial-to-mesenchymal transition. *Cardiovascular Res.* 2019;115(12):1716-1731.
20. Feinberg AP, Vogelstein B. Hypomethylation distinguishes genes of some human cancers from their normal counterparts. *Nature.* 1983;301:89–92.
21. Mann J, Mann DA. Epigenetic regulation of wound healing and fibrosis. *Curr Opin Rheumatol.* 2013;25:101–107.
22. Nakatochi M, Ichihara S, Yamamoto K, Naruse K, Yokota S, Asano H, Matsubara T, Yokota M. Epigenome-wide association of myocardial infarction with DNA methylation sites at loci related to cardiovascular disease. *Clin Epigenetics.* 2017;9:54.
23. Tampe B, Zeisberg M. Contribution of genetics and epigenetics to progression of kidney fibrosis. *Nephrol Dial Transplant.* 2014;29(suppl 4):iv72–iv79.
24. Petronis A. Epigenetics as a unifying principle in the aetiology of complex traits and diseases. *Nature.* 2010;465:721–727.
25. Yang IV, Schwartz DA. Epigenetics of idiopathic pulmonary fibrosis. *Transl Res.* 2015;165:48–60.

PART I

(EPI)GENETIC REGULATION OF ENDOTHELIAL PLASTICITY

CHAPTER

2

EPIGENETIC REGULATION OF ENDOTHELIAL-TO-MESENCHYMAL TRANSITION IN CHRONIC HEART DISEASE

HISTONE MODIFICATIONS, DNA METHYLATION, AND NONCODING RNAS

Melanie S. Hulshoff^{1,2,3}, Xingbo Xu^{1,2}, Guido Krenning^{3,†} and Elisabeth M. Zeisberg^{1,2,†}

¹*Department of Cardiology and Pneumology, University Medical Center of Göttingen, Georg-August University, Göttingen, Germany.*

²*German Centre for Cardiovascular Research (DZHK), Göttingen, Germany.*

³*Laboratory for Cardiovascular Regenerative Medicine, Department of Pathology and Medical Biology, University Medical Center Groningen, University of Groningen, The Netherlands.*

[†]*share last authorship*

ABSTRACT

Endothelial-to-mesenchymal transition (EndMT) is a process in which endothelial cells lose their properties and transform into fibroblast-like cells. This transition process contributes to cardiac fibrosis, a common feature of patients with chronic heart failure. To date, no specific therapies to halt or reverse cardiac fibrosis are available, so knowledge of the underlying mechanisms of cardiac fibrosis is urgently needed. In addition, EndMT contributes to other cardiovascular pathologies such as atherosclerosis and pulmonary hypertension, but also to cancer and organ fibrosis. Remarkably, the molecular mechanisms driving EndMT are largely unknown. Epigenetics play an important role in regulating gene transcription and translation and have been implicated in the EndMT process. Therefore, epigenetics might be the missing link in unraveling the underlying mechanisms of EndMT. Here, we review the involvement of epigenetic regulators during EndMT in the context of cardiac fibrosis. The role of DNA methylation, histone modifications (acetylation and methylation), and noncoding RNAs (microRNAs, long noncoding RNAs, and circular RNAs) in the facilitation and inhibition of EndMT are discussed, and potential therapeutic epigenetic targets will be highlighted.

INTRODUCTION

Endothelial-to-mesenchymal transition (EndMT) is a cellular transition process in which endothelial cells lose their endothelial characteristics and gain a fibroblast-like phenotype. EndMT was originally identified in cardiac development where the endocardial endothelial cells of the atrioventricular canal undergo EndMT to form the cardiac valves and septum [1]. In 2007, it was discovered that aberrant activation of the EndMT program during adult life contributes to cardiac fibrosis, a pathological scarring process which constitutes an integral component of cardiovascular disease [2]. In the years to follow, it has been shown that pathological EndMT not only plays a significant role in the initiation and progression of cardiovascular diseases such as atherosclerosis and pulmonary hypertension [3,4], but also in kidney and pulmonary fibrosis, brain vascular malformation, and cancer [5–8]. Consequently, EndMT is no longer solely associated with development but is now considered an important contributor to pathogenesis. However, different studies came to different conclusions with respect to the extent of EndMT, even in various models of pressure overload (eg, transverse aortic constriction versus ascending aortic constriction) [2,9], suggesting that EndMT is highly context-dependent and that further studies are needed to understand when exactly EndMT happens and how it is driven at a molecular level.

SIGNALING PATHWAYS AND MODULATORS OF ENDMT: TGF- β SIGNALING AS A MAJOR INDUCER OF ENDMT

Several signaling pathways have been associated with the initiation and progression of EndMT during both development and disease conditions. TGF (transforming growth factor)- β signaling is the major inducer of EndMT in both physiological and pathological conditions [10]. There are 3 isoforms of TGF- β : TGF- β 1, TGF- β 2, and TGF- β 3. Since TGF- β 1 is the most commonly studied in the context of pathological EndMT and TGF- β 2 is the most important in developmental EndMT, the effects of the TGF- β 3 isoform on EndMT are relatively unknown [11]. The TGF- β cascade is under physiological conditions in endothelial cells as follows: TGF- β binds to the TGF- β receptor type II which in turn activates

the type I TGF- β receptor ALK1 (activin receptor-like kinase-1) [12]. Subsequently, ALK1 antagonizes EndMT via activation of SMAD (SMAD family member) 1/5/8 signaling [12]. Upon increased TGF- β levels, however, signaling through the type I TGF- β receptor ALK5 is initiated [12]. ALK5 recruits and phosphorylates the transcription factors SMAD2 and SMAD3, which form a complex together with coactivator SMAD4 [12]. This complex translocates to the nucleus and interacts with transcription factors such as SNAIL (snail family transcriptional repressor 1), SLUG (snail family transcriptional repressor 2), and TWIST (twist family bHLH transcription factor 1) to regulate induction of mesenchymal gene expression and repression of endothelial gene expression, thereby facilitating EndMT (Figure 1). Other signaling pathways such as Notch signaling, independently or synergistically with TGF- β induce EndMT during both development and pathogenesis [13]. Notch signaling is initiated by ligand binding, which induces proteolytic cleavage of the transmembrane receptor and release of the intracellular domain. The intracellular domain translocates to the nucleus and associates with CSL (CBF1/Suppressor of Hairless/Lag1)-binding sites thereby recruiting coactivators to initiate transcription [14]. Other signaling pathways that induce EndMT are Ras- and BMP (bone morphogenetic protein)-signaling. Aberrant activation of signaling pathways that induce EndMT during both adult life and development can be explained by the presence of environmental factors (hits) that can trigger EndMT. Environmental factors include disturbed fluid shear stress, the frictional force of the blood flow exerted to the endothelial layer, and high blood glucose levels [15,16]. In addition, environmental factors such as hypoxia or proinflammatory cytokines, as part of the profibrotic microenvironment, contribute independently or synergistically with TGF- β signaling to EndMT [17–23]. Nevertheless, even though several signaling pathways and environmental factors have been associated with the initiation and progression of EndMT, the underlying molecular mechanisms regulating EndMT are still incompletely understood. This lack of knowledge might be explained by the presence of epigenetics as a supreme layer of regulation that aberrantly activates EndMT during disease conditions.

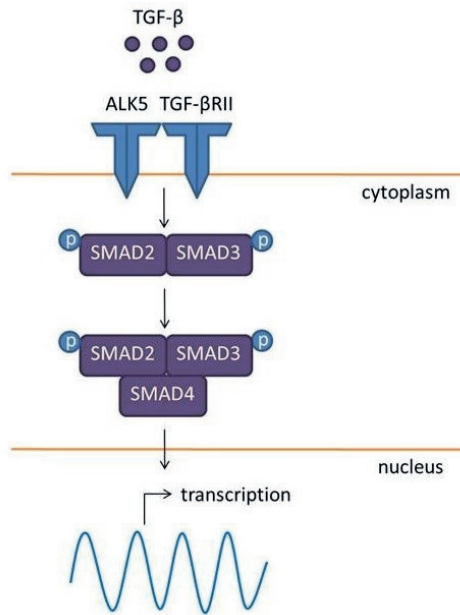


Figure 1. TGF (transforming growth factor)- β signaling as a major inducer of endothelial-to-mesenchymal transition (EndMT).

In the presence of TGF- β , the TGF- β receptor type II activates the type I TGF- β receptor ALK5 (activin receptor-like kinase-5), which in turn recruits and phosphorylates the transcription factors SMAD (SMAD family member)2 and SMAD3. The phosphorylated SMAD2 and SMAD3 then form a complex together with coactivator SMAD4 and translocate to the nucleus to affect gene transcription and drive EndMT.

EPIGENETIC REGULATION AS A STRONG CANDIDATE REGULATOR OF ENDMT

Epigenetics is a stable way of regulating gene expression independent of changes in the nucleotide sequence. The term epigenetics was already described 50 years ago, but only in the last years, there is an uprise in the field of epigenetic regulation—which aims to explain biological phenomena from a different perspective. Epigenetic regulation, and thereby regulation of gene expression, occurs at the transcriptional level via DNA methylation and histone modifications. Noncoding RNAs can affect gene expression at both the transcriptional (via long noncoding RNAs [lncRNAs] and circular RNAs [circRNAs]) and posttranscriptional

level (via microRNAs [miRNAs], lncRNAs, and circRNAs). Epigenetic regulation was originally identified as determinant for cellular differentiation during development but is increasingly recognized for its causal contribution to cardiovascular disease, organ fibrosis, and cancer [24–30]. Because EndMT (1) is originally a developmental process, (2) is a form of cellular transdifferentiation by which extensive gene expression changes are necessary, and (3) contributes to diseases which are associated with epigenetic regulation, epigenetics is considered as a strong candidate regulator of EndMT. This review will focus on the different levels of epigenetic regulation associated with EndMT and highlight potential epigenetic-based therapeutic possibilities to combat EndMT-associated pathologies with a focus on cardiovascular disease.

HISTONE METHYLATION AND (DE)ACETYLATION ARE IMPORTANT REGULATORS OF ENDMT

Histone proteins package the DNA into nucleosomes and can be modified posttranslationally resulting in either transcriptional activation (via chromatin relaxation and making the DNA accessible for transcription factors and coregulators) or transcriptional repression (via chromatin compaction). Histone modifications include phosphorylation, sumoylation, ubiquitylation, methylation, and acetylation. Only the global methylation and acetylation of lysine residues have been reported to date to be associated with EndMT and will hence be the focus of this review. Histone methylation is associated with both transcriptional activation (eg, H3K4me3) and repression (eg, H3K27me3) depending on the location of the lysine residue and the degree of methylation [31–33]. In contrast, histone acetylation is solely associated with transcriptional activation. Regulation of histone modifications occurs via homeostasis between histone-modifying enzymes which either deposit (histone methyl- or acetyltransferases) or remove modification marks (histone demethyl- or deacetylases). Consequently, histone-modifying enzymes regulate the accessibility of the chromatin thereby determining the transcriptional and thus cellular outcome. The histone-modifying enzymes that have been associated with EndMT will now be discussed in more detail.

HISTONE METHYLTRANSFERASE EZH2 AND HDAC3 ARE ESSENTIAL REGULATORS OF ENDMT DURING DEVELOPMENT AND DISEASE

EZH2 (enhancer of zeste homolog 2) is the major histone methyltransferase of the polycomb repressor complex 2 and is responsible for depositing trimethylation marks on lysine 27 of H3 (histone 3; H3K27me3) resulting in transcriptional repression [34]. EZH2 is an important modulator of EndMT during both development and disease. During second heart field development, HDAC3 (histone deacetylase 3) recruits EZH2 to the DNA to mediate silencing of TGF- β 1 transcription thereby terminating physiological EndMT, which is an essential step to complete cardiac development [35]. Lack of HDAC3 in the second heart field, and thereby the loss of EZH2 recruitment and thus transcriptional activation of TGF- β 1, results in several cardiovascular abnormalities leading to embryonic lethality because of the disruption of cardiac development [35]. This underlines the essential role of both HDAC3 and EZH2 in regulating EndMT during cardiac development [35]. At the same time, it has been reported that loss of EZH2 inhibits endothelial proliferation [36]. The definite contribution of EZH2 to EndMT is therefore still under debate. Besides physiological conditions, EZH2 also regulates EndMT during pathological conditions. Costimulation of endothelial cells with TGF- β 2 and IL (interleukin)-1 β (a proinflammatory cytokine mimicking the profibrotic microenvironment) results in decreased expression of EZH2 [17]. This loss of EZH2 expression is associated with reduced H3K27me3 marks at the TAGLN (transgelin [SM22 α]) promoter and thus with transcriptional activation of TAGLN (SM22 α), a mesenchymal gene which is upregulated during the process of EndMT, thereby facilitating EndMT [17]. Moreover, it has been shown that inhibition of HDAC3 results in epithelial-to-mesenchymal transition (EMT), a cellular transition process similar to EndMT, in a head and neck cancer cell line [37]. Altogether, this underlines the essential role of both EZH2 and HDAC3 in EndMT regulation, making them promising epigenetic targets to interfere with TGF- β -induced EndMT. In this regard, several aspects of the regulatory role of EZH2 and HDAC3 on EndMT need to be addressed. First, EZH2 can still maintain its expression on single stimulation with TGF- β 2 (without IL [interleukin]-1 β costimulation), indicating that several hits are necessary to induce the loss of EZH2. This provides the opportunity to identify the defensive mechanism by which EZH2 maintains its expression upon TGF- β 2 exposure alone, which might

result in new insights on how to reactivate or maintain EZH2 expression thereby preventing EndMT. Second, it is important to mention that several TGF- β isoforms (TGF- β 1 and TGF- β 2) are involved in the (HDAC3-) EZH2-mediated regulation of EndMT, meaning that isoform-specific effects of TGF- β on EZH2 and vice versa should be elucidated. Third, the association between HDAC3 and EZH2 displays the interaction of HDACs with histone methyltransferases. Nevertheless, the underlying mechanisms on how these different histone-modifying enzymes interact with one another remains elusive. Neither HDAC3 nor EZH2 can bind directly to the DNA, suggesting the involvement of yet to be described transcription factors and coregulators facilitating the recruitment of both HDAC3 and EZH2 to the DNA to enable transcriptional repression and regulation of EndMT. Indeed, lncRNAs, which are discussed later in this review, have been described to guide EZH2 to specific genes indicating that lncRNA context is pivotal for EZH2 function [38,39]. In short, uncovering the underlying mechanisms by which EZH2 and HDAC3 facilitate regulation of EndMT may provide important clues for novel therapeutic approaches to combat pathological EndMT.

HISTONE ACETYLATION AND THE HISTONE ACETYLASE EP300 ARE ASSOCIATED WITH ENDMT

H4 (histone 4) acetylation is involved in the synergistic upregulation of specific SMAD3 target genes (HEY1 [hes related family bHLH transcription factor with YRPW motif 1] and ANKRD1 [ankyrin repeat domain 1]) on combined TGF- β 1 stimulation and Notch activation [40]. This is facilitated via recruitment of SMAD3 to SBEs (SMAD-binding elements) and CSL (Notch) binding sites in the DNA. Interestingly, SMAD3 (and other receptor-regulated SMADs such as SMAD1, SMAD2, SMAD5, and SMAD8/9) and Notch intracellular domains can both interact with histone acetyltransferases indicating their roles in histone acetyltransferase recruitment [41,42]. Another SMAD3 target gene which is only regulated by TGF- β 1 (PAI1 [phosphoribosylanthranilate isomerase 1]) is associated with both H4 acetylation and trimethylation of a lysine residue of H3 (H3K4me3) indicating that single (regulated only by TGF- β 1) or synergistic regulation (regulated by both TGF- β 1 and Notch) of EndMT target genes can induce different epigenetic outcomes with potentially different effects in the long run. However, which histone acetyltransferase(s) or histone methyltransferase(s)

are involved remains unknown. Interestingly, because (1) TGF- β 2 treatment in mouse cardiac endothelial cells induces expression of the histone acetyltransferase p300 which (2) is also significantly upregulated in fibrotic tissues, and (3) is well-known for its role as regulator of gene transcription, the histone acetyltransferase EP300 (E1A binding protein p300) might represent an important modulator of EndMT [43–46]. Therefore, the histone acetyltransferase EP300 might be responsible for the H4 acetylation and upregulation of specific SMAD3 target genes upon TGF- β 1 stimulation and Notch activation. This makes both the histone acetyltransferase EP300 and histone acetylation interesting targets to interfere with EndMT. However, the exact role of histone acetylase EP300 and the underlying mechanisms that facilitate histone acetylation in the context of EndMT have yet to be confirmed. Therefore, more knowledge on the regulation of histone acetylation in the context of EndMT is necessary before targeting histone acetylation to inhibit EndMT.

DNA METHYLATION AS POTENTIAL TARGET TO COMBAT ENDMT

DNA methylation is the presence of ≥ 1 methyl groups on cytosine bases in CpG-islands in the DNA. These CpG-islands are mostly located in gene promoter regions, which are responsible for transcriptional activation. Addition of methyl groups via DNA methyltransferases (DNMTs) in these CpG-islands is the most potent epigenetic regulatory mechanism to stably silence gene expression [47,48]. In contrast to histone methylation, methyl groups on cytosine bases cannot be removed directly but indirectly with the help of recently discovered TET (teneleven translocation methylcytosine dioxygenase) enzymes [49]. TET enzymes catalyze the oxidation of methylcytosine to hydroxymethylcytosine, which is replaced by a naked cytosine through DNA repair mechanisms [50–52].

RASAL1 PROMOTER DEMETHYLATION INHIBITS ENDMT

TGF- β 1 treatment in human coronary endothelial cells resulted in aberrant promoter methylation and thereby reduced gene expression of RASAL1 (RAS protein activator like 1 [a Ras-signaling inhibitor]) which contributes to EndMT [53]. The aberrant promoter methylation of RASAL1 was also observed in an

experimental mouse model of cardiac fibrosis and in end-stage heart failure patients, implicating that aberrant promoter methylation of RASAL1 is an important determinant of EndMT in the context of cardiovascular disease [53]. In endocardial fibroelastosis, a subtype of cardiac fibrosis, the endogenous EndMT inhibitor BMP7 gene is aberrantly methylated, suggesting that other genes than RASAL1 are hypermethylated in the context of EndMT [54]. However, which genes are associated with aberrant methylation in the context of EndMT needs to be established. Interestingly, the antifibrotic morphogen BMP7 induces TET3-mediated hydroxymethylation of the RASAL1 promoter thereby restoring RASAL1 gene expression both *in vitro* and *in vivo* [53]. This suggests that demethylation of specific genes such as RASAL1 might provide a novel therapeutic approach to block EndMT. Although in the context of TGF- β 1-induced EndMT it remains elusive how aberrant promoter methylation of RASAL1 is facilitated [53], in renal fibrogenesis the aberrant promoter methylation of RASAL1 is shown to be mediated via DNMT1 [55]. In addition, other stimuli, such as hypoxia and inorganic phosphate, also induce aberrant promoter methylation of RASAL1 which is facilitated via DNMT3a and via HDAC2-induced recruitment of DNMT1, respectively [18,56]. Whether the underlying mechanisms of aberrant promoter methylation of different genes are similar upon the same stimuli remains unclear. Altogether, targeting of specific DNMTs or TET enzymes, or performance of gene-specific demethylation, provide therapeutic approaches to interfere with aberrant DNA methylation and thereby combat EndMT.

NONCODING RNAS AS POTENTIAL TARGETS TO INTERFERE WITH ENDMT

Noncoding RNAs are functional RNA molecules but not translated into proteins. Noncoding RNAs include miRNAs, lncRNAs, and circRNAs. miRNAs are short RNA sequences (20–25 nucleotides) which can bind to ≥ 1 mRNA targets resulting in their degradation or inhibition of their translation into protein [57]. This leads to both direct repression of gene and protein expression and indirect activation of gene and protein expression (via the downregulation of repressor molecules).

DIFFERENTIAL EXPRESSION OF MIRNAS UPON TGF- β TREATMENT: MIR-21, MIR-27B, AND MIR-155 AS INDUCERS OF ENDMT

Several miRNAs are differentially expressed upon TGF- β 2 treatment, indicating their potential role in modulating EndMT [45,58,59]. Examples of upregulated miRNAs during EndMT are miR-27b, miR-155, miR-125b, Let-7c, Let-7g, miR-21, miR-30b, and miR-195, whereas miR-122a, miR-127, miR-196, and miR-375 are downregulated upon TGF- β 2 stimulation [45,58,59]. Interestingly, blockage of miR-21 rescued the TGF- β 2-induced repression of the endothelial marker CDH5 (cadherin 5 [VE-cadherin]) and induction of the mesenchymal marker S100A4 (S100 calcium binding protein A4), identifying miR-21 as an important inducer of EndMT which is responsible for the downregulation of CDH5 (VE-Cadherin) and the induction of S100A4 in the context of TGF- β 2-induced EndMT [60]. In addition, blockage of miR-27b suppressed the TGF- β 2-induced expression of the mesenchymal markers ACTA2 (actin, alpha 2, smooth muscle, aorta [α -SMA]) and TAGLN (SM22 α), indicating a role for miR-27b in facilitating EndMT [59]. Another miRNA which has been shown to facilitate TGF- β -induced EndMT is miR-155 [58]. miR-155 inhibits SKI (SKI proto-oncogene [c-Ski]), an important inhibitor of TGF- β signaling, thereby inducing the expression of the mesenchymal gene vimentin and the EndMT transcription factors SNAIL, SLUG, and TWIST [58]. Besides miR-21, miR-27b, and miR-155, the underlying mechanisms of these differentially expressed miRNAs in regulating EndMT remain largely unknown. Interestingly, the TGF- β 2-induced differentially expressed miRNAs have also altered expression levels in cardiovascular diseases such as cardiac fibrosis and heart failure, underlining their role in regulating EndMT in pathological conditions [61–63].

LET-7B/C, MIR-20A, AND MIR-200B AS POTENTIAL TARGETS TO PREVENT ENDMT

Overexpression of miRNAs Let-7b and Let-7c represses TGF- β signaling and inhibits EndMT in human umbilical artery cells [64]. Overexpression of Let-7b also inhibits EndMT in a murine transplant arteriopathy model [64]. This indicates that Let-7b and Let-7c are potential targets to interfere with EndMT. It should be noted that Let-7c and Let-7g are, as described before, upregulated during TGF- β 2-induced EndMT in mouse cardiac endothelial cells [45]. This suggests that

these miRNAs are upregulated as a protective mechanism or that these miRNAs are differently regulated in mice and humans. Overexpression of another miRNA, miR-20a, in human umbilical vein endothelial cells inhibits the TGF- β 1-induced upregulation of the TGF- β receptor complex (TGF- β receptor 1 and 2) and SARA (Smad anchor for receptor activation) whose function is to recruit SMAD2 and SMAD3 to the TGF- β receptor complex [65]. Interestingly, miR-20a only affects TGF- β 1-signaling in authentic endothelial cells but not in cells actively undergoing EndMT, indicating that miR-20a is an important regulator in the initial phase of EndMT and an interesting target to prevent rather than reverse EndMT. Another potential target to prevent EndMT is miR-200b. Endothelial cell-specific overexpression of miR-200b prevents glucose-induced EndMT, inhibits glucose-induced cardiac expression of TGF- β and inhibits the expression of the histone acetyltransferase EP300 [66,67]. This indicates the essential role of miR-200b in preventing glucose-induced EndMT revealing miR-200b as a potential target to prevent EndMT. Whether the protective role of miR-200b is also present in TGF- β -induced EndMT needs to be established. Importantly, the inhibition of the histone acetyltransferase EP300 upon miR-200b overexpression indicates the association between different epigenetic regulators (miRNAs and histone acetyltransferases) in modulating EndMT. The underlying mechanisms of these associations and cooperation between different epigenetic modulators remain largely unknown. Altogether, miRNAs have distinct roles in the context of EndMT and can either be protective (Let-7b/c, miR-20a, and miR-200b) or inducers (miR-21, miR-27b, and miR-155) of EndMT. Suppression of upregulated miRNAs (miR-21, miR-27b, and miR-155) or overexpression of downregulated miRNAs (Let-7b/c, miR-20a, and miR-200b) might be a therapeutic approach to prevent EndMT. Important to note is that miRNAs have several targets, making it essential to carefully check off-target effects when modulating miRNA expression [68]. Also, in the case of miR-21, CDH5 (VE-Cadherin) and S100A4 might not represent direct targets of miR-21 but could reflect a secondary effect because miR-21 might target their regulators. Finding out which regulators are targeted by miRNAs might provide an approach to discover more direct regulators of EndMT and avoid the off-target effects associated with miRNAs.

LNCRNAS AS POTENTIAL MEDIATORS OF ENDMT

lncRNAs are another group of noncoding RNAs that have been described recently. In contrast to miRNAs consisting only of 20 to 25 nucleotides, lncRNAs comprise >200 nucleotides. lncRNAs regulate gene expression by a wide range of functions including (1) affection of transcription directly, (2) modulation of chromatin-modifying complexes, (3) modulation of posttranscriptional regulation via mRNA processing and stability, and (4) an effect as sponges for miRNAs to prevent them exerting their effects [69].

LNCRNAS MALAT1 AND GATA6-AS MODULATE ENDMT

To date, only 2-specific lncRNAs have been associated with EndMT: MALAT1 (metastasis-associated lung adenocarcinoma transcript 1) and GATA6-AS (GATA6 antisense RNA). The expression of MALAT1 increased upon treatment of endothelial progenitor cells with TGF- β 1, resulting in the downregulation of miR-145 and enhanced expression of the miR-145 targets SMAD3 and TGFBR2, thereby facilitating EndMT [70]. This indicates the role of lncRNAs in acting as sponges for miRNAs thereby influencing phenotypic outcome. Silencing of another lncRNA, GATA6-AS, decreases TGF- β 2-induced EndMT in human umbilical vein endothelial cells by diminishing increased TAGLN (SM22 α) and calponin expression and attenuating decreased CDH5 (VE-cadherin) expression, indicating its role in regulating EndMT [71]. Interestingly, GATA6-AS interacts with the chromatin-modifying enzyme LOXL2 (lysyl oxidase like 2) to regulate endothelial gene expression via changes in histone methylation (H3K4me3) [71]. This shows again the interaction of lncRNAs with other epigenetic modulators to modulate gene expression. In contrast to miRNAs which have been well-documented during cardiac fibrosis, lncRNAs still need to be comprehensively characterized. Therefore, it remains unknown which other lncRNAs are of importance in the regulation of EndMT. Interestingly, it has been reported that some lncRNAs are expressed more in endothelial cells as compared with fibroblasts and cardiomyocytes [72]. These endothelial-specific lncRNAs might get downregulated during the process of EndMT and likely be of importance in inhibiting EndMT. In addition, some lncRNAs have been recently described to control cardiac fibrosis, which might also play a role in facilitating EndMT.

Examples of these lncRNAs are GAS5 (growth arrest-specific 5), Wisper, and MEG3 (maternally expressed 3) [72–74]. Overexpression of GAS5 resulted in a decreased expression of miR-21 which facilitated suppression of cardiac fibrosis [74]. Because miR-21 is an inducer of EndMT, GAS5 might also exert a suppressive role on TGF- β 2-induced EndMT. Whereas overexpression of GAS5 acts as a suppressor of cardiac fibrosis, the lncRNAs Wisper and MEG3 facilitate cardiac fibrosis [72,73]. The role of these lncRNAs in regulating EndMT still needs to be confirmed, but these findings definitely point out lncRNAs as novel therapeutic targets for cardiac fibrosis. Interestingly, lncRNAs can also modulate chromatin-modifying complexes such as EZH2 and DNMTs, which are also known to be important in the regulation of EndMT [75–78]. It would therefore be interesting to explore the association of lncRNAs with EZH2 and DNMTs in the context of EndMT.

CIRC RNAS AS POTENTIAL MEDIATORS OF ENDMT

The third group of noncoding RNAs are circRNAs. Circularization of RNAs occurs because of alternative splicing where the 3' end of an exon is covalently joined to either its own 5' end or a 5' end of another exon (called back-splicing). Although most circRNAs consist of exons, circRNAs can also include other regions such as introns, untranslated regions, and intergenic regions [79]. CircRNAs were described already 26 years ago [80], but recent advancements in sequencing technologies showed us that around 5% to 20% of the human genes give rise to circRNAs, shedding new light on the importance of these noncoding RNAs [81,82]. The biological functions of circRNAs remain largely unknown, but some circRNAs have been described to (1) act as sponges for miRNAs to prevent them to exert their function, (2) act as scaffolds to regulate protein function and interactions, and (3) act as scaffolds to affect transcription [75,83,84]. Interestingly, circRNAs can even encode for proteins [85].

CIRC RNA PRODUCTION IS HIGHLY REGULATED DURING EMT

Recent data shows that the abundance of hundreds of circRNAs is widely altered during TGF- β 1-induced EMT, a cellular transition process similar to EndMT [86,87]. Several circRNAs are upregulated >20-fold after TGF- β 1 treatment (eg, SMARCA5 [SWI/SNF related, matrix associated, actin dependent regulator of chromatin, subfamily a, member 5], POLE2 [DNA polymerase epsilon 2, accessory subunit], OXNAD1 [oxidoreductase NAD-binding domain containing 1], SHPRH [SNF2 histone linker PHD RING helicase], SMAD2, and ATXN2 [ataxin 2]), whereas others are strongly decreased upon TGF- β 1 treatment (eg, DOCK1 [dedicator of cytokinesis 1] and GNB1 [G-protein subunit beta 1]) [86]. Even though this cell type-specific expression of circRNAs suggests a functional role of circRNAs during EMT, the functional outcome of how these circRNAs influence mesenchymal properties or preserve epithelial properties is still unknown. Because EMT and EndMT share many similarities, it is fair to postulate that circRNAs also play a role in EndMT. Nevertheless, only 1 circRNA has been described in EndMT to date. Overexpression of the circRNA DLGAP4 (DLG-associated protein 4) in mouse brain endothelial cells inhibits EndMT by acting as a sponge for miR-143 thereby regulating tight junction and mesenchymal marker expression [88]. Whether the circRNA DLGAP4 also inhibits TGF- β -induced EndMT in the context of cardiovascular disease remains elusive.

TARGETING EPIGENETIC MODULATORS OF ENDMT: POSSIBILITIES AND CHALLENGES

Inducers of EndMT such as nonuniform disturbed fluid shear stress and glucose and signaling pathways such as TGF- β -, Notch-, and Ras-signaling are associated with the activation of epigenetic regulators which, in turn, facilitate EndMT [89,90]. This indicates that the environmental factors and signaling pathways represent the activators, whereas epigenetic modulators are the executives who actively facilitate the activation and progression of EndMT. This makes epigenetic regulation an exciting target for the therapeutic inhibition of EndMT-contributing cardiovascular diseases. Epigenetic modulators represent histone modifications and histone-modifying enzymes, miRNAs, lncRNAs, and

DNA methylation (Figure 2; Table). HDAC3 and EZH2 represent promising targets to interfere with EndMT. In addition, suppression of upregulated miRNAs (miR-21, miR-27b, and miR-155) or overexpression of downregulated miRNAs (Let-7b/c, miR-20a, and miR-200b) and reversion of RASAL1 promoter DNA methylation result in amelioration of EndMT. The presence of EndMT-associated epigenetic regulators in the human heart is depicted in the Table. All EndMT-associated epigenetic regulators (except for the lncRNA GATA6-AS) have also been described in the human circulation [88,91,93,94,96,98–100,102,103,106,108,110,111]. This highlights the potential of using epigenetic-based therapeutic possibilities to combat EndMT. Nevertheless, some challenges need to be mentioned in the field of epigenetic regulation of EndMT. First, the possible different roles of epigenetic modifiers in different contexts and upon different stimuli represent a challenge for epigenetic-based therapeutic approaches [68,112]. It is important to mention that EndMT is not only detrimental but can also mediate beneficial effects in pathological settings. For example, partial induction of EndMT contributes to the formation of new vessels upon ischemia [113,114]. Altogether, this suggests that EndMT is a highly dynamic process which exerts differential effects in different settings which needs further elucidation. Second, off-target effects (in particular for noncoding RNAs, but also for chromatin-modifying complexes) in the context of epigenetic targeting are an important aspect which needs to be considered. Third, there are several associations between distinct epigenetic regulators such as EZH2 and HDAC3, EP300 and miR-200b, and HDAC2 and DNMT1 indicating the presence of a complex network of epigenetic regulatory mechanisms which are key to facilitate and block/reverse EndMT. Challenges in identifying both genetic and epigenetic regulatory networks are posed by different subtypes of TGF- β used in different studies, making it difficult to compare individual studies to each other. The same holds for different time points of stimulation (eg, 2 hours versus 12 days) and the use of both mouse and human cell lines. Therefore, it is important to establish the underlying mechanisms by which epigenetic modulators facilitate EndMT.

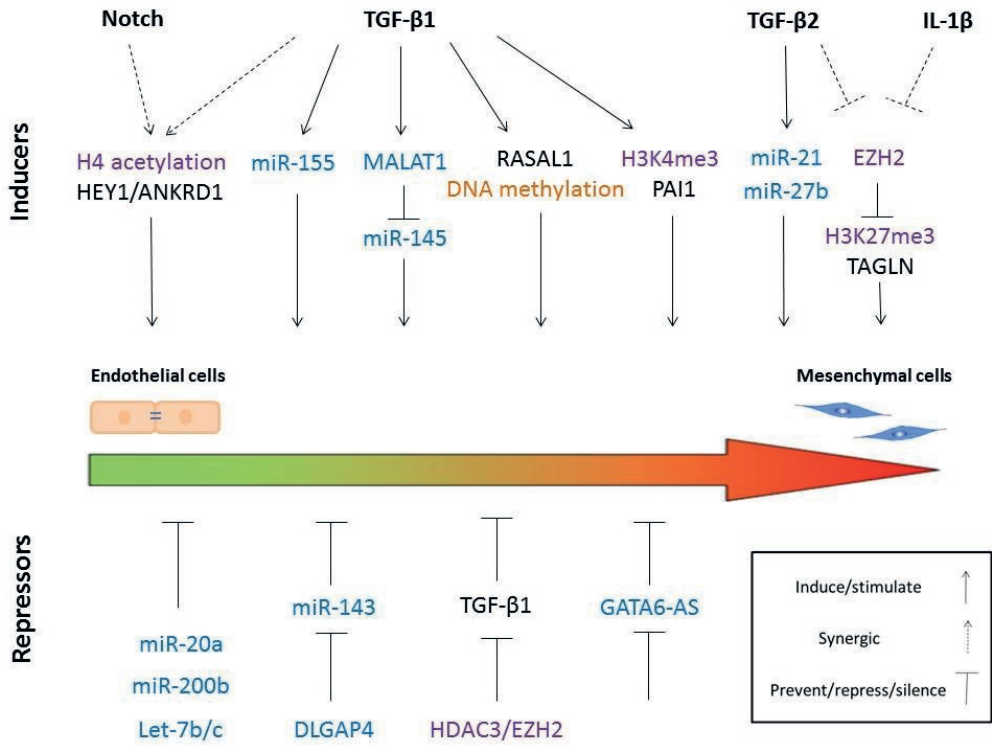


Figure 2. Overview of epigenetic regulators that are associated with endothelial-to-mesenchymal transition (EndMT).

Histone acetylation and methylation marks as well as histone-modifying enzymes are highlighted in purple, noncoding RNAs including microRNAs, long noncoding RNAs, and circular RNAs are highlighted in blue and DNA methylation is highlighted in orange. The upper row depicts epigenetic modifications and regulators associated with induction of EndMT, whereas the lower row shows the epigenetic modulators which are associated with repression of EndMT. ANKRD indicates ankyrin repeat domain 1; DLGAP4, DLG-associated protein 4; EZH2, enhancer of zeste homolog 2; GATA6-AS, GATA6 antisense RNA; H3K4me3, trimethylation of histone 3 at lysine 4; H3K27me3, trimethylation of histone 3 at lysine 27; H4, histone 4; HDAC, histone deacetylase; HEY1, hes related family bHLH transcription factor with YRPW motif 1; IL, interleukin, MALAT1, metastasis-associated lung adenocarcinoma transcript 1; PAI1, phosphoribosylanthranilate isomerase 1; RASAL1, RAS protein activator like 1; TAGLN, transgelin; and TGF, transforming growth factor.

Table. Epigenetic Regulators That Are Associated With EndMT

	Epigenetic regulators	Present in Human Heart/Circulation	Genes/miRNAs Regulated	Experimental Conditions	Species Studied	
Histone modifications	HDAC2	Y/Y	RASAL1	<i>In vitro</i>	Human	56,91,92
	HDAC3	?/Y	TGF- β 1	<i>In vivo</i>	Mouse	35,93
	EZH2	Y/Y	TGF- β 1; TAGLN (via H3K27me3)	<i>In vivo; in vitro</i>	Mouse; Human	17,35,94,95
	?	?/?	PAI1 (via H4 acetylation)	<i>In vitro</i>	Human	40
	?	?/?	PAI1 (via H3K4me3)	<i>In vitro</i>	Human	40
DNA Methylation	DNMT1	Y/Y	RASAL1	<i>In vitro; in vivo</i>	Human; mouse	55,56,96,97
	DNMT3a	Y/Y	RASAL1	<i>In vitro</i>	Human	18,97,98
	TET3	?/Y	RASAL1	<i>In vitro; in vivo</i>	Human; mouse	53,99
Noncoding RNAs	miR-20a	Y/Y	TGFBR1/2; SARA	<i>In vitro</i>	Human	65,100,101
	miR-21	Y/Y	?	<i>In vitro; in vivo</i>	Mouse/human; mouse	45,60,63,102
	miR-27b	Y/Y	ELK1, NRP2, PLXNA2, PLXND1	<i>In vitro</i>	Mouse	59,103,104
	miR-143	Y/Y	HECTD1	<i>In vitro</i>	Mouse	88,105
	miR-145	Y/Y	TGFBR2, SMAD3	<i>In vitro</i>	Human	70,100,101
	miR-155	Y/Y	SKI	<i>In vitro</i>	Human	58,106,107
	miR-200b	Y/Y	?	<i>In vitro/in vivo</i>	Mouse	66,108,109
	Let-7b/c	Y/Y	?	<i>In vitro; in vivo</i>	Human; mouse	64,101,110
	MALAT1	?/Y	miR-145	<i>In vitro</i>	Human	70,111
	GATA6-AS	?/?	POSTN, PTGS2	<i>In vitro</i>	Human	71
DLGAP4	?/Y	miR-143	<i>In vitro</i>	Mouse	88	

List of epigenetic regulators (histone-modifying enzymes, histone modifications, DNA methyltransferases, DNA hydroxymethylase, microRNAs, long noncoding RNAs, and circular RNAs) that are associated with EndMT. The presence in the human heart or circulation, the genes/miRNAs

regulated, experimental conditions, species studied, and corresponding publications are indicated. Y stands for Yes. Histone-modifying enzymes as well as histone acetylation and methylation marks are highlighted in purple, DNA methylation and hydroxymethylation are highlighted in orange, and microRNAs, long noncoding RNAs, and circular RNAs are highlighted in blue. DNMT indicates DNA methyltransferase; DLGAP4, DLG-associated protein 4; DNMT, DNA methyltransferase; ELK1, ETS transcription factor, EndMT, endothelial-to-mesenchymal transition; EZH2, enhancer of zeste homolog 2; GATA6-AS, GATA6 antisense RNA; H3K4me3, trimethylation of histone H3 at lysine 4; H3K27me3, trimethylation of histone H3 at lysine 27; H4, histone 4; HDAC, histone deacetylase; HECTD1, HECT domain E3 ubiquitin protein ligase 1; MALAT, metastasis-associated lung adenocarcinoma transcript 1; NRP2, neuropilin 2; PAI1, phosphoribosylanthranilate isomerase 1; PLXNA2, plexin A2; PLXND1, plexin D1; POSTN, periostin; PTGS2, prostaglandinendoperoxide synthase 2; RASAL1, RAS protein activator like 1, SARA, Smad anchor for receptor activation; SKI, SKI proto-oncogene; SMAD, SMAD family member; TAGLN, transgelin; TET, ten eleven translocation methylcytosine dioxygenase; TGF, transforming growth factor; and TGFBR2, transforming growth factor receptor 2.

LOOKING OUTSIDE THE BORDERS OF CARDIOVASCULAR DISEASE

When looking outside the borders of cardiovascular disease, epigenetic regulatory mechanisms have also been described in EndMT-associated pathologies such as cancer and organ fibrosis [115]. Interestingly, all epigenetic modulators which are important for driving EndMT (eg, EZH2, HDAC3, EP300, miRNAs, and DNMTs) have also been described in cancer and organ fibrosis. The role of epigenetics and the underlying regulatory mechanisms is most established in cancer where a similar process to EndMT is present: EMT. The underlying mechanisms of EMT are thought to be similar in EndMT; thus, many of the identified mechanisms in EMT might potentially play a role in EndMT as well. Also, the underlying mechanisms of EndMT are thought to be similar in different forms of organ fibrosis. Combining the knowledge of EMT and EndMT in the context of cancer and organ fibrosis with the knowledge on EndMT in the context of cardiovascular disease might enhance our knowledge on EndMT-associated pathologies leading us one step closer to perform epigenetic targeting to combat aberrant EndMT.

CONCLUSIONS

To conclude, epigenetic regulation of EndMT represents a highly promising but yet insufficiently explored field with potential for epigenetic targeting of EndMT-associated cardiovascular disease.

HIGHLIGHTS

- Histone methylation and (de)acetylation are important regulators of endothelial-to-mesenchymal transition.
- DNA methylation is a potential target to combat endothelial-to-mesenchymal transition-associated cardiovascular disease.
- Noncoding RNAs represent potential targets for interfering with endothelial-to-mesenchymal transition-associated cardiovascular disease.

SOURCES OF FUNDING

This review was supported by a Graduate School of Medical Sciences PhD Scholarship, University of Groningen (to M.S. Hulshoff). X. Xu received support from the “seed funding research program” of the Faculty of Medicine, Georg-August University Göttingen and postdoc start-up grant, German Centre for Cardiovascular Research (DZHK). G. Krenning received support from the Netherlands Organization for Scientific Research/Netherlands Organization for Health Research and Development Innovative Research Incentive number 917.16.446.

REFERENCES

1. Eisenberg LM, Markwald RR. Molecular regulation of atrioventricular valvuloseptal morphogenesis. *Circ Res.* 1995;77:1–6.
2. Zeisberg EM, Tarnavski O, Zeisberg M, Dorfman AL, McMullen JR, Gustafsson E, Chandraker A, Yuan X, Pu WT, Roberts AB, Neilson EG, Sayegh MH, Izumo S, Kalluri R. Endothelial-to-mesenchymal transition contributes to cardiac fibrosis. *Nat Med.* 2007;13:952–961.
3. Chen PY, Qin L, Baeyens N, Li G, Afolabi T, Budatha M, Tellides G, Schwartz MA, Simons M. Endothelial-to-mesenchymal transition drives atherosclerosis progression. *J Clin Invest.* 2015;125:4514–4528.
4. Ranchoux B, Antigny F, Rucker-Martin C, et al. Endothelial-to-mesenchymal transition in pulmonary hypertension. *Circulation.* 2015;131:1006–1018.
5. Hashimoto N, Phan SH, Imaizumi K, Matsuo M, Nakashima H, Kawabe T, Shimokata K, Hasegawa Y. Endothelial-mesenchymal transition in bleomycin-induced pulmonary fibrosis. *Am J Respir Cell Mol Biol.* 2010;43:161–172.
6. Maddaluno L, Rudini N, Cuttano R, et al. EndMT contributes to the onset and progression of cerebral cavernous malformations. *Nature.* 2013;498:492–496.
7. Zeisberg EM, Potenta S, Xie L, Zeisberg M, Kalluri R. Discovery of endothelial to mesenchymal transition as a source for carcinoma-associated fibroblasts. *Cancer Res.* 2007;67:10123–10128.
8. Zeisberg EM, Potenta SE, Sugimoto H, Zeisberg M, Kalluri R. Fibroblasts in kidney fibrosis emerge via endothelial-to-mesenchymal transition. *J Am Soc Nephrol.* 2008;19:2282–2287.
9. Moore-Morris T, Guimarães-Camboa N, Banerjee I, et al. Resident fibroblast lineages mediate pressure overload-induced cardiac fibrosis. *J Clin Invest.* 2014;124:2921–2934.
10. Arciniegas E, Sutton AB, Allen TD, Schor AM. Transforming growth factor beta 1 promotes the differentiation of endothelial cells into smooth muscle-like cells in vitro. *J Cell Sci.* 1992;103 (pt 2):521–529.
11. Azhar M, Runyan RB, Gard C, Sanford LP, Miller ML, Andringa A, Pawlowski S, Rajan S, Doetschman T. Ligand-specific function of transforming growth factor beta in epithelial-mesenchymal transition in heart development. *Dev Dyn.* 2009;238:431–442.
12. Goumans MJ, Liu Z, ten Dijke P. TGF-beta signaling in vascular biology and dysfunction. *Cell Res.* 2009;19:116–127.
13. Chang AC, Fu Y, Garside VC, Niessen K, Chang L, Fuller M, Setiadi A, Smrz J, Kyle A, Minchinton A, Marra M, Hoodless PA, Karsan A. Notch initiates the endothelial-to-mesenchymal transition in the atrioventricular canal through autocrine activation of soluble guanylyl cyclase. *Dev Cell.* 2011;21:288–300.
14. Wu L, Sun T, Kobayashi K, Gao P, Griffin JD. Identification of a family of mastermind-like transcriptional coactivators for mammalian notch receptors. *Mol Cell Biol.* 2002;22:7688–7700.

15. Moonen JR, Lee ES, Schmidt M, Maleszewska M, Koerts JA, Brouwer LA, van Kooten TG, van Luyn MJ, Zeebregts CJ, Krenning G, Harmsen MC. Endothelial-to-mesenchymal transition contributes to fibro-proliferative vascular disease and is modulated by fluid shear stress. *Cardiovasc Res*. 2015;108:377–386.
16. Widyantoro B, Emoto N, Nakayama K, Anggrahini DW, Adiarto S, Iwasa N, Yagi K, Miyagawa K, Rikitake Y, Suzuki T, Kisanuki YY, Yanagisawa M, Hirata K. Endothelial cell-derived endothelin-1 promotes cardiac fibrosis in diabetic hearts through stimulation of endothelial-to-mesenchymal transition. *Circulation*. 2010;121:2407–2418.
17. Maleszewska M, Gjaltema RA, Krenning G, Harmsen MC. Enhancer of zeste homolog-2 (EZH2) methyltransferase regulates transgelin/smooth muscle-22 α expression in endothelial cells in response to interleukin-1 β and transforming growth factor- β 2. *Cell Signal*. 2015;27:1589–1596.
18. Xu X, Tan X, Hulshoff MS, Wilhelmi T, Zeisberg M, Zeisberg EM. Hypoxia-induced endothelial-mesenchymal transition is associated with RASAL1 promoter hypermethylation in human coronary endothelial cells. *FEBS Lett*. 2016;590:1222–1233.
19. Mahler GJ, Farrar EJ, Butcher JT. Inflammatory cytokines promote mesenchymal transformation in embryonic and adult valve endothelial cells. *Arterioscler Thromb Vasc Biol*. 2013;33:121–130.
20. Yang M, Zheng J, Miao Y, Wang Y, Cui W, Guo J, Qiu S, Han Y, Jia L, Li H, Cheng J, Du J. Serum-glucocorticoid regulated kinase 1 regulates alternatively activated macrophage polarization contributing to angiotensin II-induced inflammation and cardiac fibrosis. *Arterioscler Thromb Vasc Biol*. 2012;32:1675–1686.
21. Li Y, Zhang C, Wu Y, Han Y, Cui W, Jia L, Cai L, Cheng J, Li H, Du J. Interleukin-12p35 deletion promotes CD4 T-cell-dependent macrophage differentiation and enhances angiotensin II-Induced cardiac fibrosis. *Arterioscler Thromb Vasc Biol*. 2012;32:1662–1674.
22. Suzuki K, Satoh K, Ikeda S, et al. Basigin promotes cardiac fibrosis and failure in response to chronic pressure overload in mice. *Arterioscler Thromb Vasc Biol*. 2016;36:636–646.
23. Fujita K, Maeda N, Sonoda M, Ohashi K, Hibuse T, Nishizawa H, Nishida M, Hiuge A, Kurata A, Kihara S, Shimomura I, Funahashi T. Adiponectin protects against angiotensin II-induced cardiac fibrosis through activation of PPAR-alpha. *Arterioscler Thromb Vasc Biol*. 2008;28:863–870.
24. Feinberg AP, Vogelstein B. Hypomethylation distinguishes genes of some human cancers from their normal counterparts. *Nature*. 1983;301:89–92.
25. Mann J, Mann DA. Epigenetic regulation of wound healing and fibrosis. *Curr Opin Rheumatol*. 2013;25:101–107.
26. Margueron R, Reinberg D. Chromatin structure and the inheritance of epigenetic information. *Nat Rev Genet*. 2010;11:285–296.
27. Nakatochi M, Ichihara S, Yamamoto K, Naruse K, Yokota S, Asano H, Matsubara T, Yokota M. Epigenome-wide association of myocardial infarction with DNA methylation sites at loci related to cardiovascular disease. *Clin Epigenetics*. 2017;9:54.
28. Tampe B, Zeisberg M. Contribution of genetics and epigenetics to progression of kidney fibrosis. *Nephrol Dial Transplant*. 2014;29(suppl 4):iv72–iv79.

29. Petronis A. Epigenetics as a unifying principle in the aetiology of complex traits and diseases. *Nature*. 2010;465:721–727.
30. Yang IV, Schwartz DA. Epigenetics of idiopathic pulmonary fibrosis. *Transl Res*. 2015;165:48–60.
31. Barski A, Cuddapah S, Cui K, Roh TY, Schones DE, Wang Z, Wei G, Chepelev I, Zhao K. High-resolution profiling of histone methylations in the human genome. *Cell*. 2007;129:823–837.
32. Heintzman ND, Stuart RK, Hon G, Fu Y, Ching CW, Hawkins RD, Barrera LO, Van Calcar S, Qu C, Ching KA, Wang W, Weng Z, Green RD, Crawford GE, Ren B. Distinct and predictive chromatin signatures of transcriptional promoters and enhancers in the human genome. *Nat Genet*. 2007;39:311–318.
33. Wang Z, Zang C, Rosenfeld JA, Schones DE, Barski A, Cuddapah S, Cui K, Roh TY, Peng W, Zhang MQ, Zhao K. Combinatorial patterns of histone acetylations and methylations in the human genome. *Nat Genet*. 2008;40:897–903.
34. Riising EM, Comet I, Leblanc B, Wu X, Johansen JV, Helin K. Gene silencing triggers polycomb repressive complex 2 recruitment to CpG islands genome wide. *Mol Cell*. 2014;55:347–360.
35. Lewandowski SL, Janardhan HP, Trivedi CM. Histone deacetylase 3 coordinates deacetylase-independent epigenetic silencing of transforming growth factor- β 1 (TGF- β 1) to orchestrate second heart field development. *J Biol Chem*. 2015;290:27067–27089.
36. Maleszewska M, Vanchin B, Harmsen MC, Krenning G. The decrease in histone methyltransferase EZH2 in response to fluid shear stress alters endothelial gene expression and promotes quiescence. *Angiogenesis*. 2016;19:9–24.
37. Giudice FS, Pinto DS Jr, Nör JE, Squarize CH, Castilho RM. Inhibition of histone deacetylase impacts cancer stem cells and induces epithelial-mesenchyme transition of head and neck cancer. *PLoS One*. 2013;8:e58672.
38. Nie FQ, Sun M, Yang JS, Xie M, Xu TP, Xia R, Liu YW, Liu XH, Zhang EB, Lu KH, Shu YQ. Long noncoding RNA ANRIL promotes non-small cell lung cancer cell proliferation and inhibits apoptosis by silencing KLF2 and P21 expression. *Mol Cancer Ther*. 2015;14:268–277.
39. Xie M, Sun M, Zhu YN, Xia R, Liu YW, Ding J, Ma HW, He XZ, Zhang ZH, Liu ZJ, Liu XH, De W. Long noncoding RNA HOXA-AS2 promotes gastric cancer proliferation by epigenetically silencing P21/PLK3/DDIT3 expression. *Oncotarget*. 2015;6:33587–33601.
40. Fu Y, Chang A, Chang L, Niessen K, Eapen S, Setiadi A, Karsan A. Differential regulation of transforming growth factor beta signaling pathways by Notch in human endothelial cells. *J Biol Chem*. 2009;284:19452–19462.
41. Itoh S, Ericsson J, Nishikawa J, Heldin CH, ten Dijke P. The transcriptional co-activator P/CAF potentiates TGF-beta/Smad signaling. *Nucleic Acids Res*. 2000;28:4291–4298.
42. Wallberg AE, Pedersen K, Lendahl U, Roeder RG. p300 and PCAF act cooperatively to mediate transcriptional activation from chromatin templates by notch intracellular domains in vitro. *Mol Cell Biol*. 2002;22:7812–7819.
43. Bugyei-Twum A, Advani A, Advani SL, Zhang Y, Thai K, Kelly DJ, Connelly KA. High glucose induces Smad activation via the transcriptional coregulator p300 and contributes to cardiac fibrosis and hypertrophy. *Cardiovasc Diabetol*. 2014;13:89.

44. Ghosh AK, Bhattacharyya S, Lafyatis R, Farina G, Yu J, Thimmapaya B, Wei J, Varga J. p300 is elevated in systemic sclerosis and its expression is positively regulated by TGF- β : epigenetic feed-forward amplification of fibrosis. *J Invest Dermatol.* 2013;133:1302–1310.
45. Ghosh AK, Nagpal V, Covington JW, Michaels MA, Vaughan DE. Molecular basis of cardiac endothelial-to-mesenchymal transition (EndMT): differential expression of microRNAs during EndMT. *Cell Signal.* 2012;24:1031–1036.
46. Ni J, Shen Y, Wang Z, Shao DC, Liu J, Kong YL, Fu LJ, Zhou L, Xue H, Huang Y, Zhang W, Yu C, Lu LM. P300-dependent STAT3 acetylation is necessary for angiotensin II-induced pro-fibrotic responses in renal tubular epithelial cells. *Acta Pharmacol Sin.* 2014;35:1157–1166.
47. Compere SJ, Palmiter RD. DNA methylation controls the inducibility of the mouse metallothionein-I gene lymphoid cells. *Cell.* 1981;25:233–240.
48. Holliday R, Pugh JE. DNA modification mechanisms and gene activity during development. *Science.* 1975;187:226–232.
49. Ito S, D’Alessio AC, Taranova OV, Hong K, Sowers LC, Zhang Y. Role of Tet proteins in 5mC to 5hmC conversion, ES-cell self-renewal and inner cell mass specification. *Nature.* 2010;466:1129–1133.
50. Bhutani N, Burns DM, Blau HM. DNA demethylation dynamics. *Cell.* 2011;146:866–872.
51. Ito S, Shen L, Dai Q, Wu SC, Collins LB, Swenberg JA, He C, Zhang Y. Tet proteins can convert 5-methylcytosine to 5-formylcytosine and 5-carboxylcytosine. *Science.* 2011;333:1300–1303.
52. Wu H, Zhang Y. Reversing DNA methylation: mechanisms, genomics, and biological functions. *Cell.* 2014;156:45–68.
53. Xu X, Tan X, Tampe B, Nyamsuren G, Liu X, Maier LS, Sossalla S, Kalluri R, Zeisberg M, Hasenfuss G, Zeisberg EM. Epigenetic balance of aberrant Rasal1 promoter methylation and hydroxymethylation regulates cardiac fibrosis. *Cardiovasc Res.* 2015;105:279–291.
54. Xu X, Friehs I, Zhong Hu T, Melnychenko I, Tampe B, Alnour F, Iacone M, Kalluri R, Zeisberg M, Del Nido PJ, Zeisberg EM. Endocardial fibroelastosis is caused by aberrant endothelial to mesenchymal transition. *Circ Res.* 2015;116:857–866.
55. Bechtel W, McGoohan S, Zeisberg EM, Müller GA, Kalbacher H, Salant DJ, Müller CA, Kalluri R, Zeisberg M. Methylation determines fibroblast activation and fibrogenesis in the kidney. *Nat Med.* 2010;16:544–550.
56. Tan X, Xu X, Zeisberg M, Zeisberg EM. DNMT1 and HDAC2 cooperate to facilitate aberrant promoter methylation in inorganic phosphate-induced endothelial-mesenchymal transition. *PLoS One.* 2016;11:e0147816.
57. Gu S, Kay MA. How do miRNAs mediate translational repression? *Silence.* 2010;1:11.
58. Wang J, He W, Xu X, Guo L, Zhang Y, Han S, Shen D. The mechanism of TGF- β /miR-155/c-Ski regulates endothelial-mesenchymal transition in human coronary artery endothelial cells. *Biosci Rep.* 2017;37:BSR20160603.
59. Suzuki HI, Katsura A, Mihira H, Horie M, Saito A, Miyazono K. Regulation of TGF- β -mediated endothelial-mesenchymal transition by microRNA-27. *J Biochem.* 2017;161:417–420.

60. Kumarswamy R, Volkman I, Jazbutyte V, Dangwal S, Park DH, Thum T. Transforming growth factor- β -induced endothelial-to-mesenchymal transition is partly mediated by microRNA-21. *Arterioscler Thromb Vasc Biol.* 2012;32:361–369.
61. Latronico MV, Catalucci D, Condorelli G. MicroRNA and cardiac pathologies. *Physiol Genomics.* 2008;34:239–242.
62. Mishra PK, Tyagi N, Kumar M, Tyagi SC. MicroRNAs as a therapeutic target for cardiovascular diseases. *J Cell Mol Med.* 2009;13:778–789.
63. Thum T, Gross C, Fiedler J, et al. MicroRNA-21 contributes to myocardial disease by stimulating MAP kinase signalling in fibroblasts. *Nature.* 2008;456:980–984.
64. Chen PY, Qin L, Barnes C, Charisse K, Yi T, Zhang X, Ali R, Medina PP, Yu J, Slack FJ, Anderson DG, Kotlianski V, Wang F, Tellides G, Simons M. FGF regulates TGF- β signaling and endothelial-to-mesenchymal transition via control of let-7 miRNA expression. *Cell Rep.* 2012;2:1684–1696.
65. Correia AC, Moonen JR, Brinker MG, Krenning G. FGF2 inhibits endothelial-mesenchymal transition through microRNA-20a-mediated repression of canonical TGF- β signaling. *J Cell Sci.* 2016;129:569–579.
66. Feng B, Cao Y, Chen S, Chu X, Chu Y, Chakrabarti S. miR-200b mediates endothelial-to-mesenchymal transition in diabetic cardiomyopathy. *Diabetes.* 2016;65:768–779.
67. McArthur K, Feng B, Wu Y, Chen S, Chakrabarti S. MicroRNA-200b regulates vascular endothelial growth factor-mediated alterations in diabetic retinopathy. *Diabetes.* 2011;60:1314–1323.
68. Wang D, Deuse T, Stubbendorff M, et al. Local microRNA modulation using a novel anti-miR-21-eluting stent effectively prevents experimental in-stent restenosis. *Arterioscler Thromb Vasc Biol.* 2015;35:1945–1953.
69. Kung JT, Colognori D, Lee JT. Long noncoding RNAs: past, present, and future. *Genetics.* 2013;193:651–669.
70. Xiang Y, Zhang Y, Tang Y, Li Q. MALAT1 modulates TGF- β -induced endothelial-to-mesenchymal transition through downregulation of miR-145. *Cell Physiol Biochem.* 2017;42:357–372.
71. Neumann P, Jaé N, Knau A, Glaser SF, Fouani Y, Rossbach O, Krüger M, John D, Bindereif A, Grote P, Boon RA, Dimmeler S. The lncRNA GATA6-AS epigenetically regulates endothelial gene expression via interaction with LOXL2. *Nat Commun.* 2018;9:237.
72. Piccoli MT, Gupta SK, Viereck J, Foinquinos A, Samolovac S, Kramer FL, Garg A, Remke J, Zimmer K, Batkai S, Thum T. Inhibition of the cardiac fibroblast-enriched lncRNA Meg3 prevents cardiac fibrosis and diastolic dysfunction. *Circ Res.* 2017;121:575–583.
73. Micheletti R, Plaisance I, Abraham BJ, Sarre A, Ting CC, Alexanian M, Maric D, Maison D, Nemir M, Young RA, Schroen B, Gonzalez A, Ounzain S, Pedrazzini T. The long noncoding RNA wisper controls cardiac fibrosis and remodeling. *Sci Transl Med.* 2017;9:eaai9118.
74. Tao H, Zhang JG, Qin RH, Dai C, Shi P, Yang JJ, Deng ZY, Shi KH. lncRNA GAS5 controls cardiac fibroblast activation and fibrosis by targeting miR-21 via PTEN/MMP-2 signaling pathway. *Toxicology.* 2017;386:11–18.

75. Guil S, Soler M, Portela A, Carrere J, Fonalleras E, Gomez A, Villanueva A, Esteller M. Intronic RNAs mediate EZH2 regulation of epigenetic targets. *Nat Struct Mol Biol.* 2012;19:664–670.
76. Kanhere A, Viiri K, Araújo CC, Rasaiyaah J, Bouwman RD, Whyte WA, Pereira CF, Brookes E, Walker K, Bell GW, Pombo A, Fisher AG, Young RA, Jenner RG. Short RNAs are transcribed from repressed polycomb target genes and interact with polycomb repressive complex-2. *Mol Cell.* 2010;38:675–688.
77. Khalil AM, Guttman M, Huarte M, Garber M, Raj A, Rivea Morales D, Thomas K, Presser A, Bernstein BE, van Oudenaarden A, Regev A, Lander ES, Rinn JL. Many human large intergenic noncoding RNAs associate with chromatin-modifying complexes and affect gene expression. *Proc Natl Acad Sci USA.* 2009;106:11667–11672.
78. Zhao J, Ohsumi TK, Kung JT, Ogawa Y, Grau DJ, Sarma K, Song JJ, Kingston RE, Borowsky M, Lee JT. Genome-wide identification of polycomb-associated RNAs by RIP-seq. *Mol Cell.* 2010;40:939–953.
79. Memczak S, Jens M, Elefsinioti A, et al. Circular RNAs are a large class of animal RNAs with regulatory potency. *Nature.* 2013;495:333–338.
80. Nigro JM, Cho KR, Fearon ER, Kern SE, Ruppert JM, Oliner JD, Kinzler KW, Vogelstein B. Scrambled exons. *Cell.* 1991;64:607–613.
81. Ebbesen KK, Hansen TB, Kjems J. Insights into circular RNA biology. *RNA Biol.* 2017;14:1035–1045.
82. Neumann DP, Goodall GJ, Gregory PA. Regulation of splicing and circularization of RNA in epithelial mesenchymal plasticity. *Semin Cell Dev Biol.* 2018;75:50–60.
83. Li Z, Huang C, Bao C, et al. Exon-intron circular RNAs regulate transcription in the nucleus. *Nat Struct Mol Biol.* 2015;22:256–264.
84. Schneider T, Hung LH, Schreiner S, Starke S, Eckhof H, Rossbach O, Reich S, Medenbach J, Bindereif A. CircRNA-protein complexes: IMP3 protein component defines subfamily of circRNPs. *Sci Rep.* 2016;6:31313.
85. Pamudurti NR, Bartok O, Jens M, et al. Translation of circRNAs. *Mol Cell.* 2017;66:9.e7–21.e7.
86. Conn SJ, Pillman KA, Toubia J, Conn VM, Salmanidis M, Phillips CA, Roslan S, Schreiber AW, Gregory PA, Goodall GJ. The RNA binding protein quaking regulates formation of circRNAs. *Cell.* 2015;160:1125–1134.
87. Liao JY, Wu J, Wang YJ, He JH, Deng WX, Hu K, Zhang YC, Zhang Y, Yan H, Wang DL, Liu Q, Zeng MS, Phillip Koeffler H, Song E, Yin D. Deep sequencing reveals a global reprogramming of lncRNA transcriptome during EMT. *Biochim Biophys Acta.* 2017;1864:1703–1713.
88. Bai Y, Zhang Y, Han B, Yang L, Chen X, Huang R, Wu F, Chao J, Liu P, Hu G, Zhang JH, Yao H. Circular RNA DLGAP4 ameliorates ischemic stroke outcomes by targeting miR-143 to regulate endothelial-mesenchymal transition associated with blood-brain barrier integrity. *J Neurosci.* 2018;38:32–50.
89. Kumar S, Kim CW, Simmons RD, Jo H. Role of flow-sensitive microRNAs in endothelial dysfunction and atherosclerosis: mechanosensitive athero-miRs. *Arterioscler Thromb Vasc Biol.* 2014;34:2206–2216.

90. Floris I, Descamps B, Vardeu A, Mitić T, Posadino AM, Shantikumar S, Sala-Newby G, Capobianco G, Mangialardi G, Howard L, Dessole S, Urrutia R, Pintus G, Emanuelli C. Gestational diabetes mellitus impairs fetal endothelial cell functions through a mechanism involving microRNA-101 and histone methyltransferase enhancer of zester homolog-2. *Arterioscler Thromb Vasc Biol.* 2015;35:664–674.
91. Tan C, Xuan L, Cao S, Yu G, Hou Q, Wang H. Decreased histone deacetylase 2 (HDAC2) in peripheral blood monocytes (PBMCs) of COPD patients. *PLoS One.* 2016;11:e0147380.
92. Colak D, Kaya N, Al-Zahrani J, Al Bakheet A, Muiya P, Andres E, Quackenbush J, Dzimir N. Left ventricular global transcriptional profiling in human end-stage dilated cardiomyopathy. *Genomics.* 2009;94:20–31.
93. Sathishkumar C, Prabu P, Balakumar M, Lenin R, Prabhu D, Anjana RM, Mohan V, Balasubramanyam M. Augmentation of histone deacetylase 3 (HDAC3) epigenetic signature at the interface of proinflammation and insulin resistance in patients with type 2 diabetes. *Clin Epigenetics.* 2016;8:125.
94. Zhou T, Sun Y, Li M, Ding Y, Yin R, Li Z, Xie Q, Bao S, Cai W. Enhancer of zeste homolog 2-catalysed H3K27 trimethylation plays a key role in acute-on-chronic liver failure via TNF-mediated pathway. *Cell Death Dis.* 2018;9:590.
95. Tschirner A, Palus S, Hetzer R, Meyer R, Anker SD, Springer J. Six1 is down-regulated in end-stage human dilated cardiomyopathy independently of Ezh2. *ESC Heart Fail.* 2014;1:154–159.
96. Deng Q, Huang W, Peng C, Gao J, Li Z, Qiu X, Yang N, Yuan B, Zheng F. Genomic 5-mC contents in peripheral blood leukocytes were independent protective factors for coronary artery disease with a specific profile in different leukocyte subtypes. *Clin Epigenetics.* 2018;10:9.
97. Shen K, Liu H, Jing R, Yi J, Zhou X. DNA methylation dysregulations in rheumatic heart valve disease. *BMC Cardiovasc Disord.* 2017;17:159.
98. Ponciano-Gómez A, Martínez-Tovar A, Vela-Ojeda J, Olarte-Carrillo I, Centeno-Cruz F, Garrido E. Mutations in TET2 and DNMT3A genes are associated with changes in global and gene-specific methylation in acute myeloid leukemia. *Tumour Biol.* 2017;39:1010428317732181.
99. de Andres MC, Perez-Pampin E, Calaza M, Santaclara FJ, Ortea I, Gomez-Reino JJ, Gonzalez A. Assessment of global DNA methylation in peripheral blood cell subpopulations of early rheumatoid arthritis before and after methotrexate. *Arthritis Res Ther.* 2015;17:233.
100. Hromadnikova I, Kotlabova K, Hymanova L, Krofta L. Gestational hypertension, preeclampsia and intrauterine growth restriction induce dysregulation of cardiovascular and cerebrovascular disease associated microRNAs in maternal whole peripheral blood. *Thromb Res.* 2016;137:126–140.
101. Ikeda S, Kong SW, Lu J, Bisping E, Zhang H, Allen PD, Golub TR, Pieske B, Pu WT. Altered microRNA expression in human heart disease. *Physiol Genomics.* 2007;31:367–373.
102. Caruso P, MacLean MR, Khanin R, McClure J, Soon E, Southgate M, MacDonald RA, Greig JA, Robertson KE, Masson R, Denby L, Dempsey Y, Long L, Morrell NW, Baker AH. Dynamic changes in lung microRNA profiles during the development of pulmonary hypertension

- due to chronic hypoxia and monocrotaline. *Arterioscler Thromb Vasc Biol.* 2010;30:716–723.
103. Ellis KL, Cameron VA, Troughton RW, Frampton CM, Ellmers LJ, Richards AM. Circulating microRNAs as candidate markers to distinguish heart failure in breathless patients. *Eur J Heart Fail.* 2013;15:1138–1147.
104. Marques FZ, Vizi D, Khammy O, Mariani JA, Kaye DM. The transcardiac gradient of cardio-microRNAs in the failing heart. *Eur J Heart Fail.* 2016;18:1000–1008.
105. Deng L, Blanco FJ, Stevens H, et al. MicroRNA-143 activation regulates smooth muscle and endothelial cell crosstalk in pulmonary arterial hypertension. *Circ Res.* 2015;117:870–883.
106. Ikitimur B, Cakmak HA, Coskunpinar E, Barman HA, Vural VA. The relationship between circulating microRNAs and left ventricular mass in symptomatic heart failure patients with systolic dysfunction. *Kardiol Pol.* 2015;73:740–746.
107. Lok SI, de Jonge N, van Kuik J, van Geffen AJ, Huibers MM, van der Weide P, Siera E, Winkens B, Doevendans PA, de Weger RA, da Costa Martins PA. MicroRNA expression in myocardial tissue and plasma of patients with end-stage heart failure during LVAD support: comparison of continuous and pulsatile devices. *PLoS One.* 2015;10:e0136404.
108. Dangwal S, Stratmann B, Bang C, Lorenzen JM, Kumarswamy R, Fiedler J, Falk CS, Scholz CJ, Thum T, Tschöepe D. Impairment of wound healing in patients with type 2 diabetes mellitus influences circulating MicroRNA patterns via inflammatory cytokines. *Arterioscler Thromb Vasc Biol.* 2015;35:1480–1488.
109. Qiang L, Hong L, Ningfu W, Huaihong C, Jing W. Expression of miR-126 and miR-508-5p in endothelial progenitor cells is associated with the prognosis of chronic heart failure patients. *Int J Cardiol.* 2013;168:2082–2088.
110. Guo L, Yang Y, Liu J, Wang L, Li J, Wang Y, Liu Y, Gu S, Gan H, Cai J, Yuan JX, Wang J, Wang C. Differentially expressed plasma microRNAs and the potential regulatory function of Let-7b in chronic thromboembolic pulmonary hypertension. *PLoS One.* 2014;9:e101055.
111. Vausort M, Wagner DR, Devaux Y. Long noncoding RNAs in patients with acute myocardial infarction. *Circ Res.* 2014;115:668–677.
112. Huang X, Yue Z, Wu J, Chen J, Wang S, Wu J, Ren L, Zhang A, Deng P, Wang K, Wu C, Ding X, Ye P, Xia J. MicroRNA-21 knockout exacerbates angiotensin II-induced thoracic aortic aneurysm and dissection in mice with abnormal transforming growth factor- β -SMAD3 signaling. *Arterioscler Thromb Vasc Biol.* 2018;38:1086–1101.
113. Manavski Y, Lucas T, Glaser SF, Dorsheimer L, Günther S, Braun T, Rieger MA, Zeiher AM, Boon RA, Dimmeler S. Clonal expansion of endothelial cells contributes to ischemia-induced neovascularization. *Circ Res.* 2018;122:670–677.
114. Welch-Reardon KM, Wu N, Hughes CC. A role for partial endothelial-mesenchymal transitions in angiogenesis? *Arterioscler Thromb Vasc Biol.* 2015;35:303–308.
115. Zeisberg EM, Zeisberg M. The role of promoter hypermethylation in fibroblast activation and fibrogenesis. *J Pathol.* 2013;229:264–273.

CHAPTER

3

HYPOXIA-INDUCED ENDOTHELIAL-MESENCHYMAL TRANSITION IS ASSOCIATED WITH RASAL1 PROMOTER HYPERMETHYLATION IN HUMAN CORONARY ENDOTHELIAL CELLS

Xingbo Xu^{1,2}, Xiaoying Tan^{1,2}, Melanie S. Hulshoff¹, Tim Wilhelmi¹, Michael Zeisberg^{2,3} and Elisabeth M. Zeisberg^{1,2}

¹*Department of Cardiology and Pneumology, University Medical Center of Göttingen, Georg-August University, Göttingen, Germany.*

²*German Centre for Cardiovascular Research (DZHK), Göttingen, Germany.*

³*Department of Nephrology and Rheumatology, University Medical Center of Göttingen, Georg-August University, Göttingen, Germany.*

ABSTRACT

Cardiac fibrosis is integral in chronic heart disease, and one of the cellular processes contributing to cardiac fibrosis is endothelial-to-mesenchymal transition (EndMT). We recently found that hypoxia efficiently induces human coronary artery endothelial cells (HCAEC) to undergo EndMT through a hypoxia inducible factor-1 α (HIF1 α)-dependent pathway. Promoter hypermethylation of Ras-Gap-like protein 1 (RASAL1) has also been recently associated with EndMT progression and cardiac fibrosis. Our findings suggest that HIF1 α and transforming growth factor (TGF)/SMAD signalling pathways synergistically regulate hypoxia-induced EndMT through both DNMT3a-mediated hypermethylation of RASAL1 promoter and direct SNAIL induction. The findings indicate that multiple cascades may be activated simultaneously to mediate hypoxia-induced EndMT.

INTRODUCTION

Endothelial-to-mesenchymal transition (EndMT), which was originally described as cellular mechanism leading to formation of the mesenchymal cushion from AV-canal endothelial cells during cardiac development [1], has emerged as causal contributor in various pathologies, including in organ fibrosis involving heart or kidney, in brain vascular malformations or as source of fibroblasts in tumour stroma [2–10]. As the contribution of EndMT to these pathologies is increasingly being recognised, there is a growing number of identified EndMT-inducing stimuli, including various growth factors, environmental factors, such as hypoxia or high glucose, inflammation, direct cell–cell interactions or shear stress [11–17]. In context of fibrosis transforming growth factor β (TGF β), hypoxia and Ras-GTP signalling have consistently emerged as inducers of EndMT; all of which are hallmarks of the fibrotic microenvironment.

Transforming growth factor β is the prototypical profibrotic growth factor, and inhibition of TGF β signaling is one of the leading targets for antifibrotic drug development. Of the three known TGF β isoforms, TGF β 1 and TGF β 2 can induce EndMT. TGF β elicits signalling responses by binding to a type II receptor (TGF β R-II) which recruits and phosphorylates a type I receptor (activin-like kinase 5, ALK5) [18,19]. In addition to ALK5, ALK4 and ALK7 have also been found to activate the SMAD 2/3 signalling pathway [20]. The activated receptors then recruit and phosphorylate SMAD 2 and SMAD 3, which then bind to the common SMAD 4. Several studies have shown that activation of these TGF β receptors type I is required for phosphorylation and consecutive action of Smad 2/3 and that Smad 2/3 alone without activation of the TGF β receptor type I does not lead to Smad 2/3-induced gene regulation [21,22]. This heterodimeric Smad-complex then enters the nucleus, where it acts as a transcription factor. Among Smad-target genes are the transcription factors TWIST, SNAIL and SLUG, which all have been identified as inducers of EndMT.

Furthermore, long-term exposure to TGF β 1 induces aberrant CpG island promoter methylation of select genes, including RASAL1, encoding for the Ras-Gaplike protein 1 (RASAL1). RASAL1 converts (active) Ras-GTP to (inactive) Ras-GDP, and its transcriptional suppression through promoter methylation causes

increased intrinsic Ras-GTP activity, ultimately contributing to EndMT and fibrosis.

Hypoxia, the state of low oxygen concentration, is another hallmark of the fibrotic microenvironment, and several studies reported that hypoxia is a stimulus for endothelial cells to undergo EndMT [15,23–25]. Cellular responses to hypoxia are mediated by hypoxia inducible factors (HIFs), most prominently by HIF1, a highly conserved heterodimeric complex composed of an alpha (HIF1 α) and a beta subunit (HIF1 β , syn. aryl hydrocarbon receptor nuclear translocator ARNT). Under normoxic conditions, the alpha subunit of HIF is hydroxylated by HIF prolyl-hydroxylases, allowing their ubiquitination and rapid degradation. In hypoxic conditions, HIF accumulates because prolyl-hydroxylase is inhibited [26,27]. HIF-1 acts by binding to HIF-responsive elements (HREs) in promoters that contain the sequence NCGTG [28]. In this regard, we had previously established that hypoxia induces EndMT via direct induction of the transcription factor SNAIL [15].

While all three EndMT pathways were identified as single EndMT stimuli in cell culture experiments, cells are simultaneously exposed to all three of them within fibrotic tissue and crosstalk between the pathways is not yet understood. Here, we explore possible contribution of TGF β -signalling and RASAL1 CpG island promoter methylation in hypoxia-induced EndMT in human coronary artery endothelial cells.

RESULTS

HYPOXIA INDUCES RASAL1 CPG ISLAND PROMOTER METHYLATION AND ENDMT

To explore possible involvement of RASAL1 CpG island promoter methylation in hypoxia-induced EndMT, we exposed human coronary artery endothelial cells (HCAEC), which have been extensively characterised as a population of homogeneous endothelial cells in previous studies [15], to hypoxia. After 3 days of hypoxia, HCAEC acquired a spindle-shaped morphology (Fig. 1A) associated with decrease in endothelial cell marker CD31 and increased expression of mesenchymal markers S100A4 and alpha-smooth muscle actin (α SMA) and accumulation of HIF1 α (Fig. 1B–D), reminiscent of endothelial cells undergoing

an EndMT. Such EndMT was associated with increased expression of transcription factors SNAIL, SLUG and TWIST (Fig. 1E), in line with previous studies. Such hypoxia-induced EndMT was further associated with increased Ras-GTP activity (Fig. 1F), decreased RASAL1 expression (Fig. 1G) and increased degree of RASAL1 CpG island promoter methylation (Fig. 1H).

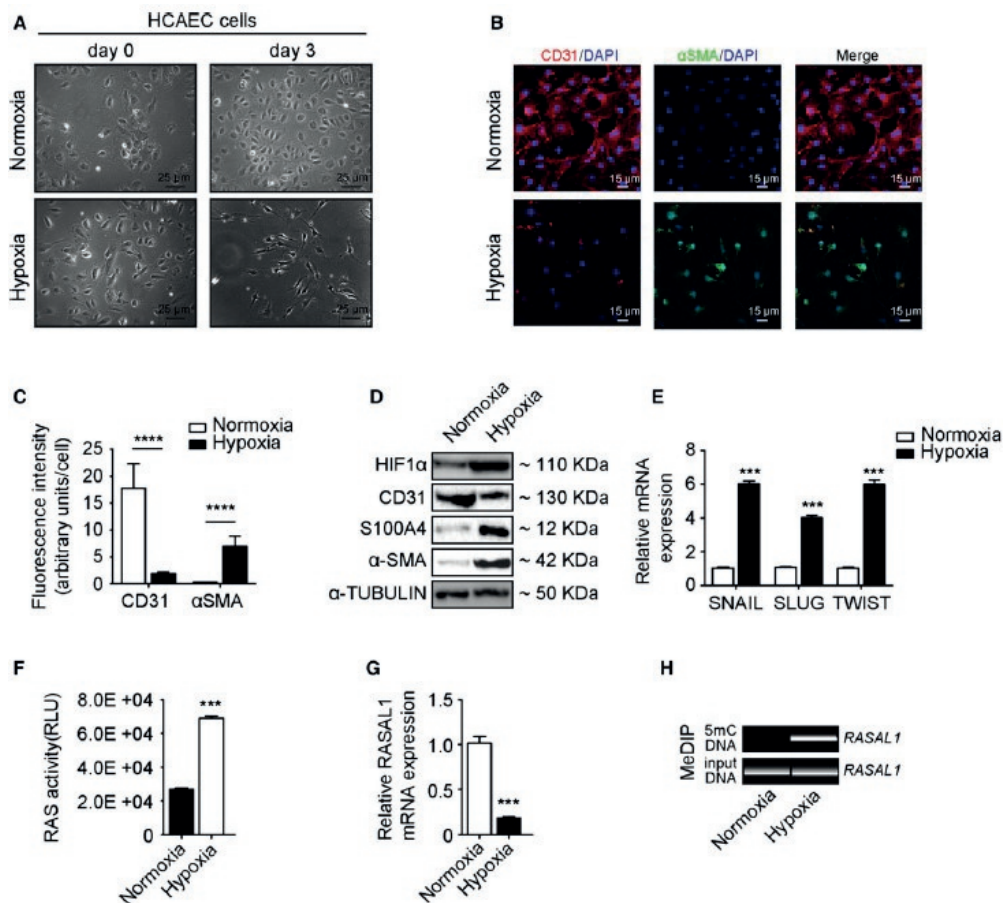


Figure 1. Hypoxia induces RASAL1 promoter hypermethylation in HCAEC.

(A) Phase-contrast microscopy pictures showing that cell morphology of HCAEC cells which were incubated under normoxic (upper) and hypoxic condition (lower) for 3 days. Scale bar equals 25 μm. (B) Representative immunofluorescence images showing CD31 (red) and α-SMA (green) staining in cell exposure to normoxia (upper panel) and hypoxia (lower panel); nuclei were counterstained with DAPI (blue). Scale bars 15 μm. (C) Densitometric measurements of the fluorescence signal of CD31 and α-SMA from images B using the IMAGEJ software. The arbitrary units of fluorescence signal were measured from single cells and represented by mean value. Error bars represent standard deviation, ****P < 0.0001. (D) Western blot analysis showing protein expression of HIF1α, CD31, S100A4, α-SMA, and α-TUBULIN. (E) Relative mRNA expression of SNAIL, SLUG, and TWIST. (F) RAS activity (RLU) in HCAEC cells. (G) Relative RASAL1 mRNA expression in HCAEC cells. (H) MeDIP assay for RASAL1 CpG island methylation in HCAEC cells.

*S100A4 and α -SMA in HCAEC cells under normoxic and hypoxic conditions. All blots were re probed with an anti- α -TUBULIN antibody as a control for equal loading. (E) qRT-PCR data showing the mRNA expression of key EndMT transcriptional factors (SNAIL, SLUG, and TWIST) in normoxic and hypoxic cells. All three genes were significantly increased upon hypoxic condition (gene expression and associated error bars, representing mean \pm SEM, $n = 3$ independent experiments, $***P < 0.001$). (F) RAS activity was measured by ELISA assay, cells cultured under normoxic condition served as controls. Hypoxia-treated cells showing RAS hyperactivity (data are presented as mean \pm SEM, $n = 6$ independent experiments, $***P < 0.001$). (G) qRT-PCR data showing the reduction in RASAL1 mRNA expression in hypoxia-treated cells (gene expression and associated error bars, representing mean \pm SEM, $n = 3$ independent experiments, $***P < 0.001$). (H) DNA virtual gel pictures showing the MeDIP results of enriched methylated DNA in RASAL1 promoter region in HCAEC cells exposed to hypoxic condition.*

Under pathological conditions, microvascular endothelial cells are a major cellular population contributing to EndMT. Therefore, in order to rule out the possibility that microvascular endothelial cells differ from macrovascular endothelial cells in response to hypoxia, we have repeated the experiments with human coronary microvascular endothelial cells (HCMEC) and obtained similar results (Fig. 2). In summary, we observed that hypoxia-induced EndMT is associated with increased RASAL1 promoter methylation and subsequent Ras-GTP activity. While this observation was in line with previous studies, which had established that RASAL1 CpG island promoter methylation is causally involved in TGF β -induced EndMT, we next aimed to gain insights into the mechanism which mediates aberrant promoter methylation in response to hypoxia.

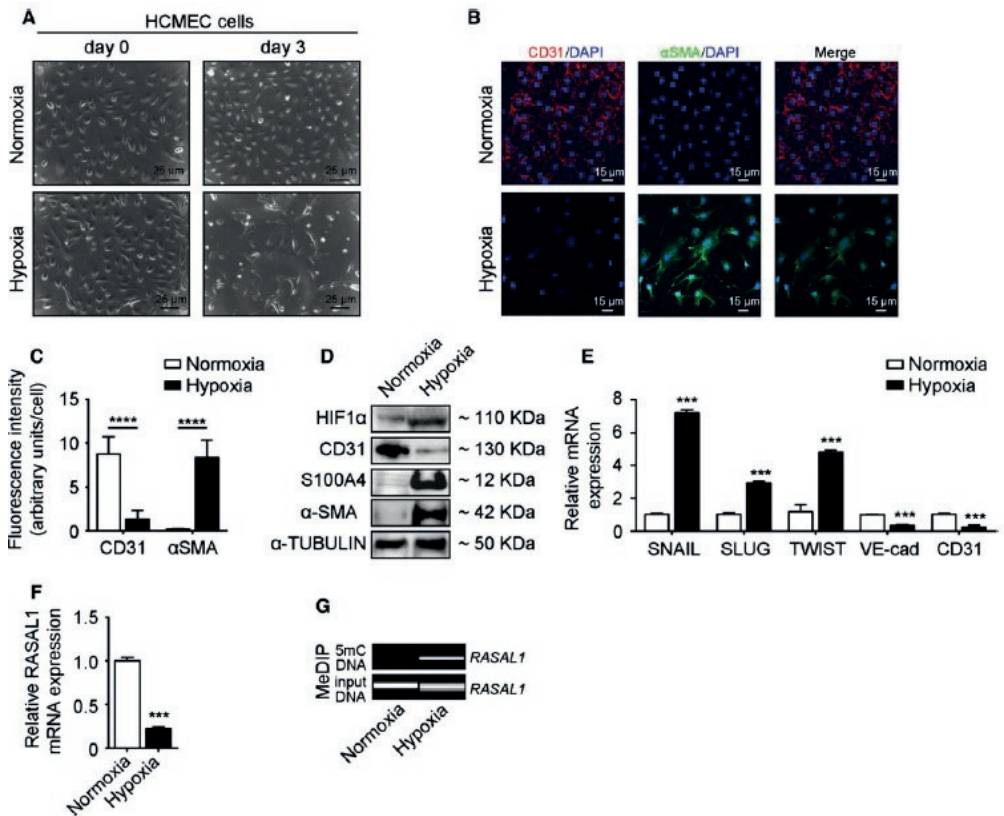


Figure 2. Hypoxia induces RASAL1 promoter hypermethylation in HCMEC.

(A) Phase-contrast microscopy pictures showing cell morphology of HCMEC cells which were incubated under normoxic (upper) and hypoxic condition (lower) for 3 days. Scale bar equals 25 μ m. (B) Representative immunofluorescence images showing CD31 (red) and α -SMA (green) staining in cells exposed to normoxia (upper panel) or hypoxia (lower panel); nuclei were counterstained with DAPI (blue). Scale bars 15 μ m. (C) Densitometric measurements of the fluorescence signal of CD31 and α -SMA from images B using IMAGEJ software. Arbitrary units of fluorescence signal were measured from single cells and represented by mean value. Error bars represent standard deviation, **** $P < 0.0001$. (D) Western blot analysis showing protein expression of HIF1 α , CD31, S100A4, α -SMA in HCAEC cells under normoxic or hypoxic conditions. All blots were reprobbed with an anti- α -TUBULIN antibody as a control for equal loading. (E) qRT-PCR data showing the mRNA expression of key EndMT transcriptional factors (SNAIL, SLUG and TWIST) and endothelial cell markers (VE-cadherin and CD31) in normoxic and hypoxic cells. (gene expression and associated error bars, representing mean \pm SEM, $n = 3$ independent experiments, *** $P < 0.001$). (F) qRT-PCR data showing the reduction in RASAL1 mRNA expression in hypoxia-treated cells (gene expression and associated error bars, representing mean \pm SEM, $n = 3$ independent experiments, *** $P < 0.001$). (G) DNA virtual gel pictures showing the MeDIP results of enriched methylated DNA in RASAL1 promoter region in HCMEC cells exposed to hypoxic condition.

HYPOXIA-INDUCED RASAL1 CPG ISLAND PROMOTER METHYLATION IS FACILITATED BY DNMT3A

In principle, four enzymes (Dnmt1, Dnmt3a, Dnmt3b and Dnmt3l) with DNA-methylating activity are known in humans. As previous studies established that DNA methylation through either of these enzymes is dependent on their transcriptional activities, we next analysed expression of DNMTs in HCAEC upon exposure to hypoxia by quantitative real-time PCR. Among the four DNMTS members, only expression of DNMT3a was substantially increased (Fig. 3A–D). To explore causal involvement of DNMT3a in hypoxia-induced RASAL1 methylation, we performed siRNA-mediated DNMT3a knockdown, sufficiently depleting intracellular DNMT3a (Fig. 3E,F) without influencing the expression of other DNMT family members (Fig. 3G). Silenced DNMT3a expression did not affect the expression of endothelial cell marker gene CD31 nor fibroblast specific genes S100A4 and α SMA (Fig. 3H) under normoxic condition. DNMT3a-depletion blunted suppression of RASAL1 expression in response to hypoxia (Fig. 3I) and RASAL1 CpG island promoter methylation (Fig. 3J), but did not completely abolish the effect of hypoxia on RASAL1 expression and promoter methylation. DNMT3a depletion also blunted induction of SNAIL, SLUG and TWIST in response to hypoxia (Fig. 3K).

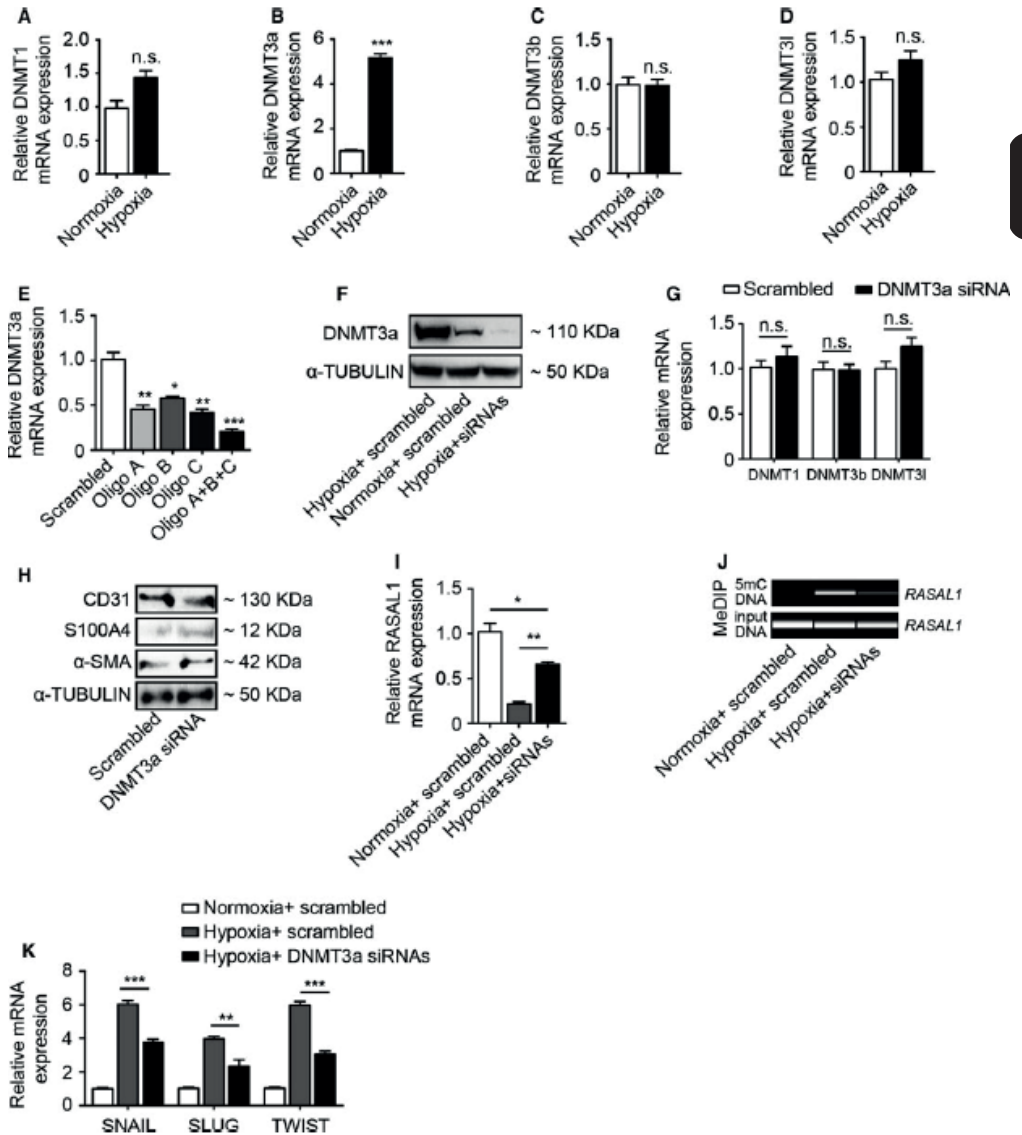


Figure 3. Silencing of DNMT3a expression alleviates hypoxia-induced EndMT.

(A–D) qRT-PCR results showing the mRNA expression of DNA methyltransferases (DNMT1, DNMT3a, DNMT3b and DNMT3l) in normoxic and hypoxic cells. DNMT3a is significantly upregulated upon hypoxia treatment. (E) qRT-PCR results showing DNMT3a mRNA expression in the cells which were transfected with different DNMT3a siRNA oligos. The combination of all three oligos contributed to over 70% reduction in DNMT3a. (F) Western blot results showing increased DNMT3a protein expression under hypoxic condition but not under normoxic condition, both transfected with combined DNMT3a. DNMT3a siRNAs treatment under hypoxic condition abolished expression of DNMT3a. (G) qRT-PCR results showing DNMT1, DNMT3b, and DNMT3l mRNA expression in HCAEC

cells transfected with DNMT3a siRNA compared to cells transfected with scrambled control. (H) Western blot analysis showing protein expression of CD31, S100A4, α -SMA in DNMT3a siRNA transfected cells compared to scrambled control transfected cells. All blots were reprobated with an anti- α -TUBULIN antibody as a control for equal loading. (I) qRT-PCR results showing DNMT3a mRNA expression in cells transfected with scrambled controls siRNA treated with normoxia and hypoxia and cells transfected with combined DNMT3a siRNAs treated with hypoxia. (J) DNA virtual gel pictures showing the MeDIP results of decreased methylation level of immunoprecipitated RASAL1 promoter in DNMT3a siRNA transfected cells compared to scrambled control transfected cells under hypoxic condition. (K) qRT-PCR data showing mRNA expression of the key EndMT transcription factors (SNAIL, SLUG, and TWIST) in DNMT3a siRNA transfected cells as compared to scrambled control transfected cells exposed to hypoxic condition (gene expression and associated error bars, representing mean \pm SEM, n = 3 independent experiments, n.s., no significance, *P < 0.05, **P < 0.01, ***P < 0.001).

HYPOXIA INDUCES AUTORCRINE TGF β SIGNALLING IN HCAEC

Because several previous studies had established TGF β signalling as prototypical stimulus for EndMT and also as inducer of RASAL1 CpG island promoter methylation, we next aimed to explore possible involvement of TGF β signalling in hypoxia-induced EndMT. For this reason, we first analysed expression of TGF β 1 (Fig. 4A), TGF β 2 (Fig. 4B) and TGF β 3 (Fig. 4C) by quantitative real-time PCR. Among the TGF β isoforms, expression of TGF β 2 was significantly increased upon exposure to hypoxic conditions. Furthermore, we also detected a significant increase in secreted TGF β 2 by ELISA assay in the supernatant of cells collected 3 days after hypoxia treatment (Fig. 4D). Corresponding with increased TGF β 2 expression, intracellular levels of phosphorylated SMAD2 (Fig. 4E) and of phosphorylated SMAD3 (Fig. 4F), both indicative of active TGF β signalling, were increased. Activated SMAD signalling was also shown by an increased expression of the SMAD-target gene PAI-I (Fig. 4G).

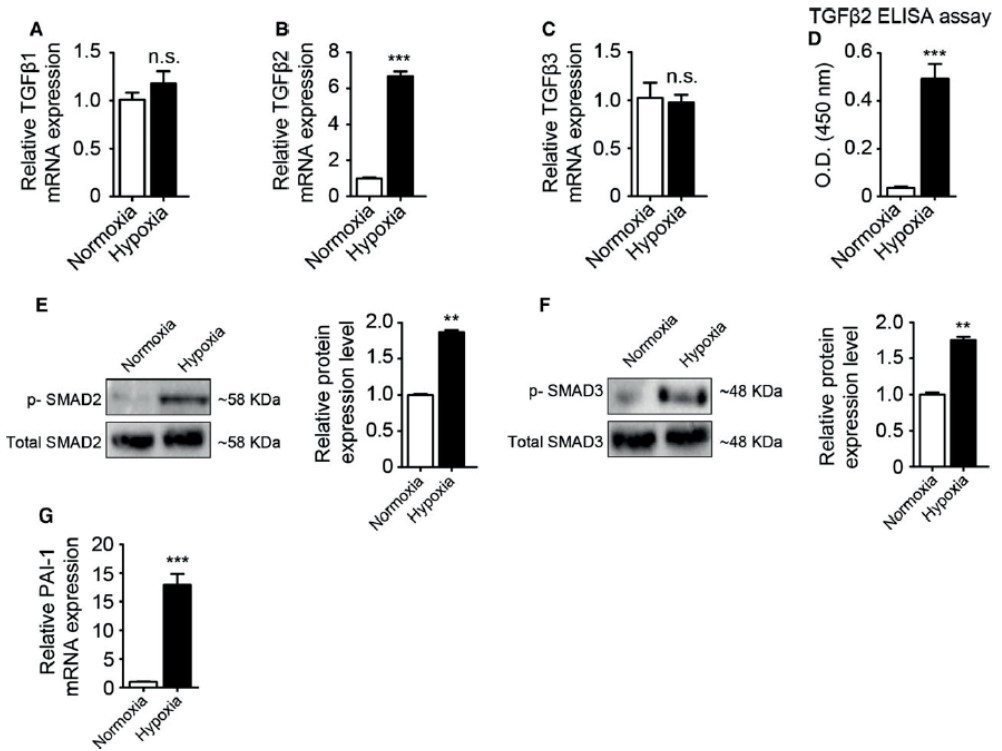


Figure 4. Hypoxia activates SMAD signaling pathway through inducing TGFβ2 expression.

(A–C) qRT-PCR results showing mRNA expression of all three TGFβ isoforms (TGFβ1, TGFβ2, and TGFβ3) in normoxic and hypoxic cells. TGFβ2 mRNA expression was significantly increased upon hypoxia treatment (gene expression and associated error bars, representing mean ± SEM, n = 3, n.s., no significance, ***P < 0.001). (D) ELISA assay measured the TGFβ2 in the cell medium secreted from cells exposed to hypoxia for 3 days. (E–F) Western blot analysis showing activated SMAD2 (E) and activated SMAD3 (F) proteins in hypoxic cells detected by specific antibodies against for phosphorylated SMADs. The membranes were reprobbed by total SMAD2 or total SMAD3 antibodies for equal-loading control. The expression levels were quantified by densitometry analysis (protein expression and associated error bars, representing mean ± SD, n = 3, **P < 0.01). (G) qRT-PCR results showing mRNA expression of a SMAD target gene, PAI-1 in normoxic and hypoxic cells. (gene expression and associated error bars, representing mean ± SEM, n = 3, ***P < 0.001).

AUTOCRINE TGF β SIGNALLING IS CAUSALLY INVOLVED IN HYPOXIA-INDUCED RASAL1 CPG ISLAND PROMOTER METHYLATION

To explore causal involvement of TGF β signalling in RASAL1 CpG island promoter methylation, we next established a system enabling us to either overexpress FLAG-tagged SMADs-2, -3 and -4 (Fig. 5A-C), and to effectively deplete SMADS by siRNA-mediated knockdown (Fig. 5D,E). Combined SMAD overexpression to enhance TGF β signalling responses further enhanced transcriptional suppression of RASAL1 (Fig. 5F) and RASAL1 CpG island promoter methylation (Fig. 5G) in response to hypoxia, whereas combined depletion of Smads-2 and -4 blunted the effect (but did not completely abolish it) on RASAL1 mRNA expression (Fig. 5H) and RASAL1 CpG island promoter methylation (Fig. 5I).

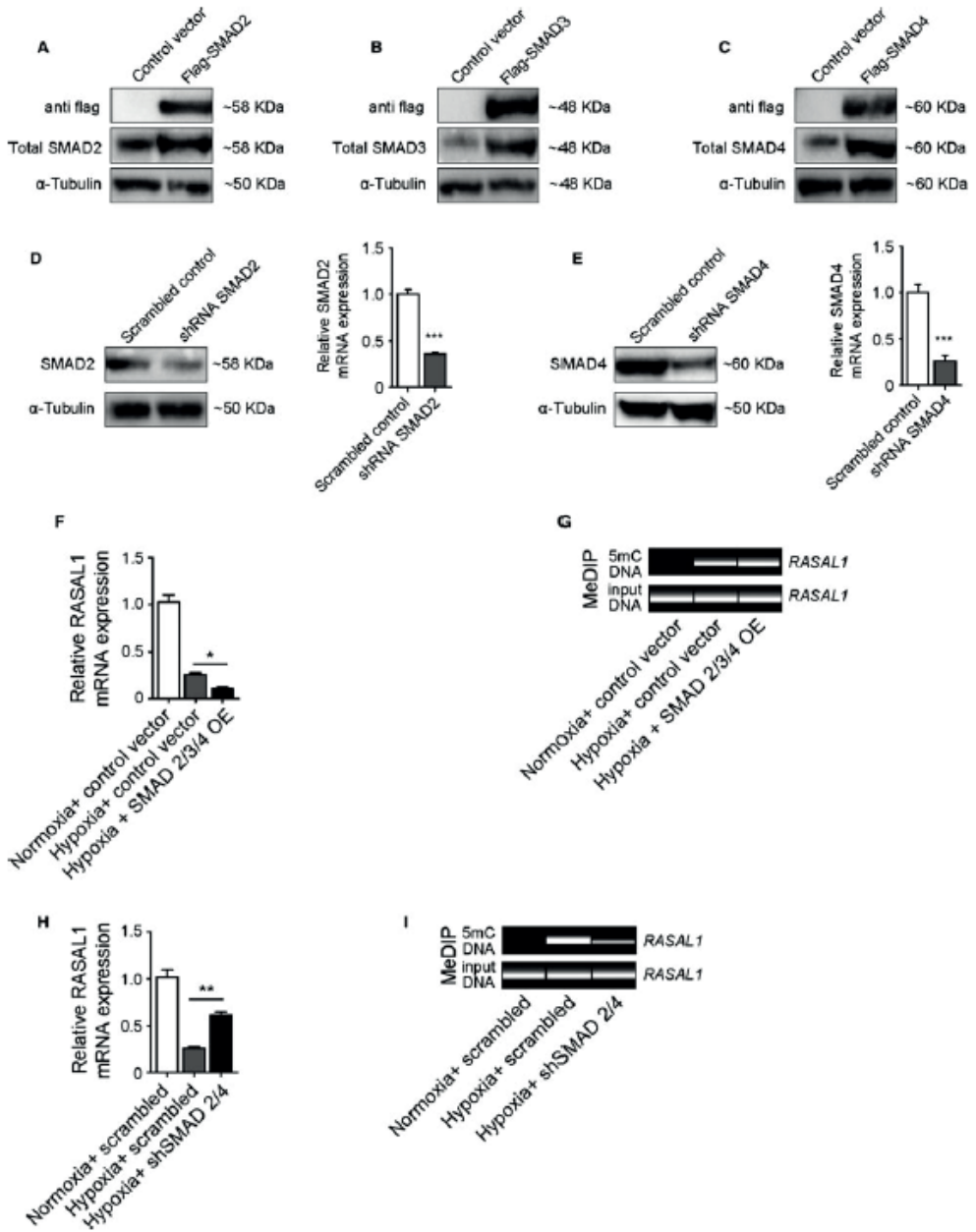


Figure 5. Silencing SMAD protein expression decreases hypoxia-induced RASAL1 promoter methylation.

(A–C) Western blot analysis showing SMAD2 (A), SMAD3 (B) and SMAD4 (C) expression in HCAEC cells which were transfected by overexpression constructs, pcDEF3-Flag(N)-hSmad2(C), pcDEF3-Flag(N)-hSmad3(D) and pcDEF3-Flag(N)-hSmad4(E). The expression levels of each protein were detected by flag antibody and corresponding antibodies. The membranes were reprobbed with a-

*Tubulin antibody for equal-loading control. (D–E) SMAD2 (D) and SMAD4 (E) expression silencing using shRNA constructs. The expression levels were analysed by qRT-PCR and Western blots analysis. The total SMAD2 and SMAD4 protein were significantly reduced upon shRNA-transfected cells compared with scrambled control shRNA-transfected cells. The protein expression levels were quantified by densitometry analysis (protein expression and associated error bars, representing mean \pm SD, n = 3, ***P < 0.001). (F) HCAEC cells were co-transfected with SMAD (SMAD2, SMAD3 and SMAD4) overexpression constructs, showing further decreased RASAL1 mRNA expression by qRT-PCR analysis (gene expression and associated error bars, representing mean \pm SEM, n = 4, *P < 0.05). (G) DNA virtual gel pictures showing increased RASAL1 promoter methylation measured by MeDIP analysis. This correlates with the decrease in RASAL1 mRNA expression. (H) qRT-PCR results showing restored RASAL1 mRNA expression after silencing SMAD (SMAD2, SMAD4) proteins (gene expression and associated error bars, representing mean \pm SEM, n = 4, ***P < 0.01). (I) DNA virtual gel pictures showing reduced RASAL1 promoter methylation measured by MeDIP analysis. This correlates with the restored RASAL1 mRNA expression.*

DISCUSSION

Our study corroborates that hypoxia induces EndMT in HCAEC and provides evidence that such EndMT in response to hypoxia is mediated by at least two distinct signalling pathways, which cannot fully compensate for each other's absence (Fig. 6). Specifically, we here demonstrate that hypoxia induces autocrine TGF β signalling, in addition to direct SNAIL activation by HIF1 α . Notably, it is specifically TGF β 2 which is upregulated among the TGF β -family members on mRNA level, and which is also detected as mature TGF β 2 in the secretome of endothelial cells upon hypoxia. While in context of fibrosis, the most abundant isoform within fibrotic tissue which had been identified as EndMT-inducing stimulus was TGF β 1 [29]. Our observation here is in line with several previous publications which identified TGF β 2 as most potent EndMT-inducing stimulus (without negating EndMT-inducing potential of TGF β 1) [30–32]. Our studies further demonstrate that hypoxia-induced autocrine TGF β signalling leads to CpG island promoter methylation of RASAL1 and subsequently increased intrinsic RAS-GTP activity. While this observation is in line with our previous studies which demonstrated that TGF β 1-induced EndMT is causally mediated by RASAL1 methylation, it is notable that in this context of hypoxia such aberrant CpG island promoter methylation was specifically mediated by the methyltransferase Dnmt3a. Knockdown of DNMT3a via siRNA on the other hand

had no effect on EndMT, suggesting that DNMT3a plays no role with respect to EndMT under normoxic condition. While this confirms previous studies which identified specifically DNMT3a to be primarily responsible for de novo promoter methylation, this is in contrast to reports which had discovered Dnmt1 as the methyltransferase responsible for aberrant RASAL1 promoter methylation in context of fibrotic kidney fibroblast activation [33–36]. While these findings are not preclusive, it is attractive to speculate that DNMT1, which was originally identified to maintain methylation patterns by copying information onto the unmethylated strand in newly synthesized hemimethylated DNA, acts predominantly in actively proliferating fibroblasts, whereas Dnmt3a acts predominantly in context of nonproliferative EndMT. Importantly, depletion of Dnmt3a or of Smad-signalling only partially inhibited RASAL1 methylation, most likely due to incomplete knockdown, but also allowing for speculation that additional mechanisms are involved. Importantly, we are aware that other genes, in addition to RASAL1, are affected. We are further aware that EndMT likely occurs context-dependent, and that robust TGF β and/or hypoxia stimulus is needed. In this context, a recent study has shown no contribution of EndMT in the model of transverse aortic constriction (TAC), 4 weeks after TAC (in this model robust hypertrophy occurred with modest fibrosis) [37], whereas in the more robust fibrosis model of ascending aortic constriction (AAC), about one-third of all fibroblasts were found to be of endothelial origin [6]. Therefore, further studies are needed to identify which stimuli induce EndMT under which circumstances.

ACKNOWLEDGEMENTS

This work was supported by DFG grants SFB1002/C01 (to EZ) and ZE523/4-1 (to MZ) and funds from the University of Göttingen Medical Center (UMG) to EZ and MZ. XX was supported by the ‘seed funding research program’ of the Faculty of Medicine, Georg-August University Göttingen and postdoc start-up grant, DZHK.

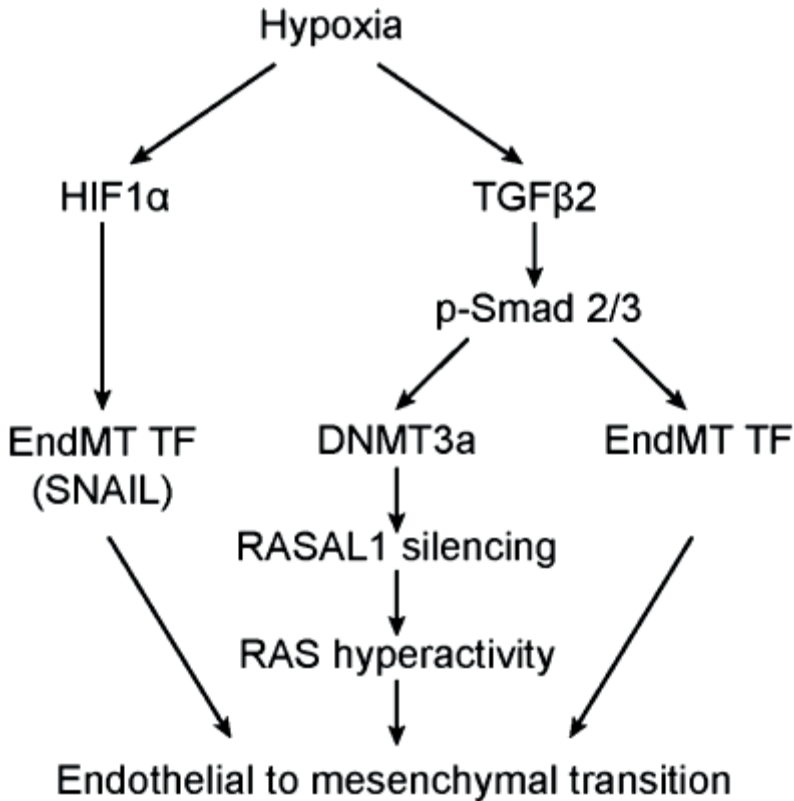


Figure 6. Hypoxia induces EndMT in HCAEC cells through different pathways. Schematic representation of hypoxia-induced endothelial-to-mesenchymal transition through different cascades. Under hypoxic condition, transcription factor HIF1 α protein is stabilised, which can directly activate EndMT transcriptional factor, Snail, to trigger the EndMT program. Besides, hypoxia can also activate TGF β 2 receptor regulated signalling pathway through SMAD2/3 proteins to induce EndMT transcription factor expression. In addition, we identified that hypoxia synergistically induces EndMT by DNMT3a-mediated hypermethylation of RASAL1 with consecutive Ras hyperactivity.

MATERIALS AND METHODS

CELL CULTURE AND HYPOXIA INCUBATIONS

Human coronary artery endothelial cells (HCAEC) were obtained from Genlantis (San Diego, CA, USA) and maintained in HCAEC growth medium (Genlantis). Human microvascular endothelial cells (HCMEC) were purchased from Promocell (Heidelberg, Germany) and maintained in endothelial cell growth medium MV (Heidelberg, Germany). Both cell types were kept in an incubator at 37 °C with 5% CO₂ and medium was changed in every other day. A total of 1x10⁶ cells were preseeded onto 10 cm plates (Griner, Frickenhausen, Germany) and were incubated for 24 h before exposure to hypoxic incubation for 72 h. Hypoxic conditions were induced as previously described. Briefly, cell dishes were placed into a hypoxia chamber (STEMCELL Technologies, Kloen, Germany), and the inside air was purged by a gas mixture (containing 1% O₂, 98% N₂) for 5 min with 1 bar flow rate. The cell morphology was examined by phase-contrast microscopy (Zeiss Axiovert200 and AXIOVISION 3.0 software (Zeiss, Goettingen, Germany)). The acquired images were processed using PHOTOSHOP CS3 software, Adobe, San Jose, CA, USA).

TRANSFECTION AND GENERATION OF PLASMID DNA CONSTRUCTS

For transfection, HCAEC cells were seeded at a confluence of 60–70% in a 10 cm dish and were cultured in growth medium overnight. Transfection was performed with Lipofectamine 2000 (Life Technologies, Paisley, UK) according to the manufacturer's instructions. Briefly, 5 µg of plasmid DNA from the respective constructs or 500 pmol of each siRNA oligo were incubated with Opti-MEM (Life Technologies) to a volume of 500 µL, and then mixed with 10 µL Lipofectamine plus Opti-MEM to a volume of 500 µL bringing the final volume to 1 mL. This mixture was incubated at room temperature for 20 min. Then the complex was added into the cell culture dish which contains 6 mL of endothelial basic medium (serum-free) for 4 h. Then, the transfection reagent-containing medium was removed and replaced by endothelial growth medium and the cells were exposed to hypoxic condition. For gene silencing experiment, DNMT3a siRNAs were purchased from OriGene (Rockville, MD, USA). pLKO.1 vector was used for

generating of pLKO.1-shSMAD2 (CCAGCAGGAATTGAGCCACAGAGTAATTA), pLKO.1-shSMAD4 (CCAACATTCCTGTGGCTCCACAAGTCAG) constructs. For gene overexpression, the DNA plasmids, pcDEF3-Flag(N)-hSmad2, pcDEF3-Flag(N)-hSmad3 and pcDEF3-Flag(N)-hSmad4, were kindly provided by Prof. Miyazono as gifts [38].

RNA EXTRACTION AND QUANTITATIVE REAL-TIME PCR

Total RNA was extracted from cells using PureLink RNA kit (Life Technologies, Carlsbad, CA, USA) following the manufacturer's protocol. A quantity of 1 µg of total RNA was first digested with DNase I (Sigma-Aldrich, St. Louis, CA, USA) and the digested product was used for cDNA synthesis using the SuperScriptII system (Life Technologies). A qRT-PCR assay was performed as previously described [35]. Briefly, 2 µL of diluted cDNA (1/20) was used as a template in Fast SYBR Master Mix (Life Technologies) and run on a StepOne Plus realtime PCR system (Life Technologies) with the real-time PCR primers (sequence listed below). Measurements were standardized to the GAPDH reaction using delta delta Ct methods.

Gene	Sequence	Supplier
CD31	F: AAGGAACAGGAGGGAGAGTATTA R: GTATTTTGCTTCTGGGGACACT	Primer design Southampton, UK
DNMT1	F: TTCTGTTAAGCTGTCTCTTTCCA R: TGCTGAAGCCTCCGAGAT	Saha et al. [39]
DNMT3a	F: ATAGATCCCGTGTGGAGCC R: ACCCAGCGCAGAAGCAG	Primer design Southampton, UK
DNMT3b	F: TCTCATTGAGATGCCTGGT R: GAGATTCGCGAGCCCAG	Saha et al. [39]
DNMT3l	F: GCCGTACACAAGATCGAAGG R: GTTCTGACCCGGGACAACCT	Minami et al. [40]
GAPDH	Undisclosed	Primer design Southampton, UK
PAI-1	F: GGCCATTACTACGACATCCTG R: GGTGATGTTGCCTTTCCAGT	Hao et al. [41]
RASAL1	F: CGTGTGGATGAGGACTG R: TCCCTGCTCAGCGAGATCTT	Primer design Southampton, UK
SLUG	F: ACTCCGAAGCCAAATGACAA R: CTCTCTGTGGGTGTGTGT	Primer design Southampton, UK
SMAD2	F: GGAGCAGAATACCGAAGGCA R: CTTGAGCAACGCACTGAAGG	Yu et al. [42]
SMAD4	F: TGGCCCAGGATCAGTAGGT R: CATCAACACCAATTCAGCA	Wang et al. [43]
SNAIL	F: GGCAATTTAACAATGTCTGAAAAGG	Primer design Southampton, UK

TGFβ1	R: GAATAGTTCTGGGAGACACATCG F: CACTCCCACTCCCTCTCTC R: GTCCTGTGCCTTGATG	Primer design Southampton, UK
TGFβ2	F: TACGCCAAGGAGGTTTACAAA R: TGAAGTAGGGTCTGTAGAAAGTG	Primer design Southampton, UK
TGFβ3	F: ACTATGCCAACTTCTGCTCAG R: CAGATGCTTCAGGGTTCAGA	Primer design Southampton, UK
TWIST	F: CTCAAGAGGTCGTGCCAATC R: CCCAGTATTTTTATTCTAAAGGTGT	Primer design Southampton, UK

PROTEIN EXTRACTION AND WESTERN BLOTTING

Proteins were extracted from cells and tissues using NP40 lysis buffer (Life Technologies), containing protease inhibitor cocktail (Roche, Mannheim, Germany). Western blotting assay was performed as previously described [44]. Protein samples were resolved on 4–12% SDS/PAGE and transferred onto nitrocellulose membrane (GE Healthcare, Buckinghamshire, UK). The membrane was incubated with 5% dry milk in TBST solution (TBS pH 7.2, 0.1% Tween-20) for 1 h blocking at room temperature, then the primary antibodies (detail and dilution factor were listed below) were diluted with washing solution (2% dry milk in TBST) at 4 °C overnight. On the second day, after 3x of washing with washing solution, the membrane was incubated with secondary horseradish peroxidase-conjugated antibodies (Cell Signaling, Danvers, MA, USA), and signals were detected using a chemiluminescent kit (Santa Cruz Biotechnology, Santa Cruz, CA, USA).

Antibody	Product code	Dilution	Company
aSMA	Ab32575	1:1000	Abcam
a-Tubulin	Sig T5168	1:5000	Sigma
CD31	553370	1:1000	BD Pharmigen
DNMT3a	IMG-268A	1:1000	IMGENEX
Flag	TA50011	1:2500	Origene
HIF1a	MA1-16504	1:1000	Thermal
p-SMAD2	3108s	1:1000	Cell Signaling
p-SMAD3	9520s	1:1000	Cell Signaling
S100A4	HPA007973-100UL	1:1000	Sigma
SMAD2	700048	1:2500	Life Technologies
SMAD3	Ab40854	1:2500	Abcam
SMAD4	Ab40759	1:2500	Abcam

MEDIP-QPCR BASED DETECTION OF METHYLATED RASAL1 PROMOTER

Methylated DNA immunoprecipitation assay was performed as previously described [2,34,35]. Briefly, the total methylated DNA was captured using Methylamp Methylated DNA capture Kit (Epigentek, Farmingdale, NY, USA). A quantity of 1.0 µg of sonicated DNA was used in each reaction and incubated at room temperature for 2 h with gently horizontal shaking. The captured DNA was purified and eluted by 100 µL of nuclease-free water. For each sample, a corresponding input sample was performed using total sonicated DNA served as control. For quantification of methylated RASAL1 promoter, 5 µL of immunoprecipitated DNA with primers (F: GCCCGCCAGCCTGCTTGTCTGG, R: GGCAGGCAGCGCGGCCCTCCACC) and 2x iQ SYBR green Supermix (Bio-Rad, Muenchen, Germany) were used for each PCR reaction in a final volume of 25 µL and ROX was served as passive reference dye (Bio-Rad). The real-time PCR reactions were performed in a 96-well plate format using the Mx3000P qPCR system (Stratagene, Foster City, CA, USA). PCR reaction was manually terminated when the fluorescent signal increased over the threshold. The electrophoresis of PCR products were performed using a Bioanalyzer 2100 (Agilent, Santa Clara, CA, USA) according to the manufacturer's protocol. Electrophoresis results are shown as virtual gel images as described in previous publications [2].

TGFβ2 ELISA ASSAY

Cell medium was collected after hypoxia treatment for 3 days. After centrifugation, the supernatant was transferred into a new tube and used for secretome measurement. The TGFβ2 ELISA assay (Abcam, Cambridge, UK) was performed according to manufacturer's protocol. Briefly, 100 µL of each sample was added into precoated wells and incubated for 3 h at room temperature with gentle shaking. After 4x washing with washing solution, 100 µL of 1x biotinylated TGFβ2 antibody was added into each well and incubated for 1 h at room temperature with gentle shaking. Then each reaction continued with adding 100 µL of 1x HRP-Streptavidin solution for 45 min followed by incubation with 100 µL tetramethylbenzidine substrate reagent for 30 min. A quantity of 50 µL of stop solution was applied to stop the reaction, and then the plate was immediately read by a spectrophotometer (Synergy2; Biotech, Bad Friedrichshall, Germany) at 450 nm wavelength.

STATISTICAL ANALYSIS

Means were calculated and plotted along with standard error bars. All statistical analyses were done using GraphPad PRISM software version 5.0 (GraphPad). All data were first analysed by Student t-test for single comparison and one-way ANOVA for multiple comparisons. Differences between means were considered statistically significant when the P-value ≤ 0.05 . Three or more biological replicates were included for all experiments, with the exception of immunofluorescence, which were tested in two independent experiments.

REFERENCES

1. Eisenberg LM and Markwald RR (1995) Molecular regulation of atrioventricular valvuloseptal morphogenesis. *Circ Res* 77, 1–6.
2. Xu X, Tan X, Tampe B, Nyamsuren G, Liu X, Maier LS, Sossalla S, Kalluri R, Zeisberg M and Hasenfuss G (2015) Epigenetic balance of aberrant *rsal1* promoter methylation and hydroxymethylation regulates cardiac fibrosis. *Cardiovasc Res* 105, 279–291.
3. Maddaluno L, Rudini N, Cuttano R, Bravi L, Giampietro C, Corada M, Ferrarini L, Orsenigo F, Papa E, Boulday G et al. (2013) EndMT contributes to the onset and progression of cerebral cavernous malformations. *Nature* 498, 492–496.
4. Zeisberg EM, Potenta S, Xie L, Zeisberg M and Kalluri R (2007) Discovery of endothelial to mesenchymal transition as a source for carcinoma-associated fibroblasts. *Cancer Res* 67, 10123–10128.
5. Zeisberg EM, Potenta SE, Sugimoto H, Zeisberg M and Kalluri R (2008) Fibroblasts in kidney fibrosis emerge via endothelial-to-mesenchymal transition. *J Am Soc Nephrol* 19, 2282–2287.
6. Zeisberg EM, Tarnavski O, Zeisberg M, Dorfman AL, McMullen JR, Gustafsson E, Chandraker A, Yuan X, Pu WT, Roberts AB et al. (2007) Endothelial-to-mesenchymal transition contributes to cardiac fibrosis. *Nat Med* 13, 952–961.
7. Cuttano R, Rudini N, Bravi L, Corada M, Giampietro C, Papa E, Morini MF, Maddaluno L, Baeyens N, Adams RH et al. (2015) *KLF4* is a key determinant in the development and progression of cerebral cavernous malformations. *EMBO Mol Med* 8, 6–24.
8. Choi SH, Nam JK, Kim BY, Jang J, Jin YB, Lee HJ, Park S, Ji YH, Cho J, Lee YJ et al. (2016) *HSPB1* inhibits the endothelial-to-mesenchymal transition to suppress pulmonary fibrosis and lung tumorigenesis. *Cancer Res* 21, 3716–3726.
9. Bravi L, Malinverno M, Pisati F, Rudini N, Cuttano R, Pallini R, Martini M, Larocca LM, Locatelli M, Levi V et al. (2016) Endothelial cells lining sporadic cerebral cavernous malformation cavernomas undergo endothelial-to-mesenchymal transition. *Stroke* 47, 886–890.
10. Peng H, Li Y, Wang C, Zhang J, Chen Y, Chen W, Cao J, Wang Y, Hu Z, Lou T et al. (2016) *ROCK1* induces endothelial-to-mesenchymal transition in glomeruli to aggravate albuminuria in diabetic nephropathy. *Sci Rep* 6, 20304.
11. Mahler GJ, Frenzl CM, Cao Q and Butcher JT (2014) Effects of shear stress pattern and magnitude on mesenchymal transformation and invasion of aortic valve endothelial cells. *Biotechnol Bioeng* 111, 2326–2337.
12. Muylaert DE, de Jong OG, Slaats GG, Nieuweboer FE, Fledderus JO, Goumans MJ, Hierck BP and Verhaar MC (2015) Environmental influences on endothelial to mesenchymal transition in developing implanted cardiovascular tissue-engineered grafts. *Tissue Eng Part B Rev* 22, 58–67.
13. Rieder F, Kessler SP, West GA, Bhilocha S, de la Motte C, Sadler TM, Gopalan B, Stylianou E and Fiocchi C (2011) Inflammation-induced endothelial-to-mesenchymal transition: a novel mechanism of intestinal fibrosis. *Am J Pathol* 179, 2660–2673.

- 14 Tang R, Li Q, Lv L, Dai H, Zheng M, Ma K and Liu B (2010) Angiotensin II mediates the high-glucose-induced endothelial-to-mesenchymal transition in human aortic endothelial cells. *Cardiovasc Diabetol* 9, 31.
- 15 Xu X, Tan X, Tampe B, Sanchez E, Zeisberg M and Zeisberg EM (2015) Snail is a direct target of HIF1a in hypoxia-induced endothelial to mesenchymal transition of human coronary endothelial cells. *J Biol Chem* 290, 16653–16664.
- 16 Muylaert DE, de Jong OG, Slaats GG, Nieuweboer FE, Fledderus JO, Goumans MJ, Hierck BP and Verhaar MC (2015) Environmental influences on endothelial to mesenchymal transition in developing implanted cardiovascular tissue-engineered grafts. *Tissue Eng Part B Rev* 22, 58–67.
- 17 Xu X, Tan X, Tampe B, Sanchez E, Zeisberg M and Zeisberg EM (2015) Snail is a direct target of hypoxia-inducible factor 1alpha (HIF1alpha) in hypoxia-induced endothelial to mesenchymal transition of human coronary endothelial cells. *J Biol Chem* 290, 16653–16664.
- 18 Guo X and Wang XF (2009) Signaling cross-talk between TGF-beta/BMP and other pathways. *Cell Res* 19, 71–88.
- 19 Krenning G, Barauna VG, Krieger JE, Harmsen MC and Moonen JR (2016) Endothelial plasticity: shifting phenotypes through force feedback. *Stem Cells Int* 2016, 9762959.
- 20 Mueller TD and Nickel J (2012) Promiscuity and specificity in BMP receptor activation. *FEBS Lett* 586, 1846–1859.
- 21 He WX, Niu ZY, Zhao SL, Jin WL, Gao J and Smith AJ (2004) TGF-beta activated Smad signalling leads to a Smad3-mediated down-regulation of DSPP in an odontoblast cell line. *Arch Oral Biol* 49, 911–918.
- 22 Zeisberg M, Hanai J, Sugimoto H, Mammoto T, Charytan D, Strutz F and Kalluri R (2003) BMP-7 counteracts TGF-beta1-induced epithelial-to-mesenchymal transition and reverses chronic renal injury. *Nat Med* 9, 964–968.
- 23 Choi SH, Hong ZY, Nam JK, Lee HJ, Jang J, Yoo RJ, Lee YJ, Lee CY, Kim KH, Park S et al. (2015) A hypoxia-induced vascular endothelial-to-mesenchymal transition in development of radiation-induced pulmonary fibrosis. *Clin Cancer Res* 21, 3716–3726.
- 24 Curci C, Castellano G, Stasi A, Divella C, Loverre A, Gigante M, Simone S, Cariello M, Montinaro V, Lucarelli G et al. (2014) Endothelial-to-mesenchymal transition and renal fibrosis in ischaemia/reperfusion injury are mediated by complement anaphylatoxins and Akt pathway. *Nephrol Dial Transplant* 29, 799–808.
- 25 Higgins DF, Kimura K, Iwano M and Haase VH (2008) Hypoxia-inducible factor signaling in the development of tissue fibrosis. *Cell Cycle* 7, 1128–1132.
- 26 Greer SN, Metcalf JL, Wang Y and Ohh M (2012) The updated biology of hypoxia-inducible factor. *EMBO J* 31, 2448–2460.
- 27 Weidemann A and Johnson RS (2008) Biology of HIF-1alpha. *Cell Death Differ* 15, 621–627.
- 28 Miyazaki K, Kawamoto T, Tanimoto K, Nishiyama M, Honda H and Kato Y (2002) Identification of functional hypoxia response elements in the promoter region of the DEC1 and DEC2 genes. *J Biol Chem* 277, 47014–47021.

- 29 Shu Y, Liu Y, Li X, Cao L, Yuan X, Li W and Cao Q (2016) Aspirin-triggered resolvin D1 inhibits TGFbeta1-induced EndMT through increasing the expression of Smad7 and is closely related to oxidative stress. *Biomol Ther (Seoul)* 24, 132–139.
- 30 Akman HO, Zhang H, Siddiqui MA, Solomon W, Smith EL and Batuman OA (2001) Response to hypoxia involves transforming growth factor-beta2 and Smad proteins in human endothelial cells. *Blood* 98, 3324–3331.
- 31 Zhang H, Akman HO, Smith EL, Zhao J, Murphy-Ullrich JE and Batuman OA (2003) Cellular response to hypoxia involves signaling via Smad proteins. *Blood* 101, 2253–2260.
- 32 Katsura A, Suzuki HI, Ueno T, Mihira H, Yamazaki T, Yasuda T, Watabe T, Mano H, Yamada Y and Miyazono K (2016) MicroRNA-31 is a positive modulator of endothelial-mesenchymal transition and associated secretory phenotype induced by TGF-beta. *Genes Cells* 21, 99–116.
- 33 Bechtel W, McGoohan S, Zeisberg EM, Muller GA, Kalbacher H, Salant DJ, Muller CA, Kalluri R and Zeisberg M (2010) Methylation determines fibroblast activation and fibrogenesis in the kidney. *Nat Med* 16, 544–550.
- 34 Tampe B, Tampe D, Muller CA, Sugimoto H, LeBleu V, Xu X, Muller GA, Zeisberg EM, Kalluri R and Zeisberg M (2014) Tet3-mediated hydroxymethylation of epigenetically silenced genes contributes to bone morphogenic protein 7-induced reversal of kidney fibrosis. *J Am Soc Nephrol* 25, 905–912.
- 35 Xu X, Friehs I, Zhong Hu T, Melnychenko I, Tampe B, Alhour F, Iascone M, Kalluri R, Zeisberg M, Del Nido PJ et al. (2015) Endocardial fibroelastosis is caused by aberrant endothelial to mesenchymal transition. *Circ Res* 116, 857–866.
- 36 Tampe B, Tampe D, Zeisberg EM, Muller GA, Bechtel-Walz W, Koziolk M, Kalluri R and Zeisberg M (2015) Induction of Tet3-dependent epigenetic remodeling by low-dose hydralazine attenuates progression of chronic kidney disease. *EBioMedicine* 2, 19–36.
- 37 Moore-Morris T, Guimaraes-Camboa N, Banerjee I, Zambon AC, Kisseleva T, Velayoudon A, Stallcup WB, Gu Y, Dalton ND, Cedenilla M et al. (2014) Resident fibroblast lineages mediate pressure overload-induced cardiac fibrosis. *J Clin Invest* 124, 2921–2934.
- 38 Kawabata M, Inoue H, Hanyu A, Imamura T and Miyazono K (1998) Smad proteins exist as monomers in vivo and undergo homo- and hetero-oligomerization upon activation by serine/threonine kinase receptors. *EMBO J* 17, 4056–4065.
- 39 Saha A, Jha HC, Upadhyay SK and Robertson ES (2015) Epigenetic silencing of tumor suppressor genes during in vitro Epstein-Barr virus infection. *Proc Natl Acad Sci USA* 112, E5199–E5207.
- 40 Minami K, Chano T, Kawakami T, Ushida H, Kushima R, Okabe H, Okada Y and Okamoto K (2010) DNMT3L is a novel marker and is essential for the growth of human embryonal carcinoma. *Clin Cancer Res* 16, 2751–2759.
- 41 Hao S, He W, Li Y, Ding H, Hou Y, Nie J, Hou FF, Kahn M, Liu Y (2011) Targeted inhibition of betacatenin/CBP signaling ameliorates renal interstitial fibrosis. *J Am Soc Nephrol* 22, 1642–1653.
- 42 Yu H, Mrowietz U and Seifert O (2009) Downregulation of SMAD2, 4 and 6 mRNA and TGFbeta receptor I mRNA in lesional and non-lesional psoriatic skin. *Acta Derm Venereol* 89, 351–356.

- 43 Wang LH, Kim SH, Lee JH, Choi YL, Kim YC, Park TS, Hong YC, Wu CF and Shin YK (2007) Inactivation of SMAD4 tumor suppressor gene during gastric carcinoma progression. *Clin Cancer Res* 13, 102–110.
- 44 Xu X, Pantakani DK, Lührig S, Tan X, Khromov T, Nolte J, Dressel R, Zechner U and Engel W (2011) Stagespecific germ-cell marker genes are expressed in all mouse pluripotent cell types and emerge early during induced pluripotency. *PLoS One* 6, e22413.

CHAPTER

4

MIR-132-3P AND KLF7 AS NOVEL POTENTIAL REGULATORS OF AORTIC STIFFENING-ASSOCIATED ENDMT IN TYPE 2 DIABETES

Melanie S. Hulshoff^{1,2,3,*}, Isabel N. Schellinger^{4,5,*}, Xingbo Xu^{1,2}, Jolien Fledderus³, Sandip K. Rath^{1,2}, Fang Cheng Wong¹, Guido Krenning³, Uwe Raaz^{1,2,4,†} and Elisabeth M. Zeisberg^{1,2,†}

¹*Department of Cardiology and Pneumology, University Medical Center of Göttingen, Georg-August University, Göttingen, Germany.*

²*German Centre for Cardiovascular Research (DZHK), Göttingen, Germany.*

³*Department of Pathology and Medical Biology, University Medical Center Groningen, University of Groningen, Groningen, The Netherlands.*

⁴*University Heart Center, Göttingen, Germany.*

⁵*Department of Endocrinology, Nephrology and Rheumatology, University of Leipzig Medical Center, Germany.*

**Authors contributed equally*

†share last authorship

Submitted

ABSTRACT

Objective – Aortic stiffening is an independent predictor of cardiovascular disease and mortality in diabetic patients. We recently showed that aortic stiffness increases prior to the development of hypertension in a mouse model of type 2 diabetes (db/db mice), making aortic stiffness an early contributor to cardiovascular disease development. We here investigated if endothelial-to-mesenchymal transition (EndMT) occurs during aortic stiffening in type 2 diabetes.

Approach and Results – We demonstrate robust co-localization of the endothelial marker CD31 with mesenchymal markers α -SMA and S100A4 in aortic sections of db/db mice. Moreover, we demonstrate an increased mRNA expression of the EndMT transcription factors (i.e. Snail, Slug and Twist) in aortic sections of db/db mice as well as of diabetic patients. As potential underlying regulator of EndMT, we identified miR-132-3p as the most consequently downregulated in aortas of db/db mice as well as in high glucose-treated human umbilical vein endothelial cells (HUVECs). Indeed, miR-132-3p was also downregulated in aortic tissue from diabetic patients. We identified Kruppel-like factor 7 (KLF7) as a target of miR-132-3p and show a significant upregulation of KLF7 in aortic sections of both db/db mice and diabetic patients as well as in high glucose-treated HUVECs.

Conclusions – We demonstrate that EndMT occurs during aortic stiffening in the context of type 2 diabetes. We identified miR-132-3p and KLF7 as novel potential regulators of EndMT in this context. Altogether, this gives us new insights in the development of aortic stiffening in type 2 diabetes.

INTRODUCTION

Throughout the world, diabetes is a growing health burden. Largely unknown in the early 20th century, type 2 diabetes (T2D) is now the 7th leading cause of death in the USA mainly due to increased cardiovascular mortality [1, 2]. One mechanism that links diabetes to increased cardiovascular risk may be accelerated arterial stiffening that is frequently observed in diabetic patients [3]. Stiffening of the large arteries leads to various adverse hemodynamic consequences, rendering arterial stiffness an independent risk factor of cardiovascular disease [4, 5]. The Hoorn emphasizes that T2D is especially associated with increased central arterial stiffness [6].

The aorta is the biggest vessel of the body and channels the blood from the heart to the periphery. Its elastic nature offers a buffering capacity (*Windkessel* function) to equalize blood flow during systole and diastole. As such, the aortic wall is an important responder to the biomechanical forces induced by the cyclic nature of the heart beating.

Elevated arterial stiffness may result from increased collagen built-up in the arterial wall [7]. However, little is known about the underlying molecular mechanisms that cause this increase in collagen.

T2D is a chronic state characterized by hyperglycemic stimuli and low-grade systemic inflammation [8]. Endothelial cells are early targets of these destructive conditions and hold a critical role in the production of extracellular matrix proteins in diabetic complications [9-11]. Endothelial-to-mesenchymal transition (EndMT) is a biologic process that forces endothelial cells to undergo a dynamic phenotypic switch (transition) in the context of sustained injury. Such changes in endothelial cells are manifested by a loss of endothelial markers and gain of mesenchymal markers [12-15]. EndMT has been shown to be a main source of fibroblasts triggering an increased production of extracellular matrix proteins in organ fibrosis [16-18].

New evidence suggests that EndMT is epigenetically regulated by a class of small non-coding RNAs called microRNA (miRs) [12, 19-22]. MiRs are short single stranded RNAs that repress the expression of messenger RNAs by binding to the 3'UTR regions that are (partially) complimentary to their own code [23]. The number of mRNAs that may be affected by a single miR is estimated to be in the hundreds [24-26].

Here, we demonstrate that EndMT occurs during aortic stiffening in T2D and identify miR-132-3p and KLF7 as novel regulators of EndMT and potentially aortic stiffening in T2D.

RESULTS

AORTAS OF DB/DB MICE AND DIABETIC PATIENTS BUT NOT OF CONTROL MICE AND SUBJECTS DISPLAY ROBUST SIGNS OF ENDMT

In aortas of db/db mice, we observed a robust co-localization of CD31 with both the mesenchymal markers α -SMA and S100A4 which was almost absent in control (db/+) mice (Fig.1A, B; for α -SMA 10 versus 2.8, $p < 0.05$, Fig.1C; for S100A4 10.6 versus 1.6, $p < 0.05$, Fig.1D). We then examined the mRNA expression of the EndMT transcription factors Snail, Slug and Twist in aortic tissue of db/db mice to further assess the presence of EndMT. Indeed, Snail, Slug and Twist were increased in aortic tissue from db/db mice when compared to control mice (Snail 13.5-fold, $p < 0.01$; Slug 9.4-fold, $p < 0.001$; Twist 6.1-fold, $p < 0.001$, Fig.1E). To investigate if EndMT is also associated with aortic stiffening in patients with T2D, we also studied aortic tissue from patients with T2D and control subjects, and we found that *SNAIL*, *SLUG* and *TWIST* are increased in T2D patients (*SNAIL* 2.6-fold, $p < 0.01$; *SLUG* 2.5-fold, $p < 0.05$; *TWIST* 3.4-fold, $p < 0.001$, Fig.1F). Altogether, this demonstrates that EndMT occurs during the pathological vascular remodeling in the context of T2D.

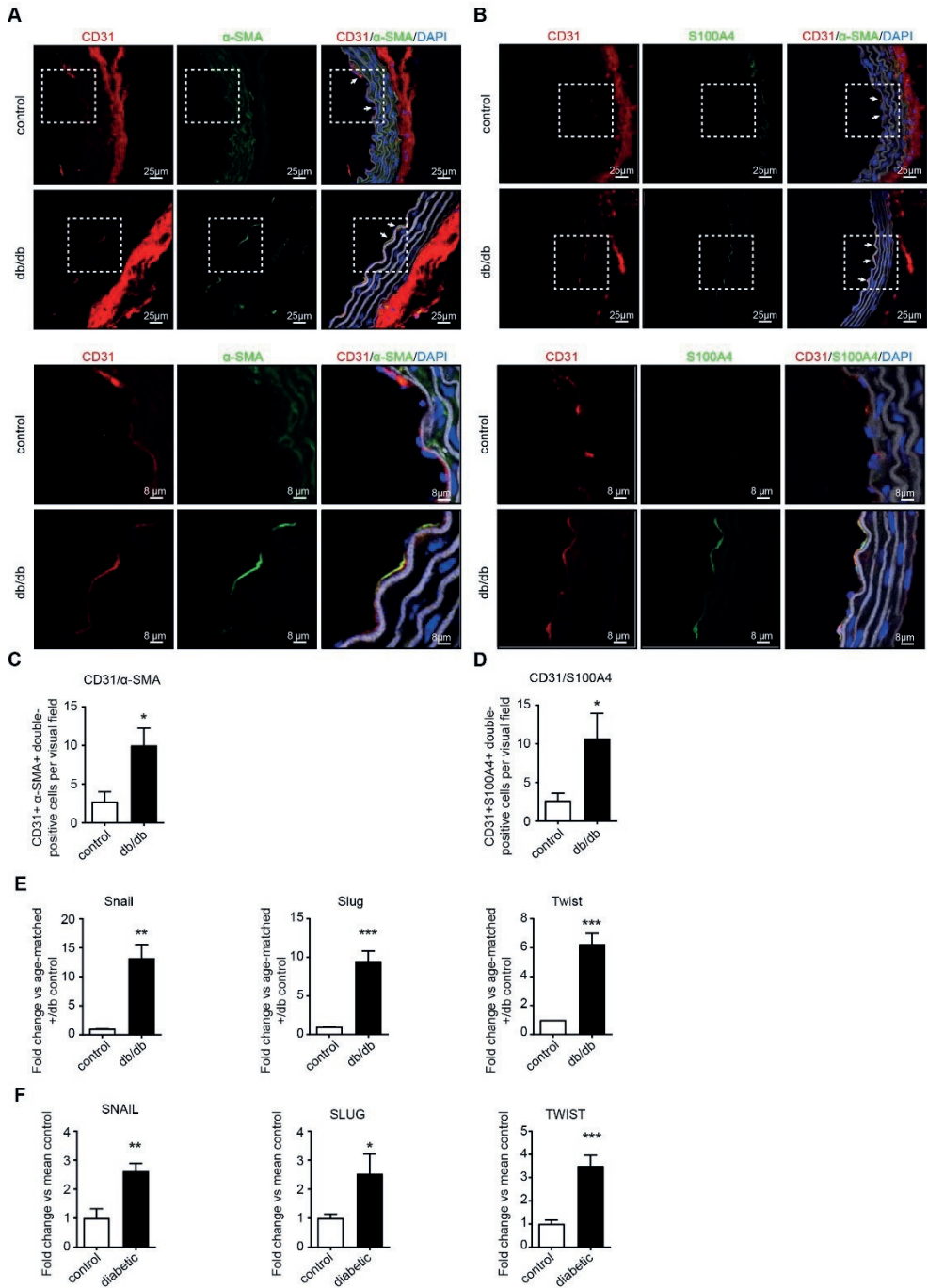


Figure 1. Endothelial-to-mesenchymal transition can be observed in aortas of db/db mice and diabetic patients.

(A) Representative images (upper panel) of co-immunofluorescent staining of CD31 (in red), α -SMA (in green) and DAPI (in blue). CD31 also stains the tunica adventitia. The elastic lamella is depicted in grey (autofluorescence). In the db/db aorta, co-localization between CD31 and α -SMA is visible at the endothelial layer (indicated by white arrows). Zoom-in (lower panel) of the tunica intima. CD31 marks the endothelial layer in the control aorta (without α -SMA expression). In the db/db aorta, robust co-localization between CD31 and α -SMA is present at the endothelial layer. (B) Representative images (upper panel) of control and db/db aortas which have been immunostained with CD31 (in red), S100a4 (in green) and DAPI (in blue). CD31 also stains the tunica adventitia. The elastic lamella depicted in grey (autofluorescence). Co-localization of CD31 and S100a4 is present in the db/db aorta (indicated by white arrows) and not in the control aorta. Zoom-in (lower panel) of the tunica intima. In the control aorta, CD31 marks the endothelial layer (without any S100a4 expression). Robust co-localization of CD31 and S100A4 is visible at the endothelial layer in the db/db aorta. (C) Quantification of co-localization of CD31 with α -SMA upon co-immunostaining in aortas from db/db mice vs age-matched control mice. The amount of co-localization of CD31 with α -SMA is significantly higher in aortas from db/db mice. (D) Quantification of co-localization of CD31 with S100A4 upon co-immunostaining in aortas from db/db mice vs age-matched control mice. The amount of co-localization of CD31 with S100A4 is significantly higher in aortas from db/db mice. (E) qRT-PCR analysis of the EndMT transcription factors *Snail*, *Slug* and *Twist* in db/db aortas vs aortas from age-matched control mice (n=4). *Snail*, *Slug* and *Twist* are significantly upregulated in aortic tissue from db/db mice. (F) qRT-PCR analysis of the EndMT transcription factors *SNAIL*, *SLUG* and *TWIST* in aortic tissue of diabetes patients vs control subjects (n=7). *SNAIL*, *SLUG* and *TWIST* are significantly upregulated in aortic tissue of diabetic patients. The data is presented as mean value; error bars represent S.E.M; *, $p < 0.05$; **, $p < 0.01$; ***, $p < 0.001$.

MIR-132-3P IS DOWNREGULATED IN AORTAS OF DB/DB MICE AND DIABETIC PATIENTS AS WELL AS IN HIGH GLUCOSE-INDUCED ENDMT IN VITRO

To identify the underlying mechanism by which EndMT is regulated in the context of T2D, we overlapped the microRNA-signature of vascular smooth muscle cells from aortas of db/db mice with the microRNA-signature of high glucose-treated human umbilical vein endothelial cells (HUVECs) (available at Gene Expression Omnibus (GEO), NCBI, GSE74296 [27] and GSE74521 [28]). Three microRNAs (miRs) were significantly downregulated in both datasets: miR-9, miR-30 and miR-132-3p (Fig.2A). Since miR-132-3p was the highest downregulated in glucose-treated HUVECs and the second highest downregulated in aortas of db/db mice, we decided to further examine the expression of this miR in aortic tissue of T2D patients. Indeed, we observed a significant downregulation of miR-

132-3p in aortic sections of T2D patients when compared to control subjects (2.4-fold, $p < 0.05$, Fig.2B). Since miR-132-3p is universally downregulated in high glucose-treated HUVECs and in aortic tissue of db/db mice and diabetic patients, we identified miR-132-3p as possible regulator of aortic stiffening-associated EndMT in T2D.

MIR-132-3P PREDICTED TARGET KLF7 IS UPREGULATED IN AORTAS OF DIABETIC PATIENTS

We identified possible targets of miR-132-3p in humans through the online prediction tool TargetScan [29]. This revealed two well-known EndMT regulators: SMAD2, which facilitates TGF- β signaling, and ZEB2, a transcription factor regulating epithelial to mesenchymal transition (EMT) (Fig.2C). SMAD2 mRNA expression was unaltered in aortas of T2D patients when compared to control subjects whereas ZEB2 was significantly downregulated (SMAD2 not significant; ZEB2, 4.1-fold, $p < 0.05$, Fig.2D). This suggests that these two predicted targets of miR-132-3p do not play a role in this context. We next examined the mRNA expression of those predicted miR-132-3p targets with the most putative binding sites for miR-132-3p in their 3'UTR: KLF7, PTEN, DNMT3a and ZBTB20 (Fig.2C). Out of these four predicted targets, only the expression of KLF7 was increased in aortas of diabetes patients whereas DNMT3a, ZBTB20 and PTEN remain unaltered when compared to control subjects (KLF7 2.2-fold, $p < 0.01$; DNMT3/ZBTB20/PTEN not significant, Fig.2E). This suggests that miR-132-3p targets KLF7 during aortic stiffening in diabetic patients.

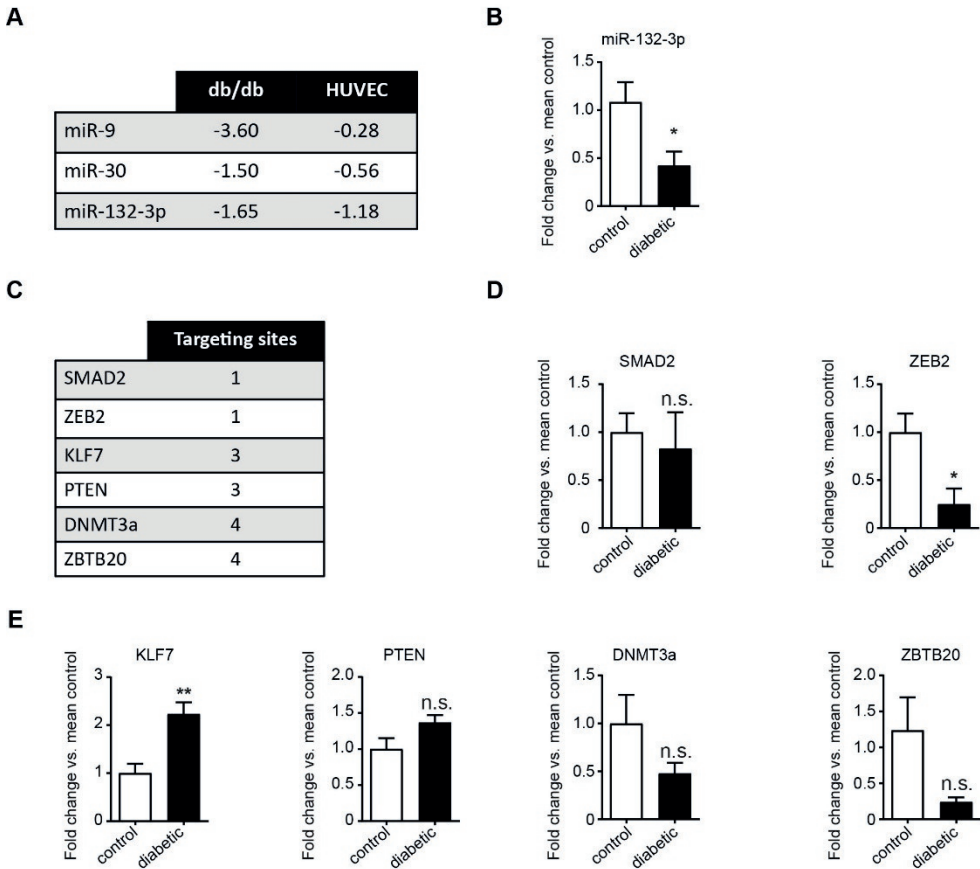


Figure 2. miR-132-3p is downregulated whereas KLF7 is upregulated in aortas of diabetic patients. (A) Overview of miRs that are downregulated in both the micronome of aortas from db/db mice and glucose-treated human umbilical vein endothelial cells (HUVECs). The values represent LogFC. (B) qRT-PCR analysis of miR-132-3p expression in aortic tissue from diabetic patients vs control subjects (n=7). miR-132-3p is downregulated in aortic tissue from diabetic patients. (C) Overview of the predicted targets of miR-132-3p with the corresponding predicted targeting sites. (D) qRT-PCR analysis of SMAD2 and ZEB2 expression in diabetic patients vs control subjects (n=7). SMAD2 remains unchanged and ZEB2 is downregulated in aortic tissue from diabetic patients. (E) qRT-PCR analysis of KLF7, PTEN, DNMT3a and ZBTB20 in aortic tissue from diabetic patients vs control subjects (n=7). KLF7 is upregulated in aortic tissue from diabetic patients whereas PTEN, DNMT3a and ZBTB20 remain unchanged. All data is presented as mean value; error bars represent S.E.M.; n.s., not significant; *, $p < 0.05$; **, $p < 0.01$.

MIR-132-3P TARGETS KLF7 WHICH IS UPREGULATED DURING HIGH GLUCOSE-INDUCED ENDMT AND AORTIC STIFFENING-ASSOCIATED ENDMT IN DB/DB MICE

We performed co-immunofluorescent staining of CD31 in combination with KLF7 in aortic sections of db/db mice. With confocal microscopy, we observed a robust co-localization of CD31 with KLF7 in aortas of db/db mice which was almost absent in control mice (Fig.3A). The observed co-localization of CD31 with KLF7 was more robust in aortas of db/db mice when compared to aortas of control mice (4.2-fold, $p < 0.05$, Fig.3B). Finally, we examined the mRNA expression of KLF7 in aortic tissue of db/db mice. We also observed an increase of KLF7 expression in aortas of db/db mice when compared to control mice (4.9-fold, $p < 0.001$, Fig. 3C). This suggests that KLF7 plays a role in aortic stiffness-associated EndMT in T2D.

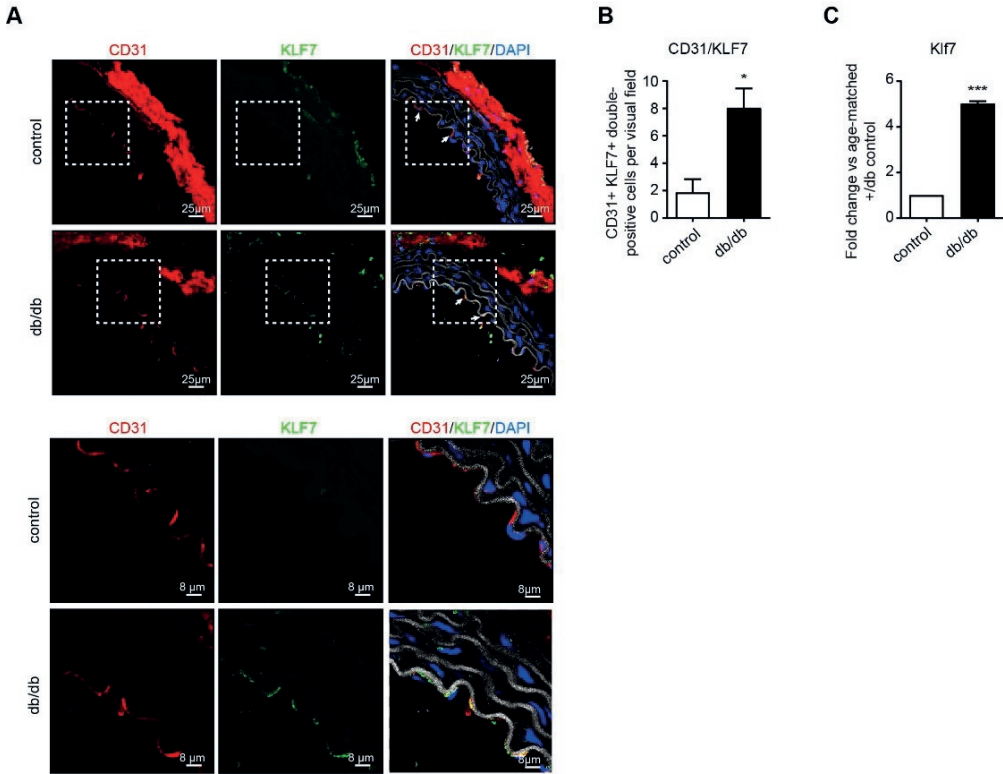


Figure 3. KLF7 is upregulated during EndMT-triggered aortic stiffening in db/db mice.

(A) Representative images (upper panel) of co-immunofluorescent staining of CD31 (in red), KLF7 (in green) and DAPI (in blue). The elastic lamella is depicted in grey (autofluorescence). In the db/db aorta, co-localization between CD31 and KLF7 is visible at the endothelial layer (indicated by white arrows). Zoom-in (lower panel) of the tunica intima. CD31 marks the endothelial layer in the control aorta (without KLF7 expression). In the db/db aorta, robust co-localization between CD31 and KLF7 is present at the endothelial layer. (B) Quantification of co-localization of CD31 with KLF7 upon co-immunostaining in aortas from db/db mice vs age-matched control mice. The amount of co-localization of CD31 with KLF7 is significantly higher in aortas from db/db mice. (C) qRT-PCR analysis of KLF7 in aortas of db/db mice (n=4) vs control. KLF7 is upregulated in aortic tissue of db/db mice. The data is presented as mean value; error bars represent S.E.M; *, $p < 0.05$; ***, $p < 0.001$.

We cloned a fragment of the human 3'UTR of KLF7 in a pMiR-REPORT luciferase vector and transfected HEK293 cells with both the pMiR-REPORT-KLF7-3'UTR and a miR-132-3p mimic or negative control (Fig.4A). We show that co-transfection with the miR-132-3p mimic results in a significant reduction of the luciferase activity of the KLF7 3'UTR when compared to the negative control, demonstrating that miR-132-3p indeed targets KLF7 (1.6-fold, $p < 0.01$, Fig.4B).

To confirm that KLF7 plays a role during EndMT in aortic stiffness, our aim was to also examine the KLF7 expression upon high glucose-induced EndMT. Therefore, we treated HUVECs with high glucose for 4 days to induce EndMT. Co-immunostaining of CD31 in combination with either α -SMA or S100A4 showed that high glucose treatment results in a decrease in the expression of CD31 and cobblestone morphology and an increase in both the α -SMA and S100A4 expression accompanied with a spindle-shaped morphology, all indicative of EndMT (Fig.4C). Moreover, qRT-PCR analysis revealed upregulation of SNAIL, SLUG and TWIST upon high glucose treatment, confirming the presence of EndMT (SNAIL 2.9-fold, $p < 0.01$; SLUG 5.4-fold, $p < 0.05$; TWIST 15.4-fold, $p < 0.001$, Fig.4D). We then demonstrated that KLF7 is significantly upregulated during high glucose-induced EndMT (2.5-fold, $p < 0.01$, Fig.4E). Altogether, this suggests that miR-132-3p regulates KLF7 in aortic stiffening-associated EndMT in T2D (Fig.5).

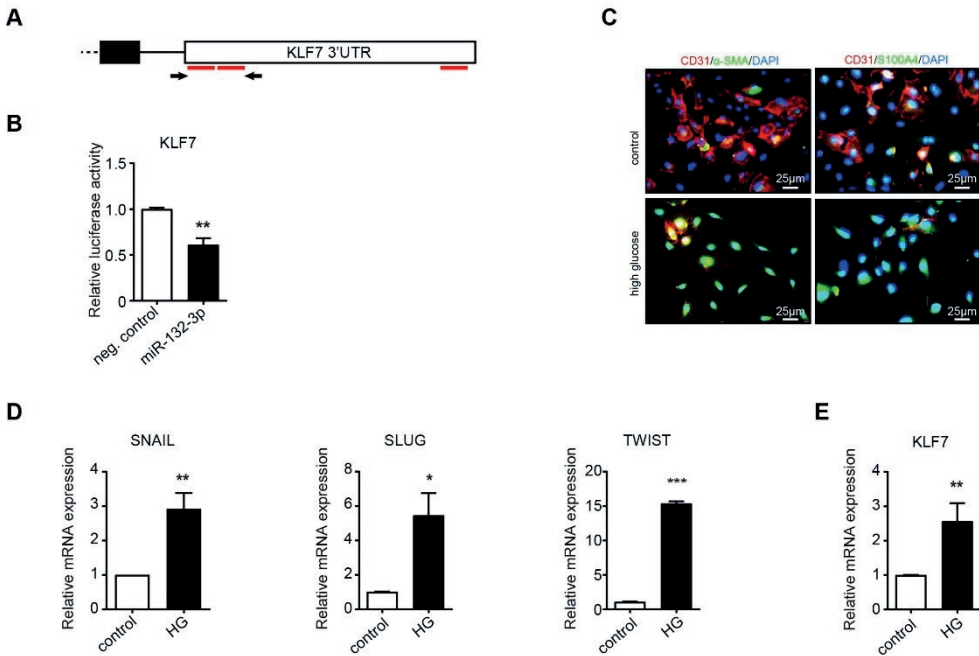


Figure 4. miR-132-3p targets KLF7 which is upregulated during high glucose-induced EndMT.

(A) Schematic demonstrating the 3'UTR of KLF7 where the predicted miR-132-3p target sites are depicted in red. The arrows represent the primers that were used to clone pMiR-REPORT-KLF7-3'UTR. (B) Luciferase assay of HEK293 cells transfected with pMiR-REPORT-KLF7-3'UTR in combination with a pGL4.73[hRLuc/SV40] (renilla) vector with either a miR-132-3p mimic or negative control. The relative luciferase activity of the KLF7 3'UTR is downregulated upon co-transfection with the miR-132-3p mimic. (C) Co-immunostaining of CD31 with either α -SMA or S100A4 in high glucose-treated human umbilical vein endothelial cells (HUVECs) vs control. High glucose treatment results in loss of CD31 and cobblestone morphology and gain of α -SMA and S100A4 accompanied by a spindle-shaped morphology. (D) qRT-PCR analysis of the EndMT transcription factors SNAIL, SLUG and TWIST in high glucose (HG)-treated HUVECs vs control. SNAIL, SLUG and TWIST are significantly upregulated in high glucose-treated HUVECs. (E) qRT-PCR analysis of KLF7 in high glucose-treated (60 mM) HUVECs vs control. KLF7 is upregulated in high glucose-treated HUVECs. The data is presented as mean value; error bars represent S.E.M.; n=4 independent biological replicates; *, $p < 0.05$; **, $p < 0.01$; ***, $p < 0.001$.

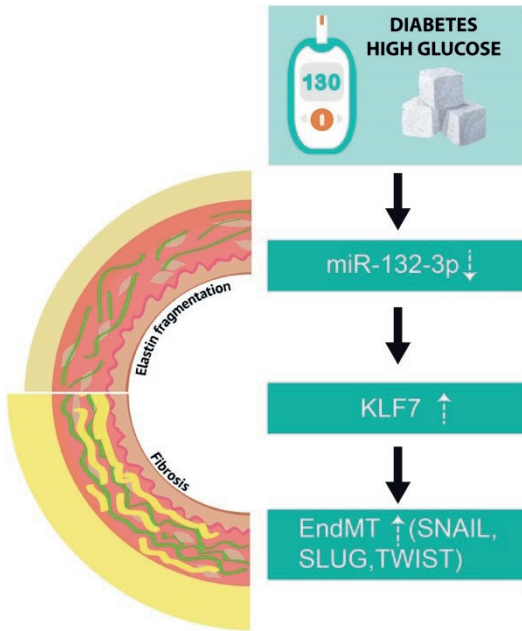


Figure 5. Proposed mechanism of aortic stiffening-related EndMT in T2D

Under diabetic or high glucose conditions, miR-132-3p is downregulated which activates the expression of its target KLF7. KLF7 is upregulated in aortas of both diabetic patients and an *in vivo* model of diabetes, as well as in high glucose-treated endothelial cells undergoing EndMT. Moreover, KLF7 co-localizes with the endothelial marker CD31 in diabetic mice, which suggests its contribution to aortic stiffening-related EndMT in T2D.

DISCUSSION

In this study, we demonstrate that aortas of db/db mice (a murine model of type 2 diabetes) and diabetes patients but not of control mice and subjects display robust signs of EndMT. We identified that miR-132-3p is downregulated in aortas of both db/db mice and diabetic patients as well as in an *in vitro* model of glucose-induced EndMT. Moreover, we demonstrate that miR-132-3p targets KLF7 which is upregulated in an *in vitro* model of diabetes-associated EndMT, during aortic stiffening-associated EndMT in db/db mice as well as in aortas of diabetes patients. A summary of the proposed mechanism is provided in Fig.5.

Cardiovascular disease and mortality in diabetes patients can be predicted by accelerated aortic stiffening. Previously, we observed aortic stiffness before hypertension in db/db mice, which makes aortic stiffness an early contributor to cardiovascular disease development [7]. We now show that EndMT occurs during aortic stiffening in T2D. This is consistent with the literature in which high glucose-induced EndMT has been demonstrated *in vitro* before [30,31], and has also been reported to be associated with diabetic cardiomyopathy [32-35].

We are aware that the observed decreased expression of miR-132-3p and increased expression of its target KLF7 in aortas of diabetic mice and patients can be contributed not only by endothelial cells but also by vascular smooth muscle cells. We therefore demonstrate in an *in vitro* model of glucose-induced EndMT that the expression levels of miR-132-3p and KLF7 are decreased and increased respectively, which indicates the role of these regulators in endothelial cells. We also demonstrate robust co-localization of KLF7 with CD31 in aortas of db/db mice, further highlighting the involvement of KLF7 in EndMT.

MicroRNAs have been shown to regulate EndMT in the context of diabetes [20,36,37]. We are the first to identify miR-132-3p as a possible regulator of EndMT and its association with both cardiovascular disease and T2D. Other studies have shown that the decrease of miR-132-3p promotes migration and proliferation in the context of carcinoma, which suggests a role for miR-132-3p in epithelial-to-mesenchymal transition, a cellular transition process similar to EndMT [38-42].

We demonstrate that miR-132-3p regulates KLF7 and thereby identify KLF7 as a novel potential regulator of EndMT. KLF7 is a member of the KLF family of zinc finger transcription factors which are known to play important role in

development and cellular differentiation processes such as epithelial-to-mesenchymal transition [43-46]. Moreover, KLF7 has been identified as one of the core transcription factors that regulate coronary artery disease-associated pathways [47]. This supports our data, as it has been shown that EndMT drives the progression of coronary artery disease [14,48]. This suggests that KLF7 might be an important player in arterial stiffness-associated EndMT in T2D.

To conclude, we demonstrate that EndMT occurs during aortic stiffening in T2D. We also identified miR-132-3p and KLF7 as novel potential regulators of EndMT in this context. Altogether, this provides new insights in the development of aortic stiffening in T2D.

HIGHLIGHTS

- Aortas of db/db mice (a murine model of type 2 diabetes) and diabetes patients but not of control mice and subjects display robust signs of endothelial-to-mesenchymal transition.
- miR-132-3p is downregulated in aortas of both diabetic patients and db/db mice, as well as in an *in vitro* model of diabetes-associated EndMT.
- miR-132-3p targets KLF7 which is upregulated in aortas from both diabetes patients and db/db mice as well as in an *in vitro* model of glucose-induced EndMT.

DISCLOSURES

I.N.S. and U.R. are cofounders of Angiolutions UG. Angiolutions UG is an academic spin-off company developing vascular devices for aneurysm diseases.

MATERIALS AND METHODS

IMMUNOFLUORESCENT STAINING OF AORTIC SECTIONS OF DB/DB MICE

Male db/db mice (BKS.Cg-Dock7m +/-Leprdb/J) and their age-matched heterozygous non-diabetic controls (+/db) were purchased from the Jackson Laboratory (Bar Harbor, ME, USA). Mice were sacrificed after 20 weeks and thoracic aortas were harvested and snap-frozen in liquid nitrogen. The cryosections were fixed with methanol at -20°C for 10 minutes and air-dried before washing three times with PBS. The sections were blocked using SEA BLOCK Blocking Buffer (Thermo Fisher Scientific, Waltham, MA, USA) and incubated at RT for 1.5 hour. The primary antibody was added to the sections and incubated at 4°C overnight. The next day, the slides were three times washed with PBS before adding the secondary antibody and incubating in the dark at RT for 45 minutes. The slides were three times washed with PBS, incubated with DAPI (1:1000 in PBS) at RT for 5 minutes. A final washing with PBS was performed before mounting the slides. The following primary antibodies and dilutions (in SEA BLOCK) were used: mouse anti-human CD31 (1:100, M0823, Dako, Carpinteria, CA, USA), rabbit anti-human S100A4 (1:50, A5114, Dako, Carpinteria, CA, USA), rabbit anti-mouse α -SMA (1:100, ab5694, Abcam, Cambridge, MA, USA) and rabbit anti-KLF7 (1:50, ab197690, Abcam, Cambridge, MA, USA). The secondary antibodies Alexa Fluor 647 goat-anti mouse (A21235, Invitrogen, Carlsbad, CA, USA) and Alexa Fluor 568 donkey anti-rabbit (A10042, Invitrogen, Carlsbad, CA, USA) were used in a 1:200 dilution. The stained slides were analysed using the Inverted Zeiss LSM 780 multiphoton laser scanning confocal microscope (Zeiss, Oberkochen, Germany).

HUMAN TISSUE SAMPLE ACQUISITION

Human aortic samples from patients who underwent replacement of the ascending aorta were collected as discarded material during surgery, snap-frozen and stored at - 80 °C. Approval for studies on human tissue samples was obtained under informed consent and conducted in accordance with the Declaration of Helsinki.

RNA EXTRACTION AND QUANTITATIVE REAL-TIME PCR

Total RNA was extracted using TRIzol Reagent (Invitrogen, Carlsbad, CA, USA) and the PureLink RNA Mini Kit (Invitrogen, Carlsbad, CA, USA) according to the manufacturer's protocol. The RNA was treated with Dnase I (Sigma-Aldrich, St. Louis, MO, USA) and the SuperScript II Reverse Transcriptase system (Invitrogen, Carlsbad, CA, USA) was used to synthesize cDNA according to the manufacturer's protocol. For qRT-PCR, Fast SYBR Green Master Mix (Applied Biosystems, Foster City, CA, USA) was used in combination with the StepOne Plus Real-Time PCR system (Applied Biosystems, Foster City, CA, USA). The primers used for qRT-PCR are listed in Table 1. The relative expression levels were standardized to GAPDH using the $\Delta\Delta C_t$ method.

Table 1. qRT-PCR primer sequences

Human		Mouse	
Name	Sequence	Name	Sequence
GAPDH	F: GTGGACCTGACCTGCCGTCT R: GGAGGAGTGGGTGTCGCTGT	GAPDH	F: TGTAGACCATGTAGTTGAGGTCA R: AGGTCGGTGTGAACGGATTGG
SNAIL	F: GGCAATTTAACAATGTCTGAAAAGG R: GAATAGTTCTGGGAGACACATCG	SNAIL	F: GTGCCACCTCCAAACCC R: AAGGACATGCGGGAGAAGG
SLUG	F: ACTCCGAAGCCAAATGACAA R: CTCTCTCTGTGGGTGTGTGT	SLUG	F: CGTCTCTTCTGGTCAAGA R: AGGTATAGGGTAACTTTCATAGAGATA
TWIST	F: CTCAAGAGGTCGTGCCAATC R: CCCAGTATTTTTATTTCTAAAGGTGTT	TWIST	F: TGATAGAAGTCTGAACACTCGTTTG R: GGCTGATTGGCAAGACTCT
SMAD2	F: GGGTTTTGAAGCCGTCTATCAGC R: CCAACCACTGTAGAGGTCCATTC	KLF7	F: GGAAGGATGCGAGTGGCGTTTT R: CGCAAGATGGTCAGACCTGGAG
ZEB2	F: AATGCACAGAGTGTGGCAAGGC R: CTGCTGATGTGCGAACTGTAGG		
KLF7	F: CTCACGAGGCACTACAGGAAAC R: TGGCAACTCTGGCCTTTCGGTT		
PTEN	F: TGAGTTCCTCAGCCGTTACCT R: GAGGTTTCCTCTGGTCCTGGTA		
ZBTB20	F: CTCTGCAACAAGACTTTCACCGC R: AGGAGAAGGAGCGCCAACAGAT		
DNMT3a	F: CCTCTTCGTGGAGGAATGTGC R: GTTCCGCACATGAGCACCTCA		

MICRONOME DATA

The micronome of glucose-treated HUVECs and the micronome of aortic vascular smooth muscle cells from db/db mice and db/+ controls are available at Gene Expression Omnibus (GEO), NCBI (GSE74296 [27] and GSE7452 [28]).

RNA QUANTIFICATION AND QRT-PCR MIR-132-3P IN HUMAN SUBJECTS

Total microRNA was isolated using a TRIzol-based (Invitrogen) RNA isolation protocol. Reverse transcription was performed by using the TaqMan microRNA Reverse Transcription kit (Applied Biosystems) according to the manufacturer's instructions. MicroRNA TaqMan assays (Applied Biosystems) for hsa-miR-132-3p was used. Amplification took place on a Fast-Real-Time PCR System (Applied Biosystems, Foster City, USA). All fold changes were calculated by the method of $\Delta\Delta Ct$.

CLONING

A fragment of the human 3'UTR of KLF7 which contains two miR-132-3p binding sites was amplified using Phusion High-Fidelity DNA Polymerase (New England Biolabs, Ipswich, MA, USA) and the primers KLF7-3'UTR -F: 5' AATTACTAGTACCATCCCTTCAAGACACGT; KLF7- 3'UTR-R: 5' AATTGTTTAAACCCAGATCTTGAAGGTTGCTG. Both the amplified PCR product and the pMiR-REPORT miRNA expression vector (Invitrogen, Carlsbad, CA, USA) were digested using SpeI and PmeI restriction enzymes (New England Biolabs, Ipswich, MA, USA). Ligation was performed using the LigaFast Rapid DNA Ligation System (Promega, Madison, WI, USA) and transformed into One Shot TOP10 Chemically Competent E. coli (Invitrogen, Carlsbad, CA, USA). Miniprep was performed using the Zippy Plasmid Miniprep Kit and the sequence of the insert was confirmed using sequencing. The generated pMiR-REPORT-KLF7-3'UTR plasmid was amplified using the HiSpeed Plasmid Midi Kit (Qiagen, Hilden, Germany).

CELL CULTURE AND GLUCOSE TREATMENT

Human embryonic kidney (HEK293) cells were cultured in DMEM medium (Gibco, Carlsbad, CA, USA) supplemented with 10% fetal bovine serum (Gibco, Carlsbad, CA, USA) and 1% penicillin-streptomycin (Gibco, Carlsbad, CA, USA). Human umbilical vein endothelial cells (Lonza, Basel, Switzerland) were cultured in Endothelial Cell Growth Medium (EGM, Lonza, Basel, Switzerland). For glucose treatment, 50,000 cells were plated and cultured as previously described [49] to induce EndMT. 60mM D-glucose was supplemented for 4 days and the medium was changed every two days. 5.5mM D-glucose plus 54.5mM D-mannitol was used as control.

4

TRANSFECTION

0.5×10^6 HEK293 cells were plated on a 6-well plate and incubated overnight. The next day, the HEK293 cells were transfected by using Lipofectamine 2000 (Thermo Fisher Scientific, Waltham, MA, USA). In short, 2 μ g of pMiR-REPORT-KLF7-3'UTR and 1 μ g of pGL4.73[hRluc/SV40] (renilla) vector (Promega, Madison, WI, USA) together with 5nM of hsa-miR-132-3p miRCURY LNA miRNA mimic (#YM00472088, Qiagen, Hilden, Germany) or negative control miRCURY LNA miRNA mimic (#YM00479902, Qiagen, Hilden, Germany) was added in a tube containing 250 μ L Opti-MEM Reduced Serum Medium (Gibco, Carlsbad, CA, USA). Another tube was prepared containing a mastermix of 250 μ L Opti-MEM and 5 μ L of Lipofectamine 2000 per transfection. The tubes were mixed at RT for 5 minutes before combining the Lipofectamine 2000 mixture with the DNA mixture. The tubes were mixed again before incubating at RT for 20 minutes. The transfection complexes were added drop-wise to the cells and incubated overnight. The next day, the medium was changed. The cells were collected 72h after transfection.

LUCIFERASE REPORTER ASSAY

The luciferase assay was performed using the Dual-Luciferase Reporter Assay System (Promega, Madison, WI, USA). In short, the cells were lysed with 1:5 diluted passive lysis buffer by shaking at RT for 30 minutes. Centrifugation at

13000 rpm for 10 minutes was performed to collect the supernatant (containing the cell lysate). The cell lysate was added in triplicates to a 96 well plate before adding Luciferase Assay Reagent II (for Firefly luciferase activity) and Sto&Glo Reagent (for Renilla luciferase activity) to detect the luminescence with the help of a luminescence plate reader.

IMMUNOFLUORESCENT STAINING OF CELLS

The cells were two times washed with PBS before being fixed with 4% PFA at RT for 30 minutes. The cells were again two times washed with PBS and incubated with 50mM NH₄Cl at 37°C for 10 minutes. After another two washes with PBS, the cells were three times washed with 0.2% Triton in PBS before incubating with the primary antibody (1:100 in 0.2% Triton in PBS) at RT for 1h. After another three washes with 0.2% Triton in PBS, the secondary antibody was added (1:100 in 0.2% Triton in PBS) and incubated in the dark at RT for 1h. The cells were washed three times with 0.2% Triton in PBS and two times washed with PBS before incubating with DAPI (1:1000 in PBS) at RT for 5 minutes. Imm-mount was added before covering the cells with a coverslip. The following primary antibodies were used: mouse anti-human CD31 (Dako, #M0823), rabbit anti-human S100A4 (Dako, #A5114), rabbit anti-mouse α -SMA (Abcam, #ab5694). Alexa Fluor 488 donkey anti-mouse (A212302, Invitrogen, Carlsbad, CA, USA) and Alexa Fluor 568 donkey anti-rabbit (A10042, Invitrogen, Carlsbad, CA, USA) were used as secondary antibodies.

STATISTICS

The data is presented as the mean \pm SEM. Co-localization was assessed with 3 aortic sections per mouse and average values of each mouse were calculated. The average values for each mouse (n=4) was then used to calculate average per group. Statistical analysis was performed using a Student's t test (two-tailed). A p value <0.05 was considered statistically significant.

REFERENCES

1. Centers for Disease Control and Prevention. National Diabetes Statistics Report, 2014. Atlanta, GA: Centers for Disease Control and Prevention, US department of Health and Human Services, 2014.
2. Ryden L, Standl E, Bartnik M et al. Guidelines on diabetes, pre-diabetes, and cardiovascular diseases: Executive summary. The task force on diabetes and cardiovascular diseases of the european society of cardiology (esc) and of the european association for the study of diabetes (easd). *European heart journal*. 2007;28:88-136
3. Stehouwer CD, Henry RM, Ferreira I. Arterial stiffness in diabetes and the metabolic syndrome: A pathway to cardiovascular disease. *Diabetologia*. 2008;51:527-539
4. Lyle AN, Raaz U. Killing me unsoftly: Causes and mechanisms of arterial stiffness. *Arteriosclerosis, thrombosis, and vascular biology*. 2017;37:e1-e11
5. Raaz U, Zollner AM, Schellinger IN et al. Segmental aortic stiffening contributes to experimental abdominal aortic aneurysm development. *Circulation*. 2015;131:1783-1795
6. Schram MT, Henry RM, van Dijk RA, Kostense PJ, Dekker JM, Nijpels G, Heine RJ, Bouter LM, Westerhof N, Stehouwer CD. Increased central artery stiffness in impaired glucose metabolism and type 2 diabetes: The hoorn study. *Hypertension*. 2004;43:176-181
7. Raaz U, Schellinger IN, Chernogubova E et al. Transcription factor runx2 promotes aortic fibrosis and stiffness in type 2 diabetes mellitus. *Circulation research*. 2015;117:513-524
8. Wellen KE, Hotamisligil GS. Inflammation, stress, and diabetes. *The Journal of clinical investigation*. 2005;115:1111-1119
9. Cao Y, Feng B, Chen S, Chu Y, Chakrabarti S. Mechanisms of endothelial to mesenchymal transition in the retina in diabetes. *Investigative ophthalmology & visual science*. 2014;55:7321-7331
10. Kaur H, Chen S, Xin X, Chiu J, Khan ZA, Chakrabarti S. Diabetes-induced extracellular matrix protein expression is mediated by transcription coactivator p300. *Diabetes*. 2006;55:3104-3111
11. Khan ZA, Cukiernik M, Gonder JR, Chakrabarti S. Oncofetal fibronectin in diabetic retinopathy. *Investigative ophthalmology & visual science*. 2004;45:287-295
12. Vanchin B, Offringa E, Friedrich J, Brinker MG, Kiers B, Pereira AC, Harmsen MC, Moonen JA, Krenning G. MicroRNA-374b induces endothelial-to-mesenchymal transition and early lesion formation through the inhibition of mapk7 signaling. *The Journal of pathology*. 2019;247:456-470
13. Evrard SM, Lecce L, Michelis KC et al. Endothelial to mesenchymal transition is common in atherosclerotic lesions and is associated with plaque instability. *Nature communications*. 2016;7:11853
14. Chen PY, Qin L, Baeyens N, Li G, Afolabi T, Budatha M, Tellides G, Schwartz MA, Simons M. Endothelial-to-mesenchymal transition drives atherosclerosis progression. *The Journal of clinical investigation*. 2015;125:4514-4528
15. Mahmoud MM, Serbanovic-Canic J, Feng S, Souilhol C, Xing R, Hsiao S, Mammoto A, Chen J, Ariaans M, Francis SE, Van der Heiden K, Ridger V, Evans PC. Shear stress induces

- endothelial-to-mesenchymal transition via the transcription factor snail. *Scientific reports*. 2017;7:3375
16. Rieder F, Kessler SP, West GA, Bhilocha S, de la Motte C, Sadler TM, Gopalan B, Stylianou E, Fiocchi C. Inflammation-induced endothelial-to-mesenchymal transition: A novel mechanism of intestinal fibrosis. *The American journal of pathology*. 2011;179:2660-2673
 17. Zeisberg EM, Potenta SE, Sugimoto H, Zeisberg M, Kalluri R. Fibroblasts in kidney fibrosis emerge via endothelial-to-mesenchymal transition. *Journal of the American Society of Nephrology : JASN*. 2008;19:2282-2287
 18. Zeisberg EM, Tarnavski O, Zeisberg M, Dorfman AL, McMullen JR, Gustafsson E, Chandraker A, Yuan X, Pu WT, Roberts AB, Neilson EG, Sayegh MH, Izumo S, Kalluri R. Endothelial-to-mesenchymal transition contributes to cardiac fibrosis. *Nature medicine*. 2007;13:952-961
 19. Correia AC, Moonen JR, Brinker MG, Krenning G. Fgf2 inhibits endothelial-mesenchymal transition through microRNA-20a-mediated repression of canonical tgf-beta signaling. *Journal of cell science*. 2016;129:569-579
 20. Feng B, Cao Y, Chen S, Chu X, Chu Y, Chakrabarti S. Mir-200b mediates endothelial-to-mesenchymal transition in diabetic cardiomyopathy. *Diabetes*. 2016;65:768-779
 21. Kumarswamy R, Volkman I, Jazbutyte V, Dangwal S, Park DH, Thum T. Transforming growth factor-beta-induced endothelial-to-mesenchymal transition is partly mediated by microRNA-21. *Arteriosclerosis, thrombosis, and vascular biology*. 2012;32:361-369
 22. Chen PY, Qin L, Barnes C, Charisse K, Yi T, Zhang X, Ali R, Medina PP, Yu J, Slack FJ, Anderson DG, Kotelianski V, Wang F, Tellides G, Simons M. Fgf regulates tgf-beta signaling and endothelial-to-mesenchymal transition via control of let-7 mirna expression. *Cell reports*. 2012;2:1684-1696
 23. Pillai RS, Bhattacharyya SN, Filipowicz W. Repression of protein synthesis by mirnas: How many mechanisms? *Trends in cell biology*. 2007;17:118-126
 24. Betel D, Wilson M, Gabow A, Marks DS, Sander C. The microRNA.Org resource: Targets and expression. *Nucleic acids research*. 2008;36:D149-153
 25. Grimson A, Farh KK, Johnston WK, Garrett-Engele P, Lim LP, Bartel DP. MicroRNA targeting specificity in mammals: Determinants beyond seed pairing. *Molecular cell*. 2007;27:91-105
 26. Krek A, Grun D, Poy MN, Wolf R, Rosenberg L, Epstein EJ, MacMenamin P, da Piedade I, Gunsalus KC, Stoffel M, Rajewsky N. Combinatorial microRNA target predictions. *Nature genetics*. 2005;37:495-500
 27. Silambarasan M, Tan JR, Karolina DS, Armugam A, Kaur C, Jeyaseelan K. MicroRNAs in hyperglycemia induced endothelial cell dysfunction. *International journal of molecular sciences*. 2016;17:518
 28. Reddy MA, Das S, Zhuo C, Jin W, Wang M, Lanting L, Natarajan R. Regulation of vascular smooth muscle cell dysfunction under diabetic conditions by mir-504. *Arteriosclerosis, thrombosis, and vascular biology*. 2016;36:864-873
 29. Agarwal V, Bell GW, Nam J, Bartel DP. Predicting effective microRNA target sites in mammalian mRNAs. *eLife*. 2015;4:e05005.

30. Tang R, Li Q, Lv L, Dai H, Zheng M, Ma K, Liu B. Angiotensin ii mediates the high-glucose-induced endothelial-to-mesenchymal transition in human aortic endothelial cells. *Cardiovascular diabetology*. 2010;9:31
31. Yu CH, Suriguga, Gong M, Liu WJ, Cui NX, Wang Y, Du X, Yi ZC. High glucose induced endothelial to mesenchymal transition in human umbilical vein endothelial cell. *Experimental and molecular pathology*. 2017;102:377-383
32. Chen XY, Lv RJ, Zhang W, Yan YG, Li P, Dong WQ, Liu X, Liang ES, Tian HL, Lu QH, Zhang MX. Inhibition of myocyte-specific enhancer factor 2a improved diabetic cardiac fibrosis partially by regulating endothelial-to-mesenchymal transition. *Oncotarget*. 2016;7:31053-31066
33. Liu X, Mujahid H, Rong B, Lu QH, Zhang W, Li P, Li N, Liang ES, Wang Q, Tang DQ, Li NL, Ji XP, Chen YG, Zhao YX, Zhang MX. Irisin inhibits high glucose-induced endothelial-to-mesenchymal transition and exerts a dose-dependent bidirectional effect on diabetic cardiomyopathy. *Journal of cellular and molecular medicine*. 2018;22:808-822
34. Tang RN, Lv LL, Zhang JD, Dai HY, Li Q, Zheng M, Ni J, Ma KL, Liu BC. Effects of angiotensin ii receptor blocker on myocardial endothelial-to-mesenchymal transition in diabetic rats. *International journal of cardiology*. 2013;162:92-99
35. Yan F, Zhang GH, Feng M, Zhang W, Zhang JN, Dong WQ, Zhang C, Zhang Y, Chen L, Zhang MX. Glucagon-like peptide 1 protects against hyperglycemic-induced endothelial-to-mesenchymal transition and improves myocardial dysfunction by suppressing poly(adp-ribose) polymerase 1 activity. *Molecular medicine*. 2015;21:15-25
36. Chen Y, Yang Q, Zhan Y, Ke J, Lv P, Huang J. The role of mir-328 in high glucose-induced endothelial-to-mesenchymal transition in human umbilical vein endothelial cells. *Life sciences*. 2018;207:110-116
37. Liu F, Zhang S, Xu R, Gao S, Yin J. Melatonin attenuates endothelial-to-mesenchymal transition of glomerular endothelial cells via regulating mir-497/rock in diabetic nephropathy. *Kidney & blood pressure research*. 2018;43:1425-1436
38. Guan H, Shang G, Cui Y, Liu J, Sun X, Cao W, Wang Y, Li Y. Long noncoding rna aprt contributes to osteosarcoma progression through repression of mir-132-3p and upregulation of yes-associated protein 1. *Journal of cellular physiology*. 2018
39. Li G, Liu K, Du X. Long non-coding rna tug1 promotes proliferation and inhibits apoptosis of osteosarcoma cells by sponging mir-132-3p and upregulating sox4 expression. *Yonsei medical journal*. 2018;59:226-235
40. Song H, He P, Shao T, Li Y, Li J, Zhang Y. Long non-coding rna xist functions as an oncogene in human colorectal cancer by targeting mir-132-3p. *Journal of B.U.ON. : official journal of the Balkan Union of Oncology*. 2017;22:696-703
41. Zhang M, Li Y, Wang H, Yu W, Lin S, Guo J. Lncrna snhg5 affects cell proliferation, metastasis and migration of colorectal cancer through regulating mir-132-3p/creb5. *Cancer biology & therapy*. 2018:1-13
42. Zhou X, Luo D, Sun H, Qi Y, Xu W, Jin X, Li C, Lin Z, Li G. Mir-132-3p regulates adamts-5 expression and promotes chondrogenic differentiation of rat mesenchymal stem cells. *Journal of cellular biochemistry*. 2018;119:2579-2587

CHAPTER 4

43. Bieker JJ. Kruppel-like factors: Three fingers in many pies. *The Journal of biological chemistry*. 2001;276:34355-34358
44. Black AR, Black JD, Azizkhan-Clifford J. Sp1 and kruppel-like factor family of transcription factors in cell growth regulation and cancer. *Journal of cellular physiology*. 2001;188:143-160
45. Ding X, Wang X, Gong Y, Ruan H, Sun Y, Yu Y. Klf7 overexpression in human oral squamous cell carcinoma promotes migration and epithelial-mesenchymal transition. *Oncology letters*. 2017;13:2281-2289
46. Zhao L, Zhang Y, Liu J, Yin W, Jin D, Wang D, Zhang W. Mir-185 inhibits cell proliferation and invasion of non-small cell lung cancer by targeting klf7. *Oncology research*. 2018
47. Vangala RK, Ravindran V, Ghatge M, Shanker J, Arvind P, Bindu H, Shekar M, Rao VS. Integrative bioinformatics analysis of genomic and proteomic approaches to understand the transcriptional regulatory program in coronary artery disease pathways. *PLoS one*. 2013;8:e57193
48. Moonen JR, Lee ES, Schmidt M, Maleszewska M, Koerts JA, Brouwer LA, van Kooten TG, van Luyn MJ, Zeebregts CJ, Krenning G, Harmsen MC. Endothelial-to-mesenchymal transition contributes to fibro-proliferative vascular disease and is modulated by fluid shear stress. *Cardiovascular research*. 2015;108:377-386
49. Neumann P, Jae N, Knau A, Glaser SF, Fouani Y, Rossbach O, Kruger M, John D, Bindereif A, Grote P, Boon RA, Dimmeler S. The lncRNA gata6-as epigenetically regulates endothelial gene expression via interaction with loxl2. *Nature communications*. 2018;9:237

CHAPTER

5

NON-CODING RNA IN ENDOTHELIAL-TO-MESENCHYMAL TRANSITION

Melanie S. Hulshoff^{1,2,3*}, Gonzalo del Monte-Nieto^{4,*}, Jason C. Kovacic⁵, Guido Krenning¹

¹*Department of Pathology and Medical Biology, University Medical Center Groningen, Hanzeplein 1, 9713 GZ, Groningen, The Netherlands.*

²*Department of Cardiology and Pneumology, University Medical Center of Göttingen, Georg-August University, Göttingen, Germany.*

³*German Centre for Cardiovascular Research (DZHK), Göttingen, Germany.*

⁴*Australian Regenerative Medicine Institute, Monash University, Victoria, Australia.*

⁵*Zena and Michael A. Wiener Cardiovascular Institute, Icahn School of Medicine at Mount Sinai, New York, New York.*

**Authors contributed equally*

ABSTRACT

Endothelial-to-mesenchymal transition (EndMT) is the process wherein endothelial cells lose their typical endothelial cell markers and functions and adopt a mesenchymal-like phenotype. EndMT is required for development of the cardiac valves, the pulmonary and dorsal aorta and arterial maturation, but activation of the EndMT program during adulthood is believed to contribute to several pathologies including organ fibrosis, cardiovascular disease and cancer. Non-coding RNAs, including microRNAs, long non-coding RNAs and circular RNAs, modulate EndMT during development and disease. Here, we review the mechanisms by which non-coding RNAs facilitate or inhibit EndMT during development and disease and provide a perspective on the therapeutic application of non-coding RNAs to treat fibroproliferative cardiovascular disease.

ENDMT DURING DEVELOPMENT AND PATHOLOGY

Endothelial cells form the inner layer of every single vessel in the body acting as a barrier between the blood or lymph and the rest of the tissues. Endothelial cells are highly plastic cells, that are able to differentiate into arterial, venous, lymphatic and endocardial cell fates during development, but also into hematopoietic lineages [1,2], or mesenchymal lineages through a process coined endothelial to mesenchymal transition (EndMT). During heart development, EndMT is essential for the formation of the valve mesenchyme [3,4]. These valvulogenic regions are located in the atrio-ventricular canal (AVC) and the outflow tract (OFT) of the developing heart and undergo differential specification programs compared to the cardiac chambers [5,6]. Besides the involvement of EndMT during valve development, EndMT is involved in embryonic pulmonary artery development [7] and in the formation of the smooth muscle component of the dorsal aorta (Figure 1) [8] Furthermore, just recently, a partial EndMT process has been suggested pivotal to physiological angiogenic sprouting (Figure 1) [9] This new concept may open new interpretations of vessel development, but also for heart development, where recent studies suggested a process similar to sprouting angiogenesis in the endocardium during ventricular trabeculation [10].

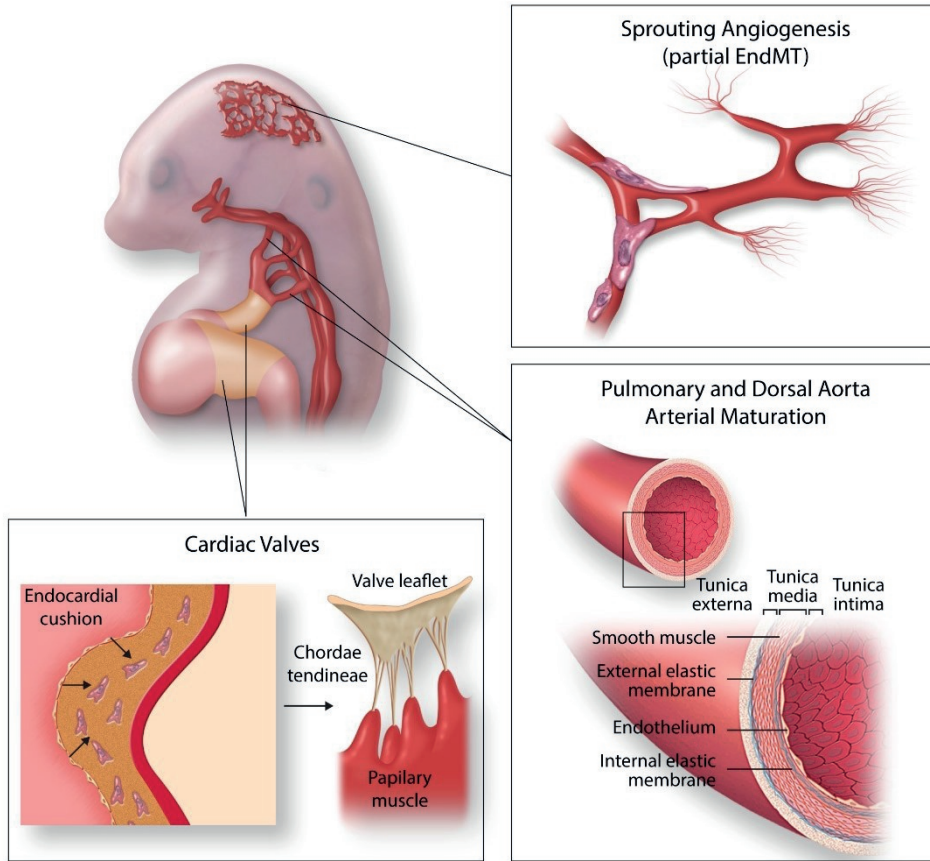


Figure 1. EndMT in development.

During embryonic development, EndMT contributes to the cardiac valves, pulmonary and dorsal aorta arterial maturation and sprouting angiogenesis (partial EndMT).

EndMT is a specific form of epithelial-to-mesenchymal transition (EMT) and the term was coined to refer specifically to the EMT affecting the endothelium, a squamous type of epithelium. The regulation of EndMT during normal developmental conditions shares many aspects with the general process of EMT, however the molecular defects promoting pathologic EndMT are less understood. EndMT is characterized by loss of endothelial markers such as VE-Cadherin and CD31, and upregulation of the EndMT transcription factors SNAIL, SLUG, TWIST, ZEB1 and ZEB2 as well as mesenchymal markers such as α -SMA (ACTA2) and S100A4. EndMT-derived mesenchymal cells acquire a highly migratory and invasive potential which is accompanied by morphological changes from a cobble-stone endothelial morphology into a spindle-shaped myofibroblast-like morphology. In recent years, the reactivation of EndMT during adult life has gained increasing attention in the cardiovascular field due to its implication in numerous adult pathologies including pulmonary hypertension [11], atherosclerosis [12,13], brain vascular malformations [14], tissue fibrosis [15-17] and cancer progression [18,19] (Figure 2). Under pathological conditions, several environmental factors induce EndMT, including high glucose, hypoxia, oxidative stress, pro-inflammatory cytokines and disturbed shear stress (the frictional force of the blood flow on the endothelial cells) [20-24]. These environmental factors trigger the activation of signaling pathways which induce EndMT such as the canonical Transforming Growth Factor Beta (TGF- β) pathway or the non-canonical pathways such as Notch and Wnt [13]. However, fibroblast growth factor (FGF) and Mitogen-activated Protein Kinase (MAPK) modulate EndMT as inhibitory pathways [25]. These signaling pathways are described in more detail below. The environmental factors and, thereby-induced signaling pathways, can also lead to the expression of non-coding RNAs, functional RNA molecules which are not translated into proteins. Non-coding RNAs include microRNAs (miRNAs), long non-coding RNAs (lncRNAs) and circular RNAs (circRNAs). These non-coding RNAs influence EndMT pathways during development and pathology [26]. In this review we summarize the current knowledge on the mechanisms by which non-coding RNAs regulate the EndMT process and outline their potential as therapeutic molecules to alleviate fibroproliferative diseases. Readers interested in further detail about the overall EndMT process, or its involvement during development or adult cardiovascular

diseases, are referred to other recent articles covering these aspects in depth [13, 27-29].

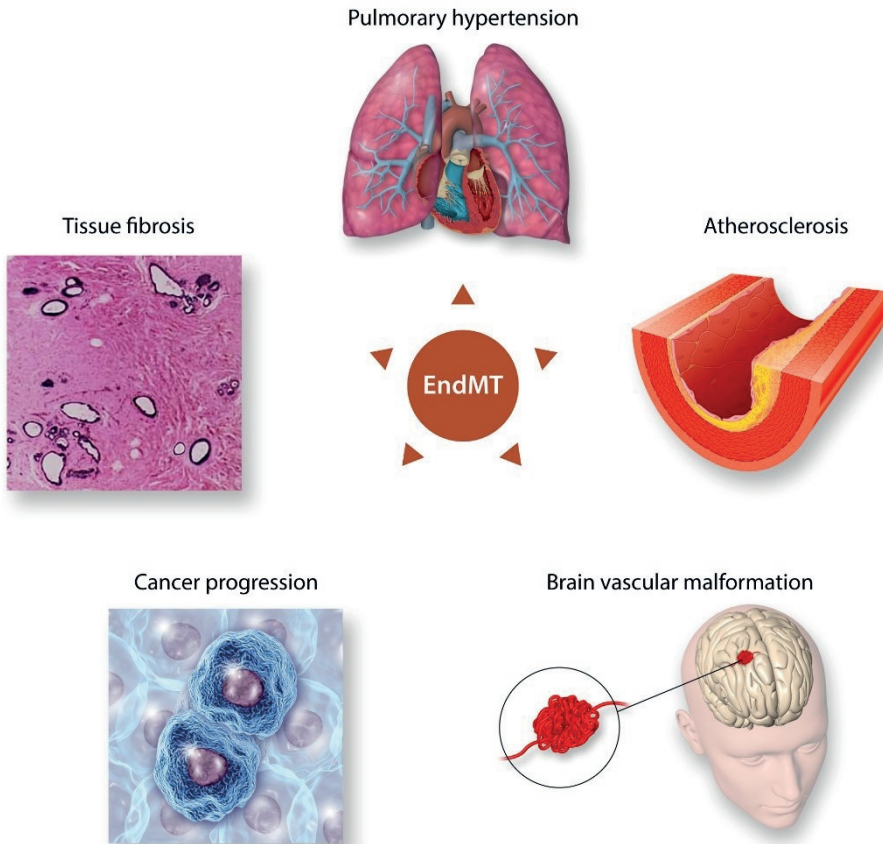


Figure 2. Pathological EndMT.

During adult life, reactivation of EndMT contributes to several pathologies such as pulmonary hypertension, atherosclerosis, brain vascular malformation, cancer progression and tissue fibrosis.

CANONICAL ENDMT PATHWAYS

THE TGF- β SIGNALING PATHWAY

When considering the molecular mechanisms controlling EndMT, the most simplistic overview is a finely regulated network integrating TGF- β , Bone Morphogenetic Proteins (BMPs) and the Notch signaling pathway (Figure 3) [30]. There are 3 ligands in the TGF- β family involved in EndMT; TGF- β 1, -2 and -3 [31]. TGF- β ligands signal through tetrameric receptors formed by two type II TGF- β receptors (TGF β R2) and two type I TGF- β receptors (ALK5 and ALK2). Once activated, they induce an intracellular signaling pathway mediated by SMAD2 and SMAD3, which then interact with SMAD4, and the entire SMAD complex translocates to the nucleus and binds DNA-associated proteins to promote the expression of mesenchymal genes. In endothelial cells, TGF- β ligands also induce the activation of the type I TGF- β receptor ALK1 which antagonizes EndMT by signaling through SMAD1, 5 and 8, allowing certain crosstalk between the TGF- β and BMP pathways. TGF- β signaling can also occur in a SMAD-independent manner by activating intracellular signaling pathways such as MAP kinase (MAPK), Rho-like GTPase, ERK1/2 or phosphatidylinositol-3-kinase (PI3K)/AKT pathways [32,33], all of which are inducers of EndMT.

TRANSCRIPTION FACTORS REGULATING ENDMT

TGF- β ligands have been described as master regulators of EndMT by promoting the expression of the transcription factors SNAIL, SLUG, TWIST, ZEB1 and ZEB2 [34]. Although all of them repress the transcription of VE-cadherin, they perform overlapping but non-redundant roles during EndMT. The transcription factors SNAIL and SLUG are pivotal to EndMT induction, whereas TWIST, ZEB1 and ZEB2 maintain the migratory phenotype [35]. Furthermore, these transcription factors cross-regulate each other and their own expression, highlighting the fine molecular regulation of EndMT [36-39]. Other transcription factors involved in the EndMT process include GATA4 and the ETS factors ERG and FLI1. Endothelial specific deletion of GATA4 culminates in reduced EndMT whereas the suppression of ERG or FLI1 expression enhances EndMT via

activation of the TGF- β pathway, in particular SMAD2/3 transcription factors [40, 41].

THE BMP SIGNALING PATHWAY

BMPs signal through four possible type I receptors (ALK1, ALK2, ALK3 and ALK6) and three type II receptors (BMPRII, ActRII or ActRIIB). During valve development, BMP2, 4, 5, 6, and 7 ligands are expressed in the valvulogenic regions. Receptor complex activation promotes intracellular signaling mediated by the SMAD1, 5 and 8, that together with SMAD4 promote the nuclear translocation of the SMAD complex and the activation of BMP-responsive genes. During development, BMPs play critical roles in the patterning the AVC/OFT myocardium to provide a pro-EndMT environment and promote the transition of endothelial cells into invasive mesenchymal cells. In particular, BMP2 and BMP4 are the two ligands described to be responsible for EndMT in the AVC and OFT [5,42,43]. It has to be noted that in contrast to its inducing role on EndMT during development, BMPs (in particular BMP7) have been described to inhibit pathological EndMT during adulthood [17, 44].

NON-CANONICAL ENDMT PATHWAYS

THE NOTCH SIGNALING PATHWAY

Notch is a cell-to-cell signaling pathway formed by 4 different receptors (Notch1-4). Notch is a key signal in the induction of EndMT during heart valve development. Notch promotes EndMT by inducing the expression of SNAIL and SLUG [45,46]. Notch1 and 2 mutant embryos show heart valve defects that arise due to defective EndMT [45]. The Notch pathway acts synergistically with the TGF- β 2 and BMP2 pathways in the control of EndMT [46, 47]. TGF- β 2 and BMP2 are able to induce SNAIL expression and to a weaker extent SLUG expression, whereas Notch activates SLUG and synergistically induces SNAIL in concert with TGF- β 2 and BMP2 [46, 47]. Furthermore, Notch controls the BMP2 expression pattern in the AVC myocardium [47].

THE WNT SIGNALING PATHWAY

Canonical Wnt signaling involves signal transduction through stabilization of β -catenin. Stabilized β -catenin translocates to the nucleus where it interacts with DNA-associated transcription factors to induce target gene expression. EndMT is strongly inhibited in endothelial-specific β -catenin mutants [48,49]. Wnt/ β -catenin acts in the AVC endocardium downstream from TGF- β to promote the acquisition of a mesenchymal phenotype during EndMT [50]. Canonical Wnt signaling induces EndMT by the induction of SNAIL and SLUG expression [51,52]. In contrast, Wnt signaling through Wnt7a inhibits EndMT53, highlighting the fine regulation of the EndMT process by the Wnt pathway.

5

INFLAMMATORY ENDMT

In general, the pathologies in which EndMT is recognized are associated with inflammatory activation in response to tissue damage. During the inflammatory response, pro-inflammatory cytokines including interleukin (IL)-1 β and Tumor necrosis factor alpha (TNF- α) activate the transcription factor Nuclear factor kappa-light-chain-enhancer of activated B cells (NF- κ B) involved in the activation of other pro-inflammatory cytokines including IL-1, IL-6, TNF- α or Interferon gamma (IFN γ), hence creating a positive feedback regulatory loop. Activation of NF- κ B promotes the induction of TGF- β 1 and TGF- β 2 and promotes EndMT [54]. But NF- κ B can also induce EndMT in a TGF- β -independent manner by directly activating SNAIL expression [55,56].

INHIBITORY ENDMT PATHWAYS

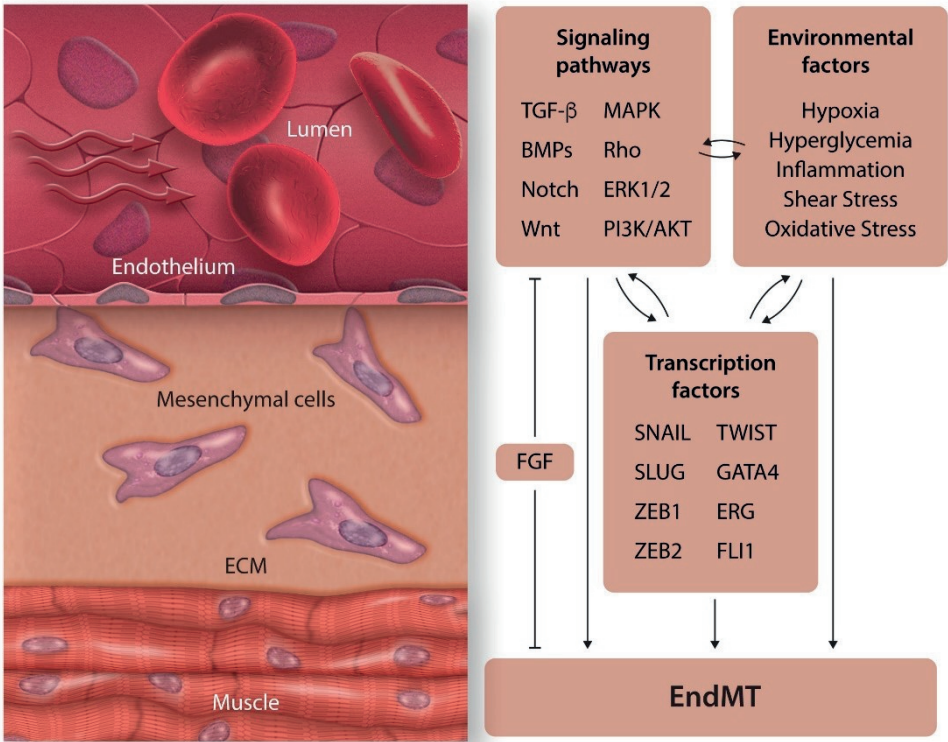
THE FGF SIGNALING PATHWAY

The FGF signaling pathway is formed by 22 different ligands that mediate their biological activity by binding to cell surface FGF receptors (FGFR1-4) [57]. Once activated, FGF receptors recruit similar intracellular signal transduction factors to other tyrosine kinase receptors including PI3K and MKK3/6, and activate similar intracellular signaling pathways including AKT-ERK1/2, Ras or MAPK (Raf, MEK).

The FGF pathway is an important regulator of endothelial TGF- β signaling mainly through FGFR1. Loss of FGFR1 signaling activates the EndMT program in a TGF- β -dependent manner culminating in intimal hyperplasia and stenosis [58].

OTHER FACTORS REGULATING ENDMT

Low oscillatory shear stress induces the expression of SNAIL, TWIST and GATA4 in the endothelium at atheroprone sites [59,60], activates TGF- β signaling and decreases FGFR1 expression [12]. Moreover, during hypoxia, HIF-1 α accumulates in the nucleus [61] where it activates hypoxia-induced genes including SNAIL, TWIST and ALK5 [62,63]. Oxidative stress also promotes EndMT and has additive effects to TGF- β [64]. Finally, the exposure to long term high glucose levels, such as in diabetic patients, also promotes EndMT through PI3K/Akt/NF- κ B pathways leading to cardiac fibrosis in diabetic patients [65]. Altogether, this shows the diversity of factors and signaling pathways that modulate EndMT (Figure 3).



5

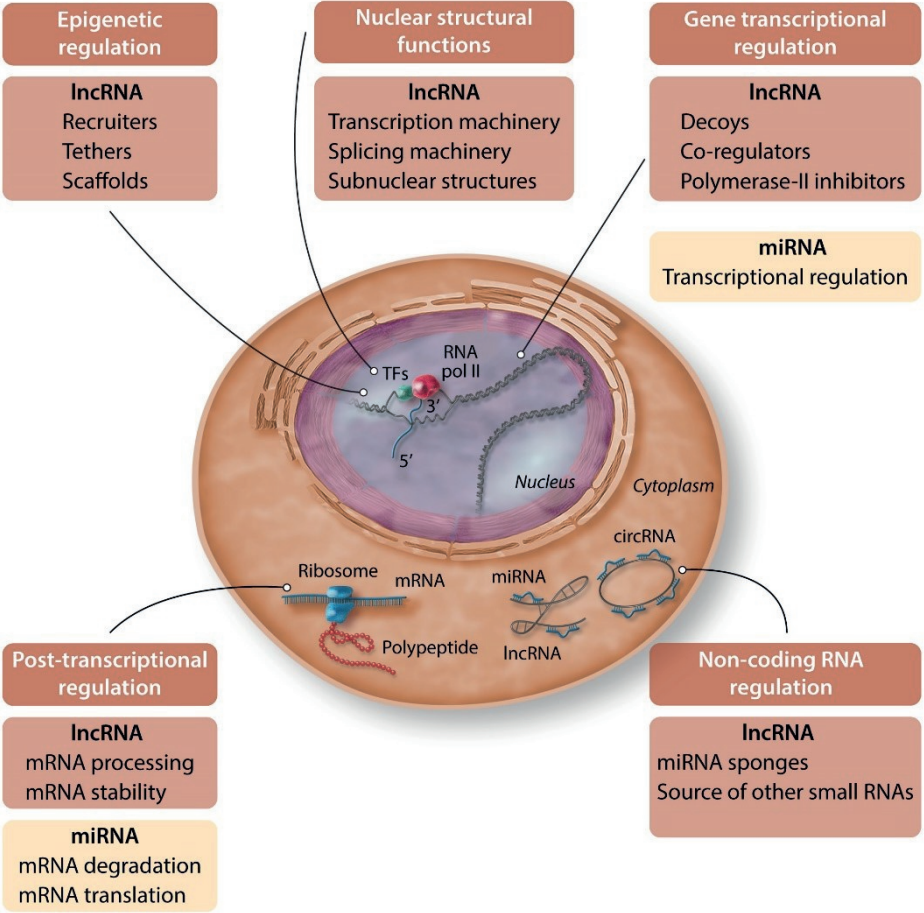
Figure 3. Molecular control of EndMT.

EndMT is induced by several environmental factors as well as signaling pathways which result in transcription of EndMT transcription factors which facilitate EndMT.

NON-CODING RNAS

microRNAs (miRNAs) are small fragments of RNA (typically 20-25 nucleotides). MiRNAs can bind to partial complementary sequences within mRNA targets and then degrade the mRNA via cleavage or destabilization or inhibit the translation of mRNAs into protein [66]. This represses gene and protein expression of direct targets of miRNAs but could also indirectly result in re-activation of gene and protein expression (because their repressors are downregulated by the miRNA). Increasing evidence describes a non-canonical role for miRNAs in transcriptional regulation as well, but the underlying mechanisms remain largely unknown. Non-coding RNAs are classified as lncRNAs when they contain more than 200 nucleotides. Their mechanism of action varies not only between different lncRNAs, but also one particular lncRNA can act using different mechanisms. They can act as recruiters, tethers and scaffolds for other regulatory factors involved in epigenetic modifications, or regulate gene transcription by acting as decoys, coregulators, or Polymerase-II inhibitors. They are also involved in the organization of the different components of the transcription and splicing machinery, as well as the organization of subnuclear structures. lncRNAs are also involved in post-transcriptional regulation, controlling processes such as mRNA processing, stability or translation, acting as sponges for miRNAs blocking their effects, or even can be the source of other small RNAs (for a review see [67]). lncRNA can be also classified according to their structural conformation. On this regard, in this review we will separate the circular lncRNAs (circRNAs) from the rest of the lncRNA described. Circular RNAs (circRNAs) are another subclass of non-coding RNAs generally formed by backsplicing that, similarly to other lncRNAs, function as miRNA sponges, RNA-binding protein sequestering factors, as well as regulators of gene expression by controlling mRNA transcription [68, 69]. Furthermore, circRNAs can also control gene transcription by interactions with phosphorylated Pol II or by competition with the pre-mRNA splicing machinery [70,71]. CircRNAs are highly stable molecules that form a covalently closed continuous loop making them resistant to RNA exonuclease digestion [72, 73]. The mechanisms of action of non-coding RNAs are summarized in Figure 4. Similar to lncRNAs, circRNAs can control EndMT by acting as sponges for miRNAs or by regulating the transcription of genes which can result in EndMT promotion or inhibition. In summary, miRNAs are important modulators as well which can

affect gene and protein expression and thus modulate EndMT. LncRNAs and circRNAs, together with miRNAs, are therefore promising targets for therapeutic applications which aim to inhibit EndMT.



5

Figure 4. Non-coding RNA mechanisms of action.
 Examples of how non-coding RNAs interfere with biological processes in cells (e.g. transcriptional regulation, post-transcriptional regulation and sponging of miRNAs).

MICRORNAS INDUCING/FACILITATING ENDMT

TGF- β 2-INDUCED ENDMT IS ASSOCIATED WITH DIFFERENTIAL EXPRESSION OF SEVERAL MIRNAS

TGF- β 2-induced EndMT is associated with increased expression of miR-21, miR-27b, miR-30b, miR-125b, miR-195, Let-7c, Let-7g and decreased expression of miR-122a, miR-127, miR-196 and miR-375 [74,75]. This suggests a role for these miRNAs in modulating EndMT. Indeed, miR-21 and miR-27b facilitate EndMT [76, 77]. Inhibition of miR-21 reverts the TGF- β 2-induced repression of VE-Cadherin and induction of S100A4 [77]. Consistently, kallistatin, an endogenous plasma protein, can reverse the TGF- β 1-induced upregulation of miR-21 and thereby inhibit EndMT [76]. Kallistatin can also reverse the expression of the EndMT transcription factor SNAIL, Akt phosphorylation, and activation of NF- κ B, emphasizing that the inhibiting effect of kallistatin on EndMT is not only due to the inhibition of miR-21 expression [76]. It has to be noted that inhibition of miR-21 did not affect ionizing radiation-induced EndMT [78]. Another miRNA that is a positive regulator of EndMT is miR-27b. Inhibition of miR-27b suppresses EndMT by preclusion of ACTA2 and TAGLN (SM22 α) expression, through an unidentified mechanism [75]. The expression of another miRNA, miR-31, is not altered upon TGF- β 2 treatment [79], yet inhibition of miR-31 suppresses both ACTA2 and TAGLN expression suggesting a role for miR-31 in facilitating EndMT [79]. However, overexpression of miR-31 has limited effects on TGF- β 2-induced EndMT suggesting that miR-31 does not induce EndMT directly but rather controls the magnitude of EndMT [79]. Let-7c and Let-7g, two other miRNAs which are upregulated upon TGF- β 2 treatment, are part of the Let-7 family which represses EndMT and will be discussed later in this review. The role of the other differentially expressed miRNAs in the regulation of EndMT remain unknown to date.

THE ROLE OF MIR-130 IN MODULATING ENDMT/EMT

miR-130b is upregulated in high proliferative and angiogenic-prone colorectal cancer, suggesting a role of miR-130b in proliferation, angiogenesis, EndMT and/or EMT [80]. Indeed, miR-130b overexpression facilitates tumor growth accompanied by enhanced proliferation, angiogenesis and EMT [80]. Overexpression of miR-130b results in decreased expression of E-Cadherin whereas EndMT transcription factors SNAIL and ZEB1 are increased [80]. miR-130a expression is increased in pulmonary hypertension as well as in TGF- β 1-treated endothelial cells, suggestive of a role for miR-130a in modulating both EndMT and EMT [81]. Indeed, miR-130a enhances the TGF- β 1-induced expression of ACTA2 and decreases CD31 expression [81]. Interestingly, NF- κ B can induce miR-130a expression and vice versa, illustrating the interplay between NF- κ B and miRNAs [81].

5

MIR-374B AND MIR-449A MODULATE ENDMT DURING ATHEROSCLEROSIS

Both miR-374b and miR-449a associate with EndMT in the context of atherosclerosis [82, 83]. Indeed, miR-449a expression culminates in reduced E-Cadherin expression and an increase in the expression of α -SMA and SMAD3 [82]. Importantly, antagonizing miR-449a expression inhibits the development of atherosclerosis in diabetic mice [82]. Similarly to miR-449a, the expression of miR-374b is elevated in atheroprone regions *in vivo*, as well as TGF- β 1-treated endothelial cells [83]. Overexpression of miR-374b results in decreased expression of the endothelial markers VE-Cadherin and eNOS whereas the expression of mesenchymal markers TAGLN and Calponin increases [83]. Interestingly, combined overexpression of miR-374b and MAPK7 (a known antagonist of EndMT) precludes the EndMT induction by miR-374b [83]. Glucose treatment induces the expression of miR-328 [84], and induces EndMT evidenced by an increase in the expression of mesenchymal markers Collagen-1 and Collagen-3 accompanied by activation of MEK1/2 and MAPK1/2 [84]. These data highlight the interplay between miRNAs and MAPK signaling, and identify MAPK signaling as a crucial regulator of EndMT.

THE ROLE OF MIR-9 AND MIR-342-5P IN MODULATING ENDMT AND ANGIOGENESIS

Contrasting effects of miR-9 and miR-342-5p highlight differential effects of miRNAs on certain biologic processes. miR-9 induces EndMT with decreased VE-Cadherin expression and a corresponding increase in N-Cadherin [85]. miR-9 also represses NF- κ B expression and inflammation whereas it promotes tube formation [85]. On the other hand, miR-342-5p also induces EndMT, but in contrast to miR-9, this inhibits lumen formation and angiogenic sprouting [86]. These data show that although there is redundancy in miRNAs that induce EndMT, there are also distinct outcomes [85,86]. Indirectly, this also suggests that pro-angiogenic conditions may or may not be pro-EndMT, and vice-versa.

MIRNAS INHIBITING ENDMT

MIR-15A, MIR-23B AND MIR-199A AS INHIBITORS OF EMT/ENDMT DURING DEVELOPMENT

While the abovementioned miRNAs function to promote EndMT, others exhibit an inhibitory effect. For example, the levels of miR-15a, miR-23b and miR-199a are elevated during AVC development in the embryonic chick heart, suggesting a role for these miRNAs in modulating both EMT and EndMT [87]. Indeed, miR-15a, miR-23b or miR-199a inhibit EMT/EndMT in AVC explants [87]. In line with this, miR-23 also inhibits TGF- β -induced EMT/EndMT by inhibiting the TGF- β -induced expression ACTA2 and SNAIL [88]. Overexpression of miR-199a-5p in HUVECs as well as irradiated HUVECs undergoing EndMT induced the expression of α -SMA and Collagen-1 in co-cultured human fetal lung fibroblasts [89]. This suggests that miR-199a-5p as well as EndMT in itself are important for myofibroblast activation of neighboring fibroblasts [89].

THE ROLE OF MIR-483 IN MODULATING ENDMT

miR-483 reduces oscillatory flow-induced EndMT by decreasing the expression of SNAIL, SLUG, TWIST and TAGLN [90], which coincides with a reduction in inflammatory activation of IL-6, ICAM-1 and VCAM-1 [90]. Concurrently, endothelial cells expressing miR-483 decrease the expression of mesenchymal markers induced by serum of Kawasaki patients, while increasing the expression of endothelial markers [91]. Interestingly, statin (atorvastatin) treatment in combination with serum of Kawasaki patients induces the expression of miR-483 and similarly represses EndMT [91]. This highlights the potential of pharmacological agents to interfere with the EndMT program through non-coding RNAs. Moreover, it is tempting to speculate that repression of EndMT is among the so-called 'pleiotropic beneficial effects' attributed to statins.

THE ROLE OF MIR-148 IN INHIBITING ENDMT

Fibrodysplasia ossificans progressiva is a congenital disorder associated with skeletal malformations and heterotopic calcification in which EndMT is involved. While gain of function mutations in ALK2 are associated with this disease, the activin A receptor type I (ACVR1) gene is also implicated. Notably, both are associated with the TGF- β pathway signaling. ACVR1 is a target of miR-148a, and the constitutive activation of ACVR1 is known to induce EndMT. Indeed, expression of miR-148a represses BMP signaling in endothelial cells [92], suggesting that miR-148a can modulate EndMT. To our knowledge, this hypothesis has not been directly examined. In contrast, the expression of miR-148b does not decrease ACVR1 expression, implying that miR-148a and miR-148b have different gene targets [93]. Overexpression of miR-148b increases migration, proliferation and angiogenesis in HUVECs [93]. On the other hand, inhibition of miR-148b induces EndMT both *in vitro* and in a mouse model of skin wound healing [93]. In line with this, TNF- α and IL-1 β treatment in HUVECs decreased miR-148b levels and induced EndMT, which is precluded by the overexpression of miR-148b [93].

LET-7, MIR-424 AND MIR-503 INHIBIT ENDMT

The inflammation-induced loss of FGF signaling decreases the expression levels of Let-7, culminating in the activation of TGF- β signaling and thus EndMT [94]. Let-7b inhibits EndMT in a murine transplant arteriopathy model.94 Moreover, the major plasma metabolite HT-3O sulfate, with antioxidant and anti-inflammatory properties, protects against IL-1 β -induced EndMT by restoring Let-7 expression [95]. IL-13 treatment induces EndMT accompanied by decreased levels of miR-424 and miR-503, suggesting a role for these miRNAs in modulating EndMT [96]. Indeed, inhibition of miR-424 increases the expression of the mesenchymal markers α -SMA and N-Cadherin [96]. Furthermore, miR-424 or miR-503 inhibit the migration of endothelial cells [96].

MIR-18A-5P AND MIR-532 INHIBIT ENDMT DURING CARDIAC FIBROSIS AND MYOCARDIAL INFARCTION

miR-18a-5p inhibits glucose-induced EndMT by decreasing the expression of the mesenchymal markers S100A4, Vimentin and Fibronectin and increasing the expression of CD31.97 miR-18a-5p attenuates both cardiac fibrosis and EndMT in diabetic mice [97]. Since miR-18a-5p targets Notch2, this might explain the underlying mechanism of how miR-18a-5p inhibits EndMT [97]. Knockdown of another miRNA, miR-532, in a mouse model of myocardial infarction elevates the abundance of Collagen-1/CD31 and α -SMA/CD31 double-positive cells, indicative of active EndMT [98]. Indeed, knockdown of miR-532 enhanced TGF- β 2-induced EndMT by increasing the expression of Collagen-3, SNAIL and ACTA2 while decreasing the expression of CD31 and vWF [98].

THE ROLE OF MIR-218, MIR-221, MIR-302C AND MIR-494 IN INHIBITING ENDMT

miR-302c inhibits EndMT *in vitro* [99]. Interestingly, co-implantation of a human hepatocellular carcinoma cell line and endothelial cells with loss- or gain of 302c drastically differed hepatocellular carcinoma growth in mice, implying that miR-302c in endothelial cells may suppress endothelial cell-mediated tumor growth [99]. Reprogramming by the RhoA-Rock-canonical BMP signaling pathways is associated with increased expression of miR-302b and miR-302c

[100]. This demonstrates the essential role of miR-302b/c in modulating endothelial cell behavior. Another miRNA, miR-218, decreases CTGF expression, thereby increasing the expression of E-Cadherin while reducing Vimentin and Fibronectin expression in a human colon cancer cell line (HCT116 cells) [101]. When HUVECs were treated with conditioned medium from miR-218 overexpressing HCT116 cells, this suppressed angiogenesis [101]. These data suggest that miR-218 not only inhibits EndMT/EMT but also angiogenesis [101]. miR-221 also suppresses angiogenesis by downregulating ZEB2 expression in HUVECs [102]. Treatment of HUVECs with conditioned medium from miR-494 overexpressing decidual-derived mesenchymal stem cells also impairs capillary formation [103]. However, the role of miR-221 and miR-494 in regulating EndMT needs further elucidation.

MIR-192, MIR-194, MIR-497, MIR-29 AND LET-7 AS INHIBITORS OF ENDMT IN KIDNEY DISEASE

miR-192 or miR-194 increase E-cadherin and decrease the expression of N-Cadherin and ZEB2 [104], suggesting that a decrease in miR-192 or miR-194 during autosomal dominant polycystic kidney disease contributes to EMT/EndMT [104]. Another miRNA which might be involved in inhibiting EndMT is miR-497 [105]. Melatonin inhibits TGF- β 2-induced EndMT by attenuating the TGF- β 2-induced reduction in miR-497 expression, thereby suppressing the expression of ROCK1 and ROCK2 [105]. Melatonin also reverses the loss of miR-497 and increase in EndMT in glomeruli of diabetic rats, showing the overall importance of miR-497 in the inhibition of EndMT in the context of kidney disease [105]. Linagliptin, a new dipeptidyl peptidase-4 (DPP-4) inhibitor that is used to treat diabetes, is another pharmacological agent that inhibits EndMT and ameliorates kidney fibrosis in diabetic mice [106, 107]. Importantly, linagliptin modulates miR-29 expression, and the miR-29 family suppresses EndMT, suggesting that linagliptin inhibits EndMT by restoring miR-29 expression levels in chronic kidney disease [106]. Diabetic mice also have decreased expression of N-acetyl-seryl-aspartyl-lysyl-proline (AcSDKP), an endogenous anti-fibrotic peptide, which is associated with insufficient levels of anti-fibrotic miRNAs in the kidney such as the miR-29 and Let-7 families [108]. Importantly, administration of AcSDKP to diabetic mice, and also to TGF- β 2-treated endothelial cells, decreases the

expression of TGF- β R1 and SMAD3 phosphorylation [108, 109]. AcSDKP restores the expression of both the miR-29 and Let-7 miRNA families [108], while Linagliptin reverses the decrease in expression of the Let-7 family via restoration of the FGF signaling [109]. This demonstrates that anti-fibrotic interventions induce a similar anti-fibrotic miRNA profile both *in vivo* and *in vitro* [106, 108]. Interestingly, overexpression of Let-7 in combination with TGF- β 2 treatment induces the expression of the miR-29 family, and vice versa [108]. This suggests a crosstalk between the miR-29 and Let-7 miRNA families in facilitating anti-fibrotic and EndMT inhibitory effects [108].

MIRNAS WHICH HAVE DIFFERENT EFFECTS ON ENDMT IN DEVELOPMENT AND PATHOLOGY

THE ROLE OF THE MIR-200 FAMILY IN MODULATING ENDMT

miR-200a inhibits TGF- β -induced EndMT [110]. Similarly, another miR-200 family member, miR-200b, prevents both glucose- and TGF- β 1-induced EndMT [111]. Endothelial cell-specific overexpression of miR-200b in diabetic mice prevents glucose-induced EndMT in the heart as well as in retinal tissues [111, 112]. In addition, overexpression of miR-200b associates with angiogenesis suppression [113]. Downregulation of the miR-200 family results in the upregulation of the EndMT transcription factors SNAIL and ZEB1 [114]. This underlines the role of the miR-200 family in inhibiting EndMT. Individuals with bicuspid aortic valves (and therefore a higher risk of developing aortic aneurysm) have lower expression of miR-200c suggesting potential activation of both EMT and EndMT [114]. Individuals with bicuspid aortic valves are also associated with a non-coding variant, called rs6601627, which is suggested to interact with GATA4 [115]. Importantly, CRISPR/Cas9-mediated disruption of GATA4 impairs TGF- β 2 and BMP2-induced EndMT in endothelial cells derived from human induced pluripotent stem cells [115]. This demonstrates that non-coding RNAs are important in regulating both EMT and EndMT in aortic valves. In contrast to the above, during development, SNAIL-induced repression of the miR-200 family promotes the generation of Flk1-positive endothelial cells, suggesting that during development the miR-200 family has an opposite role and supports

the maintenance of the endothelial character [116]. Indeed, lower levels of the miR-200 family in human embryonic stem cells is also associated with differentiation into vascular endothelial cells [117]. Furthermore, miR-200a did not affect EMT/EndMT during development of the AVC in the developing chicken heart [87]. This suggests that the miR-200 family has different roles during development and pathological conditions in different species.

THE ROLE OF MIR-126 IN REGULATING ENDMT

Combined knockdown of ERG and FLI1 induces EndMT which is accompanied by low miR-126 expression levels, suggesting a role for miR-126 in modulating EndMT [118]. Indeed, miR-126 limits the expression of ACTA2, TAGLN, Collagen-1 and SLUG and partially counteracts the reduction in VE-Cadherin and CD31 expression [118]. Interestingly, treatment of HUVECs with conditioned medium from tumors also resulted in decreased expression of both ERG and FLI1, suggesting that the decrease of these transcription factors by soluble mediators from the tumor microenvironment can promote EndMT and therewith tumor progression [118]. In line with this, miR-126 suppresses the expression of the mesenchymal genes ACTA2, TAGLN and myocardin while maintaining the expression of progenitor markers [119]. Also, miR-126 reverses the TGF- β 1-induced activation of FoxO3 and SMAD4 and decrease in PI3K and Akt, suggesting novel pathways involved in the modulation of EndMT [119]. In contrast to the above data, knockdown of miR-126a-5p reverses the hypoxia-induced decrease in CD31 and increase in α -SMA [120]. Altogether, while the majority of studies suggest that miR-126 inhibits EndMT, it appears that in specific contexts miR-126 may exert pro-EndMT effects.

THE ROLE OF MIR-155 AND MIR-20A IN MODULATING ENDMT

Inhibition of miR-155 reverses the TGF- β -induced expression of SNAIL, SLUG, TWIST and Vimentin, suggesting that miR-155 inhibits EndMT [121]. In contrast, inhibition of miR-155 does not affect TGF- β 3-induced EndMT in mouse embryonic endothelial cells [122]. Moreover, overexpression of miR-155 inhibits TGF- β 3-induced EndMT, suggesting that induction of miR-155 expression represses EndMT [122]. This demonstrates that the mechanism by which miR-155 regulates

EndMT is different during developmental and pathological contexts, which might be explained by the maturity of the cells or the difference in TGF- β isoform. miR-20a also has differential effect on EndMT in development and adult pathology. During the development of the outflow tract in the mouse embryos, deletion of BMP4/7 inhibits EMT/EndMT which could be rescued by the expression of miR-17/20a, indicative of an EndMT inductor role for this miRNA [123]. In contrast, FGF2-induced expression of miR-20a limits EndMT by reducing the expression of TGF- β receptor 1/2 and SARA (which recruits SMAD2 and SMAD3 to the TGF- β receptor complex) in adult endothelial cells [124].

In all, a remarkable number of miRNAs are associated to the EndMT regulatory program. These are summarized in Figure 5 and Table 1.

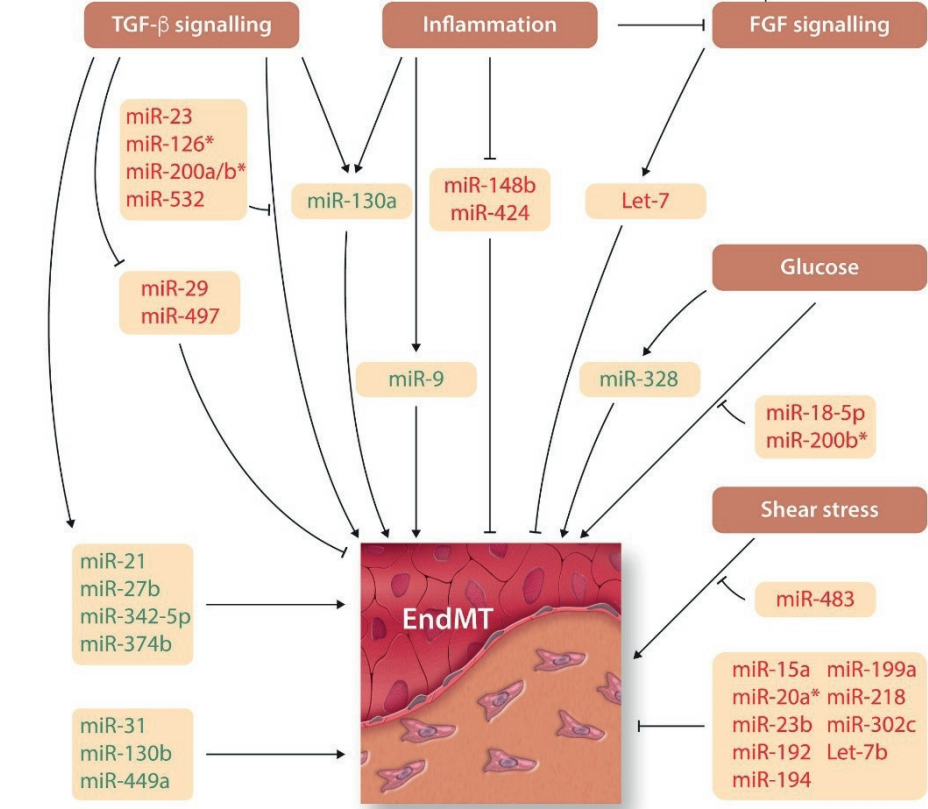


Figure 5. microRNA in EndMT.
*Overview of microRNAs (miRNAs) that induce or inhibit EndMT. miRNA inducers and inhibitors of EndMT are depicted in green and red respectively. * indicates a different role during pathology and development.*

Table 1. microRNAs in EndMT

miRNAs	Biological context	Targets	Experimental model
Inducing EndMT			
miR-9	Development/Pathology – Lymphangiogenesis/ Inflammation	NF-kB	<i>In vitro</i> – Rat mesenteric lymphatic endothelial cells [85]
miR-17	Development – OFT formation	Vegfa	<i>In vivo</i> – Mouse embryo's <i>Ex vivo</i> – OFT explant culture [123]
miR-21	Pathology – Fibrosis	?	<i>In vitro</i> – HUVECs <i>In vivo</i> – Mouse model of cardiac pressure overload [76,77]
miR-27b	Molecular characterization	Elk1, Nrp2, PlxnA2, PlxnD1	<i>In vitro</i> – Mouse pancreatic microvascular endothelial cells [75]
miR-31	Pathology – Inflammation	VAV3	<i>In vitro</i> – Mouse pancreatic microvascular endothelial cells [79]
miR-130a	Pathology – Pulmonary hypertension	BMPR2	<i>In vitro</i> – Lung microvascular endothelial cells <i>In vivo</i> – Pulmonary arterial hypertension mouse model [81]
miR-130b	Pathology – Colorectal cancer	PPAR γ	<i>In vitro</i> – Human colorectal adenocarcinoma cell lines <i>In vivo</i> – Mouse xenografts and human colorectal cancer samples [80]
miR-143	Pathology – Ischemic stroke	HECTD1	<i>In vivo</i> – Mouse brain [136]
miR-328	Pathology – Diabetes	?	<i>In vitro</i> – HUVECs [84]
miR-342-5p	Development – Angiogenesis	Endoglin	<i>In vitro</i> – HUVECs <i>In vivo</i> – Mouse retinal vasculature <i>Ex vivo</i> – Mouse aortic rings [86]
miR-374b	Pathology – Neointimal hyperplasia	RAC1, MAP3K3, MAP3K7, MAPK7, MEF2D, KLF4	<i>In vitro</i> – HUVECs <i>In vivo</i> – Porcine abdominal trifurcations and human coronary arteries [83]
miR-449a	Pathology – Atherosclerosis	AdipoR2	<i>In vitro</i> – HUVECs <i>In vivo</i> – Diabetic mice and human carotid atherosclerotic plaques [82]

Inhibiting EndMT			
miR-15a	Development – AVC formation	?	<i>Ex vivo</i> – Chicken AVC explants [87]
miR-18a-5p	Pathology – Diabetes	Notch2	<i>In vitro</i> – Human aortic valvular endothelial cells <i>In vivo</i> – Diabetic mice [97]
miR-23b	Development – AVC formation	?	<i>Ex vivo</i> – Chicken AVC explants [87]
	Development – Cardiac valve formation	Has2, Icat, Tmem2	<i>In vitro</i> – Mouse embryonic endothelial cells <i>In vivo</i> – Zebrafish [88]
miR-29a	Pathology – Bladder carcinoma	VEGFA	<i>In vitro</i> – Human bladder carcinoma cells <i>In vivo</i> – Mouse xenografts [131]
miR-29 family	Pathology – Diabetes-related kidney fibrosis	DPP-4	<i>In vitro</i> – Human dermal microvascular endothelial cells <i>In vivo</i> – Fibrotic diabetic kidney disease mouse model [106,108]
miR-30d	Pathology – Neuroinflammatory disorders	ATG5	<i>In vitro</i> – Human brain microvascular endothelial cells <i>In vivo</i> – Mouse brain [130]
miR-145	Pathology – Neointimal hyperplasia	TGFBR2, SMAD3	<i>In vitro</i> – Endothelial progenitor cells [125]
miR-148b	Physiology – Skin wound healing	TGFB2, SMAD2	<i>In vitro</i> – HUVECs <i>In vivo</i> – Mouse model of skin wound healing [93]
miR-186-5p	Pathology – Prostate cancer	Twist1	<i>In vitro</i> – Prostate cancer cells [127]
miR-192/194	Pathology – Kidney disease	ZEB2, CDH2	<i>In vitro</i> – Renal epithelial cells <i>In vivo</i> – Autosomal dominant polycystic kidney disease mouse model and human samples [104]
miR-199a	Development – AVC formation	?	<i>Ex vivo</i> – Chicken AVC explants [87]
	Pathology – Radiation induced pulmonary fibrosis	?	<i>In vitro</i> – HUVECs [89]
miR-218	Pathology – Colorectal cancer	CTGF	<i>In vitro</i> – HUVECs and human colon cancer cell line <i>In vivo</i> – Human colorectal cancer samples [101]
miR-221	Pathology – Tumor angiogenesis	ZEB2	<i>In vitro</i> – HUVECs [102]
miR-302c	Pathology – Hepatocellular	MTDH	<i>In vitro</i> – Human hepatocellular

	carcinoma		carcinoma cell line and HUVECs <i>In vivo</i> – Ectopic transplant mouse model [99]
	Pathology – Corneal blindness	?	<i>In vitro</i> – Human corneal endothelial cells [100]
miR-424/503	Pathology – Pulmonary hypertension	?	<i>In vitro</i> – Human pulmonary artery endothelial cells [96]
miR-483	Pathology – Aortic valve calcification	?	<i>In vitro</i> – Human aortic valve endothelial cells <i>In vivo</i> – Porcine aortic valve leaflets [90]
	Pathology – Kawasaki disease	CTGF	<i>In vitro</i> – Lung endothelial cells from endothelial KLF4 transgenic mice and HUVECs <i>In vivo</i> – Sera from Kawasaki disease patients [91]
miR-494	Pathology – Preeclampsia	VEGF	<i>In vitro</i> – HUVECs [103]
miR-497	Pathology – Diabetic nephropathy	ROCK1/2	<i>In vitro</i> – Human renal glomerular endothelial cells <i>In vivo</i> – Diabetic rats [105]
miR-532	Pathology – Myocardial infarction	Prss23	<i>In vitro</i> – Mouse cardiac endothelial cells <i>In vivo</i> – Mouse model of myocardial infarction [98]
Let-7 family	Pathology – Neointima formation	?	<i>In vitro</i> – Primary mouse endothelial cells <i>In vivo</i> – Mouse arterial transplant model and human coronary arteries [58]
	Pathology – Inflammation	?	<i>In vitro</i> – HUVECs and human retinal endothelial cells [95]
	Pathology – Diabetes-related kidney fibrosis	?	<i>In vitro</i> – Human dermal microvascular endothelial cells and HUVECs <i>In vivo</i> – Fibrotic diabetic kidney disease mouse model [108,109]
Differential effects on EndMT			
miR-20a	Development – Outflow tract cushion development	Vegfa	<i>In vivo</i> – Mouse embryos <i>Ex vivo</i> – Outflow tract explant culture [123]
	Pathology – Molecular characterization	TGFBR1/2, SARA	<i>In vitro</i> – HUVECs [124]

miR-126	Pathology – Tumor progression	?	<i>In vitro</i> – HUVECs <i>In vivo</i> – Tumor implantation mouse model [118]
	Pathology – Neointimal hyperplasia	PIK3R2	<i>In vitro</i> – Rat bone marrow-derived endothelial progenitor cells [119]
	Development/Pathology – Pulmonary vasculature remodeling	?	<i>In vitro</i> – Rat pulmonary microvascular endothelial cells <i>In vivo</i> – Mouse model of persistent pulmonary hypertension of the newborn [120]
miR-155	Pathology – Molecular characterization	SKI	<i>In vitro</i> – Human coronary artery endothelial cells [121]
	Development – Molecular characterization	?	<i>In vitro</i> – Mouse embryonic endothelial cells [122]
miR-200a	Pathology – Cardiac fibrosis	GRB2	<i>In vitro</i> – Human aortic endothelial cells [110]
miR-200b	Pathology – Diabetic retinopathy	?	<i>In vitro</i> – Human retinal microvascular cells <i>In vivo</i> – Diabetic mice [111]
	Pathology – Diabetic cardiomyopathy	?	<i>In vitro</i> – Mouse heart endothelial cells <i>In vivo</i> – Diabetic mice [112]
	Pathology/Physiology - Angiogenesis	Ets1	<i>In vitro</i> – Human microvascular endothelial cells [113]
miR-200c	Pathology – Aneurysm formation	?	<i>In vitro</i> – EA.hy926 endothelial cells <i>In vivo</i> – Non-dilated aortas from patients with bicuspid aortic valves [114]
miR-200 family	Development – Vasculogenesis	Flk1, Ets1	<i>In vitro</i> – Mouse embryonic stem cells [116]
	Development - Differentiation	?	<i>In vitro</i> – Human embryonic stem cells [117]

List of miRNAs regulating EndMT categorized into their inducing, inhibiting or differential role on EndMT. Question mark refers to unknown targets in this context. AdipoR2 indicates adiponectin receptor 2; ATG5, autophagy related 5; BMPR2, bone morphogenetic protein receptor 2; CDH2, cadherin-2; CTGF, connective tissue growth factor; DPP-4, dipeptidyl peptidase-4; Elk1, ETS transcription factor; Ets1, protein c-ets-1; Flk1, fetal liver kinase 1; GRB2, growth factor receptor-bound protein 2; Has2, hyaluronic acid synthase 2; Icat, beta-catenin-interacting protein; KLF4, kruppel-like factor 4; MAP3K3/7, mitogen-activated protein kinase kinase kinase 3/7; MAPK7,

mitogen-activated protein kinase 7; MEF2D, myocyte-specific enhancer factor 2D; MTDH, metadherin; NF- κ B, nuclear factor kappa-light-chain-enhancer of activated B cells; Nrp2, neuropilin 2; PIK3R2, PI3K regulatory subunit p85 beta; PlxnA2, plexin A2; PlxnD1, plexin D1; PPAR γ , peroxisome proliferator-activated receptor γ ; RAC1, ras-related C3 botulinum toxin substrate 1; ROCK, rho-associated, coiled-coil-containing protein kinase; SARA, Smad anchor for receptor activation; SKI, SKI proto-oncogene; SMAD, SMAD family member; TGFB, transforming growth factor beta; TGFBR, transforming growth factor beta receptor; Tmem2, transmembrane protein 2; Twist1, twist-related protein 1; VAV3, guanine nucleotide exchange factor VAV3; VEGF, vascular endothelial growth factor; ZEB2, zinc finger E-box-binding homeobox 2.

LNCRNAS PROMOTING ENDMT

Among all the lncRNAs identified, only a few lncRNAs have been implicated in the regulation of EndMT hitherto. Metastasis-associated lung adenocarcinoma transcript 1 (MALAT1) is a lncRNA extensively associated with cancer metastasis and recently described as an EndMT inducer. MALAT1 competitively binds to miR-145, a known miRNA that inhibits TGF- β 1-induced EndMT by directly targeting TGF- β R2 and SMAD3. Acting as a miRNA sponge, MALAT1 blocks the inhibitory activity of the miR-145 and promotes EndMT [125]. Another lncRNA identified as an EndMT promoter is GATA6-AS. The long non-coding antisense transcript of GATA6 (GATA6-AS) interacts with the epigenetic regulator LOXL2 to regulate endothelial gene expression via changes in H3K4me3 methylation, including genes encoding for periostin and cyclooxygenase-2. GATA6-AS expression is induced in endothelial cells by hypoxia. Inhibition of GATA6-AS blocks TGF- β 2-induced EndMT *in vitro* and promotes blood vessel formation in mice [126]. A third lncRNA that promotes EndMT is PVT1. PVT1 associates with tumour cell proliferation, invasion, and metastasis in different cancer models. In prostate cancer, PVT1 promotes cancer invasion and metastasis in part by the induction of EndMT. PVT1 promotes EndMT by acting as a sponge for miRNA-186-5p and positively regulating TWIST1 [127].

LNCRNAS INHIBITING ENDMT

H19 prevents glucose-induced TGF- β 1 expression and therefore, EndMT in diabetic retinopathy models. H19 controls TGF- β 1 mRNA and protein levels through a SMAD independent MAPK–ERK1/2 pathway, and this regulation is also independent of the actions of miR-200b, a known miRNA (see above) that interacts with H19 [128]. Besides the lncRNAs mentioned above, lncRNA n339260, although not directly related to EndMT, controls the expression of VE-Cadherin during the process of vascular mimicry in a human hepatocellular carcinoma [129]. Maintenance or reduction of VE-Cadherin in endothelial cells is a critical step in EndMT and therefore, future studies are needed to understand the potential role of lncRNA n339260 in EndMT. Furthermore, this study provided a number of candidate miRNAs that may be regulated by lncRNA n339260 including miR-31-3p, miR-30e-5p, miR-519c-5p, miR-520c-5p, miR-29b-1-5p, and miR-92a-1-5p. These will also require further testing to determine their potential role in the EndMT process. A summary of the currently known lncRNAs that modulate EndMT is provided in Figure 6 and Table 2. We expect this list to grow significantly in the coming years.

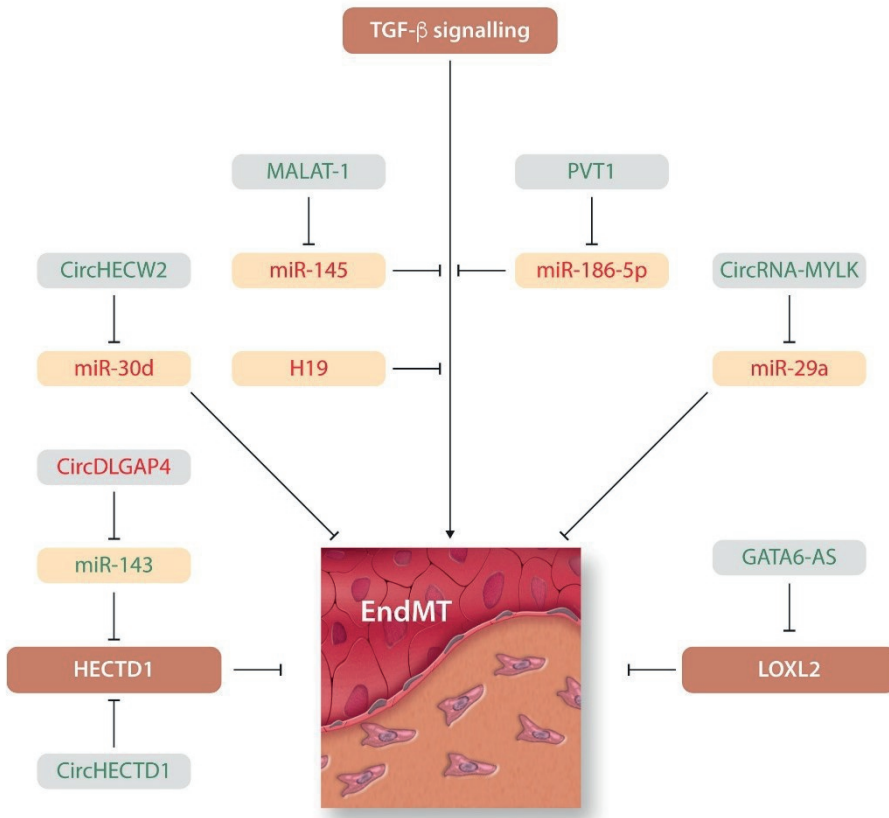


Figure 6. Long non-coding RNA in EndMT.

Overview of long non-coding RNAs (lncRNAs) that induce or inhibit EndMT. lncRNA inducers and inhibitors of EndMT are depicted in green and red respectively.

Table 2. Known lncRNAs involved in EndMT

miRNAs	Biological context	Targets	Experimental model
Inducing EndMT			
GATA6-AS	Development – Angiogenesis	LOXL2	<i>In vitro</i> – HUVECs [126]
MALAT1	Pathology – Neointimal hyperplasia	miR-145 that targets TGFBR2 and SMAD3	<i>In vivo</i> – Mouse embryo's <i>In vitro</i> – Endothelial progenitor cells [125]
PVT1	Pathology – Prostate cancer	miR-186-5p that targets Twist1	<i>In vitro</i> – Prostate cancer cells [127]
Inhibiting EndMT			
H19	Pathology – Diabetic retinopathy	TGF- β 1 through control of MAPK-ERK1/2 pathway	<i>In vitro</i> – Human retinal endothelial cells <i>In vivo</i> – Diabetic retinopathy mouse model and human samples [128]

List of lncRNAs currently known to regulate EndMT categorized into their inducing or inhibiting role on EndMT. ERK indicates extracellular signal-regulated kinase; LOXL2, lysyl oxidase homolog 2; MAPK, mitogen-activated protein kinase; SMAD, SMAD family member; TGF- β 1, transforming growth factor beta 1; TGFBR, transforming growth factor beta receptor; Twist1, twist-related protein 1.

CIRCRNAS PROMOTING ENDMT

CircRNAs that are known to promote EndMT include CircHECW2 and CircRNA-MYLK. CircHECW2 promotes EndMT by acting as a sponge for miR-30d and culminating in the increased expression of ATG5, which promotes the activation of the Notch1 pathway to induce pathologic EndMT [130]. In the case of CircRNA-MYLK, EndMT is promoted by directly binding and inhibiting miR-29a [131]. This promotes EndMT by activating the TGF- β , NF- κ B and β -catenin pathways [132, 133]. Besides acting as miRNA sponges, circRNAs can control EndMT by directly regulating the expression of genes. In this regard, circHECTD1 regulates the expression of its host gene E6-AP C-terminal domain E3 ubiquitin protein ligase 1 (HECTD1), which is implicated in the maintenance of endothelial fate and controlled by Wnt signaling through APC-Axin interactions [134]. Increased expression of circHECTD1 induces EndMT and its derivative fibroblast-like cells contribute to pulmonary fibrosis [135].

CIRCRNAS INHIBITING ENDMT

Among the circRNAs, the only currently identified EndMT inhibitor is CircRNA DLGAP4. DLGAP4 functions as an endogenous miR-143 sponge to allow for the expression of HECTD1, as mentioned above. CircRNA DLGAP4 inhibits EndMT and promotes maintenance of endothelial integrity and in the case of cerebral ischemia it maintains the integrity of the blood-brain-barrier [136]. In addition, circRNAs chr5:90817794|90827570, chr8:71336875|71337745 and chr6:22033342|22038870, were found to be increased in a circRNA screening performed on an EndMT assay [137], although their specific functions remain unknown. CircRNAs that are currently known to modulate EndMT are summarized in Figure 6 and Table 3.

Table 3. Known circRNAs involved in EndMT

miRNAs	Biological context	Targets	Experimental model
Inducing EndMT			
CircHECW2	Pathology – Neuroinflammatory disorders	miR-30d that targets ATG5	<i>In vitro</i> – Human brain microvascular endothelial cells <i>In vivo</i> – Mouse brain [130]
CircRNA- MYLK	Pathology – Bladder carcinoma	miR-29a that targets VEGFA	<i>In vitro</i> – Human bladder carcinoma cells <i>In vivo</i> – Mouse xenografts [131]
CircHECTD1	Pathology – Pulmonary disease	HECTD1	<i>In vitro</i> – Mouse microvascular lung cells <i>In vivo</i> – Lung silicosis in mouse model and human samples [135]
Inhibiting EndMT			
CircDLGAP4	Pathology – Ischemic stroke	miR-143 that targets HECTD1	<i>In vivo</i> – Mouse brain [136]

List of circRNAs regulating EndMT categorized into their inducing or inhibiting role on EndMT. ATG5 indicates autophagy related 5; HECTD, HECT domain E3 ubiquitin protein ligase; VEGF, vascular endothelial growth factor.

The identification of the functional relevance of lncRNAs and circRNAs in EndMT is a fast growing field of research. It is expected that our understanding of the regulatory roles of lncRNAs and circRNAs in EndMT will increase accordingly in the coming years and so our understanding of physiologic and pathologic EndMT.

FUTURE PERSPECTIVES: TARGETING NON-CODING RNAs TO MODULATE EndMT

As this review has highlighted, non-coding RNAs are key players in the control and modulation of EndMT (Figure 5 and 6). However, our overall knowledge of the role of non-coding RNAs in EndMT is in its infancy. Despite this, taking the data reviewed in this article as a whole, we are already able to draw several important conclusions about this field. Firstly, it is immediately clear that some non-coding RNAs inhibit EndMT such as miR-29, whereas others facilitate or induce EndMT such as miR-21, GATA6-AS and HECTD1 (Tables 1,2 and 3). Second, most of these non-coding RNAs have only been described in a single context and we do not know if their roles may differ in other contexts. In addition, different markers for EndMT are used in different studies which might not give us the full pictures of how a certain non-coding RNA affects EndMT. The difference in function of these non-coding RNAs between development and various pathological states might also be different and needs to be established. Third, non-coding RNAs also interact with other epigenetic modulators such as DNA methylation and histone modifications to affect EndMT [27]. These other epigenetic modulators affecting EndMT are not the focus of this review but are described elsewhere [27]. Fourth, it is thought that EMT and EndMT occur via similar mechanisms. Importantly, the miRNA signatures between human corneal endothelium tissues and corneal epithelium tissues did not differ much even though the gene signatures were very different [138]. This might suggest that non-coding RNAs function in similar ways in both epithelial and endothelial cells. Of course, we have to establish whether this is similar for other tissues as well. As a further point of consideration, it has been shown that the miRNA signatures of cultured human corneal endothelial cells were very different than those from fresh corneal endothelium tissue [138]. The same is true for cultured HUVECs when comparing them to freshly isolate tissue-derived umbilical cord human vascular endothelial cells [139]. Furthermore, the overall miRNA expression also decreased significantly in cultured HUVECs when compared to tissue-derived endothelial cells, and miRNA content appears to be lost during passaging of HUVECs [139]. The most downregulated miRNA during culturing is miR-126 and the most upregulated miRNA is miR-21 [139]. Also during culturing of HUVECs, the pro-fibrotic miRNAs miR-21-5p and miR-31-5p were upregulated whereas the

anti-fibrotic miRNAs miR-126-3p, Let-7 family and miR-29 family were downregulated, suggesting a transition towards a mesenchymal cell type in aging cells [139]. As a whole this indicates that the miRNA profile is highly adaptable and that cultured cells may not always represent the best model system for studying miRNA function – proper *in vivo* validation will remain as the gold standard.

It is clear in this emerging field that non-coding RNAs appear to be important players during EndMT. Indeed, as we have reviewed, non-coding RNAs interact with EndMT transcription factors, plus endothelial and mesenchymal genes and signaling pathways, ascribing them a likely pivotal role in regulating this process. As such, they represent promising future clinical targets for modulating EndMT and its accompanied pathologies [140, 141]. As a whole, the regulation of EndMT via non-coding RNAs represents a challenging but promising field with many potential opportunities for future therapeutic clinical translation.

ACKNOWLEDGEMENTS

Guido Krenning received support from the Netherlands Organization for Scientific Research/Netherlands Organization for Health Research and Development Innovational Research Incentive #917.16.446. Jason Kovacic acknowledges research support from the National Institutes of Health (R01HL130423, R01HL135093). Gonzalo del Monte-Nieto's research is supported by a Future Leader Fellowship (102036) from the National Heart Foundation of Australia, a Discovery Project (DP190101475) from the Australian Research Council, and start-up funds from Monash University. Melanie Hulshoff received support from a Graduate School of Medical Sciences (GSMS) PhD scholarship, University of Groningen.

REFERENCES

1. Aird WC. Phenotypic heterogeneity of the endothelium: I. Structure, function, and mechanisms. *Circulation research* 2007;100:158-173.
2. Aird WC. Phenotypic heterogeneity of the endothelium: II. Representative vascular beds. *Circulation research* 2007;100:174-190.
3. Markwald RR, Fitzharris TP, Manasek FJ. Structural development of endocardial cushions. *The American journal of anatomy* 1977;148:85-119.
4. Markwald RR, Fitzharris TP, Smith WN. Structural analysis of endocardial cytodifferentiation. *Developmental biology* 1975;42:160-180.
5. Ma L, Lu MF, Schwartz RJ, Martin JF. Bmp2 is essential for cardiac cushion epithelial-mesenchymal transition and myocardial patterning. *Development* 2005;132:5601-5611.
6. Yamada M, Revelli JP, Eichele G, Barron M, Schwartz RJ. Expression of chick Tbx-2, Tbx-3, and Tbx-5 genes during early heart development: evidence for BMP2 induction of Tbx2. *Developmental biology* 2000;228:95-105.
7. Arciniegas E, Neves CY, Carrillo LM, Zambrano EA, Ramirez R. Endothelial-mesenchymal transition occurs during embryonic pulmonary artery development. *Endothelium : journal of endothelial cell research* 2005;12:193-200.
8. DeRuiter MC, Poelmann RE, VanMunsteren JC, Mironov V, Markwald RR, Gittenberger-de Groot AC. Embryonic endothelial cells transdifferentiate into mesenchymal cells expressing smooth muscle actins in vivo and in vitro. *Circulation research* 1997;80:444-451.
9. Welch-Reardon KM, Wu N, Hughes CC. A role for partial endothelial-mesenchymal transitions in angiogenesis? *Arteriosclerosis, thrombosis, and vascular biology* 2015;35:303-308.
10. Del Monte-Nieto G, Ramalison M, Adam AAS, Wu B, Aharonov A, D'Uva G, et al. Control of cardiac jelly dynamics by NOTCH1 and NRG1 defines the building plan for trabeculation. *Nature* 2018;557:439-445.
11. Ranchoux B, Antigny F, Rucker-Martin C, Hautefort A, Pechoux C, Bogaard HJ, et al. Endothelial-to-mesenchymal transition in pulmonary hypertension. *Circulation* 2015;131:1006-1018.
12. Chen PY, Qin L, Baeyens N, Li G, Afolabi T, Budatha M, et al. Endothelial-to-mesenchymal transition drives atherosclerosis progression. *The Journal of clinical investigation* 2015;125:4514-4528.
13. Souilhol C, Harmsen MC, Evans PC, Krenning G. Endothelial-mesenchymal transition in atherosclerosis. *Cardiovascular research* 2018;114:565-577.
14. Maddaluno L, Rudini N, Cuttano R, Bravi L, Giampietro C, Corada M, et al. EndMT contributes to the onset and progression of cerebral cavernous malformations. *Nature* 2013;498:492-496.
15. Hashimoto N, Phan SH, Imaizumi K, Matsuo M, Nakashima H, Kawabe T, et al. Endothelial-mesenchymal transition in bleomycin-induced pulmonary fibrosis. *American journal of respiratory cell and molecular biology* 2010;43:161-172.

16. Zeisberg EM, Potenta SE, Sugimoto H, Zeisberg M, Kalluri R. Fibroblasts in kidney fibrosis emerge via endothelial-to-mesenchymal transition. *Journal of the American Society of Nephrology* : JASN 2008;19:2282-2287.
17. Zeisberg EM, Tarnavski O, Zeisberg M, Dorfman AL, McMullen JR, Gustafsson E, et al. Endothelial-to-mesenchymal transition contributes to cardiac fibrosis. *Nature medicine* 2007;13:952-961.
18. Zeisberg EM, Potenta S, Xie L, Zeisberg M, Kalluri R. Discovery of endothelial to mesenchymal transition as a source for carcinoma-associated fibroblasts. *Cancer research* 2007;67:10123-10128.
19. Hong L, Du X, Li W, Mao Y, Sun L, Li X. EndMT: A promising and controversial field. *Eur J Cell Biol* 2018;97:493-500.
20. Moonen JR, Lee ES, Schmidt M, Maleszewska M, Koerts JA, Brouwer LA, et al. Endothelial-to-mesenchymal transition contributes to fibro-proliferative vascular disease and is modulated by fluid shear stress. *Cardiovascular research* 2015;108:377-386.
21. Widyantoro B, Emoto N, Nakayama K, Anggrahini DW, Adiarto S, Iwasa N, et al. Endothelial cell-derived endothelin-1 promotes cardiac fibrosis in diabetic hearts through stimulation of endothelial-to-mesenchymal transition. *Circulation* 2010;121:2407-2418.
22. Maleszewska M, Gjaltema RA, Krenning G, Harmsen MC. Enhancer of zeste homolog-2 (EZH2) methyltransferase regulates transgelin/smooth muscle-22alpha expression in endothelial cells in response to interleukin-1beta and transforming growth factor-beta2. *Cellular signalling* 2015;27:1589-1596.
23. Xu X, Tan X, Hulshoff MS, Wilhelmi T, Zeisberg M, Zeisberg EM. Hypoxia-induced endothelial-mesenchymal transition is associated with RASAL1 promoter hypermethylation in human coronary endothelial cells. *FEBS letters* 2016;590:1222-1233.
24. Mahler GJ, Farrar EJ, Butcher JT. Inflammatory cytokines promote mesenchymal transformation in embryonic and adult valve endothelial cells. *Arteriosclerosis, thrombosis, and vascular biology* 2013;33:121-130.
25. van Meeteren LA, ten Dijke P. Regulation of endothelial cell plasticity by TGF-beta. *Cell and tissue research* 2012;347:177-186.
26. Xu S, Kamato D, Little PJ, Nakagawa S, Pelisek J, Jin ZG. Targeting epigenetics and non-coding RNAs in atherosclerosis: from mechanisms to therapeutics. *Pharmacol Ther* 2018.
27. Hulshoff MS, Xu X, Krenning G, Zeisberg EM. Epigenetic Regulation of Endothelial-to-Mesenchymal Transition in Chronic Heart Disease. *Arteriosclerosis, thrombosis, and vascular biology* 2018;38:1986-1996.
28. Kim J. MicroRNAs as critical regulators of the endothelial to mesenchymal transition in vascular biology. *BMB Rep* 2018;51:65-72.
29. Kovacic JC, Dimmeler S, Harvey RP, Finkel T, Aikawa E, Krenning G, et al. Endothelial to Mesenchymal Transition in Cardiovascular Disease: JACC State-of-the-Art Review. *J Am Coll Cardiol* 2019;73:190-209.
30. Garside VC, Chang AC, Karsan A, Hoodless PA. Co-ordinating Notch, BMP, and TGF-beta signaling during heart valve development. *Cellular and molecular life sciences : CMLS* 2013;70:2899-2917.

31. Yamagishi T, Ando K, Nakamura H. Roles of TGFbeta and BMP during valvulo-septal endocardial cushion formation. *Anatomical science international* 2009;84:77-87.
32. Derynck R, Zhang YE. Smad-dependent and Smad-independent pathways in TGF-beta family signalling. *Nature* 2003;425:577-584.
33. Zhang YE. Non-Smad pathways in TGF-beta signaling. *Cell research* 2009;19:128-139.
34. Hata A, Chen YG. TGF-beta Signaling from Receptors to Smads. *Cold Spring Harbor perspectives in biology* 2016;8.
35. Peinado H, Olmeda D, Cano A. Snail, Zeb and bHLH factors in tumour progression: an alliance against the epithelial phenotype? *Nature reviews Cancer* 2007;7:415-428.
36. Lander R, Nasr T, Ochoa SD, Nordin K, Prasad MS, Labonne C. Interactions between Twist and other core epithelial-mesenchymal transition factors are controlled by GSK3-mediated phosphorylation. *Nature communications* 2013;4:1542.
37. Peiro S, Escriva M, Puig I, Barbera MJ, Dave N, Herranz N, et al. Snail1 transcriptional repressor binds to its own promoter and controls its expression. *Nucleic Acids Res* 2006;34:2077-2084.
38. Takkunen M, Grenman R, Hukkanen M, Korhonen M, Garcia de Herreros A, Virtanen I. Snail-dependent and -independent epithelial-mesenchymal transition in oral squamous carcinoma cells. *The journal of histochemistry and cytochemistry : official journal of the Histochemistry Society* 2006;54:1263-1275.
39. Wels C, Joshi S, Koefinger P, Bergler H, Schaidt H. Transcriptional activation of ZEB1 by Slug leads to cooperative regulation of the epithelial-mesenchymal transition-like phenotype in melanoma. *The Journal of investigative dermatology* 2011;131:1877-1885.
40. Dufton NP, Peghaire CR, Osuna-Almagro L, Raimondi C, Kalna V, Chuahan A, et al. Dynamic regulation of canonical TGFbeta signalling by endothelial transcription factor ERG protects from liver fibrogenesis. *Nature communications* 2017;8:895.
41. Rivera-Feliciano J, Lee KH, Kong SW, Rajagopal S, Ma Q, Springer Z, et al. Development of heart valves requires Gata4 expression in endothelial-derived cells. *Development* 2006;133:3607-3618.
42. Rivera-Feliciano J, Tabin CJ. Bmp2 instructs cardiac progenitors to form the heart-valve-inducing field. *Developmental biology* 2006;295:580-588.
43. McCulley DJ, Kang JO, Martin JF, Black BL. BMP4 is required in the anterior heart field and its derivatives for endocardial cushion remodeling, outflow tract septation, and semilunar valve development. *Developmental dynamics : an official publication of the American Association of Anatomists* 2008;237:3200-3209.
44. Xu X, Tan X, Tampe B, Nyamsuren G, Liu X, Maier LS, et al. Epigenetic balance of aberrant Rasal1 promoter methylation and hydroxymethylation regulates cardiac fibrosis. *Cardiovascular research* 2015;105:279-291.
45. Timmerman LA, Grego-Bessa J, Raya A, Bertran E, Perez-Pomares JM, Diez J, et al. Notch promotes epithelial-mesenchymal transition during cardiac development and oncogenic transformation. *Genes & development* 2004;18:99-115.
46. Niessen K, Fu Y, Chang L, Hoodless PA, McFadden D, Karsan A. Slug is a direct Notch target required for initiation of cardiac cushion cellularization. *The Journal of cell biology* 2008;182:315-325.

47. Luna-Zurita L, Prados B, Grego-Bessa J, Luxan G, del Monte G, Benguria A, et al. Integration of a Notch-dependent mesenchymal gene program and Bmp2-driven cell invasiveness regulates murine cardiac valve formation. *The Journal of clinical investigation* 2010;120:3493-3507.
48. Hurlstone AF, Haramis AP, Wienholds E, Begthel H, Korving J, Van Eeden F, et al. The Wnt/beta-catenin pathway regulates cardiac valve formation. *Nature* 2003;425:633-637.
49. Liebner S, Cattelino A, Gallini R, Rudini N, Iurlaro M, Piccolo S, et al. Beta-catenin is required for endothelial-mesenchymal transformation during heart cushion development in the mouse. *The Journal of cell biology* 2004;166:359-367.
50. Gessert S, Kuhl M. The multiple phases and faces of wnt signaling during cardiac differentiation and development. *Circulation research* 2010;107:186-199.
51. Aisagbonhi O, Rai M, Ryzhov S, Atria N, Feoktistov I, Hatzopoulos AK. Experimental myocardial infarction triggers canonical Wnt signaling and endothelial-to-mesenchymal transition. *Disease models & mechanisms* 2011;4:469-483.
52. Thornton TM, Pedraza-Alva G, Deng B, Wood CD, Aronshtam A, Clements JL, et al. Phosphorylation by p38 MAPK as an alternative pathway for GSK3beta inactivation. *Science* 2008;320:667-670.
53. Cheng SL, Shao JS, Behrmann A, Krchma K, Towler DA. Dkk1 and MSX2-Wnt7b signaling reciprocally regulate the endothelial-mesenchymal transition in aortic endothelial cells. *Arteriosclerosis, thrombosis, and vascular biology* 2013;33:1679-1689.
54. Maleszewska M, Moonen JR, Huijckman N, van de Sluis B, Krenning G, Harmsen MC. IL-1beta and TGFbeta2 synergistically induce endothelial to mesenchymal transition in an NFkappaB-dependent manner. *Immunobiology* 2013;218:443-454.
55. Wu Y, Deng J, Rychahou PG, Qiu S, Evers BM, Zhou BP. Stabilization of snail by NF-kappaB is required for inflammation-induced cell migration and invasion. *Cancer cell* 2009;15:416-428.
56. Julien S, Puig I, Caretti E, Bonaventure J, Nelles L, van Roy F, et al. Activation of NF-kappa B by Akt upregulates Snail expression and induces epithelium mesenchyme transition. *Oncogene* 2007;26:7445-7456.
57. Johnson DE, Williams LT. Structural and functional diversity in the FGF receptor multigene family. *Advances in cancer research* 1993;60:1-41.
58. Chen PY, Qin L, Tellides G, Simons M. Fibroblast growth factor receptor 1 is a key inhibitor of TGFbeta signaling in the endothelium. *Science signaling* 2014;7:ra90.
59. Mahmoud MM, Kim HR, Xing R, Hsiao S, Mammoto A, Chen J, et al. TWIST1 Integrates Endothelial Responses to Flow in Vascular Dysfunction and Atherosclerosis. *Circulation research* 2016;119:450-462.
60. Mahmoud MM, Serbanovic-Canic J, Feng S, Souilhol C, Xing R, Hsiao S, et al. Shear stress induces endothelial-to-mesenchymal transition via the transcription factor Snail. *Scientific reports* 2017;7:3375.
61. Semenza GL. HIF-1: mediator of physiological and pathophysiological responses to hypoxia. *Journal of applied physiology* 2000;88:1474-1480.
62. Xu X, Tan X, Tampe B, Sanchez E, Zeisberg M, Zeisberg EM. Snail Is a Direct Target of Hypoxia-inducible Factor 1alpha (HIF1alpha) in Hypoxia-induced Endothelial to

- Mesenchymal Transition of Human Coronary Endothelial Cells. *The Journal of biological chemistry* 2015;290:16653-16664.
63. Yang MH, Wu MZ, Chiou SH, Chen PM, Chang SY, Liu CJ, et al. Direct regulation of TWIST by HIF-1 α promotes metastasis. *Nature cell biology* 2008;10:295-305.
 64. Evrard SM, Lecce L, Michelis KC, Nomura-Kitabayashi A, Pandey G, Purushothaman KR, et al. Endothelial to mesenchymal transition is common in atherosclerotic lesions and is associated with plaque instability. *Nature communications* 2016;7:11853.
 65. Dong WQ, Chao M, Lu QH, Chai WL, Zhang W, Chen XY, et al. Prohibitin overexpression improves myocardial function in diabetic cardiomyopathy. *Oncotarget* 2016;7:66-80.
 66. Gu S, Kay MA. How do miRNAs mediate translational repression? *Silence* 2010;1:11.
 67. Kung JT, Colognori D, Lee JT. Long noncoding RNAs: past, present, and future. *Genetics* 2013;193:651-669.
 68. Li Z, Huang C, Bao C, Chen L, Lin M, Wang X, et al. Exon-intron circular RNAs regulate transcription in the nucleus. *Nature structural & molecular biology* 2015;22:256-264.
 69. Hansen TB, Jensen TI, Clausen BH, Bramsen JB, Finsen B, Damgaard CK, et al. Natural RNA circles function as efficient microRNA sponges. *Nature* 2013;495:384-388.
 70. Zhang Y, Zhang XO, Chen T, Xiang JF, Yin QF, Xing YH, et al. Circular intronic long noncoding RNAs. *Molecular cell* 2013;51:792-806.
 71. Ashwal-Fluss R, Meyer M, Pamudurti NR, Ivanov A, Bartok O, Hanan M, et al. circRNA biogenesis competes with pre-mRNA splicing. *Molecular cell* 2014;56:55-66.
 72. Hentze MW, Preiss T. Circular RNAs: splicing's enigma variations. *The EMBO journal* 2013;32:923-925.
 73. Wilusz JE, Sharp PA. *Molecular biology*. A circuitous route to noncoding RNA. *Science* 2013;340:440-441.
 74. Ghosh AK, Nagpal V, Covington JW, Michaels MA, Vaughan DE. Molecular basis of cardiac endothelial-to-mesenchymal transition (EndMT): differential expression of microRNAs during EndMT. *Cellular signalling* 2012;24:1031-1036.
 75. Suzuki HI, Katsura A, Mihira H, Horie M, Saito A, Miyazono K. Regulation of TGF- β -mediated endothelial-mesenchymal transition by microRNA-27. *J Biochem* 2017;161:417-420.
 76. Guo Y, Li P, Bledsoe G, Yang ZR, Chao L, Chao J. Kallistatin inhibits TGF- β -induced endothelial-mesenchymal transition by differential regulation of microRNA-21 and eNOS expression. *Exp Cell Res* 2015;337:103-110.
 77. Kumarswamy R, Volkman I, Jazbutyte V, Dangwal S, Park DH, Thum T. Transforming growth factor- β -induced endothelial-to-mesenchymal transition is partly mediated by microRNA-21. *Arteriosclerosis, thrombosis, and vascular biology* 2012;32:361-369.
 78. Kwon OS, Kim KT, Lee E, Kim M, Choi SH, Li H, et al. Induction of MiR-21 by Stereotactic Body Radiotherapy Contributes to the Pulmonary Fibrotic Response. *PloS one* 2016;11:e0154942.
 79. Katsura A, Suzuki HI, Ueno T, Mihira H, Yamazaki T, Yasuda T, et al. MicroRNA-31 is a positive modulator of endothelial-mesenchymal transition and associated secretory phenotype induced by TGF- β . *Genes Cells* 2016;21:99-116.

80. Colangelo T, Fucci A, Votino C, Sabatino L, Pancione M, Laudanna C, et al. MicroRNA-130b promotes tumor development and is associated with poor prognosis in colorectal cancer. *Neoplasia* 2013;15:1086-1099.
81. Li L, Kim IK, Chiasson V, Chatterjee P, Gupta S. NF-kappaB mediated miR-130a modulation in lung microvascular cell remodeling: Implication in pulmonary hypertension. *Exp Cell Res* 2017;359:235-242.
82. Jiang L, Hao C, Li Z, Zhang P, Wang S, Yang S, et al. miR-449a induces EndMT, promotes the development of atherosclerosis by targeting the interaction between AdipoR2 and E-cadherin in Lipid Rafts. *Biomed Pharmacother* 2019;109:2293-2304.
83. Vanchin B, Offringa E, Friedrich J, Brinker MG, Kiers B, Pereira AC, et al. MicroRNA-374b induces endothelial-to-mesenchymal transition and early lesion formation through the inhibition of MAPK7 signaling. *The Journal of pathology* 2018.
84. Chen Y, Yang Q, Zhan Y, Ke J, Lv P, Huang J. The role of miR-328 in high glucose-induced endothelial-to-mesenchymal transition in human umbilical vein endothelial cells. *Life Sci* 2018;207:110-116.
85. Chakraborty S, Zawieja DC, Davis MJ, Muthuchamy M. MicroRNA signature of inflamed lymphatic endothelium and role of miR-9 in lymphangiogenesis and inflammation. *Am J Physiol Cell Physiol* 2015;309:C680-692.
86. Yan XC, Cao J, Liang L, Wang L, Gao F, Yang ZY, et al. miR-342-5p Is a Notch Downstream Molecule and Regulates Multiple Angiogenic Pathways Including Notch, Vascular Endothelial Growth Factor and Transforming Growth Factor beta Signaling. *J Am Heart Assoc* 2016;5.
87. Bonet F, Duenas A, Lopez-Sanchez C, Garcia-Martinez V, Aranega AE, Franco D. MiR-23b and miR-199a impair epithelial-to-mesenchymal transition during atrioventricular endocardial cushion formation. *Developmental dynamics : an official publication of the American Association of Anatomists* 2015;244:1259-1275.
88. Legendijk AK, Goumans MJ, Burkhard SB, Bakkers J. MicroRNA-23 restricts cardiac valve formation by inhibiting Has2 and extracellular hyaluronic acid production. *Circulation research* 2011;109:649-657.
89. Yi M, Liu B, Tang Y, Li F, Qin W, Yuan X. Irradiated Human Umbilical Vein Endothelial Cells Undergo Endothelial-Mesenchymal Transition via the Snail/miR-199a-5p Axis to Promote the Differentiation of Fibroblasts into Myofibroblasts. *Biomed Res Int* 2018;2018:4135806.
90. Esmerats JF, Villa-Roel N, Kumar S, Gu L, Salim MT, Ohh M, et al. Disturbed Flow Increases UBE2C (Ubiquitin E2 Ligase C) via Loss of miR-483-3p, Inducing Aortic Valve Calcification by the HIF-1alpha (Hypoxia-Inducible Factor-1alpha) Pathway in Endothelial Cells. *Arteriosclerosis, thrombosis, and vascular biology* 2019:ATVBAHA118312233.
91. He M, Chen Z, Martin M, Zhang J, Sangwung P, Woo B, et al. miR-483 Targeting of CTGF Suppresses Endothelial-to-Mesenchymal Transition: Therapeutic Implications in Kawasaki Disease. *Circulation research* 2017;120:354-365.
92. Song H, Wang Q, Wen J, Liu S, Gao X, Cheng J, et al. ACVR1, a therapeutic target of fibrodysplasia ossificans progressiva, is negatively regulated by miR-148a. *Int J Mol Sci* 2012;13:2063-2077.

93. Miscianinov V, Martello A, Rose L, Parish E, Cathcart B, Mitic T, et al. MicroRNA-148b Targets the TGF-beta Pathway to Regulate Angiogenesis and Endothelial-to-Mesenchymal Transition during Skin Wound Healing. *Mol Ther* 2018;26:1996-2007.
94. Chen PY, Qin L, Barnes C, Charisse K, Yi T, Zhang X, et al. FGF regulates TGF-beta signaling and endothelial-to-mesenchymal transition via control of let-7 miRNA expression. *Cell Rep* 2012;2:1684-1696.
95. Terzuoli E, Nannelli G, Giachetti A, Morbidelli L, Ziche M, Donnini S. Targeting endothelial-to-mesenchymal transition: the protective role of hydroxytyrosol sulfate metabolite. *Eur J Nutr* 2019.
96. Takagi K, Yamakuchi M, Matsuyama T, Kondo K, Uchida A, Misono S, et al. IL-13 enhances mesenchymal transition of pulmonary artery endothelial cells via down-regulation of miR-424/503 in vitro. *Cellular signalling* 2018;42:270-280.
97. Geng H, Guan J. MiR-18a-5p inhibits endothelial-mesenchymal transition and cardiac fibrosis through the Notch2 pathway. *Biochem Biophys Res Commun* 2017;491:329-336.
98. Bayoumi AS, Teoh JP, Aonuma T, Yuan Z, Ruan X, Tang Y, et al. MicroRNA-532 protects the heart in acute myocardial infarction, and represses prss23, a positive regulator of endothelial-to-mesenchymal transition. *Cardiovascular research* 2017;113:1603-1614.
99. Zhu K, Pan Q, Jia LQ, Dai Z, Ke AW, Zeng HY, et al. MiR-302c inhibits tumor growth of hepatocellular carcinoma by suppressing the endothelial-mesenchymal transition of endothelial cells. *Scientific reports* 2014;4:5524.
100. Zhu YT, Li F, Han B, Tighe S, Zhang S, Chen SY, et al. Activation of RhoA-ROCK-BMP signaling reprograms adult human corneal endothelial cells. *The Journal of cell biology* 2014;206:799-811.
101. Lun W, Wu X, Deng Q, Zhi F. MiR-218 regulates epithelial-mesenchymal transition and angiogenesis in colorectal cancer via targeting CTGF. *Cancer Cell Int* 2018;18:83.
102. Chen Y, Banda M, Speyer CL, Smith JS, Rabson AB, Gorski DH. Regulation of the expression and activity of the antiangiogenic homeobox gene GAX/MEOX2 by ZEB2 and microRNA-221. *Mol Cell Biol* 2010;30:3902-3913.
103. Chen S, Zhao G, Miao H, Tang R, Song Y, Hu Y, et al. MicroRNA-494 inhibits the growth and angiogenesis-regulating potential of mesenchymal stem cells. *FEBS letters* 2015;589:710-717.
104. Kim DY, Woo YM, Lee S, Oh S, Shin Y, Shin JO, et al. Impact of miR-192 and miR-194 on cyst enlargement through EMT in autosomal dominant polycystic kidney disease. *FASEB J* 2019;33:2870-2884.
105. Liu F, Zhang S, Xu R, Gao S, Yin J. Melatonin Attenuates Endothelial-to-Mesenchymal Transition of Glomerular Endothelial Cells via Regulating miR-497/ROCK in Diabetic Nephropathy. *Kidney Blood Press Res* 2018;43:1425-1436.
106. Kanasaki K, Shi S, Kanasaki M, He J, Nagai T, Nakamura Y, et al. Linagliptin-mediated DPP-4 inhibition ameliorates kidney fibrosis in streptozotocin-induced diabetic mice by inhibiting endothelial-to-mesenchymal transition in a therapeutic regimen. *Diabetes* 2014;63:2120-2131.

107. Shi S, Kanasaki K, Koya D. Linagliptin but not Sitagliptin inhibited transforming growth factor-beta2-induced endothelial DPP-4 activity and the endothelial-mesenchymal transition. *Biochem Biophys Res Commun* 2016;471:184-190.
108. Srivastava SP, Shi S, Kanasaki M, Nagai T, Kitada M, He J, et al. Effect of Antifibrotic MicroRNAs Crosstalk on the Action of N-acetyl-seryl-aspartyl-lysyl-proline in Diabetes-related Kidney Fibrosis. *Scientific reports* 2016;6:29884.
109. Nagai T, Kanasaki M, Srivastava SP, Nakamura Y, Ishigaki Y, Kitada M, et al. N-acetyl-seryl-aspartyl-lysyl-proline inhibits diabetes-associated kidney fibrosis and endothelial-mesenchymal transition. *Biomed Res Int* 2014;2014:696475.
110. Zhang H, Hu J, Liu L. MiR-200a modulates TGF-beta1-induced endothelial-to-mesenchymal shift via suppression of GRB2 in HAECs. *Biomed Pharmacother* 2017;95:215-222.
111. Cao Y, Feng B, Chen S, Chu Y, Chakrabarti S. Mechanisms of endothelial to mesenchymal transition in the retina in diabetes. *Invest Ophthalmol Vis Sci* 2014;55:7321-7331.
112. Feng B, Cao Y, Chen S, Chu X, Chu Y, Chakrabarti S. miR-200b Mediates Endothelial-to-Mesenchymal Transition in Diabetic Cardiomyopathy. *Diabetes* 2016;65:768-779.
113. Chan YC, Khanna S, Roy S, Sen CK. miR-200b targets Ets-1 and is down-regulated by hypoxia to induce angiogenic response of endothelial cells. *The Journal of biological chemistry* 2011;286:2047-2056.
114. Maleki S, Cottrill KA, Poujade FA, Bhattachariya A, Bergman O, Gadin JR, et al. The mir-200 family regulates key pathogenic events in ascending aortas of individuals with bicuspid aortic valves. *J Intern Med* 2019;285:102-114.
115. Yang B, Zhou W, Jiao J, Nielsen JB, Mathis MR, Heydarpour M, et al. Protein-altering and regulatory genetic variants near GATA4 implicated in bicuspid aortic valve. *Nature communications* 2017;8:15481.
116. Gill JG, Langer EM, Lindsley RC, Cai M, Murphy TL, Murphy KM. Snail promotes the cell-autonomous generation of Flk1(+) endothelial cells through the repression of the microRNA-200 family. *Stem Cells Dev* 2012;21:167-176.
117. Kim Y, Kim N, Park SW, Kim H, Park HJ, Han YM. Lineage-specific Expression of miR-200 Family in Human Embryonic Stem Cells during In Vitro Differentiation. *Int J Stem Cells* 2017;10:28-37.
118. Nagai N, Ohguchi H, Nakaki R, Matsumura Y, Kanki Y, Sakai J, et al. Downregulation of ERG and FLI1 expression in endothelial cells triggers endothelial-to-mesenchymal transition. *PLoS Genet* 2018;14:e1007826.
119. Zhang J, Zhang Z, Zhang DY, Zhu J, Zhang T, Wang C. microRNA 126 inhibits the transition of endothelial progenitor cells to mesenchymal cells via the PI3K2-PI3K/Akt signalling pathway. *PloS one* 2013;8:e83294.
120. Xu YP, He Q, Shen Z, Shu XL, Wang CH, Zhu JJ, et al. MiR-126a-5p is involved in the hypoxia-induced endothelial-to-mesenchymal transition of neonatal pulmonary hypertension. *Hypertens Res* 2017;40:552-561.
121. Wang J, He W, Xu X, Guo L, Zhang Y, Han S, et al. The mechanism of TGF-beta/miR-155/c-Ski regulates endothelial-mesenchymal transition in human coronary artery endothelial cells. *Biosci Rep* 2017;37.

122. Bijkerk R, de Bruin RG, van Solingen C, Duijs JM, Kobayashi K, van der Veer EP, et al. MicroRNA-155 functions as a negative regulator of RhoA signaling in TGF-beta-induced endothelial to mesenchymal transition. *Microna* 2012;1:2-10.
123. Bai Y, Wang J, Morikawa Y, Bonilla-Claudio M, Klysik E, Martin JF. Bmp signaling represses Vegfa to promote outflow tract cushion development. *Development* 2013;140:3395-3402.
124. Correia AC, Moonen JR, Brinker MG, Krenning G. FGF2 inhibits endothelial-mesenchymal transition through microRNA-20a-mediated repression of canonical TGF-beta signaling. *J Cell Sci* 2016;129:569-579.
125. Xiang Y, Zhang Y, Tang Y, Li Q. MALAT1 Modulates TGF-beta1-Induced Endothelial-to-Mesenchymal Transition through Downregulation of miR-145. *Cell Physiol Biochem* 2017;42:357-372.
126. Neumann P, Jae N, Knau A, Glaser SF, Fouani Y, Rossbach O, et al. The lncRNA GATA6-AS epigenetically regulates endothelial gene expression via interaction with LOXL2. *Nature communications* 2018;9:237.
127. Chang Z, Cui J, Song Y. Long noncoding RNA PVT1 promotes EMT via mediating microRNA-186 targeting of Twist1 in prostate cancer. *Gene* 2018;654:36-42.
128. Thomas AA, Biswas S, Feng B, Chen S, Gonder J, Chakrabarti S. lncRNA H19 prevents endothelial-mesenchymal transition in diabetic retinopathy. *Diabetologia* 2019.
129. Zhao X, Sun B, Liu T, Shao B, Sun R, Zhu D, et al. Long noncoding RNA n339260 promotes vasculogenic mimicry and cancer stem cell development in hepatocellular carcinoma. *Cancer Sci* 2018;109:3197-3208.
130. Yang L, Han B, Zhang Y, Bai Y, Chao J, Hu G, et al. Engagement of circular RNA HECW2 in the nonautophagic role of ATG5 implicated in the endothelial-mesenchymal transition. *Autophagy* 2018;14:404-418.
131. Zhong Z, Huang M, Lv M, He Y, Duan C, Zhang L, et al. Circular RNA MYLK as a competing endogenous RNA promotes bladder cancer progression through modulating VEGFA/VEGFR2 signaling pathway. *Cancer letters* 2017;403:305-317.
132. Luo M, Hou L, Li J, Shao S, Huang S, Meng D, et al. VEGF/NRP-1axis promotes progression of breast cancer via enhancement of epithelial-mesenchymal transition and activation of NF-kappaB and beta-catenin. *Cancer letters* 2016;373:1-11.
133. Park HY, Kim JH, Park CK. VEGF induces TGF-beta1 expression and myofibroblast transformation after glaucoma surgery. *The American journal of pathology* 2013;182:2147-2154.
134. Tran H, Bustos D, Yeh R, Rubinfeld B, Lam C, Shriver S, et al. HectD1 E3 ligase modifies adenomatous polyposis coli (APC) with polyubiquitin to promote the APC-axin interaction. *The Journal of biological chemistry* 2013;288:3753-3767.
135. Fang S, Guo H, Cheng Y, Zhou Z, Zhang W, Han B, et al. circHECTD1 promotes the silica-induced pulmonary endothelial-mesenchymal transition via HECTD1. *Cell Death Dis* 2018;9:396.
136. Bai Y, Zhang Y, Han B, Yang L, Chen X, Huang R, et al. Circular RNA DLGAP4 Ameliorates Ischemic Stroke Outcomes by Targeting miR-143 to Regulate Endothelial-Mesenchymal Transition Associated with Blood-Brain Barrier Integrity. *J Neurosci* 2018;38:32-50.

137. Huang X, Chen Y, Xiao J, Huang Z, He L, Xu D, et al. Identification of differentially expressed circular RNAs during TGF- β 1-induced endothelial-to-mesenchymal transition in rat coronary artery endothelial cells. *Anatol J Cardiol* 2018;19:192-197.
138. Ueno M, Asada K, Toda M, Schlotzer-Schrehardt U, Nagata K, Montoya M, et al. Gene Signature-Based Development of ELISA Assays for Reproducible Qualification of Cultured Human Corneal Endothelial Cells. *Invest Ophthalmol Vis Sci* 2016;57:4295-4305.
139. Kuosmanen SM, Kansanen E, Sihvola V, Levenon AL. MicroRNA Profiling Reveals Distinct Profiles for Tissue-Derived and Cultured Endothelial Cells. *Scientific reports* 2017;7:10943.
140. Jackson AO, Zhang J, Jiang Z, Yin K. Endothelial-to-mesenchymal transition: A novel therapeutic target for cardiovascular diseases. *Trends Cardiovasc Med* 2017;27:383-393.
141. Chen PY, Simons M. Future Targets in Endothelial Biology: Endothelial Cell to Mesenchymal Transition. *Curr Drug Targets* 2016;17:1707-1713.

CHAPTER

6

STAGE-SPECIFIC MAPPING OF THE ENDOTHELIAL-TO-MESENCHYMAL TRANSITION

Melanie S. Hulshoff^{1,2,3,*}, Xingbo Xu^{1,2,*}, Jirko Kühnisch^{4,5}, Xiaoying Tan^{2,6}, Michael Zeisberg^{2,6}, Guido Krenning³, Sabine Klaassen^{4,5,7}, Elisabeth M. Zeisberg^{1,2}

¹*Department of Cardiology and Pneumology, University Medical Center of Göttingen, Georg-August University, Göttingen, Germany.*

²*German Centre for Cardiovascular Research (DZHK), Göttingen, Germany.*

³*Department of Pathology and Medical Biology, University Medical Center Groningen, Hanzeplein 1, 9713 GZ, Groningen, The Netherlands.*

⁴*Experimental and Clinical Research Center, Charite University Medicine Berlin, Humboldt University of Berlin, Berlin, Germany.*

⁵*German Centre for Cardiovascular Research (DZHK), Berlin, Germany.*

⁶*Department of Nephrology and Rheumatology, University Medical Center of Göttingen, Georg-August University, Göttingen, Germany.*

⁷*Department of Pediatric Cardiology, Charite University Medicine Berlin, Humboldt University of Berlin, Berlin, Germany.*

**Authors contributed equally*

In preparation

ABSTRACT

Endothelial-to-mesenchymal transition (EndMT) is a process in which endothelial cells change into mesenchymal cells. EndMT was initially identified during the development of the heart, but is now increasingly recognized to occur during adult life where it contributes to several pathologies such as organ fibrosis and cardiovascular disease. So far, investigations on EndMT have primarily focused on the initiating events that induce EndMT (the naive endothelial cells) and the final stage of EndMT (the fully transitioned endothelial-derived myofibroblast-like cells). The cells actively undergoing EndMT is not or less often investigated. The aim of this study is to discover the transcriptional patterns that highlight the “active stage” of transformation of EndMT. We established an in vitro system (based on CD31 and CD90 expression) to identify different stages of EndMT: naive endothelial cells (CD31+CD90-), cells actively undergoing EndMT (CD31+CD90+) and endothelial-derived myofibroblasts (CD31-CD90-). We determined the transcriptome of each population by next generation sequencing and identified Rap1 signaling to be primarily involved in the active stage of EndMT. We demonstrate that inhibition of Rap1 signaling in part alleviates EndMT.

INTRODUCTION

Endothelial-to-mesenchymal transition (EndMT) is a cellular transition process in which endothelial cells lose their cell-specific properties and transform into myofibroblast-like cells. This transition process is accompanied by the repression of endothelial markers whereas the expression of mesenchymal markers is induced. EndMT was originally identified in cardiac development [1], but has recently also been described postnatally where it contributes not only to organ fibrosis and cardiovascular disease but also to cancer [2-8]. Remarkably, the underlying mechanisms of EndMT are largely unknown. Moreover, there are no specific inhibitors of EndMT available hitherto.

So far, investigations on EndMT have primarily focused on the final stage of EndMT (the fully transitioned endothelial-derived myofibroblast-like cells). The cells that actively undergo EndMT are not or less often investigated. Moreover, the transcriptional signature and/or markers for the active stage of EndMT are unknown even though these cells might be the most 'targetable' population to combat EndMT in disease context since (1) they have an unique phenotype and (2) patients with chronic illnesses most likely already have ongoing EndMT. Our aim was therefore to discover the transcriptional patterns that highlight the "active stage" of transformation.

We therefore established an *in vitro* marker-based cell sorting system to identify the different stages which was followed by RNA-sequencing to identify the gene signature of the active stage of EndMT. Our results demonstrate the successful separation of the different stages in which we can appreciate different gene signatures. We identified Rap1 signaling to be primarily involved in the active stage of EndMT and demonstrate that inhibition of Rap1 signaling in part alleviates EndMT.

RESULTS

ESTABLISHMENT OF AN *IN VITRO* SYSTEM TO ACHIEVE STAGE-SPECIFIC MAPPING OF ENDMT

We established an *in vitro* system to achieve stage-specific mapping of EndMT. Since cell passage number can greatly influence the expression of endothelial-lineage markers, we made use of early-passage human umbilical vein endothelial cells (HUVECs; passage 3). We first examined two well-known endothelial markers: VE-Cadherin and CD31 [10,11]. The criteria for the endothelial marker should be (1) high expression in endothelial cells under basal conditions. With flow cytometry we observed that 37% of the HUVECs were low-positive for VE-Cadherin whereas 99% of the HUVECs were high-positive for CD31 (Suppl. Fig. 1). Therefore, we decided to continue with CD31 as endothelial marker. CD31 (also known as PECAM1) is a well-known endothelial marker and loss of CD31 expression has been shown to be associated with EndMT [8].

We then continued to examine the expression of different mesenchymal cell markers including CD56, CD90, N-Cadherin, Periostin, α -SMA and S100A4. The criteria for the mesenchymal marker should be (1) absence of or low expression in endothelial cells under basal conditions, (2) increased expression upon induction of EndMT and (3) high expressed in cardiac fibroblasts. HUVECs were treated with TGF- β 1 for 4 days to induce EndMT and subsequently immunostained with CD31 in combination with one of the mentioned mesenchymal markers and then analyzed using flow cytometry. All mesenchymal markers, except for N-Cadherin, were low expressed in HUVECs under basal conditions (Suppl.Fig.2). The expression of the cell-surface marker CD90 increased the most upon TGF- β 1 treatment, but also the expression of the cell-surface marker CD56 and the intracellular marker Periostin were substantially increased after 4 days of TGF- β 1 treatment. The well-known mesenchymal markers S100A4 (FSP1) and α -SMA are also increased upon TGF- β 1 treatment, but to a lesser extent. Since CD56 and CD90 are (1) one of the highest upregulated mesenchymal markers upon TGF- β 1 treatment and (2) are cell-surface proteins, which means that the membrane does not have to be permeabilized for the staining, we selected CD56 and CD90 as possible mesenchymal markers. We then examined the expression of these two markers

in human cardiac fibroblasts (HCFs) and identified that CD56 is low expressed in HCFs whereas 95% of the HCFs is positive for CD90 (Suppl.Fig.3). CD90 (also known as Thy-1) is also known for its expression on fibroblasts [12,13]. Altogether, we selected CD90 as mesenchymal marker.

STAGE-SPECIFIC MAPPING OF ENDMT

After having established our *in vitro* system, our aim was to distinguish three different stages based on CD31 and CD90 expression. Naive endothelial cells are marked by the endothelial marker (CD31+/CD90- population) whereas endothelial-derived myofibroblast-like cells are marked by the mesenchymal marker (CD31-/CD90+ population). The active stage of EndMT is marked by both the endothelial and mesenchymal marker (CD31+/CD90+ population) since these cells gained already expression of the mesenchymal marker CD90 but did not lose their endothelial CD31 expression (Fig.1A). Therefore, we treated HUVECs with TGF- β 1 for four days to induce EndMT and performed live-cell immunostaining for the endothelial marker CD31 and the mesenchymal marker CD90 (Fig. 1B). Upon TGF- β 1-induced EndMT, the naive endothelial cells decreased from 89% to 49% whereas the active EndMT stage and endothelial-derived myofibroblast-like cells increased from 5% to 17% and 0,6% to 6% respectively (Fig.1C). We then isolated RNA from these different stages (n=3) and performed RNA-sequencing to profile the transcriptome of each population. Altogether, this system allows stage-specific analysis of the genetic mechanisms facilitating EndMT.

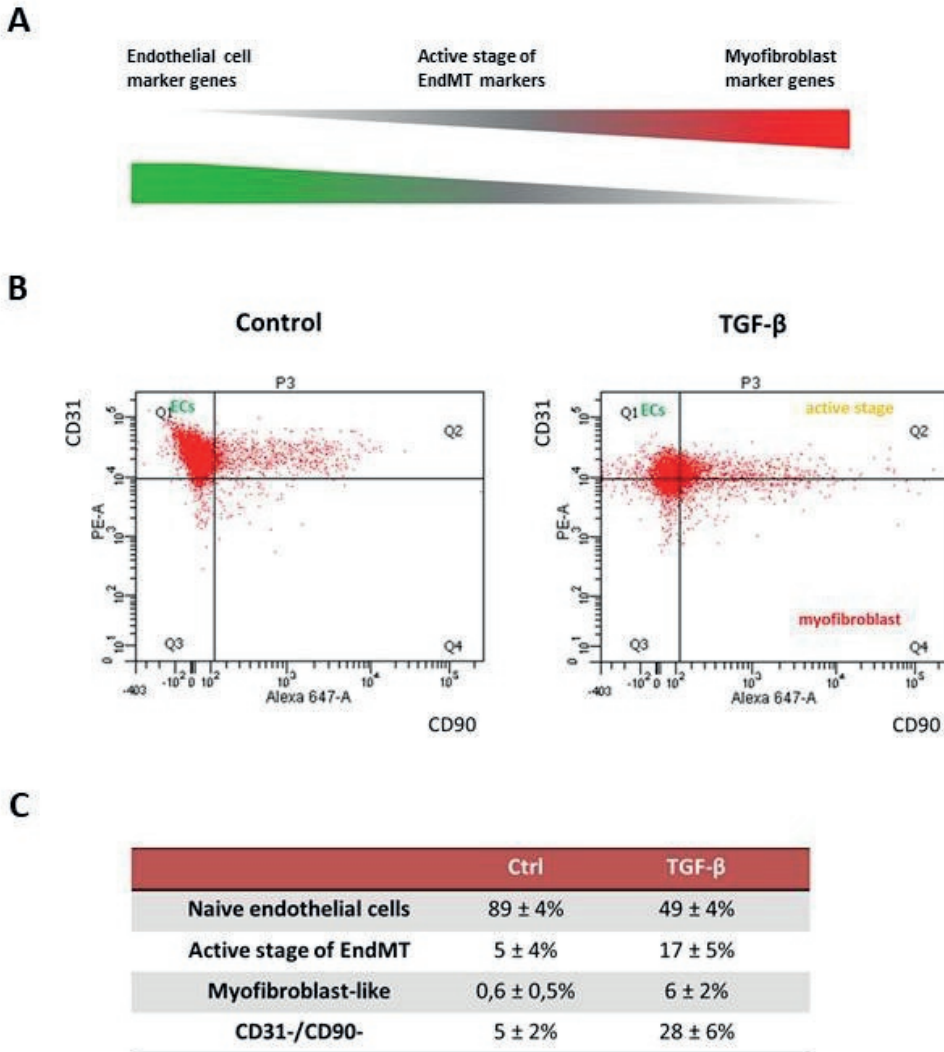


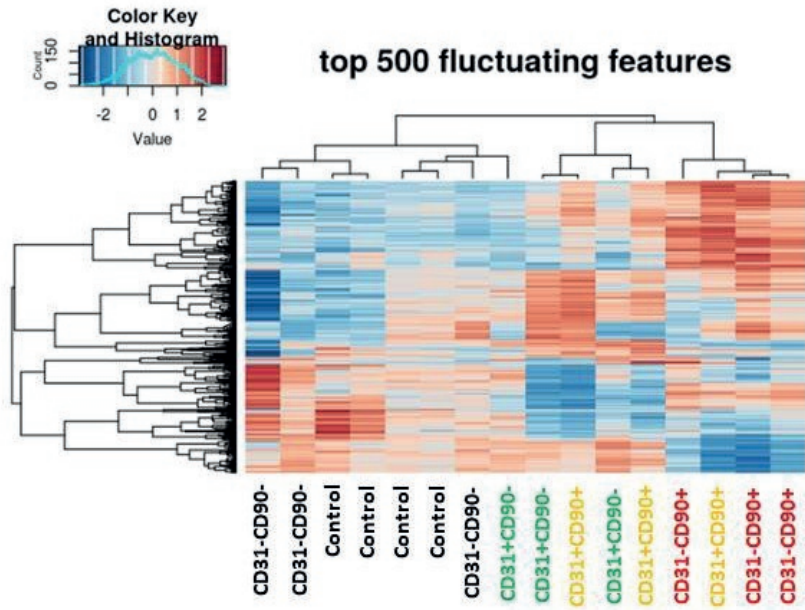
Figure 1. Stage-specific mapping of EndMT.

(A) Schematic demonstrating our hypothesis that naive endothelial cells express the endothelial marker CD31 and lack mesenchymal CD90 expression, cells actively undergoing EndMT express both CD31 and CD90 and endothelial-derived myfibroblasts express solely CD90. (B) Fluorescence-activated cell sorting (FACS) of control and TGF- β -treated HUVECs which are live-cell immunostaining with CD31 and CD90. Upon TGF- β treatment, the population shifts down (losing CD31 expression) and towards the right (towards CD90 expression). (C) Overview of the percentage of cells which are assigned (based on their CD31 and CD90 expression) as naive endothelial cells, cells active undergoing EndMT, endothelial-derived myfibroblast-like cells or the population which is negative for both CD31 and CD90 expression. Upon TGF- β treatment, there is a marked decrease in the naive endothelial cell population, whereas the percentage of the other three stages increases. The data is presented as mean value \pm S.D.; n=3 independent biological replicates.

CLUSTERING AND IDENTIFICATION OF DIFFERENT STAGES OF ENDMT

We first clustered the different stages based on the top 500 fluctuating features (Fig.2A). When moving towards the other end of the spectrum, we can observe the naive endothelial cells (CD31+CD90-) first indicating that these cells closely resemble untreated HUVECs (as well as the CD31-CD90- cells). We could also demonstrate that indeed the endothelial-derived myofibroblast-like cells (CD31-CD90+) are at the far end of the spectrum, indicating that they indeed differ the most from the untreated HUVECs (as well as CD31+CD90-). Interestingly, the CD31+CD90+ cells are clustered in between the CD31+CD90- and CD31-CD90+ cells which may confirm our hypothesis that CD31+CD90+ cells represent the active stage of EndMT since they are closely related to both CD31+CD90- and CD31-CD90+ cells. We then continued to pre-identify the different stages based on well-known EndMT markers such as α -SMA (ACTA2), Snail (SNAI1), Vimentin (VIM) and TGF- β (TGFB), the novel fibroblast marker periostin (POSTN), as well as CD90 (THY1) and some epigenetic modifiers (TET2, DNMT3A) known to be associated with EndMT. When comparing the different stages with untreated HUVECs (untreated CD31+CD90-), we demonstrate that the active stage of EndMT has increased expression of ACTA, THY1 as well as POSTN whereas TGFB2 expression is decreased (Fig.2B). The endothelial-derived myofibroblast-like cells have increased expression of ACTA2 and THY1 but also of TGFB1/3, SNAI, VIM and DNMT3A whereas TET2 and TGFB2 are decreased. This might indicate that ACTA2 and POSTN resemble markers of the active stage of EndMT. Also, this fits our hypothesis since the CD31-CD90+ cells expresses more mesenchymal markers than the CD31+CD90+ cells.

A



B

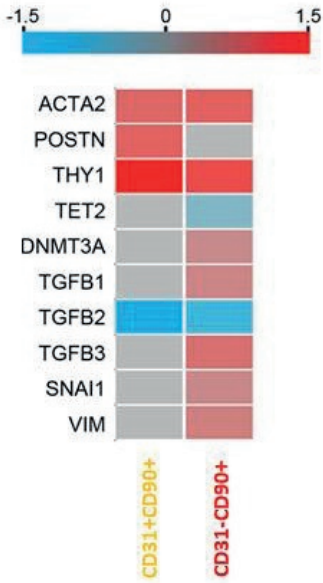


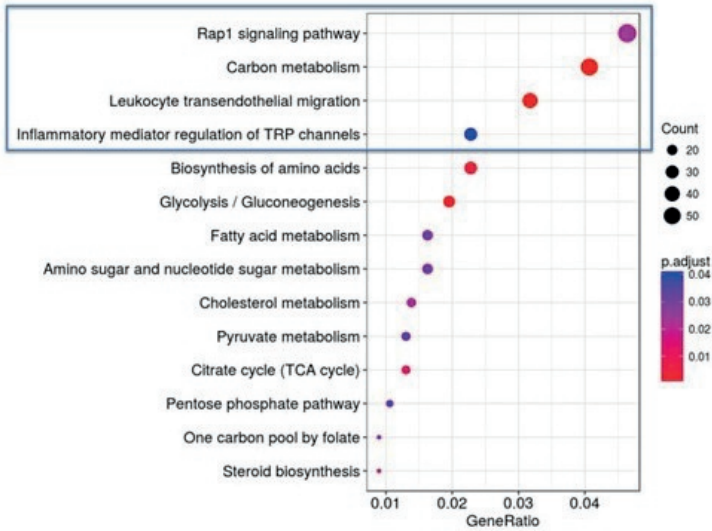
Figure 2. Clustering and identification of different stages of EndMT.

(A) Heatmap of the clustering analysis based on the top 500 fluctuating features upon RNA-sequencing. The CD31-CD90- population is most closely related to untreated HUVECs (Control). When moving toward the end of the spectrum, we can observe naïve endothelial cells (CD31+CD90-), the active stage of EndMT (CD31+CD90+) and at the far end the endothelial-derived myofibroblasts (CD31-CD90-). Interestingly, the CD31+CD90+ stage closely resemble both naïve endothelial cells (CD31+CD90-) as well as endothelial-derived myofibroblasts (CD31-CD90+). (B) Heatmap indicating the expression of mesenchymal genes and epigenetic regulators in the different stages when compared to untreated HUVECs. Interestingly, the active stage of EndMT (CD31+CD90-) exhibit increased expression of α -SMA (ACTA2), Periostin (POSTN) and CD90 (THY1) when compared to untreated HUVECs. The endothelial-derived myofibroblasts (CD31-CD90+) have an increased expression of the mesenchymal genes ACTA2 and THY1 but also of TGF- β 1 and TGF- β 3 (TGFB1/TGFB3), Snail (SNAI1), Vimentin (VIM) as well as the epigenetic modifier DNA methyltransferase 3A (DNMT3A) when compared to untreated HUVECs. Endothelial-derived myofibroblasts (CD31-CD90+) exhibit decreased expression of TGF- β 2 as well as the epigenetic modifier Tet Methylcytosine Dioxygenase 2 (TET2).

THE ACTIVE STAGE OF ENDMT IS CHARACTERIZED BY CHANGES IN THE RAP1 SIGNALING PATHWAY

KEGG enrichment analysis revealed that the changes in gene expression in the active stage of EndMT are associated with the Rap1 signaling pathway (50 genes) as well as carbon metabolism (40 genes), leukocyte transendothelial migration (30 genes) and inflammatory mediator regulation of TRP channels (20 genes, Fig.3A). Interestingly, the Rap1 signaling pathway, leukocyte transendothelial migration and inflammatory mediator regulation of TRP are all interconnected (Fig.3B). This indicates that cells actively undergoing EndMT are possibly depending on the Rap1 signaling pathway and highlights that inflammatory conditions are potential important features for the active stage of EndMT.

A



B

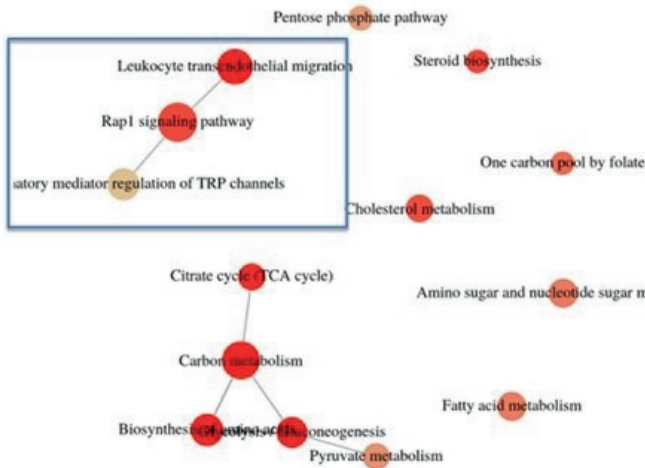
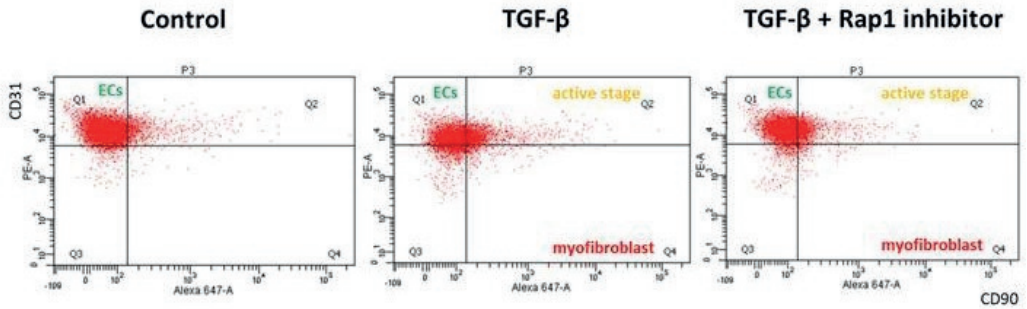


Figure 3. The active stage of EndMT is characterized by changes in the Rap1 signaling pathway (A) KEGG enrichment analysis revealed gene expression changes in the Rap1 signaling pathway (50 genes), carbon metabolism (40 genes), leukocyte transendothelial migration (30 genes) and inflammatory mediator regulation of TRP channels (20 genes). (B) Interestingly, Rap1 signaling pathway is associated with both leukocyte transendothelial migration as well as inflammatory mediator regulation of TRP channels.

THE RAP1 INHIBITOR GGTI 298 IN PART INHIBITS ENDMT

We continued to inhibit the Rap1 signaling pathway and assess its effect on EndMT. Treatment with the Rap1 inhibitor GGTI 298 (in combination with TGF- β 1 treatment) results in a shift towards CD31 expression (Fig.4A). Upon treatment with GGTI 298, the naive endothelial cells increased from 53% to 72% whereas no difference could be observed in the percentage of cells in the active stage of EndMT (22% vs 21%; Fig.4B). The endothelial-derived myofibroblast-like cells and CD31-CD90- cells decreased from 5% to 2% and 20% to 5% respectively (Fig.4B). This suggests that Rap1 inhibition results in partial inhibition of EndMT, and that the cells are less likely to lose/decrease their CD31 expression.

A**B**

	Ctrl	TGF- β	TGF- β + Rap1 inhibitor
Naive endothelial cells	91 \pm 6%	53 \pm 5%	72 \pm 1%
Active stage of EndMT	6 \pm 5%	22 \pm 1%	21 \pm 2%
Myofibroblast-like	0,2 \pm 0,1%	5 \pm 1%	2 \pm 0,5%
CD31-/CD90-	3 \pm 1%	20 \pm 5%	5 \pm 1%

Figure 4. Inhibition of Rap1 signaling results in partial inhibition of EndMT.

(A) Fluorescence-activated cell sorting (FACS) of control, TGF- β -treated HUVECs and TGF- β -treated HUVECs in combination with the Rap1 inhibitor GGTI 298 which are live-cell immunostaining with CD31 and CD90. Upon treatment with the Rap1 inhibitor, the cells shift up (gaining CD31 expression). (B) Overview of the percentage of cells which are assigned (based on their CD31 and CD90 expression) as naive endothelial cells, actively undergoing EndMT, endothelial-derived myofibroblast-like or the cells which are negative for both CD31 and CD90 expression. Upon Rap1 inhibition, there is a marked increase in the naive endothelial cells whereas the myofibroblast-like cells and CD31-CD90- cells are decreased. There is no difference in the percentage of cells in the active stage of EndMT. The data is presented as mean value \pm S.D.; n=3 independent biological replicates.

DISCUSSION

In this study we established an *in vitro* system to identify different stages of EndMT. We identified a combination of markers, using CD31 as an endothelial cell marker and CD90 as an mesenchymal cell marker, which can be used to perform live-cell immunostaining in order to sort out cells at defined stages of EndMT. RNA sequencing and clustering analysis indicated that we were able to sort out different stages: naive endothelial cells (CD31+CD90-), cells actively undergoing EndMT (CD31+CD90+) and endothelial-derived myofibroblasts (CD31-CD90+). Since there is a high heterogeneity in (myo)fibroblasts, not all (myo)fibroblasts express CD90 (Suppl.Fig.3). This indicates that the CD31-CD90-cells could also represent endothelial-derived myofibroblasts (which lack CD90 expression).

CD90 is substantially expressed in cardiac fibrosis and more specifically in cardiac fibroblasts, but its association with EndMT has only received minor attention so far [14]. It is important to note that there might be different and/or more stages of EndMT when other/additional mesenchymal markers would be used. Moreover, the sorting of more distinct populations would provide a deeper understanding of which processes start first (and are thus most important) and which follow. The recent development of single cell sequencing would therefore enhance our analysis since it is not dependent on an endothelial and mesenchymal marker, but takes into account each individual cell as a whole (even though it is limited by its sequencing depth). Nevertheless, to the best of our knowledge, this is the first study to allow real-time mapping of genetic changes that facilitate different stages of EndMT.

We identified that the active stage of EndMT is primarily characterized by changes in the Rap1 signaling pathway. We also demonstrate that inhibition of Rap1 signaling partially alleviates EndMT. Even though the RNA-seq analysis suggests that the Rap1 signaling pathway affects the active stage of EndMT, the percentage of cells in the active stage of EndMT (CD31+CD90+) remained the same. Nevertheless, we show that Rap1 signaling inhibition reduced the percentage of both CD31-CD90- and CD31-CD90+ cells which together results in an EndMT inhibiting effect from 25% to 7%.

Rap1 signaling consists of the RAS signaling pathway, the calcium signaling pathway, the T cell receptor signaling pathway, the MAPK signaling pathway, the

PI3K-Akt signaling pathway, adherens junctions, focal adhesion and regulation of actin cytoskeleton. We and others have previously demonstrated the importance of the RAS signaling pathway as well as the MAPK signaling pathway in the regulation of EndMT [15-20]. The understanding of genes/signaling pathways which facilitate the active stage of EndMT might allow us to block EndMT in a specific way. Especially since (1) no specific inhibitors for EndMT are available and (2) the active stage of EndMT might represent the most targetable population.

Interestingly, the Rap1 signaling pathway, leukocyte transendothelial migration and inflammatory mediator regulation of TRP are all interconnected. Since inflammation is also involved in EndMT, future research could be directed on the interplay between the Rap1 signaling pathway and inflammatory mediator regulation.

To conclude, we identified via a stage-specific mapping strategy that the active stage of EndMT is primarily characterized by changes in the Rap1 signaling pathway. Indeed, we show that inhibition of Rap1 partially alleviates EndMT.

MATERIALS AND METHODS

Cell Culture and induction of EndMT

Human umbilical vein endothelial cells (HUVECs, Lonza, Basel, Switzerland) were cultured in EBM medium (Lonza, Basel, Switzerland) in 0.2% gelatin-coated flasks (Sigma, St. Louis, MO, USA). Trypsin-EDTA Solution (Sigma, St. Louis, Mo, USA) was used to detach the cells. Passages 3-4 were used for sequencing experiments. 4.9×10^5 cells were seeded to a T75 flask. Induction of EndMT was performed by addition of 10 ng/mL TGF- β 1 (R&D Systems, Minneapolis, MN, USA) as described before [9]. HUVECs were stimulated for four days. The ECM medium (containing TGF- β 1) was changed every day.

Fluorescence Activated Cell Sorting (FACS)

HUVECs were harvested and incubated with the antibodies on ice for 30 minutes and washed with FACS-buffer (1% 0.2M EDTA and 0.5% FCS in PBS). The following antibodies were used: CD31-R-PE (#IQP-552R, IQ Products, Groningen, The Netherlands) and APC mouse anti-human CD90 (#561971, BD Biosciences, San Jose, CA, USA). For analysis, cells were resuspended in FACS-buffer. Both antibodies were used in a 1:10 dilution in FACS-buffer. For analysis, the FACS ARIA II (BD Biosciences, Franklin Lakes, NJ, USA) in combination with the blue laser (488 nm) for CD31-R-PE and red laser (633 nm) for APC mouse anti-human CD90 was used.

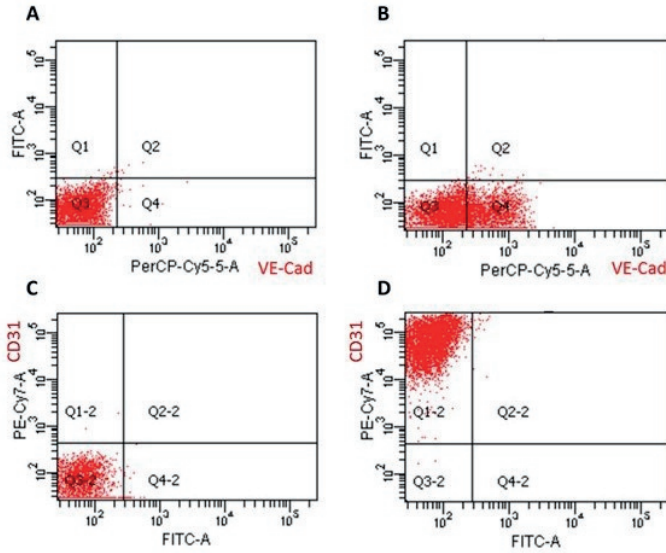
RNA sequencing

Library preparation was performed using the high throughput v2 kit for 150 cycles single read. RNA sequencing was performed on a NextSeq with a high output kit where 24 samples were run on all 4 flow cell lanes (around 25 million reads per sample).

Rap1 inhibitor experiment

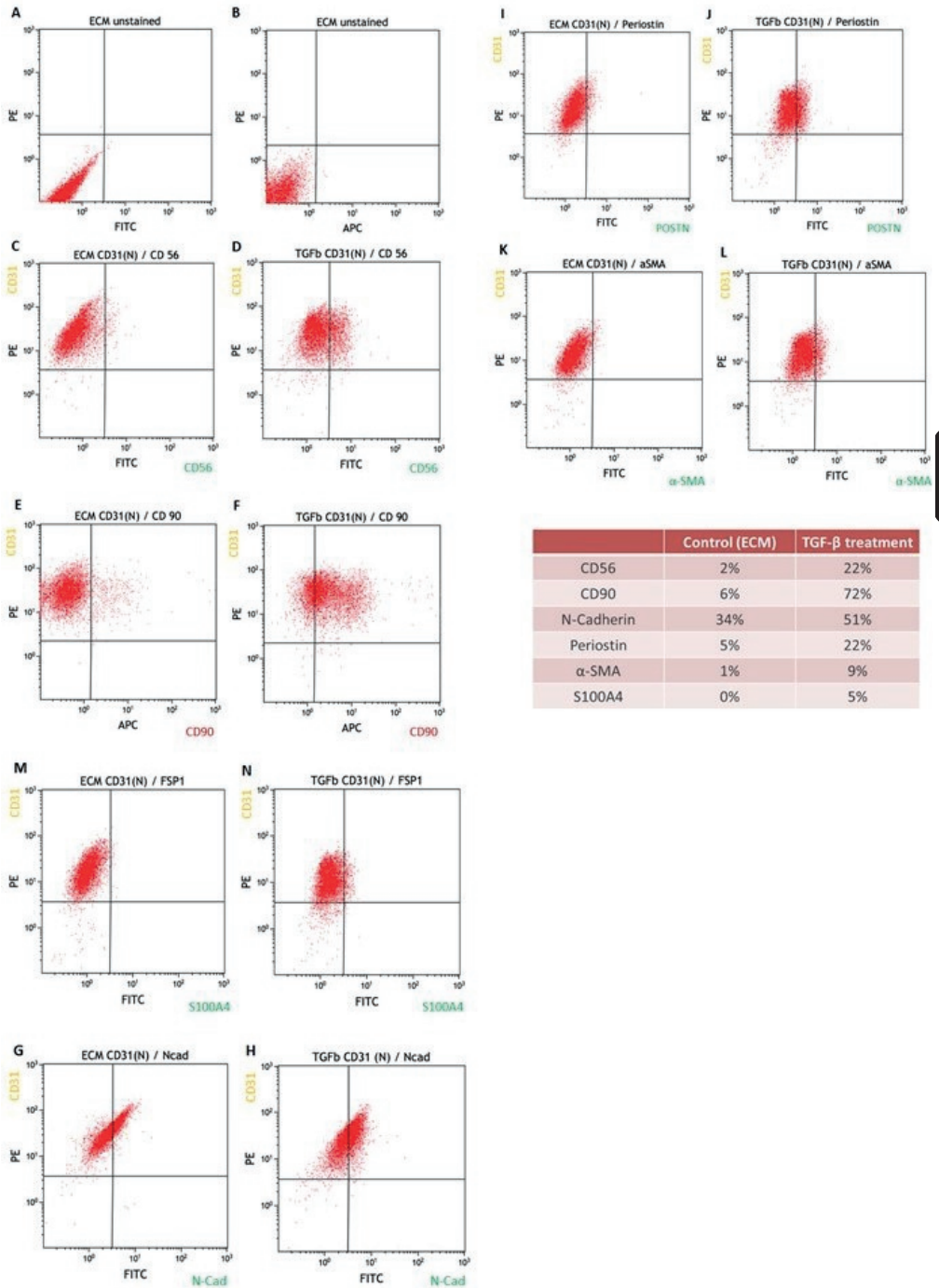
HUVECs were treated for 48 hours with TGF- β 1 followed by 48 hours of TGF- β 1 treatment in combination with 5 μ M of the Rap1 inhibitor GGTI 298 (Selleckchem, Houston, TX, USA).

SUPPLEMENTARY DATA



Supplementary Figure 1. Identification of CD31 as endothelial marker for live-cell immunostaining.

Live-cell immunostaining of HUVECs with VE-Cadherin and CD31 was performed under basal conditions to identify an endothelial marker which can be used for the stage-specific mapping of EndMT. (A) Negative control for VE-Cadherin staining. (B) HUVECs were stained with VE-Cadherin. Flow cytometry indicates that 37% of the HUVECs were low-positive for VE-Cadherin. (C) Negative control for CD31 staining. (D) HUVECs were stained with CD31. HUVECs are high-positive for CD31, making CD31 a reliable endothelial marker for the stage-specific mapping of EndMT.

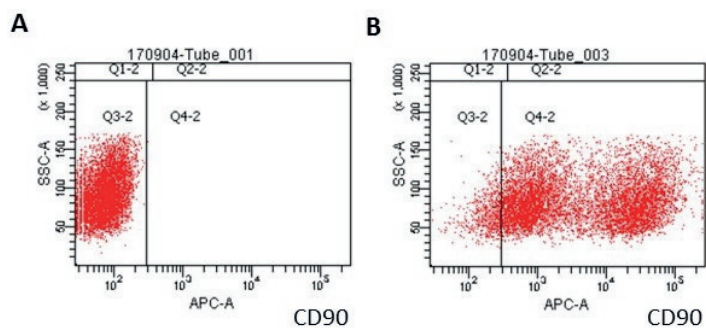


6

Supplementary Figure 2. Identification of a mesenchymal marker for live-cell immunostaining. HUVECs under basal conditions (ECM) or treated for 4 days with TGF- β 1 (TGF β) were stained with CD31 in combination with one of the following mesenchymal markers: CD56 (C,D), CD90 (E,F), N-

CHAPTER 6

Cadherin (G,H), Periostin (I,J), α -SMA (K,L) or FSP1 (S100A4; M,N). Unstained HUVECs were used as a negative control (A,B). An overview of the change in expression (in %) of the different mesenchymal markers upon TGF- β 1 treatment is shown.



Supplementary Figure 3. CD90 expression in human cardiac fibroblasts.

Human Cardiac Fibroblasts under basal conditions were stained with CD90. (A) Negative control for CD90 staining. (B) Human cardiac fibroblasts are high positive for CD90 expression (95%).

REFERENCES

1. Eisenberg LM, Markwald RR. Molecular regulation of atrioventricular valvuloseptal morphogenesis. *Circulation research*. 1995;77:1-6
2. Chen PY, Qin L, Baeyens N, Li G, Afolabi T, Budatha M, Tellides G, Schwartz MA, Simons M. Endothelial-to-mesenchymal transition drives atherosclerosis progression. *The Journal of clinical investigation*. 2015;125:4514-4528
3. Hashimoto N, Phan SH, Imaizumi K, Matsuo M, Nakashima H, Kawabe T, Shimokata K, Hasegawa Y. Endothelial-mesenchymal transition in bleomycin-induced pulmonary fibrosis. *American journal of respiratory cell and molecular biology*. 2010;43:161-172
4. Maddaluno L, Rudini N, Cuttano R, Bravi L, Giampietro C, Corada M, Ferrarini L, Orsenigo F, Papa E, Boulday G, Tournier-Lasserre E, Chapon F, Richichi C, Retta SF, Lampugnani MG, Dejana E. Endmt contributes to the onset and progression of cerebral cavernous malformations. *Nature*. 2013;498:492-496
5. Ranchoux B, Antigny F, Rucker-Martin C, Hautefort A, Pechoux C, Bogaard HJ, Dorfmueller P, Remy S, Lecerf F, Plante S, Chat S, Fadel E, Houssaini A, Anegon I, Adnot S, Simonneau G, Humbert M, Cohen-Kaminsky S, Perros F. Endothelial-to-mesenchymal transition in pulmonary hypertension. *Circulation*. 2015;131:1006-1018
6. Zeisberg EM, Potenta S, Xie L, Zeisberg M, Kalluri R. Discovery of endothelial to mesenchymal transition as a source for carcinoma-associated fibroblasts. *Cancer research*. 2007;67:10123-10128
7. Zeisberg EM, Potenta SE, Sugimoto H, Zeisberg M, Kalluri R. Fibroblasts in kidney fibrosis emerge via endothelial-to-mesenchymal transition. *Journal of the American Society of Nephrology : JASN*. 2008;19:2282-2287
8. Zeisberg EM, Tarnavski O, Zeisberg M, Dorfman AL, McMullen JR, Gustafsson E, Chandraker A, Yuan X, Pu WT, Roberts AB, Neilson EG, Sayegh MH, Izumo S, Kalluri R. Endothelial-to-mesenchymal transition contributes to cardiac fibrosis. *Nature medicine*. 2007;13:952-961
9. Neumann P, Jae N, Knau A, Glaser SF, Fouani Y, Rossbach O, Kruger M, John D, Bindereif A, Grote P, Boon RA, Dimmeler S. The lncrna gata6-as epigenetically regulates endothelial gene expression via interaction with loxl2. *Nature communications*. 2018;9:237
10. van Mourik JA, Leeksa OC, Reinders JH, de Groot PG, Zandbergen-Spaargaren J. Vascular endothelial cells synthesize a plasma membrane protein indistinguishable from the platelet membrane glycoprotein iia. *The Journal of biological chemistry*. 1985;260:11300-11306
11. Suzuki S, Sano K, Tanihara H. Diversity of the cadherin family: Evidence for eight new cadherins in nervous tissue. *Cell regulation*. 1991;2:261-270
12. Lupatov AY, Vdovin AS, Vakhrushev IV, Poltavtseva RA, Yarygin KN. Comparative analysis of the expression of surface markers on fibroblasts and fibroblast-like cells isolated from different human tissues. *Bulletin of experimental biology and medicine*. 2015;158:537-543

13. Ali SR, Ranjbarvaziri S, Talkhabi M, Zhao P, Subat A, Hojjat A, Kamran P, Muller AM, Volz KS, Tang Z, Red-Horse K, Ardehali R. Developmental heterogeneity of cardiac fibroblasts does not predict pathological proliferation and activation. *Circulation research*. 2014;115:625-635
14. Medici D, Shore EM, Lounev VY, Kaplan FS, Kalluri R, Olsen BR. Conversion of vascular endothelial cells into multipotent stem-like cells. *Nature medicine*. 2010;16:1400-1406
15. Correia AC, Moonen JR, Brinker MG, Krenning G. Fgf2 inhibits endothelial-mesenchymal transition through microrna-20a-mediated repression of canonical tgf-beta signaling. *Journal of cell science*. 2016;129:569-579
16. Maleszewska M, Vanchin B, Harmsen MC, Krenning G. The decrease in histone methyltransferase ezh2 in response to fluid shear stress alters endothelial gene expression and promotes quiescence. *Angiogenesis*. 2016;19:9-24
17. Xu X, Tan X, Hulshoff MS, Wilhelmi T, Zeisberg M, Zeisberg EM. Hypoxia-induced endothelial-mesenchymal transition is associated with rasal1 promoter hypermethylation in human coronary endothelial cells. *FEBS letters*. 2016;590:1222-1233
18. Tan X, Xu X, Zeisberg M, Zeisberg EM. Dnmt1 and hdac2 cooperate to facilitate aberrant promoter methylation in inorganic phosphate-induced endothelial-mesenchymal transition. *PLoS one*. 2016;11:e0147816
19. Xu X, Tan X, Tampe B, Nyamsuren G, Liu X, Maier LS, Sossalla S, Kalluri R, Zeisberg M, Hasenfuss G, Zeisberg EM. Epigenetic balance of aberrant rasal1 promoter methylation and hydroxymethylation regulates cardiac fibrosis. *Cardiovascular research*. 2015;105:279-291
20. Vanchin B, Offringa E, Friedrich J, Brinker MG, Kiers B, Pereira AC, Harmsen MC, Moonen JA, Krenning G. Microrna-374b induces endothelial-to-mesenchymal transition and early lesion formation through the inhibition of mapk7 signaling. *The Journal of pathology*. 2019;247:456-470

PART II

(EPI)GENETICS AS A THERAPEUTIC TARGET IN ORGAN FIBROSIS

CHAPTER

7

SERELAXIN ALLEVIATES CARDIAC FIBROSIS THROUGH INHIBITING ENDOTHELIAL-TO-MESENCHYMAL TRANSITION VIA RXFP1

Tim Wilhelm^{1,3,*}, Xingbo Xu^{1,3,*}, Xiaoying Tan^{2,3}, Melanie S. Hulshoff^{1,3,4}, Sabine Maamari¹, Samuel Sossalla^{1,3,5}, Michael Zeisberg^{2,3} and Elisabeth M. Zeisberg^{1,3}

¹*Department of Cardiology and Pneumology, University Medical Center of Göttingen, Georg-August University, Göttingen, Germany.*

²*Department of Nephrology and Rheumatology, University Medical Center of Göttingen, Georg-August University, Göttingen, Germany.*

³*German Centre for Cardiovascular Research (DZHK), Göttingen, Germany.*

⁴*Laboratory for Cardiovascular Regenerative Medicine, Department of Pathology and Medical Biology, University Medical Center Groningen, University of Groningen, Groningen, The Netherlands.*

⁵*Department of Internal Medicine II, University Medical Center Regensburg, Regensburg, Germany*

**Authors contributed equally*

Theranostics 2020; 10(9): 3905-3924.

ABSTRACT

Rationale: Cardiac fibrosis is an integral constituent of every form of chronic heart disease, and persistence of fibrosis reduces tissue compliance and accelerates the progression to heart failure. Relaxin-2 is a human hormone, which has various physiological functions such as mediating renal vasodilation in pregnancy. Its recombinant form Serelaxin has recently been tested in clinical trials as a therapy for acute heart failure but did not meet its primary endpoints. The aim of this study is to examine whether Serelaxin has an anti-fibrotic effect in the heart and therefore could be beneficial in chronic heart failure.

Methods: We utilized two different cardiac fibrosis mouse models (ascending aortic constriction (AAC) and Angiotensin II (ATII) administration via osmotic minipumps) to assess the anti-fibrotic potential of Serelaxin. Histological analysis, immunofluorescence staining and molecular analysis were performed to assess the fibrosis level and indicate endothelial cells which are undergoing EndMT. In vitro TGF β 1-induced endothelial-to-mesenchymal transition (EndMT) assays were performed in human coronary artery endothelial cells and mouse cardiac endothelial cells (MCECs) and were examined using molecular methods. Chromatin Immunoprecipitation-qPCR assay was utilized to identify the Serelaxin effect on chromatin remodeling in the Rxfp1 promoter region in MCECs.

Results: Our results demonstrate a significant and dose-dependent anti-fibrotic effect of Serelaxin in the heart in both models. We further show that Serelaxin mediates this effect, at least in part, through inhibition of EndMT through the endothelial Relaxin family peptide receptor 1 (RXFP1). We further demonstrate that Serelaxin administration is able to increase its own receptor expression (RXFP1) through epigenetic regulation in form of histone modifications by attenuating TGF β -pSMAD2/3 signaling in endothelial cells.

Conclusions: This study is the first to identify that Serelaxin increases expression of its own receptor RXFP1 and that this mediates inhibition of EndMT and cardiac fibrosis, suggesting that Serelaxin may have a beneficial effect as anti-fibrotic therapy in chronic heart failure.

INTRODUCTION

Cardiac fibrosis is an integral constituent of every form of chronic heart disease and leads to an increased wall stiffness and diastolic dysfunction. Regardless of the pathogenesis of cardiac fibrosis, activated fibroblasts mediate fibrogenesis by excessive extracellular matrix production [1–3]. However, currently there is no specific therapy available to block the progression of cardiac fibrosis, albeit several groups have shown different anti-fibrotic strategies in proof-of-concept studies [4-8].

Serelaxin is a recombinant form of the human hormone Relaxin-2, which is a 6kDa polypeptide hormone known to have various physiological functions such as mediating renal vasodilation during pregnancy. Furthermore, it is able to soften the cervix, increase both the flexibility of the interpubic ligament and motility of male sperm and is, most importantly, involved in organ remodeling (of the skin, lung, liver, kidney and heart) by inducing degradation of extracellular matrix [9-13]. Relaxin peptides bind to one of their cognate receptors called Relaxin family peptide receptors (RXFPs) 1-4. RXFPs are expressed in heart tissue, blood vessels, and the kidneys [12-14] and trigger various pathways resulting in an induction of multiple functional products such as Vascular endothelial growth factor (VEGF), endothelial nitric oxide synthase (eNOS) and Matrix metalloproteinases (MMPs) [13,15]. In Relaxin-knockout mice, an increased deposition of collagen I was observed in the left ventricle [16]. In another study, an anti-fibrotic effect of Relaxin could be confirmed; however the molecular mechanisms have not yet been addressed [12,17,18]. Nevertheless, with its vasodilating, anti-inflammatory and anti-fibrotic effects, Relaxin has gained attention in cardiovascular research as this single compound targets different aspects of heart failure.

In an international, double-blinded and placebo-controlled study, the effect of Serelaxin was examined in 1161 hospitalized patients with acute heart failure. Patients received an intravenous infusion of Serelaxin (30 µg/kg per day) or placebo infusion for 48 hours. In this study, the administration of Serelaxin showed a significant improvement of dyspnea (shortness of breath) and a 37% reduction in both cardiovascular and overall mortality within 6 months as compared to the placebo control group. Furthermore, worsening of heart failure events could be reduced by 47% after day 5 [19,20]. Cardiac output was not significantly changed by Serelaxin [21]. An additional phase III trial (RELAX-AHF 2)

including 6,600 patients hospitalized for acute heart failure was designed to confirm whether Serelaxin has significant effects on reducing cardiovascular death and worsening heart failure episodes. However, it failed to reduce the previous reported cardiovascular death after 6 months or worsening of heart failure after 5 days [22]. We here explored the effect of Serelaxin on cardiac fibrosis. In this respect, an anti-fibrotic effect of Relaxin has been observed in both kidney and heart using an experimental model of spontaneously hypertensive rats [23]. However, no pathomechanistic insights were provided by this study. *In vitro* studies demonstrated an anti-Transforming growth factor β (TGF β)/ Smad3-mediated protective effect of Relaxin on fibroblast activation [24]. Because the pro-fibrotic mechanism of endothelial mesenchymal transition (EndMT) is also Smad3-mediated, these studies further suggest an inhibitory and anti-fibrotic effect of Serelaxin with respect to EndMT.

Besides the TGF β pathway, several other molecular signaling pathways such as Notch, Wnt, Erk1/2, p38, NF- κ B, etc. can also independently or synergistically regulate EndMT [25]. Notch signaling is involved in developmental EndMT during embryonic formation of the heart [26,27] but also in pathogenic EndMT during tumor development and fibrogenesis [28,29]. In this aspect, Notch has been reported to preserve endothelial cell properties and attenuate EndMT, and that this can be affected by Relaxin [30,31]. The Notch signaling pathway is activated via its ligand Jagged1 binding to the extracellular domain of the Notch1 receptor. This leads to cleavage of the Notch intracellular domain (NICD) by a γ -secretase and to translocation into the nucleus where downstream target genes are activated.

EndMT is a cellular transformation process by which endothelial cells lose endothelial and gain mesenchymal cell characteristics (e.g. loss of CD31 expression and gain of α -SMA). While this mechanism is a physiological cell transformation process during embryonic heart development (which allows the formation of the endocardial cushion and the heart valves from endocardial cells of the atrioventricular canal), EndMT has recently gained attention because of its contribution to cardiac fibrosis and fibrogenesis of other organs such as the lung, kidney and liver [7,32-38].

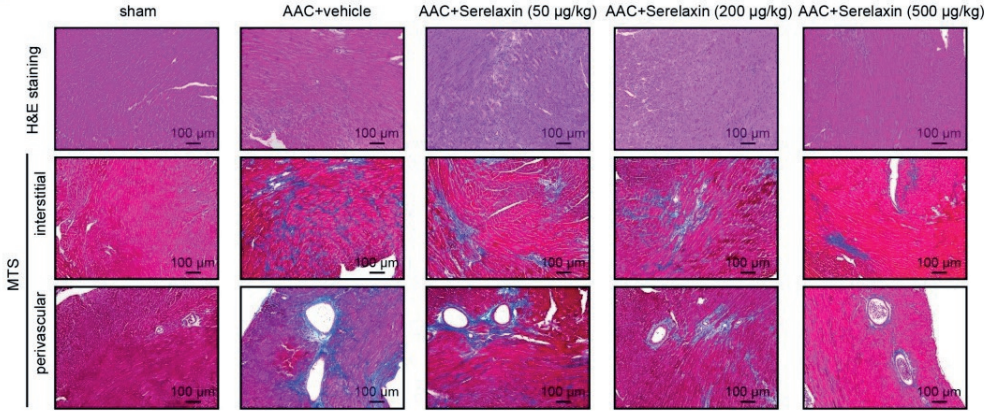
Here we aimed to explore the anti-fibrotic potential of Serelaxin and its function in inhibiting EndMT both *in vitro* and *in vivo*.

RESULTS

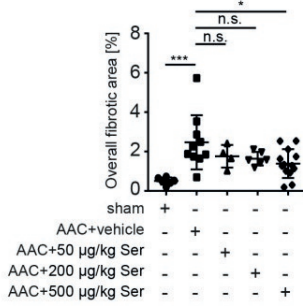
SERELAXIN AMELIORATES CARDIAC FIBROSIS IN TWO INDEPENDENT MOUSE MODELS OF PRESSURE OVERLOAD

Following clinical studies as well as previous animal studies, which suggested an anti-fibrotic effect of Serelaxin, we aimed to systematically assess the effect of Serelaxin at different doses in two established mouse models of cardiac fibrosis. For this purpose, we induced pressure overload in mice by ascending aortic constriction (AAC) and administered either a vehicle or Serelaxin at 3 different doses at the same time (details are described in the methods section). Echocardiography was performed to verify aortic constriction, and mice were sacrificed after 4 weeks. Quantitative assessment of overall left ventricular fibrotic area by Masson Trichrome staining showed a dose-dependent anti-fibrotic effect of Serelaxin with significant reduction of overall fibrosis by 50% in the high dose Serelaxin group when compared to vehicle (Figure 1A-B). We further performed a sub analysis of perivascular fibrosis (defined as fibrotic lesions surrounding vessels of $>100\ \mu\text{m}$) and interstitial fibrosis (defined as all other fibrotic lesions), and demonstrate that while both forms of fibrosis were ameliorated by Serelaxin, the effect of Serelaxin was relatively higher on perivascular as compared to interstitial lesions (Figure 1A, 1C-D). Amelioration of cardiac fibrosis was associated with a significantly reduced mortality in mice which had received the high dose of Serelaxin as compared to vehicle treated mice (Figure 1E). Analysis of the heart weight in relation to body weight (Figure 1F) and tibia length (Figure 1G) showed an elevated heart weight in AAC-operated compared to sham mice. Administration of high dose Serelaxin significantly prevented the increase in heart weight. AAC-operated hearts showed an enlarged phenotype. Echocardiography parameters suggested a dilated left ventricle. Serelaxin could not significantly reverse the heart performance but the heart weight upon high dose administration (Supplementary Figure 1).

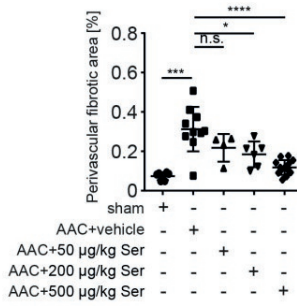
A



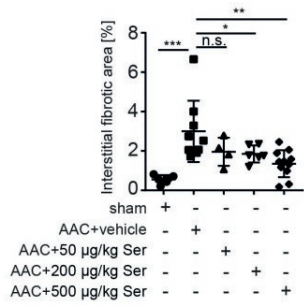
B



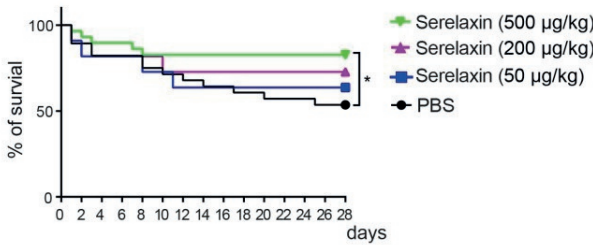
C



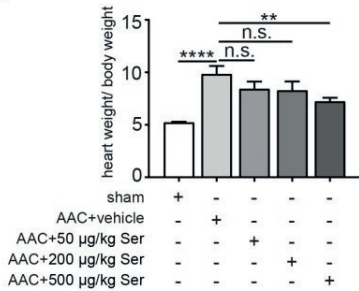
D



E



F



G

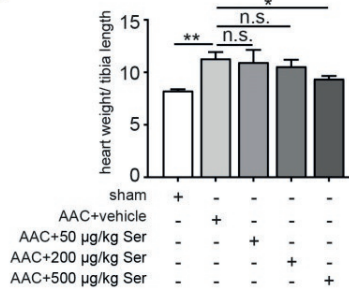


Figure 1. Serelaxin ameliorates cardiac fibrosis.

(A) HE and Masson's Trichrome Staining microphotography of sham and AAC-operated mouse heart showing the reduction of interstitial and perivascular fibrosis in Serelaxin-treated (500 µg/kg/day) hearts compared to sham and vehicle-treated hearts. (B-D) Graphs showing a significant reduction of fibrosis in Serelaxin-treated hearts. The dot plots represent the percentage of overall, interstitial and perivascular fibrotic area in the sham (n=6), vehicle-treated (n=10) and low (n=4), middle (n=6) and high dose (n=13) Serelaxin-treated AAC mouse hearts. (E) Kaplan-Meier survival curve summarizes survival rates of mice from the AAC operation date until 4 weeks after operation in vehicle-treated (n=28), low (13), middle (13) and high dose Serelaxin-treated (n=29) groups. Administration of high dose Serelaxin substantially increased survival. (F)-(G) Bar graphs showing heart weight related to body weight and tibia length. AAC-operation increased the heart weight compared to sham group, while administration of high but not low and middle dose Serelaxin prevented the increase in heart weight. Student t-test was used for single comparison and one-way ANOVA with Bonferroni post-hoc analysis was used for multiple group comparisons. Overall survival was analyzed by using a Kaplan-Meier survival method with a log rank test to determine statistical differences. Error bars represent mean ± SEM, n.s. no significance, * p<0.05, ** p<0.01, *** p<0.001, **** p<0.0001.

As a second independent mouse model, we additionally tested the effect of Serelaxin in an ATII-induced cardiac fibrosis model at two different time points. Mice received 1.5 mg/kg/day ATII and either Serelaxin (500 µg/kg/day) or vehicle for 2 or 4 weeks respectively (Supplementary Figure 2A). Vehicle administered ATII mice developed cardiac fibrosis after 2 weeks and even more pronounced after 4 weeks, which was significantly reduced in mice which were administered with Serelaxin (Supplementary Figure 2B-C). Both perivascular and interstitial fibrosis were ameliorated by Serelaxin, but the effect of Serelaxin was relatively higher on perivascular as compared to interstitial lesions (Supplementary Figure 2D). This shows that Serelaxin ameliorates cardiac fibrosis in two independent mouse models of cardiac fibrosis.

SERELAXIN ALLEVIATES CARDIAC FIBROSIS THROUGH INHIBITION OF ENDMT

Because Relaxin acts primarily on vascular cells [42], and because our results indicated a higher effect of Serelaxin on perivascular fibrosis as compared to interstitial fibrosis, we next examined if Serelaxin inhibits EndMT and preserves the endothelial phenotype *in vivo*. We therefore performed immunofluorescence labelling of the endothelial marker CD31 in combination with the mesenchymal markers α -SMA and collagen I (Figure 2A-D). Confocal analysis confirmed abundance of CD31/ α -SMA double-positive cells in AAC-challenged hearts indicating the presence of EndMT, as previously described [7,38]. In Serelaxin-administered mice, these double positive cells were reduced from 12% to 7% as compared to vehicle-treated mice, suggesting an EndMT-inhibiting effect of Serelaxin (Figure 2A-B). We also analysed the expression of CD31 as well as EndMT transcription factors Snail, Twist and Slug in hearts of vehicle- or Serelaxin-administered mice which underwent AAC surgery (Figure 2E). Overall, while AAC is associated with a reduction of CD31-positive cells and a reduction of CD31 expression in the heart, indicating a loss of microvasculature, this reduction was ameliorated in Serelaxin-treated mice, associated with a decrease of collagen I and α -SMA (Figure 2A-D). Moreover, the EndMT transcription factors were upregulated in AAC-challenged and ATII-treated hearts as compared to sham animals and vehicle-treated mice respectively. This upregulation was partially blocked in Serelaxin-administered mice (Figure 2E, Supplementary Figure 2E). To exclude that the observed reduction in CD31 is due to apoptosis, we performed an immunohistochemistry staining of cleaved Caspase 3 which is a critical executioner of apoptosis. The staining showed an increased level of cleaved Caspase 3 (3.6%) in AAC-operated hearts compared to sham operated. Serelaxin could not significantly affect cleaved Caspase 3 levels (Supplementary Figure 3). Together with the report of Park et al. who showed that during heart failure endothelial cells contribute less than 19% to all apoptotic cells of the heart [43], our results suggest an apoptosis-independent effect of Serelaxin.

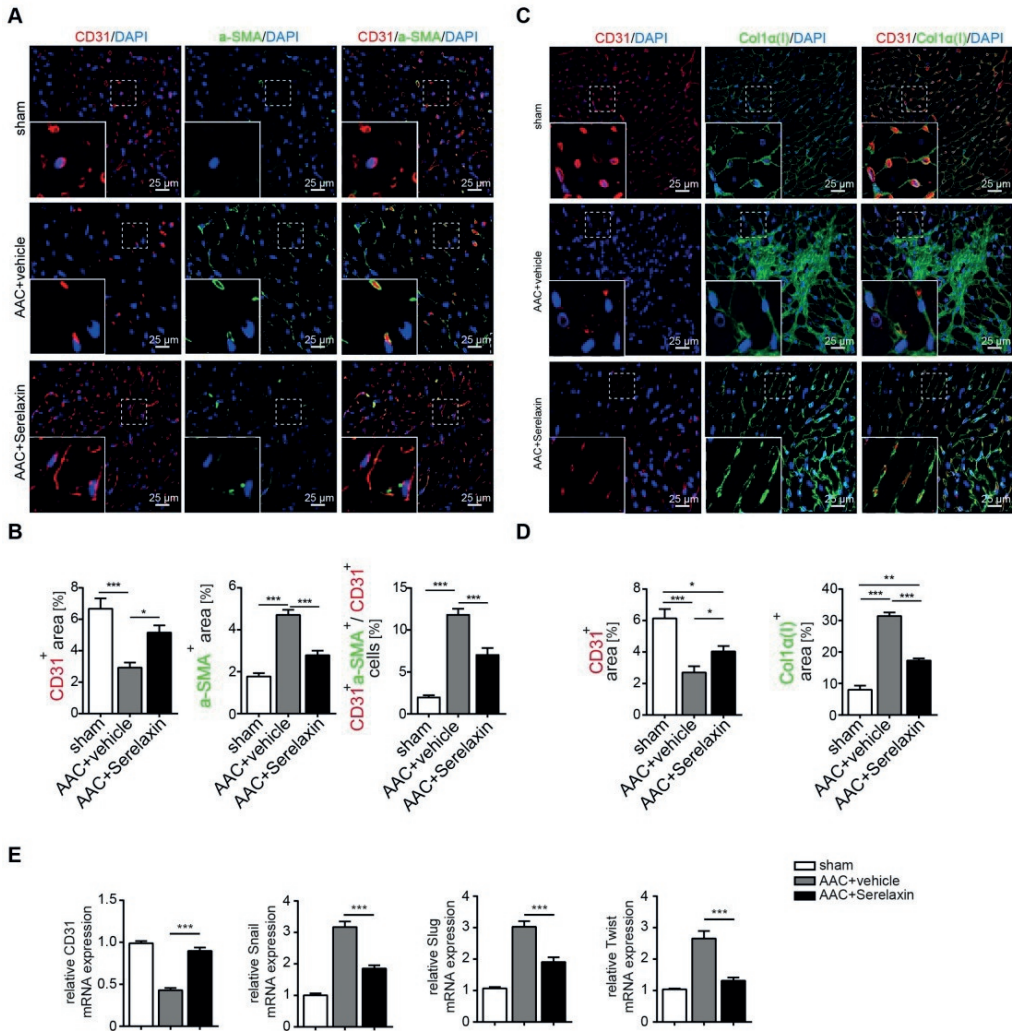


Figure 2. Serelaxin blocks EndMT in a mouse model of pressure overload.

(A) Immunofluorescence staining of endothelial cell marker CD31, mesenchymal marker α -SMA and DAPI. (B) Quantifications of CD31 and α -SMA positive area and ratio of CD31+ α -SMA+ / CD31+ cells. Compared to sham, vehicle-treated hearts showed an increased expression of α -SMA but a decreased protein expression of CD31, while treatment with Serelaxin showed reduced α -SMA and restored CD31 protein expression. Double positive cells significantly increased in AAC-operated animals and were reduced by Serelaxin administration. (C) Immunofluorescence staining of endothelial cell marker CD31, fibrotic marker alpha-1 type I collagen (Col1 α (I)) and DAPI. (D) Quantifications of CD31 and Col1 α (I) positive area: Col1 α (I) expression was upregulated in AAC hearts and is inhibited by Serelaxin. Compared to sham, vehicle-treated hearts showed a decreased protein expression of CD31, while treatment with Serelaxin again restored CD31 expression. (E) qPCR analysis showing the relative mRNA expression level of CD31 and EndMT key regulators Snail,

*Slug, and Twist in AAC hearts treated with vehicle or Serelaxin. Vehicle-treated AAC-operated hearts showed an increased expression of Snail, Slug and Twist but a decreased expression of CD31, while Serelaxin treatment reduced Snail, Slug and Twist expression and restored CD31 expression. Student t-test was used for single comparison and one-way ANOVA with Bonferroni post-hoc analysis was used for multiple group comparisons. Gene expression and associated error bars represent mean \pm SEM, $n \geq 3$, n.s. no significance, * $p < 0.05$, ** $p < 0.01$, *** $p < 0.001$.*

SERELAXIN INHIBITS TGF β 1-INDUCED ENDMT THROUGH RXFP1

To gain mechanistic insights into Serelaxin-induced inhibition of EndMT, we used *in vitro* assays of EndMT in human and mouse endothelial cells. We first induced EndMT in HCAECs by TGF β 1 (10 ng/ml), and additionally applied four different concentrations of Serelaxin (ranging from 20 ng/ml to 200 ng/ml). Expression levels of CD31 and of EndMT transcription factors Snail, Twist and Slug were analyzed after 2 and 4 days respectively. Addition of Serelaxin showed a significant restored CD31 expression as well as a decrease in TGF β 1-induced expression of Snail, Twist and Slug at the doses of 100 and 200 ng/ml, indicating inhibition of EndMT (Figure 3A, Supplementary Figure 4). This effect could be observed after 2 days (Supplementary Figure 4A) and was more pronounced after 4 days (Figure 3A). Similar to human endothelial cells, addition of 100 ng/ml of Serelaxin was also effective in inhibiting TGF β 1-induced EndMT in MCECs (Figure 3B).

In order to identify the receptor type which mediates the EndMT-inhibitory effect of Serelaxin, we analyzed the mRNA expression level of each Relaxin receptor (type 1-4) in HCAECs. We only detected Relaxin receptor 1 (RXFP1) and 4 (RXFP4) to be expressed in these cells (Figure 3C). We next performed shRNA-mediated knockdown of RXFP1 and RXFP4 with up to 40% transfection efficiency and successfully decreased expression of both receptors by 80% (Supplementary Figure 5A-B). We next tested the effect of Serelaxin on TGF β 1-induced EndMT in HCAECs upon RXFP1 and RXFP4 knockdown respectively.

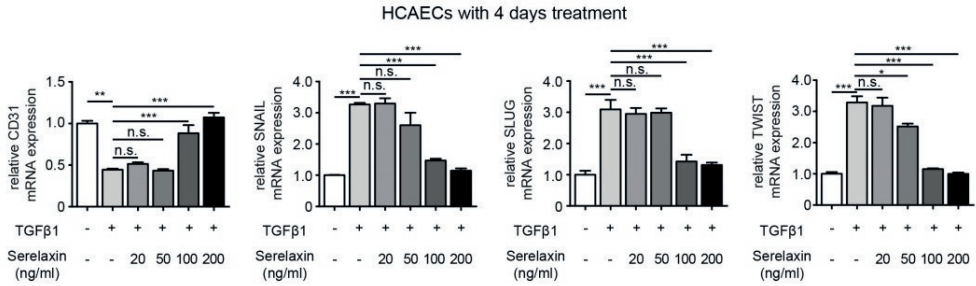
Upon knockdown of RXFP4, Serelaxin was still able to reduce the TGF β 1-induced expression of the key EndMT regulators SNAIL, SLUG, and TWIST. However, upon knockdown of RXFP1, the expression levels of the key EndMT regulators were not significantly altered by Serelaxin treatment (Figure 3D). Moreover, overexpression of RXFP1 enhanced the inhibitory effect of Serelaxin

on EndMT in HCAECs (Supplementary Figure 6A). These results demonstrate that the inhibitory effect of Serelaxin on EndMT is mediated by RXFP1.

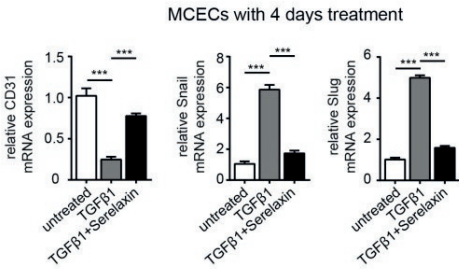
In order to gain insights if the anti-fibrotic effect of Serelaxin observed in the mouse models of cardiac fibrosis is also due to RXFP1-mediated inhibition of EndMT, we performed quantitative real time PCR for the different Relaxin receptors in MCECs. In MCECs, only Rxfp1 could be detected (Figure 3E).

We silenced Rxfp1 expression by a siRNA technique with three different oligos after which the Rxfp1 expression was reduced by 90% (Figure 3F). As in HCAECs, upon knockdown of Rxfp1, the expression levels of CD31 and the key EndMT regulators were not significantly altered by Serelaxin treatment in MCECs (Figure 3G). This data suggests that Serelaxin inhibits TGF β 1-induced EndMT through binding to Rxfp1 in both human and mouse endothelial cells.

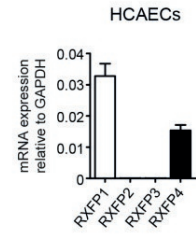
A



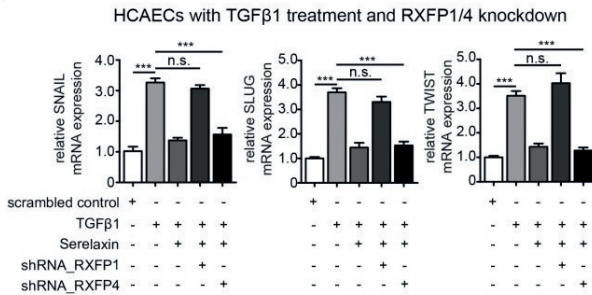
B



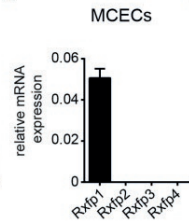
C



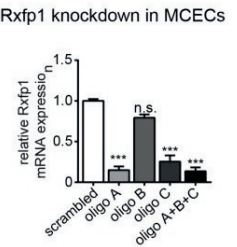
D



E



F



G

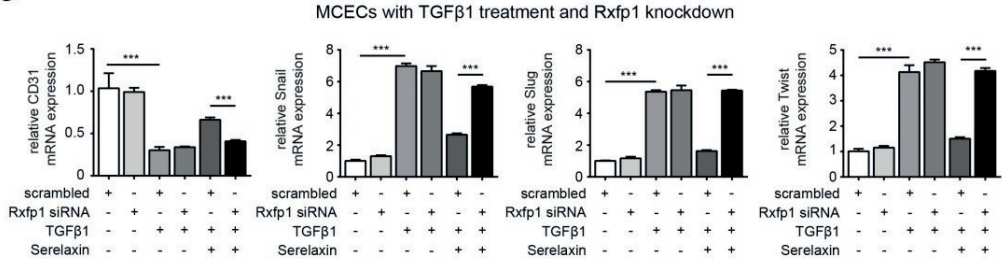


Figure 3. Serelaxin partially inhibits TGF β 1-induced EndMT in human coronary artery endothelial cells (HCAECs) and mouse cardiac endothelial cells (MCECs) via RXFP1.

(A) qPCR analysis showing the expression of endothelial cells marker CD31 and expression of EndMT key regulators SNAIL, SLUG, and TWIST in TGF β 1-treated HCAECs supplemented with different doses of Serelaxin after 4 days. Cells without any treatment were used as control. Serelaxin treatment significantly rescues expression of CD31 (100 and 200 ng/ml) and decreases expression of SNAIL, SLUG and TWIST (100 and 200 ng/ml). (B) qPCR analysis showing the mRNA expression of EndMT transcriptional factors Snail, Slug and Twist and of endothelial cell marker CD31 in TGF β 1-treated MCECs. Upon TGF β 1 treatment Snail, Slug and Twist expression increased and CD31 expression decreased. Treatment of Serelaxin showed a reduced expression of Snail, Slug and Twist and a restored expression of CD31. (C) qPCR analysis showing the relative mRNA expression level of RXFP1-4 in HCAECs. Among all four genes, only RXFP1 and RXFP4 expression is detectable. (D) qPCR analysis showing the expression of EndMT key regulators SNAIL, SLUG and TWIST in TGF β 1 and Serelaxin-treated HCAECs in combination with knockdown of RXFP1 or RXFP4. Cells without any treatment were used as control. Serelaxin treatment showed a reversal effect on TGF β 1-induced EndMT but not in RXFP1 knockdown cells. (E) qPCR analysis showing the relative mRNA expression level of Rxfp1-4 in MCECs. Among all 4 genes, only Rxfp1 expression is detectable but not the others. (F) qPCR analysis showing the relative mRNA level of Rxfp1 in scrambled and siRNA-mediated Rxfp1 knockdown cells. (G) qPCR analysis showing the expression of EndMT key regulators Snail, Slug and Twist in TGF β 1 and Serelaxin-treated MCECs upon Rxfp1 knockdown. Cells without any treatment were used as control. Serelaxin treatment showed a reversal effect on TGF β 1-induced EndMT but not upon Rxfp1 knockdown. Student t-test was used for single comparison and one-way ANOVA with Bonferroni post-hoc analysis was used for multiple group comparisons. Gene expression and associated error bars represent mean \pm SEM, $n \geq 3$, n.s. no significance, * $p < 0.05$, ** $p < 0.01$, *** $p < 0.001$.

We next analyzed RXFP1 protein expression by immunofluorescence staining (Figure 4A-D) and Western blot (Figure 4E) and mRNA expression by qPCR (Figure 4F) *in vivo* in the AAC-induced cardiac fibrosis model. In sham control mice, RXFP1 is largely colocalized (91%) with CD31 expression (Figure 4D). Interestingly, the expression level of Rxfp1 was decreased in diseased hearts as compared to healthy controls, but upregulated upon Serelaxin treatment (Figure 4D-F). In human heart tissue from healthy controls, RXFP1 is also the most abundant among all four receptors (Figure 4G), and is significantly decreased in tissue of patients with end stage heart failure (obtained at the time of heart transplantation) (Figure 4H).

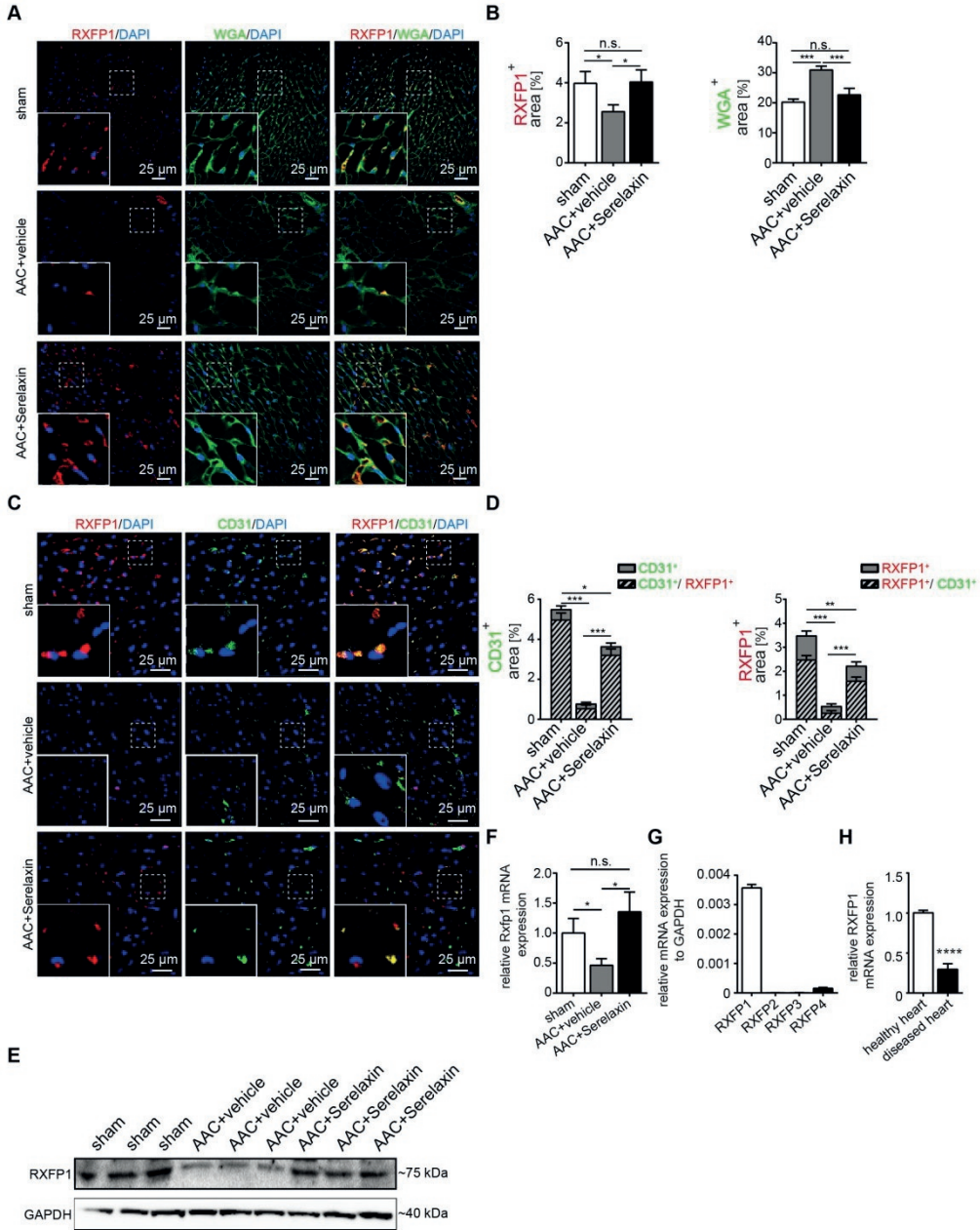


Figure 4. Serelaxin inhibits EndMT via RXFP1 *in vitro* and *in vivo*.

(A) Immunofluorescence staining of WGA, RXFP1 and DAPI in sham and AAC-operated hearts treated with vehicle or high dose Serelaxin. (B) Quantification of RXFP1 and WGA positive area showed a decreased RXFP1 and increased WGA protein expression in AAC-operated hearts compared to sham. Upon treatment with Serelaxin, RXFP1 expression was restored and WGA

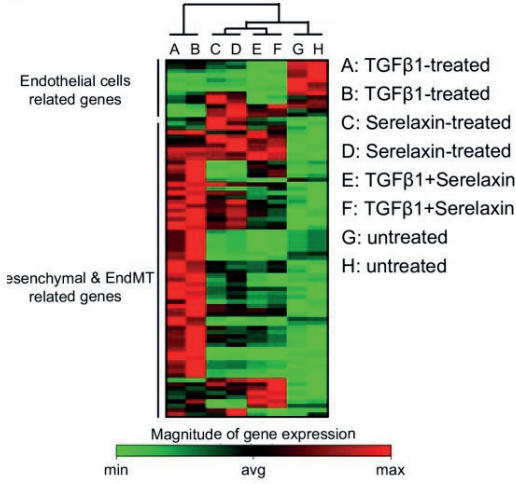
expression decreased. (C) Immunofluorescence staining of endothelial cell marker CD31, RXFP1 and DAPI. (D) Quantifications of CD31 (left panel) and RXFP1 (right panel) positive area. Compared to sham, AAC-operated vehicle-treated hearts showed a decreased expression of RXFP1 and CD31, while treatment with Serelaxin showed increased protein expressions of both CD31 and RXFP1. Each bar shows both the double positive area (streak lines) as well as single positive area (gray). The information on significance refers to the total CD31 (left panel) or RXFP1 (right panel) positive area. (E) Western blot analysis showing protein levels of RXFP1 in sham, AAC-operated and AAC-operated+Serelaxin-treated mouse hearts. Reduction of RXFP1 expression in AAC-operated animals compared to sham. Upon administration of Serelaxin, the protein level of RXFP1 was increased. (F) qPCR analysis showing the relative mRNA expression level of *Rxfp1* in sham and AAC-operated hearts treated with vehicle or Serelaxin. *Rxfp1* expression is decreased in AAC-operated hearts but restored upon Serelaxin treatment. (G) qPCR analysis showing the relative mRNA expression level of RXFP1-4 in human hearts. RXFP1 and RXFP4 expression were detected whereas RXFP2 was mainly expressed. (H) qPCR analysis showing a reduced relative mRNA expression level of RXFP1 in diseased human hearts compared to healthy control hearts. Student t-test was used for single comparison and one-way ANOVA with Bonferroni post-hoc analysis was used for multiple group comparisons. Gene expression and associated error bars, representing mean \pm SEM, $n \geq 3$, n.s. no significance, * $p < 0.05$, ** $p < 0.01$, *** $p < 0.001$, **** $p < 0.0001$.

SERELAXIN INHIBITS TGF β 1-INDUCED ENDMT THROUGH PRESERVATION OF NOTCH SIGNALING IN ENDOTHELIAL CELLS

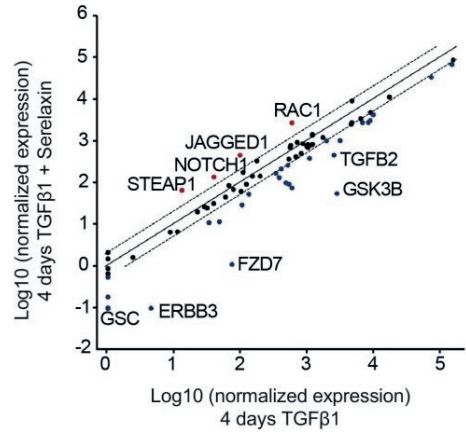
In order to gain insight into the downstream signaling pathways affected by Serelaxin treatment, we performed an EndMT qPCR array analysis (containing 84 key genes that either change their expression during the EndMT process or regulate those gene expression changes). This assay was performed in HCAECs after 4 days with either no treatment, TGF β 1 treatment alone, Serelaxin treatment alone or both TGF β 1 and Serelaxin treatment. The overall gene expression profile of TGF β 1/Serelaxin combination treatment was closest to that of Serelaxin-treated samples and then to the untreated sample group in hierarchy analysis (Figure 5A). We then compared the differentially expressed genes between TGF β 1 treatment alone and TGF β 1/Serelaxin combination treatment (Figure 5B) and between Serelaxin treatment alone and TGF β 1 treatment alone (Supplementary Figure 7). Four genes (STEAP1, NOTCH1, JAGGED1 and RAC1) were selectively upregulated in the Serelaxin treatment alone and TGF β 1/Serelaxin combination group and six genes (GSC, ERBB3, FZD7, GSK3B and TGFB2) in the TGF β 1 group. Notably, Serelaxin ameliorated the effects of TGF β 1 on these genes in HCAECs.

To validate those candidate genes in mice, we analyzed their expression in MCECs and in mouse heart tissue. In Serelaxin supplemented TGF β 1-treated MCECs Rac1, Steap1, Notch1 and Jagged1 were all significantly upregulated whereas Gsk3b, Gsc, Fzd7 and Erbb3 were significantly decreased as compared with TGF β 1-treated cells (Figure 5C-D), which is in line with the experiments in HCAECs. In hearts of AAC-challenged mice which received Serelaxin, three of the upregulated genes (Rac1, Jagged1 and Notch1) and three of the downregulated genes (Erbb3, Gsk3b and Fzd7) could be validated (Figure 5E). Unlike Erbb3, Steap1 (which is reduced both in endothelial cells upon TGF β 1 *in vitro*, and also in whole AAC hearts *in vivo*) is rescued by Serelaxin only *in vitro* but not *in vivo* (where Serelaxin even further decreases Steap1 expression). This discrepancy is likely due to different regulation of Steap1 in different cell types.

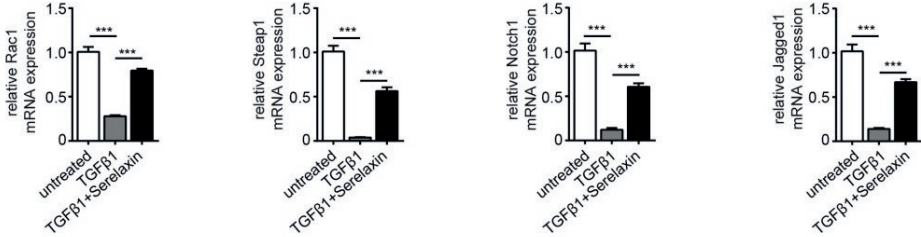
A



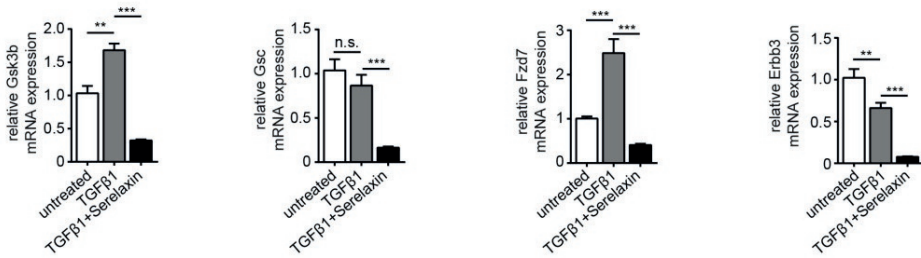
B



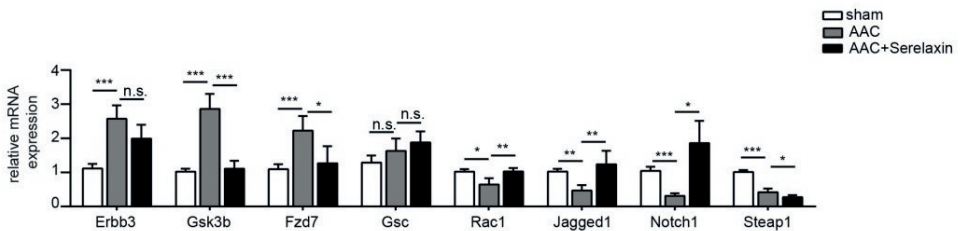
C



D



E



7

Figure 5. Serelaxin promotes the preservation of endothelial cell properties in both *in vivo* and *in vitro* by regulating candidate genes.

(A) Heat map and (B) scatter plot show the genes with altered mRNA expression level in only TGF β 1-treated (x-axis) or in both TGF β 1- and Serelaxin-treated (y-axis) HCAECs. STEAP1, NOTCH1, JAGGED1, RAC1, DSP, GSC, ERBB3, FZD7, GSK3B and TGF β 2 are significantly regulated are significantly regulated by Serelaxin treatment, which is shown by separation from dot lines (cut-off by 4 folds). (C-D) qPCR analysis showing the expression of candidate genes, which were identified from qPCR array in TGF β 1- and Serelaxin-treated MCECs. Cells without any treatment were used as control. (E) qPCR analysis of the panel of candidate genes *in vivo* in sham and AAC-operated mice treated with vehicle or Serelaxin. Serelaxin significantly rescued the effects of AAC on all genes except for Gsc and Steap1. Student t-test was used for single comparison and one-way ANOVA with Bonferroni post-hoc analysis was used for multiple group comparisons. Gene expression and associated error bars, representing mean \pm SEM n \geq 3, n.s. no significance, * p<0.05, ** p<0.01, *** p<0.001.

Because out of these genes Notch1 and its ligand Jagged1 (both upregulated by Serelaxin treatment) have well-known protective roles for maintaining the endothelial phenotype, we focused on studying the effect of Serelaxin on Notch signaling. Immunofluorescence staining of AAC-challenged hearts revealed fewer Jagged1, Notch1 and NICD-positive cells (indicating reduced Notch1 intracellular signaling) as compared to sham operated mice, especially within fibrotic areas (as indicated by wheat germ agglutinin staining, WGA, Figure 6A-C).

In Serelaxin-administered mice, Jagged1, Notch1 and NICD-positive areas were all increased as compared to vehicle-treated mice (Figure 6D-F), indicating that the effect of Serelaxin which we observed during EndMT *in vitro* also occurs during fibrogenesis *in vivo*. To test if this effect of Serelaxin is similarly mediated by Rxfp1, we performed siRNA knockdown of Rxfp1 in MCECs. Afterwards we induced EndMT by TGF β 1 and tested the effect of Serelaxin with respect to Notch1 and Jagged1 expression (Supplementary Figure 6B-D). While Serelaxin rescued Notch1 and Jagged1 expression in TGF β 1-induced EndMT, this effect was gone upon knockdown of Rxfp1. In order to further elucidate the link between Serelaxin, Rxfp1 and Notch1, we have additionally transfected TGF β 1-treated MCECs with a NICD overexpression construct (to mimic Notch1 activation), which resulted in reduction of EndMT marker genes (Supplementary Figure 6E). On the other hand, supplementation of DAPT (an indirect Notch inhibitor) to Serelaxin + TGF β 1-treated MCECs leads to a significantly decreased EndMT-inhibitory effect of Serelaxin as compared to supplementation of DMSO as a control

(Supplementary Figure 6F). This data implies that Serelaxin ameliorates TGF β 1-induced EndMT, at least in part, via activation of the Notch pathway.

Because Jagged1 mediates Notch1 activation only after being secreted, we also measured Jagged1 secretion from MCECs. We therefore collected medium from TGF β 1-treated and control MCECs and precipitated all soluble proteins by acetone. Western blot analysis confirmed a significant decrease of secreted Jagged1 soluble protein in MCECs upon TGF β 1 treatment when compared to untreated MCECs (Figure 6G). To sum up, our results suggest that the Notch1 signaling pathway is partially inhibited in AAC operated hearts and TGF β 1-treated MCECs. These effects were attenuated by supplementation of Serelaxin.

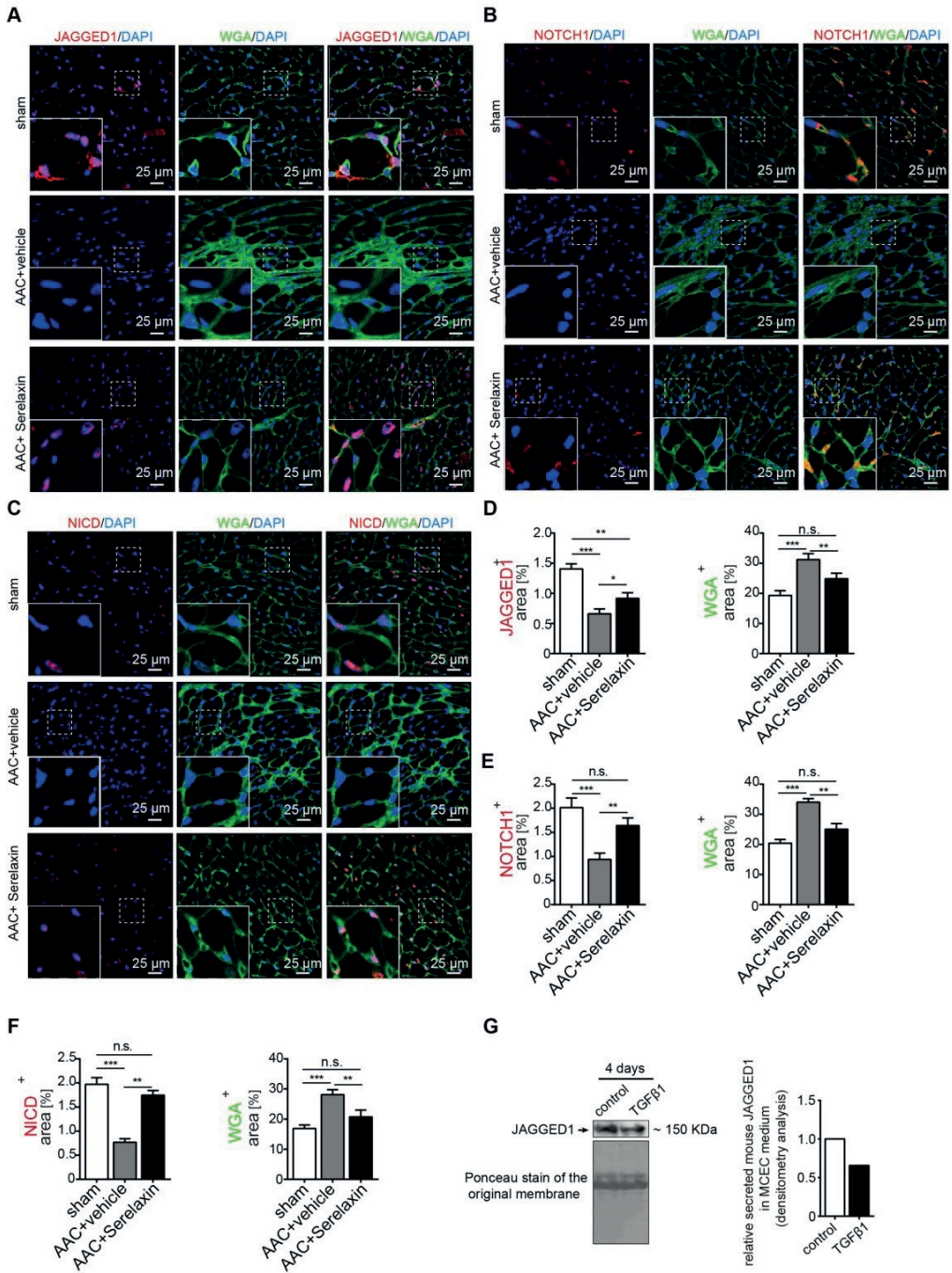


Figure 6. Serelaxin rescues the Notch1 pathway in AAC operated hearts.

Immunofluorescence staining of (A) *Jagged1*, (B) *Notch1* and (C) *NICD* in combination with WGA and DAPI in sham and AAC-operated hearts treated with vehicle or Serelaxin. Quantifications showed that protein expressions of (D) *Jagged1*, (E) *Notch1* and (F) *NICD* were downregulated in AAC-operated hearts and could be restored by Serelaxin. (G) Western blot analysis shows the amount of the soluble form of *Jagged1* in the medium of *TGFβ1*-treated MCECs. Ponceau-S stained membrane picture indicates that an equal amount of total precipitated protein was loaded for both the control and *TGFβ1*-treated MCECs. Soluble *Jagged1* is reduced in *TGFβ1*-treated MCECs as quantified by densitometry analysis (right panel). Student *t*-test was used for single comparison and one-way ANOVA with Bonferroni post-hoc analysis was used for multiple group comparisons. Gene expression and associated error bars, representing mean \pm SEM, $n \geq 3$, n.s. no significance, * $p < 0.05$, ** $p < 0.01$, *** $p < 0.001$.

SERELAXIN RESCUES RXFP1 EXPRESSION BY MODULATING HISTONE MODIFICATIONS

Overall, the results thus far imply that Serelaxin exerts its anti-fibrotic effect at least in part by inhibition of EndMT via the Notch1 signaling pathway, which is mediated by Rxfp1. However, we have observed, that in AAC-challenged mouse hearts (Figure 4E-F), human diseased hearts (Figure 4H) as well as in *TGFβ1*-treated endothelial cells (Supplementary Figure 6B); RXFP1 is downregulated as compared to healthy hearts or native endothelial cells. In mice which were administered with Serelaxin on the other hand, this receptor downregulation was rescued (Figure 4E-F). In this respect, it has been shown that *TGFβ1* induces epigenetic silencing of gene expression via methylation of CpG islands within the promoter as well as via histone modifications. We therefore aimed to investigate if the silencing of Rxfp1 could be due to one of these epigenetic mechanisms and if Serelaxin is able to inhibit such modifications. However, within 5kb upstream of the transcription start site (TSS) of murine Rxfp1 we have not found a CpG island, indicating that silencing of Rxfp1 is not mediated by promoter hypermethylation.

In order to identify potential histone modifications facilitated by *TGFβ1* and/or Serelaxin, we performed ChIP analysis of gene specific histone modification profiles (activating: H3K4me3, H3K27ac; and repressive: H3K9me3, H3K27me3) at the promoter region (1kb upstream of TSS) of Rxfp1 (Figure 7A). Real-time PCR showed that the promoter region of Rxfp1 was enriched for the activating modifications H3K4me3 and H3K27ac and depleted for the repressive

modifications H3K9me3 and H3K27me3 in untreated cells, indicating a transcriptionally active chromatin (Figure 7B). In contrast, after TGF β 1 treatment, the repressive modifications were increased whereas activating modifications were reduced (Figure 7B). After supplementation with Serelaxin, the activating modifications could be significantly increased and repressive modification marks were significantly decreased (Figure 7B). The qPCR analysis with primer targeting intron 10 did not show any significant differences among all the histone marks. To further explore the dependence of histone modification changes on Rxfp1 expression, we repeated ChIP analysis with Rxfp1-knockdown MCECs and found that Serelaxin was no longer able to increase the activating modifications nor to decrease the repressive modifications (Figure 7C). Collectively, these results suggest that restored Rxfp1 expression upon Serelaxin treatment is mediated at least in part through a histone modification regulatory mechanism facilitated by Serelaxin on the remaining Rxfp1 expression.

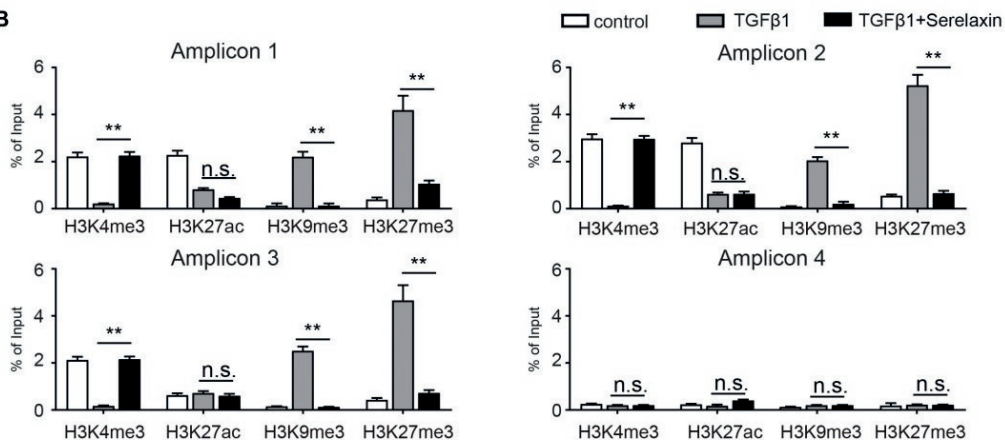
Since it is known that Relaxin inhibits the TGF β pathway [44–46], we hypothesized that activation of RXFP1 expression by Serelaxin might be through blocking the TGF β pathway. We performed Western blot analysis of pSMAD2 and pSMAD3 in sham, AAC-operated and AAC-operated + Serelaxin-treated mouse hearts and showed an increase of pSMAD2 and pSMAD3 protein levels in AAC-operated animals compared to sham. Upon administration of Serelaxin, the protein levels of pSMAD2 and pSMAD3 were decreased (Figure 7D). pSMAD2/3 are transcription factors which bind to DNA, regulate the target gene expression and are known to mediate histone marks (H3K27me3, H3K9me3, H3K4me3, H3K27ac). In order to further elucidate the link between Serelaxin, pSMAD2/3 and RXFP1 expression, we performed a pSMAD2/3 immunoprecipitation experiment at the promoter region of Rxfp1 and showed that the enrichment of pSMAD2/3 at the Rxfp1 promoter region was significantly compromised by treatment with TGF β 1+Serelaxin when compared to TGF β 1 treatment alone (Figure 7E). The qPCR analysis with primer targeting intron 10 did not show any significant differences between these groups.

SERELAXIN ALLEVIATES CARDIAC FIBROSIS THROUGH INHIBITING ENDMT

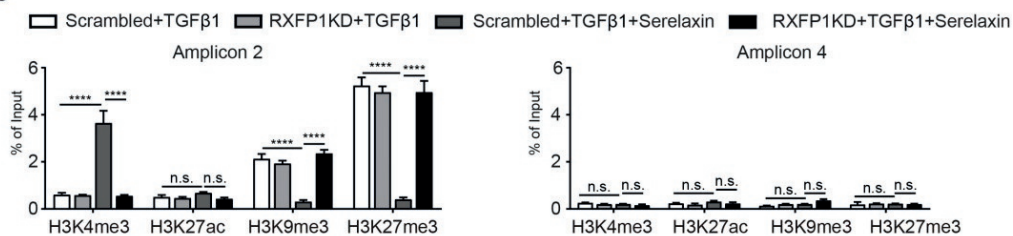
A



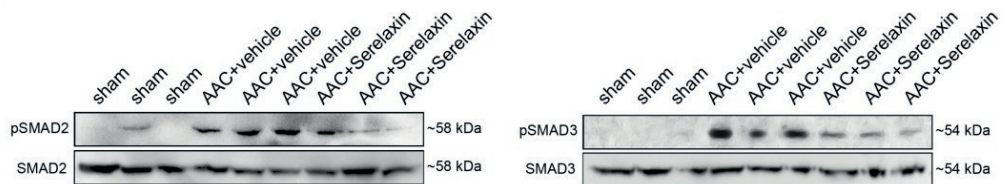
B



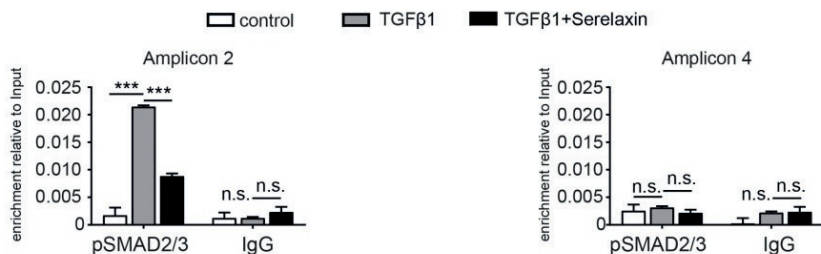
C



D



E



7

Figure 7. Serelaxin reactivates Rxfp1 expression via histone modifications.

(A) Schematic representing the mouse *Rxfp1* locus with locations of CHIP-qPCR primers. (B) qPCR analysis showing the enrichment of 4 different histone modification marks (active: H3K4me3 and H3K27ac, repressive: H3K9me3, H3K27me3) in the *Rxfp1* promoter region (Amplicon 1-3) and intron 10 (Amplicon 4). The enrichment of TGF β 1-influenced H3K4me3, H3K9me3 and H3K27me3 marks were significantly compromised by Serelaxin if performed with amplicons 1-3 targeting the promoter region but not with amplicon 4 targeting intron10. (C) ChIP-qPCR analysis showing the enrichment of histone modification marks in the *Rxfp1* promoter region after RXFP1 knockdown. Upon RXFP1 knockdown, treatment with Serelaxin did not significantly increase the activating modifications or decrease the repressive modification marks. (D) Western blot analysis showing protein levels of pSMAD2 and pSMAD3 in sham, AAC-operated and AAC-operated+Serelaxin-treated mouse hearts, total SMAD2 and SMAD3 were used as protein loading controls. AAC-operated(E) qPCR analysis showing the enrichment of pSMAD2/3 in the *Rxfp1* promoter region (Amplicon 2) and intron 10 (Amplicon 4). The enrichment of TGF β 1-induced pSMAD2/3 was significantly compromised by Serelaxin. The qPCR analysis with primer targeting intron10 did not show any significant differences between these groups. Student t-test was used for single comparison and one-way ANOVA with Bonferroni post-hoc analysis was used for multiple group comparisons. Gene expression and associated error bars, representing mean \pm SEM, $n \geq 3$, n.s. no significance, ** $p < 0.01$, *** $p < 0.001$, **** $p < 0.0001$.

These results suggest that Serelaxin initiates a positive feedback loop: Serelaxin induces Rxfp1 expression by partially inhibiting TGF β -induced histone modifications at the Rxfp1 promoter (Figure 8).

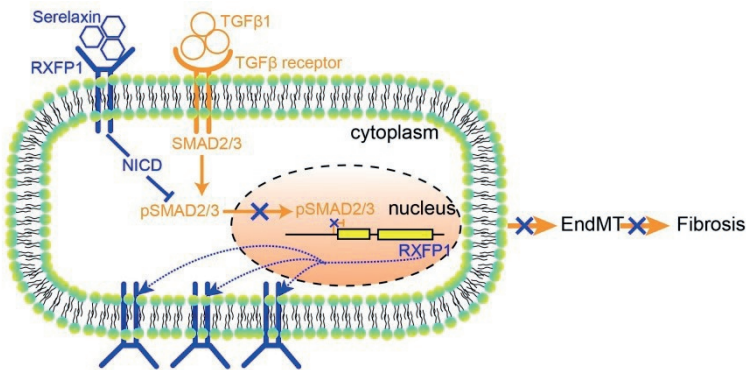


Figure 8. A proposed model depicting the molecular mechanism by which Serelaxin activates the Notch signaling pathway to inhibit TGF β -induced SMAD2/3 phosphorylation to restore the RXFP1 expression via histone modifications.

DISCUSSION

This study demonstrates an anti-fibrotic effect of Serelaxin in two independent mouse models of pressure overload, AAC and the ATII infusion via osmotic minipumps. We also showed that the anti-fibrotic effect is associated with reduced mortality in mice. We further demonstrate that the anti-fibrotic effect of Serelaxin is at least in part due to inhibition of EndMT via activation of Notch1 signaling, and that this effect is mediated by the Relaxin receptor Rxfp1. Finally, we provide data which suggest that Serelaxin is able to rescue low Rxfp1 levels in diseased hearts by blocking the TGF β pathway and consequently mediating Rxfp1 gene histone modifications.

With respect to controversial reports on the relevance of EndMT in pressure overload models, it is important to note that in this study we used constriction of the ascending aorta ("AAC", a more pronounced model of pressure overload, where EndMT has been previously demonstrated [38]) but not constriction of the transverse aorta ("TAC" a milder model, where EndMT has not been reported [47]). Interestingly, we found downregulation of Notch1 signaling (which has been linked to increased EndMT by several studies [30,31]) 4 weeks after AAC accordingly, whereas increased Notch1 signaling has been reported one week after TAC (where no EndMT is present). As a second model we used Angiotensin II infusion via osmotic minipumps, which yielded similar results. We are aware however, that this model (while in general well-accepted to induce pressure-overload and cardiac fibrosis) also exerts direct pro-fibrotic stimuli to the heart, e.g. via direct activation of the TGF β 1/Smad signaling pathway in cardiac fibroblasts [48]. Thus, an additional influence of Serelaxin on these stimuli cannot be excluded in this model.

Nevertheless, in both animal models, Serelaxin showed consistent results in the sense that the reduction of perivascular fibrosis was more significant than interstitial fibrosis, which guided our focus on studying the effect of Serelaxin with respect to EndMT. Since perivascular fibrosis is also a contributor to reduction of myocardial and arterial compliance [49], the therapeutic effect of Serelaxin on perivascular observed by us is in line with a recent study which showed a vascular-protective effect of Serelaxin in an ATII mouse model [50].

This study is in line with several other studies which reported an anti-fibrotic effect of Serelaxin in various organs including the heart [51-53]. While most other

studies focused on studying effects of Serelaxin on fibroblasts, in our study Serelaxin showed a microvasculature stabilizing and profound EndMT-inhibitory effect on endothelial cells. We could prove that Serelaxin is indeed able to ameliorate fibrosis, at least in part, via inhibition of EndMT. Both mechanisms, inhibition of fibroblast to myofibroblasts activation [54] and inhibition of EndMT, likely affect fibrosis in parallel and synergistically.

In line with this, Wu et al. recently showed that Serelaxin inhibits TGF β 1/Smad2/3 signaling pathway through inhibiting the expression of ALK5 in TGF β 1-treated cardiac fibroblasts [55].

That EndMT contributes to fibrogenesis was first reported in cardiac fibrosis in a model of pressure overload, but in subsequent studies it was shown that EndMT is also relevant in fibrosis of other organs including the kidney, the lung and the intestinal tract [33,37,56]. Besides EndMT contributes to cancer-associated fibroblasts in the tumor stroma, where it is associated with metastasis [36]. It could therefore be speculated that Serelaxin has an effect on fibrosis in all organs where EndMT is involved and potentially, that it affects progression of tumors associated with EndMT.

Several tumor studies describe that Relaxin promotes matrix invasion by affecting the Wnt/ β -Catenin and GSK3 β pathway [57–59]. These studies found that supplementation of Relaxin increased protein levels of phosphorylated GSK3 β but not of total GSK3 β . We have studied mRNA of total GSK3 β (which we find decreased in cardiac endothelial and whole heart tissue upon Serelaxin). In general, this supports Thanasupawat et al., who summarized in 2019 that the positive or negative effect of Relaxin on cells depends on the cell model chosen, the exposure time, and on the Relaxin concentration used [60].

Our study identified Notch1 signaling to be reactivated by Serelaxin both *in vitro* and *in vivo*. Because Notch1 signaling is able to both induce and to inhibit EndMT (depending on the context), we performed NICD overexpression to study the effect of Notch1 in the context of adult coronary artery endothelial cells. Our results suggest that Notch1 protects the endothelial phenotype in this context. Our study is supported by a study in a rat model of heart failure, where a link between Relaxin and Notch1 signaling has also been observed [30]. The effect of TGF β 1 on Notch1 is equally context-dependent: a positive regulatory role of TGF β 1 in activating Notch signaling pathway has been reported in other cells. Blokzijl et al. showed a cross-talk between the Notch1 and TGF β signaling

pathways in mouse neural stem cells and mouse myoblasts [61]. Upon TGF β 1 treatment, Hes1 (the target for Notch pathway) expression was increased. Hajdu et al. also showed an increased HES1 and TIEG expression in human non-Hodgkin B-cell lymphoma cell lines [62]. Both studies focused on the effect of TGF β 1 treatment on Notch1 target gene expression rather than on Notch1 expression itself. In contrast to these studies, Wu et al. showed (similar to our results) a reduced Notch1 target gene expression by TGF β 1 in adult human Mueller stem cells [63]. Interestingly, a reduction of Notch1 by TGF β 1 in cardiac fibroblast has also been reported by Sassoli et al [24]. The discrepancy between these various studies underlines the cell-type specific regulation of Notch1 signaling, and potential cell-type specific effects of Serelaxin.

Furthermore, our study is the first to identify Rxfp1 to mediate the anti-EndMT effect of Serelaxin. We identified this receptor in *in vitro* studies of EndMT, and found this receptor to be downregulated in diseased hearts as compared to healthy hearts *in vivo* accordingly. The fact that administration of Serelaxin to mice which had undergone AAC was able to rescue expression of this receptor to the level of sham operated animals is potentially one of the most important and novel findings of this study. Our data suggests that in diseased hearts, Rxfp1 is downregulated through histone modifications and that Serelaxin is able to influence these chromatin modifications in a favorable way. This study is the first to report that Serelaxin affects histone modifications by an anti-TGF β -SMAD2/3 cascade (Figure 8). The recent phase III trial (RELAX-AHF 2), testing short-term intravenous Serelaxin administration for acute decompensated heart failure, did not show a reduced cardiovascular mortality after 6 months nor reduced worsening of heart failure after 5 days and therefore failed. However, our results suggest that Serelaxin may have long-term beneficial effects in chronic heart failure through its anti-fibrotic and epigenetic gene re-activating effects.

FUNDING

This work was supported by Novartis Pharma AG, Basel, Switzerland for providing Serelaxin and for funding to support the project. XX received support from the “seed funding research program” of the Faculty of Medicine, Georg August University Goettingen and postdoc start-up grant, DZHK.

ACKNOWLEDGEMENTS

The authors thank Annika Erdmann, Sarah Rinkleff and Anika Krueger for technical assistance.

MATERIALS AND METHODS

ANIMAL WELFARE AND ETHICS STATEMENT

All animal experiments complied with ethical regulations and were conducted according to the animal experimental protocols, which were approved by the Institutional Review Board of the University of Göttingen and the responsible government authority of Lower Saxony (Germany). All animal procedures conformed to the guidelines from Directive 2010/63/EU of the European Parliament on the protection of animals used for scientific purposes. Animal surgery experimental protocols are described in the following texts.

ASCENDING AORTIC CONSTRICTION

Ascending aortic constriction (AAC) was performed under anesthesia in 12-week-old C57BL/6N mice (each group was composed of half male and half female mice), weighing between 25-30 g with a mixture of medetomidine (0.5 mg/kg), midazolam (5 mg/kg) and fentanyl (10 mg/kg) at 0.1 ml NaCl intraperitoneally before the surgery. In these mice constriction of the ascending aorta was performed with a 24-gauge needle as previously described [38]. Sham operation was performed under the same conditions except for the aortic banding. Echocardiography of the aortic pressure gradient was performed to verify aortic constriction, and all mice were sacrificed four weeks after operation by cervical dislocation under anesthesia.

ECHOCARDIOGRAPHIC MEASUREMENT OF THE PRESSURE GRADIENT

Pressure gradients were measured according to the previously described protocol [39] using a Vevo 2100 (FUJIFILM VisualSonics, Toronto, Canada) system with a 30-MHz respiration- and ECG-controlled probe under anesthesia with 1.5% isoflurane by inhalation during the whole procedure. The ascending aorta was visualized with 2-D and color flow imaging. The distal ascending aortic flow velocity (distal to constriction in AAC mice) was measured by pulsed wave (PW) Doppler to assess the pressure gradient, which was estimated using the modified

Bernoulli equation (pressure gradient = $4 \times \text{velocity}^2$). The investigator was blinded with respect to treatment.

APPLICATION OF SERELAXIN AND PBS VIA OSMOTIC MINIPUMP IMPLANTATION

Serelaxin was applied at three different dosages (50, 200 and 500 $\mu\text{g}/\text{kg}$ bodyweight/day) for 28 days. PBS was used as a vehicle. Both Serelaxin and PBS were administered to animals using an osmotic minipump (Model 1004 ALZET, Cupertino, CA, USA). The minipumps were implanted during AAC operation by cutting the skin median of the dorsal neck. Skin was mobilized carefully from the muscle fascia. Afterwards the minipump was put into the skin pocket and the wound closed by three sutures.

APPLICATION OF ANGIOTENSIN II VIA OSMOTIC MINIPUMP IMPLANTATION

14- to 16-week-old C57BL/6N mice between 25-30 g were used for Angiotensin II (ATII) experiments. ATII (1.5 mg/kg per day) plus Serelaxin (500 $\mu\text{g}/\text{kg}$ bodyweight) or PBS as vehicle control were administered to animals at the same time using an osmotic minipump (ALZET Model 1002 for 2 weeks and 1004 for 4 weeks). The mice were anesthetized with 3% to 4% of isoflurane by inhalation during the whole procedure.

HISTOLOGICAL ASSESSMENT OF CARDIAC FIBROSIS

The percent area of left ventricular myocardial fibrosis was quantified using cellSens software. Perivascular fibrosis was defined as fibrotic lesions surrounding vessels of $>100 \mu\text{m}$.

IMMUNOFLOUORESCENT STAINING

Paraffin-embedded heart tissues were sectioned at 3 μm thickness, deparaffinized and rehydrated by xylol and graded alcohol series prior to staining. Antigen retrieval was performed with citrate buffer (Dako Retrieval Solution (10x) pH6, Agilent Dako, Santa Clara, CA, USA) for 40 minutes and thereafter washed with PBS for 10 minutes. The slides were blocked in 1% BSA in PBS at room

temperature for 30 minutes before incubating with a primary antibody at 4°C overnight. The fluorescence labeled secondary antibodies were added and incubated at room temperature for 45 minutes. The cell nucleus was visualized with DAPI (1 mg/ml, #6335.1, Carl Roth, Karlsruhe, Germany) with 1:1000 dilution in PBS at room temperature for 5 minutes. Microscopic pictures were acquired using an Olympus Confocal Microscope FV-1000 and Fluoview program. The acquired pictures were processed using Photoshop CS6 software. The primary and secondary antibodies used in this study with dilution factors are listed below.

Antibody	Dilution	Company	Catalog No.
Anti-Mouse wheat germ agglutinin	1:1000	Life technologies	W11261
Alexa Fluor 488 conjugated			
Rabbit Anti-Mouse RXFP1	1:50	Santa Cruz	SC50528
Rabbit Anti-Mouse α SMA	1:100	Abcam	Ab32575
Goat Anti-Mouse CD31	1:50	Santa Cruz	SC1306
Rabbit Anti-Mouse Col1 α (I)	1:200	Abcam	Ab34710
Rabbit Anti-Mouse Notch1	1:100	Abcam	Ab8925
Rabbit Anti-Mouse Jagged1	1:50	Santa Cruz	SC8303
Rabbit Anti-Mouse NICD	1:50	Abcam	Ab52627
Alexa Fluor 568 donkey anti rabbit	1:200	Life technologies	A10042
Alexa Fluor 568 donkey anti mouse	1:200	Life technologies	A10037
Alexa Fluor 568 donkey anti goat	1:200	Life technologies	A11057
Alexa Fluor 488 donkey anti rabbit	1:200	Life technologies	R37118

CHROMATIN IMMUNOPRECIPITATION (CHIP) - QPCR

Chromatin immunoprecipitation for histone modifications was performed as previously described [40]. Briefly, the chromatin was cross-linked with paraformaldehyde for 10 minutes and immunoprecipitation was performed with antibodies dilutions listed below. The pull-down DNA was dissolved with 100 μ l of elution buffer and 2 μ l of DNA sample was used for each qPCR reaction with the real-time PCR primers (sequence listed below).

Antibody	Dilution	Company	Catalog No.
H3K4me3	1:400	ActiveMotif	39159
H3K9me3	1:400	ActiveMotif	39765
H3K27me3	1:400	ActiveMotif	39155

CHAPTER 7

H3K27ac	1:400	ActiveMotif	39133
pSMAD2/3	1:300	Cell Signaling	5678

ChIP-qPCR assay for Rxfp1

Amplicon	Sequence
1	F: TGCTCAACTTCCAAACAGA R: ATGCTTTTGTGGCACAGCTA
2	F: CCATGCTTGGGATTACCTC R: TGCTCTGACAAAGCCTTCAC
3	F: ATGAGGGAGGGACACAGAGA R: ACAGCTCACAGTGGTTGTGC
4	F: TGGTGTGGGGATTGAACTCA R: GACTTCATGCATGTGGAGGC

CELL CULTURE EXPERIMENTS AND TRANSFECTION

Human coronary artery endothelial cells (HCAECs, PromoCell, Heidelberg, Germany) and mouse cardiac endothelial cells (MCECs, CellLutions, Burlington, Ontario, Canada) were kept at 37 °C supplemented with 5% CO₂. Every other day the cell medium was changed and supplemented with 10 ng/mL TGFβ1 (R&D Systems, Minneapolis, USA) or 20- 200 ng/ml Serelaxin (Novartis, Switzerland). For Notch inhibition experiment, DAPT (Sigma-Aldrich, St. Louis, CA, USA) was supplemented into the cell culture medium (20 µg/ml) and replaced every second day. A total cell number of 2 x 10⁵ was seeded onto 6-well-plates, incubated for 24 hours and starved with basal medium before treatment. Cell samples were collected at 2 or 4 days after treatment.

For transfection experiments, HCAECs and MCECs were seeded onto 10 cm plates (Griner), cultured overnight and transfected with Lipofectamine 2000 (Life Technologies, Carlsbad, CA, USA) according to the manufacturer's instructions [41]. Briefly, 2.5 µg of shRNA-plasmid or 40 pmol of siRNA (Origene, Rockville, MD, USA) and Lipofectamine 2000 were mixed in a ratio of 1:2 in a total volume of 500 µl of Opti-MEM (Life Technologies), what forms the complex by incubating 20 minutes at room temperature. Then, the DNA–Lipofectamine complex was added to the cells in endothelial cell basic medium. After 3 hours of incubation, the medium was replaced by growth medium. TGFβ1 treatment started one day after transfection, and cells were collected for gene expression analysis after 4 days of TGFβ1 treatment.

RNA EXTRACTION AND QUANTITATIVE REAL-TIME PCR

Tissue was first shredded using TissueLyser LT (Qiagen, Hilden, Germany). Total RNA was extracted from cells or shredded tissue by PureLink RNA kit (Life Technologies, Carlsbad, USA) following the manufacturer's protocol. Prior to cDNA synthesis using the SuperScript II system (Life Technologies, Carlsbad, USA), 1 µg of total RNA was digested with DNase I (Sigma Aldrich, St. Louis, CA, USA). qRT-PCR was performed with SYBR Master Mix (Life Technologies, Carlsbad, USA) in 20 µl of final reaction volume, and 2 µl of diluted cDNA (1:20) was used as a template and run on a StepOne Plus real-time PCR system (Life Technologies) with real-time PCR primers (sequence listed below). Measurements were standardized to the GAPDH reaction using delta delta Ct methods.

Name	Sequence	Reference
Mouse		
CD31	F: CCAAAGCCAGTAGCATCATGGTC R: GATGGTGAAGTTGGCTACAGG	Primer design
Erb3	F: TCACACTCAGCCCGTTTAGA R: AGGTGCTGGGTTTCCTTCTC	Origene
Fzd7	F: TCAGCTGGAGGAAAAGACG R: GTGCTGGACGCGGAGAGT	Origene
Gapdh	undisclosed	Primer design
Gsc	F: CATGTAGGGCAGCATCTGGT R: CAGCAGTGCTCCTGCGTC	Origene
Gsk3b	F: GTGGTTACCTTGCTGCCATC R: GACCGAGAACCACCTCCTTT	Origene
Jagged1	F: AACCTGTAACATAGCCCGAAAC R: GTAAAGGACTCGCCGTTGAC	Primer design
Notch1	F: TGCCCGTTCTTGAAATGTAGG R: GGCAGTGTCTTTCCCAGA	Primer design
Rac1	F: CTCCAGGAAATGCATTGGT R: AGATGCAGGCCATCAAGTGT	Origene
Rln1	F: GGCAACCATCATTACCAGAGC R: TCCAAGCCTAAGTATTTAATTCTGAA	Primer design
Rxfp1	F: ATTTCTCTGCTGTGCTGACT R: CGGCTGTGCGTGCTTATTG	Primer design
Rxfp2	F: ACGAACTCCACCTTCTAACG R: AAAATGTCTTCTCTGGAACAAAACC	Primer design
Rxfp3	F: AACCCGATCCTCTACTGCTTAG R: GCATGTTGGTGAGCGAAGG	Primer design

CHAPTER 7

Rxfp4	F: AGGTAAGTGTGGTCAGCGTGTG R: CCAGTGGAAAGTCCATTGCTGAC	Origene
Slug	F: CGCTCCTTCTGGTCAAGA R: AGGTATAGGGTAACTTTCATAGAGATA	Primer design
Snail	F: GTGCCACCTCCAAACCC R: AAGGACATGCGGGAGAAGG	Primer design
Steap1	F: CAAACCCAGAACAACCTTTGGA R: TCGTCTCTCCCAGAGCTCTTA	Origene
Twist	F: TGATAGAAGTCTGAACACTCGTTTG R: GGCTGATTGGCAAGACCTCT	Primer design
Human		
CD31	F: AAGGAACAGGAGGGAGAGTATTA R: GTATTTTGCTTCTGGGGACACT	Primer design
GAPDH	undisclosed	Primer design
RLN1	F: GGCAACCATCATTACCAGAGC R: TCCAAGCCTAAGTATTTTAATTCTGAA	Primer design
RLN2	F: GCTCCTCAGACACCTAGACC R: CTGTGGCAAATTAGCAACAAATTC	Primer design
RXFP1	F: GCTGTATGCCATGTCAATCATT R: TCTCCACGAACTTTAGGTCAA	Primer design
RXFP2	F: GATCACTCCTTCATGCCAAAAG R: TGTCACCACAGTTCTTTCGT	Primer design
RXFP3	F: ACCAAATCAGTGACCATCGTT R: GCGTTGAACTTGATGAGGATG	Primer design
RXFP4	F: CCTGTCACTACTTGCTTGGCAC R: TCAACCGCAGATCCCTGAAGGT	Origene
SLUG	F: ACTCCGAAGCCAAATGACAA R: CTCTCTCTGTGGGTGTGTGT	Primer design
SNAIL	F: GGCAATTTAACAATGTCTGAAAAGG R: GAATAGTTCTGGGAGACACATCG	Primer design
TWIST	F: CCAAGAGGTCGTGCCAATC R: CCCAGTATTTTATTTCTAAAGGTGTT	Primer design

QPCR ARRAY

A human EMT Signaling Pathway PCR array (PAHS-090Z, SABiosciences, Frederick, MD, USA) was used to analyze the expression changes of genes related to EndMT in HCAECs. Briefly, 5 µg of total RNA was used for first-strand cDNA synthesis with the RT² first strand kit (Qiagen). The PCR array was carried out following the manufacturer's instructions using the ready-to-use RT²-qPCR master mix (RT²-SYBR® Green/Fluorescein qPCR master mix, SABiosciences). 20µl master mix was added into each well containing pre-dispensed, gene-specific primer pairs and run on a StepOne Plus realtime PCR system (Life technologies). Data analysis was performed using the web-based standard RT PCR array suite (SABiosciences).

PROTEIN EXTRACTION AND WESTERN BLOTTING

Cells and tissue were lysed with NP40 lysis buffer (Life Technologies) containing protease inhibition cocktail (Roche, Mannheim, Germany). Tissue was shredded by Tissue Lyser LT (Qiagen). Protein samples were loaded on a 4-12% SDS/PAGE gel and transferred onto a nitrocellulose membrane (GE Healthcare, Buckinghamshire, UK). After blocking with 5% dry milk in TBST solution (TBS pH 7.2, 0.1% Tween-20), the membrane was incubated with primary antibody solution (diluted in 2% dry milk in TBST, dilution factors are indicated in the following table) at 4 °C overnight. Next day, after three time washing with 2% dry milk in TBST, the membrane was incubated with secondary antibody (horseradish peroxidase-conjugated antibodies (Cell Signaling, Danvers, MA, USA)) diluted in 2% dry milk in TBST for 1 hour at room temperature and finally washed three times. Signals were detected using a chemiluminescent kit (Santa Cruz Biotechnology, Santa Cruz, CA, USA).

Antibody	Dilution	Company
RXFP1	1:1000	Abnova
RXFP4	1:1000	Sigma-Aldrich
CD31	1:1000	Abcam
TGFβ1	1:1000	Abcam
Smad2/3	1:1000	Cell Signaling

HUMAN TISSUE

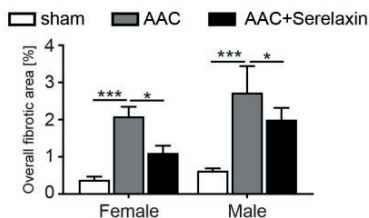
All procedures were performed conform to the World Medical Association Declaration of Helsinki and the permission of human tissue usage was approved by the local ethics committee. Left ventricular myocardial tissue was obtained from end-stage heart failure patients at the time of heart transplantation or from donors without heart disease in cases when the heart could not be transplanted for technical reasons.

STATISTICAL ANALYSIS

Means were calculated and plotted along with standard error bars. All statistical analyses were done using GraphPad Prism software version 6.0 (GraphPad). All data were first analyzed by Student t-test for single comparison and one-way ANOVA with Bonferroni post-hoc analysis was used for comparing multiple groups. Significant differences between means were considered statistically significant when the p-value is smaller or equal to 0.05. Three or more biological replicates were included for all experiments. Overall survival was analyzed by using a Kaplan-Meier survival method with a log rank test to determine statistical differences.

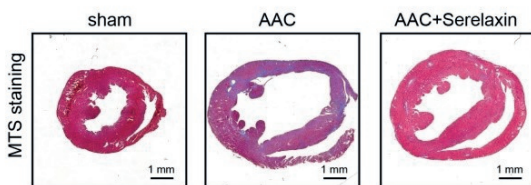
SUPPLEMENTARY DATA

A

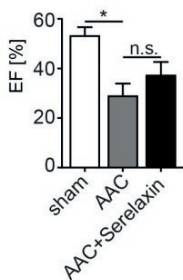


	sham		AAC+vehicle		AAC+Serelaxin	
	Female	Male	Female	Male	Female	Male
day 0	3	3	14	14	15	14
day 28	3	3	8	7	12	11
Survival (%)	100	100	57.14286	50	80	78.57142
Significance	n.s.		n.s. (p=0.8208)		n.s. (p=0.7994)	

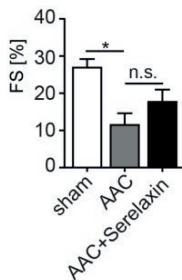
B



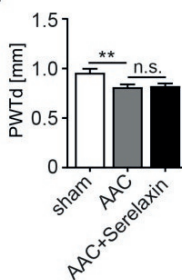
C



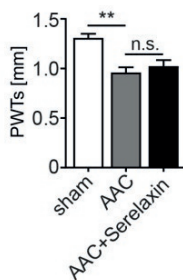
D



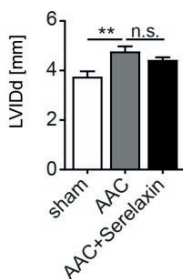
E



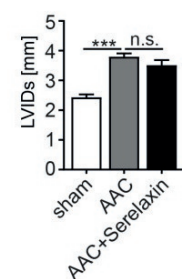
F



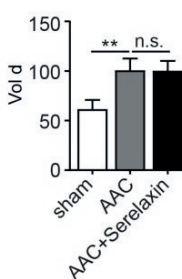
G



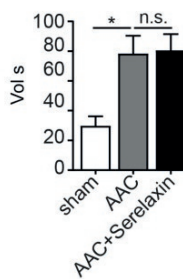
H



I



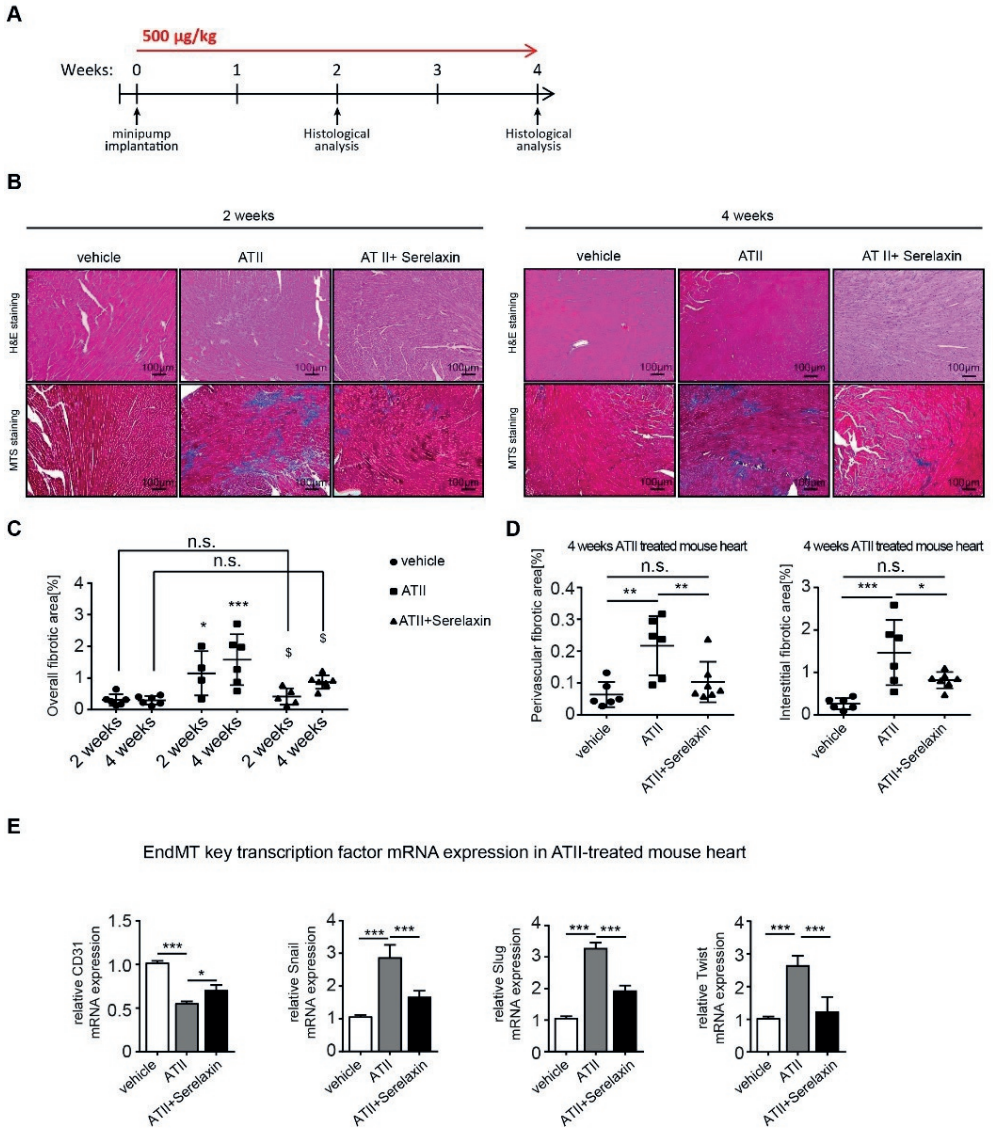
J



Supplementary Figure 1. AAC-operated mouse hearts showed an enlarged phenotype.

(A) Bar graphs showing the differences of total fibrotic area between male and female groups (left panel). Table summarizing the difference between male and female groups (right panel). (B) Masson's trichrome stained images of sham, AAC-operated and AAC-operated + Serelaxin-treated mouse hearts. The AAC-operated heart shows an enlarged phenotype and an increased area of fibrosis as compared to sham. Serelaxin reduced the area of fibrosis but did not reverse the enlarged phenotype. (C) – (J) Bar graphs show the echocardiographic parameters at 28 days after AAC

operation. EF, FS, PWTd and PWTs were significantly reduced upon AAC surgery and were not significantly reversed by administration of Serelaxin. LVIDd, LVIDs, Vol d and Vol s were significantly increased upon AAC surgery but were not significantly reduced by application of Serelaxin. EF: ejection fraction; FS: fractional shortening; PWTd: diastolic posterior wall thickness, PWTs: systolic posterior wall thickness; LVIDd: diastolic left ventricular inner diameter; LVIDs: systolic left ventricular inner diameter; Vol d: diastolic left ventricular volume; Vol s: systolic left ventricular volume. Student t-test was used for single comparison and one-way ANOVA with Bonferroni post-hoc analysis was used for multiple group comparisons. Gene expression and associated error bars, representing mean \pm SEM, n \geq 3, n.s. no significance, * $p < 0.05$, ** $p < 0.01$, *** $p < 0.001$.

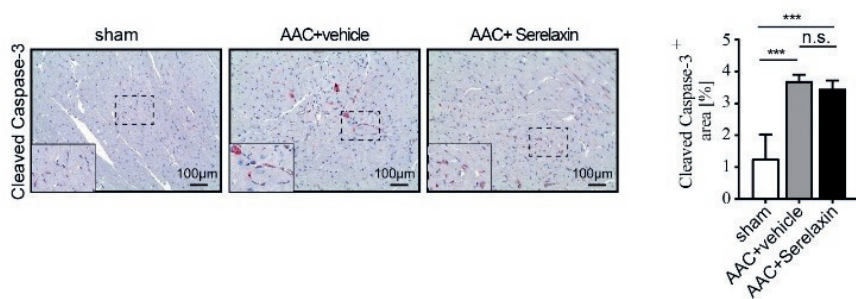


Supplementary Figure 2. Serelaxin ameliorates Angiotensin II (ATII) - induced cardiac fibrosis.

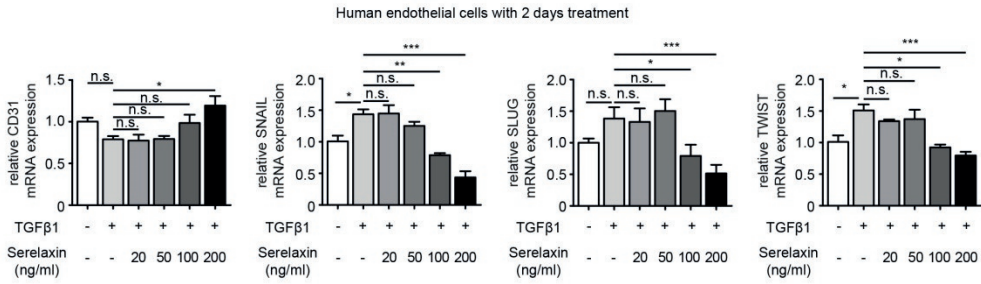
(A) Experimental plan for ATII-induced cardiac fibrosis. (B) HE and Masson's Trichrome Staining microphotography of vehicle, ATII and ATII + Serelaxin-treated mouse hearts showing the significant reduction of overall fibrosis in Serelaxin-treated (500 µg/kg/day) hearts compared to ATII-treated hearts at two different time points (2 weeks and 4 weeks). (C) Bar graphs showing the percentage of overall fibrotic area in the control (vehicle), ATII-treated and ATII + Serelaxin-treated mouse hearts after 2 weeks and 4 weeks. (D) Graphs showing the percentage of interstitial and perivascular fibrotic area in vehicle, ATII and ATII + Serelaxin-treated mouse hearts after 4 weeks. There is a significant reduction of interstitial and perivascular fibrosis in ATII and Serelaxin-treated (500 µg/kg/day) hearts compared to ATII-treated hearts. (E) qPCR analysis showing the relative mRNA

CHAPTER 7

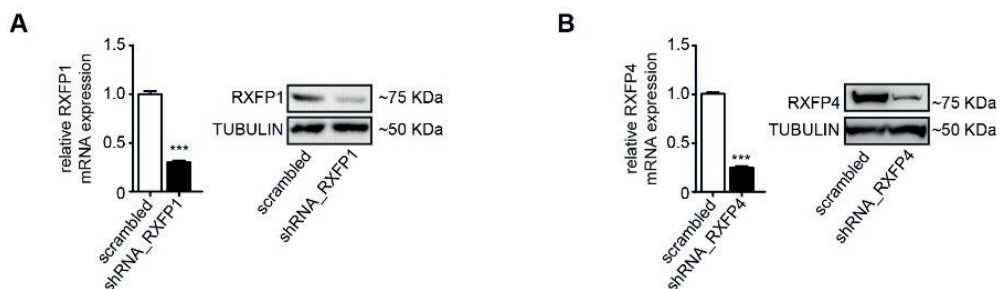
*expression level of CD31 and EndMT key regulators Snail, Slug, and Twist in vehicle, ATII and ATII + Serelaxin-treated mouse hearts. ATII-treated hearts showed an increased expression of Snail, Slug and Twist but a decreased expression of CD31 compared to vehicle-treated hearts, while ATII in combination with Serelaxin treatment reduced Snail, Slug and Twist expression and restored CD31 expression when compared to ATII-treated hearts. Student t-test was used for single comparison and one-way ANOVA with Bonferroni post-hoc analysis was used for multiple group comparisons. Gene expression and associated error bars, representing mean \pm SEM n \geq 3, n.s. no significance, * $p < 0.05$, ** $p < 0.01$, *** $p < 0.001$.*



Supplementary Figure 3. Serelaxin does not affect apoptosis in AAC-operated mouse hearts. Immunohistochemistry staining of cleaved Caspase 3, which is a critical executioner of apoptosis. The staining showed an increased level of cleaved Caspase 3 in AAC-operated hearts compared to sham operated hearts. Serelaxin could not significantly affect cleaved Caspase 3 levels. Student t-test was used for single comparison and one-way ANOVA with Bonferroni post-hoc analysis was used for multiple group comparisons. Error bars represent mean \pm SEM, $n \geq 3$, n.s. no significance, *** $p < 0.001$.

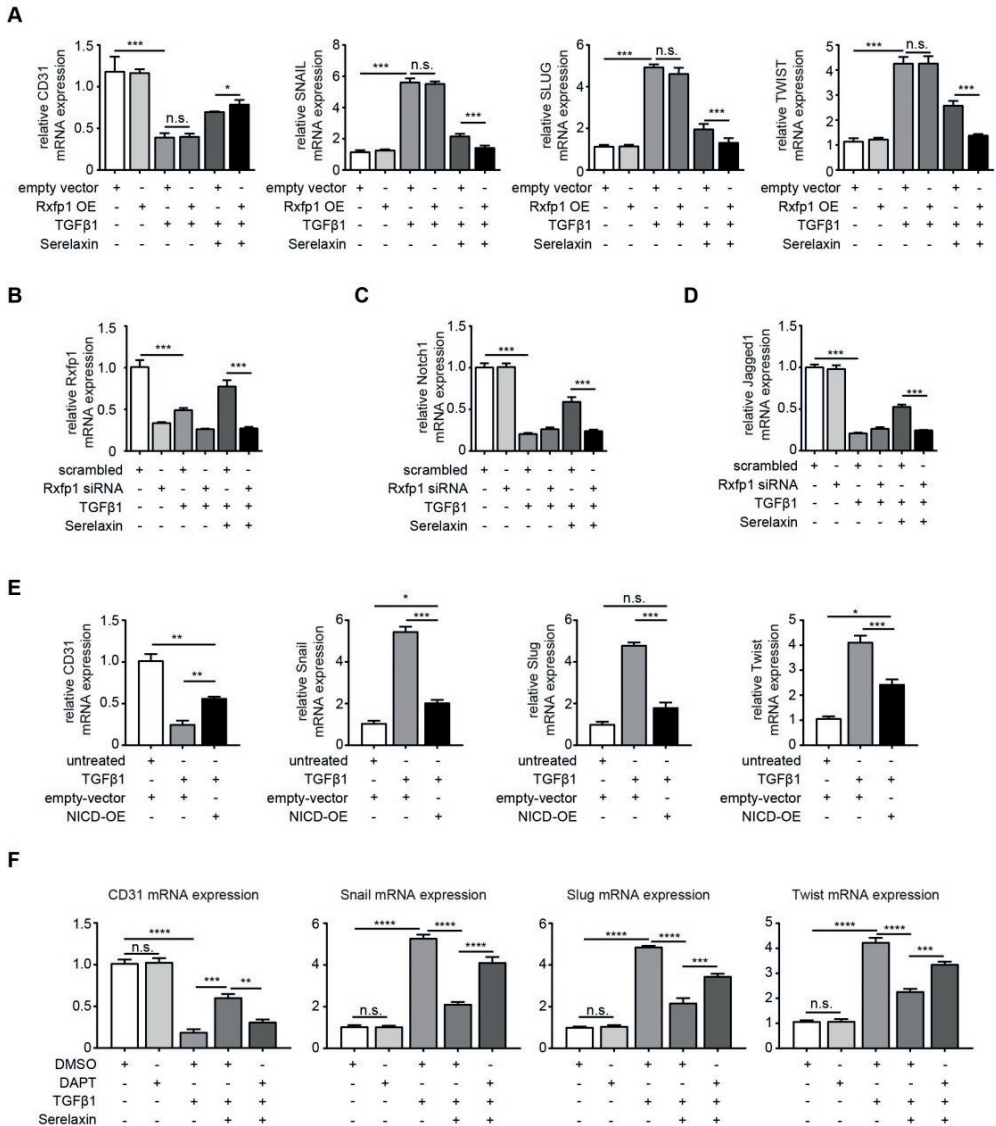


Supplementary Figure 4. Serelaxin alleviates EndMT in HCAECs upon TGFβ1 treatment after 2 days. qPCR analysis showing the expression of endothelial cells marker CD31 and expression of EndMT key regulators SNAIL, SLUG, and TWIST in TGFβ1-treated HCAECs supplemented with different doses of Serelaxin after 2 days. Cells without any treatment were used as control. Serelaxin treatment significantly rescues expression of CD31 (200 ng/ml) and decreases expression of SNAIL, SLUG and TWIST (100 and 200 ng/ml). Student t-test was used for single comparison and one-way ANOVA with Bonferroni post-hoc analysis was used for multiple group comparisons. Error bars represent mean ± SEM, n≥3, n.s. no significance, * p<0.05, ** p<0.01, *** p<0.001.



Supplementary Figure 5. Validation of specificity of RXFP1- and RXFP4 shRNA knockdown.

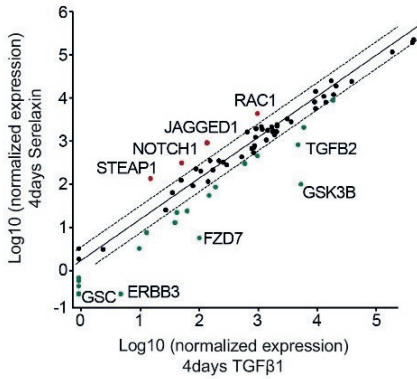
(A-B) qPCR analysis showing the relative mRNA level and Western blot analysis showing the protein level of RXFP1 (A) and RXFP4 (B) in scrambled compared to shRXFP1 and shRXFP4-mediated knockdown in HCAECs. Student *t*-test was used for single comparison and one-way ANOVA with Bonferroni post-hoc analysis was used for multiple group comparisons. Gene expression and associated error bars, representing mean \pm SEM, $n \geq 3$, *** $p < 0.001$.



Supplementary Figure 6. Serelaxin mediates effects on EndMT by activation of the Notch1 pathway via Rxfp1.

(A) qPCR analysis showing the expression of endothelial cell marker CD31 and EndMT transcriptional factors Snail, Slug and Twist in TGFβ1 and Serelaxin-treated MCECs upon Rxfp1 overexpression. Cells transfected with empty vector were used as control. In cells with Rxfp1 overexpression, Serelaxin enhanced its inhibitory effect on TGFβ1-induced EndMT as shown by increased CD31 expression and decreased expression of EndMT key transcriptional factor genes Snail, Slug and Twist. (B-D) qPCR analysis showing the expression of Rxfp1, the Notch1 receptor and its ligand Jagged1 in TGFβ1- and Serelaxin-treated, shRNA knocked down MCECs. Scrambled cells were used as control. The

expression of all three genes was partly restored in Serelaxin-supplemented, TGF β 1-treated cells, but not in *Rxfp1* knockdown cells. (E) qPCR analysis showing that NICD overexpression could partially block TGF β 1-induced EndMT as shown by increased expression of endothelial marker gene CD31 and decreased expression of EndMT transcriptional factors Snail, Slug and Twist. Cells transfected with an empty vector were used as control. (F) qPCR analysis showing an increased expression of endothelial marker gene CD31 and decreased expression of EndMT transcriptional factors Snail, Slug and Twist upon treatment with TGF β 1 and Serelaxin compared to TGF β 1 alone. When the cells were additionally treated with Notch-inhibitor DAPT this effect was abolished. Cells transfected with DMSO were used as control. Student t-test was used for single comparison and one-way ANOVA with Bonferroni post-hoc analysis was used for multiple group comparisons. Gene expression and associated error bars, representing mean \pm SEM, $n \geq 3$, n.s. no significance, * $p < 0.05$, ** $p < 0.01$, *** $p < 0.001$, **** $p < 0.0001$.



Supplementary Figure 7. Identification of Serelaxin-regulated genes in TGFβ1-treated HCAECs.

(A) Scatter plot showing the genes with altered mRNA expression level in only TGFβ1-treated (x-axis) or only Serelaxin-treated (y-axis) HCAECs. STEAP1, NOTCH1, JAGGED1, RAC1, DSP, GSC, ERBB3, FZD7, GSK3B and TGFB2 are significantly regulated are significantly regulated by Serelaxin treatment, which is shown by separation from dot lines (cut-off by 4 folds).

REFERENCES

1. Zeisberg EM, Kalluri R. Origins of cardiac fibroblasts. *Circ Res.* 2010;107(11): 1304-12.
2. Krenning G, Zeisberg EM, Kalluri R. The origin of fibroblasts and mechanism of cardiac fibrosis. *J Cell Physiol.* 2010;225(3): 631-7.
3. Khan R, Sheppard R. Fibrosis in heart disease: Understanding the role of transforming growth factor-beta in cardiomyopathy, valvular disease and arrhythmia. *Immunology.* 2006;118(1): 10-24.
4. Chen Z, Li Y, Dian K, Rao L. Modulating microRNAs as Novel Therapeutic Targets in Cardiac Fibrosis. *Theranostics.* 2017;7(8): 2287-8.
5. Hao K, Lei W, Wu H, Wu J, Yang Z, Yan S, et al. LncRNA-Safe contributes to cardiac fibrosis through Safe-Sfrp2-HuR complex in mouse myocardial infarction. *Theranostics.* 2019;9(24): 7282-97.
6. Wang B, Zhang A, Wang H, Klein JD, Tan L, Wang Z-M, et al. miR-26a Limits Muscle Wasting and Cardiac Fibrosis through Exosome-Mediated microRNA Transfer in Chronic Kidney Disease. *Theranostics.* 2019;9(7): 1864-77.
7. Xu X, Friehs I, Zhong Hu T, Melnychenko I, Tampe B, Alnour F, et al. Endocardial fibroelastosis is caused by aberrant endothelial to mesenchymal transition. *Circ Res.* 2015;116(5): 857-66.
8. Yuan J, Liu H, Gao W, Zhang L, Ye Y, Yuan L, et al. MicroRNA-378 suppresses myocardial fibrosis through a paracrine mechanism at the early stage of cardiac hypertrophy following mechanical stress. *Theranostics.* 2018;8(9): 2565-82.
9. Novak J, Danielson LA, Kerchner LJ, Sherwood OD, Ramirez RJ, Moalli PA, et al. Relaxin is essential for renal vasodilation during pregnancy in conscious rats. *J Clin Invest.* 2001;107(11): 1469-75.
10. Seibold JR, Korn JH, Simms R, Clements PJ, Moreland LW, Mayes MD, et al. Recombinant human relaxin in the treatment of scleroderma. A randomized, double-blind, placebo-controlled trial. *Ann Intern Med.* 2000;132(11): 871-9.
11. Unemori EN, Pickford LB, Salles AL, Piercy CE, Grove BH, Erikson ME, et al. Relaxin induces an extracellular matrix-degrading phenotype in human lung fibroblasts in vitro and inhibits lung fibrosis in a murine model in vivo. *J Clin Invest.* 1996;98(12): 2739-45.
12. Dschietzig T, Bartsch C, Baumann G, Stangl K. Relaxin-a pleiotropic hormone and its emerging role for experimental and clinical therapeutics. *Pharmacol Ther.* 2006;112(1): 38-56.
13. Bathgate RAD, Halls ML, van der Westhuizen ET, Callander GE, Kocan M, Summers RJ. Relaxin family peptides and their receptors. *Physiol Rev.* 2013;93(1): 405-80.
14. Hsu SY, Nakabayashi K, Nishi S, Kumagai J, Kudo M, Sherwood OD, et al. Activation of orphan receptors by the hormone relaxin. *Science.* 2002;295(5555): 671-4.
15. Nistri S, Bani D. Relaxin receptors and nitric oxide synthases: Search for the missing link. *Reprod Biol Endocrinol.* 2003;1: 5.
16. Samuel CS, Unemori EN, Mookerjee I, Bathgate RAD, Layfield SL, Mak J, et al. Relaxin modulates cardiac fibroblast proliferation, differentiation, and collagen production and reverses cardiac fibrosis in vivo. *Endocrinology.* 2004;145(9): 4125-33.

17. Bani D, Yue SK, Bigazzi M. Clinical profile of relaxin, a possible new drug for human use. *Curr Drug Saf.* 2009;4(3): 238-49.
18. Samuel CS, Hewitson TD, Unemori EN, Tang ML-K. Drugs of the future: The hormone relaxin. *Cell Mol Life Sci.* 2007;64(12): 1539-57.
19. Ponikowski P, Metra M, Teerlink JR, Unemori E, Felker GM, Voors AA, et al. Design of the RELAXin in acute heart failure study. *Am Heart J.* 2012;163(2): 149-55.e1.
20. Teerlink JR, Cotter G, Davison BA, Felker GM, Filippatos G, Greenberg BH, et al. Serelaxin, recombinant human relaxin-2, for treatment of acute heart failure (RELAX-AHF): A randomised, placebo-controlled trial. *The Lancet.* 2013;381(9860): 29-39.
21. Ponikowski P, Mitrovic V, Ruda M, Fernandez A, Voors AA, Vishnevsky A, et al. A randomized, double-blind, placebo-controlled, multicentre study to assess haemodynamic effects of serelaxin in patients with acute heart failure. *Eur Heart J.* 2014;35(7): 431-41.
22. Teerlink JR, Voors AA, Ponikowski P, Pang PS, Greenberg BH, Filippatos G, et al. Serelaxin in addition to standard therapy in acute heart failure: rationale and design of the RELAX-AHF-2 study. *Eur J Heart Fail.* 2017;19(6): 800-9.
23. Leggabe ED, Kiriazis H, Zhao C, Xu Q, Moore XL, Su Y, et al. Relaxin reverses cardiac and renal fibrosis in spontaneously hypertensive rats. *Hypertension.* 2005;46(2): 412-8.
24. Sassoli C, Chellini F, Pini A, Tani A, Nistri S, Nosi D, et al. Relaxin prevents cardiac fibroblast-myofibroblast transition via notch-1-mediated inhibition of TGF- β /Smad3 signaling. *PLoS ONE.* 2013;8(5): e63896.
25. Roy O, Leclerc VB, Bourget J-M, Thériault M, Proulx S. Understanding the process of corneal endothelial morphological change in vitro. *Invest Ophthalmol Vis Sci.* 2015;56(2): 1228-37.
26. High FA, Epstein JA. The multifaceted role of Notch in cardiac development and disease. *Nat Rev Genet.* 2008;9(1): 49-61.
27. Luxán G, D'Amato G, MacGrogan D, La Pompa JL de. Endocardial Notch Signaling in Cardiac Development and Disease. *Circ Res.* 2016;118(1): e1-e18.
28. Inder S, O'Rourke S, McDermott N, Manecksha R, Finn S, Lynch T, et al. The Notch-3 receptor: A molecular switch to tumorigenesis? *Cancer Treat Rev.* 2017;60: 69-76.
29. Nistri S, Sassoli C, Bani D. Notch Signaling in Ischemic Damage and Fibrosis: Evidence and Clues from the Heart. *Front Pharmacol.* 2017;8: 187.
30. Zhou X, Chen X, Cai JJ, Chen LZ, Gong YS, Wang LX, et al. Relaxin inhibits cardiac fibrosis and endothelial-mesenchymal transition via the Notch pathway. *Drug Des Devel Ther.* 2015;9: 4599-611.
31. Rodriguez-Vita J, Tetzlaff F, Fischer A. Notch controls endothelial cells. *Oncoscience.* 2017;4(5-6): 45-6.
32. Eisenberg LM, Markwald RR. Molecular regulation of atrioventricular valvuloseptal morphogenesis. *Circ Res.* 1995;77(1): 1-6.
33. Choi S-H, Nam J-K, Kim B-Y, Jang J, Jin Y-B, Lee H-J, et al. HSPB1 Inhibits the Endothelial-to-Mesenchymal Transition to Suppress Pulmonary Fibrosis and Lung Tumorigenesis. *Cancer Res.* 2016;76(5): 1019-30.

34. Peng H, Li Y, Wang C, Zhang J, Chen Y, Chen W, et al. ROCK1 Induces Endothelial-to-Mesenchymal Transition in Glomeruli to Aggravate Albuminuria in Diabetic Nephropathy. *Sci Rep.* 2016;6: 20304.
35. Piera-Velazquez S, Li Z, Jimenez SA. Role of endothelial-mesenchymal transition (EndoMT) in the pathogenesis of fibrotic disorders. *Am J Pathol.* 2011;179(3): 1074-80.
36. Zeisberg EM, Potenta S, Xie L, Zeisberg M, Kalluri R. Discovery of endothelial to mesenchymal transition as a source for carcinoma-associated fibroblasts. *Cancer Res.* 2007;67(21): 10123-8.
37. Zeisberg EM, Potenta SE, Sugimoto H, Zeisberg M, Kalluri R. Fibroblasts in kidney fibrosis emerge via endothelial-to-mesenchymal transition. *J Am Soc Nephrol.* 2008;19(12): 2282-7.
38. Zeisberg EM, Tarnavski O, Zeisberg M, Dorfman AL, McMullen JR, Gustafsson E, et al. Endothelial-to-mesenchymal transition contributes to cardiac fibrosis. *Nat Med.* 2007;13(8): 952-61.
39. Toischer K, Zhu W, Hünlich M, Mohamed BA, Khadjeh S, Reuter SP, et al. Cardiomyocyte proliferation prevents failure in pressure overload but not volume overload. *J Clin Invest.* 2017;127(12): 4285-96.
40. Nagarajan S, Benito E, Fischer A, Johnsen SA. H4K12ac is regulated by estrogen receptor-alpha and is associated with BRD4 function and inducible transcription. *Oncotarget.* 2015;6(9): 7305-17.
41. Xu X, Tan X, Tampe B, Sanchez E, Zeisberg M, Zeisberg EM. Snail Is a Direct Target of Hypoxia-inducible Factor 1 α (HIF1 α) in Hypoxia-induced Endothelial to Mesenchymal Transition of Human Coronary Endothelial Cells. *J Biol Chem.* 2015;290(27): 16653-64.
42. Jeyabalan A, Shroff SG, Novak J, Conrad KP. The vascular actions of relaxin. *Adv Exp Med Biol.* 2007;612: 65-87.
43. Park M, Shen Y-T, Gaussin V, Heyndrickx GR, Bartunek J, Resuello RRG, et al. Apoptosis predominates in nonmyocytes in heart failure. *Am J Physiol Heart Circ Physiol.* 2009;297(2): H785-91.
44. Heeg MHJ, Koziolok MJ, Vasko R, Schaefer L, Sharma K, Müller GA, et al. The antifibrotic effects of relaxin in human renal fibroblasts are mediated in part by inhibition of the Smad2 pathway. *Kidney Int.* 2005;68(1): 96-109.
45. Mookerjee I, Hewitson TD, Halls ML, Summers RJ, Mathai ML, Bathgate RAD, et al. Relaxin inhibits renal myofibroblast differentiation via RXFP1, the nitric oxide pathway, and Smad2. *FASEB J.* 2009;23(4): 1219-29.
46. Yuan Y, Zhang Y, Han X, Li Y, Zhao X, Sheng L, et al. Relaxin alleviates TGF β 1-induced cardiac fibrosis via inhibition of Stat3-dependent autophagy. *Biochem Biophys Res Commun.* 2017;493(4): 1601-7.
47. Moore-Morris T, Guimarães-Camboa N, Banerjee I, Zambon AC, Kisseleva T, Velayoudon A, et al. Resident fibroblast lineages mediate pressure overload-induced cardiac fibrosis. *J Clin Invest.* 2014;124(7): 2921-34.
48. Campbell SE, Katwa LC. Angiotensin II stimulated expression of transforming growth factor-beta1 in cardiac fibroblasts and myofibroblasts. *J Mol Cell Cardiol.* 1997;29(7): 1947-58.

49. Biernacka A, Frangogiannis NG. Aging and Cardiac Fibrosis. *Aging Dis.* 2011;2(2): 158-73.
50. McCarthy JC, Aronovitz M, DuPont JJ, Calamaras TD, Jaffe IZ, Blanton RM. Short-Term Administration of Serelaxin Produces Predominantly Vascular Benefits in the Angiotensin II/L-NAME Chronic Heart Failure Model. *JACC Basic Transl Sci.* 2017;2(3): 285-96.
51. Bennett RG, Simpson RL, Hamel FG. Serelaxin increases the antifibrotic action of rosiglitazone in a model of hepatic fibrosis. *World J Gastroenterol.* 2017;23(22): 3999-4006.
52. Lam M, Royce SG, Samuel CS, Bourke JE. Serelaxin as a novel therapeutic opposing fibrosis and contraction in lung diseases. *Pharmacol Ther.* 2018;187: 61-70.
53. Wang D, Luo Y, Myakala K, Orlicky DJ, Dobrinskikh E, Wang X, et al. Serelaxin improves cardiac and renal function in DOCA-salt hypertensive rats. *Sci Rep.* 2017;7(1): 9793.
54. Sassoli C, Chellini F, Pini A, Tani A, Nistri S, Nosi D, et al. Relaxin Prevents Cardiac Fibroblast-Myofibroblast Transition via Notch-1-Mediated Inhibition of TGF- β /Smad3 Signaling. *PLoS ONE.* 2013;8(5).
55. Wu X-P, Wang H-J, Wang Y-L, Shen H-R, Tan Y-Z. Serelaxin inhibits differentiation and fibrotic behaviors of cardiac fibroblasts by suppressing ALK-5/Smad2/3 signaling pathway. *Exp Cell Res.* 2018;362(1): 17-27.
56. Rieder F, Kessler SP, West GA, Bhilocha S, La Motte C de, Sadler TM, et al. Inflammation-induced endothelial-to-mesenchymal transition: a novel mechanism of intestinal fibrosis. *Am J Pathol.* 2011;179(5): 2660-73.
57. Fue M, Miki Y, Takagi K, Hashimoto C, Yaegashi N, Suzuki T, et al. Relaxin 2/RXFP1 Signaling Induces Cell Invasion via the β -Catenin Pathway in Endometrial Cancer. *Int J Mol Sci.* 2018;19(8).
58. Thompson VC, Morris TGW, Cochrane DR, Cavanagh J, Wafa LA, Hamilton T, et al. Relaxin becomes upregulated during prostate cancer progression to androgen independence and is negatively regulated by androgens. *Prostate.* 2006;66(16): 1698-709.
59. Astuti Y, Nakabayashi K, Deguchi M, Ebina Y, Yamada H. Human recombinant H2 relaxin induces AKT and GSK3 β phosphorylation and HTR-8/SVneo cell proliferation. *Kobe J Med Sci.* 2015;61(1): E1-8.
60. Thanasupawat T, Glogowska A, Nivedita-Krishnan S, Wilson B, Klonisch T, Hombach-Klonisch S. Emerging roles for the relaxin/RXFP1 system in cancer therapy. *Mol Cell Endocrinol.* 2019;487: 85-93.
61. Blokzijl A, Dahlqvist C, Reissmann E, Falk A, Moliner A, Lendahl U, et al. Cross-talk between the Notch and TGF-beta signaling pathways mediated by interaction of the Notch intracellular domain with Smad3. *J Cell Biol.* 2003;163(4): 723-8.
62. Hajdu M, Kopper L, Sebestyén A. Notch-regulation upon Dll4-stimulation of TGF β -induced apoptosis and gene expression in human B-cell non-Hodgkin lymphomas. *Scand J Immunol.* 2010;71(1): 29-37.
63. NA WU, Joseph Wiseman, Yuan Lei, Karen Eastlake, Xinghuai Sun, G Astrid Limb. Modulation of the Notch and Wnt signalling by TGF- β in adult human Müller stem cells. *Invest Ophthalmol Vis Sci.* 2014(55): 1373.

CHAPTER

8

CAUSAL CONNECTIONS FROM CHRONIC KIDNEY DISEASE TO CARDIAC FIBROSIS

Melanie S. Hulshoff^{1,2,3}, Sandip K. Rath^{1,2}, Xingbo Xu^{1,2}, Michael Zeisberg²,
Elisabeth M. Zeisberg^{1,2}

¹*Department of Cardiology and Pneumology, University Medical Center of Göttingen, Georg-August University, Göttingen, Germany.*

²*German Centre for Cardiovascular Research (DZHK), Göttingen, Germany.*

³*Department of Pathology and Medical Biology, University Medical Center Groningen, Hanzeplein 1, 9713 GZ, Groningen, The Netherlands.*

⁴*Department of Nephrology and Rheumatology, University Medical Center of Göttingen, Robert-Koch-Str. 40, 37075, Göttingen, Germany.*

ABSTRACT

Cardiovascular disease and heart failure are the primary cause of morbidity and mortality in patients with chronic kidney disease. Because impairment of kidney function correlates with heart failure and cardiac fibrosis, a kidney–heart axis is suspected. Although our understanding of the underlying mechanisms still is evolving, the possibility that kidney–heart messengers could be intercepted offers ample reason to focus on this clinically highly relevant problem. Here, we review the current knowledge of how kidney injury causes heart failure and fibrosis.

INTRODUCTION

Patients with chronic kidney disease (CKD) are more likely to get heart disease, and in fact cardiovascular disease is the primary cause of morbidity and mortality in these patients, even by early stages of CKD [1]. Because approximately 35% of all individuals older than 70 years are affected by early stages of CKD, the health care burden is dramatic [2]. Although common comorbidities such as hypertension and diabetes undeniably contribute to both the progression of CKD and cardiovascular disease, the presence of CKD is an independent risk factor for cardiovascular morbidity and mortality, suggesting that mechanisms specific for CKD patients are at play. More specifically, CKD is linked to augmented atherosclerosis, arrhythmias, heart failure, and cardiac fibrosis. This review summarizes the current knowledge of CKD-associated heart failure and cardiac fibrosis.

CARDIAC FIBROSIS

Although all forms of chronic heart disease are associated with cardiac fibrosis, CKD patients are especially prone to cardiac fibrogenesis [3]. Several post-mortem studies have shown that the stage of CKD directly correlates to the extent of cardiac fibrosis [4,5]. Typically, patients with CKD have significantly more fibrotic tissue in the heart as compared with subjects without CKD (Fig. 1).

Cardiac fibrosis in general is defined as a disproportional increment of the connective tissue compartment in the heart. Although all forms of chronic heart disease are associated with cardiac fibrosis, it may be of specific relevance in heart failure with preserved ejection fraction, contributing to increased stiffness and impaired diastolic filling of the heart [6-8]. Fibrosis is characterized by excessive accumulation of fibrillar extracellular matrix, rarefaction of microvessels, a sterile mononuclear infiltrate, and accumulation of fibroblasts, the main mediators of fibrosis [5,6,8]. As opposed to the essential process of scar formation after acute myocardial infarction, pathologic fibrosis is a continuous process affecting all areas of the heart, which also commonly is referred to as remodeling. Fibroblasts are the main source of extracellular matrix and thus mechanisms that induce extracellular matrix production by fibroblasts are of the highest interest [8,9]. Because not all fibroblasts proliferate, alternate sources

contribute to accumulation of activated fibroblasts such as invasion of bone marrow-derived fibrocytes and conversion of endothelial cells into fibroblasts through a process termed endothelial-mesenchymal transition (EndMT). EndMT in the context of fibrosis first was identified in the heart [10]. In consecutive studies, EndMT also was found to contribute to fibrogenesis of other organs such as kidney, lung, and gut, and also to the tumor stroma [11-14]. Meanwhile, hundreds of studies have studied EndMT in different settings (and thus provided indisputable evidence for this process). However, controversy has arisen about when exactly EndMT happens and what the extent of EndMT (and its relevance) is in different models, which likely reflects the fact that EndMT is highly context-dependent and a process that is still only partially understood. Apart from the cellular source for fibroblasts, numerous mediators of cardiac fibrosis have been identified including growth factors (eg, transforming growth factor β 1 [TGF β 1], connective tissue growth factor [CTGF] [15,16]), cytokines (eg, tumor necrosis factor- α [TNF- α], interleukin [IL]-1 β [17,18]), and metabolic products (eg, the reduced form of nicotinamide adenine dinucleotide phosphate oxidases [NOXs], reactive oxygen species [ROS] [19-21]). Because of the direct correlation of the degree of impaired kidney function and the severity of cardiac fibrosis, it is plausible that profibrotic mechanisms specific for chronic kidney disease exist, which are reviewed later.

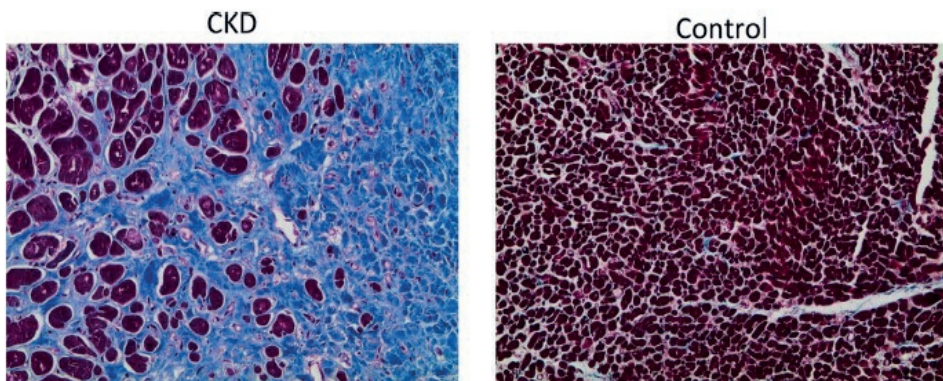


Figure 1. Representative light microscopy images from post-mortem heart tissue from a patient with CKD (left) and a control subject without CKD (right). Heart tissue was stained for collagen (in blue) by Masson trichrome staining. CKD patients show more fibrosis in the heart compared with non-CKD subjects.

ENDMT AS MODULATOR OF CARDIAC FIBROSIS AND VASCULAR LOSS

EndMT is a cellular transition process in which endothelial cells lose their endothelial characteristics and gain a myofibroblast-like phenotype. EndMT not only contributes to cardiac fibrosis [10], but also plays a pivotal role in myocardial vascular loss owing to loss of microvascular density. EndMT is mediated by a set of master-transcription factors including Twist, Snail, and Slug [22]. Several stimuli have been identified to induce EndMT, including TGF β 1, which is abundantly present within the fibrotic microenvironment, and intrinsic mechanisms such as aberrant promoter methylation of Rasal1 [10,23]. Because in patients with impaired kidney function the incidence of EndMT within the heart is 17% higher in comparison with healthy controls, it is tempting to speculate that a direct kidney–heart axis exists and that the chronically diseased kidney releases EndMT inducers [5]. In this regard, treatment of endothelial cells with serum derived from CKD patients resulted in a change toward a myofibroblast-like, spindle-shaped morphology and increased expression of EndMT transcription factors [5]. This indicates the presence of factors in the serum of patients with CKD that can induce EndMT.

Because TGF β 1 is an important profibrotic growth factor in heart and kidney, and because TGF β 1 is a well-established inducer of EndMT, it also is attractive to speculate that kidney-derived TGF β 1 is responsible for the EndMT observed in the heart of CKD patients. However, the literature is mixed with regard to increased TGF β 1 serum levels within CKD patients. Although in an African American study population TGF β 1 serum levels correlated with the incidence of CKD [24], such correlation is not always observed [25].

Nitric oxide (NO) is not only a modulator of vasodilatation but also of angiogenesis, the de novo development of new blood vessels, which has been linked to partial EndMT of the tip cells (the leading cells of vascular sprouts that mediate angiogenesis) and therefore NO could play a role in the EndMT phenotype induced by CKD. Indeed, in CKD the overall production of NO is decreased [26]. There are several factors such as the NO synthase inhibitor asymmetric dimethylarginine (ADMA) and the angiogenesis inhibitors angiopoietin-2 (ANG-2), thrombospondin-2 (TSP-2), and endostatin, which are associated with lower NO levels and increased cardiovascular disease [27-34]. All

of these factors are increased in the serum of CKD patients, and all could induce the expression of at least one of the EndMT transcription factors, indicating their involvement in EndMT [5]. The serum of patients with CKD also induced endothelial cell apoptosis *in vitro*, showing another mechanism that contributes to vascular loss [5]. Three of four factors that affect EndMT (ADMA, ANG-2, and TSP-2) also are responsible for increased endothelial cell apoptosis [5]. Altogether, this shows the interplay of NO and its regulators with EndMT, which contributes to both vascular loss and cardiac fibrosis in the context of CKD. Importantly, these results are in line with prior studies that showed that ADMA, ANG-2, and endostatin are increased in CKD and are associated with higher risks of cardiovascular and overall mortality [29,34-37]. High levels of circulating TSP-2 similarly are associated with a poor prognosis in patients with heart failure with preserved ejection fraction, a patient group in which CKD is common and cardiac fibrosis is an important pathomechanistic factor [38-40]. EndMT and fibrogenesis induced by these factors therefore at least may contribute to the observed increased overall mortality in patients with CKD.

OXIDATIVE STRESS AS INDUCER OF CARDIAC FIBROSIS IN CKD

CKD is characterized by enhanced ROS production in the kidneys and enhanced ROS levels in the plasma [41,42]. The presence of ROS is beneficial under physiological conditions, but growing evidence supports that pathophysiological accumulation of ROS (such as H₂O₂, O₂⁻, OH, and ONOO⁻) influences fibrotic remodeling [43-45]. ROS is produced not only as a by-product during oxidative phosphorylation in mitochondria, but also from a variety of enzymatic and nonenzymatic process such as xanthine oxidase, NOXs, cytochrome P450; by auto-oxidation of catecholamines; and by uncoupling of NO synthase [44,46,47]. Among the variety of ROS sources, the one generated by NOXs has gained much attention in fibrotic remodeling [48,49]. Of the seven members of this family, NOX4 (highly expressed in the kidney) and NOX2 (also expressed in the kidney, but may be compensated by NOX4) are studied predominantly [50]. In cardiac fibroblasts, NOX2-induced ROS accumulation together with TGFβ drives fibrotic progression via up-regulation of collagen I and II [19,49,51]. Moreover, NOX4–Smad family member (Smad) 2/3 signaling also is involved in driving fibrotic progression of cardiac fibroblasts and NOX4 induces

cardiac fibrosis via nuclear factor κ light-chain- enhancer of activated B cells signaling, a signaling pathway also important in inflammation [52]. In addition to cardiac fibroblasts, ROS also affects endothelial cells. Endothelial-specific overexpression of NOX2 in an angiotensin II-induced fibrotic mouse model results in enhanced EndMT, thereby exacerbating cardiac fibrosis [53]. Interestingly, NOX4 expression in endothelial cells mediates protection against fibrotic remodeling in transverse aortic constriction mouse models of cardiac fibrosis [54]. This indicates that NOX4 has a cell-specific role in mediating cardiac fibrosis: NOX4 drives fibrosis progression in cardiac fibroblasts whereas NOX4 expression in endothelial cells has a protective role. It is important to note that the ROS-induced changes in cardiac fibrosis have been studied only in mouse models of cardiac fibrosis to date and not in mouse models of chronic kidney disease. However, because there is increased ROS production in the kidney and increased ROS levels in the plasma of CKD patients, it is plausible to speculate that the circulating ROS levels affect the endothelial cells and cardiac fibroblast activation in the heart.

ACTIVATION OF THE RENIN-ANGIOTENSIN SYSTEM IN CKD

Hyperactivity of the renin-angiotensin system is associated with CKD [55]. In short, angiotensinogen is produced by the liver and is converted into angiotensin I by renin, and further converted into angiotensin II by angiotensin-converting enzyme. Angiotensin II is responsible for systemic arterial vasoconstriction and the release of aldosterone, resulting in increased systemic blood pressure. Chronic activation of the renin-angiotensin system is known to result in both myocardial fibrosis and inflammation, and therefore is very likely involved in CKD-associated cardiovascular disease and angiotensin II-releasing pumps are used to induce both kidney and heart fibrosis in mice [49]. Although hyperactivity of the renin-angiotensin-aldosterone system (RAAS) typically is associated with increased blood pressure, local blood pressure-independent mechanisms contribute to the profibrotic activity of RAAS. One of the underlying mechanisms of angiotensin II-induced cardiac fibrosis is NOX2-mediated perivascular fibrosis via the production of ROS [53]. NOX2 also is important in the angiotensin II-induced expression of adhesion molecules on endothelial cells, which are responsible for leukocyte attachment to the endothelium and subsequent

perivascular infiltration [56]. Knockout of NOX2 attenuated angiotensin II-induced myocardial fibrosis in mice, indicating its importance in facilitating myocardial fibrosis [57]. Whether angiotensin II and NOX2 induce cardiac fibrosis in the context of CKD has yet to be established. Nevertheless, this indicates the synergistic effect of angiotensin II and NOX2 in mediating cardiac fibrosis, and underlines the possible link of both mediators with inflammation.

INFLAMMATION AS A MODULATOR OF CARDIOVASCULAR DISEASE

Inflammation is an important mediator of both CKD and cardiovascular disease, and therefore could represent a mechanism by which CKD induces cardiovascular disease. In CKD, a spectrum of proinflammatory and anti-inflammatory cytokines are secreted into the circulation and thereby influence pathologic remodeling in the heart. One example is NACHT, LRR, and PYD domain-containing protein 3 (NLRP3), a cytokine that is more abundant in the circulation during CKD and that, together with other molecules, can activate the proinflammatory cytokines IL-1 β and IL-18 [58]. Oral administration of theracurmin, a novel formulation of curcumin (a naturally occurring chemical compound that is found in the spice turmeric with antioxidant and anti-inflammatory properties), in a rat model of subtotal nephrectomy (which induces cardiac fibrosis and diastolic dysfunction) decreases NLRP3 expression and thereby reduces proinflammatory IL-1 β levels in the heart [58]. In addition, theracurmin-induced inhibition of NLRP3 resulted in decreased expression of collagen type 1 (an extracellular matrix protein involved in fibrosis) and decreased phosphorylation of Smad2 (a protein involved in canonical TGF β 1 signaling) in the heart [58]. Together, this results in decreased cardiac fibrosis and decreased expression of TGF β 1, an important modulator of fibroblast activation and EndMT [58]. This indicates that individual components of inflammation can contribute to cardiovascular disease in the context of CKD. What should be noted is that additional but as yet unknown mechanisms of theracurmin also could be responsible for the antifibrotic effect observed in the heart. Interestingly, theracurmin does not influence kidney fibrosis, indicating that NLRP3 specifically targets the heart [58].

It also has been reported that circulating proinflammatory TNF- α receptors are associated with cardiovascular disease in the context of CKD [59]. Interestingly, TNF- α has been described to be involved in ROS, mitogen-activated protein kinase (MAPK) cascade, and the renin-angiotensin system, underlining the link between oxidative stress, inflammation, and the renin-angiotensin system [60-62]. This indicates that TNF- α and its receptors could have pleiotropic functions in facilitating cardiovascular disease in the context of CKD. Interestingly, both proinflammatory IL-1 β and TNF- α can induce the expression of another proinflammatory cytokine: IL-33. IL-33 is expressed in both cardiac endothelial cells and cardiac fibroblasts, suggesting an essential role of IL-33 in modulating cardiovascular disease in the context of CKD [63]. IL-33 activates the MAPK signaling pathways, which in turn activates the proinflammatory nuclear factor κ light-chain-enhancer of activated B cells signaling [64]. Interestingly, IL-33 has been shown to induce endothelial dysfunction by promoting inflammatory infiltration (via increased intracellular adhesion molecule expression) and increased endothelial permeability (via decreased vascular endothelial cadherin [VE-cadherin] expression), resulting in adverse myocardial remodeling [65]. Decreased VE-cadherin expression is also a sign of EndMT, suggesting IL-33 can influence EndMT directly. This shows that besides NLRP3 and TNF- α receptors, IL-33 also has pleiotropic functions in the heart, suggesting that inflammation is an important component of CKD-induced cardiovascular disease. Other examples of up-regulated proinflammatory cytokines are C-reactive protein, pentraxin 3, and IL-6, whereas the anti-inflammatory cytokine IL-10 also is up-regulated in the context of CKD [66-68]. These cytokines all are associated with the risk of cardiovascular events in CKD patients and therefore are likely to impact the heart [67,68]. In mice, C-reactive protein and IL-6 both have been described to promote cardiac fibrosis [69,70], whereas IL-10 has been described to inhibit cardiac fibrosis, suggesting that not all factors increased in CKD are detrimental to the heart [71]. The specific role of pentraxin 3 on affecting the heart also has yet to be described. Importantly, the exact impact of these cytokines on the heart in the clinical setting of CKD has yet to be defined. Interestingly, the proinflammatory cytokines IL-1 β , IL-6, and TNF- α stimulate angiotensin II-mediated ROS production, again showing the interplay of different factors in stimulating cardiovascular disease in the context of CKD [72,73]. To conclude, inflammation seems to be tightly connected to oxidative stress and RAAS, which together

induce pathologic cardiac remodeling in the context of CKD. In addition, the MAPK signaling pathway seems pivotal in exerting the inflammation-mediated effects on cardiovascular disease during CKD.

FIBROBLAST GROWTH FACTOR 23 AS A POTENTIAL MODULATOR OF CARDIAC FIBROSIS

Fibroblast growth factor 23 (FGF23) is an endocrine hormone that regulates phosphate excretion and vitamin D metabolism under physiological conditions [74]. FGF23 binds to the FGF receptor and the co-receptor Klotho, to exert its effects in both the kidney and parathyroid glands [74-76]. Under pathophysiological conditions, a decrease of renal function and loss of klotho expression results in increased serum levels of FGF23, which has been associated with greater risks of cardiovascular events and mortality [77-80]. Indeed, increased serum levels of FGF23 are associated independently with left ventricle hypertrophy, one of the underlying characteristics of chronic heart failure in CKD patients [81]. It has been shown *in vitro* that, in the heart, FGF23 is expressed the most highly in cardiac fibroblasts in comparison with cardiomyocytes, suggesting a role of FGF23 in cardiac fibrosis [82]. In this respect, FGF23 induces the proliferation of adult mouse cardiac fibroblasts and increases the expression of collagens [82]. *In vivo* myocardial injection of FGF23 together with myocardial infarction or ischemia/reperfusion surgery exacerbated left ventricular diastolic dysfunction and cardiac fibrosis via increased TGF β and collagen levels [82]. Interestingly, this effect was mediated partially by β -catenin, indicating that as yet to be defined other regulators also are involved in FGF23-induced cardiac dysfunction [82]. A possible regulator is angiotensin II, which is a well-known inducer of cardiac fibrosis and stimulates FGF23 expression [82]. Another possible regulator would be parathyroid hormone, because FGF23 directly affects the parathyroid glands. However, there was no difference observed in parathyroid hormone serum levels, indicating that FGF23 and parathyroid hormone work independently of each other. Another possible regulator is inflammation, because it has been reported that FGF23 expression in cardiac fibroblasts can be up-regulated by systemic inflammation [83]. Because MAPK signaling is involved in the FGF23-mediated effect on cardiac hypertrophy, and MAPK signaling also is pivotal in inflammation associated with CKD-induced cardiovascular disease,

MAPK signaling might represent an important modulator with pleiotropic functions in facilitating CKD-induced cardiovascular disease. Although numerous studies have shown an association of FGF23 with cardiovascular disease in CKD, the direct effect of FGF23 on the heart in the context of CKD still is unclear. However, because FGF23 levels are increased in CKD patients, and FGF23 induces cardiac fibrosis at least in the context of myocardial infarction, it is reasonable to postulate that FGF23 induces cardiac fibrosis in the context of kidney disease.

KLOTHO DEFICIENCY INDUCES CARDIAC FIBROSIS

Besides functioning as a co-receptor for FGF23, the extracellular domain of Klotho also can be cleaved, resulting in circulating Klotho. CKD patients show decreased expression of Klotho in the kidney and decreased serum levels [84]. Klotho deficiency (kl/+) in mice results in cardiac hypertrophy and decreased cardiac function, indicating its role in cardiovascular disease [84]. Moreover, complete knock-out of klotho results in both cardiac fibrosis and hypertrophy [84]. This is associated with increased phosphorylation of Smad2/3, modulators of the canonical TGF β pathway, which is important for fibrosis and suggestive of EndMT, and extracellular signal-regulated kinase, which is pivotal in MAPK signaling, again underlining the interplay of different mediators in facilitating CKD-mediated cardiovascular disease. Interestingly, administration of phosphate to non-CKD mice resulted in decreased Klotho serum levels and decreased Klotho expression in the kidney, indicating the role of phosphate in regulating Klotho and Klotho-induced cardiovascular disease [84]. Klotho in turn attenuated TGF β 1-, angiotensin II-, and phosphate-induced collagen expression and extracellular signal-regulated kinase phosphorylation in cardiac fibroblasts *in vitro* [84]. This suggests that Klotho interferes at different levels to mediate a cardioprotective effect in the context of CKD. In this respect, indoxyl sulfate is an important uremic solute that induces cardiac hypertrophy, and Klotho inhibits indoxyl sulfate-induced cardiac hypertrophy by counteracting oxidative stress via reduced NOX2 and NOX4 expression and by counteracting MAPK signaling [85]. Although in these studies the contribution of FGF23 to Klotho-mediated cardiac dysfunction is not addressed, they underline the importance of FGF23/Klotho/phosphate-mediated cardiovascular disease in the context of CKD. Extensive research is necessary to identify the interplay between FGF23, Klotho,

and phosphate to be able to specifically target these mediators of cardiovascular disease.

CONTRIBUTION OF INCREASED PHOSPHATE CONCENTRATIONS TO CARDIAC FIBROSIS

Both FGF23 and Klotho are phospho-regulatory hormones, and, as discussed in detail earlier, although numerous studies corroborated their relevance on cardiovascular morbidity, high phosphate levels still decreased lifespan when FGF23 and Klotho were absent in FGF23^{-/-} and Klotho^{-/-} knockout mice, suggesting an independent role of phosphate in heart failure and cardiac fibrosis. In this regard, hyperphosphatemia is a hallmark of chronically impaired excretory kidney function [86]. Plasma phosphate levels, ranging typically between 0.8 and 1.5 mmol/L, are a reflection of the body's phosphate balance and in advanced CKD insufficient renal phosphate excretion causes phosphate overload, as reflected by hyperphosphatemia (and altered levels of phospho-regulatory hormones) [87]. Although in absence of known phosphate-sensitive receptors phosphate had been long considered biologically inert, exposure of cultured fibroblasts to media supplemented with high phosphate recapitulated all features of fibroblast activation and EndMT when endothelial cells were cultured within high phosphate media [88,89]. This was dependent on increased phosphate uptake and subsequently increased phosphorylation of the DNA methyltransferase Dnmt1, resulting in its increased activity. Although the underlying cause of observed aberrant Dnmt1 phosphorylation remained unclear in these studies, it is tempting to speculate that excessively increased intracellular phosphate concentrations within CKD patients could serve as a nonspecific phosphate donor, bringing inorganic phosphate to life. Phosphate is an essential constituent of critical cellular functions, including energy metabolism, nucleic acid synthesis, and phosphorylation-dependent cell signaling. Increased plasma phosphate levels are an independent risk factor for decreased life expectancy as well as for heart and kidney failure [89,90]. In summary, insights into the mechanisms underlying the detrimental effect of high phosphate on cardiovascular morbidity in the context of CKD still are emerging and may provide an important novel therapeutic target.

MICRORNAS AS PROFIBROTIC KIDNEY-HEART MESSENGERS

MicroRNAs are small endogenously transcribed regulatory RNAs that modulate gene expression by binding to untranslated regions of messenger RNA or to promoter sequences. MicroRNAs have been reported to regulate various pathogenic processes in the heart and kidney [91,92]. There is considerable overlap of profibrotic microRNAs in heart and kidney, and microRNA-21 and microRNA-29 are among the most abundantly expressed microRNAs in the heart and kidney and both are known to regulate fibrosis by their action on messenger RNA of extracellular matrix proteins and TGF β 1 [91,92]. In a mouse model of cardiorenal syndrome, both microRNA-21 and microRNA-29 were shown to be increased in the heart after myocardial infarction associated with an increase of uremic toxins [93]. Because microRNAs are present in the circulation [94], this conceptually offers the possibility that microRNAs are released by the injured kidney and directly induce fibrosis in the heart, possibly via exosome-mediated RNA transfer [95,96]. Another possible explanation for the synchronized increase of microRNA-21 and microRNA-29 in the heart and kidney is an increase of common inducing factors such as uremic toxins. In this regard, it was shown in the earlier-mentioned mouse model of myocardial infarction that treatment with uremic toxin-adsorbent AST-120 inhibited the increase of microRNA-21 and microRNA-29 levels in the heart [93].

SUMMARY

The progression of chronic heart failure and cardiac fibrosis is a complex process, which involves numerous cell types, soluble factors, and novel mechanisms that still are evolving (Fig. 2). Augmented heart disease through kidney failure via a kidney–heart axis adds further complexity to this process. Although our understanding of the underlying mechanisms still is evolving, the possibility that kidney–heart messengers could be intercepted offers ample reason to focus on this clinically highly relevant problem.

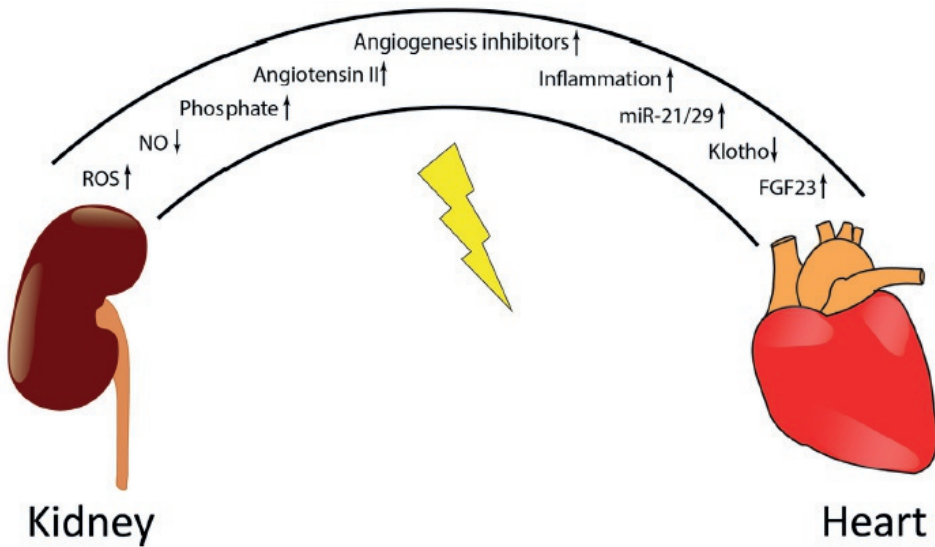


Figure 2. Mediators of CKD-associated cardiac fibrosis.

The mediators of CKD-associated cardiac fibrosis include increased levels of ROS, phosphate, angiotensin II, angiogenesis inhibitors, inflammation, FGF23, microRNA-21 (miR-21) and microRNA-29 (miR-29), and decreased levels of NO and Klotho. The lightning bolt indicates damage.

REFERENCES

1. Hill NR, Fatoba ST, Oke JL, et al. Global prevalence of chronic kidney disease - a systematic review and meta-analysis. *PLoS One*. 2016;11:e0158765.
2. O'Callaghan CA, Shine B, Lasserson DS. Chronic kidney disease: a large-scale population-based study of the effects of introducing the CKD-EPI formula for eGFR reporting. *BMJ Open*. 2011;1:e000308.
3. Charytan DM, Cinelli A, Zeisberg EM. Association of circulating angiogenesis inhibitors and asymmetric dimethyl arginine with coronary plaque burden. *Fibrogenesis Tissue Repair*. 2015;8:13.
4. Mall G, Huther W, Schneider J, Lundin P, Ritz E. Diffuse intermyocardiocytic fibrosis in uraemic patients. *Nephrol Dial Transplant*. 1990;5:39-44.
5. Charytan DM, Padera R, Helfand A, et al. Increased concentration of circulating angiogenesis and nitric oxide inhibitors induces endothelial to mesenchymal transition and myocardial fibrosis in patients with chronic kidney disease. *Int J Cardiol*. 2014;176:99-109.
6. Lim GB. Heart failure: macrophages promote cardiac fibrosis and diastolic dysfunction. *Nat Rev Cardiol*. 2018;15:196-7.
7. Sorop O, Heinonen I, van Kranenburg M, et al. Multiple common comorbidities produce left ventricular diastolic dysfunction associated with coronary microvascular dysfunction, oxidative stress, and myocardial stiffening. *Cardiovasc Res*. 2018;114:954-64.
8. Krenning G, Zeisberg EM, Kalluri R. The origin of fibroblasts and mechanism of cardiac fibrosis. *J Cell Physiol*. 2010;225:631-7.
9. Tallquist MD, Molkenin JD. Redefining the identity of cardiac fibroblasts. *Nat Rev Cardiol*. 2017;14:484-91.
10. Zeisberg EM, Tarnavski O, Zeisberg M, et al. Endothelial-to-mesenchymal transition contributes to cardiac fibrosis. *Nat Med*. 2007;13:952-61.
11. Zeisberg EM, Potenta S, Xie L, Zeisberg M, Kalluri R. Discovery of endothelial to mesenchymal transition as a source for carcinoma-associated fibroblasts. *Cancer Res*. 2007;67:10123-8.
12. Zeisberg EM, Potenta SE, Sugimoto H, Zeisberg M, Kalluri R. Fibroblasts in kidney fibrosis emerge via endothelial-to-mesenchymal transition. *J Am Soc Nephrol*. 2008;19:2282-7.
13. Rieder F, Kessler SP, West GA, et al. Inflammation-induced endothelial-to-mesenchymal transition: a novel mechanism of intestinal fibrosis. *Am J Pathol*. 2011;179:2660-73.
14. Hashimoto N, Phan SH, Imaizumi K, et al. Endothelial-mesenchymal transition in bleomycin-induced pulmonary fibrosis. *Am J Respir Cell Mol Biol*. 2010;43:161-72.
15. Teekakirikul P, Eminaga S, Toka O, et al. Cardiac fibrosis in mice with hypertrophic cardiomyopathy is mediated by non-myocyte proliferation and requires Tgf-beta. *J Clin Invest*. 2010;120:3520-9.
16. Ahmed MS, Øie E, Vinge LE, et al. Connective tissue growth factor—a novel mediator of angiotensin II-stimulated cardiac fibroblast activation in heart failure in rats. *J Mol Cell Cardiol*. 2004;36:393-404.

17. Duerschmid C, Crawford JR, Reineke E, et al. TNF receptor 1 signaling is critically involved in mediating angiotensin-II-induced cardiac fibrosis. *J Mol Cell Cardiol.* 2013;57:59-67.
18. Fedulov AV, Ses TP, Gavrisheva NA, et al. Serum TGF-beta 1 and TNF-alpha levels and cardiac fibrosis in experimental chronic renal failure. *Immunol Invest.* 2005;34:143-52.
19. Liu Y, Zhang J. Nox2 contributes to cardiac fibrosis in diabetic cardiomyopathy in a transforming growth factor-beta dependent manner. *Int J Clin Exp Pathol.* 2015;8:10908-14.
20. Takuwa N, Ohkura S, Takashima S, et al. S1P3-mediated cardiac fibrosis in sphingosine kinase 1 transgenic mice involves reactive oxygen species. *Cardiovasc Res.* 2010;85:484-93.
21. Liu X, Gai Y, Liu F, et al. Trimetazidine inhibits pressure overload-induced cardiac fibrosis through NADPH oxidase-ROS-CTGF pathway. *Cardiovasc Res.* 2010;88:150-8.
22. Xu X, Tan X, Tampe B, et al. Snail is a direct target of hypoxia-inducible factor 1alpha (HIF1alpha) in hypoxia-induced endothelial to mesenchymal transition of human coronary endothelial cells. *J Biol Chem.* 2015;290:16653-64.
23. Xu X, Tan X, Tampe B, et al. Epigenetic balance of aberrant Rasal1 promoter methylation and hydroxymethylation regulates cardiac fibrosis. *Cardiovasc Res.* 2015;105:279-91.
24. Suthanthiran M, Gerber LM, Schwartz JE, et al. Circulating transforming growth factor-beta1 levels and the risk for kidney disease in African Americans. *Kidney Int.* 2009;76:72-80.
25. Kilis-Pstrusinska K, Mastalerz-Migas A, Zwolinska D, et al. The rs1800471 polymorphism of TGFbeta1 gene, serum TGF-beta1 level and chronic kidney disease progression. *Adv Exp Med Biol.* 2015;833:37-46.
26. Baylis C. Nitric oxide deficiency in chronic kidney disease. *Am J Physiol Renal Physiol.* 2008;294:F1-9.
27. Bhandari V, Choo-Wing R, Harijith A, et al. Increased hyperoxia-induced lung injury in nitric oxide synthase 2 null mice is mediated via angiotensin 2. *Am J Respir Cell Mol Biol.* 2012;46:668-76.
28. Daniel C, Amann K, Hohenstein B, Bornstein P, Hugo C. Thrombospondin 2 functions as an endogenous regulator of angiogenesis and inflammation in experimental glomerulonephritis in mice. *J Am Soc Nephrol.* 2007;18:788-98.
29. David S, John SG, Jefferies HJ, et al. Angiotensin-2 levels predict mortality in CKD patients. *Nephrol Dial Transplant.* 2012;27:1867-72.
30. MacLauchlan S, Yu J, Parrish M, et al. Endothelial nitric oxide synthase controls the expression of the angiogenesis inhibitor thrombospondin 2. *Proc Natl Acad Sci U S A.* 2011;108:E1137-45.
31. O'Riordan E, Mendeleev N, Patschan S, et al. Chronic NOS inhibition actuates endothelial-mesenchymal transformation. *Am J Physiol Heart Circ Physiol.* 2007;292:H285-94.
32. Reinecke H, Robey TE, Mignone JL, et al. Lack of thrombospondin-2 reduces fibrosis and increases vascularity around cardiac cell grafts. *Cardiovasc Pathol.* 2013;22:91-5.
33. Watorek E, Paprocka M, Duś D, Kopeć W, Klinger M. Endostatin and vascular endothelial growth factor: potential regulators of endothelial progenitor cell number in chronic kidney disease. *Pol Arch Med Wewn.* 2011;121:296-301.

34. Zoccali C, Bode-Böger S, Mallamaci F, et al. Plasma concentration of asymmetrical dimethylarginine and mortality in patients with end-stage renal disease: a prospective study. *Lancet*. 2001;358:2113-7.
35. Fleck C, Janz A, Schweitzer F, et al. Serum concentrations of asymmetric (ADMA) and symmetric (SDMA) dimethylarginine in renal failure patients. *Kidney Int Suppl*. 2001;78:S14-8.
36. David S, Kümpers P, Lukasz A, et al. Circulating angiotensin-2 levels increase with progress of chronic kidney disease. *Nephrol Dial Transplant*. 2010;25:2571-6.
37. Chen J, Hamm LL, Kleinpeter MA, et al. Elevated plasma levels of endostatin are associated with chronic kidney disease. *Am J Nephrol*. 2012;35:335-40.
38. Lewis GA, Schelbert EB, Williams SG, et al. Biological phenotypes of heart failure with preserved ejection fraction. *J Am Coll Cardiol*. 2017;70:2186-200.
39. Kimura Y, Izumiya Y, Hanatani S, et al. High serum levels of thrombospondin-2 correlate with poor prognosis of patients with heart failure with preserved ejection fraction. *Heart Vessels*. 2016;31:52-9.
40. Lofman I, Szummer K, Dahlström U, Jernberg T, Lund LH. Associations with and prognostic impact of chronic kidney disease in heart failure with preserved, mid-range, and reduced ejection fraction. *Eur J Heart Fail*. 2017;19:1606-14.
41. Hirata Y, Yamamoto E, Tokitsu T, et al. The pivotal role of a novel biomarker of reactive oxygen species in chronic kidney disease. *Medicine (Baltimore)*. 2015;94:e1040.
42. Ramos LF, Shintani A, Ikizler TA, Himmelfarb J. Oxidative stress and inflammation are associated with adiposity in moderate to severe CKD. *J Am Soc Nephrol*. 2008;19:593-9.
43. Angelos MG, Kutala VK, Torres CA, et al. Hypoxic reperfusion of the ischemic heart and oxygen radical generation. *Am J Physiol Heart Circ Physiol*. 2006;290:H341-7.
44. Giordano FJ. Oxygen, oxidative stress, hypoxia, and heart failure. *J Clin Invest*. 2005;115:500-8.
45. Zhao W, Zhao T, Chen Y, Ahokas RA, Sun Y. Oxidative stress mediates cardiac fibrosis by enhancing transforming growth factor-beta1 in hypertensive rats. *Mol Cell Biochem*. 2008;317:43-50.
46. Sugamura K, Keaney Jr JF. Reactive oxygen species in cardiovascular disease. *Free Radic Biol Med*. 2011;51:978-92.
47. Panth N, Paudel KR, Parajuli. Reactive oxygen species: a key hallmark of cardiovascular disease. *Adv Med*. 2016;2016:9152732.
48. Zhao QD, Viswanadhapalli S, Williams P, et al. NADPH oxidase 4 induces cardiac fibrosis and hypertrophy through activating Akt/mTOR and NFκB signaling pathways. *Circulation*. 2015;131:643-55.
49. Bache RJ, Chen Y. NOX2-induced myocardial fibrosis and diastolic dysfunction: role of the endothelium. *J Am Coll Cardiol*. 2014;63:2742-4.
50. Sirker A, Zhang M, Shah AM. NADPH oxidases in cardiovascular disease: insights from in vivo models and clinical studies. *Basic Res Cardiol*. 2011;106:735-47.
51. Numaga-Tomita T, Kitajima N, Kuroda T, et al. TRPC3-GEF-H1 axis mediates pressure overload-induced cardiac fibrosis. *Sci Rep*. 2016;6:39383.

52. Rocic P, Lucchesi. NAD(P)H oxidases and TGF-beta-induced cardiac fibroblast differentiation: Nox-4 gets Smad. *Circ Res.* 2005;97:850-2.
53. Murdoch CE, Chaubey S, Zeng L, et al. Endothelial NADPH oxidase-2 promotes interstitial cardiac fibrosis and diastolic dysfunction through proinflammatory effects and endothelial-mesenchymal transition. *J Am Coll Cardiol.* 2014;63:2734-41.
54. Zhang M, Mongue-Din H, Martin D, et al. Both cardiomyocyte and endothelial cell Nox4 mediate protection against hemodynamic overload-induced remodeling. *Cardiovasc Res.* 2018;114:401-8.
55. Santos PC, Krieger JE, Pereira. Renin-angiotensin system, hypertension, and chronic kidney disease: pharmacogenetic implications. *J Pharmacol Sci.* 2012;120:77-88.
56. Liu J, Yang F, Yang XP, Jankowski M, Pagano PJ. NAD(P)H oxidase mediates angiotensin II-induced vascular macrophage infiltration and medial hypertrophy. *Arterioscler Thromb Vasc Biol.* 2003;23:776-82.
57. Looi YH, Grieve DJ, Siva A, et al. Involvement of Nox2 NADPH oxidase in adverse cardiac remodeling after myocardial infarction. *Hypertension.* 2008;51:319-25.
58. Bugyei-Twum A, Abadeh A, Thai K, et al. Suppression of NLRP3 inflammasome activation ameliorates chronic kidney disease-induced cardiac fibrosis and diastolic dysfunction. *Sci Rep.* 2016;6:39551.
59. Bae E, Cha RH, Kim YC, et al. Circulating TNF receptors predict cardiovascular disease in patients with chronic kidney disease. *Medicine (Baltimore).* 2017;96:e6666.
60. Takei Y, Di Tullio MR, Homma S, et al. Soluble tumor necrosis factor receptor 1 level is associated with left ventricular hypertrophy: the northern Manhattan study. *Am J Hypertens.* 2009;22:763-9.
61. Higuchi Y, Otsu K, Nishida K, et al. Involvement of reactive oxygen species-mediated NF-kappa B activation in TNF-alpha-induced cardiomyocyte hypertrophy. *J Mol Cell Cardiol.* 2002;34:233-40.
62. Park JK, Fischer R, Dechend R, et al. p38 mitogen-activated protein kinase inhibition ameliorates angiotensin II-induced target organ damage. *Hypertension.* 2007;49:481-9.
63. Demyanets S, Kaun C, Pentz R, et al. Components of the interleukin-33/ST2 system are differentially expressed and regulated in human cardiac cells and in cells of the cardiac vasculature. *J Mol Cell Cardiol.* 2013;60:16-26.
64. Gungor O, Unal HU, Guclu A, et al. IL-33 and ST2 levels in chronic kidney disease: associations with inflammation, vascular abnormalities, cardiovascular events, and survival. *PLoS One.* 2017;12:e0178939.
65. Chalubinski M, Wojdan K, Luczak E, et al. IL-33 and IL-4 impair barrier functions of human vascular endothelium via different mechanisms. *Vascul Pharmacol.* 2015;73:57-63.
66. Taslipinar A, Yaman H, Yilmaz MI, et al. The relationship between inflammation, endothelial dysfunction and proteinuria in patients with diabetic nephropathy. *Scand J Clin Lab Invest.* 2011;71:606-12.
67. Yilmaz MI, Solak Y, Saglam M, et al. The relationship between IL-10 levels and cardiovascular events in patients with CKD. *Clin J Am Soc Nephrol.* 2014;9:1207-16.

68. Yilmaz MI, Sonmez A, Ortiz A, et al. Soluble TWEAK and PTX3 in nondialysis CKD patients: impact on endothelial dysfunction and cardiovascular outcomes. *Clin J Am Soc Nephrol.* 2011;6:785-92.
69. Ma F, Li Y, Jia L, et al. Macrophage-stimulated cardiac fibroblast production of IL-6 is essential for TGF beta/Smad activation and cardiac fibrosis induced by angiotensin II. *PLoS One.* 2012;7:e35144.
70. Zhang R, Zhang YY, Huang XR, et al. C-reactive protein promotes cardiac fibrosis and inflammation in angiotensin II-induced hypertensive cardiac disease. *Hypertension.* 2010;55:953-60.
71. Verma SK, Garikipati VNS, Krishnamurthy P, et al. Interleukin-10 inhibits bone marrow fibroblast progenitor cell-mediated cardiac fibrosis in pressure-overloaded myocardium. *Circulation.* 2017;136:940-53.
72. Wassmann S, Stumpf M, Strehlow K, et al. Interleukin-6 induces oxidative stress and endothelial dysfunction by overexpression of the angiotensin II type 1 receptor. *Circ Res.* 2004;94:534-41.
73. Ijsselmuiden AJ, Musters RJ, de Rooter G, et al. Circulating white blood cells and platelets amplify oxidative stress in heart failure. *Nat Clin Pract Cardiovasc Med.* 2008;5:811-20.
74. Quarles LD. Role of FGF23 in vitamin D and phosphate metabolism: implications in chronic kidney disease. *Exp Cell Res.* 2012;318:1040-8.
75. Kurosu H, Ogawa Y, Miyoshi M, et al. Regulation of fibroblast growth factor-23 signaling by klotho. *J Biol Chem.* 2006;281:6120-3.
76. Urakawa I, Yamazaki Y, Shimada T, et al. Klotho converts canonical FGF receptor into a specific receptor for FGF23. *Nature.* 2006;444:770-4.
77. Gutierrez OM, Mannstadt M, Isakova T, et al. Fibroblast growth factor 23 and mortality among patients undergoing hemodialysis. *N Engl J Med.* 2008;359:584-92.
78. Isakova T, Xie H, Yang W, et al. Fibroblast growth factor 23 and risks of mortality and end-stage renal disease in patients with chronic kidney disease. *JAMA.* 2011;305:2432-9.
79. Jean G, Bresson E, Lorriaux C, et al. Increased levels of serum parathyroid hormone and fibroblast growth factor-23 are the main factors associated with the progression of vascular calcification in long-hour hemodialysis patients. *Nephron Clin Pract.* 2012;120:c132-8.
80. Parker BD, Schurgers LJ, Brandenburg VM, et al. The associations of fibroblast growth factor 23 and uncarboxylated matrix Gla protein with mortality in coronary artery disease: the Heart and Soul Study. *Ann Intern Med.* 2010;152:640-8.
81. Faul C, Amaral AP, Oskoueï B, et al. FGF23 induces left ventricular hypertrophy. *J Clin Invest.* 2011;121:4393-408.
82. Hao H, Li X, Li Q, et al. FGF23 promotes myocardial fibrosis in mice through activation of beta-catenin. *Oncotarget.* 2016;7:64649-64.
83. Yan L, Bowman MA. Chronic sustained inflammation links to left ventricular hypertrophy and aortic valve sclerosis: a new link between S100/RAGE and FGF23. *Inflamm Cell Signal.* 2014;1.
84. Hu MC, Shi M, Cho HJ, et al. Klotho and phosphate are modulators of pathologic uremic cardiac remodeling. *J Am Soc Nephrol.* 2015;26:1290-302.

85. Yang K, Wang C, Nie L, et al. Klotho protects against indoxyl sulphate-induced myocardial hypertrophy. *J Am Soc Nephrol*. 2015;26:2434-46.
86. Kuro OM. A phosphate-centric paradigm for pathophysiology and therapy of chronic kidney disease. *Kidney Int Suppl*. 2013;3:420-6.
87. Blaine J, Chonchol M, Levi. Renal control of calcium, phosphate, and magnesium homeostasis. *Clin J Am Soc Nephrol*. 2015;10:1257-72.
88. Tan X, Xu X, Zeisberg M, et al. DNMT1 and HDAC2 cooperate to facilitate aberrant promoter methylation in inorganic phosphate-induced endothelial-mesenchymal transition. *PLoS One*. 2016;11:e0147816.
89. Tan X, Xu X, Zeisberg EM, et al. High inorganic phosphate causes DNMT1 phosphorylation and subsequent fibrotic fibroblast activation. *Biochem Biophys Res Commun*. 2016;472:459-64.
90. Ritz E, Hahn K, Ketteler M, et al. Phosphate additives in food—a health risk. *Dtsch Arztebl Int*. 2012;109:49-55.
91. Thum T. Noncoding RNAs and myocardial fibrosis. *Nat Rev Cardiol*. 2014;11:655-63.
92. Chung AC, Lan HY. MicroRNAs in renal fibrosis. *Front Physiol*. 2015;6:50.
93. Rana I, Kompa AR, Skommer J, et al. Contribution of microRNA to pathological fibrosis in cardio-renal syndrome: impact of uremic toxins. *Physiol Rep*. 2015;3.
94. Martino F, Lorenzen J, Schmidt J, et al. Circulating microRNAs are not eliminated by hemodialysis. *PLoS One*. 2012;7:e38269.
95. Valadi H, Ekström K, Bossios A, et al. Exosome-mediated transfer of mRNAs and microRNAs is a novel mechanism of genetic exchange between cells. *Nat Cell Biol*. 2007;9:654-9.
96. Gonzalez-Calero L, Martin-Lorenzo M, Alvarez-Llamas G. Exosomes: a potential key target in cardio-renal syndrome. *Front Immunol*. 2014;5:465.

CHAPTER

9

CRISPR/CAS DERIVATIVES AS NOVEL GENE MODULATING TOOLS: POSSIBILITIES AND *IN VIVO* APPLICATIONS

Xingbo Xu^{1,2,*}, Melanie S. Hulshoff^{1,2,3,*}, Xiaoying Tan^{2,4}, Michael Zeisberg^{2,4} and Elisabeth M. Zeisberg^{1,2}

¹*Department of Cardiology and Pneumology, University Medical Center Göttingen, Robert-Koch-Str. 40, 37075, Göttingen, Germany.*

²*German Centre for Cardiovascular Research (DZHK), Göttingen, Germany.*

³*Department of Pathology and Medical Biology, University Medical Center Groningen, Hanzeplein 1, 9713 GZ, Groningen, The Netherlands.*

⁴*Department of Nephrology and Rheumatology, University Medical Center of Göttingen, Robert-Koch-Str. 40, 37075, Göttingen, Germany.*

**Authors contributed equally*

ABSTRACT

The field of genome editing started with the discovery of meganucleases (e.g. the LAGLIDADG family of homing endonucleases) in yeast. After the discovery of transcription activator-like effector nucleases and zinc finger nucleases, the recently discovered CRISPR/Cas system has opened a new window of applications in the field of gene editing. Here, we review different Cas proteins and their corresponding features including advantages and disadvantages and we provide an overview of the different dCas derivatives. These dCas derivatives consist of an endonuclease-deficient Cas9 which can be fused to different effector domains to perform distinct in vitro applications such as tracking, transcriptional activation and repression, as well as base editing. Finally, we review the in vivo applications of these dCas derivatives and discuss their potential to perform gene activation and repression in vivo, as well as their potential future use in human therapy.

INTRODUCTION

In the last ten years, major breakthroughs have been made in the field of gene editing, which is the process where DNA is modified, deleted, inserted or replaced. The most recent discovery of the clustered regularly interspaced short palindromic repeats (CRISPR)/CRISPR associated proteins (Cas) system has opened up many novel opportunities as well as applications for gene editing both *in vitro* and *in vivo*. In this review, we provide an overview of the different gene editing techniques including the CRISPR/Cas system, which was discovered in 2012. After this finding, different Cas proteins were developed with unique features that allow for distinct gene editing approaches. Here, we summarize these different Cas proteins and detail their specific features. Besides the development of different Cas proteins, endonuclease-deficient Cas proteins allow for additional applications of the CRISPR/Cas system. These endonuclease-deficient Cas proteins (dCas) can be fused to effector domains which exert additional functions such as transcriptional activation or repression, but also tracking and base-editing. These dCas-effectors as well as their functions and *in vivo* applications will be the main focus of this perspective.

GENE EDITING TECHNIQUES

Gene editing started with the discovery of meganucleases in yeast as well as in other small organisms. There are hundreds of meganucleases which each contain a recognition sequence (homing site) between 14 and 40 base pairs (Figure 1) [1]. This large recognition site ensures great locus specificity together with low off-target effects. At the same time, the large recognition site is also the main limitation of meganucleases since their recognition site only occurs once (or sometimes not at all) in the genome of a given organism. This limitation can be circumvented by modifying the recognition site of the particular meganuclease [2], which is time-consuming and labor-intensive.

In 1994, the zinc finger nucleases (ZFN) were discovered as first modulated gene editing tools [3]. ZFN consist of nucleases which are coupled to certain zinc fingers which each recognize triplets of base pairs (codons; Figure 1) [4]. To increase the binding specificity, several zinc fingers are attached together (usually 3) to reach a binding site of 9 nucleotides (3 codons). The same holds for the

complementary strand, so in total an 18-nucleotide specificity is reached. These zinc fingers can be engineered in a specific way to recognize the DNA region of interest. These connected zinc fingers are then fused to cleavage domains of endonucleases (usually to FokI nuclease monomers) [5]. The sequence in between the two ZFN binding sites is the so-called spacer region consisting of 5-7 nucleotides where FokI monomers form a catalytically active dimer, which cleaves the DNA resulting in double-strand breaks [6]. The production of an efficient ZFN might require multiple rounds of re-designing and optimizations (because each of the selected ZF might affect the binding affinity of the adjacent ZFs), which is labor-intensive, time consuming and most importantly expensive.

In 2009, the transcription activator-like effector nucleases (TALEN) were developed which function in a similar way but have increased specificity when compared to ZFN [7, 8]. Transcription activator-like effectors (TALE) were discovered in bacteria and are able to bind to single nucleotides (instead of triplets of nucleotides by zinc fingers) [9]. Similar to ZFN, several TALE are attached together (i.e. 12-31 repeats per TALEN) to target the DNA sequence of interest and are fused to FokI nuclease monomers (Figure 1) [10]. Similarly, the second TALEN monomer is designed for the complementary strand. FokI nuclease monomers will again form a catalytically active dimer in the spacer region and cleave the DNA. The procedure of producing new ZFN and TALEN is labor-intensive since for every DNA target region of interest, novel ZFN and TALEN have to be generated.

In 2012, the most recent gene editing tool was discovered: Clustered regularly interspaced short palindromic repeats (CRISPR) and CRISPR associated genes (Cas) [11]. The CRISPR genomic locus consist of Cas genes (which code e.g. for the nuclease Cas9) and a leader sequence followed by repeat sequences which are flanked by spacer regions. Originally, CRISPR was discovered in bacteria and contributes to the immune defense system where foreign DNA from viruses or fungi is inserted within the repeat sequences of the CRISPR genomic locus [12,13]. These repeat sequences are subsequently transcribed into so-called CRISPR RNAs (crRNAs) which recognize foreign DNA and recruit a Cas protein to cleave the foreign DNA. This system can be adapted by the design of a so-called single guide RNA (sgRNA) which is a custom-designed short crRNAs fused to the scaffold trans-activating crRNA sequence (tracrRNA) and guides the Cas9 nuclease to a specific DNA region of interest. Another essential element for the

Cas nuclease is the protospacer adjacent motif (PAM) which is a short specific sequence following the target DNA sequence that is needed for Cas nuclease-mediated cleavage [11]. The precise location of the Cas nuclease can be adapted by changing the sgRNA to a specific locus. This sgRNA molecule is cheaper and easier to generate compared to the production of ZFN and TALEN, which is an advantage of the CRISPR/Cas system. The limitation of CRISPR, but also of ZFN and TALEN, is the presence of off-target effects. These off-target effects have been reduced by the discovery of the so-called high-fidelity CRISPR/Cas system where four amino acids have been substituted in *Streptococcus pyogenes* Cas9 (SpCas9) by Kleinstiver and his colleagues. These four amino acid substitutions alter the energetics of the binding of SpCas9 to the DNA and thereby the specificity, which diminished off-target effects [14]. A comparison of the different gene editing techniques is provided in Table 1.

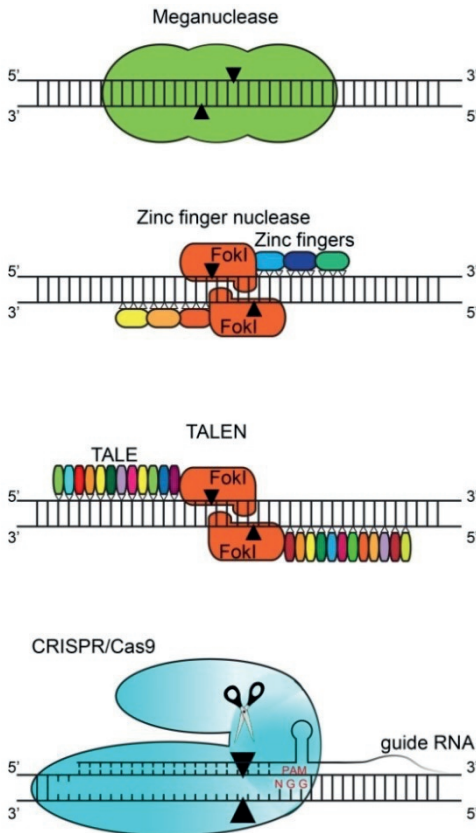


Figure 1. Gene editing techniques.

Overview of the different gene editing designer nucleases. This figure depicts the initially discovered meganucleases. In addition, the zinc finger and TALE (transcription activator-like effectors) are

depicted which are fused to FokI nuclease monomers which cleave the DNA upon dimerization. The most recently discovered RNA-guided CRISPR/Cas9 system is illustrated as well. Black arrows represent the cleavage site.

Table 1. Comparison of gene editing techniques

	Meganucleases	ZFN	TALEN	CRISPR/Cas9
Flexible localization	Complex	Limited	Average	Almost total
Nuclease construction	Laborious	Significant	Significant	Simple
<i>In vitro</i> testing	Laborious	Significant	Significant	Simple
Targeting efficiency	Not reported	Limiting factor	Average	Good
Off-target effects	Low	Moderate	Moderate	High
Multiplexing	No	No	No	Yes
Time investment	Very high	High	Moderate	Low
Cost	Very high	High	Average	Low

Comparison of the different gene editing techniques based on different components such as flexible localization, nuclease construction, targeting efficiency and time investment. CRISPR/Cas9 has several advantages over meganucleases, ZFN and TALEN: it has an almost total flexible localization, it is simple to construct and test *in vitro*, it has a good targeting efficiency with the ability for multiplexing whereas the time investment and costs are low. Off-target effects are the main limitation of the CRISPR/Cas9 system, but also for ZFN and TALEN.

VARIETY OF CAS PROTEINS

The most commonly used Cas9 protein is derived from *Streptococcus pyogenes* (SpCas9) [11]. The use of SpCas9 is limited by its 5'-NGG-3' (where N = G, C, T or A) PAM motif which constricts the range of targetable sites in the DNA [15]. The wild-type SpCas9 is therefore engineered to gain different PAM specificities which enable targeting of previously inaccessible sites. These engineered SpCas9 mutants include VQR (D1135V/R1335Q/T1337R) with 5'-NGAN-3' as PAM, EQR (D1135E/R1335Q/T1337R) with 5'-NGAG-3' as PAM and VRER (D1135V/G1218R/R1335E/T1337R) with 5'-NGCG-3' as PAM motif respectively (Table 2) [15]. spCas9 consists of 1,368 amino acids, which restricts its use in adeno-associated virus (AAV) vector-based therapeutic applications (which will be discussed later in this review). More than 1kb shorter than SpCas9 are the Cas9 proteins derived from *Staphylococcus aureus* (SaCas9), *Neisseria meningitidis* (NmCas9), *Streptococcus thermophilus* (St1Cas9) and *Brevibacillus*

laterosporus (BlatCas9; Table 2) [16-19]. The targeting range of SaCas9 is also increased by a modified PAM recognition site (from 5'-NNGRRT-3' to 5'-NNNRRT-3') [19,20]. NmCas9 recognizes a 5'-NNNNGATT-3' PAM whereas St1Cas9 and BlatCas9 recognize 5'-NNAGAAW-3' and 5'-NNNNCNDD-3' (where D = A, G or T) respectively [16-18]. SaCas9, NmCas9 and St1Cas9 all have a strict PAM [16,17,19,20], whereas the PAM of BlatCas9 is less restrictive since it has a strong preference for just a single nucleotide [18]. Cas9 derived from *Francisella novicida* (FnCas9) also has a less restrictive PAM but with 1,629 amino acids it is significantly larger than the other Cas9 orthologs [21]. FnCas9 consist of a wild-type and a mutated form which recognize 5'-NGG-3' and 5'-YG-3' (where Y = C or T) respectively (Table 2) [21]. Even though BlatCas9 and FnCas9 have a less restrictive PAM, there are less application examples when compared to the other Cas9 orthologs (most likely because they were discovered later).

Besides different Cas9 orthologs, other Cas proteins are discovered as well including Cpf1 (CRISPR from *Prevotella* and *Francisella* 1 aka Cas12), Cas13 and Cas14 [22]. Cpf1 has various unique characteristics: (1) it is a single RNA-guided endonuclease which lacks tracrRNA, (2) it has a strict T-rich PAM (5'-TTTN-3') when compared to the more G-rich PAM of Cas9 proteins, and (3) where Cas9 facilitates blunt ends, Cpf1 facilitates sticky ends with a 4 or 5 nucleotide 5' overhang [22]. To date, there are several known Cpf1 orthologs with robust nuclease activity: *Acidaminococcus* sp. Cas12 (AsCpf1), *Lachnospiraceae bacterium* Cas12 (LbCpf1) and *Bacillus hisashii* Cas12b (BhCas12b; Table 2) [22,23]. In addition, Cas12c, Cas12g, Cas12h and Cas12i have been characterized which demonstrate RNA-guided dsDNA interference activity [24].

In addition to Cas9 and Cpf1, CasX enzymes represent a distinct family of RNA-guided genome editors. CasX enzymes use unique structures for programmable dsDNA binding and cleavage [25].

Where Cas9 and Cpf1 are widely used to induce DNA breaks (as well as the recently discovered CasX enzymes), Cas13a (previously called C2c2) cleaves single-stranded RNA [25-27]. Similar to Cpf1, Cas13a lacks tracrRNA and is guided by a single crRNA [27]. RNA cleavage is mediated by catalytic residues in the two conserved Higher Eukaryotes and Prokaryotes Nucleotide-binding (HEPN) domains and is dependent on a 3' H (non-G) protospacer flanking site (PFS) following the RNA target site [27]. The first characterized Cas13 protein derived from the bacterium *Leptotrichia shahii* (LshCas13a) [27]. The later characterized

Leptotrichia wadei Cas13a (LwaCas13a) exhibits higher cleavage activity than LshCas13a and does not require a PFS (Table 2) [26]. After the discovery of LwaCas13a, researchers identified *Prevotella sp. P5-125* Cas13b (PspCas13b) which also does not require a PFS (Table 2) [28]. PspCas13b-mediated mRNA knockdown is more efficient when compared to LwaCas13a [28]. The most recent discovered Cas13 protein is *Ruminococcus flavefaciens* Cas13d (RfxCas13d) and is also not dependent on a PFS (Table 2) [29]. This Cas13 protein has the smallest protein size which allows packaging into AAV vectors and thus enables AAV vector-based therapeutic applications (will be discussed later in this review) [29]. In summary, the main differences between Cas9 and Cas13 include the PAM motif, the length of the sgRNA and the cleavage of RNA vs DNA.

Cas9 and Cas13 can both serve as gene silencing tools for protein coding genes. The Cas9 system utilizes non-homologous end joining-based DNA damage repair to create a DNA insertion/deletion (indel) mutation to generate a frame shift or a point mutation (e.g. premature stop codon, non-functional protein) [11]. In this way, a premature stop codon is very likely to form and a functional protein will not be translated. However, for non-protein coding genes such as long non-coding RNAs, utilizing Cas9 is unlikely to show gene silencing effects whereas Cas13 can target and cleave RNA thereby triggering the RNA degradation pathway [26, 28]. In addition to programmable RNase activity, Cas13 exhibits collateral activity after recognition and cleavage of a target transcript, leading to non-specific degradation of any nearby transcripts regardless of complementarity to the spacer [30, 31]. This property enables Cas13 to be well suited for nucleic acid detection. When the enzyme recognizes its target in vitro, it becomes activated and promiscuously cleaves RNA species in solution. Cas13-based detection is specific and can be tuned for single-nucleotide distinction at any position on the target. This nucleic acid detection technology is called SHERLOCK (Specific High-Sensitivity Enzymatic Reporter unLOCKing) [30, 31].

The most recently discovered Cas14 family consists of the smallest RNA-guided nucleases which depend on a tracrRNA and, in contrast to the other Cas proteins, targets single-stranded DNA (Table 2) [32]. Cleavage of single-stranded DNA by Cas14 is not dependent on restrictive sequence requirements (PAM) [32]. Altogether, these different Cas proteins enable a wide range of targeting sites and applications to perform CRISPR/Cas-mediated gene editing at either the DNA or RNA level (Table 2).

Table 2. Comparison of Cas proteins

Name	Protein size (aa)	WT/mutants	PAM (5'-3')	Protospacer length	Target / Type of DSB	Pros/Cons	<i>In vivo/in vitro</i>
Cas9 (HNH, RuvC)							
SpCas9	1368	WT	NGG	20	DNA/Be	Most commonly used, Large protein size	<i>In vitro, in vivo</i> [11]
		VQR	NGAN	20	DNA/Be	Different PAM specificities, Large protein size	<i>In vitro, in vivo</i> [15]
		EQR	NGAG	20	DNA/Be		
		VRER	NGCG	20	DNA/Be		
SaCas9	1053	WT KKH	NNGRRT NNNRRT	20 20	DNA/Be DNA/Be	Small protein size, Relatively strict PAM	<i>In vitro, in vivo</i> [19,20]
FnCas9	1629	WT RHA	NGG YG	20 20	DNA/Be DNA/Be	Less restrictive PAM, Large protein size, Less application examples	<i>In vitro, in vivo</i> [21]
NmCas9	1082	WT	NNNNG ATT	24	DNA/Be	Small protein size, Strict PAM	<i>In vitro, in vivo</i> [17]
St1Cas9	1121	WT	NNAGA AW	20	DNA/Be	Small protein size, Strict PAM	<i>In vitro</i> [16]
BlatCas9	1092	WT	NNNNC NDD	21	DNA/Be	Less restrictive PAM, Small protein size, Less application examples	<i>In vitro</i> [18]

CHAPTER 9

Cas12/Cpf1 (RuvC-like)

AsCpf1	1307	WT	TTTN	23	DNA/Se	Various unique characteristics , Restrict PAM with 5'overhang	<i>In vitro, in vivo</i> [22]
LbCpf1	1228	WT	TTTN	23	DNA/Se		
BhCas12b	1140	WT	ATTN	23	DNA/Se	High specificity	<i>In vitro</i> [23]
Cas12c	1253	WT	TG/TN	n.a.	DNA	Less restrictive	<i>In vitro</i> [24]
Cas12g	768	WT	*	24			
Cas12h	871	WT	RTR	n.a.		PAM, small protein size	
Cas12i	1055	WT	TTN	28			
CasX	987	WT	TTCN	20	DNA/Se	Very small protein size	<i>In vitro</i> [25]
Cas14 (RuvC)							
Cas14a	529	WT	*	25	DNA	Very small protein size, target ssDNA	<i>In vitro</i> [32]
Cas13 (2xHEPN)							
LshCas13a	1427	WT	3' A, U	28	RNA	Very flexible	<i>In vitro</i> [26,27]
LwaCas13a	1152	WT	or C**	28	RNA	PFS, target RNA	
PspCas13b	1124	WT		30	RNA		
RfxCas13d	979	WT	3' A, U or C**	30	RNA	Very small protein size, target RNA	<i>In vitro</i> [29]

*Overview of different Cas proteins, both wildtype (WT) and mutants, characteristics such as length, protospacer adjacent motif (PAM), DNA end and DNA/RNA targeted. Their advantages and disadvantages (pros and cons) are mentioned as well as their respective reference. Be=Blunt end, Se=Staggered End, *=Not required, **=Not required by all orthologs, n.a.=Not applicable. A: Adenine, C: Cytosine, G: Guanine, T: Thymine, D: A or G or T, R: A or G, W: A or T, Y: C or T, N: any base.*

DCAS DERIVATIVES AND THEIR FUNCTIONS

The CRISPR/Cas system can be repurposed in several ways by modification into an endonuclease-deficient Cas protein (dCas). dCas9 is generated via the introduction of two mutations in the cleavage domains of Cas9 (D10A and H840A). dCas9 is still capable to bind to the DNA in a sgRNA-mediated manner but does no longer cleave the DNA. Different effector domains with distinct gene regulatory functions such as transcriptional activators, repressors or base editing domains, can be fused to dCas9. Subsequent introduction into cells results in sgRNA-guided gene activation, gene repression or base editing of the targeted locus. dCas9 can also be used to perform fluorescent imaging. These Cas9 derivatives will be discussed in more detail below.

CHROMATIN VISUALIZATION AND FLUORESCENT IMAGING WITH DCAS9 DERIVATIVES

One possibility is to use a sgRNA-dependent enhanced green fluorescent protein (EGFP)-tagged dCas9 protein to dynamically image repetitive elements in both telomeres and coding genes (Figure 2) [33]. This system is composed of three components: cells stably expressing a doxycycline-inducible EGFP-tagged dCas9 and Tet-On 3G/BFP trans-activator which are transduced with lentiviral vectors expressing the respective sgRNAs [33]. Non-repetitive sequences can be imaged as well by the design of different sgRNAs at multiple adjacent site of the locus of interest [33]. This strategy was used to visualize a non-repetitive region of the *MUC4* locus [33]. Importantly, the Cas9 fusion protein did not disrupt telomere dynamics. Genomic labeling by dCas9-EGFP is not destructive and also allows to observe native chromatin dynamics. The authors designed sgRNAs targeting exon 2 and intron 3 of the *MUC4* gene in HeLa cells to investigate the chromosome reorganization dynamics during cell replication. Therefore, dCas9-fluorescent imaging represents a new approach to study chromatin conformation and dynamics in both short time frames and long-term processes such as mitosis. [33] Another possibility for fluorescent imaging is the so-called dCas9-SunTag system. This is a protein-tagging system for signal amplification in fluorescent imaging [34]. This system consists of a protein scaffold, which is a repeating peptide array called SunTag (10xGCN4), which can recruit multiple copies of an

antibody (single-chain variable fragment [scFV]-fused protein such as GFP) [34]. This system can be used for fluorescent imaging, where SunTag can recruit up to 24 copies of GFP which results in long-term imaging of single protein molecules in living cells [32]. This system can also be used to recruit multiple copies of effector domains responsible for transcriptional activation, which will be discussed in more detail below.

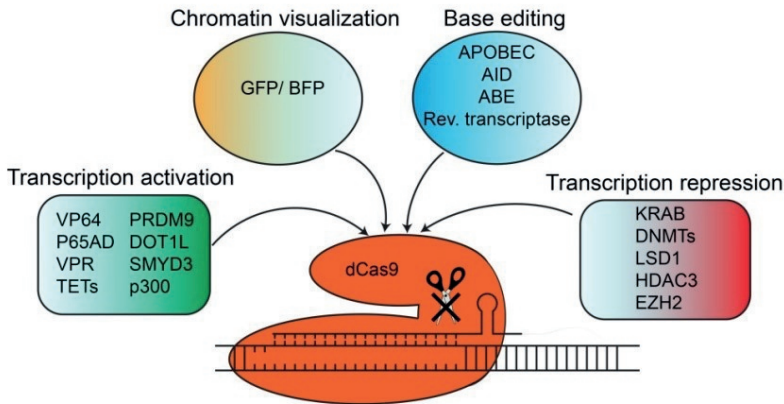


Figure 2. dCas9 derivatives and their purpose.

Overview of the different dCas9 derivatives. Their purpose includes transcriptional activation (via transcriptional activators or epigenetic modifiers), chromatin visualization, base editing and transcriptional repression (via repressor domains or epigenetic modifiers).

TRANSCRIPTIONAL ACTIVATION WITH DCAS9 DERIVATIVES

Recruitment of transcriptional factors or activation domains to initiate gene expression can be achieved by fusion of various activation domains to dCas9 (Figure 2). dCas9-based gene reactivation methods which upregulate the expression of endogenous genes have the advantage over gene over-expression techniques since 95% of the human genes are alternatively spliced, and forced expression of any single mRNA transcript would distort the original homeostatic ratios of the endogenous transcripts [35]. Examples of these activation domains are the C-terminal of the VP64 acidic transactivation domain [36,37] or the p65 activation domain (p65AD) [36]. To enhance the transcriptional activity, these transcriptional activators can also be combined into a tripartite activator called

VPR (which is a combination of VP64, p65 and Rta) [38]. These activation domains are capable to activate both endogenous coding and non-coding genes and can target several genes at the same time by using multiple sgRNAs [38]. The previous mentioned dCas9-SunTag system is also used to recruit multiple copies of VP64 to dCas9-VP64 which enhances transcriptional activation by dCas9-VP64 [34]. Since these methods are based on over-recruitment of transcription factors, this often leads to gene expression levels much higher than physiological levels which largely limits the *in vivo* applications.

Besides fusing transcriptional activators to dCas9, it is also possible to fuse dCas9 to epigenetic-modifying domains. Here, the gene is activated via their endogenous transcription system and is therefore expressed at physiological levels [39,40]. In general, gene regulation via dCas9-based epigenetic effectors includes DNA promoter methylation and histone modifications. DNA promoter methylation is responsible for gene silencing whereas histone modifications induce either gene activation (via histone acetylation or trimethylation of histone H3 lysine 4) or gene silencing (e.g. dimethylation of histone H3 lysine 4). Examples of epigenetic-modifying domains responsible for gene activation are the catalytic domain of Ten-eleven translocation methylcytosine dioxygenases (TETs) or the histone acetyltransferase p300. TETs are responsible for reversing DNA promoter methylation via hydroxymethylation thereby re-activating gene expression. We and others have shown that fusion of dCas9 to the catalytic domain of TET1 [41-43] and TET3 [44] enables gene-specific demethylation which results in re-activation of gene expression [41-44]. The dCas9-SunTag system is also used to recruit multiple copies of the catalytic domain of TET1 to dCas9-TET1CD to perform targeted DNA demethylation [42]. Another strategy includes the recruitment of multiple copies of the catalytic domain of TET1 by using a MS2 coat protein [36]. Another possibility of epigenetic editing is the fusion of dCas9 to the catalytic core of the histone acetyltransferase p300 [40]. P300 acetylates histone H3 lysine 27 which induces transcriptional activation of target genes from promoters and both proximal and distal enhancers [40]. dCas9 can also be fused to the histone methyltransferase SMYD3 (SET and MYND domain containing protein 3) to facilitate trimethylation of histone H3 lysine 4 (H3K4me3) which results in transcriptional activation of silenced target genes [45]. The catalytic core of the histone methyltransferase PRDM9 also induces H3K4me3 marks when fused to dCas9 which results in transcriptional activation [46]. The H3K79

methyltransferase DOT1L also enables re-expression of genes when fused to dCas9 [46]. The mix of both PRDM9 and DOT1L enabled stable induction of gene re-expression [46]. Interestingly, the presence of DNA methylation hampers gene re-expression induced by both PRDM9 and DOT1L [46]. This raises the possibility to combine DNA demethylation effector domains with histone modifying effector domains to enhance the efficacy of dCas9-based transcriptional activation. Altogether, this demonstrates that both VP64-based artificial transcription factors as well as epigenetic effectors can be fused to dCas9 to perform gene activation.

dCas9-based gene activation systems (by fusing dCas9 to different activator such as VP64, p65, Rta or HSF1) showed great gene reactivation effects, but they mainly depend on using a pool of different guide RNAs, which makes it more difficult to use effectively in genome-wide screens. Additionally, these ectopic transcription factors increase the gene reactivation level beyond physiological conditions which is likely to bring unwanted side effects. Also, VP64 and Rta are derived from Herpes Simplex Viral Protein 16 and Epstein-Barr Virus Rta Protein respectively, which might lead to cell type-specific efficiency and toxicity issues [47].

TET protein-mediated DNA demethylation and histone modification enzyme-induced chromatin remodeling can also reactivate gene expression. These methods rely on increasing the chromatin accessibility of gene promoter/enhancer regions to recruit endogenous transcription factors thereby enhancing the transcription. These methods have the advantage over dCas9 fusion with activators such as VP64, p65, Rta or HSF1 since they maintain the reactivated gene expression within a physiological level [39,40]. However, dCas9-TET fusion-mediated gene reactivation techniques can only reactivate those genes which are silenced by promoter hypermethylation, and it is also important to know the critical CpG sites whose methylation controls the gene expression in order to design effective guide RNAs to reactivate gene expression [44]. Moreover, dCas9-derived histone modifiers usually need a pool of different guide RNAs in order to successfully restore gene expression [40].

TRANSCRIPTIONAL REPRESSION WITH dCAS9 DERIVATIVES

Besides transcriptional activation, effector domains which facilitate transcriptional repression can also be fused to dCas9 (Figure 2). Examples of these repressor domains are KRAB (kruppel-associated box) domain of Kox1 [36,48]. Also here, epigenetic modifiers can be used as well to perform sgRNA-guided dCas9-based transcriptional repression. These include the catalytic domain of DNA methyltransferases (DNMTs) such as DNMT3A and DNMT3L, which induce site-specific DNA promoter methylation which results in gene silencing and is heritable across mitotic division [48-50]. Methylation of a larger part of the promoter can be achieved via the design of multiple sgRNAs at adjacent sites [49]. In addition, combination of several repressor domains such as KRAB, DNMT3A and DNMT3L allows stable and stimulation-resistant gene silencing [48]. Besides inducing DNA promoter methylation, histone-modifying enzymes can also be used to induce dCas9-based transcriptional repression. The histone demethylases LSD1 and KDM1A can be fused to dCas9 to allow transcriptional silencing [51]. LSD1 demethylates H3K4me2 histone modifications that correlate with active enhancers, which results in loss of H3K4me2 as well as H3K27Ac (which is indicative of active enhancers) [51]. LSD1 can therefore be used to identify which enhancers are critical for the appropriate expression of genes in for example the stem cell state [51]. Also, the histone methyltransferase EZH2 can be fused to dCas9 to facilitate gene silencing [52]. Besides histone demethylases/methyltransferases, histone deacetylases can also be fused to dCas9 to induce transcriptional repression. An example of this is the histone deacetylase 3 (HDAC3) which, when fused to dCas9, can induce locus-specific histone deacetylation which results in gene silencing [53]. Here, the location of the sgRNA is critical for dCas9-HDAC3 activity: only sgRNAs located adjacent to H3K27ac marks promoted a dCas9-HDAC3-dependent effect on transcription [53]. This shows that both repressor domains such as KRAB as well as epigenetic-modifying enzymes such as DNMTs and histone demethylases and deacetylases can be fused to dCas9 to induce sgRNA-guided gene silencing of the desired locus. It is important to note that different combinations of histone demethylases/methyltransferases and DNA methyltransferases are required to achieve maximal repression at different loci (e.g. the requirement of histone methyltransferases can be locus specific) [54].

The advantage of dCas9-based gene repression modules (fused with KRAB, LSD1, KDM1A or HDAC) is that it can efficiently and specifically decrease gene expression by up to 99% [55]. As compared to the conventional RNA interference (RNAi) method, dCas9-based gene silencing methods are easy to modify and can be used in *ex-vivo* cell therapy as well [56]. These repression modules-mediated silencing of target gene expression are facilitated by histone modifications of the cell itself. This means that long-term suppression of gene expression results in additional DNA methylation marks which leads to enhanced robustness of gene suppression [48, 57].

Notably, dCas9-fused DNMTs also hold a great ability in gene silencing, however, this is only applicable for those genes which have CpG-rich regions in the promoter (half of all human genes contain a CpG-rich region). In addition, Galonska et al. have reported that dCas9-DNMT modules have global off-target effects by adding methylation footprints that are independent of sgRNA and delivery methods [58].

BASE EDITING WITH DCAS9 DERIVATIVES

The CRISPR/Cas9 system can also be repurposed to perform base editing in the DNA to correct mutations relevant to human disease (Figure 2). This enables the direct and irreversible conversion of a target base in the DNA into another one. Notably, Cas9-dependent base editing functions in a programmable manner (sgRNA-guided) and no longer requires double-stranded DNA cleavage or a donor template. The fusion of different effector domains to dCas9 enables base editing of different bases. These effector domains include single-strand specific deaminases that convert cytosine (C) into uracil (U), which pairs with adenine during replication resulting in a C-to-T conversion. The cytidine deaminase enzyme APOBEC1 enables C-to-T substitution [59-61] whereas the activation-induced cytidine deaminase (AID) enables C-to-T/G substitution [62,63]. An additional uracil glycosylase inhibitor (UGI) is added to the dCas9-cytidine deaminase fusion-protein to prevent excision of uracil (and thus uracil base excision repair) and thereby increases base editing efficiency and product purity. Nickase activity of the Cas9(D10A) protein manipulates cellular mismatch repair into replacing the G in the non-edited strand [63]. These components can also be delivered as an all-in-one ribonucleoprotein (RNP) complex to establish DNA-free

base editing [61]. Another possibility is to mutate cytidine deaminase domains to narrow the width of the base editing window from approximately 5 nucleotides to either 1 or 2 nucleotides [59]. This results in increased specificity since it excludes neighboring cytosines in the 5 nucleotide-window which would otherwise be base-edited as well. The addition of dCas9 to AID can be achieved via either direct fusion or by attaching a SH3 (Src 3 homology) domain to the C terminus of dCas9 and a SHL (SH3 interaction ligand) to the C terminus of AID [62]. Additional blockage of uracil N-glycosylase (UNG), which is also responsible for uracil cleavage and thus initiation of uracil base excision repair, was used to develop the fourth generation of base editors (BE4 [*S. pyogenes* Cas9-derived base editor] and SaBE4 [*Staphylococcus aureus* Cas9-derived BE4]) [63]. Also, fusion of these fourth generation of base editors to the bacteriophage Mu dsDNA end-binding protein Gam reduced the formation of undesired base editing-induced indels and increased the product purity [63]. Another effector domain that can be fused to dCas9 are the so-called adenine base editors (ABE) which facilitate A-to-G substitution in the DNA [64]. Here, dCas9 is fused to tRNA adenosine deaminase which performs efficient and high-purity base editing while generating a low rate of indels [64]. It is important to note that DNA base editing induces off-target RNA mutations which can be eliminated by engineering deaminases (e.g. cytosine base editors [CBE] or ABE variants) [65]. Altogether, this demonstrates the multiple applications of Cas9 derivatives including fluorescent imaging, transcriptional activation or repression, and base editing.

PRIME EDITING

Base editing ingeniously avoids DNA breaks and was thought to minimize inaccuracy [66]. However, this strategy only offers limited options as it can only make four out of the 12 possible base pair changes and some recent works have suggested it is not as precise as scientists first thought [67]. Recently, David R. Liu's group has discovered a new type of gene editing which is called prime editing. Prime editing steers around shortcomings of Cas9 and base editing by modifying both the Cas9 protein and the gRNA. Here, the nickase Cas9(H840A) cleaves only one strand of DNA, leaving the other intact. An engineered prime editing guide RNA (pegRNA) contains an RNA template for a new DNA sequence to be incorporated into the cleaved strand of DNA at the target location. In

addition, a reverse transcriptase enzyme which is fused to the Cas9 protein enables to synthesize a new DNA strand from the RNA template to be inserted at the cleaved site. Prime editing is considered a promising novel part of the CRISPR tool kit [66]. Nevertheless, its robustness needs to be established in different *in vitro* models as well as *in vivo*.

FUNCTIONS OF CAS13 DERIVATIVES

Where Cas9 derivatives can be used to induce transcriptional activation or repression at the DNA level, Cas13 derivatives can be used for RNA targeting. Similar to dCas9, dCas13 is able to bind to the target RNA but unable to cleave it. Also similar to dCas9, an EGFP-tagged dCas13 can be used to track transcripts in living cells [26]. Moreover, dCas13a can be also fused to a KRAB domain to repress transcription [26]. In addition, dCas13 proteins can also be repurposed for adenine (A)-to-inosine (I) base editing [28,68]. Inosine can base pair with cytidine and can therefore be corrected to guanine resulting in an A-to-G conversion. Base editing at the RNA level holds promise for treating genetic diseases, where disease-relevant sequences containing pathogenic mutations can be edited to yield functional proteins [28]. Both dCas13a and dCas13b can be fused to the deaminase domain of ADAR 2 (adenosine deaminase acting on RNA type 2) which enables direct A-to-I deaminase activity to transcripts in mammalian cells [28,68]. The ADAR2 deaminase domain can also be mutated (E488Q) to increase the A-to-I editing rates [28]. This system is called RNA Editing for Programmable A to I Replacement (REPAIR). This system has recently evolved into RNA Editing for Specific C-to-U Exchange (RESCUE), which is capable of both C-to-U and A-to-I editing [69,70]. Finally, Cas13-based derivatives are able to promote mRNA translation and mRNA decay [71]. Fusion of dCas13b to the two most well-characterized m⁶A (which is the most prevalent mRNA modification) reader proteins YTDHF1 and YTDHF2 results in enhanced translation and induction of mRNA degradation respectively [71]. Taken together, this demonstrates the versatile use of Cas derivatives to perform several cellular applications such as imaging, transcriptional modulation and base editing (Table 3).

Table 3. dCas derivatives: functions and purpose

Effector domains	Function	Purpose	Reference
dCas9			
GFP/BFP	Gene visualization	Tracking	[33]
SunTag (10xGCN4)	Adapter domain	Recruitment of other effector domains	[34]
APOBEC	C to T substitution	Base editing	[53,60]
AID	C to T/G substitution	Base editing	[62,63]
ABE	A to G substitution	Base editing	[64]
Rev. Transcriptase	Reverse transcription	Base editing	[66]
VP64	Transcriptional activation	Activation	[34,36,37]
P65AD	Transcriptional activation	Activation	[36]
VPR	Transcriptional activation	Activation	[38]
P300	Histone acetylation	Activation	[40]
TETs	DNA demethylation	Activation	[41-44]
PRDM9	Histone methylation	Activation	[46]
DOT1L	Histone methylation	Activation	[46]
SMYD3	Histone methylation	Activation	[45]
KRAB	Chromatin remodeling	Repression	[36,48,51]
LSD1/KDM1A	Histone demethylation	Repression	[51]
DNMTs	DNA methylation	Repression	[48-50]
EZH2	Histone methyltransferase	Repression	[52]
HDAC3	Histone deacetylation	Repression	[53]
dCas13			
GFP	RNA visualization	Tracking	[26]
ADAR	A-to-I substitution	Base editing (REPAIR)	[28,65,68,69,72]
YTHDF1	Promote mRNA translation	Activation	[71]
YTHDF2	Promote mRNA decay	Repression	[71]
KRAB	Transcriptional repression	Repression	[26]

Overview of the function and purpose of different dCas derivatives and their respective reference(s). The main purpose of dCas derivatives (both dCas9 and dCas13) include tracking, base editing, activation and repression. These purposes can be achieved via different functions such as DNA demethylation or chromatin remodeling (for dCas9 derivatives) but also to promote mRNA translation or decoy (for dCas13 derivatives).

IN VIVO APPLICATIONS OF DCAS9 DERIVATIVES

The CRISPR/Cas derivatives have distinct effects *in vitro*, such as transcriptional activation or repression, but only some of them have been demonstrated to function *in vivo*. The first description of dCas9-mediated transcriptional activation was *in vivo* in drosophila [73]. Here, dCas9-VPR enabled activation of endogenous genes in drosophila which induced dominant phenotypes [73,74]. dCas9-VPR was the most optimal for transcriptional activator in drosophila and outperformed dCas9-VP64 and dCas9-SAM (synergistic activation mediator) [73,74]. dCas9-SAM includes dCas9-VP64 in combination with two MS2 protein-fused additional activator domains, p65 and HSF1 (heat shock factor 1), which are recruited to the sgRNA tail [74]. dCas9-VPR-based transcriptional activation in drosophila holds great potential for overexpression studies where tissue-specific Gal4 driven dCas9-VPR can be crossed to flies expressing distinct sgRNAs, which is both cheap and scalable [73,74]. Transcriptional activation using dCas derivatives has also been shown in mice in several studies. Here, a neuron-optimized dual lentiviral dCas9-VPR system is used for robust and gene specific regulation in rats [75]. Also, light-sensitive gene transcriptional activation was performed using dCas9-SAM which is delivered into the muscles of mice via electroporation [76]. In a different study, dCas9-VP64 was used to perform transcriptional activation in a cancer mouse model [56]. Interestingly, it was suggested that targeting of dCas9-VP64 downstream of the transcriptional start site results in gene silencing instead of gene activation [56]. This might be due to dCas9-VP64 acting as a transcriptional roadblock by interfering with transcriptional initiation/elongation [65]. In another cancer mouse model, dCas9-SunTag (with recruiting VP64 domains) is used to induce transcriptional activation [77]. Altogether, CRISPR/dCas9 derivatives allow to study the impact of individual genes on disease phenotype such as cancer *in vivo*. CRISPR/dCas9 derivatives are also used to perform simultaneous transcriptional activation of multiple genes and long noncoding RNAs, which are more than 200 nucleotides long which belong to the non-coding RNA group of epigenetic modifiers, in the mouse brain [78]. This study combines two CRISPR/dCas9 derivatives into one: it uses dCas9-SunTag but replaces VP64 with p65-HSF1 (which were previously used in dCas9-SAM) now called dCas9-SunTag-p65-HSF1 (SPH) [78]. The targeted activation of three endogenous neurogenic transcription

factors resulted in the efficient conversion of astrocytes into functional neurons *in vivo* via AAV8 vectors [78]. Robust activation of multiple genes was also achieved in the liver using dCas9-SPH [78].

As described before, dCas9-based transcriptional activation can not only occur via fusion of dCas9 to transcriptional activators but also to epigenetic modifiers such as TETs which induce DNA demethylation and thus re-activation of gene expression. The dCas9-SunTag (with recruiting TET1CDs) is used to perform targeted demethylation and thus upregulation of genes in the brain of mouse fetuses via *in utero* electroporation [42]. dCas9-TET1 is also used in another study to facilitate demethylation *in vivo* in the brain and skin of mice via lentiviral vectors [79]. We have also demonstrated that dCas9-TET3CD induces gene-specific re-activation and demethylation which results in amelioration of kidney fibrosis *in vivo* via lentiviral vectors [44].

Besides transcriptional activation, CRISPR-dCas9-based transcriptional repression has also been reported in a few *in vivo* studies. In general, CRISPR-dCas9 derivatives are delivered *in vivo* via lentiviral vectors [44], electroporation [69] but mostly AAV vectors [77,78,81,82] because of its low toxicity and immunogenicity. However, AAV vectors are associated with delivery challenges since the large size of CRISPR-dCas9 derivatives exceeds the packaging limit of AAV. To circumvent the AAV packaging limitation, *in vivo* studies made use of Cre-dependent Cas9 activation (which also allows cell-type specific activation) [77,78], the so-called split-intein system [82] or a smaller Cas9 protein (SaCas9) [81]. The split-intein system enables fusion of two separate parts of CRISPR-dCas9 derivatives. Here, the N-terminal of a CRISPR/Cas9 derivative is fused to N-intein whereas the C-terminal is fused to C-intein. Upon transduction, the two intein proteins recognize and excise themselves, resulting in a complete and functional dCas9 protein. This system was used for the transcriptional activator dCas9-VP64-RTA as well as the transcriptional repressor dCas9-KRAB and allowed *in vivo* gene activation and repression, respectively [82]. Utilization of additional activator domains (VP64 or p65) improved gene activation whereas additional repressor domains (KRAB, DNMT3A or DNMT3L) did not [82]. This system was also applied in a mouse model of heritable eye disease (retinitis pigmentosa) where AAV vector-based delivery of dCas9-KRAB induced gene repression which prevented degradation of photoreceptors and improved visual function [82]. The transcriptional repressor dCas9-KRAB was packaged into lentiviral vectors and

infused into the mouse brain to perform multiplex gene silencing [83]. In another study, KRAB was fused to the smaller dSaCas9, which is compatible with AAV vector-based delivery, and induced gene silencing *in vivo* which was associated with reduced cholesterol levels [81]. The gene silencing was still observed after 24 weeks, which indicates the long-term potential of using CRISPR/Cas9 derivatives in adult mice [81].

The dCas9-KRAB, but also dCas9 fused to the epigenetic repressor LSD1 (lysine-specific demethylase 1) are electroporated in the chick embryo to inactivate enhancers [80]. dCas9-VP64 in combination with the SAM system (MS2 protein-fused additional VP-64 domains) was used as well in the chick embryo to activate gene expression [80]. dCas9 can also be fused to an engineered prokaryotic DNA methyltransferase MQ1 to achieve locus-specific methylation in mice via zygote microinjection [84]. This indicates its potential use in early development [73]. Interestingly, the increased methylation is still observed after birth indicating its heritability for at least 3 weeks [84].

Altogether, this shows the *in vivo* applications of different CRISPR/Cas derivatives (summarized in Table 4). Both transcriptional activation and repression are achieved in different species such as drosophila and mice, in both the embryonic and adult state, which can induce alterations in phenotype *in vivo*. This can be used to study gene function and the associated phenotype in disease settings *in vivo*, and aid unraveling novel pathology-contributing genes as well as potential novel therapies.

Table 4. dCas derivatives: *in vivo* applications

Module	Species	Delivery method	Feature	Ref
dCas9-VPR	Drosophila / Rat	Cross breeding transgenic lines / Lentiviral vectors	Gene activation Increased protein levels of a target gene in the brain	[73,74,75]
dCas9 with MS2- p65-HSF1	Mouse	Electroporation	Light-mediated gene activation in muscle	[76]
dCas9-VP64	Mouse	Tail-vein injection of transgenic B-ALL cells	Gene activation/repression in cancer	[56]

CRISPR/CAS DERIVATIVES AS NOVEL GENE MODULATING TOOLS

dCas9-VP64 / MS2-p65-HSF1	Mouse	AAV vectors	Multiplexed activation of endogenous genes	[54]
dCas9-SunTag (VP64)	Mouse	AAV vectors	Gene activation / growth and tumorigenesis assay	[77]
dCas9-10xGCN4 with p65-HSF1-SAM	Mouse	AAV8 vectors	Simultaneous transcriptional activation of multiple genes in the brain	[78]
dCas9-TET1CD	Mouse	In utero electroporation / lentiviral vectors	Demethylation in brain of mouse fetuses / demethylation of skin and brain	[42,79]
dCas9-TET3CD	Mouse	Lentiviral vectors	Gene re-activation and amelioration of kidney fibrosis	[44]
dCas9-KRAB	Mouse	AAV vectors / lentiviral vectors	Split-intein-mediated gene repression in retinitis pigmentosa / multiplex gene silencing in the brain	[82,83]
dSaCas9-KRAB	Mouse / Chicken	AAV8 vectors / Electroporation	Gene silencing and lowering of cholesterol / inactivation of enhancers in the embryo	[80,81]
dCas9-LSD1/VP64	Chicken	Electroporation	Inactivation of enhancers in the embryo	[80]
dCas9-MQ1	Mouse	Zygote microinjection	Methylation in zygote	[84]

Overview of the in vivo applications of dCas derivatives including species, delivery method, their unique features and the corresponding reference(s). In vivo applications are performed in drosophila and chicken, but mostly in mice. The common delivery methods are electroporation or AAV/lentivirus delivery. The features of in vivo applications of dCas derivatives involve both gene activation (via transcriptional activation or demethylation) and repression (via transcriptional repression or methylation).

EFFECTIVE GENE DELIVERY *IN VIVO*

Safety and effectiveness are the two major concerns for delivering dCas9 derivatives into the affected cells and thus influence treatment efficacy. Basically, three different formats can be used as delivery methods: gene expression plasmids, viral vectors, and ribonuclear complexes. The selection of the delivery system ideally should provide: (1) tissue-specificity, (2) target cell entry ability, and (3) without/low immunogenicity. Initially, as proof-of-concept many of the therapeutic applications of dCas9 derivatives were performed on animal models via electroporation of plasmid DNA [42,76]. Electroporation can be highly toxic since it can harm the cell membrane. In some cases, this leads to permanent permeabilization of the membrane [85]. Viral vector-based gene delivery systems have been widely used in gene therapy and even entered clinical trials in some cases [86]. The most widely used are lentiviral and AAV vectors, each one having its own advantages and disadvantages. For example, a lentiviral vector has a large packaging capacity up to 8.5 kB, long-lasting transgene expression and is capable of transducing non-dividing cells [87]. However, a lentiviral vector is oncogenic, immunogenic and is likely to make a transgene insertion into the host genome, which largely constrained its applications [87]. On the other hand, AAV vectors have a large variety of target tissues with low immunogenicity and non-oncogenicity [88]. AAV vectors have a very small genome size however, and therefore a low packaging capacity, which makes it unable to deliver a large transgene within a virus [88]. Instead of delivering DNA into the cells, the dCas9 derivatives can also be first transcribed into mRNA and delivered into cells via ribonucleoproteins. The transient nature of this approach favors controlling gene expression level and minimizes the window of immune activation [87]. Moreover, from a pharmaceutical point of view, ribonucleoproteins are much easier to scale up for clinical use and can be chemically functionalized with ligands to obtain target cell specificity [87].

CONCLUSION

The discovery of the CRISPR/Cas9 system has revolutionized the field of epigenetic and genetic editing in the pre-clinic. This is a fast-growing field where different Cas9 proteins have been discovered with each their distinct features (e.g. length and recognition sites). The discovery of endonuclease-deficient Cas9 has led to the development of different CRISPR/dCas9 derivatives which can be used to perform distinct functions such as tracking, transcriptional activation and repression, and base editing. Some of these dCas9-based derivatives have also been applied *in vivo* where they contribute to transcriptional activation or repression which can lead to changes in disease phenotype. This holds great promise for genetic screens to identify novel genes which are associated with a disease phenotype, and of course for potential therapies. Even though the discovery of high-fidelity Cas9 has significantly improved off-target effects, future research needs to be directed to improve methods to detect off-target effects (e.g. a recent study has demonstrated that engineering a hairpin secondary structure onto the spacer region of single guide RNAs [hp-sgRNAs] can increase the specificity by several orders of magnitude) [89]. In addition, recent advancements in the unbiased detection of CRISPR off-target effects (DISCOVER-Seq) in patient-derived induced pluripotent stem cells directs us towards *in situ* off-target discovery within individual patient genotypes during therapeutic genome modulation. [90]. Also, future research needs to be directed at optimizing delivery methods for clinical use of CRISPR/Cas (e.g. a recent study showed proof of concept of a self-deleting AAV-CRISPR system) [91]. Altogether, the CRISPR/Cas-based epigenetic and genetic editing is a fast-growing field with opportunities to develop novel applications altogether and increase the scale of already existing CRISPR/Cas-based applications.

REFERENCES

1. Chevalier, B. S.; Stoddard, B. L., Homing endonucleases: structural and functional insight into the catalysts of intron/intein mobility. *Nucleic Acids Res* 2001, 29, (18), 3757-74.
2. Seligman, L. M.; Chisholm, K. M.; Chevalier, B. S.; Chadsey, M. S.; Edwards, S. T.; Savage, J. H.; Veillet, A. L., Mutations altering the cleavage specificity of a homing endonuclease. *Nucleic Acids Res* 2002, 30, (17), 3870-9.
3. Choo, Y.; Sanchez-Garcia, I.; Klug, A., In vivo repression by a site-specific DNA-binding protein designed against an oncogenic sequence. *Nature* 1994, 372, (6507), 642-5.
4. Mandell, J. G.; Barbas, C. F., 3rd, Zinc Finger Tools: custom DNA-binding domains for transcription factors and nucleases. *Nucleic Acids Res* 2006, 34, (Web Server issue), W516-23.
5. Kim, Y. G.; Cha, J.; Chandrasegaran, S., Hybrid restriction enzymes: zinc finger fusions to Fok I cleavage domain. *Proc Natl Acad Sci U S A* 1996, 93, (3), 1156-60.
6. Bitinaite, J.; Wah, D. A.; Aggarwal, A. K.; Schildkraut, I., FokI dimerization is required for DNA cleavage. *Proc Natl Acad Sci U S A* 1998, 95, (18), 10570-5.
7. Boch, J.; Scholze, H.; Schornack, S.; Landgraf, A.; Hahn, S.; Kay, S.; Lahaye, T.; Nickstadt, A.; Bonas, U., Breaking the code of DNA binding specificity of TAL-type III effectors. *Science* 2009, 326, (5959), 1509-12.
8. Moscou, M. J.; Bogdanove, A. J., A simple cipher governs DNA recognition by TAL effectors. *Science* 2009, 326, (5959), 1501.
9. Boch, J.; Bonas, U., Xanthomonas AvrBs3 family-type III effectors: discovery and function. *Annu Rev Phytopathol* 2010, 48, 419-36.
10. Li, T.; Huang, S.; Jiang, W. Z.; Wright, D.; Spalding, M. H.; Weeks, D. P.; Yang, B., TAL nucleases (TALNs): hybrid proteins composed of TAL effectors and FokI DNA-cleavage domain. *Nucleic Acids Res* 2011, 39, (1), 359-72.
11. Jinek, M.; Chylinski, K.; Fonfara, I.; Hauer, M.; Doudna, J. A.; Charpentier, E., A programmable dual-RNA-guided DNA endonuclease in adaptive bacterial immunity. *Science* 2012, 337, (6096), 816-21.
12. Barrangou, R.; Fremaux, C.; Deveau, H.; Richards, M.; Boyaval, P.; Moineau, S.; Romero, D. A.; Horvath, P., CRISPR provides acquired resistance against viruses in prokaryotes. *Science* 2007, 315, (5819), 1709-12.
13. Marraffini, L. A.; Sontheimer, E. J., CRISPR interference limits horizontal gene transfer in staphylococci by targeting DNA. *Science* 2008, 322, (5909), 1843-5.
14. Kleinstiver, B. P.; Pattanayak, V.; Prew, M. S.; Tsai, S. Q.; Nguyen, N. T.; Zheng, Z.; Joung, J. K., High-fidelity CRISPR-Cas9 nucleases with no detectable genome-wide off-target effects. *Nature* 2016, 529, (7587), 490-5.
15. Kleinstiver, B. P.; Prew, M. S.; Tsai, S. Q.; Topkar, V. V.; Nguyen, N. T.; Zheng, Z.; Gonzales, A. P.; Li, Z.; Peterson, R. T.; Yeh, J. R.; Aryee, M. J.; Joung, J. K., Engineered CRISPR-Cas9 nucleases with altered PAM specificities. *Nature* 2015, 523, (7561), 481-5.

16. Esvelt, K. M.; Mali, P.; Braff, J. L.; Moosburner, M.; Yaung, S. J.; Church, G. M., Orthogonal Cas9 proteins for RNA-guided gene regulation and editing. *Nat Methods* 2013, 10, (11), 1116-21.
17. Hou, Z.; Zhang, Y.; Propson, N. E.; Howden, S. E.; Chu, L. F.; Sontheimer, E. J.; Thomson, J. A., Efficient genome engineering in human pluripotent stem cells using Cas9 from *Neisseria meningitidis*. *Proc Natl Acad Sci U S A* 2013, 110, (39), 15644-9.
18. Karvelis, T.; Gasiunas, G.; Young, J.; Bigelyte, G.; Silanskas, A.; Cigan, M.; Siksnys, V., Rapid characterization of CRISPR-Cas9 protospacer adjacent motif sequence elements. *Genome Biol* 2015, 16, 253.
19. Ran, F. A.; Cong, L.; Yan, W. X.; Scott, D. A.; Gootenberg, J. S.; Kriz, A. J.; Zetsche, B.; Shalem, O.; Wu, X.; Makarova, K. S.; Koonin, E. V.; Sharp, P. A.; Zhang, F., In vivo genome editing using *Staphylococcus aureus* Cas9. *Nature* 2015, 520, (7546), 186-91.
20. Kleinstiver, B. P.; Prew, M. S.; Tsai, S. Q.; Nguyen, N. T.; Topkar, V. V.; Zheng, Z.; Joung, J. K., Broadening the targeting range of *Staphylococcus aureus* CRISPR-Cas9 by modifying PAM recognition. *Nat Biotechnol* 2015, 33, (12), 1293-1298.
21. Hirano, H.; Gootenberg, J. S.; Horii, T.; Abudayyeh, O. O.; Kimura, M.; Hsu, P. D.; Nakane, T.; Ishitani, R.; Hatada, I.; Zhang, F.; Nishimasu, H.; Nureki, O., Structure and Engineering of *Francisella novicida* Cas9. *Cell* 2016, 164, (5), 950-61.
22. Zetsche, B.; Gootenberg, J. S.; Abudayyeh, O. O.; Slaymaker, I. M.; Makarova, K. S.; Essletzbichler, P.; Volz, S. E.; Joung, J.; van der Oost, J.; Regev, A.; Koonin, E. V.; Zhang, F., Cpf1 is a single RNA-guided endonuclease of a class 2 CRISPR-Cas system. *Cell* 2015, 163, (3), 759-71.
23. Strecker, J.; Jones, S.; Koopal, B.; Schmid-Burgk, J.; Zetsche, B.; Gao, L.; Makarova, K. S.; Koonin, E. V.; Zhang, F., Engineering of CRISPR-Cas12b for human genome editing. *Nat Commun* 2019, 10, (1), 212.
24. Yan, W. X.; Hunnewell, P.; Alfonse, L. E.; Carte, J. M.; Keston-Smith, E.; Sothiselvam, S.; Garrity, A. J.; Chong, S.; Makarova, K. S.; Koonin, E. V.; Cheng, D. R.; Scott, D. A., Functionally diverse type V CRISPR-Cas systems. *Science* 2019, 363, (6422), 88-91.
25. Liu, J. J.; Orlova, N.; Oakes, B. L.; Ma, E.; Spinner, H. B.; Baney, K. L. M.; Chuck, J.; Tan, D.; Knott, G. J.; Harrington, L. B.; Al-Shayeb, B.; Wagner, A.; Brotzmann, J.; Staahl, B. T.; Taylor, K. L.; Desmarais, J.; Nogales, E.; Doudna, J. A., CasX enzymes comprise a distinct family of RNA-guided genome editors. *Nature* 2019, 566, (7743), 218-223.
26. Abudayyeh, O. O.; Gootenberg, J. S.; Essletzbichler, P.; Han, S.; Joung, J.; Belanto, J. J.; Verdine, V.; Cox, D. B. T.; Kellner, M. J.; Regev, A.; Lander, E. S.; Voytas, D. F.; Ting, A. Y.; Zhang, F., RNA targeting with CRISPR-Cas13. *Nature* 2017, 550, (7675), 280-284.
27. Abudayyeh, O. O.; Gootenberg, J. S.; Konermann, S.; Joung, J.; Slaymaker, I. M.; Cox, D. B.; Shmakov, S.; Makarova, K. S.; Semenova, E.; Minakhin, L.; Severinov, K.; Regev, A.; Lander, E. S.; Koonin, E. V.; Zhang, F., C2c2 is a single-component programmable RNA-guided RNA-targeting CRISPR effector. *Science* 2016, 353, (6299), aaf5573.
28. Cox, D. B. T.; Gootenberg, J. S.; Abudayyeh, O. O.; Franklin, B.; Kellner, M. J.; Joung, J.; Zhang, F., RNA editing with CRISPR-Cas13. *Science* 2017, 358, (6366), 1019-1027.

29. Konermann, S.; Lotfy, P.; Brideau, N. J.; Oki, J.; Shokhirev, M. N.; Hsu, P. D., Transcriptome Engineering with RNA-Targeting Type VI-D CRISPR Effectors. *Cell* 2018, 173, (3), 665-676 e14.
30. Gootenberg, J. S.; Abudayyeh, O. O.; Kellner, M. J.; Joung, J.; Collins, J. J.; Zhang, F., Multiplexed and portable nucleic acid detection platform with Cas13, Cas12a, and Csm6. *Science* 2018, 360, (6387), 439-444.
31. Gootenberg, J. S.; Abudayyeh, O. O.; Lee, J. W.; Essletzbichler, P.; Dy, A. J.; Joung, J.; Verdine, V.; Donghia, N.; Daringer, N. M.; Freije, C. A.; Myhrvold, C.; Bhattacharyya, R. P.; Livny, J.; Regev, A.; Koonin, E. V.; Hung, D. T.; Sabeti, P. C.; Collins, J. J.; Zhang, F., Nucleic acid detection with CRISPR-Cas13a/C2c2. *Science* 2017, 356, (6336), 438-442.
32. Harrington, L. B.; Burstein, D.; Chen, J. S.; Paez-Espino, D.; Ma, E.; Witte, I. P.; Cofsky, J. C.; Kypides, N. C.; Banfield, J. F.; Doudna, J. A., Programmed DNA destruction by miniature CRISPR-Cas14 enzymes. *Science* 2018, 362, (6416), 839-842.
33. Chen, B.; Gilbert, L. A.; Cimini, B. A.; Schnitzbauer, J.; Zhang, W.; Li, G. W.; Park, J.; Blackburn, E. H.; Weissman, J. S.; Qi, L. S.; Huang, B., Dynamic imaging of genomic loci in living human cells by an optimized CRISPR/Cas system. *Cell* 2013, 155, (7), 1479-91.
34. Tanenbaum, M. E.; Gilbert, L. A.; Qi, L. S.; Weissman, J. S.; Vale, R. D., A protein-tagging system for signal amplification in gene expression and fluorescence imaging. *Cell* 2014, 159, (3), 635-46.
35. Pan, Q.; Shai, O.; Lee, L. J.; Frey, B. J.; Blencowe, B. J., Deep surveying of alternative splicing complexity in the human transcriptome by high-throughput sequencing. *Nat Genet* 2008, 40, (12), 1413-5.
36. Gilbert, L. A.; Larson, M. H.; Morsut, L.; Liu, Z.; Brar, G. A.; Torres, S. E.; Stern-Ginossar, N.; Brandman, O.; Whitehead, E. H.; Doudna, J. A.; Lim, W. A.; Weissman, J. S.; Qi, L. S., CRISPR-mediated modular RNA-guided regulation of transcription in eukaryotes. *Cell* 2013, 154, (2), 442-51.
37. Perez-Pinera, P.; Kocak, D. D.; Vockley, C. M.; Adler, A. F.; Kabadi, A. M.; Polstein, L. R.; Thakore, P. I.; Glass, K. A.; Ousterout, D. G.; Leong, K. W.; Guilak, F.; Crawford, G. E.; Reddy, T. E.; Gersbach, C. A., RNA-guided gene activation by CRISPR-Cas9-based transcription factors. *Nat Methods* 2013, 10, (10), 973-6.
38. Chavez, A.; Scheiman, J.; Vora, S.; Pruitt, B. W.; Tuttle, M.; E, P. R. I.; Lin, S.; Kiani, S.; Guzman, C. D.; Wiegand, D. J.; Ter-Ovanesyan, D.; Braff, J. L.; Davidsohn, N.; Housden, B. E.; Perrimon, N.; Weiss, R.; Aach, J.; Collins, J. J.; Church, G. M., Highly efficient Cas9-mediated transcriptional programming. *Nat Methods* 2015, 12, (4), 326-8.
39. Parsi, K. M.; Hennessy, E.; Kearns, N.; Maehr, R., Using an Inducible CRISPR-dCas9-KRAB Effector System to Dissect Transcriptional Regulation in Human Embryonic Stem Cells. *Methods Mol Biol* 2017, 1507, 221-233.
40. Hilton, I. B.; D'Ippolito, A. M.; Vockley, C. M.; Thakore, P. I.; Crawford, G. E.; Reddy, T. E.; Gersbach, C. A., Epigenome editing by a CRISPR-Cas9-based acetyltransferase activates genes from promoters and enhancers. *Nat Biotechnol* 2015, 33, (5), 510-7.
41. Xu, X.; Tao, Y.; Gao, X.; Zhang, L.; Li, X.; Zou, W.; Ruan, K.; Wang, F.; Xu, G. L.; Hu, R., A CRISPR-based approach for targeted DNA demethylation. *Cell Discov* 2016, 2, 16009.

42. Morita, S.; Noguchi, H.; Horii, T.; Nakabayashi, K.; Kimura, M.; Okamura, K.; Sakai, A.; Nakashima, H.; Hata, K.; Nakashima, K.; Hatada, I., Targeted DNA demethylation in vivo using dCas9-peptide repeat and scFv-TET1 catalytic domain fusions. *Nat Biotechnol* 2016, 34, (10), 1060-1065.
43. Choudhury, S. R.; Cui, Y.; Lubecka, K.; Stefanska, B.; Irudayaraj, J., CRISPR-dCas9 mediated TET1 targeting for selective DNA demethylation at BRCA1 promoter. *Oncotarget* 2016, 7, (29), 46545-46556.
44. Xu, X.; Tan, X.; Tampe, B.; Wilhelmi, T.; Hulshoff, M. S.; Saito, S.; Moser, T.; Kalluri, R.; Hasenfuss, G.; Zeisberg, E. M.; Zeisberg, M., High-fidelity CRISPR/Cas9- based gene-specific hydroxymethylation rescues gene expression and attenuates renal fibrosis. *Nat Commun* 2018, 9, (1), 3509.
45. Kim, J. M.; Kim, K.; Schmidt, T.; Punj, V.; Tucker, H.; Rice, J. C.; Ulmer, T. S.; An, W., Cooperation between SMYD3 and PC4 drives a distinct transcriptional program in cancer cells. *Nucleic Acids Res* 2015, 43, (18), 8868-83.
46. Cano-Rodriguez, D.; Gjaltema, R. A.; Jilderda, L. J.; Jellema, P.; Dokter-Fokkens, J.; Ruiters, M. H.; Rots, M. G., Writing of H3K4Me3 overcomes epigenetic silencing in a sustained but context-dependent manner. *Nat Commun* 2016, 7, 12284.
47. La Russa, M. F.; Qi, L. S., The New State of the Art: Cas9 for Gene Activation and Repression. *Mol Cell Biol* 2015, 35, (22), 3800-9.
48. Amabile, A.; Migliara, A.; Capasso, P.; Biffi, M.; Cittaro, D.; Naldini, L.; Lombardo, A., Inheritable Silencing of Endogenous Genes by Hit-and-Run Targeted Epigenetic Editing. *Cell* 2016, 167, (1), 219-232 e14.
49. Vojta, A.; Dobrinic, P.; Tadic, V.; Bockor, L.; Korac, P.; Julg, B.; Klasic, M.; Zoldos, V., Repurposing the CRISPR-Cas9 system for targeted DNA methylation. *Nucleic Acids Res* 2016, 44, (12), 5615-28.
50. McDonald, J. I.; Celik, H.; Rois, L. E.; Fishberger, G.; Fowler, T.; Rees, R.; Kramer, A.; Martens, A.; Edwards, J. R.; Challen, G. A., Reprogrammable CRISPR/Cas9-based system for inducing site-specific DNA methylation. *Biol Open* 2016, 5, (6), 866-74.
51. Kearns, N. A.; Pham, H.; Tabak, B.; Genga, R. M.; Silverstein, N. J.; Garber, M.; Maehr, R., Functional annotation of native enhancers with a Cas9-histone demethylase fusion. *Nat Methods* 2015, 12, (5), 401-403.
52. O'Geen, H.; Bates, S. L.; Carter, S. S.; Nisson, K. A.; Halmaj, J.; Fink, K. D.; Rhie, S. K.; Farnham, P. J.; Segal, D. J., Ezh2-dCas9 and KRAB-dCas9 enable engineering of epigenetic memory in a context-dependent manner. *Epigenetics Chromatin* 2019, 12, (1), 26.
53. Kwon, D. Y.; Zhao, Y. T.; Lamonica, J. M.; Zhou, Z., Locus-specific histone deacetylation using a synthetic CRISPR-Cas9-based HDAC. *Nat Commun* 2017, 8, 15315.
54. Wang, G.; Chow, R. D.; Bai, Z.; Zhu, L.; Errami, Y.; Dai, X.; Dong, M. B.; Ye, L.; Zhang, X.; Renauer, P. A.; Park, J. J.; Shen, L.; Ye, H.; Fuchs, C. S.; Chen, S., Multiplexed activation of endogenous genes by CRISPRa elicits potent antitumor immunity. *Nat Immunol* 2019, 20, (11), 1494-1505.
55. Qi, L. S.; Larson, M. H.; Gilbert, L. A.; Doudna, J. A.; Weissman, J. S.; Arkin, A. P.; Lim, W. A., Repurposing CRISPR as an RNA-guided platform for sequence-specific control of gene expression. *Cell* 2013, 152, (5), 1173-83.

56. Braun, C. J.; Bruno, P. M.; Horlbeck, M. A.; Gilbert, L. A.; Weissman, J. S.; Hemann, M. T., Versatile in vivo regulation of tumor phenotypes by dCas9-mediated transcriptional perturbation. *Proc Natl Acad Sci U S A* 2016, 113, (27), E3892-900.
57. Stepper, P.; Kungulovski, G.; Jurkowska, R. Z.; Chandra, T.; Krueger, F.; Reinhardt, R.; Reik, W.; Jeltsch, A.; Jurkowski, T. P., Efficient targeted DNA methylation with chimeric dCas9-Dnmt3a-Dnmt3L methyltransferase. *Nucleic Acids Res* 2017, 45, (4), 1703-1713.
58. Galonska, C.; Charlton, J.; Mattei, A. L.; Donaghey, J.; Clement, K.; Gu, H.; Mohammad, A. W.; Stamenova, E. K.; Cacchiarelli, D.; Klages, S.; Timmermann, B.; Cantz, T.; Scholer, H. R.; Gnirke, A.; Ziller, M. J.; Meissner, A., Genome-wide tracking of dCas9-methyltransferase footprints. *Nat Commun* 2018, 9, (1), 597.
59. Kim, Y. B.; Komor, A. C.; Levy, J. M.; Packer, M. S.; Zhao, K. T.; Liu, D. R., Increasing the genome-targeting scope and precision of base editing with engineered Cas9-cytidine deaminase fusions. *Nat Biotechnol* 2017, 35, (4), 371-376.
60. Komor, A. C.; Kim, Y. B.; Packer, M. S.; Zuris, J. A.; Liu, D. R., Programmable editing of a target base in genomic DNA without double-stranded DNA cleavage. *Nature* 2016, 533, (7603), 420-4.
61. Rees, H. A.; Komor, A. C.; Yeh, W. H.; Caetano-Lopes, J.; Warman, M.; Edge, A. S. B.; Liu, D. R., Improving the DNA specificity and applicability of base editing through protein engineering and protein delivery. *Nat Commun* 2017, 8, 15790.
62. Nishida, K.; Arazoe, T.; Yachie, N.; Banno, S.; Kakimoto, M.; Tabata, M.; Mochizuki, M.; Miyabe, A.; Araki, M.; Hara, K. Y.; Shimatani, Z.; Kondo, A., Targeted nucleotide editing using hybrid prokaryotic and vertebrate adaptive immune systems. *Science* 2016, 353, (6305).
63. Komor, A. C.; Zhao, K. T.; Packer, M. S.; Gaudelli, N. M.; Waterbury, A. L.; Koblan, L. W.; Kim, Y. B.; Badran, A. H.; Liu, D. R., Improved base excision repair inhibition and bacteriophage Mu Gam protein yields C:G-to-T:A base editors with higher efficiency and product purity. *Sci Adv* 2017, 3, (8), eaao4774.
64. Gaudelli, N. M.; Komor, A. C.; Rees, H. A.; Packer, M. S.; Badran, A. H.; Bryson, D. I.; Liu, D. R., Programmable base editing of A*T to G*C in genomic DNA without DNA cleavage. *Nature* 2017, 551, (7681), 464-471.
65. Zhou, C. Y.; Sun, Y. D.; Yan, R.; Liu, Y. J.; Zuo, E. W.; Gu, C.; Han, L. X.; Wei, Y.; Hu, X. D.; Zeng, R.; Li, Y. X.; Zhou, H. B.; Guo, F.; Yang, H., Off-target RNA mutation induced by DNA base editing and its elimination by mutagenesis. *Nature* 2019, 571, (7764), 275-+.
66. Anzalone, A. V.; Randolph, P. B.; Davis, J. R.; Sousa, A. A.; Koblan, L. W.; Levy, J. M.; Chen, P. J.; Wilson, C.; Newby, G. A.; Raguram, A.; Liu, D. R., Search-and-replace genome editing without double-strand breaks or donor DNA. *Nature* 2019, 576, (7785), 149-157.
67. Grunewald, J.; Zhou, R.; Garcia, S. P.; Iyer, S.; Lareau, C. A.; Aryee, M. J.; Joung, J. K., Transcriptome-wide off-target RNA editing induced by CRISPR-guided DNA base editors. *Nature* 2019, 569, (7756), 433-437.
68. Jing, X.; Xie, B.; Chen, L.; Zhang, N.; Jiang, Y.; Qin, H.; Wang, H.; Hao, P.; Yang, S.; Li, X., Implementation of the CRISPR-Cas13a system in fission yeast and its repurposing for precise RNA editing. *Nucleic Acids Res* 2018, 46, (15), e90.

69. Grunewald, J.; Zhou, R.; Iyer, S.; Lareau, C. A.; Garcia, S. P.; Aryee, M. J.; Joung, J. K., CRISPR DNA base editors with reduced RNA off-target and self-editing activities. *Nat Biotechnol* 2019, 37, (9), 1041-1048.
70. Lee, C.; Hyun Jo, D.; Hwang, G. H.; Yu, J.; Kim, J. H.; Park, S. E.; Kim, J. S.; Kim, J. H.; Bae, S., CRISPR-Pass: Gene Rescue of Nonsense Mutations Using Adenine Base Editors. *Mol Ther* 2019, 27, (8), 1364-1371.
71. Rauch, S.; He, C.; Dickinson, B. C., Targeted m(6)A Reader Proteins To Study Epitranscriptomic Regulation of Single RNAs. *J Am Chem Soc* 2018, 140, (38), 11974-11981.
72. Abudayyeh, O. O.; Gootenberg, J. S.; Franklin, B.; Koob, J.; Kellner, M. J.; Ladha, A.; Joung, J.; Kirchgatterer, P.; Cox, D. B. T.; Zhang, F., A cytosine deaminase for programmable single-base RNA editing. *Science* 2019, 365, (6451), 382-386.
73. Lin, S.; Ewen-Campen, B.; Ni, X.; Housden, B. E.; Perrimon, N., In Vivo Transcriptional Activation Using CRISPR/Cas9 in *Drosophila*. *Genetics* 2015, 201, (2), 433-42.
74. Ewen-Campen, B.; Yang-Zhou, D.; Fernandes, V. R.; Gonzalez, D. P.; Liu, L. P.; Tao, R.; Ren, X.; Sun, J.; Hu, Y.; Zirin, J.; Mohr, S. E.; Ni, J. Q.; Perrimon, N., Optimized strategy for in vivo Cas9-activation in *Drosophila*. *Proc Natl Acad Sci U S A* 2017, 114, (35), 9409-9414.
75. Savell, K. E.; Bach, S. V.; Zipperly, M. E.; Revanna, J. S.; Goska, N. A.; Tuscher, J. J.; Duke, C. G.; Sultan, F. A.; Burke, J. N.; Williams, D.; Ianov, L.; Day, J. J., A Neuron-Optimized CRISPR/dCas9 Activation System for Robust and Specific Gene Regulation. *eNeuro* 2019, 6, (1).
76. Shao, J.; Wang, M.; Yu, G.; Zhu, S.; Yu, Y.; Heng, B. C.; Wu, J.; Ye, H., Synthetic far-red light-mediated CRISPR-dCas9 device for inducing functional neuronal differentiation. *Proc Natl Acad Sci U S A* 2018, 115, (29), E6722-E6730.
77. Wangenstein, K. J.; Wang, Y. J.; Dou, Z.; Wang, A. W.; Mosleh-Shirazi, E.; Horlbeck, M. A.; Gilbert, L. A.; Weissman, J. S.; Berger, S. L.; Kaestner, K. H., Combinatorial genetics in liver repopulation and carcinogenesis with a in vivo CRISPR activation platform. *Hepatology* 2018, 68, (2), 663-676.
78. Zhou, H.; Liu, J.; Zhou, C.; Gao, N.; Rao, Z.; Li, H.; Hu, X.; Li, C.; Yao, X.; Shen, X.; Sun, Y.; Wei, Y.; Liu, F.; Ying, W.; Zhang, J.; Tang, C.; Zhang, X.; Xu, H.; Shi, L.; Cheng, L.; Huang, P.; Yang, H., In vivo simultaneous transcriptional activation of multiple genes in the brain using CRISPR-dCas9-activator transgenic mice. *Nat Neurosci* 2018, 21, (3), 440-446.
79. Liu, X. S.; Wu, H.; Ji, X.; Stelzer, Y.; Wu, X.; Czauderna, S.; Shu, J.; Dadon, D.; Young, R. A.; Jaenisch, R., Editing DNA Methylation in the Mammalian Genome. *Cell* 2016, 167, (1), 233-247 e17.
80. Williams, R. M.; Senanayake, U.; Artibani, M.; Taylor, G.; Wells, D.; Ahmed, A. A.; Sauka-Spengler, T., Genome and epigenome engineering CRISPR toolkit for in vivo modulation of cis-regulatory interactions and gene expression in the chicken embryo. *Development* 2018, 145, (4).
81. Thakore, P. I.; Kwon, J. B.; Nelson, C. E.; Rouse, D. C.; Gemberling, M. P.; Oliver, M. L.; Gersbach, C. A., RNA-guided transcriptional silencing in vivo with *S. aureus* CRISPR-Cas9 repressors. *Nat Commun* 2018, 9, (1), 1674.

82. Moreno, A. M.; Fu, X.; Zhu, J.; Katrekar, D.; Shih, Y. V.; Marlett, J.; Cabotaje, J.; Tat, J.; Naughton, J.; Lisowski, L.; Varghese, S.; Zhang, K.; Mali, P., In Situ Gene Therapy via AAV-CRISPR-Cas9-Mediated Targeted Gene Regulation. *Mol Ther* 2018, 26, (7), 1818-1827.
83. Zheng, Y.; Shen, W.; Zhang, J.; Yang, B.; Liu, Y. N.; Qi, H.; Yu, X.; Lu, S. Y.; Chen, Y.; Xu, Y. Z.; Li, Y.; Gage, F. H.; Mi, S.; Yao, J., CRISPR interference-based specific and efficient gene inactivation in the brain. *Nat Neurosci* 2018, 21, (3), 447-454.
84. Lei, Y.; Zhang, X.; Su, J.; Jeong, M.; Gundry, M. C.; Huang, Y. H.; Zhou, Y.; Li, W.; Goodell, M. A., Targeted DNA methylation in vivo using an engineered dCas9-MQ1 fusion protein. *Nat Commun* 2017, 8, 16026.
85. Hui, S. W., Overview of drug delivery and alternative methods to electroporation. *Methods Mol Biol* 2008, 423, 91-107.
86. Lundstrom, K., Viral Vectors in Gene Therapy. *Diseases* 2018, 6, (2).
87. Wilbie, D.; Walther, J.; Mastrobattista, E., Delivery Aspects of CRISPR/Cas for in Vivo Genome Editing. *Acc Chem Res* 2019, 52, (6), 1555-1564.
88. Zetsche, B.; Volz, S. E.; Zhang, F., A split-Cas9 architecture for inducible genome editing and transcription modulation. *Nat Biotechnol* 2015, 33, (2), 139-42.
89. Kocak, D. D.; Josephs, E. A.; Bhandarkar, V.; Adkar, S. S.; Kwon, J. B.; Gersbach, C. A., Increasing the specificity of CRISPR systems with engineered RNA secondary structures. *Nat Biotechnol* 2019, 37, (6), 657-666.
90. Wienert, B.; Wyman, S. K.; Richardson, C. D.; Yeh, C. D.; Akcakaya, P.; Porritt, M. J.; Morlock, M.; Vu, J. T.; Kazane, K. R.; Watry, H. L.; Judge, L. M.; Conklin, B. R.; Maresca, M.; Corn, J. E., Unbiased detection of CRISPR off-targets in vivo using DISCOVER-Seq. *Science* 2019, 364, (6437), 286-289.
91. Li, A.; Lee, C. M.; Hurley, A. E.; Jarrett, K. E.; De Giorgi, M.; Lu, W.; Balderrama, K. S.; Doerfler, A. M.; Deshmukh, H.; Ray, A.; Bao, G.; Lagor, W. R., A Self-Deleting AAV-CRISPR System for In Vivo Genome Editing. *Mol Ther Methods Clin Dev* 2019, 12, 111-122.

HIGH-FIDELITY CRISPR/CAS9-BASED GENE-SPECIFIC HYDROXYMETHYLATION RESCUES GENE EXPRESSION AND ATTENUATES RENAL FIBROSIS

Xingbo Xu^{1,2,*}, Xiaoying Tan^{2,3,*}, Björn Tampe³, Tim Wilhelmi^{1,2}, Melanie S. Hulshoff^{1,2,4}, Shoji Saito³, Tobias Moser⁵, Raghu Kalluri⁶, Gerd Hasenfuss^{1,2}, Elisabeth M. Zeisberg^{1,2,†} and Michael Zeisberg^{2,3,†}

¹*Department of Cardiology and Pneumology, University Medical Center Göttingen, Robert-Koch-Str. 40, 37075, Göttingen, Germany.*

²*German Centre for Cardiovascular Research (DZHK), Partner Site Göttingen, Germany.*

³*Department of Nephrology and Rheumatology, University Medical Center of Göttingen, Robert-Koch-Str. 40, 37075, Göttingen, Germany.*

⁴*Department of Pathology and Medical Biology, University Medical Center Groningen, Hanzeplein 1, 9713 GZ, Groningen, The Netherlands.*

⁵*Institute for Auditory Neuroscience & Inner Ear Lab, University Medical Center Göttingen, Robert-Koch-Str. 40, 37075, Göttingen, Germany.*

⁶*Department of Cancer Biology, Metastasis Research Center, University of Texas, MD Anderson Cancer Center, 1881 East Road, Houston, TX, 77054-1901, USA.*

**Authors contributed equally*

†share last authorship

ABSTRACT

While suppression of specific genes through aberrant promoter methylation contributes to different diseases including organ fibrosis, gene-specific reactivation technology is not yet available for therapy. TET enzymes catalyze hydroxymethylation of methylated DNA, reactivating gene expression. We here report generation of a high-fidelity CRISPR/Cas9-based gene-specific dioxygenase by fusing an endonuclease deactivated high-fidelity Cas9 (dHFCas9) to TET3 catalytic domain (TET3CD), targeted to specific genes by guiding RNAs (sgRNA). We demonstrate use of this technology in four different anti-fibrotic genes in different cell types in vitro, among them RASAL1 and Klotho, both hypermethylated in kidney fibrosis. Furthermore, in vivo lentiviral delivery of the Rasal1-targeted fusion protein to interstitial cells and of the Klotho-targeted fusion protein to tubular epithelial cells each results in specific gene reactivation and attenuation of fibrosis, providing gene-specific demethylating technology in a disease model.

INTRODUCTION

Aberrant CpG island promoter methylation of select genes leads to silencing of these genes and thus contributes to various pathologies such as cancer, neuronal degeneration, and organ fibrosis [1–3]. Well-studied examples of such genes are *RASAL1* (which encodes for a Ras-GAP-like Ras-GTP inhibitor, and hypermethylation of the *RASAL1* promoter leads to silencing of *RASAL1* expression and increased RAS-GTP activity) [4–6] and *KL1* (which encodes for Klotho, a transmembrane protein working as a co-receptor for fibroblast growth factor-23), both of which have been associated with cancer and also fibrogenesis [7–11]. The *RASAL1* promoter is consistently hypermethylated in tissue fibrosis including kidney, heart, and liver and also in gastrointestinal cancers [4–6,9,13]. The extent of *RASAL1* promoter methylation correlates with progression of kidney fibrosis in patients and mice [14], and rescue of *RASAL1* transcription through transgenic overexpression attenuates progression of experimental fibrosis in the kidney [14]. This suggests that reversal of aberrant *RASAL1* methylation and rescue of *RASAL1* expression are new therapeutic targets to inhibit progression of kidney fibrosis. *RASAL1* was originally identified as one of three genes (including also *EYA1* encoding for a member of the eyes absent (*EYA*) family of proteins, which plays a key role in the kidney development [15,16] and *LRFN2*, encoding for leucine-rich repeat and fibronectin type III domain-containing protein, which functions in presynaptic differentiation [17]) in a genome-wide methylation screen comparing normal and fibrotic kidney fibroblasts, which were consistently downregulated and hypermethylated in fibrotic but not healthy fibroblasts both in humans and mouse [4].

Hypermethylation of the *KLOTHO* promoter has been shown to be associated with progression of various forms of cancer and to correlate with kidney fibrosis in both humans and experimental fibrosis mouse models [18–22]. In the kidney, Klotho is predominantly expressed in tubular epithelial cells. Reversal of hypermethylated Klotho promoter associated Klotho suppression by a lipophilic anthraquinone compound, Rhein, has been demonstrated to ameliorate renal fibrosis in unilateral ureter obstruction (UUO)-induced fibrotic kidney mouse model. This results through effectively reducing aberrant DNMT1/3a expression and thereby maintaining secreted and membrane Klotho levels [22].

It has long been known that DNA methylation can be inhibited through administration of nucleotide analogs such as 5'azacytidine, which is incorporated into the DNA thereby causing DNA damage and subsequent DNA repair by replacement with unmethylated DNA. While nucleotide analogs are in clinical use in several malignant diseases such as myelodysplastic syndrome as demethylating therapies, they are highly unspecific and their utility is limited to second line therapies due to side effects, highlighting the need for gene-specific, less toxic demethylating therapies.

In this regard, members of the ten-eleven translocation (TET) family of zinc finger proteins (ZFPs) catalyze oxidation of methylated cytosine residues (so-called hydroxymethylation), which subsequently leads to replacement of methylated cytosine residues with naked cytosine [23]. Both hydroxymethylated and demethylated promoters result in re-expression of genes that had been silenced through CpG promoter methylation. We previously demonstrated that (1) TET3 is the predominant TET protein in the kidney [5], (2) kidney fibrosis is associated with decreased TET3 expression [5], and (3) induction of endogenous TET3 expression leads to hydroxymethylation, demethylation, and thereby reactivation of various genes, including *RASAL1*, within diseased kidneys and attenuates experimental kidney fibrosis [5,14]. TET3 only induces transcription of genes that had been previously methylated, and it is recruited to select genes (including *RASAL1*) through recognition of a common CXXC motif in proximity to gene promoter CpG islands, providing enhanced specificity as compared to nucleotide analogs. As opposed to silencing of DNMTs, activation of TET enzymes is an active way of reducing aberrant gene methylation. However, there are more than 9000 genes targeted by TET proteins within the human genome, suggesting gene-specific delivery of TET as an attractive approach to rescue expression of aberrantly methylated genes [24].

Previous studies demonstrated that by fusion of the TET methylcytosine dioxygenase catalytic domain (in which the CXXC binding domain is lacking) to the programmable DNA-binding domains of ZFPs or transcription activator-like effectors (TALE), enhanced gene-specificity of hydroxymethylation and re-expression of methylated genes could be achieved as compared to globally increased TET expression [25,26]. However, utility of these approaches was limited due to off-target effects, high labor intensity, and lack of evidence for

disease modifying activities *in vivo*, revealing that a technique with further enhanced specificity was needed.

Here we aimed to utilize both the high target specificity of sgRNA-guided *Streptococcus pyogenes* dCas9 and the enzymatic effectiveness of TET3. We demonstrate gene-specific targeting and successful re-expression of hypermethylated genes *RASAL1*, *EYA1*, *LRFN2*, and *KLOTHO* through all-in-one constructs in which either dCas9 or high-fidelity dCas9, respectively, is fused to the TET3 catalytic domain which is specifically targeted to the promoters of these genes by single-guide RNA (sgRNA). We further systematically established viral targeting of different cell populations in the kidney *in vivo* and demonstrate that by expression of dCas9/dHFCas9-TET3CD-*RASAL1*-sgRNA in kidney fibroblasts and of dHFCas9-TET3CD-*KLOTHO*-sgRNA in epithelial cells, fibrosis is significantly attenuated in a mouse model of kidney fibrosis. In summary, we show that CRISPR/Cas9-based gene-specific hydroxymethylation can rescue gene expression. This technology therefore has a broad application spectrum and may be useful to combat other diseases induced by aberrant gene methylation, such as various forms of cancer and neurodegenerative diseases.

RESULTS

TARGETED HYDROXYMETHYLATION RESCUES GENE EXPRESSION *IN VITRO*

In order to generate a gene-specific hydroxymethylation system, we created a chimeric hydroxymethylase by fusing the TET3 catalytic domain (TET3CD) [24,27] to the C-terminal domain of a double mutated Cas9 (dCas9), in which endonuclease catalytic residues D10A and H840A have been mutated to avoid cutting of the DNA (Figs. 1a, b, Supplementary Fig. 1) [28–33]. We next introduced TET3CD (aa851–aa1795) to generate a hydroxymethylation vector (pLenti-dCas9-TET3CD) (Supplementary Figs. 1, 2) [24,34]. We have also generated a control vector (pLenti-dCas9-TETCDi) in which catalytic residue mutations H1077Y and D1079A have been created to abolish the hydroxymethylation activity of TET3CD (Supplementary Fig. 2) [35]. As proof-of-principle, we aimed to reactivate the genes *RASAL1*, *EYA1*, *LRFN2*, and *KLOTHO* whose expressions are silenced due to promoter hypermethylation in fibrotic human renal fibroblasts and human tubular epithelial cells, respectively [4,36,37].

To identify applicable sgRNA to enable specific targeting of the dCas9-TET3CD fusion protein to the gene promoters, we designed 10 sgRNAs (five guiding RNAs targeting each strand) targeting the *RASAL1* promoter, six sgRNAs (three guiding RNAs targeting each strand) targeting the *EYA1* promoter, eight sgRNAs (four guiding RNAs targeting each strand) targeting the *LRFN2* promoter and the Klotho promoter, respectively. Those sgRNAs were inserted into the pLenti-dCas9-TET3CD vector to generate gene-specific demethylation constructs for *RASAL1* (pLenti-dCas9-*RASAL1*-sgRNA1-10), *EYA1* (pLenti-dCas9-*EYA1*-sgRNA1-6), *LRFN2* (pLenti-dCas9-*LRFN2*-sgRNA1-8), and *KLOTHO* (pLenti-dCas9-TET3CD-KL-sgRNA1-8). *LacZ* sgRNA [38] was introduced into pLenti-dCas9-TET3CD (pLenti-dCas9-*LacZ*-sgRNA) vector serving as control construct.

Upon establishing the demethylation constructs, we tested their demethylation activities utilizing TK188 fibrotic human renal fibroblasts with known robust CpG island promoter methylation for *RASAL1*, *EYA1*, and *LRFN2* and HK2 epithelial cells with known CpG island promoter methylation for Klotho upon stimulation with TGF β 1. Fibrotic fibroblasts, which were treated with dCas9-TET3CD-*RASAL1*-sgRNA2/3, showed significant reactivated *RASAL1* expression (Fig.1c). Cells that were treated with dCas9-TET3CD-*EYA1*-sgRNA1/3 showed reactivated *EYA1* expression (Fig. 1d). Cells that were treated with dCas9-TET3CD-*LRFN2*-sgRNA3/6 showed restored *LRFN2* expression (Fig. 1e). Restored expression does not occur with *LacZ* nor with the respective pLenti-dCas9-TET3CD vectors, in which hydroxymethylation activity of TET3CD was abolished (Fig. 1c–e). HK2 epithelial cells showed reduced expression of Klotho upon TGF β 1 treatment, which was restored upon pLenti-dCas9-TET3CD-KL-sgRNA1-2 vectors (Fig. 1i). To rule out the possibility that demethylation is due to overexpression of TET3CD, we performed experiments only using TET3CD vectors without guiding RNA. No significant gene induction was observed in any of these 4 genes indicating that demethylation is not due to overexpression of TET3CD (Supplementary Fig. 3). Among the three tested genes in fibroblasts, cells that were treated with dCas9-TET3CD-*RASAL1*-sgRNA3 showed the highest induction level which was comparable to *RASAL1* mRNA expression in control (non-fibrotic) human kidney fibroblasts.

We hence performed methylation- and hydroxymethylationspecific MeDIP and hMeDIP assays (immunoprecipitation of methylated or hydroxymethylated DNA, respectively, followed by qPCR) of the *RASAL1* promoter for dCas9-TET3CD

guided by *RASAL1*-sgRNA3, *LacZ*-sgRNA, and dCas9-TET3CDi guided by *RASAL1*-sgRNA3, revealing that among those different vectors, only dCas9-TET3CD-*RASAL1*-sgRNA3 significantly induced *RASAL1* promoter hydroxymethylation and reduced methylation (Fig. 1f, g). To determine if and which CpG sites could be demethylated in the *RASAL1* promoter region after expression of dCas9-TET3CD-*RASAL1*-sgRNA3, bisulfite sequencing was performed. In contrast to dCas9-TET3CD-*LacZ*-sgRNA transduced cells, cells transduced with dCas9-TET3CD-*RASAL1*-sgRNA3 demonstrated demethylation in the promoter region between -114 to +1 (Fig. 1h, Supplementary Fig. 4), suggesting this to be a “critical promoter region”. To gain single base-pair resolution for hydroxymethylation within the critical region, we performed glucosylation-mediated restriction enzyme sensitive PCR (gRES-PCR) revealing that upon treatment with T4-BGT and *MspI* the uncleaved *RASAL1* PCR amplicon was only detectable in the cells transduced with dCas9-TET3CD-*RASAL1*-sgRNA3 (Supplementary Fig. 5d) but not in the other samples (Supplementary Fig. 5b, c, e), confirming site-specific hydroxymethylation of the *RASAL1* promoter by dCas9-TET3CD-*RASAL1*-sgRNA3. Upon establishing that dCas9-TET3CD-*RASAL1*-sgRNA3 effectively induced *RASAL1* CpG promoter hydroxymethylation and demethylation and subsequent rescue of *RASAL1* expression, we identified all genes which were predicted to be targeted by sgRNA3 via the online program CCTop [39]. We hence performed qRT-PCR for these genes, but no significant difference in mRNA expression could be detected for any of the predicted genes other than *RASAL1* when comparing cells transduced with dCas9-TET3CD-*RASAL1*-sgRNA3 with cells transduced with dCas9-TET3CD-*LacZ*-sgRNA (Supplementary Fig. 6, Supplementary Table 8). This suggests that none of these predicted off-targeted genes was hypermethylated and hence they were not affected by our demethylation system.

Just as for *RASAL1*, we rescued *KL* expression corresponding with enhanced *KL* promoter hydroxymethylation and decreased promoter methylation (Fig. 1j, k). We also performed qRT-PCR for those genes that were predicted to be *KL* sgRNA2 off-targets. Other than *KL* no significant difference in mRNA expression could be detected when comparing cells transduced with sgRNA2 with cells transduced with *LacZ*-sgRNA (Supplementary Fig. 7, Supplementary Table 9).

In summary, we demonstrate successful targeted demethylation of 4 different aberrantly methylated gene promoters (*RASAL1*, *EYA1*, *LRFN1*, and *KL*) and in two different cell types (fibroblasts and epithelial cells) through lentiviral delivery of a

construct encoding a fusion protein of dCas9-TET3CD, which is targeted to the promoter CpG through specific single-guide RNA. Notably, we realized that demethylation proteins guided by sgRNAs that are targeting the DNA antisense strand are more efficient as compared to those where the DNA sense strand was targeted.

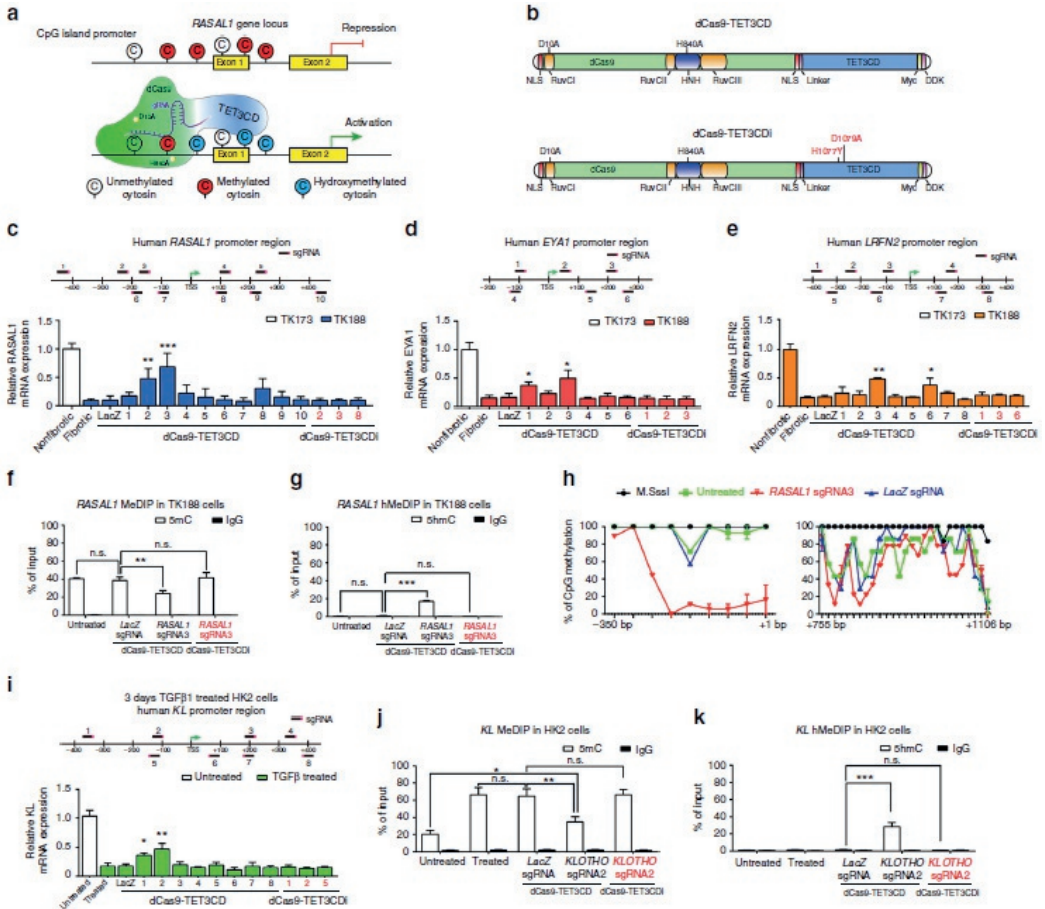


Figure 1. Targeted hydroxymethylation of four different aberrantly methylated genes by dCas9-TET3CD fusion protein in human kidney cells.

(a) Schematic representing hypermethylated RASAL1 promoter region (upper panel) and reactivated RASAL1 expression through induction of RASAL1 promoter hydroxymethylation by dCas9-TET3CD fusion protein in complex with a sgRNA binding to its target region (lower panel). (b) Schematic of domain structure of the dCas9-TET3CD (upper panel) and dCas9-TET3CDi (lower panel) fusion protein. (c–e) Locations for RASAL1/EYA1/LRFN2-sgRNAs are indicated by thick lines with corresponding PAM in magenta within the human RASAL1/EYA1/LRFN2 gene locus, respectively. Human fibrotic

TK188 fibroblasts were transduced with lentivirus expressing demethylation constructs guided by RASAL1-sgRNAs 1–10, EYA1-sgRNA 1–6, LRFN2-sgRNA 1–8, or by LacZ control sgRNA. Results were normalized to reference gene GAPDH. (f, g) MeDIP and hMeDIP analysis of TK188 cells were transduced with dCas9-TET3CD-RASAL1-sgRNA3. The results were calculated relative to the input. (h) Bisulfite sequencing summary of promoter methylation status of the RASAL1 gene in TK188 cells transduced with demethylation constructs guided by RASAL1-sgRNA3, by LacZ control sgRNA or DNA treated with *M.SssI* serving as positive control. Each data point represents the mean of three independent transduction experiments with error bars indicating the standard error of the mean for six or more bisulfite sequencing results. (i) Locations for KL-sgRNAs are indicated by thick lines with corresponding PAM in magenta within the human KL gene locus. Three days TGFβ1-treated HK2 cells were transduced with lentivirus expressing demethylation constructs guided by KL-sgRNAs 1–8 or by LacZ control sgRNA. (j, k) MeDIP and hMeDIP analysis of HK2 cells were transduction with dCas9-TET3CD-KL-sgRNA2. The results were calculated relative to the input. All data are presented as mean value; error bars represent S.D.; n = 3 independent biological replicates, n.s. not significant; *p < 0.05, **p < 0.01, ***p < 0.001.

In order to explore the possibility of utilizing this demethylation system in mice *in vivo*, we next tested our system in primary mouse kidney fibroblasts (mKFs) and in mouse renal tubular epithelial cells (MCT cells), where *Rasal1* and *Kl* expressions are reduced, respectively, via promoter hypermethylation by prolonged exposure to TGFβ1 treatment (Fig. 2a–f, Supplementary Fig. 8a, b) [4,5]. We designed eight different sgRNAs (four sgRNAs targeting each strand) targeting the *Rasal1* promoter and six different sgRNAs (all sgRNAs targeting antisense strand) targeting the *Kl* promoter, and introduced them into a pLentiCas9-TET3CD vector (pLenti-dCas9-TET3CD-*Rasal1*-sgRNA1-8 or pLenti-dCas9-TET3CD-*Kl*-sgRNA1-6) to transduce 10 days TGFβ1-treated mKFs or three days TGFβ1-treated MCT cells, respectively. We identified that three of the constructs (dCas9-TET3CD-*Rasal1*-sgRNA2-4) rescued *Rasal1* expression (Fig. 2a, Supplementary Fig. 8d) and three of the constructs (dCas9-TET3CD-*Kl*-sgRNA1-3) restored *Kl* expression (Fig. 2b). Moreover, rescued *Rasal1* and *Kl* expression corresponded with enhanced hydroxymethylation and attenuated promoter methylation for both genes (Fig. 2a–f). Bisulfite sequencing identified –323 bp to –179 bp as the critical region within the murine *Rasal1* promoter which has been demethylated (Fig. 2d, Supplementary Fig. 9) and –101 bp to +98 bp as the critical region within the murine *Kl* promoter which has been effectively demethylated (Fig. 2f, Supplementary Fig. 10).

In order to test off-target effects (a problem immanent to the Cas9 technology, which has thus far limited therapeutic utility [40]), we performed chromatin immunoprecipitation followed by sequencing (ChIP-seq) for dCas9-TET3CD-*Rasal1*-sgRNA4 binding sites in mKFs. Our data reveal the targeted region of the *Rasal1* promoter and a large number of 159 off-target binding sites within 48 different genes (Table 1). Importantly, these off-target genes included genes with known pro-fibrotic effects (which are commonly silenced by promoter methylation in normal tissue) such that therapeutic efficacy by rescue of (anti-fibrotic) *RASA1* could be counteracted by newly induced expression of pro-fibrotic genes through our dCas9-TET3CD construct. We therefore next aimed to improve our technique to reduce off-target effects. Among all methods to reduce off-target effects of Cas9, the use of high-fidelity CRISPR-spCas9 has been shown to be the most efficient [41]. We hence introduced catalytic domain deactivation amino acid mutations (D10A and H840A) into high-fidelity spCas9 to abolish its cleavage properties and we generated a new dHFCas9-TET3CD demethylation construct (Fig. 2g, Supplementary Fig. 11).

We used mouse *Rasal1* sgRNA4 and Kl sgRNA2 (which effectively induced gene expression in dCas9-TET3CD constructs) to generate dHFCas9-TET3CD-*Rasal1*-sgRNA4 and dHFCas9-TET3CD-*Kl*-sgRNA2 and transduced them into mKFs or MCT cells, respectively. Both *Rasal1* and *Kl* expressions were significantly reactivated to the same level as induced by the dCas9-TET3CD vectors (Fig. 2h). Furthermore, rescued *Rasal1* and *Kl* gene expression corresponded with attenuated promoter methylation to the same level as induced by the dCas9-TET3CD vectors (Fig. 2i). To compare off-target binding sites between dCas9-TET3CD and dHFCas9-TET3CD, we performed ChIP-seq on cells transfected with dCas9-TET3CD-*LacZ*-sgRNA/-*Rasal1*-sgRNA4, or dHFCas9-TET3CD-*LacZ*-sgRNA/-*Rasal1*-sgRNA4. Using this approach, only eight genes were common for both dCas9-TET3CD and dHFCas9-TET3CD (Table 1), besides 40 peaks specific only for dCas9-TET3 where many of the off-target peaks showed quite high binding levels, as defined by the peak height relative to on-target peaks after subtracting dCas9-TET3CD-*LacZ*-sgRNA reads at that site (Fig. 2j, Table 1).

Table 1. Off-target genes identified by CHIP-sequencing analysis

Targets of dCas9-TET3CD-Rosafl-sgRNA4									
Chrom	Start	End	Score	ThickStart	ThickEnd	ItemRGB	BlockCount	Gene symbol	
1	chr5	114153103	114153177	65	6.52912	11.72342	6.56068	89	1700069116Rik
2	chr12	112968908	112969072	47	5.59639	9.73582	4.71895	68	2810002N01Rik
3	chr16	57391581	57391772	173	9.89721	23.05536	17.33657	48	2610528E23Rik
4	chr6	67692952	67693120	140	10.66121	19.54378	14.08762	37	abfParts
5	chr8	125333034	125333227	47	5.59639	9.73582	4.71895	96	Acdf3
6	chr2	33906296	33906460	65	6.52912	11.72342	6.56068	112	AK048710
7	chr6	4764451	4764703	65	6.52912	11.72342	6.56068	92	AK076963
8	chr7	69254460	69254632	180	12.43808	23.6066	18.03127	30	AK086712
9	chr6	50557448	50557617	30	4.66366	7.81498	3.03828	84	AK144624
10	chr5	4053134	4053342	47	5.59639	9.73582	4.71895	104	Akap9
11	chr3	126852658	126852848	59	6.87729	10.96568	5.9056	56	Ank2
12	chr6	86698604	86698768	47	5.59639	9.73582	4.71895	82	Anxa4
13	chr1	50872914	50873114	465	23.98771	52.41908	46.51371	49	BC029710
14	chr17	13745750	13745921	114	4.18092	16.85615	11.47872	45	BC068229
15	chr10	58926851	58927510	247	36.82354	254.31743	247.07439	36	Ccdc109a
16	chr10	94456808	94456973	105	8.39458	15.86543	10.50555	90	Ccdc41
17	chr11	51843853	51844017	30	4.66366	7.81498	3.03828	55	Cdk13
18	chr11	12213679	12213882	65	6.52912	11.72342	6.56068	45	Cobl
19	chr7	26797237	26797401	76	7.92883	12.87339	7.67306	27	Cyp2b6
20	chr3	102939715	102939879	47	5.59639	9.73582	4.71895	114	Dennd2c
21	chr5	121098768	121099300	840	15.6069	13.73752	8.49179	341	Rasall
22	chr14	8703442	8703750	40	6.77979	9.17137	4.05255	190	Flnb
23	chr7	34880923	34881149	150	11.29756	20.53988	15.0373	140	Gml2776
24	chr6	142752466	142752630	47	5.59639	9.73582	4.71895	76	Gm766
25	chr8	96357751	96357949	105	8.39458	15.86543	10.50555	95	Gnao1
26	chr5	104423124	104423288	65	6.52912	11.72342	6.56068	70	Hsd17b11
27	chr13	13846763	13846961	65	6.52912	11.72342	6.56068	82	Lyst
28	chr2	4930750	4931328	282	15.85643	33.99368	28.26957	289	Mcm10
29	chr18	7609200	7609768	168	11.19277	22.41256	16.85413	149	Mpp7
30	chr13	100159145	100159461	84	7.46185	13.7689	8.49179	232	Mps27
31	chr10	6271609	6271773	84	7.46185	13.7689	8.49179	76	Mshfdll
32	chr14	58173518	58173682	84	7.46185	13.7689	8.49179	94	N6amt2
33	chr5	95099096	95099260	65	6.52912	11.72342	6.56068	142	Nell2
34	chr9	121151	12115	47	5.59639	9.73582	4.71895	111	Nlrp4g
35	chr7	2421257	24212603	213	13.05824	26.95684	21.33005	163	Nlrp5
36	chr12	83086950	83087140	47	5.59639	9.73582	4.71895	35	Pcmx
37	chr3	96646134	96646506	65	6.52912	11.72342	6.56068	181	Pdk1
38	chr3	152449257	152449918	190	12.12551	24.66862	19.07566	340	Pigk
39	chr9	66725484	66725736	84	7.9959	13.71865	8.4867	126	Rab8b
40	chr4	120536872	120537036	84	7.46185	13.7689	8.49179	82	Rims3
41	chr17	8149373	8149587	47	5.59639	9.73582	4.71895	57	Raph3a
42	chr4	112068812	112069093	213	13.05824	26.95684	21.33005	143	Skint9
43	chr6	142181926	142182108	378	19.58736	43.71904	37.89215	36	Slic21a7
44	chr1	57911770	57911934	47	5.59639	9.73582	4.71895	35	Spats21
45	chr10	5264302	5264480	47	6.52912	11.72342	6.56068	99	Syne1
46	chr5	64639102	64639266	65	6.52912	11.72342	6.56068	66	Tbc1d1
47	chr4	74361648	74361927	187	13.99224	24.4904	18.76297	145	Tmem56
48	chr1	43834505	43834730	65	6.52912	11.72342	6.56068	124	Uxt1

Targets of dHFCas9-TE3CD-Rosafl-sgRNA4									
Chrom	Start	End	Score	ThickStart	ThickEnd	ItemRGB	BlockCount	Gene symbol	
1	chr1	50872919	50873111	322	19.47483	38.10745	32.22037	39	BC029710
2	chr17	13745609	13745912	88	3.17695	14.27044	8.84702	170	BC068229
3	chr10	58926856	58927475	359	23.74614	193.00722	185.91823	82	ccdc109a
4	chr14	8703110	8703279	73	8.12621	12.74668	7.36305	122	Flnb
5	chr7	34880926	34881147	169	13.16969	22.59302	16.90299	132	Gml2776
6	chr5	121098997	121099271	1273	1.52457	12.67083	7.3371	425	Rasall
7	chr3	120952807	120952979	152	11.73355	20.8748	15.21403	37	Tmem56
8	chr10	5264302	5264480	47	5.59639	9.73582	4.71895	57	Syne1

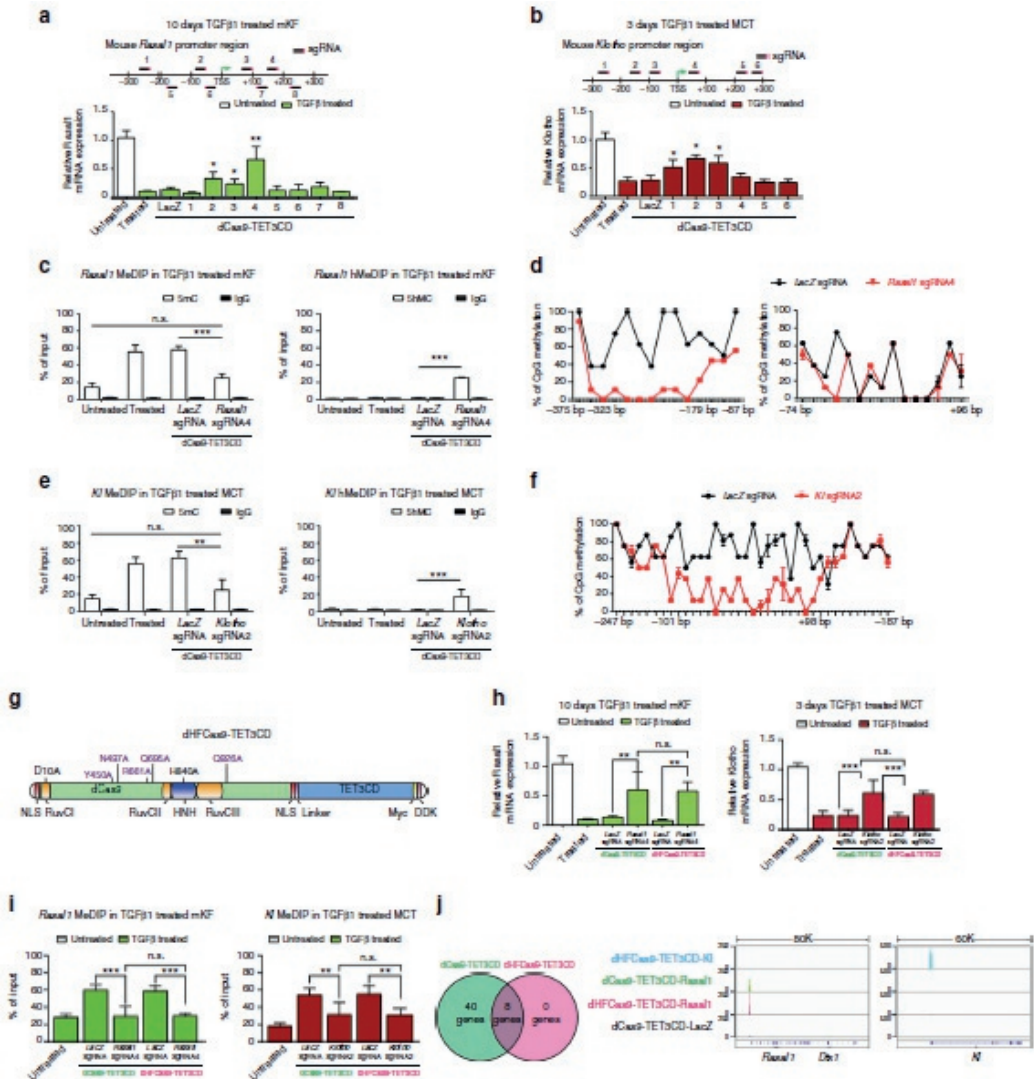


Figure 2. dCas9-TET3CD and dhFCas9-TET3CD fusion proteins induce targeted *Rasal1*/*Kl* promoter demethylation in mouse kidney cells and dhFCas9-TET3CD largely reduced off-target effects.

(a) Locations for *Rasal1*-sgRNAs are indicated by thick lines with corresponding PAM in magenta within the mouse *Rasal1* gene locus. 10 days TGFβ1-treated mKF were transduced with dCas9-TET3CD-*Rasal1*-sgRNAs1-8 or by LacZ control sgRNA. (b) Locations for *Klotho*-sgRNAs are indicated by thick lines with corresponding PAM in magenta within the mouse *Klotho* gene locus. Three days TGFβ1-treated MCT were transduced with dCas9-TET3CD-*Klotho*-sgRNAs1-6 or by LacZ control sgRNA. (c) MeDIP and hMeDIP analysis of TGFβ1-treated mKF were transduced with dCas9-TET3CD-*Rasal1*-sgRNA4. (d) Bisulfite sequencing summary of promoter methylation status of the *Rasal1* gene in TGFβ1-treated cells transduced with dCas9-TET3CD-*Rasal1*-sgRNA4 or by LacZ control sgRNA. (e) MeDIP and hMeDIP analysis of TGFβ1-treated MCT cells transduced with dCas9-TET3CD-

*Kl1-sgRNA2 or with LacZ control sgRNA. (f) Bisulfite sequencing summary of promoter methylation status of the Klotho gene in TGFβ1-treated MCT cells transduced with dCas9-TET3CD-sgRNA2 or by LacZ control sgRNA. (g) Schematic of domain structure of the dHFCas9-TET3CD fusion protein. (h) TGFβ1-treated mKFs were transduced with dCas9/dHFCas9-TET3CD-Rasal1-sgRNA4 or LacZ control sgRNA (left panel). TGFβ1-treated MCT cells were transduced with dCas9/dHFCas9-TET3CD-Klotho-sgRNA2 or LacZ control sgRNA (right panel). (i) MeDIP-qPCR analysis of TGFβ1-treated mKFs transduced with dCas9/dHFCas9-TET3CD-Rasal1-sgRNA4 or LacZ control sgRNA (left panel) and TGFβ1-treated MCT cells transduced with dCas9/dHFCas9-TET3CD-Klotho-sgRNA2 or LacZ control sgRNA (right panel). (j) Venn diagram summarizes the common off-targets identified by ChIP-seq analysis between dCas9-TET3CD and dHFCas9-TET3CD transduced mKF (left panel). Tracks indicate the binding regions and the enrichment of dCas9/dHFCas9-TET3CD-Rasal1/Klotho/LacZ sgRNA protein-RNA complexes in mKF cells as visualized in the IGV browser (right panel). Genomic coordinates are shown below the tracks (build mm9). All data are presented as mean value; error bars represent S.D, n = 3 independent biological replicates, n.s. not significant, *p < 0.05, **p < 0.01, ***p < 0.001. qRT-PCR results were normalized to reference gene Gapdh. MeDIP and hMeDIP results were calculated relative to input. For bisulfate sequencing each data point represents the mean of three independent biological replicates with error bars indicating the standard error of the mean for six or more bisulfite sequencing results*

RASAL1 KNOCKDOWN AGGRAVATES KIDNEY FIBROSIS *IN VIVO*

To perform proof-of principle experiments for a therapeutic efficacy of Rasal1 demethylation constructs, we next generated a *Rasal1* knockout mouse model to validate that loss of Rasal1 is pro-fibrotic. It has been demonstrated by different research groups that fibrosis in the kidney, heart and liver, and also gastrointestinal cancers are associated with *RASAL1* promoter hypermethylation, and that *RASAL1* promoter hypermethylation leads to decreased *RASAL1* expression [4–6,9,13]. Also, the extent of *RASAL1* promoter methylation correlates with progression of kidney fibrosis in patients and mice [14], and rescue of *RASAL1* transcription through transgenic overexpression attenuates experimental fibrosis in the kidney [14]. However, whether loss of Rasal1 expression per se contributes to kidney fibrosis has not yet been addressed.

We therefore generated *Rasal1*^{tm1a/tm1a} mice that harbor a gene-trap DNA cassette consisting of a splice acceptor site, an internal ribosome entry site and a β-galactosidase reporter, inserted into the second intron of the gene as described extensively in the methods section (Fig. 3a and Supplementary Fig. 12). In these mice Rasal1 expression is reduced by 80% on mRNA and protein level as

compared to wild-type littermate control mice (Fig. 3b, c). Kidneys of *Rasal1^{tm1a/tm1a}* mice appeared unchanged as compared to wild-type littermate control mice under baseline condition. However, after challenge with UUO, a model of obstructive nephropathy, which results in severe kidney fibrosis through increased parenchymal pressure, ensuing ischemia, tubular epithelial cell death, and inflammation 7 days after surgery. *Rasal1^{tm1a/tm1a}* mice displayed significantly higher levels of kidney fibrosis as compared to wild-type littermate controls, associated with higher levels of Collagen-1 deposition and abundance of α -SMA-positive fibroblasts (Fig. 3d).

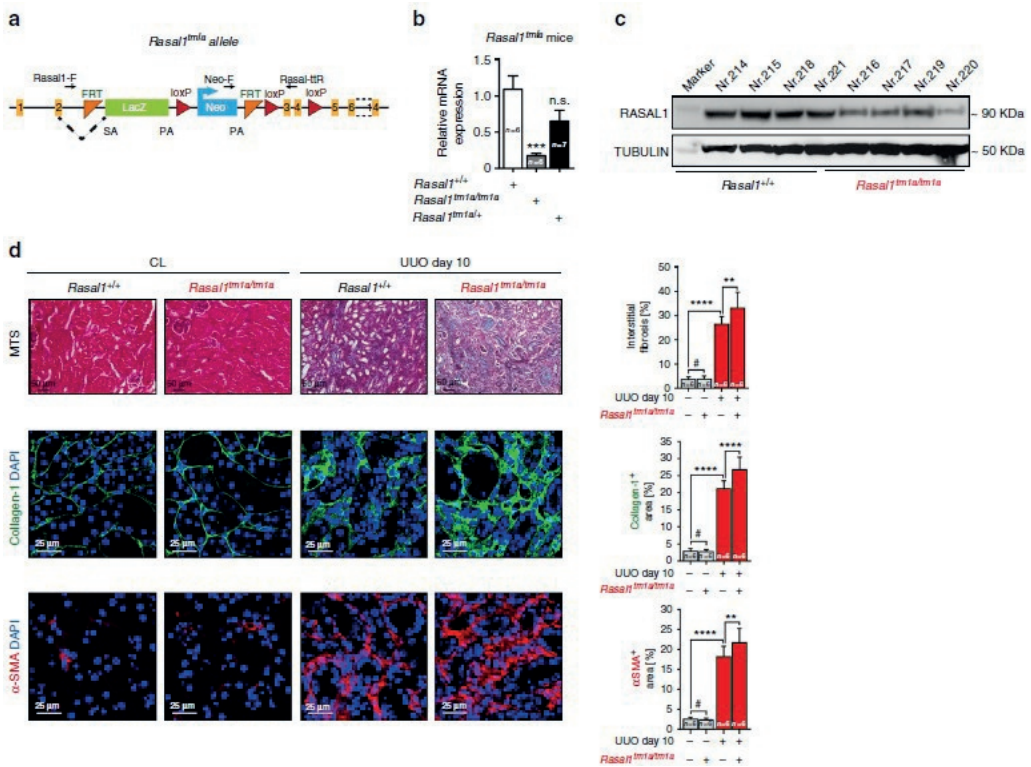


Figure 3. *Rasal1* gene disruption results in aggravated fibrosis level in the UUO model. (a) Schematic of knockout-first strategy for *Rasal1* gene. The gene trapping *LacZ* cassette is alternatively spliced with exon 2 mediated by a splicing acceptor (*SA*). A promoter-driven Neomycin cassette is inserted after *LacZ*. The targeted exon 3 and 4 are flanked by *loxP* sites. Black arrows indicate the location of genotyping primers. (b) qRT-PCR analysis shows the *Rasal1* mRNA expression in homozygous mice are significantly reduced as compared with wild-type mice, while there is no significant reduction in heterozygous mice. The data are presented as mean value, error bars represent S.D., n.s. not significant, ***p < 0.001. (c) Western blot analysis shows the RASAL1

protein expression is largely decreased in homozygous mice as compared with wild-type mice. (d) Kidney sections of wild type and homozygous *Rasal1tm1a* mutant mouse which were either sham controls (CL) or challenged with UUO were stained for Masson's Trichrome (MTS) (representative light microscopy images are shown in the top row), Collagen-1 or α -SMA (representative confocal images are shown in the middle and bottom row, respectively.) (Scalebars: 25 μ m or 50 μ m). Quantification of the percentage of total interstitial fibrosis and immunostained positive cells in each group are depicted (data are presented as mean value, error bars represent S.E.M., # not significant, *** $p < 0.0001$).

VIRAL DELIVERY MODE AFFECTS CELLULAR TARGETING *IN VIVO*

After establishing that lack of *Rasal1* aggravates kidney fibrosis and in light of known causality of lack of *Klotho* as another contributor to kidney fibrosis and importantly because both genes are silenced by hypermethylation during kidney fibrosis, we decided to test if targeted hydroxymethylation of *Rasal1* and *Klotho*, respectively, ameliorates kidney fibrosis *in vivo*. Because *Rasal1* is primarily expressed in fibroblasts and *Klotho* in tubular epithelial cells, we first established if different modes of lentiviral delivery impact what cells are primarily targeted.

We therefore used green and red fluorescence protein (GFP and RFP) labeled control lentivirus to transduce kidneys by different delivery routes. Transduction efficiency was > 95% in mouse kidney fibroblasts and > 95% in mouse kidney epithelial cells *in vitro* (Fig. 4a, b). Next, we analyzed which cells are targeted *in vivo* by testing four different delivery methods (using 10^8 TU/80 μ l virus particles each) in both healthy and UUO kidneys: via the renal artery, intraparenchymal (4 sites with 20 μ l/site), via the renal vein, and via retrograde infusion into the ureter. Ten days after virus injection, mice were sacrificed and GFP and RFP expression was visualized by immunohistochemistry using antibodies against GFP and RFP, respectively (Fig. 4c–f). Injection of lentivirus into the renal artery transduced the fewest cells overall among all four techniques in both healthy and UUO kidneys (Fig. 4c). Venous injection leads to transduction of interstitial cells (Fig. 4e), albeit to a lower extent as compared to intraparenchymal injection (Fig. 4d). In contrast, retrograde injection into the ureter predominantly transduced tubular epithelial cells with high efficacy (Fig. 4f).

In order to quantify percentage of transduced fibroblasts we next performed further analysis by double labeling of α -smooth muscle actin (α SMA)-positive fibroblasts and GFP. Ten days after lentiviral intraparenchymal CMV-GFP

construct delivery and UUO surgery, an average of 46% of all α SMA-positive fibroblasts were also positive for GFP indicating successful transduction (Fig. 4g).

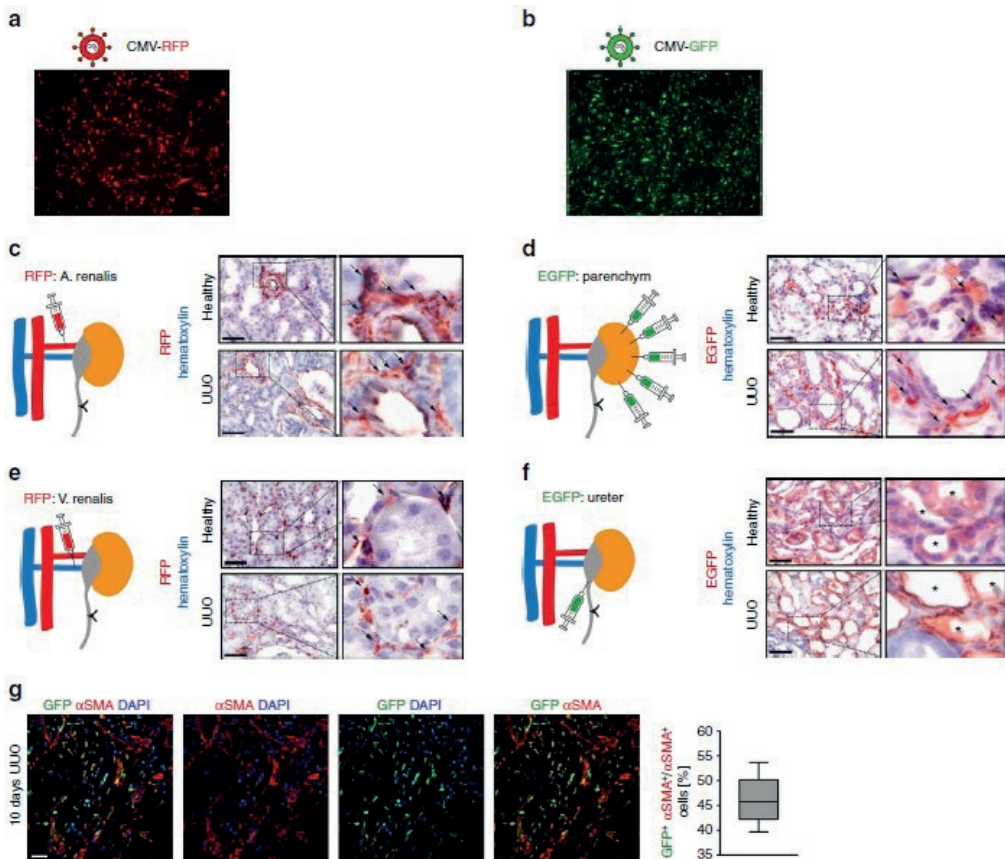


Figure 4. *In vivo* gene delivery to mouse kidney by Lentivirus transduction.

(a, b) Immunofluorescence pictures show that mouse kidney fibroblasts and kidney epithelial cells were efficiently transduced with lentivirus containing a RFP (a) or EGFP (b) gene, respectively. (c–f) Immunohistochemistry pictures show RFP/EGFP-positive cells in kidney sections which were transduced with lentivirus containing RFP (c, e) or EGFP (d, f) through different delivery routes: renal artery (c), parenchyma (d), renal vein (e), and infusion into retrograde ureter (f) with 80 μ l (108TU) virus particles for each method. $n = 6$ in each injection group. (g) Representative confocal photomicrographs of UUO kidneys transduced with GFP-labeled lentivirus via parenchymal injection. The sections were double stained for GFP (in green) and myofibroblast marker α SMA (in red). Nuclei were counterstained with DAPI (in blue). The boxwhisker plot (right panel) shows the percentage of GFP and α SMA double positive cells out of all α SMA-positive cells. $n = 3$ mice

HYDROXYMETHYLATION OF RASAL1 AND KLOTHO IMPROVES KIDNEY FIBROSIS

To test the efficacy of the established dCas9-TET3CD-*Rasal1*-sgRNA and dCas9-TET3CD-*Klotho*-sgRNA systems *in vivo*, we utilized the mouse model of UUO. This model displays robust *Rasal1* promoter methylation within interstitial fibroblasts and *Klotho* methylation in tubular epithelial cells, resulting in transcriptional suppression of *Rasal1* and *Klotho*, which causes disease progression [4,5]. Based on our previous results which demonstrated effective lentiviral transduction of kidney interstitial cells upon vector delivery through intraparenchymal injection and of epithelial cells upon vector delivery through retrograde ureter infusion, we first injected lentivirus harboring either dCas9-TET3CD-/*Rasal1* sgRNA4 or dHFCas9-TET3CD-/*Rasal1* sgRNA4 with dCas9-TET3CD-*LacZ*-sgRNA or dHFCas9-TET3CD-*LacZ*-sgRNA as controls, respectively, into the renal parenchyme of UUO-challenged and contralateral control kidneys (Fig. 5a, b).

Restored *Rasal1* expression upon UUO was observed exclusively in mice which received either dCas9-TET3CD-*Rasal1*-sgRNA4 or dHFCas9-TET3CD-*Rasal1*-sgRNA4, but not in mice injected with the dCas9/dHFCas9-TET3CD-*LacZ*-sgRNA control vectors (Fig. 5c, d). Increased *Rasal1* expression correlated with increased *Rasal1* hydroxymethylation and reduced methylation (Fig. 5e, f). Most importantly, renal fibrosis, accumulation of fibroblasts and type I collagen were significantly attenuated in dCas9/dHFCas9-TET3CD-*Rasal1*-sgRNA4 treated mice, but not in mice administered with the dCas9/dHFCas9-TET3CD-*LacZ*-sgRNA control vectors (Fig. 5g–j). Interestingly, even though *Rasal1* hydroxymethylation and restoration of *Rasal1* expression was equally effective, attenuation of kidney fibrosis was almost 50% and thereby more effective in dHF- as compared to less than 30% in dCas9-TET3CD-*Rasal1*-sgRNA treated mice (Fig. 5c–j), which is likely due to the reduction of off-target effects in the dHFCas9-TET3CD as compared to the dCas9-TET3CD system (Fig. 2j).

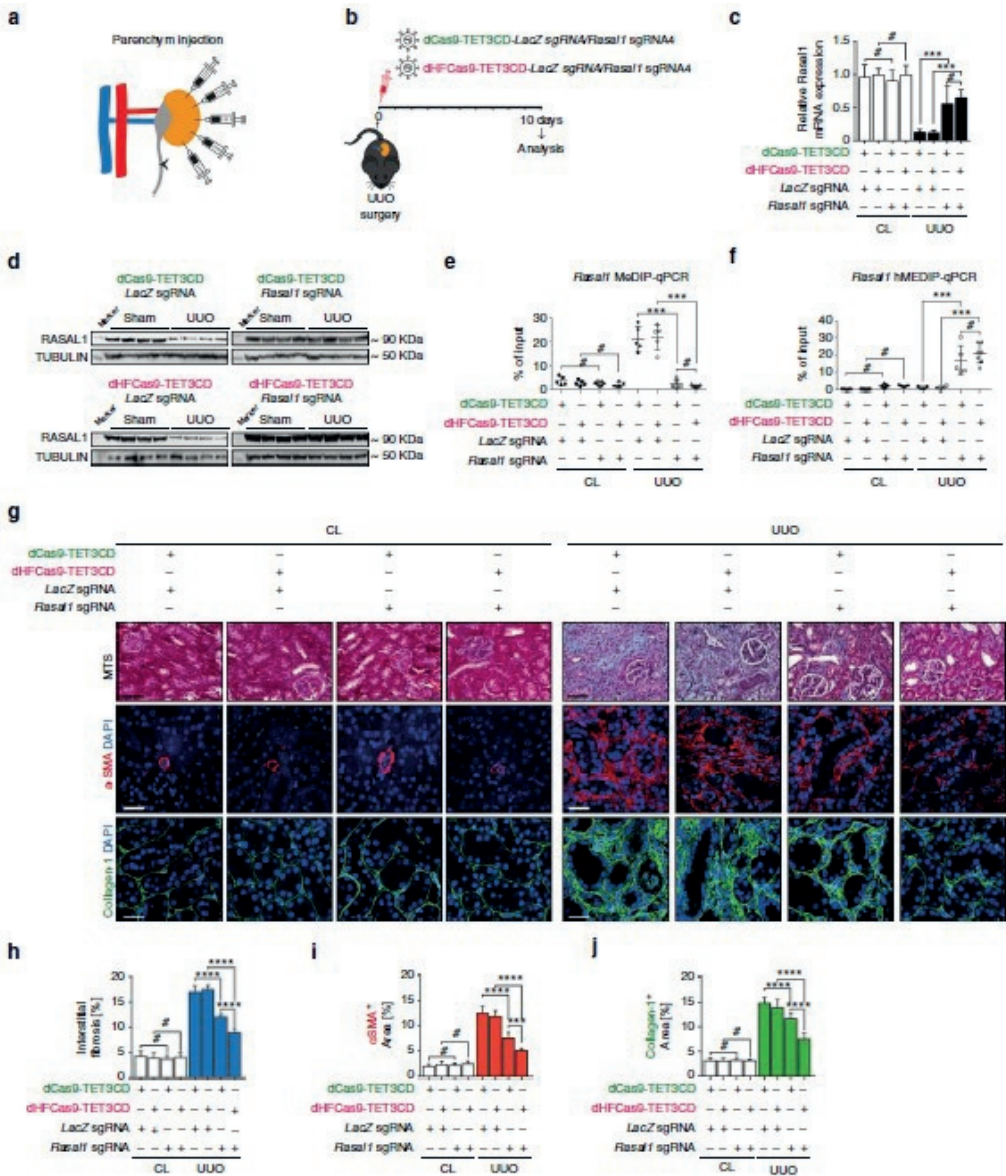


Figure 5. Targeted Rasal1 promoter demethylation by dCas9/dHFCas9-TET3CD-Rasal1-sgRNA fusion protein ameliorates kidney fibrosis.

(a) Schematic showing the parenchymal injection of lentiviral particles containing dCas9/dHFCas9-TET3CD fusion protein into UUO-challenged kidneys. (b) Schedule of UUO mouse surgery, lentivirus injection, and analysis. (c) qRT-PCR results showing that Rasal1 mRNA expression was significantly induced in UUO-challenged kidneys transduced with dCas9/dHFCas9-TET3CD-Rasal1-sgRNA, but not in UUO-challenged kidneys transduced with control dCas9/dHFCas9-TET3CD-LacZ-sgRNA. There is no significant difference between dCas9-TET3CD and dHFCas9-TET3CD constructs. Results were normalized to reference gene *Gapdh* (expression is presented as mean value; error bars represent

S.D., $n \geq 5$ in each group, # not significant, $***p < 0.001$). (d) Western blots showing restored RASAL1 protein expression in UUO-challenged kidneys which were transduced with lentivirus expressing dCas9/dHFCas9-TET3CD-Rasal1-sgRNA. The membranes were restriped and re-probed with α -TUBULIN antibody to serve as equal loading control. (e, f) UUO-challenged kidneys which were transduced with lentivirus expressing dCas9/dHFCas9-TET3CD-Rasal1-sgRNA show significantly reduced Rasal1 promoter methylation by MeDIPqPCR assay (e) and increased hydroxymethylation by hMeDIP-qPCR assay (f). There is no significant difference between dCas9-TET3CD and dHFCas9-TET3CD constructs. The results were calculated relative to input. The data are presented as mean value, error bars represent *S.D.*, $n \geq 5$; # not significant, $***p < 0.001$. (g) Kidney sections from UUO- and sham-operated mice which were transduced with lentivirus expressing dCas9/dHFCas9-TET3CD-Rasal1-sgRNA or dCas9/dHFCas9-TET3CD-LacZ-sgRNA were stained for Masson's trichrome (MTS) (representative light microscopy images are shown in the top row), Collagen-1 or α -SMA (representative confocal images are shown in the middle and bottom row, respectively) (Scale bars: 25 μ m or 50 μ m). (h–j) Quantification of the percentage of total interstitial fibrosis and immunostained positive cells in each group is depicted (data are presented as mean value, error bars represent *S.E.M.*, $n \geq 5$ in each group, # not significant, $***p < 0.001$, $****p < 0.0001$). Both dCas9-TET3CD and dHFCas9-TET3CD lentivirus transduced UUO-operated kidneys show significantly decreased interstitial fibrosis level and a significantly decreased number of α -SMA- and Collagen-1-positive cells. HFCas9-TET3CD shows significantly better efficacies when compared to dCas9-TET3CD.

After establishing that dHFCas9-TET3CD is superior to the dCas9-TET3CD system, we continued to use the dHFCas9-TET3CD system for targeted hydroxymethylation of *Klotho* in tubular epithelial cells in order to test its anti-fibrotic potential *in vivo*. To target methylated *Klotho* in tubular epithelial cells, we performed retrograde injection of dHFCas9-TET3CD-*Klotho*-sgRNA and dHFCas9-TET3CD-*LacZ*-sgRNA control viruses into the ureters of UUO-challenged and of contralateral control kidneys and analyzed the kidneys after 10 days (Fig. 6a, b). Similar as with Rasal1, *Klotho* expression was successfully restored to ~50% of the physiological level by dHFCas9-TET3CD-*Klotho*-sgRNA but not with *LacZ*-sgRNA and restoration correlated with reduced *Klotho* promoter methylation levels (Fig. 6c–f). Kidney fibrosis was significantly reduced by 25.4% by dHFCas9-*Klotho*-sgRNA as compared to dHF-TET3CD-*LacZ*-sgRNA injection (Fig. 6f), and this reduction in fibrosis correlated with blunted accumulation of fibroblasts and of type I Collagen (Fig. 6g, h), correlating with *Klotho* demethylation and rescued *Klotho* expression.

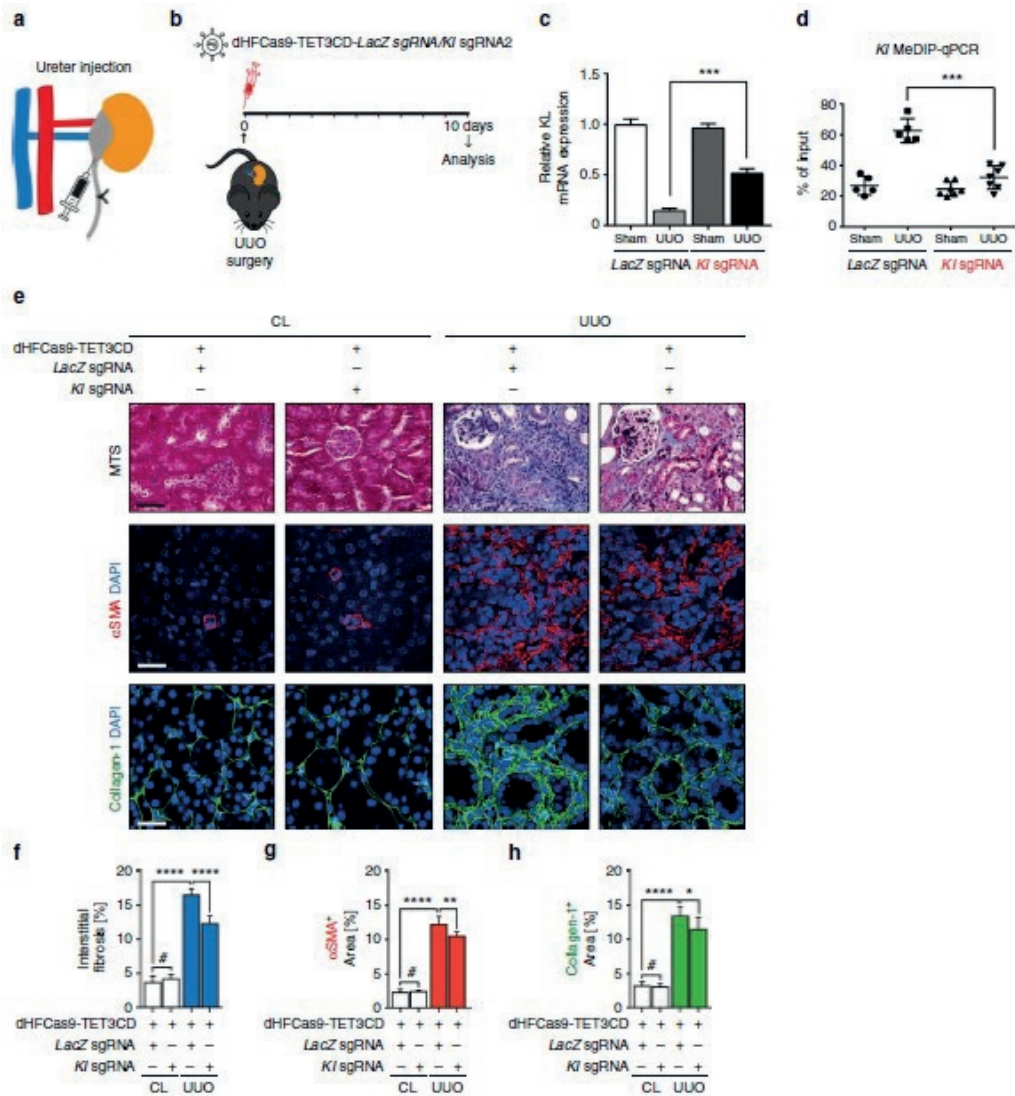


Figure 6. Induction of Klotho promoter hydroxymethylation by dhFCas9-TET3CD-Klotho-sgRNA in tubular epithelial cells ameliorates kidney fibrosis.

(a) Schematic shows retrograde ureter injection of lentiviral particles containing dhFCas9-TET3CD-Klotho-sgRNA into UUO-operated kidneys. (b) Schedule of UUO mouse surgery, lentivirus injection, and analysis. (c) qRT-PCR results showing that KI mRNA expression was significantly induced in UUO-operated kidneys transduced with dhFCas9-TET3CD-KI-sgRNA but not in UUO-challenged kidneys transduced with LacZ-sgRNA control. Results were normalized to reference gene *Gapdh* (expression is presented as mean value, error bars represent S.E.M., $n=6$ in each group, $***p < 0.001$). (d) UUO-operated kidneys which were transduced with lentivirus expressing dhFCas9-TET3CD-KI-sgRNA show significantly reduced KI promoter methylation level by MeDIP-qPCR assay. The results were calculated relative to input. The data are presented as mean value, error bars

represent S.D., $n \geq 5$, $***p < 0.001$. (e) Kidney sections from UUO- and sham-operated mice which were transduced with lentivirus expressing dHFCas9-TET3CD-KI-sgRNA or LacZ-sgRNA were stained for Masson's trichrome (MTS) (representative light microscopy images are shown in the top row), Collagen-1 or α -SMA (representative confocal images are shown in the middle and bottom row, respectively) (Scale bars: 25 μm or 50 μm). (f–h) Quantification of the percentage of total interstitial fibrosis and immunostained positive cells in each group are depicted (data are presented as mean value, error bars represent S.E.M., $n \geq 5$ in each group, # not significant, $*p < 0.05$, $**p < 0.01$, $***p < 0.0001$). UUO-challenged kidneys transduced with lentivirus expressing dHFCas9-TET3CD-KI-sgRNA show significantly decreased interstitial fibrosis level and a significantly decreased number of α -SMA- and Collagen-1-positive cells.

DISCUSSION

In this study, we provide proof-of-principle that by using a novel dCas9/dHFCas9-TET3CD all-in-one fusion protein approach, single methylated genes can be specifically targeted and transcriptionally reactivated *in vitro* as well as *in vivo* in a disease model. Based on the example of four different genes (*RASAL1*, *EYA1*, *LRFN2*, and *KL*) that are known to be hypermethylated in specific cell types or upon stimulation with TGF β 1, we demonstrate that targeted TET3-mediated hydroxymethylation is a feasible, reliable, and fast technology which results in demethylation and transcriptional reactivation of these genes. Because we also demonstrate that use of the mutated wild-type SpCas9 in this technology results in substantial off-target effects we developed a new high-fidelity Cas9-based approach which reduced off-target genes by 85%. The relevance of reduction of off-target genes was proven by testing our gene-specific demethylation technologies in a disease model *in vivo*, which to our knowledge has not been done before.

Among the four genes for which we established gene-specific hydroxymethylation vectors, we selected *Rasal1* and *Klotho* for *in vivo* studies, as both genes have been well studied in context of kidney fibrosis in both human and mouse models: *Klotho* has been shown to be hypermethylated and transcriptionally silenced in kidney fibrosis patients and in corresponding mouse models, and lack of *Klotho* is causally linked to kidney fibrosis in mice. *Rasal1* has been shown to be transcriptionally silenced and hypermethylated in both human and mouse kidney fibrosis. Because the causality between *Rasal1* and kidney fibrosis had not yet been addressed, we generated *Rasal1* knockout mice in

which *Rasal1* expression was reduced by 70%. In these mice, kidney fibrosis was substantially increased upon challenge with UUO, thus causally linking lack of *Rasal1* with kidney fibrosis.

Predominant expression of *Rasal1* occurs in kidney fibroblasts and of *Klotho* in tubular epithelial cells. Both cell types are separated by a basal membrane. Because it has been shown that lentiviral constructs do not cross basal membranes [42], we established different routes of lentiviral delivery to primarily target interstitial cells (via parenchymal injection) or epithelial cells (via the ureter). By these respective modes of injection we were able to specifically reactivate *Klotho* expression in tubular epithelial cells by dHFCas9-TET3CD-*Klotho*-sgRNA and *Rasal1* expression in interstitial cells by dCas9/dHFCas9-TET3CD-*Rasal1*-sgRNA constructs in the UUO mouse model of kidney fibrosis and to ameliorate kidney fibrosis. Interestingly, the therapeutic anti-fibrotic effect of dCas9-TET3CD-*Rasal1*-sgRNA construct was much smaller (less than 30% fibrosis reduction) as compared to the dHFCas9-TET3CD-*Rasal1*-sgRNA (almost 50% reduction in total interstitial fibrosis) despite a complete reactivation of *Rasal1* expression by both constructs. It appears likely that this is due to off-target effects of dCas9-TET3CD which reactivated pro-fibrotic genes *Anxa4*, and *Nlrp5* (off-targeted by dCas9-TET3CD but not by dHFCas9-TET3CD, Table 1) along with *Rasal1*, thus limiting the therapeutic effect and highlighting the need for the use of high-fidelity Cas9 in this context.

In general, by fusing dCas9 with the TET3 catalytic domain, we achieved superior specificity and reached a more extended region of demethylation from the target site as compared to previous Zinc finger and TALE-based approaches. Previous studies showed that TET3 mediates hydroxymethylation of cytosine bases (e.g., within the *Rasal1* promoter) followed by consecutive Tdg-mediated base excision, and subsequent replacement with naked cytosine [14]. siRNA-mediated depletion of Tdg effectively prevented *Rasal1* demethylation, suggesting that Tdg is needed for the return to baseline gene expression upon hydroxymethylation [14]. Our study is in line with previous reports which demonstrated gene-specific reactivation of epigenetically silenced genes within cultured cells using dCas9-p300, dCas9-LSD1, dCas9-VP64, and dCas9-TET1CD fusion constructs *in vitro* [28–30,43,44]. Unlike our approach those studies did not use an all-in-one fusion protein but two individual components, which are

only functional when both are delivered and expressed simultaneously in the same cell, thus thereby limiting their utility *in vivo*.

Our study is further in line with a very recent report, where a demethylating system based on dCas9 is fused to the repeating peptide GCN4, which recruits an anti-GCN4 single-chain variable fragment (scFv) fused to the effector domain of TET1CD [45]. This system was successfully introduced into the embryonic mouse brain by *in utero* electroporation and thereby reactivated expression of specific genes including *Gfap in vivo*. Our application is in contrast by lentiviral delivery and is made possible through a considerably smaller size of the construct in our study as compared to constructs utilized in that study and thus presents a more feasible therapeutic approach *in vivo* as compared to electroporation-based gene delivery. Thus, although there are previous reports with respect to gene-specific demethylation both *in vitro* and *in vivo*, to our knowledge, this study is the first to describe an effective CRISPR-based epigenetic therapy in a disease model. Unlike all previously published reports where only catalytic domain of TET1 or TET2 have been fused with DNA-binding domains ZNF, TALE, or dCas9 [25,26,45], to our knowledge we are the first to validate gene-specific demethylation by TET3CD by the use of dCas9-TET3CD.

Even more importantly, none of the previous studies used a high-fidelity Cas9. Off-target effects largely hinder the utility of CRISPR/Cas9 technology therapeutically. Through substitution of four amino acids, Kleinstiver and his colleagues developed a high-fidelity Cas9, which abolishes the redundant energetics of SpCas9-sgRNA with the consequence of diminished off-target effects [41]. Thus, as long as number of off-target genes is kept low through the use of HFCas9, adverse effects of our strategy in cells other than the target cells are unlikely since only methylated genes which were originally actively transcribed within target cells can be reactivated. This provides a conceptual advantage over other therapies based on e.g. AAV-delivered overexpression constructs where the targeting of specific cell types still remains a challenge.

ACKNOWLEDGEMENTS

This work was supported by DFG grants SFB1002/C01 (to E.M.Z.) and DFG ZE523/4-1, SFB1002/D03 (to M.Z.) and funds from the University of Göttingen Medical Center (UMG) to E.M.Z. and M.Z. X.X. received support from the “seed funding research program” of the Faculty of Medicine, Georg August University Göttingen and postdoc start-up grant, DZHK. This work was further supported by the German Ministry of Research and Education (BMBF) through the DZHK (German Centre for Cardiovascular Research). The authors thank Dr. Wanhua Xie for helping with ChIP-sequencing data analysis and Annika Faust, Sarah Rinkleff, and Anika Krueger for technical assistance.

MATERIALS AND METHODS

PLASMIDS

The sgRNA sequences (*RASAL1*, *EYA1*, *LRFN2*, *KL*, *Rasal1*, and *Kl*) were designed by the online tool Blueheronbio (Origene, Herford, Germany). The control *LacZ* sgRNA sequence was the same as previously used³⁸. The sgRNA sequences (Supplementary Table 1) were inserted into the pLenti-Cas-Guide plasmid (Origene, Herford, Germany) with BamHI and BsmBI restriction sites to generate pLenti-Cas-sgRNA (*RASAL1*, *EYA1*, *LRFN2*, *KL*, *Rasal1*, and *Kl*) constructs and confirmed by DNA sequencing. The wild-type Cas9 open reading frame was removed from the vector with Age1 and Not1 restriction sites. The plasmids encoding H840A SpCas9 and encoding high-fidelity SpCas9-HF4 were gifts from Jennifer Doudna and Keith Joung, respectively (Addgene plasmids #39316 [46] and #72249 [41].) The pLenti-dCas9-sgRNA gene demethylation constructs were generated by cloning H840 SpCas9 in frame into the digested pLenti-sgRNA vectors by PCR using Phusion high-fidelity DNA polymerase (NEB, Ipswich, USA) with Age1 (5') and Xba1, Not1 (3') restriction sites with two NLS (nuclear localization signal) peptides at the N- and C-terminus each with a primer pair that introduced the D10A mutation [30] (Supplementary Table 6). The TET3CD (catalytic domain, aa850-1795) [24] was amplified from a human TET3 ORF (Origene, Herford, Germany) with a primer pair which introduced Age1, a start codon, Xba1, a Gly-Gly-Gly-Ser-Gly linker (5'), and Not1 (3') and then inserted into the digested pLentidCas-*LacZ* vector to generate pLenti-dCas9-TET3CD-*LacZ*. The sequence and the coding frame for dCas9 and for TET3CD were confirmed by DNA sequencing and by western blot (Supplementary Fig. 1). The final constructs pLenti-dCas9-TET3CD-sgRNA (*RASAL1*, *EYA1*, *LRFN2*, *KL*, *Rasal1*, and *Kl*) were generated by removing TET3CD from pLenti-dCas9-TET3CD-*LacZ*, subsequently inserted into pLenti-dCas9-sgRNA (*RASAL1*, *EYA1*, *LRFN2*, *KL*, *Rasal1*, and *Kl*) with Xba1 and Not1 restriction sites. The primer sequences used for PCR cloning are listed in Supplementary Table 2.

DNA ISOLATION, MEDIP and HMedIP ASSAY

Animal tissues or cell pellets were lysed by DNA lysis buffer (Qiagen, Hilden, Germany) and precipitated and purified using DNeasy Blood & Tissue Kit (Qiagen, Hilden, Germany) according to the manufacturer's protocol. Prior to immunoprecipitation, genomic DNA was sonicated (Qsonica, Newtown, USA) to produce DNA fragments ranging in size from 200 to 1000 bp, with a mean fragment size of around 300 bp. Methylated DNA was captured using Methylamp Methylated DNA Capture Kit (Epigentek, Farmingdale, USA). In total 1.0 µg of fragmented DNA was applied in every antibody-coated well and incubated at room temperature on a horizontal shaker for 2 h. The immunoprecipitated DNA was released by proteinase K. The DNA was eluted and adjusted to a final volume of 100 µl with nuclease-free water. For each sample, an input vial was included using total sonicated DNA as loading control. Hydroxymethylated DNA was captured using EpiQuick Hydroxymethylated Immunoprecipitation (hMeDIP) Kit (Epigentek, Farmingdale, USA) according to the manufacturer's protocol. A volume of 0.5 µg of sonicated DNA was added to each antibody-coated well and incubated at room temperature on a horizontal shaker for 90 min. The immunoprecipitated DNA was released by proteinase K. The DNA was eluted and diluted to a final volume of 200 µl with nuclease-free water. For each sample, an input vial was included using total sonicated DNA as loading control. The primer sequences used for MeDIP/hMeDIP-qPCR cloning are listed in Supplementary Table 3.

GLUCOSYLATION-MEDIATED RESTRICTION ENZYME SENSITIVE PCR

The EpiMark Kit (NEB, Ipswich, USA) was used to validate the conversion from 5'mC to 5'hmC at the selected *RASAL1* promoter region. The assay was performed according to the manufacturer's protocol. Briefly, 10 µg of genomic DNA was used and equally divided into two reactions, one treated with T4-phage βGT at 37 °C for 12 h, the other one was kept as untreated control. Both the βGT-treated and untreated samples were then divided into three PCR tubes and digested with either MspI, HpaII, or left uncut at 37 °C for an additional 12 h. Samples were treated with proteinase K at 40 °C for 10 min prior to dilution to a final volume of 100 µl with nuclease-free water and heating to 95 °C for 5 min.

PCR was carried out in a volume of 5 μ l for each sample on a PCR cycler (Eppendorf, Hamburg, Germany) with a standard PCR program. The primer sequences used for PCR are listed in Supplementary Table 4. To visualize the PCR products, samples were loaded into the Bioanalyzer 2100 electrophoresis system (Agilent Technologies, California, USA). Electrophoresis results are shown as a virtual gel as previously described [47].

BISULFATE SEQUENCING

Purified cellular DNA was bisulfite-treated using the EZ DNA Methylation-Lightning Kit (Zymoresearch, Irvine, USA) according to the manufacturer's protocol. To amplify the *Rasal1* and *Kl* promoter fragments, a touchdown PCR program was performed using Taq DNA Polymerase (Sigma-Aldrich, St. Louis, USA). The first round of PCR consisted of the following cycling conditions: 94 °C for 2 min, 6 cycles consisting of 30 s at 94 °C, 30 s at 60–55 °C (reduce 1 °C after each cycle), and 30 s at 72 °C. The second round of PCR consisted of the following cycling conditions: 32 cycles consisting of 30 s at 94 °C, 30 s at 55 °C, and 30 s at 72 °C. The final elongation consisted of 72 °C for 6 min. The sequences of the PCR primers are listed in Supplementary Table 5. The PCR products were purified using the QIAEX II Gel Extraction Kit (Qiagen, Hilden, Germany), cloned into the pGEM-T Vector (Promega, Wisconsin, United States) and transformed into Top10 Competent E.coli Cells (Life Technologies, Carlsbad, USA). The plasmid DNA was then purified with DNA Plasmid Miniprep Kit (Qiagen, Hilden, Germany) and sequenced (Seqlab, Göttingen, Germany).

CELL CULTURE AND TRANSFECTION

TK173 and TK188 kidney fibroblasts were isolated from human kidney biopsies [4]. HEK293 and HK2 cells were purchased from ATCC (Teddington, UK). Mouse kidney fibroblasts were generated in our lab. Murine MCT cells were kindly provided by Dr. Eric G. Neilson (Northwestern University, Evanston, IL). Human TK188, HK2, HEK293, 293 T, MCT, and mKF (passages between 3 and 5) were cultured in DMEM (Gibco, Carlsbad, USA) supplemented with 2 mmol/l L-glutamine, 100 g/ml penicillin, 100 g/ml streptomycin and 10% heat-inactivated fetal bovine serum (FBS, Cellgro, Manassas, USA) at 37 °C in 5% CO₂. For

transfection experiments, cells were pre-plated and cultured overnight and transfected with Lipofectamine 2000 (Life Technologies, Carlsbad, USA) according to the manufacturer's protocol. Briefly, the plasmid DNA (2.5 µg each) and Lipofectamine 2000 were mixed in a ratio of 1:2 in a total volume of 500 µl of Opti-MEM (Life Technologies, Carlsbad, USA) and incubated at room temperature to form complexes for 20 min. The transfection complex was added to the cells in basic medium without serum. After overnight incubation, the medium was replaced back to complete growth medium.

CHROMATIN IMMUNOPRECIPITATION-NEXT GENOMIC SEQUENCING

ChIP assay was performed using 1 Day ChIP kit and Shearing ChIP kit (Diagenode, Denville, USA) according to the manufacturer's protocol. After lentiviral transduction and crosslinking, mouse kidney fibroblasts were fixed with formaldehyde and the DNA was sheared into small fragments. After incubation with a Myc-tag antibody (Cell signaling, Beverly, USA), the pulled-down complexes were de-crosslinked and treated with proteinase K. The purified DNA samples were proceeded further for library preparation by TruSeq RNA Library Prep Kit v2 (Illumina, USA) and quality control and library validation were performed by Fragment Analyzer and Kapa PCR (Illumina, USA), respectively. The fragments were sequenced by an Illumina HiSeq4000 instrument. For data analysis, a previous established protocol [48] was followed. Briefly, the raw reads from two independent biological replicates were first concatenated and then peak calling was performed with MACSII in order to obtain the count numbers. We used settings for narrow peaks (200 bp window size, 200 bp gap size, and false discovery rate of 0.01) in all cases.

VIRUS PACKAGING AND TITRATION

Lentiviruses were produced using 293 T virus packaging cells upon transfection with a combination of 2nd Generation Packaging System Mix (Abmgood, Richmond, Canada), pLenti-dCas9-TET3CD-sgRNA (*RASAL1*, *EYA1*, *LRFN2*, *KL*, *Rasa1*, and *Kl*), and Lentifectin (Abmgood, Richmond, Canada) according to the manufacture's protocol. Lentiviral supernatant was collected 2 and 3 days after transfection, filtered through a 0.45 µm filter and concentrated

with Lenti-X Concentrator (Clontech, Heidelberg, Germany). The viral particles were resuspended in PBS and stored at -80°C . Lentivirus titration was determined by the Lenti-X qRT-PCR Titration Kit (Clontech, Heidelberg, Germany) and $8\ \mu\text{g}/\text{ml}$ Polybrene (Sigma- Aldrich, Munich, Germany) was added to the viral solution for the *in vivo* and *in vitro* transduction experiments.

RASAL1 MUTANT MOUSE PRODUCTION

Two different mouse embryonic stem cell clones (A03, H03) carrying targeted gene knockout alleles were received from EUCOMM international knockout mouse consortium. Stem cells were from the JM8 line on a C57BL/6 N genetic background reference. The targeted *Rasal1*^{tm1a(KOMP)WTSI} allele carried a gene-trap DNA cassette, inserted into the second intron of the gene, consisting of a splice acceptor site, an internal ribosome entry site, and a β -galactosidase reporter. The use of the splice acceptor site is purposely to generate a truncated non-functional transcript. After confirming the correct genome targeting by long range PCR (Supplementary Fig. 12a), *Rasal1* mutant ESCs were injected into blastocysts to generate chimera mice which were further bred with C57BL/6 N mice to generate *Rasal1*^{tm1a/+} mice. Homozygous *Rasal1*^{tm1a/tm1a} mice were then generated by inbreeding (Supplementary Fig. 12b). Copy number variation analysis of *Rasal1*^{tm1a} mouse kidneys confirmed that mutant mice carried the correct copy number of gene-trap DNA cassette (Supplementary Fig. 12c). The sequence of primers used for characterizing the *Rasal1*^{tm1a/+} mice are listed in Supplementary Table 6. Mice were euthanized at 12–14 weeks of age under isoflurane anesthesia with cervical dislocation. Tissues were rapidly harvested and quick-frozen in liquid nitrogen, and stored at -80°C . All animal work followed the Guide of the Institutional Review Board of the University of Göttingen and the responsible government authority of Lower Saxony (Germany).

UNILATERAL URETERAL OBSTRUCTION

All animal experiments complied with ethical regulations and were conducted according to the animal experimental protocols which were approved by the Institutional Review Board of the University of Göttingen and the responsible government authority of Lower Saxony (Germany). Eight-to-twelve-week-old

wild-type C57BL/6 N mice were used for the study. After anesthesia with isoflurane inhalation, analgesia was performed by subcutaneous Buprenorphine injection. The ureter was separated from the surrounding tissues and the left ureter was clamped distal to the infusion site by two ligatures [14]. The abdominal muscles were sutured with absorbable suture, and the skin was closed with non-absorbable suture [49,50]. Mice were sacrificed 10 days after ureter ligation and viral solution injection. The UUO-operated and the contralateral kidney were removed for histological analysis.

INTRARENAL ARTERY/VEIN INFUSION

After anesthesia, the aorta, inferior vena cava, and the right renal vessels were visualized through a midline incision. After completing the UUO surgery, the left renal artery/vein was clamped and the renal artery/vein was cannulated with a 27-gauge needle. Either control *LacZ*-sgRNA or *Rasal1/Kl*-sgRNA lentiviral solution (80 μ l about 1×10^8 TUs) was slowly injected under gentle pressure to avoid leaking of the injection solution. As the needle was removed, a clamp was placed around the renal artery to trap the solution in the kidney. Blood flow was stopped for 15 min and then the clamps were removed, thus restoring blood flow to the kidney.

RETROGRADE URETERAL INFUSION

Upon completion of the UUO surgery, the left ureter-pelvic junction was cannulated with a 27-gauge needle. Viral solution (80 μ l about 1×10^8 TUs) was infused under gentle pressure to avoid renal pelvic distention and leaking of the viral solution.

INTRAPARENCHYMAL INJECTION

Once completing the UUO surgery, the left kidney was locally injected with viral solution (80 μ l about 1×10^8 TUs in total) into four different sites.

HISTOLOGY AND IMMUNOFLOUORESCENCE

Paraffin-embedded kidneys were sectioned at 3 μm and Masson's Trichrome Stain (MTS) was performed. We assessed the fibrotic area using CellSens (Olympus, Tokyo, Japan) software, as previously described [14]. For immunofluorescent staining, primary antibodies against α -smooth muscle actin (1:100 diluted, Abcam, Cambridge, UK), Collagen-1 (1:100 diluted, Abcam, Cambridge, UK), and Collagen-4 (1:100 diluted, BD/Pharmingen, San Diego, USA), and Alexa Fluor 488, 568 (1:300 diluted, Life Technologies, USA, Carlsbad, USA) secondary antibodies were used. Nuclear staining was performed using 4', 6-diamidino-2-phenylindole (DAPI, Vector Labs, Burlingame, USA). Relative areas positive for α -SMA and Collagen-1 per visual fields were analyzed at magnification $\times 40$.

RNA EXTRACTION, CDNA SYNTHESIS, AND REAL-TIME PCR ANALYSIS

Animal tissues were shredded by TissueLyser LT (Qiagen, Hilden, Germany). Total RNA was extracted from the shredded tissues or cells by direct lysis with TRIzol reagent (Life Technologies, Carlsbad, USA) and RNA isolation was performed using the Pure-Link RNA Mini Kit (Life Technologies, Carlsbad, USA) according to the manufacturer's protocol. For first-strand cDNA synthesis, 1 μg of total RNA was treated with DNase I (Sigma- Aldrich, Munich, Germany) and then converted into complementary DNA (cDNA) using the SuperScript II System (Life Technologies, Carlsbad, USA). For qRT-PCR analysis, 2 μl of diluted cDNA (1:10) as a template and the Fast SYBR Green Master Mix (Life Technologies, Carlsbad, USA) were used in a final volume of 20 μl for each reaction. Real-time PCR was performed in triplicate in a 96-well format by StepOne Plus Real-Time PCR system (Life Technologies, Carlsbad, USA). The real-time PCR primers are listed in Supplementary Table 7. The relative expression levels were standardized to GAPDH using $2^{-\Delta\Delta\text{Ct}}$ methods.

WESTERN BLOT

Animal tissues were shredded by TissueLyser LT (Qiagen, Hilden, Germany). The shredded tissues and cells were lysed in NP40 buffer (Life Technologies, Carlsbad, USA) containing protease inhibitor cocktail (Roche, Mannheim, Germany). Lysates were mixed with loading buffer and heated at 95 $^{\circ}\text{C}$ for 5 min.

Protein samples were resolved on 4–12% SDS–PAGE gels (Life Technologies, Carlsbad, USA) and transferred onto nitrocellulose membranes (GE Healthcare, Freiburg, Germany). Non-specific antibody binding was blocked with 5% nonfat milk in TBST buffer (50mM Tris/150mM NaCl/0.1% Tween-20) for 1 h. The membranes were incubated with primary antibodies in incubation solution (2% milk in TBST) overnight. Myc-tag antibody (Cell Signaling #5605, Danvers, USA) was diluted 1:2500; Tubulin antibody (Sigma-Aldrich #T5168, Munich, Germany) was diluted 1:5000; RASAL antibody (Abcam #ab168610, Cambridge, UK; Biorbyt #orb101674, Cambridge, UK) was diluted 1:1000. The membranes were washed three times with 2% milk in TBST and incubated with HRP conjugated secondary antibody for 1 h. Membranes were visualized using LumiGLO chemiluminescence (Cell Signaling, Danvers, USA) and images were documented by a ChemiDoc MP System and processed using ImageLab software (Bio-Rad, Munich, Germany). All uncropped blots are included in Supplementary Fig. 13.

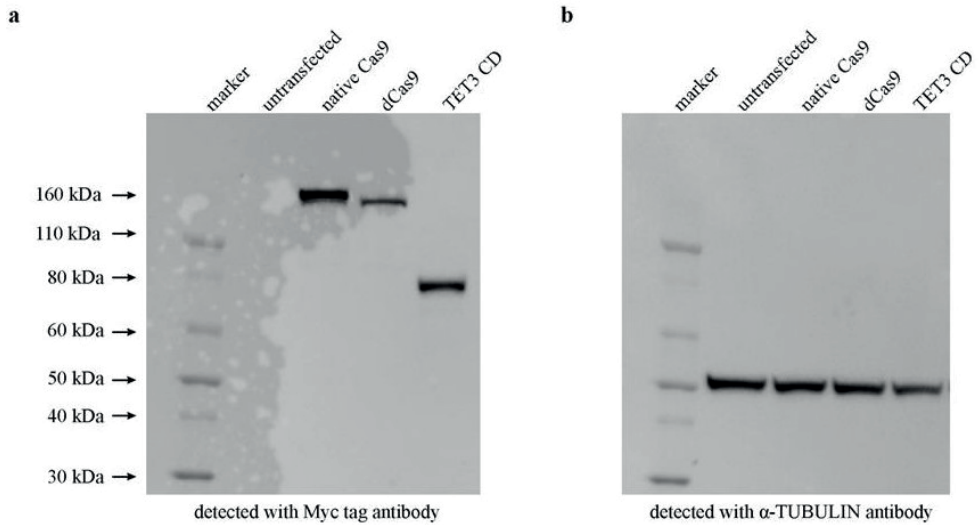
STATISTICAL ANALYSIS

All qRT-PCR data for RNA expression analysis are presented as the mean \pm SD and represent a minimum of three independent experiments. As for MeDIP-qPCR, two biological replicates with three technical replicates each were analyzed, and the average of six values was used for further statistical analysis. Histological analysis was assessed as 10 visual fields per mouse and average values of each mouse were calculated. The average values for each mouse ($n = 6$) was then used to calculate average per group. Statistical analysis was then performed on these averages using One-way ANOVA with Bonferroni post-hoc analysis comparing selected pairs of columns.

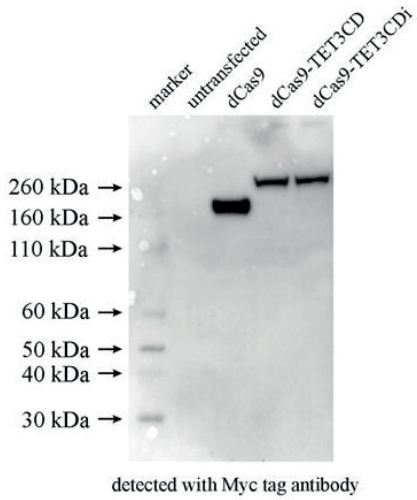
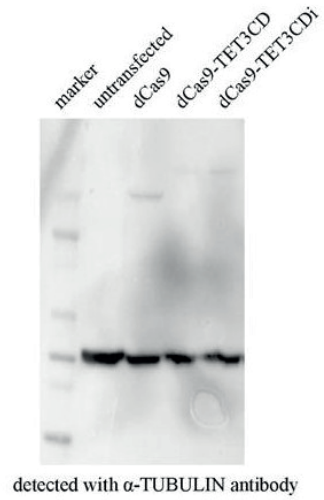
DATA AVAILABILITY

The authors declare that all relevant data supporting the findings of this study are available within the paper and its supplementary information files. All the figures and graphics were created by the authors. Complete ChIP-sequencing data has been deposited in BioProject <https://submit.ncbi.nlm.nih.gov/subs/bioproject/SUB3776305/biosample> with accession number [SUB3776305].

SUPPLEMENTARY INFORMATION

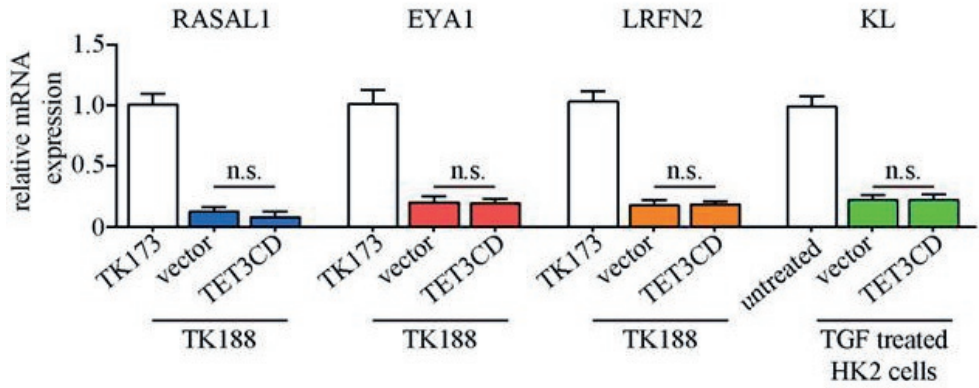
**Supplementary Figure 1. Expression of mutated Cas9 protein and TET3 catalytic domain.**

(a) Western blot analysis showing the expression of native and mutated Myc-tagged Cas9 (dCas9) protein as well as human TET3 catalytic domain by Myc antibody in HEK293 cells. (b) Untransfected cells served as negative control. The membrane was restripped and re-probed with anti-TUBULIN antibody to serve as loading control.

a**b**

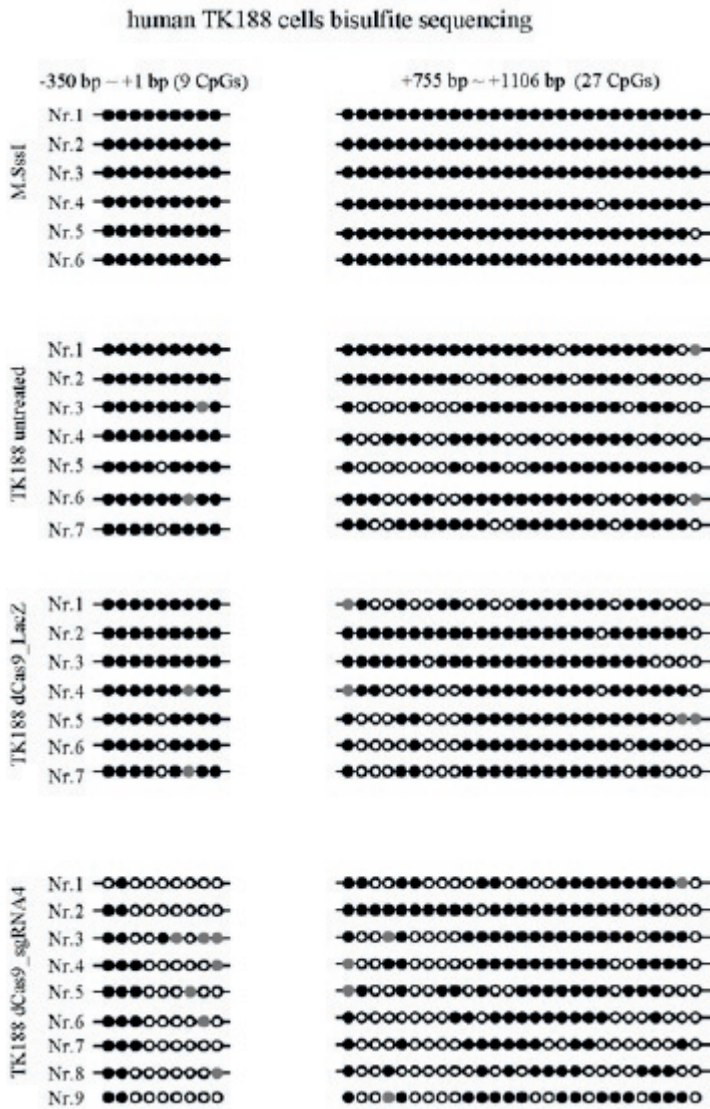
Supplementary Figure 2. Expression of dCas9, dCas9-TET3CD or dCas9-TET3CDi fusion proteins in HEK293 cells.

(a) Western blot analysis showing the expression of dCas9, dCas9-TET3CD or dCas9-TET3CDi fusion proteins by Myc antibody in HEK293 cells. Untransfected cells served as negative control. (b) The membrane was restriped and re-probed with anti-TUBULIN antibody to serve as loading control.



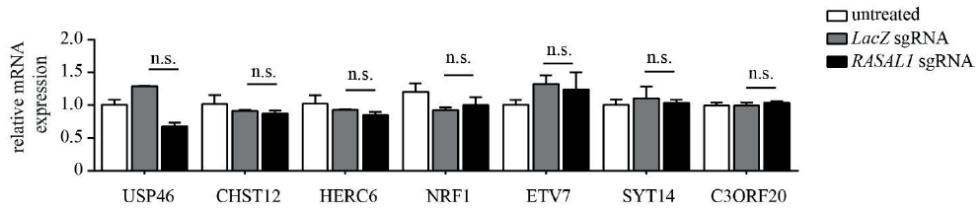
Supplementary Figure 3. Overexpression of TET3 catalytic domain does not restore the expression of 4 different aberrantly methylated genes.

qRT-PCR results showing that only overexpression of TET3 catalytic domain does not induce the expression of 3 different aberrantly methylated genes RASAL1, EYA1, LRFN2 in TK188 fibrotic human kidney fibroblasts and does not induce the expression of KL in TGF β 1-treated HK2 cells. Results were normalized to reference gene GAPDH (expression is presented as mean value; error bars represent S.E.M.; n=3 independent biological replicates).



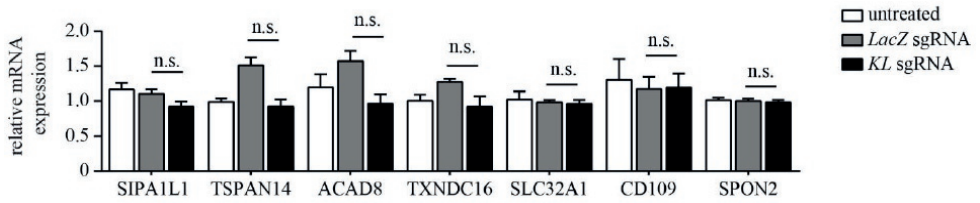
Supplementary Figure 4. Sanger sequencing of bisulfite PCR products of RASAL1 promoter region in TK188 cells.

Bisulfite sequencing analysis showing the methylation status of CpGs in two different regions (region 1: from -350 bp to +1 bp; region 2: from + 755 bp to +1106 bp) within the RASAL1 promoter in TK188 cells transduced with lentivirus expressing dCas9-RASAL1-sgRNA and control dCas9-LacZ-sgRNA constructs. M.SssI treated cell genomic DNA served as bisulfite conversion control. Each panel shows at least six different sequencing results derived from three independent biological replicates. Closed circles indicate methylated, open circles indicate un-methylated and grey circles indicate undetermined CpGs.



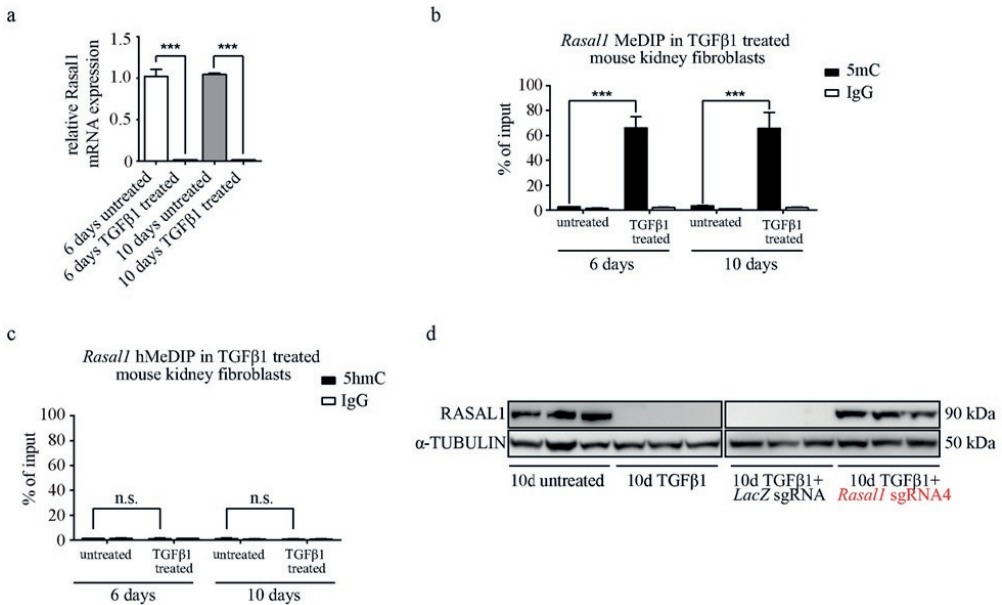
Supplementary Figure 6. Assessment of the off-target effects of the dCas9-TET3CD-RASAL1-sgRNA3 demethylation in TK188 cells.

Human fibrotic TK188 cells were transduced with lentivirus expressing demethylation constructs guided by RASAL1-sgRNA3 or by LacZ-sgRNA. The mRNA expression of predicted off-target genes was assessed by qRT-PCR analysis, but there is a not significant difference between RASAL1-sgRNA3 and LacZ-sgRNA transduced cells for all tested genes. Results were normalized to reference gene GAPDH (expression is presented as mean value; error bars represent S.D.; $n = 3$ independent biological replicates; n.s., not significant).



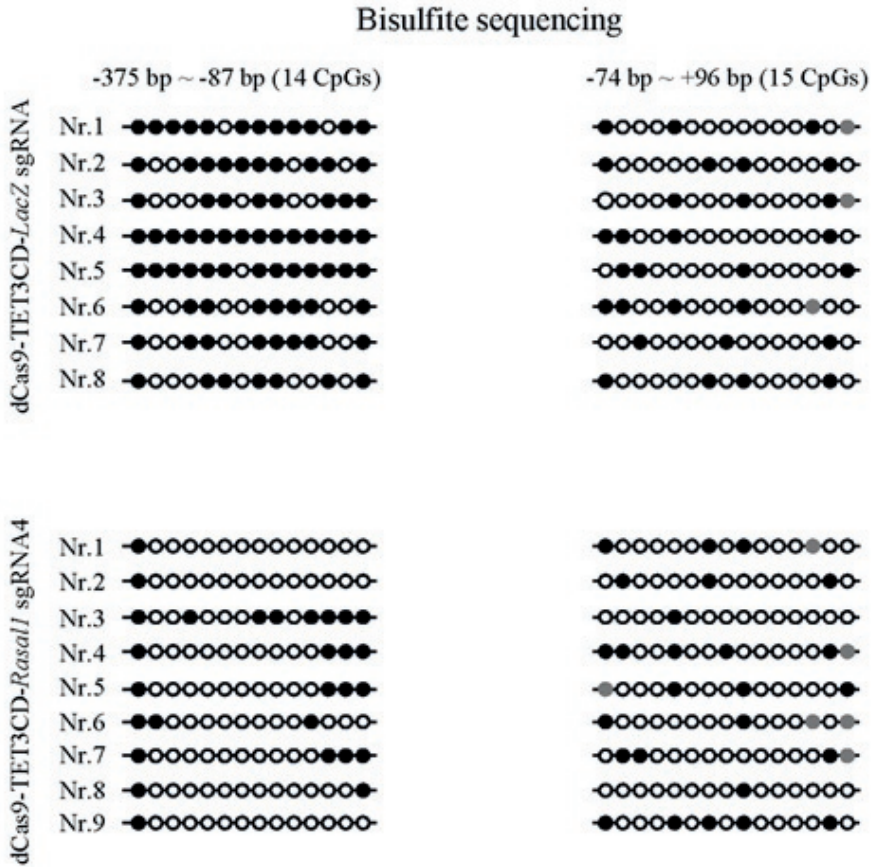
Supplementary Figure 7. Assessment of the off-target effects of the dCas9-TET3CD-KL-sgRNA2 demethylation in HK2 cells.

TGFβ1-treated HK2 cells were transduced with lentivirus expressing demethylation constructs guided by KL-sgRNA2 or by LacZ-sgRNA. The mRNA expression of predicted off-target genes was assessed by qRT-PCR analysis, but there is no significant difference in gene expression between KL-sgRNA2 and LacZ-sgRNA transduced cells for all tested genes. Results were normalized to reference gene GAPDH (expression is presented as mean value; error bars represent S.D.; n = 3 independent biological replicates; n.s., not significant).



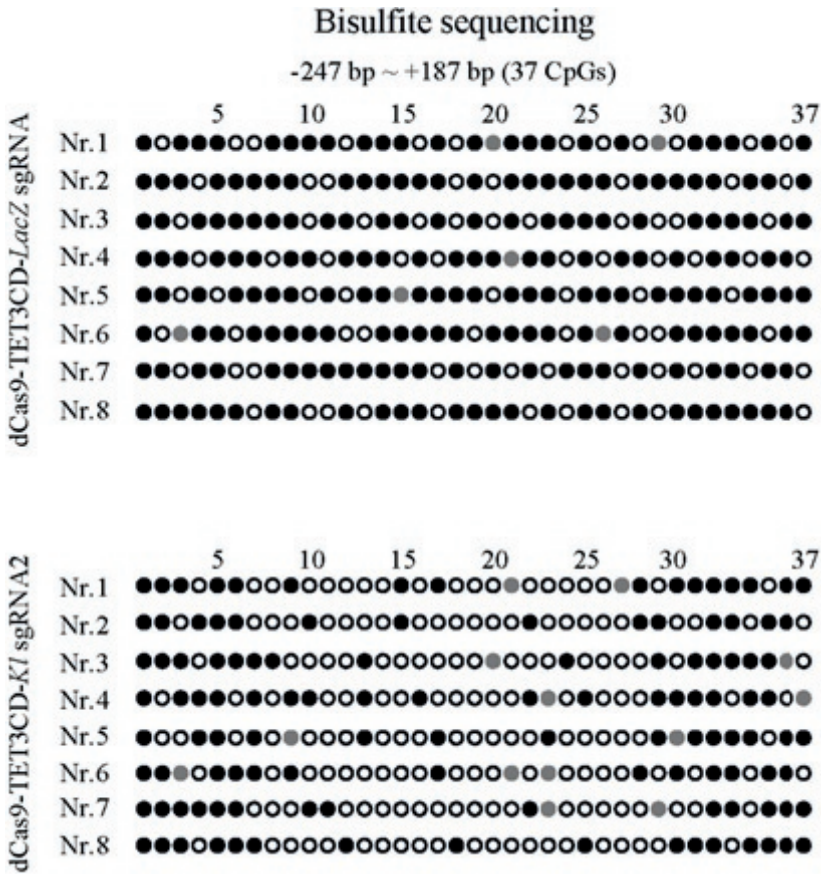
Supplementary Figure 8. TGFβ1 induces decreased Rasal1 expression through promoter hypermethylation in mKF.

(a) Mouse kidney fibroblasts (mKF) were treated with TGFβ1 for 6 and 10 days. The Rasal1 mRNA expression was analysed by qRT-PCR assay. Results were normalized to reference gene *Gapdh* (expression is presented as mean value; error bars represent S.D.; n = 3 independent biological replicates; ***, p < 0.001). (b) MeDIP-qPCR analysis showing a significant increase of Rasal1 promoter methylation in TGFβ1-treated mKF compared to non-treated control mKF. The results were calculated relative to input. The data is presented as mean value; error bars represent S.D.; n=3 independent biological replicates; ***, p < 0.001. (c) hMeDIP-qPCR analysis shows no significant change in Rasal1 promoter hydroxymethylation levels in TGFβ1-treated mKF in comparison to non-treated control mKF. (d) Western blot analysis shows the restored RASAL1 protein expression in TGFβ1-treated mKF which are transduced with lentivirus expressing Rasal1-sgRNA but not with control LacZ-sgRNA.



Supplementary Figure 9. Sanger sequencing of bisulfite PCR products of Rasal1 promoter region in TGFβ1-treated mKF.

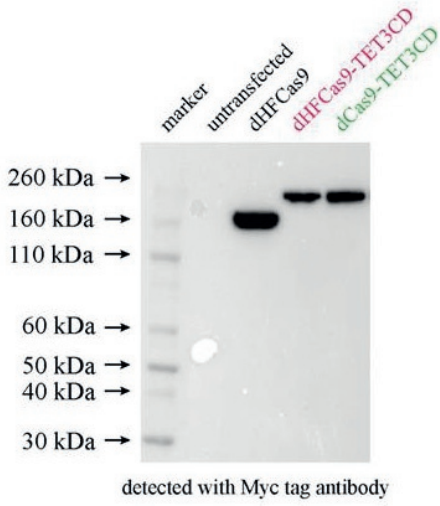
Bisulfite sequencing analysis showing the methylation status of CpGs in two different regions (region 1: from -375 bp to -87 bp; region 2: from -74 bp to +96 bp) within the Rasal1 promoter in TGFβ1-treated mKF transduced with lentivirus expressing dCas9-Rasal1-sgRNA4 and control dCas9-LacZ-sgRNA constructs. Each panel shows at least six different sequencing results derived from three independent biological replicates. Closed circles indicate methylated, open circles un-methylated and grey circles undetermined CpGs.



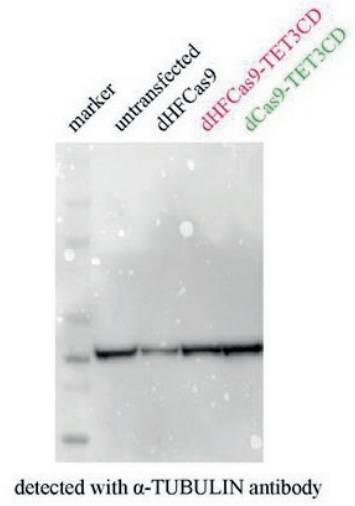
Supplementary Figure 10. Sanger sequencing of bisulfite PCR products of Klotho promoter region in TGFβ1-treated MCT cells.

Bisulfite sequencing analysis showing the methylation status of CpGs in Klotho promoter regions from -247 bp to +187 bp in TGFβ1-treated renal tubular epithelial cell (MCT) cells transduced with lentivirus expressing pLenti-dCas9-Klotho-sgRNA2 and control pLenti-dCas9-LacZ-sgRNA constructs. Each panel shows at least six different sequencing results derived from three independent biological replicates. Closed circles indicate methylated, open circles un-methylated and grey circles undetermined CpGs.

a

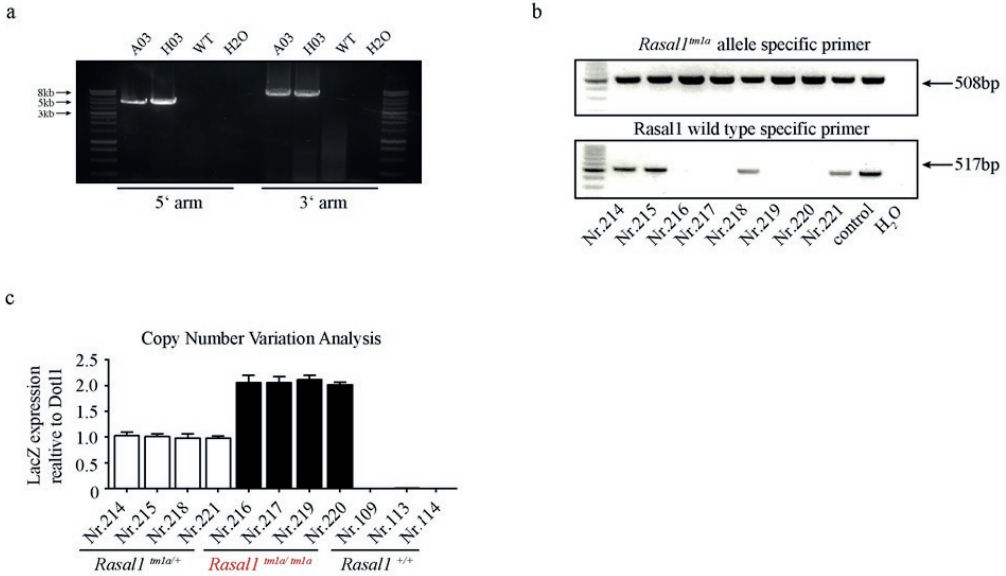


b



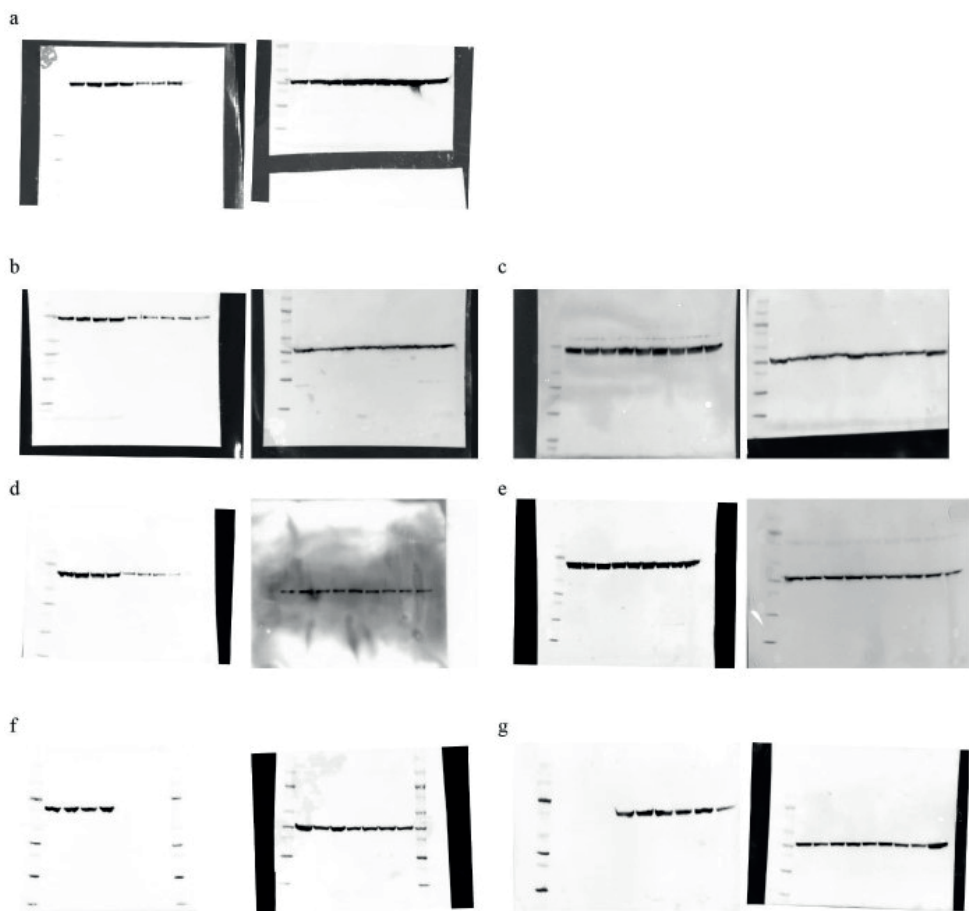
Supplementary Figure 11. Expression of dHFCas9, dHFCas9-TET3CD in HEK293 cells.

(a) HEK293 cells were transfected with dHFCas9, dHFCas9-TET3CD or dCas9-TET3CD constructs and detected with Myc antibody. Untransfected cells served as negative control. (b) The membrane was restripped and re-probed with anti-TUBULIN antibody to serve as loading control.



Supplementary Figure 12. Characterization of *Rasal1tm1a/tm1a* mutant mice.

(a) Agarose gel picture shows the expected size of long-range PCR products from *Rasal1tm1a* mutant ES cells (2 different clones A03, H03) tested from both 5' and 3' directions. (b) Agarose gel picture shows the genotyping PCR products from genomic DNA of *Rasal1 tm1a* homozygous and heterozygous mice. (c) qRT-PCR analysis shows the copy number variation in *Rasal1 tm1a* mice assayed with a *LacZ* probe. Results were normalized to reference gene *Dot11* (expression is presented as mean value; error bars represent S.D.).

**Supplementary Figure 13. Uncropped Western blots.**

(a) Original Western blots for Main Figure 3c, RASAL1 protein (left) and α -TUBULIN protein (right).
(b-e) Original Western blots for Main Figure 5d, RASAL1 protein (left) and α -TUBULIN protein (right).
(f-g) Original Western blots for Supplementary Figure 8d, RASAL1 protein (left) and α -TUBULIN protein (right).

Supplementary Table 1: DNA sequences used for guiding RNA

Human		Mouse	
Name	Sequence	Name	Sequence
RASAL1		Rasal1	
sgRNA1	CAAAGCACAGAGAGGTTGAA	sgRNA1	CATGACATACAGAGTTGCCGAGG
sgRNA2	ATCCATAAACTGCGGATAATGGG	sgRNA2	CGCAGTGGCAGCCGGTGACGTGG
sgRNA3	ACTTTTTATCATCGCTGTAGTGG	sgRNA3	GCCCAGAGAGAGTACTGTTCCGG
sgRNA4	GGAACATGCGACCTCTCTCTGG	sgRNA4	GAGACACCCGGGTTCTTGAGGG
sgRNA5	AAGCCCAATGCCAACTCACCAGG	sgRNA5	CGAACACTTAACCAAGTCCAGG
sgRNA6	ACTGTTCTAAGCGCTTACTGGG	sgRNA6	TTAAACCCGGAGTGTGCCAGCGG
sgRNA7	CACTGCGGGGAGGAAGCCGCGG	sgRNA7	CAACACCAGCCTCGGGGTCCCGG
sgRNA8	GGTCCAGGAGCAAGTATTAGTGG	sgRNA8	GAGCAGTCAAGCAGGGCTGCAGG
sgRNA9	GGCATTGGGCTTAAAGACATGG		
sgRNA 10	AGTACTCACACGTCCTTGCCAGG		
EYA1			
sgRNA1	AGCTGTTTATTCAGATAGCGTGG		
sgRNA2	TTAGGACAAGAGAATAGCTGTGG		
sgRNA3	TCTGCCGCTGCTGTTTGGTGGGG		
sgRNA4	AGAATAACTTCTCTGAGACGTGG		
sgRNA5	ATTTGTTTGCGCAGCCTGTAGG		
sgRNA6	TCAGCTCCCACCGTTCTGTTGG		
LRFN2			
sgRNA1	CCCACCTCCCTCCGCGACTGCGG		
sgRNA2	CTTCGGCTCCTGCAGCTCCGCGG		
sgRNA3	CGCCCGACTCCCTCCAGATTGG		
sgRNA4	ATGCCTGGGGTTCTTCGATCCGG		
sgRNA5	AACACCGCCGCGAAACCAGAGG		
sgRNA6	GCCAGAGGCGCCAGGAACCCGG		
sgRNA7	TCAAGTTCAGACGAGCCTGCCGG		
sgRNA8	TGGCATTTAGCAAGAAGAAGGGG		
KL		KI	
sgRNA1	CTCCCGACGAAGCCGCTCCAGG	sgRNA1	CTCCCTGAGCTGGCTGCAGCAGG
sgRNA2	TCGCAGTAATTATTGCCAGCGG	sgRNA2	TGTGCTCTCTCTGGGCACCCTGG
sgRNA3	TTCCAGGGCACCTTCCCGACGG	sgRNA3	CCCCCGTGCAGGCCGGAGTGGG
sgRNA4	TACGTTACCCACCACCCCTGG	sgRNA4	AGCGGGGTGGGCACCGCTAGG
sgRNA5	CGTCCCCGGCGGGCTCCGCTGG	sgRNA5	CGCTGCCTGAGCGCTGAGCCGGG
sgRNA6	ACCAGCAGCAGCGACAGCGACGG	sgRNA6	GCTCCTGCCAGAGGCCGCTGG
sgRNA7	CCAGAGGAAGCCGTCGGGGAAAGG		
sgRNA8	GACGTTGTTGTAGCTGTCGCTGG		

Supplementary Table 2: Primer sequences used for PCR cloning

Name	Sequence
Cas9 cloning primer	
NlsmutCas9_F	TTAAACCGGTGAGGAGATCTGCCGCCGCGATCGCCATGGCGCCGAAAAAAA AACGCAAAGTGGGCCGCGGCATGGATAAGAAATACTCAATAGGCTTAGCTA TCGGCACAATAGCGTCGGAT
NlsmutCas9_R	TTAAGCGGCCGCTTCTAGACACTTTGCGTTTTTTTTTCGGGTCACCTCCTAG CTGACTCAAATC
TET3 catalytic domain cloning primer	
hTet3CDAge1Xba1_F	TTAAACCGGTATGTCTAGAGGCGGAGGCTCGGGCTATTATACTCACTTGGGA TCTGGCCCA
hTET3CD_R1	TTAAGCGGCCGCTAGCCCCAACAGCTTCTCGCTGGAT
TET3 catalytic domain mutation primers	
hTET3CDTM_F	TGTGCCACGCCTACAAGGCCAGCATAAC
hTET3CDTM_R	GAAGTCCATGCAGGCCGTGACCC

Supplementary Table 3: MeDIP/hMeDIP primer sequences

Name	Sequence	Reference
Human MeDIP/hMeDIP primer		
hRasal1_MeDIP_F1	GCCAACTCACCAGGAGCCAGCGGC	Tampe et al., <i>Ebiomedicine</i> , 2015
hRasal1_MeDIP_R1	CTACCGGCACCCAGTCATGCGC	Tampe et al., <i>Ebiomedicine</i> , 2015
hKL_MeDIPF1	CCAGTCCCTAATTGGCTCCA	
hKL_MeDIPR1	GACCAACTTCCCGACTTG	
Mouse MeDIP/hMeDIP primer		
mRasal1_MeDIP_F1	TGCAGATGGCTCTTATCGTG	
mRasal1_MeDIP_R1	CCAATTAACCCGGAGTGTG	
MeDIP_mKL_F1	AAACCTCGCAAAGTCCACC	
MeDIP_mKL_R1	CAGAAACAGCTGCCCACTT	

Supplementary Table 4: Primer sequences used for RASAL1 gRES PCR

Name	Sequence
<i>RASAL1</i> gRES-PCR primers	
hRasal1_EpiMrkF1	ACTGGGGTGCCGGTAGAG
hRasal1_EpiMrkR1	AGGGACCTCCCCACAATC

Supplementary Table 5: Bisulfite sequencing primer sequences

Name	Sequence	Reference
Human bisulfate sequencing primers		
human RASAL1 BGS2 F	TAGTTTGTTTGTTGGAGTTTTAGA	Bechtel et al., <i>Nat Med</i> , 2015
human RASAL1 BGS2 R	ACCTACTTCAAACCTAACTCCCTAC	Bechtel et al., <i>Nat Med</i> , 2015
human RASAL1 bisu F2	AGTTAGGATTCGAATTTTTGGAAGGT AAATTAG	
human RASAL1 bisu R2	TTTCCAATTAACACAAAACCCAAAC TCTACTC	
human RASAL1 bisu F5	GCGTTATGGTTAAGAGTAGTTTTTTG AATG	
human RASAL1 bisu R5	CTCTAAACAACCCCTTTAATACATCC C	
Mouse bisulfate sequencing primers		
mouse Rasal1 bisu F4	ATTGGAGACGAAGAGAAGATGTAAG GGGATG	
mouse Rasal1 bisu R4	AACGCCCCCTACTAACACCCCAA ACTAC	
mouse Rasal1 bisu F9	GGGGGTTTTCGGTTGAGTGTAGTAG TTTGGG	
mouse Rasal1 bisu R9	AACATACGTCCAAA ACTACAATAAC TATAC	
BismKLF3	GGATTGTGTGATGTGGAATAGTTTG TTTTTTGAG	
BismKLR3	AACAACAACAATAACAACAACA AAC	
BismKLF6	TTTTAGGAATATTAGTTTTAGGAAGG TAAAGGG	
BismKLR6	CCCACGAACAATAATTATCCAAAACA AAC	

Supplementary Table 6: Primer sequence for genotyping Rasal1^{tm1a} mutant mouse

Name	Sequence	Reference
Rasal1 F	TGTCTGGCTTTGACTTGACCCTAGC	IMPC
Neo-F	GGGATCTCATGCTGGAGTTCTTCG	IMPC
Rasal1-ttR	ACACATCCAGACATGCAAAGGAAGC	IMPC
LacZ assay-F	CTCGCCACTTCAACATCAAC	IMPC
LacZ assay-R	TATCAGCCGGAAAACCTACC	IMPC
LacZ assay-Probe	TCGCCATTTGACCACTACCATCAATCC	IMPC
Dot1l control-F	GCCCCAGCACGACCATT	IMPC
Dot1l control-R	TAGTTGGCATCCTTATGCTTCATC	IMPC
Dot1l control-Probe	CCAGCTCTCAAGTCG	IMPC
CSD-RAF5-F	CACACCTCCCCTGAACCTGAAAC	IMPC
GF2	GTCTTACAGGACGGGTTAAAGGAG	IMPC
LR-5En2frt-R	GGTGGTGTGGGAAAGGGTTCGAAG	IMPC
GR1	GAGCCAAGGGTCCAATGAGATGAC	IMPC

Supplementary Table 7: qRT PCR primer sequences

Name	Sequence	Reference
Human		
qRT_hUSP46_F	TCCGGGAGAATGTGTTGGC	Primer bank
qRT_hUSP46_R	GTGTGGCAATGCTGTGGAAAA	Primer bank
qRT_hCHST12_F	CTTCTACTTGACACGCCTT	Primer bank
qRT_hCHST12_R	CTCCGTCTCCTTTCTGGGAA	Primer bank
qRT_hHERC6_F	CCACTCCCTGGCATTATCAAAA	Primer bank
qRT_hHERC6_R	GCCAAACGAAGTCCCACAGA	Primer bank
qRT_hNRF1_F	AGGAACACGGAGTGACCCAA	Primer bank
qRT_hNRF1_R	TATGCTCGGTGTAAGTAGCCA	Primer bank
qRT_hETV7_F	CTGCTGTGGGATTACGTGTATC	Primer bank
qRT_hETV7_R	GTTCTTGTGATTTCCCAGAGTC	Primer bank
qRT_hSYT14_F	AAATACAGTCCTCTATCGGCAGA	Primer bank
qRT_hSYT14_R	TTGGGCACTTGTTATATGAGCAT	Primer bank
qRT_hc3ORF20_F	GGAAAGAGTCCCTCGCAAACA	Primer bank
qRT_hc3ORF20_R	GGGGTTCCTCCTCGAT	Primer bank
qRT_mSIPA1L1_F	GTCGCAGACCGAAAGACCTG	Primer bank
qRT_mSIPA1L1_R	GGTTGAGGTGATATGGTGAGGG	Primer bank
qRT_mTSPAN14_F	GGCTGGCTGGAGTTGTCTTC	Primer bank
qRT_mTSPAN14_R	GGTCGATTCCATGCAACCG	Primer bank
qRT_mACAD8_F	TCCTGGGGCTAAATGAAGAAC	Primer bank
qRT_mACAD8_R	TCCCAGCTGCAAAGTCAAAG	Primer bank
qRT_mTXNDC16_F	AGAAGCGTCAAGGTACTGTGG	Primer bank
qRT_mTXNDC16_R	GAAGTCTTCCAGGGTGGTAA	Primer bank
qRT_mSLC32A1_F	ACCTCCGTGTCCAACAAGTC	Primer bank
qRT_mSLC32A1_R	CAAAGTCGAGATCGTCGAGT	Primer bank
qRT_mCD109_F	TCCCGCTTTCTGGTGACAG	Primer bank
qRT_mCD109_R	ACCTGAGCCTTTACAAGGACC	Primer bank
qRT_mSPON2_F	ATGGAAAACGTGAGTCTTGCC	Primer bank
qRT_mSPON2_R	TGATGCTGTATCTAGCCAGAGG	Primer bank
Mouse		
qRT mRasal1_F	CTCACAAGGCGTGAGGTGG	Bechtel et al., <i>Nat Med</i> , 2010
qRT mRasal1_R	TGCCAAGGAGTTAGAACGGAA	Bechtel et al., <i>Nat Med</i> , 2010
qRT mKl_F	ACTACGTTCAAGTGGACACTACT	Primer bank
qRT mKl_R	GATGGCAGAGAAATCAACACAGT	Primer bank

Supplementary Table 8: Gene list of predicted off-targets for human RASAL1 sgRNA3

Coordinates	strand	Mismatches	target_seq	PAM	distance		gene name
chr12:113574133-113574155	-	0	ACTTTTTATCATCGCTGTAG	TGG	89	-	RASAL1
chr20:57696895-57696917	-	3	AGTATTTATCATTGCTGTAG	AGG	8209	-	MRPS16P2
chr4:53515136-53515158	-	4	TCTTCAATCATTGCTGTAG	TGG	1980	I	USP46
chr7:2467215-2467237	-	4	TTTTTCTATCATCTCTGTAG	GGG	4961	I	CHST12
chr11:88418860-88418882	-	3	ACTTTTAGTCATGGCTGTAG	TGG	32289	I	GRM5
chr9:3046135-3046157	+	4	TCATTTTATCTTAGCTGTAG	AGG	7130	I	CARM1P1
chr2:123688625-123688647	+	4	TATTTTTATAATCTCTGTAG	GGG	NA	-	NA
chr4:89329458-89329480	-	4	ACAATTTATTATCTCTGTAG	TGG	196	I	HERC6
chr7:129298490-129298512	-	4	AATTTGATTATCCCTGTAG	AGG	1076	I	NRF1
chr13:85978922-85978944	+	4	GCTATTTATCACCCCTGTAG	AGG	40692	I	LINC00351
chr17:70613720-70613742	+	4	AGTTTTTCTCGTCTCTGTAG	AGG	713	I	LINC00511
chr6:36343417-36343439	-	4	ACTTGTTTTCAGAGCTGTAG	GGG	209	I	ETV7
chr1:29280765-29280787	+	4	GCTATTTATCATTGTTGTAG	AGG	28003	I	RP4-604A2.1
chr1:210327126-210327148	-	4	ACTTTTAGTCAACTGTAG	TGG	1918	I	SYT14
chr8:105743730-105743752	+	4	ATCTTTTATCATCATTGTAG	CGG	16527	I	RP11-127H5.1
chr13:106601077-106601099	-	4	ACTTCAGATCATCGCTGAAG	AGG	51085	-	SNORA25
chr3:14725729-14725751	+	4	GCTTTCATCATTGCTTTAG	TGG	0	E	C3orf20
chr11:4224812-4224834	+	4	CCTTTTCATCTTCGCTGGAG	CGG	927	-	RP11-23F23.2
chr17:69852904-69852926	+	4	TCTTTATATCATCTCTTTAG	GGG	NA	-	NA
chr13:54376908-54376930	+	4	ACAATTTATCATGGCTGGAG	AGG	12624	-	LINC00558

Potential off-target sites predicted for RASAL1-sgRNA3 by the online program CCTop were listed according to the number of mismatched nucleotides. The genome location and the nearby genes are included in the list (E: exonic; I: intronic; -: intergenic).

Supplementary Table 9: Gene list of predicted off-targets for human KL sgRNA2

Coordinates	strand	Mismatches	target_seq	PAM	distance	gene name
chr13:33590446-33590468	+	0	TCGCAGGTAATTATTGCCAG	CGG	0	E KL
chr14:71977318-71977340	+	4	TGCTGGGAATTATTGCCAG	GGG	2120	I SIPA1L1
chr5:102757803-102757825	-	4	GCTCAGTTGATTATTGCCAG	TGG	8282	- AC010423.1
chr20:50965499-50965521	+	4	TTGCAAGATATTATTGCCAG	AGG	6340	I RP4-723E3.1
chr3:2481671-2481693	-	4	TCTCATTTACTTATTGCCAG	AGG	71341	I CNTN4
chr6:46878083-46878105	+	4	TTGTGGGTAATAATTGCCAG	TGG	1268	I RP3-365O12.2
chr10:82250548-82250570	+	4	TAGCATGTGTTTATTGCCAG	TGG	1478	I TSPAN14
chr11:27423007-27423029	-	4	TTGCATGTGTTTATTGCCAG	AGG	8942	I LGR4
chrX:134831527-134831549	-	4	TGGCAGTCAAGTATTGCCAG	AGG	11661	- RP11-432N13.4
chrX:134783498-134783520	-	4	TGGCAGTCAAGTATTGCCAG	AGG	23786	- RP11-432N13.4
chr4:132263571-132263593	-	4	TAGCTGTTAATTTTGGCCAG	TGG	37575	- RP11-314N14.1
chr11:134132511-134132533	+	4	TAGAAGGTAAAAATTGCCAG	AGG	0	E ACAD8
chr14:52901283-52901305	+	4	TCTCAAGTAAGAATTGCCAG	TGG	1978	I TXNDC16
chr8:54810698-54810720	-	4	AGGCAGGGAATTATAGCCAG	GGG	10894	I RP11-1070A24.1
chr20:37350290-37350312	+	4	TGGCATCTAATTATAGCCAG	CGG	2793	- SLC32A1
chr10:84162887-84162909	+	4	TGCTAGGTAATTATTCAG	AGG	44263	I NRG3
chr11:8234267-8234289	+	4	TCAAAGCTAATTATACCAG	AGG	11562	- LMO1
chr6:74411096-74411118	+	4	CAGCAGGTAATAATTACCAG	AGG	3801	I CD109
chrX:65593743-65593765	-	4	TCACAGCTAAATATTACCAG	AGG	12125	- RP13-238N7.2
chr4:1193268-1193290	-	4	TTCCAGGTGATTATTGCTAG	AGG	0	E SPON2

Potential off-target sites predicted for KL-sgRNA2 by the online program CCTop were listed according to the number of mismatched nucleotides. The genome location and the nearby genes are included in the list (E: exonic; I: intronic; -: intergenic).

REFERENCES

1. Tampe, D., & Zeisberg, M. Potential approaches to reverse or repair renal fibrosis. *Nat. Rev. Nephrology* 10, 226–237 (2014).
2. Bergman, Y. & Cedar, H. DNA methylation dynamics in health and disease. *Nat. Struct. Mol. Biol.* 20, 274–281, (2013).
3. Yao, B. et al. Epigenetic mechanisms in neurogenesis. *Nat. Rev. Neurosci.* 17, 537–549 (2016).
4. Bechtel, W. et al. Methylation determines fibroblast activation and fibrogenesis in the kidney. *Nat. Med.* 16, 544–550, (2010).
5. Tampe, B. et al. Tet3-mediated hydroxymethylation of epigenetically silenced genes contributes to bone morphogenic protein 7-induced reversal of kidney fibrosis. *J. Am. Soc. Nephrol.* 25, 905–912 (2014).
6. Xu, X. et al. Epigenetic balance of aberrant Rasal1 promoter methylation and hydroxymethylation regulates cardiac fibrosis. *Cardiovasc. Res.* 105, 279–291 (2015).
7. Ligumsky, H. et al. Tumor suppressor activity of klotho in breast cancer is revealed by structure-function analysis. *Mol. Cancer Res.* 13, 1398–1407, (2015).
8. Qiao, F. et al. Enforced expression of RASAL1 suppresses cell proliferation and the transformation ability of gastric cancer cells. *Oncol. Rep.* 28, 1475–1481 (2012).
9. Liu, D., Yang, C., Bojdani, E., Murugan, A. K. & Xing, M. Identification of RASAL1 as a major tumor suppressor gene in thyroid cancer. *J. Natl. Cancer Inst.* 105, 1617–1627, (2013).
10. Xie, B., Chen, J., Liu, B. & Zhan, J. Klotho acts as a tumor suppressor in cancers. *Pathol. Oncol. Res.* 19, 611–617, (2013).
11. Chen, H. et al. Hypermethylation and clinicopathological significance of RASAL1 gene in gastric cancer. *Asian Pac. J. Cancer Prev.* 14, 6261–6265 (2013).
12. Wolf, I. et al. Klotho: a tumor suppressor and a modulator of the IGF-1 and FGF pathways in human breast cancer. *Oncogene* 27, 7094–7105 (2008).
13. Tao, H. et al. MeCP2 controls the expression of RASAL1 in the hepatic fibrosis in rats. *Toxicology* 290, 327–333 (2011).
14. Tampe, B. et al. Induction of Tet3-dependent epigenetic remodeling by lowdose hydralazine attenuates progression of chronic kidney disease. *EBioMedicine* 2, 19–36, (2015).
15. Sajithlal, G., Zou, D., Silviu, D., & Xu, P. X. Eya 1 acts as a critical regulator for specifying the metanephric mesenchyme. *Dev. Biol.* 284, 323–336 (2005).
16. Johnson, K. R. et al. Inner ear and kidney anomalies caused by IAP insertion in an intron of the Eya1 gene in a mouse model of BOR syndrome. *Hum. Mol. Genet.* 8, 645–653 (1999).
17. Thevenon, J. et al. Heterozygous deletion of the LRFN2 gene is associated with working memory deficits. *Eur. J. Hum. Genet.* 24, 911–918, (2016).
18. Satoh, M. et al. Klotho protects against mouse renal fibrosis by inhibiting Wnt signaling. *Am.J. Physiol. Renal Physiol.* 303, F1641–F1651 (2012).
19. Zhou, L., Li, Y., Zhou, D., Tan, R. J. & Liu, Y. Loss of Klotho contributes to kidney injury by derepression of Wnt/beta-catenin signaling. *J. Am. Soc. Nephrol.* 24, 771–785, (2013).

20. Sugiura, H. et al. Reduced Klotho expression level in kidney aggravates renal interstitial fibrosis. *Am.J. Physiol. Renal Physiol.* 302, F1252–F1264 (2012).
21. Zhang, Q., Yin, S., Liu, L., Liu, Z. & Cao, W. Rhein reversal of DNA hypermethylation-associated Klotho suppression ameliorates renal fibrosis in mice. *Sci. Rep.* 6, 34597, (2016).
22. Azuma, M. et al. Promoter methylation confers kidney-specific expression of the Klotho gene. *FASEB J.* 26, 4264–4274, (2012).
23. Pastor, W. A., Aravind, L. & Rao, A. TETonic shift: biological roles of TET proteins in DNA demethylation and transcription. *Nat. Rev. Mol. Cell Biol.* 14, 341–356, (2013).
24. Bian, C. & Yu, X. PGC7 suppresses TET3 for protecting DNA methylation. *Nucleic Acids Res.* 42, 2893–2905, (2014).
25. Chen, H. et al. Induced DNA demethylation by targeting ten-eleven translocation 2 to the human ICAM-1 promoter. *Nucleic Acids Res.* 42, 1563–1574, (2014).
26. Maeder, M. L. et al. Targeted DNA demethylation and activation of endogenous genes using programmable TALE-TET1 fusion proteins. *Nat. Biotechnol.* 31, 1137–1142, (2013).
27. Solary, E., Bernard, O. A., Tefferi, A., Fuks, F. & Vainchenker, W. The teneleven translocation-2 (TET2) gene in hematopoiesis and hematopoietic diseases. *Leukemia* 28, 485–496, (2014).
28. Hilton, I. B. et al. Epigenome editing by a CRISPR-Cas9-based acetyltransferase activates genes from promoters and enhancers. *Nat. Biotechnol.* 33, 510–517, (2015).
29. Kearns, N. A. et al. Functional annotation of native enhancers with a Cas9-histone demethylase fusion. *Nat. Methods* 12, 401–403, (2015).
30. Perez-Pinera, P. et al. RNA-guided gene activation by CRISPR-Cas9-based transcription factors. *Nat. Methods* 10, 973–976, (2013).
31. Polstein, L. R. & Gersbach, C. A. A light-inducible CRISPR-Cas9 system for control of endogenous gene activation. *Nat. Chem. Biol.* 11, 198–200, (2015).
32. Thakore, P. I. et al. Highly specific epigenome editing by CRISPR-Cas9 repressors for silencing of distal regulatory elements. *Nat. Methods* 12, 1143–1149, (2015).
33. Vojta, A. et al. Repurposing the CRISPR-Cas9 system for targeted DNA methylation. *Nucleic Acids Res.* 44, 5615–5628, (2016).
34. Tahiliani, M. et al. Conversion of 5-methylcytosine to 5-hydroxymethylcytosine in mammalian DNA by MLL partner TET1. *Science* 324, 930–935, (2009).
35. Jiang, D., Wei, S., Chen, F., Zhang, Y. & Li, J. TET3-mediated DNA oxidation promotes ATR-dependent DNA damage response. *EMBO Rep.* 18, 781–796, (2017).
36. Eisenberg, L. M. & Markwald, R. R. Molecular regulation of atrioventricular valvuloseptal morphogenesis. *Circ. Res.* 77, 1–6 (1995).
37. Sun, C. Y., Chang, S. C. & Wu, M. S. Suppression of Klotho expression by protein-bound uremic toxins is associated with increased DNA methyltransferase expression and DNA hypermethylation. *Kidney Int.* 81, 640–650, (2012).
38. Platt, R. J. et al. CRISPR-Cas9 knockin mice for genome editing and cancer modeling. *Cell* 159, 440–455 (2014).

39. Stemmer, M., Thumberger, T., Del Sol Keyer, M., Wittbrodt, J., & Mateo, J.L. CCTop: an intuitive, flexible and reliable CRISPR/Cas9 target prediction tool. *PLoS ONE* 10, e0124633 (2015).
40. Zhang, X. H., Tee, L. Y., Wang, X. G., Huang, Q. S., & Yang, S. H. Off-target effects in CRISPR/Cas9-mediated genome engineering. *Mol. Ther. Nucleic Acids* 4, e264 (2015).
41. Kleinstiver, B. P. et al. High-fidelity CRISPR-Cas9 nucleases with no detectable genome-wide off-target effects. *Nature* 529, 490–495, (2016).
42. Beronja, S., Livshits, G., Williams, S. & Fuchs, E. Rapid functional dissection of genetic networks via tissue-specific transduction and RNAi in mouse embryos. *Nat. Med.* 16, 821–827, (2010).
43. Choudhury, S. R., Cui, Y., Lubecka, K., Stefanska, B., & Irudayaraj, J. CRISPRdCas9 mediated TET1 targeting for selective DNA demethylation at BRCA1 promoter. *Oncotarget* 7, 46545–46556 (2016).
44. Xu, X. et al. A CRISPR-based approach for targeted DNA demethylation. *Cell Discov* 2, 16009 (2016).
45. Morita, S. et al. Targeted DNA demethylation in vivo using dCas9-peptide repeat and scFv-TET1 catalytic domain fusions. *Nat. Biotechnol.* 34, 1060–1065 (2016).
46. Jinek, M. et al. A programmable dual-RNA-guided DNA endonuclease in adaptive bacterial immunity. *Science* 337, 816–821, (2012).
47. Xu, X. et al. Endocardial fibroelastosis is caused by aberrant endothelial to mesenchymal transition. *Circ. Res.* 116, 857–866, (2015).
48. Xie, W. et al. RNF40 regulates gene expression in an epigenetic contextdependent manner. *Genome Biol.* 18, 32, (2017).
49. Gusella, G. L., Fedorova, E., Marras, D., Klotman, P. E., & Klotman, M. E. In vivo gene transfer to kidney by lentiviral vector. *Kidney Int* 61, S32–S36 (2002).
50. Gusella, G. L. et al. Lentiviral gene transduction of kidney. *Hum. Gene Ther.* 13, 407–414, (2002).

CHAPTER

11

SPLIT-INTEIN MEDIATED AAV DELIVERY OF DCAS9-TET3 AS ANTIFIBROTIC THERAPY

Xingbo Xu^{1,2,*}, Melanie S. Hulshoff^{1,2,3,*}, Xiaoying Tan^{2,4,*}, Sabine Maamari^{1,2}, Guido Krenning³, Oliver Müller⁵, Gerd Hasenfuss^{1,2}, Michael Zeisberg^{2,4} and Elisabeth M. Zeisberg^{1,2}

¹*Department of Cardiology and Pneumology, University Medical Center Göttingen, Robert-Koch-Str. 40, 37075, Göttingen, Germany.*

²*German Centre for Cardiovascular Research (DZHK), Göttingen, Germany.*

³*Department of Pathology and Medical Biology, University Medical Center Groningen, Hanzeplein 1, 9713 GZ, Groningen, The Netherlands.*

⁴*Department of Nephrology and Rheumatology, University Medical Center of Göttingen, Robert-Koch-Str. 40, 37075, Göttingen, Germany.*

⁵*Department of Internal Medicine III, University of Kiel and University Medical Center Schleswig-Holstein and German Center for Cardiovascular Research (DZHK), Partner Site Hamburg/Kiel/Lübeck, Arnold-Heller-Straße 3, 24105 Kiel, Germany*

**Authors contributed equally*

Submitted

ABSTRACT

Cardiac fibrosis is characterized by excessive deposition of extracellular matrix in the heart, resulting in a progressive loss of cardiac function for which no specific therapy is available as of yet. Gene methylation of anti-fibrotic genes such as Rasal1 play an important role in the progression of organ fibrosis. However, it is not clear whether Rasal1 depletion per se induces organ fibrosis. Here we show that Rasal1 deficient mice do not display spontaneous organ fibrosis development, but are more susceptible to cardiac fibrosis progression upon Angiotensin-II treatment. To examine whether reactivated RASAL1 expression hinders cardiac fibrosis progression, we performed CRISPR/Cas9-based gene-specific hydroxymethylation via adeno associated virus (AAV). While AAV-mediated delivery of CRISPR/Cas9 holds great therapeutic potential, its utility is limited because most constructs exceed the viral packaging capacity. We here demonstrate AAV delivery of two fragments of a Cas9 derivative (dHFCas9 fused to the catalytic domain of TET3 and gene-specific guide RNA) and subsequent split-intein-mediated fusion of the N-terminus and C-terminus in situ. The fused dHFCas9-TET3CD protein leads to gene-specific demethylation of RASAL1 and attenuates cardiac fibrosis in mice.

INTRODUCTION

Fibrosis is a scarring process which is characterized by excessive deposition of extracellular matrix that often happens in repeated or chronic organ injury, and may lead to the disruption of organ structure and organ failure [1-4]. Fibrosis involving organs such as heart, liver and kidney, is an unsolved biomedical challenge, as specific therapies are not yet available for clinical use. Because transcriptional silencing of specific genes through promoter methylation contributes causally to fibrogenesis, gene-specific demethylation is an attractive therapeutic approach [5]. Previously, we and others have shown that promoter hypermethylation of the RASAL1 gene (which encodes for a RAS- GTP like Ras-GTP inhibitor, which suppresses RAS-GTP activity) leads to silencing of RASAL1 expression which regulates different forms of organ fibrosis including heart and kidney [6,7]. Silencing of RASAL1 expression is therefore believed to be causative to organ fibrosis. We previously reported that reduced RASAL1 expression results in increased kidney fibrosis [8]. So far, it is known that RASAL1 knockout mice are more susceptible to liver fibrosis, but is unknown whether Rasal1-deficient mice exhibit systemic development and/or progression of organ fibrosis in the kidney, lung and heart.

Gene reactivation of RASAL1 is beneficial in the kidney where it ameliorates kidney fibrosis [9]. Not only reactivation of RASAL1, but also overexpression of other genes has been demonstrated as beneficial in the context of organ fibrosis. For example, Jeong et al. reported that adeno-associated virus (AAV)-mediated overexpression of CCN5 results in alleviation of cardiac fibrosis [10].

Gene-specific demethylation by combining a deactivated high-fidelity Cas9 protein (dHFCas9), which lost its nuclease activity, to the catalytic domain of methylcytosine dioxygenase TET3 (TET3CD) can reverse methylation via so-called hydroxymethylation in an all-in-one fusion protein [8]. A gene-specific guiding RNA can locate this dHFCas9-TET3CD protein to a gene-specific location to perform targeted demethylation of anti-fibrotic genes such as RASAL1 [8]. Other groups have established similar strategies such as fusing TET1 to dCas9 [11], or the fusion of dCas9 with either TET1 or DNMT3a [12], a methyl transferase, which enables targeted DNA demethylation or methylation both *in vitro* and *in vivo* in mice. In our previous report, we demonstrated that this technique can not only

reactive gene expression of e.g. Rasal1 *in vitro* and *in vivo*, but also ameliorate kidney fibrosis progression [8].

We now aimed to establish a method to deliver such protein via AAVs as a broader application form, and to rescue Rasal1 expression through gene-specific hydroxymethylation of the Rasal1 gene in fibroblasts and experimental fibrotic mouse hearts as proof of concept. However, the all-in-one dHFCas9-TET3CD fusion protein is 7.2kb and thus exceeds the packaging capacity for AAVs (approximately 4.8 kb).

To circumvent the packaging limit of AAV, we made use of the so-called split-intein proteins to be able to divide large constructs into two parts to be later fused inside the cell. Split-intein proteins are regulators of protein splicing in smaller organisms such as bacteria and yeast [13]. Split-intein proteins can recognize each other and excise themselves, thereby fusing adjacent proteins into one functional protein [14,15]. We applied this split-intein system by splitting our dHFCas9-TET3CD into two parts (N- and C-terminal) and fusing N- and C-intein proteins to each part respectively. This split-intein strategy allowed packaging our dHF-Cas9-TET3CD into two AAVs thereby enabling, targeted demethylation in the context of cardiac fibrosis for the first time.

Altogether, we demonstrated that Rasal1 deficient mice do not develop spontaneous organ fibrosis (in the kidney, heart, liver and lung) but display an increased susceptibility for cardiac fibrogenesis upon Angiotensin II (ATII) treatment. We also established an AAV-based strategy which enables split-intein mediated gene activation of RASAL1 in the heart and alleviates cardiac fibrosis *in vivo*. This technique holds potential to be applied for future AAV delivery-mediated therapeutic applications.

RESULTS

RASAL1 DEFICIENT MICE DEVELOP NO SPONTANEOUS ORGAN FIBROSIS BUT DISPLAY ENHANCED CARDIAC FIBROSIS UPON ANGIOTENSIN II-TREATMENT

We generated *Rasal1* deficient mice by breeding conditional *Rasal1*^{tm1c} mice (in which the targeted exon 3 and 4 are flanked by two loxP sites) with E2a-Cre mice resulting in *Rasal1*^{tm1d} mice with excision of exon 3 and 4 (Figure 1A). Genotyping PCR validates the *Rasal1* knockout as shown by absence of the wildtype allele (Figure 1B). The *Rasal1* knockout is also validated by qRT-PCR demonstrating the complete loss of *Rasal1* mRNA expression in the heart, kidney, liver and lung of *Rasal1*^{tm1d} knockout mice (Figure 1C). We then systematically analyzed whether knockout of *Rasal1* induced any spontaneous fibrosis in these organs, but this was not the case (Figure 1D-H, Suppl.Fig.1).

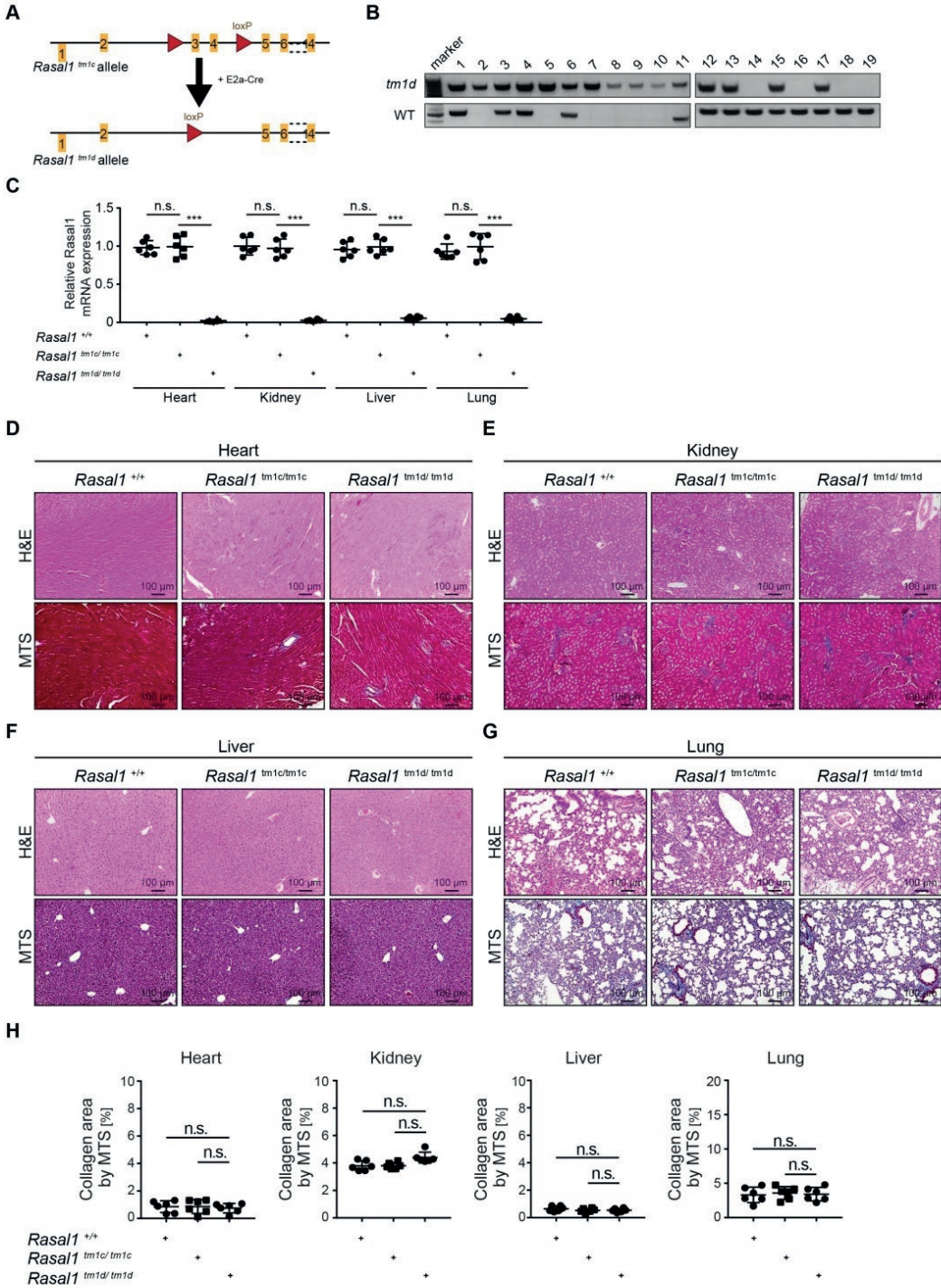


Figure 1. Rasal1 knockout mice do not display spontaneous organ fibrosis development.

(A) Schematic demonstrating the generation of Rasal1 knockout mice. Rasal1^{tm1c} mice are bred with E2a-Cre mice, resulting in depletion of exon number 3 and 4. (B) Genotyping PCR for both the wildtype and Tm1d allele shows that several mice are negative for the wildtype allele and thus represent Rasal1^{tm1d/tm1d} knockout mice (nr. 2, 5 and 7-10). Heterozygous mice are positive for both the wildtype and Tm1d allele (nr. 1, 3, 4, 6, 11-13, 15 and 17). (C) qRT-PCR analysis of Rasal1 mRNA expression in the heart, kidney liver and lung of Rasal1^{+/+} (wildtype), Rasal1^{tm1c/tm1c} and Rasal1 knockout mice (Rasal1^{tm1d/tm1d}). Rasal1^{tm1d/tm1d} mice are completely depleted of Rasal1 mRNA expression in the heart, kidney, liver and lung, whereas Rasal1^{tm1c/tm1c} mice have same expression level as wildtype mice. (D) H&E staining and MTS staining of the heart, kidney (E), liver (F) and lung (G) of Rasal1^{+/+} (wildtype), Rasal1^{tm1c/tm1c} and Rasal1 knockout mice (Rasal1^{tm1d/tm1d}). No spontaneous fibrosis development is detected in these organs upon Rasal1 knockout. (H) Quantification of the total fibrotic area (in percentage) based on the MTS staining in the heart, kidney, liver and lung of Rasal1^{+/+} (wildtype), Rasal1^{tm1c/tm1c} and Rasal1 knockout mice (Rasal1^{tm1d/tm1d}). There is no significant difference in collagen content between these groups, indicating that Rasal1 knockout does not induce spontaneous organ fibrosis development. The data is presented as mean value; error bars represent S.E.M.; *, $p < 0.05$; **, $p < 0.01$, ***, $p < 0.001$.

We then focused on Rasal1 function in the heart, and on Rasal1^{tm1c} mice versus Rasal1^{tm1d} knockout mice, and further characterized fibrosis in the heart via immunofluorescence staining of Collagen-1 and α -SMA (Figure 2A). This confirmed that there is no spontaneously increase in collagen deposition nor activated myofibroblasts in Rasal1^{tm1d} knockout mice (Figure 2B,C).

We treated both Rasal1^{tm1c} and Rasal1^{tm1d} knockout mice with either vehicle or Angiotensin II (ATII) treatment for 4 weeks. Interestingly, Rasal1^{tm1d} knockout mice developed more fibrosis when compared to Rasal1^{tm1c} mice (Figure 2D-G). Altogether, this indicates that Rasal1 deficient mice develop no spontaneous organ fibrosis but are more susceptible to cardiac fibrosis development and/or progression upon pro-fibrotic stimuli (in this case ATII).

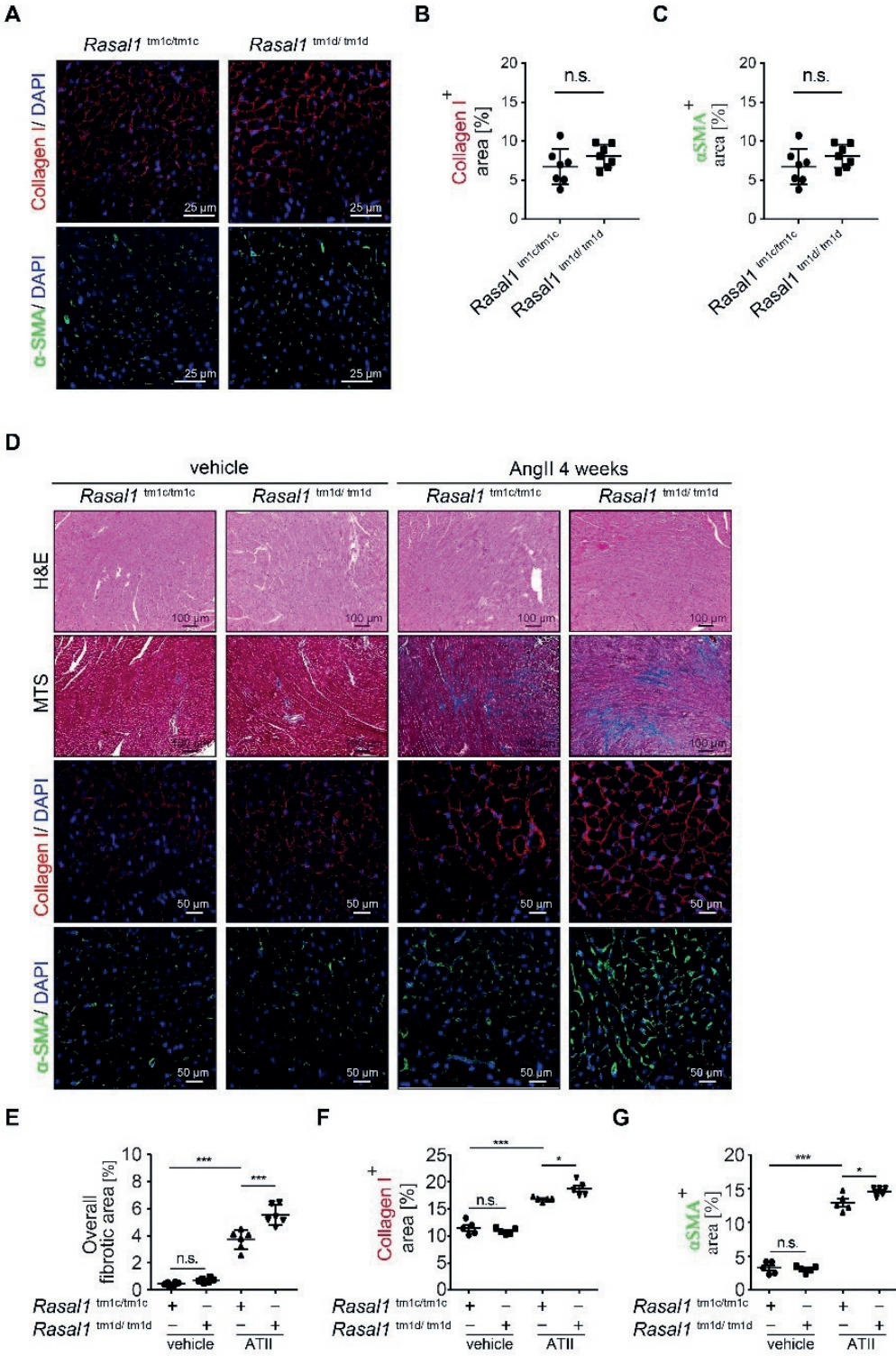


Figure 2. Rasal1 knockout mice develop more cardiac fibrosis upon Angiotensin II-induction.

Immunofluorescent staining of Collagen-1 and α SMA in Rasal1^{tm1c/tm1c} versus Rasal1 knockout mice (Rasal1^{tm1d/tm1d}). (B) Quantification of the Collagen-1 positive area and (C) quantification of the α SMA positive area. No significant difference in Collagen-1 or α SMA positive area is detected between Rasal1^{tm1c/tm1c} versus Rasal1 knockout mice (Rasal1^{tm1d/tm1d}). (D) H&E staining, MTS staining and immunofluorescent staining of Collagen-1 and α SMA in Rasal1^{tm1c/tm1c} versus Rasal1^{tm1d/tm1d} mice upon vehicle and Angiotensin II (ATII) treatment. (E-G) Quantification demonstrates that there is no significant difference between vehicle treated Rasal1^{tm1c/tm1c} and Rasal1^{tm1d/tm1d} mice. ATII treatment results in fibrosis in both Rasal1^{tm1c/tm1c} and Rasal1^{tm1d/tm1d} mice based on quantification of the overall fibrotic area, Collagen-1⁺ area and α SMA⁺ area. However, ATII treatment induces significant more fibrosis in Rasal1^{tm1d/tm1d} than in Rasal1^{tm1c/tm1c} mice. The data is presented as mean value; error bars represent S.E.M.; *, $p < 0.05$; **, $p < 0.01$, ***, $p < 0.001$.

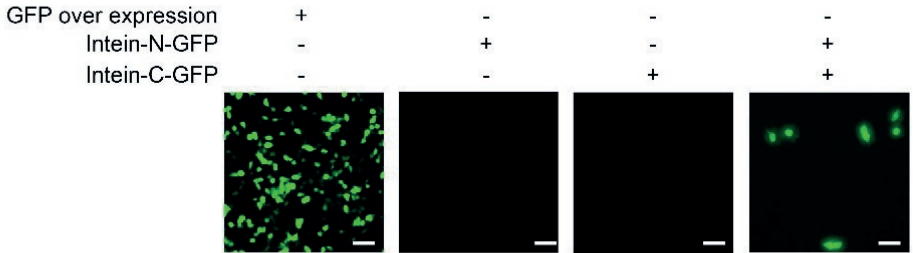
SUCCESSFUL FUSION OF GREEN FLUORESCENT PROTEIN (GFP) BY USING THE SPLIT INTEIN SYSTEM

The augmented cardiac fibrosis upon ATII treatment in Rasal1 deficient mice confirmed our hypothesis that Rasal1 expression protects against fibrogenesis. We have previously shown that in experimental fibrosis of non-transgenic animals Rasal1 expression is reduced through promoter hypermethylation. Therefore, we now aimed to rescue Rasal1 expression through gene-specific hydroxymethylation of the Rasal1 gene in experimental fibrotic hearts of Rasal1^{tm1c} mice. Experimental cardiac fibrosis of Rasal1^{tm1d} knockout mice served as control experiment (as no Rasal1 gene is present in these mice and hence Rasal1-gene-specific hydroxymethylation cannot be performed). To establish the split-intein strategy we first divided the green fluorescent protein (GFP) into two parts (N- and C-terminal) and cloned it adjacent to Intein-N and Intein-C respectively. This results in the generation of the constructs: pCMV6-GFP-Intein-N and pCMV6-Intein-GFP-C (Figure 3A). Upon transfection of both constructs into HEK293 cells, GFP could be observed by fluorescent microscopy and could also be detected via Western Blot (Figure 3B-C), whereas single transfection did not result in green fluorescence (Figure 3B-C). This indicates successful fusion of the N- and C-terminal part of GFP via the split intein system. We continued by cloning the GFP-Intein-N and Intein-GFP-C into an AAV backbone to generate pAAV-GFP-Intein-N and pAAV-Intein-GFP-C respectively (Figure 3D). We then packaged these constructs into AAV (AAV9-SLRSPPS) and transduced mouse cardiac fibroblasts (MCFs). Upon co-transduction of both constructs, GFP again could be observed by light microscopy and detected via Western blot, whereas single transduction did not (Figure 3E-F). This shows that we successfully established the split-intein strategy.

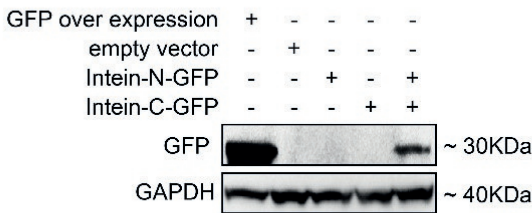
A



B



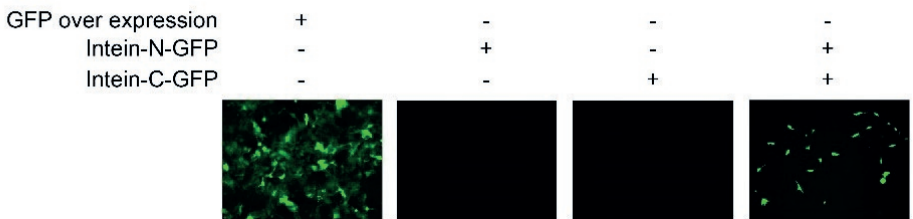
C



D



E



F

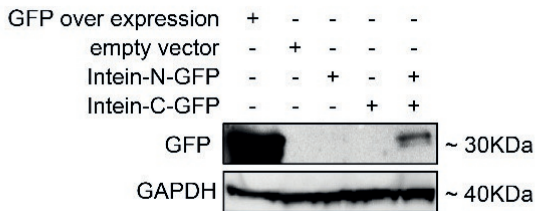


Figure 3. Successful fusion of green fluorescent protein (GFP) by using the split intein system.

Schematic representation of the split-intein GFP constructs. The left construct represents the N-terminal part of GFP fused to N-intein (pCVM6-GFP-Intein-N) whereas the right construct represents the C-terminal part of GFP fused to C-intein (pCMV6-Intein-GFP-C). (B). HEK293 cells transfected with both pCMV6-GFP-Intein-N and pCMV6-Intein-GFP-C results in a green fluorescent signal. Single transfection of either one of these constructs did not result in a green fluorescent signal. GFP overexpression serves as positive control. (C) Western Blot of HEK293 cells co-transfected with pCMV6-GFP-Intein-N and pCMV6-Intein-GFP-C reveals the presence of the GFP protein. Single transfection did not result in detection of the GFP protein. GFP overexpression was used as a positive control. (D). Schematic representation of the split-intein GFP constructs when packaged into AAV. The constructs are similar as before, but now cloned into an AAV-backbone. The two constructs include pAAV-GFP-Intein-N, representing the N-terminal of GFP, and pAAV-Intein-GFP-C, representing the C-terminal of GFP. (E) Transduction of both constructs in mouse cardiac fibroblasts (MCFs) results in the appearance of a green fluorescent signal whereas single transduction did not. GFP overexpression served as positive control. (F). Western blot of MCFs transduced with both split-intein GFP constructs resulting in the appearance of the GFP protein. Single transduction did not reveal a band for GFP. GFP overexpression was used as positive control.

SPLIT INTEIN-MEDIATED FUSION OF DHFCAS9-TET3CD RESCUES RASAL1 EXPRESSION IN A GENE-SPECIFIC WAY *IN VITRO*

After having established the split-intein strategy using a GFP labeling construct, we divided the dHFCas9-TET3CD into two parts (N- and C-terminal) and cloned it adjacent to Intein-N and Intein-C respectively. This resulted in the generation of pCMV6-dHFCas9-TET3CD-Intein-N and pAAV-Intein-dHFCas9-TET3CD-C (Figure 4A). We identified several possible splitting sites (amino acid number 909, 1004, 1115, 1153 and 1246) in the middle of our dHFCas9-TET3CD construct (to ensure that each half fits into AAV) [18], and generated the corresponding construct accordingly (Figure 4B).

We show that co-transfection of both the dHFCas9-TET3CD fusion constructs 909 or 1246 in combination with sgRNA-*Rasal1* rescued the mRNA expression of *Rasal1* in mouse cardiac fibroblasts (MCFs), in which *Rasal1* methylation is induced by TGF- β 1 [5-7,9,19,20], while co-transfection of both the dHFCas9-TET3CD fusion constructs in combination with sgRNA-*LacZ* did not have this effect (Figure 4C). Since split site 909 (in combination with sgRNA-*Rasal1*) was the most efficient in rescuing the mRNA levels of *Rasal1*, we continued with this split site in our next experiments focusing on the demethylation efficacy of the dHFCas9-TET3CD fusion constructs.

We demonstrate that co-transfection of both the dHFCas9-TET3CD fusion constructs in combination with sgRNA-*Rasal1* rescues the mRNA expression of *Rasal1* by decreasing *Rasal1* promoter methylation (Figure 4D). Even though we made use of high-fidelity Cas9 (which is associated with less off-target effects when compared to native Cas9), we wanted to confirm the gene-specificity of our split intein-mediated fusion of dHFCas9-TET3CD. We therefore examined the mRNA levels of potential off-target genes which are identified from our previous study [8] as well as an online prediction program [8,21]. Co-transfection of both the dHFCas9-TET3CD fusion constructs with either sgRNA-*Rasal1* or sgRNA-*LacZ* did not show expression changes of the predicted off-target genes. (Figure 4E). This confirms that our split intein-mediated fusion of dHFCas9-TET3CD together with sgRNA-*Rasal1* reactivates *Rasal1* via hydroxymethylation in a gene-specific manner *in vitro*.

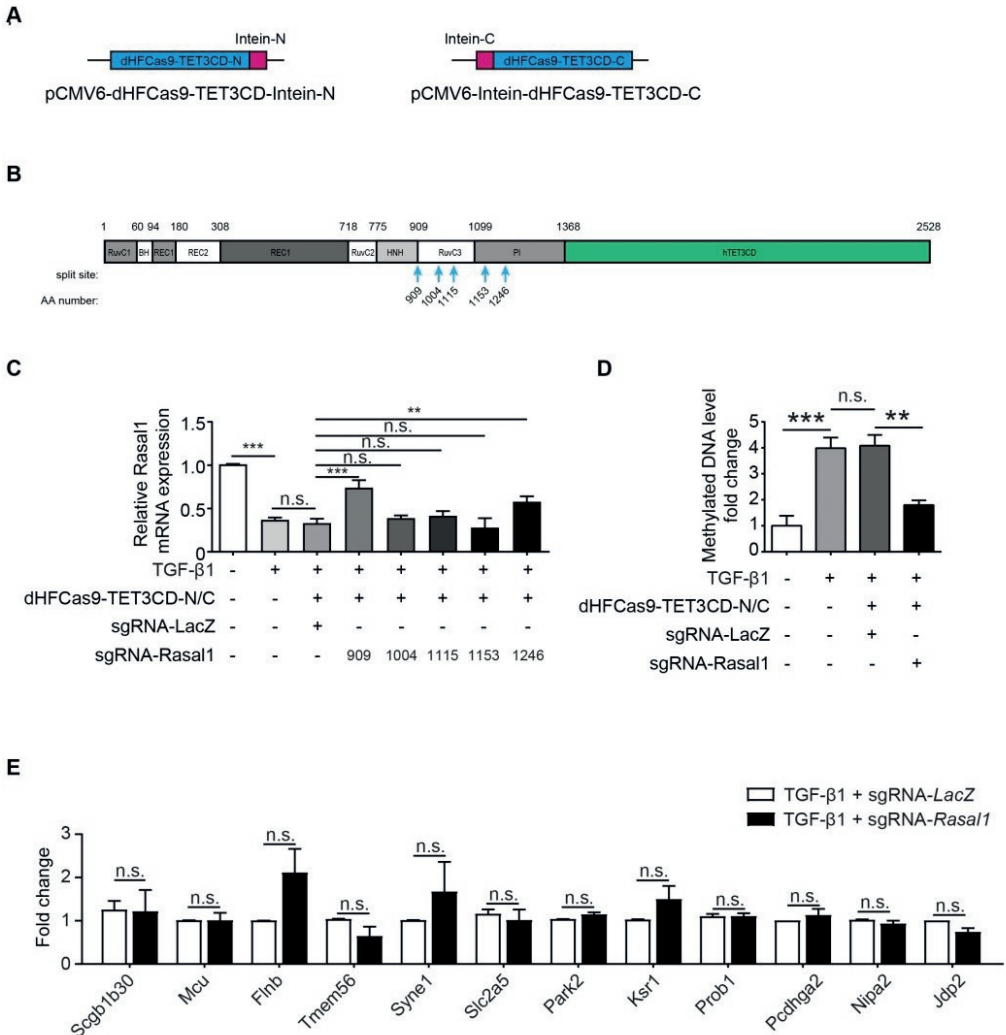


Figure 4. Split intein-mediated fusion of dHFCas9-TET3CD rescues Rasal1 expression in a gene-specific way *in vitro*

(A) Schematic representation of the split-intein dHFCas9-TET3CD constructs. The left construct represents the N-terminal part of dHFCas9-TET3CD fused to N-intein (pCMV6-dHFCas9-TET3CD-Intein-N) whereas the right construct represents the C-terminal of dHFCas9-TET3CD fused to C-intein (pCMV6-Intein-dHFCas9-TET3CD-C). (B) Schematic representation of the different potential split sites (indicated by arrows) in the dHFCas9-TET3CD protein. (C) qRT-PCR analysis of mouse cardiac fibroblasts (MCFs) treated with TGF-β1 for 4 days and transfected with different split-intein dHFCas9-TET3CD constructs in combination with a sgRNA for Rasal1 or LacZ (as negative control). TGF-β1 treatment decreases the mRNA expression of Rasal1. Transfection of MCFs with both split-intein-dHFCas9-TET3CD (splitting sites 909 or 1246) in combination with the sgRNA-Rasal1 rescues the TGF-β-induced decrease in Rasal1 mRNA expression. (D). Methylated DNA Immunoprecipitation

analysis of MCFs treated with TGF- β 1 for 4 days and transfected with both split-intein dHFCas9-TET3CD constructs in combination with a sgRNA for Rasal1 or LacZ. TGF- β 1 treatment increases the methylation of Rasal1. Transfection of both split-intein-dHFCas9-TET3CD constructs in combination with sgRNA Rasal1 rescues the TGF- β 1-induced methylation of Rasal1. (E). qRT-PCR analysis of the predicted off-target genes for sgRNA Rasal1. MCFs treated with TGF- β 1 for 4 days and transfected with the split-intein dHFCas9-TET3CD constructs in combination with a sgRNA for Rasal1 or LacZ (as negative control). sgRNA-Rasal1 did not affect the predicted off-target genes. The data is presented as mean value; error bars represent S.E.M.; **, $p < 0.01$, ***, $p < 0.001$.

SPLIT INTEIN-MEDIATED FUSION OF DHFCAS9-TET3CD RESCUES RASAL1 EXPRESSION AND AMELIORATES CARDIAC FIBROSIS *IN VIVO*

After having established the split-intein strategy *in vitro*, we continued by testing if this also functions *in vivo*, and assessed its efficacy in ameliorating cardiac fibrosis. We chose to make use of the recently discovered AAV serotype AAV9-SLRSPPS, which has been shown to effectively target cardiac fibroblasts *in vitro* [22]. To establish the cardiac fibroblast transduction competency of AAV9-SLRSPPS *in vivo*, we packaged EGFP into AAV9-SLRSPPS, injected it with a titer of 1.8×10^{10} vg/g into the tail vein and examined its cell type specificity after 7 days and 4 weeks. Immunofluorescence staining of GFP in combination with WGA indicates the cell borders and gave us the hint that AAV9-SLRSPPS targets predominantly interstitial cells including fibroblasts and endothelial cells (Figure 5A). This was confirmed with immunofluorescence of GFP together with the fibroblast marker α -SMA, where we could demonstrate robust overlap of GFP with α -SMA (Figure 5B). Quantification of the GFP and α -SMA-positive cells revealed that 51% and 32% of the fibroblasts express GFP after 7 days and 4 weeks respectively (Figure 5C).

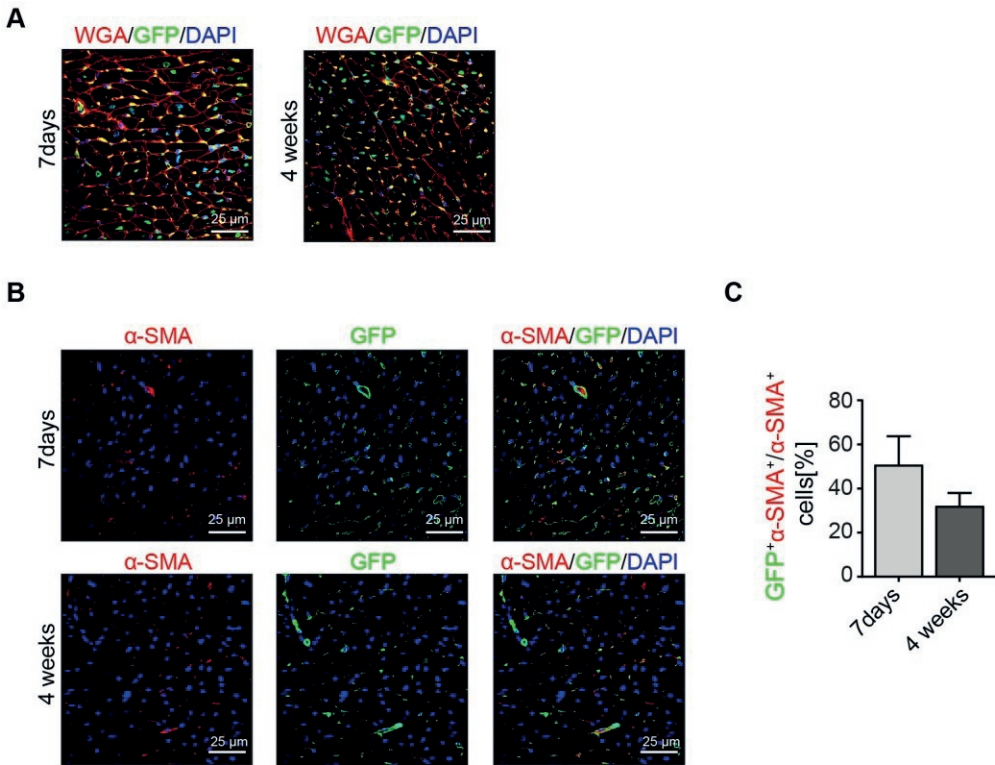
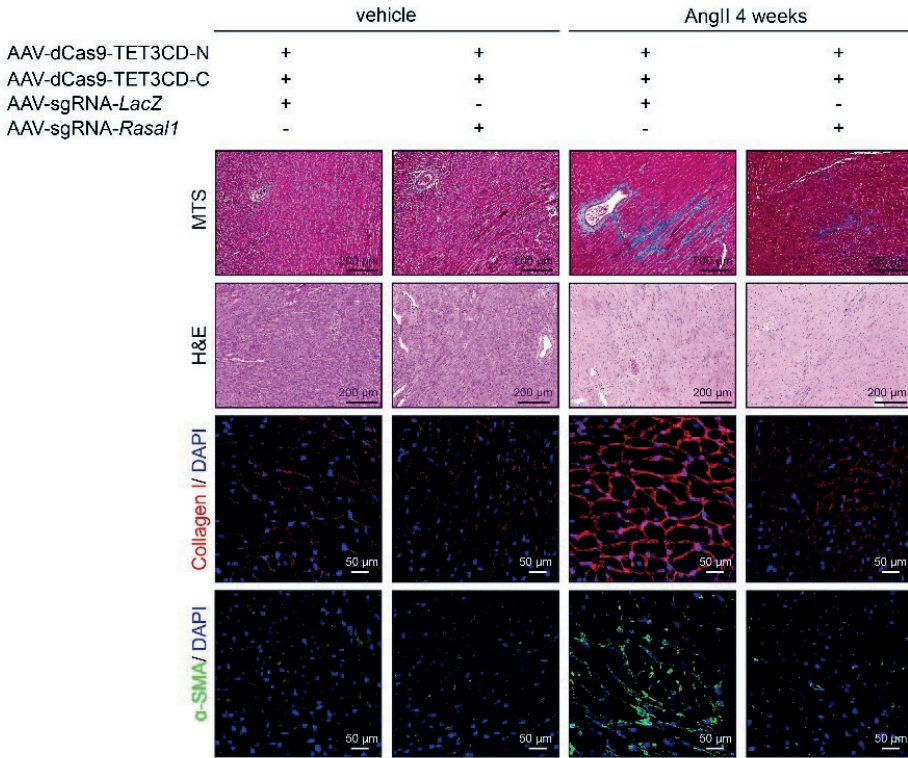


Figure 5. AAV9-SLRSPPS targets fibroblasts *in vivo*.

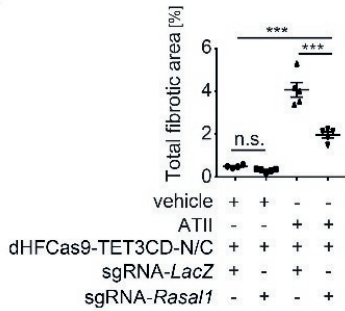
To establish the cardiac fibroblast transduction competency of AAV9-SLRSPPS *in vivo*, we packaged EGFP into AAV9-SLRSPPS, injected it with a titer of 1.8×10^{10} vg/g into the tail vein and examined its cell type specificity after 7 days and 4 weeks. (A) Immunofluorescence staining of GFP in combination with WGA indicates the cell borders and suggested that AAV9-SLRSPPS targets predominantly interstitial cells including fibroblasts and endothelial cells. (B) The targeting of fibroblasts (our primary cells of interest) was confirmed with immunofluorescence of GFP together with the fibroblast marker α -SMA, where we could demonstrate robust overlap of GFP with α -SMA. (C) Quantification of the GFP and α -SMA-positive cells revealed that 51% and 32% of the fibroblasts express GFP after 7 days and 4 weeks respectively.

After having established that AAV9-SLRSPPS efficiently targets fibroblasts *in vivo*, we continued to assess the efficiency of the split-intein strategy *in vivo*. Therefore, we packaged the dHFCas9-TET3CD fusion constructs, sgRNA-*Rasal1* and sgRNA-*LacZ* into AAV. We used ATII administration via osmotic minipumps as a model of pressure overload to induce cardiac fibrosis and injected the AAV-packed dHFCas9-TET3CD fusion constructs in combination with either sgRNA-*Rasal1* or sgRNA-*LacZ* in *Rasal1*^{tm1c} mice. ATII treatment results in methylation and decreased expression of *Rasal1*. However, this effect was reversed when injecting the AAV-packed dHFCas9-TET3CD fusion constructs in combination with a sgRNA-*Rasal1* (but not with sgRNA-*LacZ*) (Figure 6E,F). We next assessed whether the split-intein mediated reactivation of *Rasal1* expression ameliorates cardiac fibrosis. The ATII-induced cardiac fibrosis was significantly decreased when the mice were injected with the AAV-packed dHF-Cas9-TET3CD fusion constructs in combination with the sgRNA-*Rasal1* (but not with sgRNA-*LacZ*, Figure 6A-D). Altogether, this suggests that the split-intein mediated fusion of dHF-Cas9-TET3CD in combination with sgRNA-*Rasal1* reactivates *Rasal1* expression *in vivo* and alleviates cardiac fibrosis.

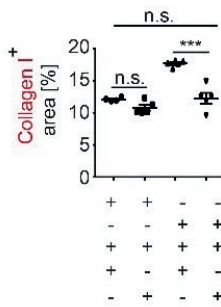
A



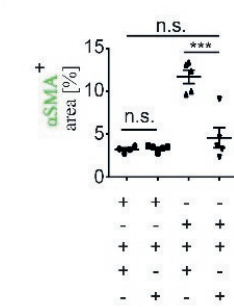
B



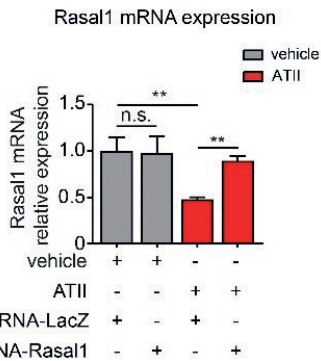
C



D



E



F

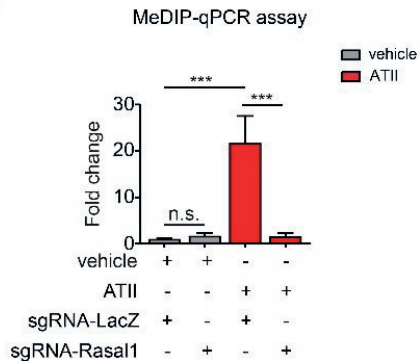


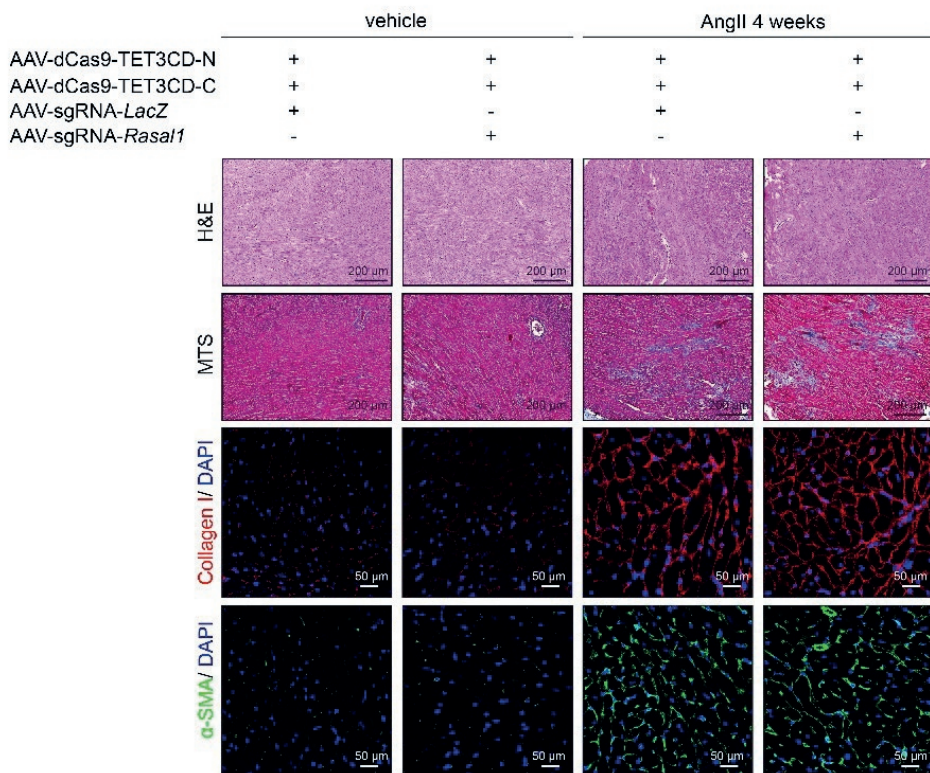
Figure 6. Split intein-mediated fusion of dHFCas9-TET3CD rescues Rasal1 expression and ameliorates cardiac fibrosis *in vivo*.

(A-D) Mice were treated with Angiotensin II (ATII) or PBS as vehicle control for 4 weeks and injected with AAV-dHF-Cas9-TET3CD-Intein-N and AAV-Intein-dHF-Cas9-TET3CD-C in combination with AAV-sgRNA-Rasal1 or AAV-sgRNA-LacZ (as negative control). Vehicle control in combination with injection of AAV-dHF-Cas9-TET3CD-Intein-N and AAV-Intein-dHF-Cas9-TET3CD-C with either AAV-sgRNA-Rasal1 or AAV-sgRNA-LacZ did not result in fibrosis and has similar effects on the expression of fibrotic markers Collagen-1 (in red) and α -SMA (in green). ATII treatment in combination with injection of AAV-dHF-Cas9-TET3CD-Intein-N, AAV-Intein-dHF-Cas9-TET3CD-C and AAV-sgRNA-LacZ results in increased fibrosis as shown by Masson-Trichrom-Staining (MTS, in blue), Hematoxylin and eosin (HE) staining and immunofluorescent staining for Collagen-1 (in red) and α -SMA (in green). The nucleus was stained with DAPI (in blue). ATII treatment in combination with injection of AAV-dHF-Cas9-TET3CD-Intein-N, AAV-Intein-dHF-Cas9-TET3CD-C and AAV-sgRNA-Rasal1 ameliorates cardiac fibrosis as shown by reduced fibrotic area (MTS and H&E staining) and reduced expression of the fibrotic markers α -SMA and Collagen-1. (E) qRT-PCR analysis of Rasal1 mRNA expression. ATII treatment reduces the mRNA expression of Rasal1 which is rescued by injection of our dHFCas9-TET3CD fusion constructs in combination with sgRNA-Rasal1 but not sgRNA-LacZ. (F) MeDIP analysis of the Rasal1 promoter demonstrating that ATII treatment induces methylation of the Rasal1 promoter. Injection of our dHFCas9-TET3CD fusion constructs together with sgRNA-Rasal1 rescues the methylation of the Rasal1 promoter *in vivo*. The data is presented as mean value; error bars represent S.E.M.; **, $p < 0.01$, ***, $p < 0.001$.

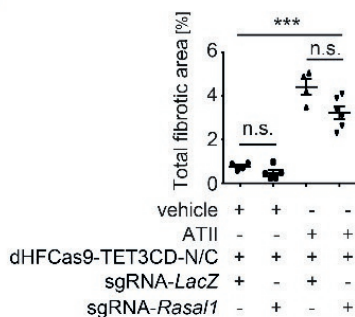
THE RASAL1 SPLIT-DEMETHYLATION TECHNIQUE IS DEPENDENT ON RASAL1 EXPRESSION

To confirm that our Rasal1 split-intein strategy is dependent on Rasal1 expression, we performed control *in vivo* experiments in Rasal1 knockout mice (Rasal1^{tm1d}, in which Rasal1 exons 3 and 4 are lacking). Even though promoter methylation of Rasal1 is induced upon ATII treatment in Rasal1 knockout mice and has been successfully rescued upon injection with the dHF-Cas9-TET3CD fusion constructs together with sgRNA-*Rasal1* (but not together with sgRNA-*LacZ*), this has no further impact on Rasal1 expression since the critical exons 3 and 4 are lacking (Figure 7E,F). Next, we assessed the effect of our split-demethylation technique on cardiac fibrosis in Rasal1 knockout mice. ATII treatment significantly induced cardiac fibrosis in Rasal1 knockout mice (Figure 7A-D). However, injection of the dHF-Cas9-TET3CD fusion constructs together with sgRNA-*Rasal1* did not ameliorate cardiac fibrosis in Rasal1 knockout mice (Figure 7A-D). This confirms that our Rasal1 split demethylation technique is gene-specific and indeed dependent on Rasal1 expression.

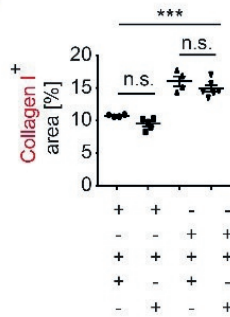
A



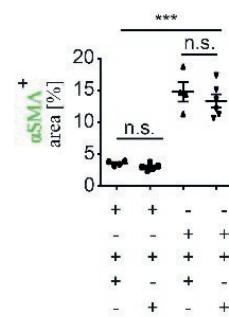
B



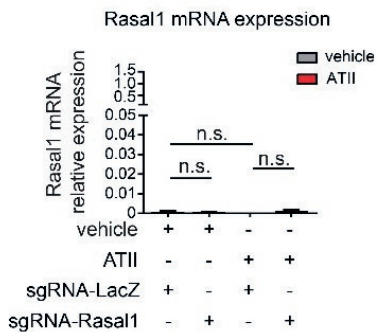
C



D



E



F

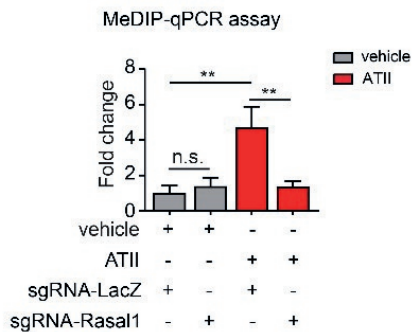


Figure 7. The split Rasal1 demethylation technique is dependent on Rasal1 expression.

(A) *Rasal1* knockout mice were treated with Angiotensin II (ATII) or PBS as vehicle control for 4 weeks and injected with AAV-dHF-Cas9-TET3CD-Intein-N and AAV-Intein-dHF-Cas9-TET3CD-C in combination with AAV-sgRNA-*Rasal1* or AAV-sgRNA-LacZ (as negative control). Vehicle control in combination with injection of AAV-dHF-Cas9-TET3CD-Intein-N and AAV-Intein-dHF-Cas9-TET3CD-C with either AAV-sgRNA-*Rasal1* or AAV-sgRNA-LacZ did not result in fibrosis and has similar effects on the expression of fibrotic markers Collagen-1 (in red) and α -SMA (in green). ATII treatment in combination with injection of AAV-dHF-Cas9-TET3CD-Intein-N, AAV-Intein-dHF-Cas9-TET3CD and AAV-sgRNA-LacZ or AAV-sgRNA-*Rasal1* both results in increased fibrosis as shown by Masson-Trichrom-Staining (MTS, in blue), Hematoxylin and eosin (HE) staining and immunofluorescent staining for Collagen-1 (in red) and α -SMA (in green) and there was no significant difference between the two groups. The nucleus was stained with DAPI (in blue). (B) Quantification of the total fibrotic area (in percentage) based on the MTS staining, (C) quantification of the Collagen-1 positive area and (D) quantification of the α -SMA positive area. (E) qRT-PCR analysis of *Rasal1* mRNA expression shows the lack of *Rasal1* expression in *Rasal1* knockout mice. (F) MeDIP analysis of the *Rasal1* promoter demonstrating that ATII treatment induces methylation of the *Rasal1* promoter. Injection of our dHFCas9-TET3CD fusion constructs together with sgRNA-*Rasal1* rescues the methylation of the *Rasal1* promoter in vivo. The data is presented as mean value; error bars represent S.E.M.; **, $p < 0.01$, ***, $p < 0.001$.

TRANSLATION OF OUR SPLIT-DEMETHYLATION TECHNIQUE TO HUMAN FIBROTIC CELL LINES

To explore whether the split intein-mediated demethylation technique also has future perspectives for use in humans, we transduced three human (fibrotic) cell lines with split-intein mediated fusion of green fluorescent protein via AAV delivery. Indeed, co-transduction of both constructs in human cardiac fibroblasts (HCFs), healthy human kidney fibroblasts (TK173) and fibrotic human kidney fibroblasts (TK188) efficiently transduces human fibroblasts as shown by the appearance of GFP (Suppl. Fig.2). This indicates that our split-mediated fusion of dHFCas9-TET3CD in combination with AAV delivery has also implications for future translation in humans.

DISCUSSION

Here, we demonstrate that Rasal1-deficiency does not result in spontaneous organ fibrogenesis but increases the progression of cardiac fibrosis upon Angiotensin-II (ATII) treatment. We performed gene-specific demethylation of Rasal1 by establishing split-intein mediated fusion of dHFCas9-TET3CD in a cardiac fibrosis mouse model. This split-intein mediated fusion of dHFCas9-TET3CD rescues Rasal1 expression *in vitro* whereas predicted off-target genes were not affected. Our split-intein strategy of dHFCas9-TET3CD in combination with AAV also allowed us to perform gene-specific demethylation of Rasal1 in the context of cardiac fibrosis. Importantly, our generated split-intein strategy also ameliorated cardiac fibrosis *in vivo*. Cardiac fibrosis is not ameliorated in Rasal1 knockout mice (due to lack of Rasal1 expression), confirming that our split-intein mediated reduction in cardiac fibrosis is gene-specific and dependent on Rasal1 expression.

Our results are in line with a previous study, where Takata et al. demonstrated that RASAL1-deficient mice do not show spontaneous liver fibrosis development but display exacerbated chemical-induced liver fibrosis [23]. Here, we systematically analyzed Rasal1 expression in different organs in Rasal1 deficient mice. We show that Rasal1 deficiency does not spontaneously induce organ fibrosis in the kidney, heart and lung, and that Rasal-deficient mice are more susceptible to cardiac fibrosis upon ATII treatment.

In our recent publication, we showed that lentiviral delivery of the dHFCas9-TET3CD construct could re-activate anti-fibrotic genes such as Rasal1 and ameliorates kidney fibrosis [8]. In this study, we made use of Rasal1^{tm1a} mice in which the Rasal1 gene expression is decreased upon insertion of a gene trapping cassette, resulting in around 70% Rasal1 mRNA reduction. Considerations of these Rasal1^{tm1a} mice are that (1) alternative splicing is not efficient enough to completely deplete the gene expression, and (2) that the insertion of the trapping cassette, which contains a human β -actin promoter, may influence the expression of neighboring genes and thus side effects cannot be ruled out. Now, we made use of complete Rasal1 knockout mice for the first time. The split-intein system in combination with AAV has been used for dCas9-based transcriptional repression before in a mouse model of heritable eye disease [24].

Recently, several studies highlighted the use of CRISPR/Cas9 in combination with AAV as potential therapy for Duchenne muscular dystrophy and Hutchinson-Gilford progeria syndrome [25-27]. This highlights the possibilities of CRISPR/Cas9 in combination with AAV for interfering with or prevention of disease progression. It was recently demonstrated that use of the split-intein system in combination with Cas9 can be used to treat metabolic liver disease by *in vivo* genome base editing [28]. Also, the split-intein system in combination with dCas9 was used to perform *in vivo* gene repression which prevented degradation of photoreceptors and improved visual function [24]. We now demonstrate the use of a Cas9 derivative (dHFCas9 fused to the catalytic domain of TET3) in combination with the split-intein technology to perform targeted demethylation both *in vitro* and *in vivo* and that this results in amelioration of cardiac fibrosis *in vivo*.

Other gene-splitting strategies include the use of “oversized” AAV but its limitation is that the packaged genome is as large as 6.0 kb but the larger genome-containing virions are highly heterogenous in size and are preferentially degraded by the proteasome [29]. Another strategy is the so-called dual vector AAV strategy which includes either trans-splicing [30], overlapping [31] or a combination of both (hybrid) dual AAV vectors. Another strategy to delivery large genes via AAV is spliceosome-mediated pre-mRNA trans-splicing [32,33]. Major limitations of these strategies include requirement of identification of optimal splitting points or overlapping regions which lead to reduced efficacy and high labor intensity. Among all those strategies, we made use of the split-intein approach to pack our demethylation system (~7.2 kb), since split-intein mediated CRISPR delivery by AAV has been successfully demonstrated before [24,28].

Altogether, we show that Rasal1 deficient mice exacerbate the progression of cardiac fibrosis in an experimental pressure-overload model, but that they do not display spontaneous fibrosis development in the heart, kidney, liver or lung. Also, we established a split-intein mediated gene-specific reactivation of Rasal1 expression through hydroxymethylation both *in vitro* and *in vivo* which ameliorates cardiac fibrosis. We here demonstrate the use of a new technology which holds promise not only for cardiac disease but for any disease associated with hypermethylation as well as for other applications where CRISPR/Cas9 in combination with AAV is useful.

MATERIALS AND METHODS

CLONING

All inserts were amplified by PCR with Phusion High-Fidelity DNA Polymerase (New England Biolabs, Ipswich, MA, USA) (sequences are listed in Table 1). The RmaIntein-C and RmaIntein-N (gBlocks® Gene Fragments, Integrated DNA Technologies, Coralville, IA, USA) PCR products were cloned into a pCMV6-Entry Vector (Origene, Rockville, MD, USA) at SgfI/MluI and XhoI/PmeI restriction sites (New England Biolabs, Ipswich, MA, USA) respectively. This resulted in generation of a pCMV6-RmaIntein-N and a pCMV6-RmaIntein-C construct. The EGFP(N-terminal) PCR product was cloned into the pCMV6-RmaIntein-N vector at SgfI/XhoI restriction sites (New England Biolabs, Ipswich, MA, USA) resulting in a pCMV6-EGFP(N)-RmaIntein-N construct. The EGFP(C-terminal) PCR product was cloned into the pCMV6-RmaIntein-C vector at MluI/XhoI restriction sites (New England Biolabs, Ipswich, MA, USA) generating a pCMV6-RmaIntein-C-EGFP(C) construct. Following the same strategy as with EGFP, the N- and C-terminal part of dHFCas9-TET3CD were inserted into pCMV6-RmaIntein-N and pCMV6-RmaIntein-C using AscI/XhoI and MluI/XhoI restriction sites respectively, thereby generating pCMV6-dHFCas9-TET3CD(N)-RmaIntein-N and pCMV6-RmaIntein-C-dHFCas9-TET3CD(C). The inserts were then shifted into vectors which are suitable for AAV transduction. The EGFP(N)-RmaIntein-N and RmaIntein-C-EGFP(C) PCR products were inserted into a pAAV-MCS Expression Vector (Cell Biolabs, San Diego, CA, USA) using EcoRI/HindIII restriction sites to generate pAAV-MCS-EGFP(N)-RmaIntein-N and pAAV-MCS-RmaIntein-C-EGFP(C) respectively. The dHFCas9-TET3CD(N)-RmaIntein-N was inserted into a pAAV-MCS Expression Vector at ClaI/BamHI cutting sites to generate a pAAV-MCS-dHFCas9-TET3CD(N)-RmaIntein-N vector. The RmaIntein-C-dHFCas9-TET3CD(C) was inserted into a pAAV-CMV-iCre vector (Addgene, Watertown, MA, USA) at KpnI/ClaI restriction sites to generate a pAAV-CMV-RmaIntein-C-dCas9-TET3CD(C) construct. The sgRNA sequences for *Rasal1* were designed by the online tool Blueheronbio (Origene, Herford, Germany). *Rasal1*-sgRNA-AARI was inserted into an AARI-digested pAAV-U6gRNA-U6gRNA vector (in which the TNT-Cre was removed) to generate a pAAV-*Rasal1*-sgRNA vector. *Rasal1*-sgRNA-SAPI was inserted into a SAPI-digested pAAV-*Rasal1*-sgRNA vector to generate a pAAV-*Rasal1*-sgRNA-*Rasal1*-sgRNA vector. The sgRNA sequences for LacZ were the same as previously

used [16,17], and the strategy for cloning was the same as for sgRasal1, thereby generating a pAAV-*LacZ*-sgRNA-*LacZ*-sgRNA vector. The oligo sequences are depicted in Table 2.

Table 1: Cloning primers

Name	Sequence
RmalIntein-C	F: AATT GCGATCGC CATGGCGGCGGCGTGCCCGGAA R: AATT ACGCGT GTTATGCGCAATAATATCGT
RmalIntein-N	F: AATT CTCGAG TGTCTGGCTGGCGATACTCT R: AATT GTTTAAAC GGAGGCAGTAGGGATTCTC
EGFP-N	F: TTAA GCGATCGC CATGGTGAGCAAGGGCGAGGA R: TTAA CTCGAG CTCCTGAAGTCGATGCCCTT
EGFP-C	F: TTAA ACGCGT GACGGCAACATCCTGGGG R: TTAA CTCGAG CTTGTACAGCTCGTCCATGC
dCas9-TET3CD-N	F: AATT GGCGCGCC ACCGGTGAGGAGATCTGCCG R: AATT CTCGAG AGTTTCAACCAATTGGCGTT
dCas9-TET3CD-C	F: AATT ACGCGT CGCCAAATCACTAAGCATGT R: AATT CTCGAG GATCCAGCGGCTGTAGGGGC
EGFP-N-RmalIntein-N	F: AATT GAATTC ATGGTGAGCAAGGGCGAGGA R: AATT TTAGTTATGCGCAATAATATCGT
RmalIntein-C-EGFP-C	F: AATT GAATTC ATGGCGGCGGCGTGCCCGGAA R: AATT AAGCTT TTAAGTGTACAGCTCGTCCATGC
dCas9-TET3CD-N-RmalIntein-N	F: AATT ATCGAT ATG ACCGGTGAGGAGATCTGCCG R: AATT GGATCC TTA GGAGGCAGTAGGGATTCTC
RmalIntein-C-dCas9-TET3CD-C	F: AATT GGTACC GCCATGTTGACATTGATTATTG R: AATT ATCGAT TAAAGCCCCAAACAGCTTCTCGCTGGA
Intein-N_AAV for pAAV-MCS-Intein-N-basic	F: AATT GTCGAC TGTCTGGCTGGCGATACTCT R: AATT AGATCT GGAGGCAGTAGGGATTCTC
pAAV-MCS-Intein-N-dCas9-TET3CD-N2-5	F: TTAA ATCGAT ATGGCGCCGAAAAAAAAACGC R2: TTAA GTCGAC TCCATTTGCAAGTGAATTTCTGT R3: TTAA GTCGAC ATTTCTTTTTGGTAAAATTGACT R4: TTAA GTCGAC TTTCCCTTTTTCCACCTTAG R5: TTAA GTCGAC CTTCAACTTTTCATAATGACTAGC
pAAV-CMV-Intein-C-dCas9-TET3CD-C2-5	F2: TTAA ACGCGT GAGATTCGCAAACGCCCT F3: TTAA ACGCGT TCGGACAAGCTTATTGCTCGTAA F4: TTAA ACGCGT TCGAAGAAGTTAAAATCCGTT F5: TTAA ACGCGT GGTAGTCCAGAAGATAACGAA R: TTAA ATCGAT CTTATCGTCGCATCCTTGTA

Table 2: Oligo sequences

Name	Sequence	Reference
sgRasal1-AARI	F: CACC CGCAGTGGCAGCCGGTGACGTGG	Self-designed
	R: AAC CGTCACCGGCTGCCACTGCG	Self-designed
sgRasal1-SAPI	F: ACC GAGACACCCGGTCTTGAGGG	Self-designed
	R: AAC TCCAAGAACCCGGGTGTCTC	Self-designed
sgLacZ-AARI	F: CACC TGCGAATACGCCACGCGAT	Platt et al., Cell, 2014
	R: AAAC ATCGCGTGGGCGTATTGCA	Platt et al., Cell, 2014
sgLacZ-SAPI	F: ACC CCCGAATCTCTATCGTGGG	Hart et al., Cell, 2015
	R: AAC CCGCACGATAGAGATTCGGG	Hart et al., Cell, 2015

The generated constructs were confirmed using sequencing (primer sequences are listed in Table 3). The CMV-based and AAV-based constructs were propagated in competent E.Coli (Invitrogen, Carlsbad, CA, USA) and STBL3 competent cells (Thermo Fisher Scientific, Waltham, MA, USA) respectively and isolated using the HiSpeed Plasmid Midi Kit (Qiagen, Hilden, Germany) according to the manufacturer's protocol

Table 3: Sequencing primers

Name	Sequence
For pCMV6 and AAV-MCS vector:	
Forward	GGACTTTCAAAATGTCG
Reverse	ATTAGGACAAGGCTGGTGGG
For pAAV-CMV-iCre and AAV-sgRNA vector:	
Forward	CGGCCGCACGCGCCGTACC
Reverse	AGGAGAGGCACTGGGGAGGG

CELL CULTURE, TGF- β TREATMENT AND TRANSFECTION

Mouse cardiac fibroblasts (MCFs), human embryonic kidney (HEK) 293 cells, human healthy kidney fibroblasts (TK173) and human fibrotic kidney fibroblasts (TK188) were cultured in Dulbecco's modified Eagle's medium (DMEM; Gibco, Carlsbad, CA, USA). HEK293T cells were cultured in high glucose DMEM (Gibco, Carlsbad, CA, USA). The DMEM medium contained 10% Fetal Calf Serum (FCS) (Sigma-Aldrich, St. Louis, MO, USA) and 1% penicillin/streptomycin (Gibco, Carlsbad, CA, USA). Human cardiac fibroblasts (HCFs) were cultured in Fibroblast

Medium-2 (ScienCell Research Laboratories, Carlsbad, CA, USA). Trypsin-EDTA Solution (Sigma-Aldrich, St. Louis, MO, USA) was used to detach the cells. For TGF- β 1 experiments, 1×10^5 MCFs were seeded to a 6-well plate, cultured overnight and treated with 10 ng/mL TGF- β 1 (R&D Systems, Minneapolis, MN, USA) for 4 days. The MCFs were then transfected overnight and treated for an additional 2 days with 10 ng/mL TGF- β 1. For other transfection experiments, 1×10^6 HEK293 cells were seeded to a 6-well plate and cultured overnight. The cells were transfected with Lipofectamine 2000 (Invitrogen, Carlsbad, CA, USA) according to the manufacturer's instructions. Briefly, 2 μ g of plasmid DNA and 5 μ L Lipofectamine 2000 were mixed in a total volume of 500 μ L Opti-MEM Reduced Serum medium (Gibco, Carlsbad, CA, USA) and allowed to form complexes at room temperature (RT) for 20 min. The plasmid DNA-Lipofectamine complex was added to the cells in DMEM growth medium. After overnight incubation, the medium was changed into complete DMEM growth medium.

AAV PACKAGING, PURIFICATION AND TRANSDUCTION

For AAV packaging, 2.5×10^7 HEK293T cells were plated in a 15 cm² dish. The next day, the medium was replaced by antibiotic free DMEM medium for two hours followed by transfection. For transfection, 7 μ g of AAV9-SLRSPPS (AAV serotype, kindly provided by Prof. Oliver Müller), 7 μ g of AAV genome (pAAV-dCas9-TET3CD(N)-N-intein, pAAV-C-intein-dCas9-TET3CD(C), pAAV-Rasal1-sgRNA-Rasal1-sgRNA or pAAV-LacZ-sgRNA-LacZ-sgRNA) and 20 μ g of helper plasmid (Cell Biolabs, San Diego, CA, USA) were added to 1.8 ml of Opti-MEM Reduced Serum medium and mixed. 170 μ l of PEI (Sigma-Aldrich, St. Louis, MO, USA) was added and the solution was again mixed before incubating at room temperature for 20 min. The solution was then added to the cells and incubated overnight. The following day, the medium was replaced by DMEM medium without FCS. Three days after transfection, the HEK293T cells were harvested. For harvesting, the media and cells were collected separately. The cells were resuspended with 10ml AAV lysis buffer (20mM Tris pH8.0, 1mM MgCl₂ and 150mM NaCl) and stored at -80 °C. To every 40 ml of media, 0.93g NaCl and 10ml of 40% PEG was added and kept at 4 °C overnight. The next day, the media was centrifuged to precipitate the AAV. The media was removed and the pellet was resuspended in 4 ml AAV lysis buffer and combined with the cells at -80 °C. For cell lysis and DNA digestion, 14ul of MgCl₂ and 5ul of Benzonase nuclease (Sigma-Aldrich, St. Louis, MO, USA) was

added followed by three cycles of freezing (-80 °C) and thawing (37 °C). Another 5ul of Benzonase nuclease was added before digestion was performed at 37 °C for 15 min. After centrifugation, the supernatant was transferred to a new tube. AAV was concentrated using the iodixanol density gradient (Optiprep, Sigma-Aldrich, St. Louis, MO, USA). Viral genome extraction was performed by treatment with DNase I and 10x DNase buffer at 37°C for 30 min and 95°C for 10 min. Proteinase K and DNase I was added before incubating at 37°C for 15 min and 95°C for 10 min to release the vector DNA from the AAV capsid. AAV titration primers are listed in Table 4. Serial dilutions were used to generate a standard curve for absolute quantification of AAV. For transduction experiments, 3x10⁵ MCFs, HCFs, TK173 or TK188 cells were seeded to a 6-well plate and cultured overnight. The cells were transduced by using 100.000 MOI (multiplicity of infection) and were collected after 48 hours.

Table 4: AAV titration primers

Name	Sequence
AAV-dHF-Cas9-TET3CD-Intein-N and AAV-Intein-dHFCas9-TET3CD-C	F: TTCCTACTTGGCAGTACATCTTACG R: GTCAATGGGGTGGAGACTTGG
AAV-sgRNA-Rasal1 and AAV-sgRNA-LacZ	F: TGGGCTTATATGGGCTCCTG R: GCAACACTTGTGAGCTGCTA

WESTERN BLOT

Proteins were extracted using Np40 lysis buffer (Invitrogen, Carlsbad, CA, USA) supplemented with proteinase inhibitor cocktail (Roche, Basel, Switzerland) and phosphatase inhibitor cocktail 2 (Sigma-Aldrich, St. Louis, MO, USA) and incubation on ice for 30 min. Sonication was performed to destroy protein complex and the lysate was mixed with SDS and incubated at 95 °C for 5 min. Protein samples were resolved on a NuPage 4-12% Bis-Tris gel (Invitrogen, Carlsbad, CA, USA) together with the Novex Sharp Pre-Stained Protein Standard (Invitrogen, Carlsbad, CA, USA) and transferred onto a nitrocellulose membrane (GE Healthcare, Buckinghamshire, UK) using 20x NuPAGE Transfer buffer (Invitrogen, Carlsbad, CA, USA) and 10% methanol in ddH₂O. The membrane was blocked with 5% milk in TBS-T (containing TBS pH 7.2 and 0.1% Tween-20) at RT for 1h and incubation with the primary antibody in 2% milk in TBS-T was

performed at 4 °C overnight. The following primary antibodies and dilutions were used: Anti-GAPDH (#5G4 Mab 6C5, HyTest, Turku, Finland) 1:5000 and GFP Tag Monoclonal Antibody (#MA5-15256, Thermo Fisher Scientific, Waltham, MA, USA) 1:2000. The next day the membrane was washed with 2% milk in TBS-T before incubation with secondary horseradish peroxidase-conjugated antibodies (Cell Signaling, Danvers, MA, USA) 1:2500 in 2% milk in TBS-T at RT for 1h. The membrane was washed with 2% milk in TBS-T and with PBS before detection using 20x LumiGLO Reagent and 20x Peroxide (Cell Signaling Technology, Cambridge, UK).

RNA EXTRACTION AND QUANTITATIVE REAL-TIME PCR

RNA was extracted using PureLink RNA Mini Kit (Life Technologies, Carlsbad, CA, USA) according to the manufacturer's protocol. cDNA synthesis was performed using DNaseI (Sigma-Aldrich, St. Louis, MO, USA) and the SuperScriptII Reverse Transcriptase system (Invitrogen, Carlsbad, CA, USA) according to the manufacturer's protocol. The diluted cDNA (1:10) together with Fast SYBR Green Master Mix (Applied Biosystems, Waltham, MA, USA) was run on a StepOnePlus Real-Time PCR System (Applied Biosystems, Waltham, MA, USA). Quantitative Real-Time PCR (qRT-PCR) reactions were performed using a 10 min holding stage at 95°C and 40 cycles of 95°C for 15 sec and 60°C for 1 min. Ct values were normalized to GAPDH using the $\Delta\Delta Ct$ method. Primer sequences are listed in Table 5.

Table 5: qRT-PCR primers

Name	Sequence	Reference
mGapdh	F: TGTAGACCATGTAGTTGAGGTCA	Origene
	R: AGGTCGGTGTGAACGGATTTG	Origene
mRasal	F: CTCACAAGGCGTGAGGTGG	Bechtel et al., Nat. Med, 2010
	R: TGCCAAGGAGTTAGAACGGAA	Bechtel et al., Nat. Med, 2010
mScgb1b30	F: TTGTGGCCTTTGCCAGTTTTAC	Origene
	R: GCCAACATCCTATCGGAACAT TTC	Origene
mMcu	F: GAGCCGCATATTGCACTACGGT	Origene
	R: AAACACGCCGACTGAGTCAGAG	Origene
mFlnb	F: CCTGGACTGAAAGAGGCGTTTAC	Origene
	R: CTGCCATCCTTGTTGTCTCTGC	Origene
mTmem56	F: CGTGCCACTCTTTGTTAGTTG GG	Origene

	R: TGAGGTAGCCTGAAGCAGTTGC	Origene
mSyne1	F: CAGCCATTCAGTGTGAGCAGCT	Origene
	R: CACCATCCAGACCTCTAAGGCT	Origene
mSlc2a5	F: ATCGCTGCCTTTGGCTCATCCT	Origene
	R: AGCAGCGTCAAGGTGAAGGACT	Origene
mPark2	F: GAGGTCGATTCTGACACCAGC	Primer bank
	R: CCGGCAAAAATCACACGCAG	Primer bank
mKsr1	F: ACATGACTGGCTGTGCTACCTG	Origene
	R: GCCAGTCTCTTGCTGTAGTTC	Origene
mProb1	F: TCACAAGCACTCTGGACGAC	Self-designed
	R: TAACCATCTTGCGCACGTCT	Self-designed
mPcdhga2	F: CCAACACTGACTGGCGTTTCTC	Origene
	R: GATCATGGCTTGACAGCATCTCTG	Origene
mNipa2	F: TGCTCCGGCCACATTAGTG	Primer bank
	R: GCA AAC ACC CAATTTCCCATGA	Primer bank
mJdp2	F: CACTTCTGGAGGTGAAACTGG	Origene
	R: GCAGCGACTTTGTCTTTCCCG	Origene

DNA ISOLATION AND METHYLATION DNA IMMUNOPRECIPITATION

DNA isolation of cells and tissues was performed using the DNeasy Blood & Tissue Kit (Qiagen, Hilden, Germany) according to the manufacturer's protocol. Methylated DNA immunoprecipitation (Epigentek, Farmingdale, NY, USA) was performed according to the manufacturer's protocol as well. In short, wells were incubated with MC1 buffer in combination with anti-5-methylcytosine or normal mouse IgG (as negative control) at RT for 1h. The wells were washed with MC1 buffer and MC3 buffer before the sonicated DNA was added to the wells (5% of sonicated DNA was left aside as input). The wells were incubated at RT for 2h while shaking and washed three times with MC3 buffer. MC4 buffer in combination with Proteinase K was added to the wells and incubated at 65°C for 1h. Finally, methylated DNA was eluted and methylation was quantified using qRT-PCR (primer sequences are listed in Table 6).

Table 6: MeDIP primers

Name	Sequence
mRasal1	F: TGCAGATGGCTCTTATCGTG R: CCAATTAACCCGGAGTGTG

ANIMAL EXPERIMENTS

The targeted $Rasal1^{tm1a(KOMP)}$ WTSI mouse line was generated as described previously [8], after breeding with a CAG-FlpO line (Jackson Laboratory, Bar Harbor, ME, USA), a $Rasal1$ floxed mouse line ($Rasal1^{tm1c}$) was generated. These mice were bred with wildtype C57Bl/6N mice to eliminate the FlpO transgene. To obtain a ubiquitously $Rasal1$ -knockout mouse line, $Rasal1^{tm1c}$ was bred with a E2a-Cre line (The Jackson Laboratory, Bar Harbor, ME, USA). The $Rasal1^{tm1c/+}$ allele was produced by crossing $Rasal1^{tm1a/tm1a}$ with a global Flp transgenic mouse strain [C57BL/6N-Tg(CAG-Flpo)1Afst/Mmucd, UCDavis Stock No: 036512]. The $Rasal1^{tm1d/+}$ allele was generated by mating $Rasal1^{tm1c/tm1c}$ with a global Cre transgenic mouse strain [B6.FVB-Tg(Ella-cre)C5379Lmgd/J, The Jackson Laboratory Stock No: 003724]. After breeding with wild type C57Bl/6N mice, the Cre transgene was eliminated. PCR primers used for genotyping are listed in table 7. All the animal experiments complied with the ethical regulations and were approved by the Institutional Review Board of the University of Göttingen and the responsible government authority of Lower Saxony (Germany). Anesthesia with isoflurane inhalation was performed with 8-12 weeks-old mice before the ATII osmotic mini pump (Alzet, Cupertino, CA, USA) was inserted into a skin pocket of the dorsal neck. The mice were injected with AAV using tail vein injection. Analgesia was performed via subcutaneous injection. The mice were sacrificed after 4 weeks and hearts were embedded in paraffin.

Table 7: $Rasal1^{tm1d}$ mice genotyping primers

Name	Sequence
PostFlp	F: TGTCTGGCTTTGACTTGACCCTAGC R: ACACATCCAGACATGCAAAGGAAGC
PostFlp & Cre	F: TGTCTGGCTTTGACTTGACCCTAGC R: CTTAGAGGCAAAGTGCTTGCTAGGC
FlpO	F: GCTATCGAATTCCACCATGGCTCCTAAGAAGAA R: CAATGCGATGAATTCTCAGATCCGCCTGTTGATGTA
Cre	F: GCATTACCGTTCGATGCAACGAGTGATGAG R: GAGTGAACGAACCTGGTCGAAATCAGTGCG

HISTOLOGY AND IMMUNOFLUORESCENCE STAINING OF TISSUE

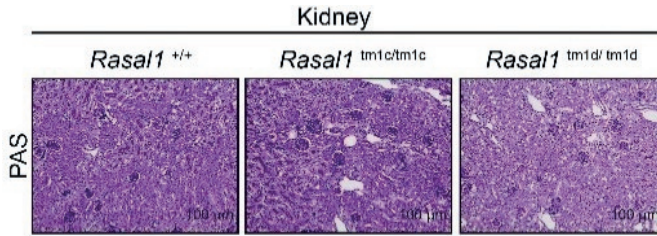
Paraffin-embed hearts were sectioned and Masson's Trichrome Staining (MTS) was performed as described previously [9]. The fibrotic area was assessed by the CellSens software (Olympus, Tokyo, Japan) as previously described [9]. For immunofluorescent stainings, paraffin-embedded heart tissue was put into xylene for 2x 10 min, put into 100% EtOH for 2x 5 min and put into 95%, 70%, 50% and 30% EtOH for 5 min each to complete the deparaffinization. The tissue was washed with distilled water and PBS before being boiled in 1:10 diluted Target Retrieval Solution (#S1699, Dako, Jena, Germany) in dH₂O for 40 min. The tissue was washed 2x with PBS and blocked using 1% BSA in PBS at RT for 30 min. The primary antibodies were added in 1% BSA in PBS and incubated at 4 °C overnight. The following primary antibodies were used: anti-collagen 1 (#ab34710, 1:200, Abcam, Cambridge, UK), anti-alpha smooth muscle Actin antibody (#ab32575, 1:100, Abcam, Cambridge, UK), GFP Tag Monoclonal Antibody (#MA5-15256, 1:2000, Thermo Fisher Scientific, Waltham, MA, USA) and anti-Mouse wheat germ agglutinin Alexa Fluor 595 conjugated (#W11262; 1:100, Life Technologies, Carlsbad, CA, USA). The next day, the slides were washed with PBS before the secondary antibody was added in 1% BSA in PBS at RT for 45 min. The following secondary antibodies were used: Alexa Fluor 488 donkey anti-mouse (#A21202, 1:200, Thermo Fisher Scientific, Waltham, MA, USA) and Alexa Fluor 568 donkey anti-rabbit (#A10042, 1:200, Thermo Fisher Scientific, Waltham, MA, USA). The tissue was washed with PBS and 1mg/mL DAPI 1:1000 diluted in PBS was added at RT for 5 min. Mounting medium was added and the slides were topped with coverslips. The stained slides were examined by the Inverted Zeiss LSM 780 multiphoton laser scanning confocal microscope (Zeiss, Oberkochen, Germany).

STATISTICAL ANALYSIS

The data is presented as the mean \pm SEM and represents a minimum of four independent experiments. Quantification of histology and immunofluorescence staining was assessed with 3 slides (5 visual fields each) per mouse and average values of each mouse were calculated. The average values for each mouse (n=5) was then used to calculate average per group. Statistical analysis was performed by a Student's t test (two-tailed) for the comparison of two groups. For the

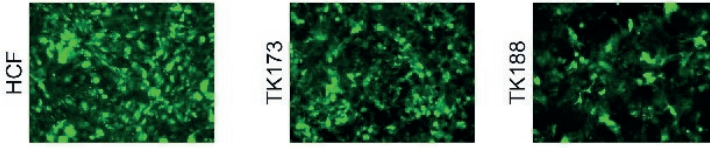
comparison of four groups, One-way ANOVA in combination with a Bonferroni post-hoc analysis was performed. A p value <0.05 was considered statistically significant.

SUPPLEMENTARY INFORMATION

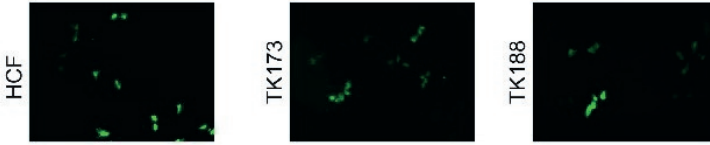
**Supplementary Figure 1. No change in glomerular structure in *Rasa1* knockout mice.**

PAS staining in kidneys of wildtype (*Rasa1*^{+/+}), *Tm1c* (*Rasa1*^{tm1c/tm1c}) and *Tm1d* *Rasa1* knockout mice (*Rasa1*^{tm1d/tm1d}) demonstrates no difference in glomerular structure.

GFP signal intensity 72 hours after AAV-SLRSPPS-EGFP transduction



GFP signal intensity 3 weeks after AAV-SLRSPPS-EGFP transduction



Supplementary Figure 2. The split-demethylation technique also functions in human fibrotic cell lines. *Human cardiac fibroblasts (HCFs), human healthy kidney fibroblasts (TK173) and human fibrotic kidney fibroblasts (TK188) were efficiently transduced with AAV-SLRSPPS-EGFP.*

REFERENCES

1. Khan, R. and Sheppard, R. (2006) Fibrosis in heart disease: understanding the role of transforming growth factor-beta in cardiomyopathy, valvular disease and arrhythmia. *Immunology*, 118, 10-24.
2. Sabbah, H.N., Sharov, V.G., Lesch, M. and Goldstein, S. (1995) Progression of heart failure: a role for interstitial fibrosis. *Mol Cell Biochem*, 147, 29-34.
3. Eddy, A.A. (1996) Molecular insights into renal interstitial fibrosis. *J Am Soc Nephrol*, 7, 2495-2508.
4. Kuncio, G.S., Neilson, E.G. and Haverty, T. (1991) Mechanisms of tubulointerstitial fibrosis. *Kidney Int*, 39, 550-556.
5. Zeisberg, E.M. and Zeisberg, M. (2013) The role of promoter hypermethylation in fibroblast activation and fibrogenesis. *J Pathol*, 229, 264-273.
6. Bechtel, W., McGoohan, S., Zeisberg, E.M., Muller, G.A., Kalbacher, H., Salant, D.J., Muller, C.A., Kalluri, R. and Zeisberg, M. (2010) Methylation determines fibroblast activation and fibrogenesis in the kidney. *Nat Med*, 16, 544-550.
7. Xu, X., Tan, X., Tampe, B., Nyamsuren, G., Liu, X., Maier, L.S., Sossalla, S., Kalluri, R., Zeisberg, M., Hasenfuss, G. et al. (2015) Epigenetic balance of aberrant Rasal1 promoter methylation and hydroxymethylation regulates cardiac fibrosis. *Cardiovasc Res*, 105, 279-291.
8. Xu, X., Tan, X., Tampe, B., Wilhelmi, T., Hulshoff, M.S., Saito, S., Moser, T., Kalluri, R., Hasenfuss, G., Zeisberg, E.M. et al. (2018) High-fidelity CRISPR/Cas9- based gene-specific hydroxymethylation rescues gene expression and attenuates renal fibrosis. *Nat Commun*, 9, 3509.
9. Tampe, B., Tampe, D., Zeisberg, E.M., Muller, G.A., Bechtel-Walz, W., Koziolok, M., Kalluri, R. and Zeisberg, M. (2015) Induction of Tet3-dependent Epigenetic Remodeling by Low-dose Hydralazine Attenuates Progression of Chronic Kidney Disease. *EBioMedicine*, 2, 19-36.
10. Jeong, D., Lee, M.A., Li, Y., Yang, D.K., Kho, C., Oh, J.G., Hong, G., Lee, A., Song, M.H., LaRocca, T.J. et al. (2016) Matricellular Protein CCN5 Reverses Established Cardiac Fibrosis. *J Am Coll Cardiol*, 67, 1556-1568.
11. Morita, S., Noguchi, H., Horii, T., Nakabayashi, K., Kimura, M., Okamura, K., Sakai, A., Nakashima, H., Hata, K., Nakashima, K. et al. (2016) Targeted DNA demethylation in vivo using dCas9-peptide repeat and scFv-TET1 catalytic domain fusions. *Nat Biotechnol*, 34, 1060-1065.
12. Liu, X.S., Wu, H., Ji, X., Stelzer, Y., Wu, X., Czauderna, S., Shu, J., Dadon, D., Young, R.A. and Jaenisch, R. (2016) Editing DNA Methylation in the Mammalian Genome. *Cell*, 167, 233-247 e217.
13. Wu, H., Hu, Z. and Liu, X.Q. (1998) Protein trans-splicing by a split intein encoded in a split DnaE gene of *Synechocystis* sp. PCC6803. *Proc Natl Acad Sci U S A*, 95, 9226-9231.
14. Shah, N.H. and Muir, T.W. (2014) Inteins: Nature's Gift to Protein Chemists. *Chem Sci*, 5, 446-461.

15. Novikova, O., Topilina, N. and Belfort, M. (2014) Enigmatic distribution, evolution, and function of inteins. *J Biol Chem*, 289, 14490-14497.
16. Hart, T., Chandrashekar, M., Aregger, M., Steinhart, Z., Brown, K.R., MacLeod, G., Mis, M., Zimmermann, M., Fradet-Turcotte, A., Sun, S. et al. (2015) High-Resolution CRISPR Screens Reveal Fitness Genes and Genotype-Specific Cancer Liabilities. *Cell*, 163, 1515-1526.
17. Platt, R.J., Chen, S., Zhou, Y., Yim, M.J., Swiech, L., Kempton, H.R., Dahlman, J.E., Parnas, O., Eisenhaure, T.M., Jovanovic, M. et al. (2014) CRISPR-Cas9 knockin mice for genome editing and cancer modeling. *Cell*, 159, 440-455.
18. Zetsche, B., Volz, S.E. and Zhang, F. (2015) A split-Cas9 architecture for inducible genome editing and transcription modulation. *Nat Biotechnol*, 33, 139-142.
19. Xu, X., Tan, X., Hulshoff, M.S., Wilhelmi, T., Zeisberg, M. and Zeisberg, E.M. (2016) Hypoxia-induced endothelial-mesenchymal transition is associated with RASAL1 promoter hypermethylation in human coronary endothelial cells. *FEBS Lett*, 590, 1222-1233.
20. Tampe, B., Tampe, D., Muller, C.A., Sugimoto, H., LeBleu, V., Xu, X., Muller, G.A., Zeisberg, E.M., Kalluri, R. and Zeisberg, M. (2014) Tet3-mediated hydroxymethylation of epigenetically silenced genes contributes to bone morphogenic protein 7-induced reversal of kidney fibrosis. *J Am Soc Nephrol*, 25, 905-912.
21. Stemmer, M., Thumberger, T., Del Sol Keyer, M., Wittbrodt, J. and Mateo, J.L. (2015) CCTop: An Intuitive, Flexible and Reliable CRISPR/Cas9 Target Prediction Tool. *PLoS One*, 10, e0124633.
22. Varadi, K., He, T., Sacher, A., Müller, M., Grimm, D., Katus, H.A., Backs, J. and Müller, O., J. (2013) [Abstracts of the 79th Annual Meeting of the German Cardiac Society. April 3-6, 2013. Mannheim, Germany]. *Clin Res Cardiol*, 102 Suppl 1, 1.
23. Takata, A., Otsuka, M., Kishikawa, T., Yamagami, M., Ishibashi, R., Sekiba, K., Suzuki, T., Ohno, M., Yamashita, Y., Abe, T. et al. (2017) RASAL1 is a potent regulator of hepatic stellate cell activity and liver fibrosis. *Oncotarget*, 8, 64840-64852.
24. Moreno, A.M., Fu, X., Zhu, J., Katrekar, D., Shih, Y.V., Marlett, J., Cabotaje, J., Tat, J., Naughton, J., Lisowski, L. et al. (2018) In Situ Gene Therapy via AAV-CRISPR-Cas9-Mediated Targeted Gene Regulation. *Mol Ther*, 26, 1818-1827.
25. Beyret, E., Liao, H.K., Yamamoto, M., Hernandez-Benitez, R., Fu, Y., Erikson, G., Reddy, P. and Izpisia Belmonte, J.C. (2019) Single-dose CRISPR-Cas9 therapy extends lifespan of mice with Hutchinson-Gilford progeria syndrome. *Nat Med*, 25, 419-422.
26. Nelson, C.E., Wu, Y., Gemberling, M.P., Oliver, M.L., Waller, M.A., Bohning, J.D., Robinson-Hamm, J.N., Bulaklak, K., Castellanos Rivera, R.M., Collier, J.H. et al. (2019) Long-term evaluation of AAV-CRISPR genome editing for Duchenne muscular dystrophy. *Nat Med*, 25, 427-432.
27. Santiago-Fernandez, O., Osorio, F.G., Quesada, V., Rodriguez, F., Basso, S., Maeso, D., Rolas, L., Barkaway, A., Nourshargh, S., Folgueras, A.R. et al. (2019) Development of a CRISPR/Cas9-based therapy for Hutchinson-Gilford progeria syndrome. *Nat Med*, 25, 423-426.

28. Villiger, L., Grisch-Chan, H.M., Lindsay, H., Ringnalda, F., Pogliano, C.B., Allegri, G., Fingerhut, R., Haberle, J., Matos, J., Robinson, M.D. et al. (2018) Treatment of a metabolic liver disease by in vivo genome base editing in adult mice. *Nat Med*, 24, 1519-1525.
29. Grieger, J.C. and Samulski, R.J. (2005) Packaging capacity of adeno-associated virus serotypes: impact of larger genomes on infectivity and postentry steps. *J Virol*, 79, 9933-9944.
30. Hirsch, M.L., Li, C., Bellon, I., Yin, C., Chavala, S., Pryadkina, M., Richard, I. and Samulski, R.J. (2013) Oversized AAV transduction is mediated via a DNA-PKcs-independent, Rad51C-dependent repair pathway. *Mol Ther*, 21, 2205-2216.
31. Halbert, C.L., Allen, J.M. and Miller, A.D. (2002) Efficient mouse airway transduction following recombination between AAV vectors carrying parts of a larger gene. *Nat Biotechnol*, 20, 697-701.
32. Tornabene, P., Trapani, I., Minopoli, R., Centrulo, M., Lupo, M., de Simone, S., Tiberi, P., Dell'Aquila, F., Marrocco, E., Iodice, C. et al. (2019) Intein-mediated protein trans-splicing expands adeno-associated virus transfer capacity in the retina. *Sci Transl Med*, 11.
33. Dooley, S.J., McDougald, D.S., Fisher, K.J., Bennicelli, J.L., Mitchell, L.G. and Bennett, J. (2018) Spliceosome-Mediated Pre-mRNA trans-Splicing Can Repair CEP290 mRNA. *Mol Ther Nucleic Acids*, 12, 294-308.

CHAPTER 12

RESEARCH SUMMARY

RESEARCH SUMMARY

(EPI)GENETIC REGULATION OF ENDOTHELIAL PLASTICITY

Endothelial-to-mesenchymal transition (EndMT) is the hallmark of endothelial plasticity and is the main focus of the first part of this thesis. EndMT can be induced via several signaling pathways, including TGF- β , and modulators, including hypoxia (lack of oxygen) and high glucose concentrations. These signaling pathways and modulators play a crucial role in the activation of epigenetic modifiers which in part regulate EndMT. In **Chapter 2** we summarize epigenetic changes that are associated with EndMT in the context of chronic heart disease. We identified histone methylation and (de)acetylation, DNA methylation as well as noncoding RNAs as important regulators and thus potential epigenetic targets of EndMT. An example of this is demonstrated in **Chapter 3** where hypoxia induces TGF- β signaling which in turn causes DNMT3a-mediated promoter methylation of *Rasal1*, thereby contributing to EndMT.

The primary cause of morbidity and mortality in diabetes patients is cardiovascular disease. Diabetes patients exhibit accelerated aortic stiffening which precedes hypertension development and is therefore believed to be an early contributor to cardiovascular disease. In **Chapter 4** we identified robust EndMT in aortas of type 2 diabetic mice and patients which might contribute to aortic stiffening in type 2 diabetes. We also identified miR-132-3p as well as *KLF7* as potential novel regulators in this context. This shows that EndMT does not only play a role in the context of cardiac fibrosis, but is also associated with other pathologies.

Therefore, we continued by summarizing the non-coding RNAs which are known to regulate EndMT in different contexts such as atherosclerosis, myocardial fibrosis but also of kidney disease in **Chapter 5**. We also highlight non-coding RNAs which have different effects on EndMT in development and pathology. In all, we could show that a remarkable number of non-coding RNAs is associated to the EndMT regulatory program.

In **Chapter 6** we performed stage-specific mapping of EndMT to get insights in the genetic regulatory mechanisms that facilitate the active stage of EndMT. We identified that the active stage of EndMT is characterized by changes in the Rap1 signaling pathway, and that Rap1 inhibition in part alleviates EndMT.

Altogether, the first part of this thesis highlights the interplay between the different signaling pathways, modulators as well as epigenetic modifiers in regulating EndMT.

(EPI)GENETICS AS A THERAPEUTIC TARGET IN FIBROSIS

In the second part of this thesis, we focus on (epi)genetics as a therapeutic target in fibrosis. In **Chapter 7** we show that Serelaxin, a recombinant form of the human hormone Relaxin-2, inhibits EndMT and ameliorates cardiac fibrosis. Serelaxin reversed the TGF- β -mediated histone modifications at the RXFP1 promoter thereby restoring the expression of RXFP1 which enabled RXFP1-mediated inhibition of EndMT.

Cardiovascular disease and heart failure are the primary cause of morbidity and mortality in patients with chronic kidney disease. In **Chapter 8** we review the current knowledge of how kidney injury causes heart failure and fibrosis. Different components such as inflammation but also EndMT and non-coding RNAs are potential regulators which facilitate chronic kidney disease-induced cardiac fibrosis.

In **Chapter 9** we summarize genomic editing tools including the recent discovered CRISPR/Cas9 system. We describe distinct functions of CRISPR/Cas9 derivatives including tracking, transcriptional activation and repression, and base editing. We also discuss the *in vivo* applications and potential of CRISPR/Cas9 derivatives which results in changes in (disease) phenotype. In **Chapter 10** we make use of the CRISPR/Cas system by deactivating the Cas9 nuclease and fusing it to the catalytic domain of TET3. This enabled gene-specific hydroxymethylation and thus reactivation which ameliorates kidney fibrosis. In **Chapter 11** we use split-intein mediated AAV delivery of the established system (deactivated Cas9 nuclease fused to the catalytic domain of TET3) to perform gene-specific reactivation of Rasal1 expression which ameliorates cardiac fibrosis. This shows the possibilities of targeting epigenetic modifications thereby ameliorating organ fibrosis.

In conclusion, in this thesis we have shown that endothelial plasticity is highly regulated by epigenetic modifications. Besides, we have shown that epigenetic

modifications can be targeted *in vivo* which results in the amelioration of organ fibrosis.

CHAPTER 13

EPILOGUE

EPILOGUE

OUTCOME OF THIS THESIS

Fibrosis is an underlying cause of chronic illnesses such as heart failure and chronic kidney disease [1]. As of yet, no effective treatment for fibrosis is available. In *part I* of this thesis, we gained insight into the (epi)genetic regulation of endothelial plasticity, as an underlying cause of fibrosis. In *part II*, we established proof-of-concept to perform (epi)genetic targeting in experimental fibrosis. In this chapter, we discuss the future challenges for (1) the field of EndMT and (2) for the therapeutic targeting of (epi)genetics in fibrosis that originate from this thesis.

FUTURE GOALS TO IMPROVE OUR UNDERSTANDING OF ENDMT

The field of EndMT research is an emerging and exciting field since it provides opportunities for future (epi)genetic therapeutic applications in several diseases such as organ fibrosis and cardiovascular disease. Nevertheless, several challenges, open questions and limitations concerning EndMT need to be overcome in the future.

First, standardization of *in vitro* models of EndMT is key to unraveling the underlying (epi)genetic mechanisms of EndMT. So far, *in vitro* models of EndMT are inconsistent because of the use of different types of media and inducers, which affect the extent and phenotype of EndMT, and making it difficult to compare individual studies to each other [2]. The same holds for different time points of stimulation (*e.g.* 2 hours versus 12 days) and the use of both mouse and human cell lines. Moreover, one study showed that passage number as well as culturing versus freshly isolated endothelial cells affects the non-coding RNA expression [3]. This highlights that non-coding RNA expression is highly adaptable and that proper *in vivo* validation is key. It is safe to speculate that the same holds for other epigenetic modifiers such as DNA promoter methylation and histone modifications. In my opinion, it would be key to develop consortia with researchers which focus on endothelial plasticity with the aim to achieve a consensus about standardization of *in vitro* EndMT protocols. We, as EndMT researchers, would largely benefit from this agreement, since we can then focus

on unraveling EndMT under standard conditions and from there move towards a broader understanding of EndMT. Also, the role of epigenetics and the underlying regulatory mechanisms is most established in cancer where a similar process to EndMT is present: epithelial-to-mesenchymal transition (EMT). Therefore, I believe that close collaboration between EndMT and EMT researchers is key to improve our understanding of endothelial/epithelial plasticity.

Second, our understanding of EndMT is limited by the lack of *in vivo* models which allow specific inhibition or depletion of EndMT. This restricts our understanding of the causative role that EndMT has in disease pathology. From my perspective, after the identification of EndMT inhibitors in standardized assays, these could then also be applied to develop proper *in vivo* models of EndMT. Proper standardization of *in vitro* models and development of *in vivo* models might also help to explain why different studies came to different conclusions with respect to the extent of EndMT in different *in vivo* contexts (eg transverse aortic constriction versus ascending aortic constriction) [4,5]. Future stage-specific mapping strategies as well as the recent development of the single-cell sequencing technology would potentially help on this part (even though it is currently limited by its sequencing depth).

Third, EndMT is not a process that all endothelial cells go through and most end-stage studies report on heterogenous cell populations containing EndMT-derived myofibroblasts and EndMT-resistant endothelial cells. Therefore, an open question about EndMT is why certain endothelial cells undergo EndMT whereas others are resistant to EndMT. This might be explained by clonality (which directs endothelial cells from the same clone towards EndMT-prone or EndMT-resistant). The recent established Rainbow system might help to answer this question. The Rainbow system enables to mark different cells and their progeny with distinct fluorescent colors thereby allowing to trace cellular expansion *in vivo* [6,7]. When driven under an endothelial-specific promoter, the Rainbow system could identify individual endothelial cells and their progeny. This endothelial-specific Rainbow system, in combination with mesenchymal marker analysis, might help to examine whether certain clones are more prone towards EndMT than others. This might help us to identify novel therapeutic strategies aimed at EndMT-prone and/or EndMT-resistant cells.

Future research and perhaps the discovery of novel technologies, will potentially help to overcome the current challenges and limitations concerning

EndMT. This will help us to reach a better understanding of the (epi)genetic regulation of EndMT, as an underlying cause of fibrosis.

CURRENT CHALLENGES TO TARGET (EPI)GENETICS IN FIBROSIS

(Epi)genetic targeting to combat fibrosis has exciting opportunities for future use in the clinic. Nevertheless, several questions and challenges concerning (epi)genetic targeting in the context of fibrosis need to be addressed.

One of the questions that need to be answered before performing (epi)genetic targeting to combat fibrosis, is whether to perform cell-specific or general treatment. Cell-specific treatment has most likely the advantage that it has less adverse effects since it is specifically focused on one cell type. However, since endothelial-derived myofibroblast-like cells and (myo)fibroblasts are believed to express the same markers and exhibit common mechanisms to secrete extracellular matrix, general treatment could result in targeting two aspects of fibrosis at the same time which I believe might potentially have a stronger and pleiothropic effect on the disease pathology.

Concerning the targeting of cell types, it is important to note the matter of balance. Fibroblasts are not only detrimental but also exert beneficial effects (*e.g.* during initial insults). The same holds for (partial) EndMT which contributes to the formation of new vessels upon ischemia [8,9]. Therefore, I believe that future strategies should be directed towards elimination of some, but definitely not all (myo)fibroblasts and cells that are prone to undergo EndMT, which should be a point of consideration for each future therapy that targets fibrosis.

When focusing specifically on EndMT, it is likely that we have to make a choice which cells we want to target: the cells actively undergoing EndMT or the endothelial cells that have already fully transformed into myofibroblast-like cells. I personally believe that the cells that actively undergo EndMT represent the most targetable population to combat EndMT since (1) they are unique in their phenotype and (2) patients with chronic illnesses most likely have ongoing EndMT as part of the chronic disease pathology. However, gene signatures and marker expression of the active stage of EndMT remain largely unknown which remains a challenge for now.

Also, we have to make a decision whether we want to direct cells that undergo EndMT into a so-called mesenchymal-to-endothelial transition (MEndT)

to reverse their phenotype. It has been recently described that cardiac fibroblasts adopt an endothelial cell phenotype upon ischemic cardiac injury [10]. However, it is unclear until now whether MEndT also occurs during chronic disease states (such as heart failure) and whether (full) reversal of EndMT via MEndT is possible. Even though MEndT might be beneficial, we can also speculate that when we force EndMT-derived myofibroblast-like cells into MEndT, they could become more prone to (again) undergo EndMT at a later time point. Therefore, future knowledge about how both EndMT and fibrosis are regulated will hopefully guide us towards the right direction.

The lack of effective therapies for fibrosis also suggests that the current experimental models are not efficient enough to translate the *in vivo* findings to the patient. Concerning EndMT, it is important to mention that there is a lack of robust human data on EndMT [2]. Nevertheless, almost all factors that induce EndMT via epigenetic mechanisms have also been described in the human circulation [11]. This emphasizes the future potential of therapeutically targeting epigenetic modulators in order to combat EndMT-associated pathologies.

The platforms to perform (epi)genetic targeting in the context of fibrosis are already available. The recent discovery of the CRISPR/Cas system allows gene-specific (epi)genetic targeting when deactivated (nuclease deficient) Cas9 is fused to different epigenetic adaptor domains. This, together with a so-called guiding RNA can result in gene-specific epigenetic editing. Currently, there are two major limitations to the CRISPR/Cas system which need to be overcome before performing epigenetic targeting in fibrosis. The first limitation is the off-target effects of the CRISPR/Cas system. The discovery of the so-called high-fidelity Cas9 has significantly improved the off-target effects that were associated with the Cas9 technology [12]. Nevertheless, screening and understanding of potential off-target effects is still key for future therapeutic use of the CRISPR/Cas technology. It is not only the CRISPR/Cas technology in itself which has potential off-target effects, but the same holds when targeting epigenetic modifiers (in particular for non-coding RNAs, but also for chromatin-modifying complexes). Therefore, future research needs to be directed to understand the network of non-coding RNAs and other epigenetic modifiers, to prevent adverse effects when performing epigenetic targeting.

Another aspect which needs to be considered for future use of the CRISPR/Cas technology for fibrosis treatment is the delivery method. Adeno associated virus

(AAV) is considered to be the safest virus so far and therefore often used in experimental models of fibrosis [13]. However it is safe to speculate that any virus, in particular in combination with a bacteria-derived Cas protein, could have potential disastrous effects in patients. Therefore, future research on alternatives to viral delivery of the CRISPR/Cas technology (eg synthetic vectors) is key for future use of this technology in the clinic.

CONCLUDING REMARKS

To conclude, (epi)genetic regulation of EndMT represents a highly promising but yet insufficiently explored field with the potential for future (epi)genetic targeting of EndMT-associated diseases such as fibrosis.

The field of EndMT as well as (epi)genetic targeting in fibrosis is currently challenged by several limitations and open questions. Future research dedicated to solving these limitations is key to develop (epi)genetic targeting tools which are compatible with the clinic.

REFERENCES

1. Rockey DC, Bell PD and Hill JA. Fibrosis-a common pathway to organ injury and failure. *N Engl J Med* 372, 1138-1149 (2015)
2. Kovacic JC, Dimmeler S and Harvey RP et al. Endothelial to mesenchymal transition in cardiovascular disease: JACC state-of-the-art review. *J Am Coll Cardiol* 73(2), 190-209 (2019)
3. Kuosmanen SM, Kansanen E and Sihvola V et al. MicroRNA Profiling Reveals Distinct Profiles for Tissue-Derived and Cultured Endothelial Cells. *Scientific reports* 7,10943 (2017)
4. Zeisberg EM, Tarnavski O and Zeisberg M et al. R. Endothelial-to-mesenchymal transition contributes to cardiac fibrosis. *Nat Med.* 13, 952–961 (2007)
5. Moore-Morris T, Guimarães-Camboa N, Banerjee I, et al. Resident fibroblast lineages mediate pressure overload-induced cardiac fibrosis. *J Clin Invest* 124, 2921–2934 (2014)
6. Sereti KI, Nguyen NB and Kamran P et al. Analysis of cardiomyocyte clonal expansion during mouse heart development and injury. *Nat Comm* 9(1), 754 (2018)
7. Rinkevich Y, Lindau P and Ueno H et al. Germ and lineage restricted stem/progenitors regenerate the mouse digit tip. *Nature* 476(7361), 409-13 (2011)
8. Manavski Y, Lucas T and Glaser SF et al. Clonal expansion of endothelial cells contributes to ischemia-induced neovascularization. *Circ Res.* 122, 670–677 (2018)
9. Welch-Reardon KM, Wu N and Hughes CC. A role for partial endothelial-mesenchymal transitions in angiogenesis? *Arterioscler Thromb Vasc Biol.* 35, 303–308 (2015)
10. Ubil E, Duan J and Pillai IC et al. Mesenchymal-endothelial transition contributes to cardiac neovascularization. *Nature* 514(7524), 585-90 (2014)
11. Hulshoff MS, Xu X and Krenning G et al. Epigenetic regulation of endothelial-to-mesenchymal transition in chronic heart disease. *Arterioscler Thromb Vasc Biol.* 38(9), 1986-1996 (2018)
12. Vakulskas CA, Dever DP and Rettig GR et al. A high-fidelity Cas9 mutant delivered as a ribonucleoprotein complex enables efficient gene editing in hematopoietic stem and progenitor cells. *Nat Med.* 24(8), 1216-1224 (2018)
13. Naso MF, Tomkowicz B and Perry WL et al. Adeno-associated virus (AAV) as a vector for gene therapy. *BioDrugs* 31(4), 317-334 (2017)

CHAPTER

14

NEDERLANDSE SAMENVATTING
(OOK VOOR NIET INGEWIJDEN)

NEDERLANDSE SAMENVATTING

De doelen van dit proefschrift zijn om (1) nieuwe (epi)genetische mechanismen te ontdekken die de plasticiteit van het endotheel beïnvloeden als onderliggende oorzaak van fibrose, en (2) om therapieën te richten op (epi)genetische mechanismen om fibrose tegen te gaan. We hebben relevante (epi)genetische veranderingen geïdentificeerd gedurende de endotheel-naar-mesenchym transitie (EndMT), een specifieke vorm van plasticiteit van het endotheel, in verschillende ziektes en hebben de impact van verschillende EndMT triggers (zoals hypoxie en een hoog glucose concentratie) onderzocht en de epigenetische veranderingen die zij teweeg brengen. Bovendien hebben we hun relevantie voor de inductie en progressie van EndMT onderzocht. Ook hebben we verschillende fasen van EndMT in kaart gebracht om genetische mechanismen te identificeren die verantwoordelijk zijn voor de actieve fase van transitie. Voor het tweede doel hebben we laten zien dat Serelaxin, een recombinante vorm van het Relaxin-2 hormoon in de mens, fibrose in het hart verlicht door het gedeeltelijk remmen van EndMT. We hebben ook de mechanismen besproken die betrokken zijn bij de wederzijdse relatie tussen chronische nierziekten en fibrose in het hart, en hebben microRNAs als potentiële profibrotische nier-hart boodschappers geïdentificeerd. Ook hebben we relevante mogelijkheden en in vivo applicaties van CRISPR/Cas derivaten geïdentificeerd. Dit gen modulerend hulpmiddel is toegepast om zich op epigenetische modificaties te richten wat leidt tot verlichting van fibrose in de nieren en het hart. Om samen te vatten, in dit proefschrift hebben we laten zien dat de plasticiteit van het endotheel in fibroproliferatieve ziektes gereguleerd is door epigenetische veranderingen (deel I). Het aangrijpen van deze epigenetische veranderingen zou nieuwe therapeutische benaderingen teweeg kunnen brengen. We laten inderdaad zien dat we therapeutische benaderingen kunnen richten op epigenetische veranderingen, wat leidt tot verlichting van fibrose (deel II).

NEDERLANDSE SAMENVATTING VOOR NIET INGEWIJDEN

Endotheel cellen zijn de cellen aan de binnenkant van bloedvaten, die in direct contact staan met het bloed. Deze cellen zijn belangrijk omdat ze een barriere vormen tussen het bloed en de ernaast liggende weefsels. Echter, door verschillende stimuli kunnen deze endotheelcellen beschadigd raken waardoor ze zich veranderen in meer uitgerekte (mesenchymale) cellen en verschillende stoffen beginnen uit te scheiden. Dit leidt tot een verlies van barriere functie en draagt bij aan verschillende ziektes zoals hart- en nierziekten.

Deze verandering van endotheel cellen naar meer uitgerekte (mesenchymale) cellen komt tot stand doordat bepaalde genen ´aan´ worden gezet terwijl andere worden uitgezet. Deze aan- en uitschakeling van genen wordt gereguleerd door een groep eiwitten en wordt epigenetica genoemd.

In dit proefschrift onderzoeken we hoe deze eiwitten (epigenetica) het veranderen van endotheelcellen in meer uitgerekte (mesenchymale) cellen beïnvloedt. Er wordt een overzicht gegeven van alle eiwitten die hier een rol in spelen, en er worden nieuwe eiwitten ontdekt die hier een mogelijke rol in spelen.

Tot slot worden er in dit proefschrift therapieën ontwikkelt om deze eiwitten (epigenetica) te veranderen wat leidt tot de vermindering van hart- en nierziekten in muizen. De in dit proefschrift-opgedane kennis kan hopelijk in de toekomst ook worden toegepast op mensen.

CHAPTER 15

DEUTSCHE ZUSAMMENFASSUNG

DEUTSCHE ZUSAMMENFASSUNG

Diese Arbeit hat zum Ziel, (1) neue (epi)genetische Regulationsmechanismen für endotheliale Plastizität zu identifizieren, welche ursächlich zur Organfibrose beiträgt und (2) diese (epi)genetischen Regulationsmechanismen und damit Organfibrose therapeutisch zu beeinflussen. Wir konnten relevante epigenetische Veränderungen während der endothelial-mesenchymalen Transition (EndMT, welche eine besondere Form der endothelialen Plastizität darstellt) im Kontext verschiedener Krankheiten identifizieren und den Einfluss von verschiedenen Auslösefaktoren für EndMT (wie z.B. Hypoxie oder ein hoher Glucosespiegel) sowie die epigenetischen Veränderungen, die sie induzieren, offenlegen. Zusätzlich haben wir deren Relevanz hinsichtlich der Induktion und Aufrechterhaltung der EndMT untersucht. Weiterhin haben wir EndMT in verschiedenen Stadien untersucht, um genetische Regulationsmechanismen, die das aktive Stadium der Transition steuern, zu identifizieren. Für das zweite Ziel konnten wir zeigen, dass Serelaxin, eine rekombinante Form des humanen Relaxin-2-Hormons, Herzfibrose zumindest teilweise durch die Inhibition der EndMT reduzieren kann. Außerdem haben wir die Mechanismen betrachtet, welche in den reziproken Zusammenhang zwischen chronischer Nierenerkrankung und Herzfibrose involviert sind und haben microRNAs identifiziert, die möglicherweise als pro-fibrotische Nieren-Herz-Botenstoffe wirken. Ebenfalls konnten wir neue relevante Möglichkeiten und in-vivo-Applikationen von CRISPR/Cas-Derivaten identifizieren. Diese Möglichkeit der Genmodulation wirkt gezielt auf epigenetische Modifikationen, welche sowohl Nieren- als auch Herzfibrose reduzieren können. Zusammenfassend haben wir in dieser Arbeit gezeigt, dass die endotheliale Plastizität bei fibroproliferativen Erkrankungen durch epigenetische Modifikationen stark beeinflusst wird (Teil 1). Diese epigenetischen Modifikationen könnten neue therapeutische Angriffspunkte darstellen. Diesbezüglich konnten wir zeigen, dass epigenetische Modifikationen *in vivo* gezielt verändert und damit Organfibrose reduziert werden kann (Teil 2).

APPENDICES

ABBREVIATIONS

ABBREVIATIONS

α -SMA	alpha smooth muscle actin
AAC	ascending aortic constriction
AAV	adeno associated virus
AcSDKP	n-acetyl-seryl-aspartyl-lysyl-proline
ADMA	asymmetric dimethylarginine
ANG-2	angiopoietin-2
ATII	angiotensin II
AVC	atrio-ventricular canal
BMP	bone morphogenetic protein
CD31	cluster of differentiation 31
ChIP	chromatin immunoprecipitation
circRNA	circular RNA
CKD	chronic kidney disease
dCas9	deactivated Cas9
dHFCas9	deactivated high-fidelity Cas9
DNMT	dna methyltransferase
EMT	epithelial-to-mesenchymal transition
EndMT	endothelial-to-mesenchymal transition
eNOS	endothelial nitric oxide synthase
EZH2	enhancer of zeste homolog 2
FACS	fluorescence-activated cell sorting
FGF	fibroblast growth factor
GAS5	growth arrest-specific 5
GFP	green fluorescent protein
H3	histone 3
HCAEC	human coronary artery endothelial cells
HDAC	histone deacetylase
HIF1 α	hypoxia inducible factor-1 α
HUVECs	human umbilical vein endothelial cells
IL	interleukin
lncRNA	long non-coding RNA
ITR	inverted terminal repeat
KLF7	kruppel-like factor 7

MALAT1	metastasis-associated lung adenocarcinoma transcript 1
MAPK	mitogen-activated protein kinase
MCEC	mouse cardiac endothelial cells
MEndT	mesenchymal-to-endothelial transition
MeDIP	methylated DNA immunoprecipitation
miR	microRNA
miRNA	microRNA
MMP	matrix metalloproteinase
NF- κ B	nuclear factor kappa-light-chain-enhancer of activated B cells
NLRP3	NACHT, LRR, and PYD domain-containing protein 3
NO	Nitric oxide
NOX	nicotinamide adenine dinucleotide phosphate oxidase
OFT	outflow tract
RAAS	renin-angiotensin-aldosterone system
RASAL1	ras-gap-like protein 1
RFP	red fluorescent protein
ROS	reactive oxygen species
RXFP	relaxin family peptide receptor
S100A4	s100 calcium-binding protein A4
SARA	smad anchor for receptor activation
SBEs	SMAD-binding elements
TAC	transverse aortic constriction
TALE	transcription activator-like effectors
TET	ten-eleven translocation methylcytosine dioxygenase
TET3CD	TET3 catalytic domain
TGF- β	transforming growth factor beta
TNF- α	tumor necrosis factor alpha
TSP-2	thrombospondin-2
TSS	transcription start site
T2D	type 2 diabetes
UUO	unilateral ureteral obstruction
VE-Cadherin	vascular endothelial cadherin
VEGF	vascular endothelial growth factor
ZFP	zinc finger protein

ACKNOWLEDGMENTS

ACKNOWLEDGEMENTS

First of all, I would like to thank my supervisors Elisabeth Zeisberg and Guido Krenning. Elisabeth, thank you for the possibilities you gave to me, thank you for believing in me, and thank you for your ultimate support. Your leadership has been a great inspiration. Thank you. Guido, thank you for promoting my independency, thank you for your trust and thank you for your support. Your great scientific insights have always inspired me. Thank you.

Also, I would like to thank my promotor Marco Harmsen for his trust and for acquainting me with the field of endothelial plasticity. I would like to thank Michael Zeisberg for his great scientific insights as well as for his ultimate support. And, I would like to acknowledge Steven Johnsen for his support and scientific insights during my thesis committee meetings.

I am grateful to the manuscript assessment committee, consisting of Prof. Steven A. Johnsen, Prof. Bernd Wollnik, Prof. Jan-Luuk Hillebrands and Prof. Marie-José T. H. Goumans, for taking the time and effort to assess this thesis. I am also grateful to the examining committee, consisting of Prof. Steven A. Johnsen, Prof. Bernd Wollnik, Prof. Jan-Luuk Hillebrands, Prof. Marie-José T. H. Goumans, Prof. Dr. Viacheslav O. Nikolaev, Prof. André Fischer, Prof. Robert H. Henning and Prof. Marianne G. Rots for taking the time and effort to assess the thesis defence.

Thank you to all lab members in Göttingen for providing a great scientific environment. In particular, I would like to thank Xingbo Xu for his great scientific input, for giving me opportunities and for believing in me. Thank you. I am grateful to Xiaoying Tan for her support during my PhD. Also, I would like to acknowledge Gunsmaa Nyamsuren, Sandip Rath, Sabine Maamari and Tim Wilhelmi for their support in the lab. I am also grateful to Sarah Rinkleff, Annika Erdmann and Anika Krueger for their technical assistance.

I would also like to thank all lab members in Groningen who supported me whenever necessary. In particular, I would like to thank Byambaa Nyamsuren and

Jolien Fledderus for their support in the lab. The Topmaster program Medical and Pharmaceutical Drug Innovation in Groningen stands out for its scientific education which is focused on becoming a top scientist. This training was essential for the successful completion of this PhD, for which I am very grateful.

Of course, I would also like to acknowledge the financial support of this PhD. I am grateful to the Graduate School of Medical Sciences in Groningen who provided a PhD scholarship. Also, I would like to thank the U4 network, and in particular Marco Lange, for financially supporting the exchange between Groningen and Göttingen. And last but not least, I would like to thank the lab in Göttingen as well as in Groningen for their financial support.

CURRICULUM VITAE & PUBLICATION LIST

CURRICULUM VITAE

The author of this thesis, Melanie Hulshoff, was born on December 12th 1992 in



Groningen, The Netherlands. She studied a Bachelor program in Biomedical Sciences at the University of Groningen, The Netherlands which she completed with distinction. She was also enrolled in the so-called Honours College, an additional extracurricular program for talented students. She then continued with the selective Topmaster program in Medical and Pharmaceutical Drug Innovation at the University of

Groningen, which she completed with distinction as well. After completing her Master studies, she was selected for a joint double degree PhD Scholarship in which she could perform her self-designed research proposal. This PhD work was performed at the University of Groningen and the University of Göttingen, Germany under supervision of Dr. Guido Krenning and Prof. Elisabeth M. Zeisberg respectively. During her PhD she has published and prepared several manuscripts on the topic of fibrosis, epigenetics and endothelial plasticity.

PUBLICATION LIST

Xu X, Tan X, **Hulshoff MS**, Wilhelmi T, Zeisberg M, Zeisberg EM. Hypoxia-induced endothelial-mesenchymal transition is associated with RASAL1 promoter hypermethylation in human coronary endothelial cells. *FEBS Lett.* 2016, 590(8):1222-33.

Xu X, Tan X, Tampe B, Wilhelmi T, **Hulshoff MS**, Saito S, Moser M, Kalluri R, Hasenfuss G, Zeisberg EM, Zeisberg M. High-fidelity CRISPR/Cas9-based gene-specific hydroxymethylation rescues gene expression and attenuates renal fibrosis. *Nat Commun.* 2018, 9(1):3509.

Hulshoff MS, Xu X, Krenning G, Zeisberg EM. Epigenetic regulation of endothelial-mesenchymal transition in chronic heart disease: histone modifications, DNA

methylation and non-coding RNAs.

Arterioscler Thromb Vasc Biol. 2018, 38:1986-96.

Hulshoff MS, Rath S, Xu X, Zeisberg M, Zeisberg EM. Causal connections from chronic kidney disease to cardiac fibrosis.

Semin Nephrol. 2018, 38(6):629-636.

Hulshoff MS*, Del Monte-Nieto G*, Kovacic J, Krenning G. Non-coding RNA in endothelial-to-mesenchymal transition.

Cardiovasc Res. 2019, 115(12):1716-1731.

Wilhelmi T, Xu X, Tan X, **Hulshoff MS**, Maamari S, Sossalla S, Zeisberg M and Zeisberg EM. Serelaxin alleviates cardiac fibrosis through inhibiting endothelial-to-mesenchymal transition via RXFP1.

Theranostics. 2020, 10(9):3905-3924.

Xu X*, **Hulshoff MS***, Tan X, Zeisberg M, Zeisberg EM. CRISPR/Cas derivatives as novel gene modulating tools: possibilities and in vivo applications.

Int J Mol Sci. 2020, 21(9). pii:E3038.

Xu X*, **Hulshoff MS***, Tan X*, Maamari S, Krenning G, Mueller O, Hasenfuss G, Zeisberg M, Zeisberg EM. Split-intein mediated AAV delivery of dCas9-TET3 as antifibrotic therapy.

Submitted.

Hulshoff MS*, Schellinger IN*, Xu X, Fledderus J, Rath SK, Wong FC, Krenning G, Raaz U, Zeisberg EM. miR-132-3p and KLF7 as novel potential regulators of aortic stiffening-associated EndMT in type 2 diabetes.

Submitted.

Hulshoff MS*, Xu X*, Kühnisch J, Tan X, Zeisberg M, Krenning G, Klaassen S, Zeisberg EM. Stage-specific mapping of the endothelial-to-mesenchymal transition. In preparation.

*These authors contributed equally to these studies

